

MECHANOCHEMICAL TRANSFORMATIONS OF α -CHITIN

by

© Georgios Margoutidis

A thesis submitted to the

School of Graduate Studies

in partial fulfillment of the requirements for the degree of

Doctor of Philosophy

Department of Chemistry

Memorial University of Newfoundland

March 2019

St. John's, Newfoundland

Abstract

Comprising 20–30% of the shells of crustaceans, α -chitin has been shown to provide a wide range of valuable products such as therapeutic substances, platform molecules and functional materials. However, the polysaccharide's crystallinity has been poorly studied, and this has limited its widespread utilization thus far.

Filling that research gap, this thesis reports a new mechanochemical method of ball milling which amorphizes α -chitin in a controlled way. Using powder XRD to measure the polysaccharide's crystallinity index (CrI%), a low balls-to-chitin (BtC) steel system was found to reduce CrI by an average of 6.0 units in regular milling times with good precision (± 2.5 CrI units). That data set was correlated for the first time with FT-IR intensity ratios showing an unaffected degree of acetylation (DA), a steady decrease of glycosidic linkage content and α -chitin's characteristic amide I split. The behaviour of the latter was rationalized as an experimental indicator for the weakening of the polysaccharide's intermolecular hydrogen bonding network which is hypothesized to arise from the distribution of the average collision force within the nanofibril structure.

The combination of increased collision frequency along with the presence of a solid acid catalyst (kaolinite) provided optimum mechanochemical conditions for efficient conversion of α -chitin into water-soluble products. The latter were analysed with a MALDI-TOF-MS method developed in Memorial University revealing oligomers of *N*-acetyl-D-glucosamine (NAG) with degrees of polymerization (DP)

of 1 to 5. The monomer and dimer reached yields of 5.1 and 3.9 wt.%, respectively, within 6 h, which compare well with yields of glucose and cellobiose from literature for cellulose ball milling. The products of this solvent-free oligomerization process were complemented by colorimetric approximations of reducing ends as well as size exclusion chromatography observations. This analysis is expected to stimulate future research for the sustainable production of these likely biologically active chitooligosaccharides.

In parallel, the inevitable fraction of higher MW chitin resulting from the ball milling process has been shown to conveniently solubilize in cold NaOH. An optimum concentration of 19 wt.% of the alkali was found to dissolve ~5 wt.% high MW/crystallinity α -chitin via a freeze-thaw process at $-28\text{ }^{\circ}\text{C}$ and give films of acceptable mechanical properties after a simple casting treatment with HCl. Practically, this method avoids some of the disadvantages of organic-salt-solution solvents like the need for a costly recycling/purification treatment, their life cycle issues, the high temperatures, and the long stirring times. At the same time, it can quickly create homogeneous solutions of predictable viscosities in the 1–10 wt.% range allowing for more efficient and controlled chitin deacetylation.

Publications arising from this work

Peer reviewed

Margoutidis, G.; Parsons, V. H.; Bottaro, C. S.; Yan, N.; Kerton, F. M. Mechanochemical amorphization of α -chitin and conversion into oligomers of *N*-acetyl-D-glucosamine. *ACS Sustainable Chemistry & Engineering* **2018**, 6 (2), 1662-1669.

Conference

Maini; Halasz; Takacs; James; Belenguer; Frišćic; Jones; Stolle; Boldyreva; Blair; Galembeck; Suslick; Margoutidis; Mack; Jörres; Nagapudi; Beyer; Brekalo; Lamaty; Irikura; Khripin; Hamilton; Zhang Mechanistic understanding, catalysis and scaling up of mechanochemistry: General discussion. *Faraday Discussions* **2014**, 170, 287-310.

Grants

Part of the work contained in Chapter 4 of this thesis has been supported financially by a "Researcher Mobility Grant", which was awarded by the Royal Society of Chemistry (RSC) on 2016 to work at the Centre for Sustainable Chemical Technologies (CSCT) of the University of Bath (UK).

Presentations on international conferences

Part of the work contained in this thesis has been presented in posters in the following international conferences:

- American Chemical Society (ACS) Summer School on Green Chemistry and Sustainable Energy, Golden, Colorado, USA (June 2017)
- International Symposium on Green Chemistry (ISGC), La Rochelle, France (May 2017)
- Faraday Discussion 170 on "Mechanochemistry: from functional solids to single molecules", Montreal, Canada (May 2014)

Acknowledgements

The writing of this study was carried out while I had the honour and privilege to follow Memorial University's PhD program and work as a researcher in The Green Chemistry and Catalysis Group in Newfoundland. I feel particularly fortunate that Professor Francesca Kerton entrusted me with this new and effectively innovative method to briefly investigate one of the island's most beautiful and powerful resources. Thanks to her shrewd selection of this topic, I was able to fully engage with the ups and downs of the 5-year research project captured in this thesis. Yet, more importantly, I am grateful for the freedom she gave me to take any turn I wanted for my experiments and literature readings (this should not be taken for granted in these days of ever-limited research funding). We sometimes had our disagreements on the project's kinetics, the thermodynamics however have always benefited from a team spirit; the routes taken showed me a silky way of refusing to go beyond the fact. Raising some new research questions in the future will surely allow me to reciprocate a valuable gift.

This same devotion to science, which has no connection with a materialistic view of life, has been a source of inspiration for me coming from Professor Christopher Kozak as well. With his enthusiasm for laboratory work, and attention to detail in group meetings and in thesis drafts, Chris supported me when my doubts were no longer fertile but corrosive. This positive energy was also generated by my lab-mates Kata, Jen, Dalal, Jenna, Hart, Kenson, Tim, Kori, Juliana, Ali, Yi (my role model), Charlene, Jue, Kaijie, Craig, Shafaet, Quentin, Erika, Coralie, Keegan, and Courtney

who not only helped me, but also kept me motivated, organized, safe in the lab and the Department, and generally made the days pass quickly. I am particularly thankful to Valerie Parsons for preparing and sharing a convenient and reliable MALDI-TOF-MS method for sugar analysis. Her quality work and scientific curiosity allowed me to make a smooth and dynamic start with a significant set of experiments. Here, I would like to thank Professor Robert Helleur who became another important source of encouragement through his willingness to regularly listen to my findings and generously offer his perspective. Many thanks also to Professor Erika Merschrod for the thesis writing club sessions and supervision, as well as to Dr. Wanda Aylward and Nick Ryan who have been particularly supportive with my XRD, FT-IR and viscometry investigations.

Special thanks to Erin Alcock from MUN's library for her help with literature hunt, the late Colin Antle for willingly preparing ammonium acetate, Anne Shepard, David Murphy, Bernie Rice, Tiber Reardon, and Jenny Kim for being excellent teaching instructors, Steve, Mike and the rest of the Machine Shop team for the "fistful of steel", and also for gracefully repairing the ball mill several times, the tireless and reliable Technical Services, the Centre for Chemical Analysis, Research and Training (C-CART), the University's Writing Centre, and the entire staff of the Chemistry Department for providing a wonderful environment for research and teaching. The School of Graduate Studies (SGS), Natural Sciences and Engineering Research Council (NSERC) of Canada, and the Research & Development Corporation (RDC) of Newfoundland are acknowledged for their financial support.

This is a good place to extend my gratitude to Professor Janet Scott who elegantly arranged for me to be hosted in “the cellulose group” within the Centre for Sustainable Chemical Technologies (CSCT) of the University of Bath (UK). One of the most rewarding aspects of that experience was to realize the potential of the “waste” material that I’ve been studying so far to be transformed into a high-value product. I am therefore grateful to Professor Scott for giving me the freedom to try various solvents on α -chitin and reviewing my experimental results with dedication (again this should not be taken for granted today). Special thanks to Dr. Ram Sharma, Dr. Tim Woodman, Dr. Rémi Castaing, Marcus, Reggie, Jamie, James, Alvaro, Nick, Georgina, Kasia, Magdalena, and Giovanna for the scientific support and good company during those three months. I would also like to acknowledge the Royal Society of Chemistry (RSC) for the financial support of the work in Bath through its “Researcher Mobility Grants”.

Finally, my most heartfelt thanks go to Paris Georghiou for being a good friend on that side of the ocean, Tatsuo Izawa for having his coffee breaks with me and offering his physics perspective, Meghan Farrell for being my “partner in crime”, Peter Barnes for being my “father” in Newfoundland and introducing me to his lifetime friends from the beautiful west coast of the island, my brother Socrates and my mother Zoe for their unconditional affection and devotion, sometimes at great sacrifice to themselves.

Table of contents

Abstract	ii
Publications arising from this work	iv
Acknowledgements	v
Table of contents	viii
List of figures	xiii
List of tables	xxiii
List of abbreviations	xxiv
Chapter 1 Introduction	1
1.1 Irreversible environmental changes and societal timescales.....	1
1.2 Green Chemistry	3
1.3 Renewable resources, food waste and biorefineries.....	7
1.4 Chitin.....	9
1.5 Valuable products from chitin.....	17
1.5.1 Therapeutic substances	18
1.5.2 Products for agricultural systems.....	19
1.5.3 Platform molecules.....	22
1.5.4 Fuels.....	23
1.5.5 Personal care products	23
1.5.6 Functional materials.....	25
1.6 Natural polysaccharides and valorization methods	28
1.7 Mechanochemistry.....	38
1.8 Summary, research objectives and thesis structure	42
1.9 References.....	45
Chapter 2 Mechanochemical amorphization of α-chitin	62
2.1 Introduction	62
2.1.1 Mechanical force and organic macromolecules	62
2.1.2 Reduction of polysaccharide crystallinity via ball milling	65
2.1.3 Ball milling essentials and collision frequency.....	70
2.1.4 Amorphization-solubilization of polysaccharides via collisional forces	74

2.1.5	Methodological approach to the problem	76
2.2	Experimental	77
2.2.1	Materials	77
2.2.2	Mechanochemical treatment of α -chitin	78
2.2.3	Gravimetric analysis to determine the mass of soluble products (sample solubility%)	78
2.2.4	X-ray diffraction (XRD)	79
2.2.5	Fourier transform infrared (FT-IR) spectroscopy	79
2.3	Results and Discussion	80
2.3.1	X-ray diffraction of native α -chitin	80
2.3.2	Effect of the milling ball diameter on crystallinity	83
2.3.3	Effect of chitin mixing load on crystallinity	88
2.3.4	Effect of milling time on particle size and morphology	95
2.3.5	FT-IR investigation into molecular origins of changes in crystallinity.....	98
2.3.5.1	<i>Qualitative analysis and weakening of α-chitin's hydrogen bonding network.....</i>	<i>98</i>
2.3.5.2	<i>Quantitative analysis and a force distribution hypothesis.....</i>	<i>101</i>
2.3.5.3	<i>Comparison with literature data.....</i>	<i>112</i>
2.3.6	Effect of milling on the solubility of α -chitin in water.....	115
2.4	Conclusions	121
2.5	References.....	123
Chapter 3	Mechanochemical conversion of α-chitin to oligomers of <i>N</i>- acetyl-D-glucosamine.....	134
3.1	Introduction	134
3.1.1	Relevant ball milling methods in polysaccharide literature	134
3.1.2	Mechanistic considerations	136
3.1.3	Summary and methodological approach to the problem	139
3.2	Experimental	140
3.2.1	Materials	140
3.2.2	Mechanochemical treatment of α -chitin	141

3.2.3	Gravimetric analysis to determine the mass of soluble products (sample solubility %)	141
3.2.4	X-ray diffraction (XRD) and Fourier transform infrared (FT-IR) spectroscopy	141
3.2.5	Chitin conversion to levulinic acid (LA)	142
3.2.6	Colorimetric approximation of reducing ends of soluble products	143
3.2.6.1	<i>Dinitrosalicylic acid (DNS) method</i>	143
3.2.6.2	<i>Schales' method</i>	144
3.2.7	Derivatization of soluble products, GlcNAc and (GlcNAc) ₂ for quantification using MALDI-TOF MS analysis	145
3.2.8	MALDI-TOF instrumentation and mass spectra processing	145
3.2.9	Size Exclusion Chromatography (SEC) analyses	146
3.3	Results and discussion	147
3.3.1	Effect of kaolinite on α -chitin's amorphization/solubility	147
3.3.2	Effect of increased packing and balls-to-chitin (BtC) ratios (intense ball milling) on α -chitin	153
3.3.2.1	<i>Fast amorphization</i>	153
3.3.2.2	<i>Fast solubilization</i>	156
3.3.2.3	<i>Fast and deep depolymerization, deacetylation trend, and a liquid assisted grinding (LAG) test</i>	159
3.3.2.4	<i>Depolymerization of chitosan</i>	163
3.3.2.5	<i>A hypothesis on α-chitin molecular weight (MW)</i>	166
3.3.2.6	<i>Proposed mechanistic considerations</i>	167
3.3.3	Effect of intense ball milling on α -chitin's conversion to levulinic acid (LA)	170
3.3.4	Effect of the combination of intense ball milling and kaolinite on α -chitin solubility	173
3.3.5	Colorimetric approximation of reducing ends of soluble products	179
3.3.5.1	<i>Dinitrosalicylic acid (DNS) method</i>	181
3.3.5.2	<i>Schales' method</i>	192
3.3.6	Mass spectrometry analysis of soluble products with matrix assisted laser desorption ionization (MALDI)	197

3.3.6.1	<i>Qualitative analysis</i>	199
3.3.6.2	<i>Quantitative analysis</i>	202
3.3.7	Size Exclusion Chromatography (SEC) analysis of soluble products	207
3.4	Conclusions	208
3.5	References.....	211
Chapter 4	α-Chitin dissolution studies towards film casting.....	218
4.1	Introduction and methodological approach to the problem	218
4.2	Experimental	221
4.2.1	Mechanochemical treatment of α -chitin	221
4.2.2	X-ray diffraction (XRD)	221
4.2.3	Fourier transform infrared (FT-IR) spectroscopy	221
4.2.4	Relative viscosity of chitin in 1-ethyl-3-methylimidazolium acetate.....	221
4.2.5	Chitin dissolution studies and preliminary film casting.....	222
4.2.6	Ultrasound assisted heterogeneous deacetylation of α -chitin.....	223
4.2.7	Determination of degree of acetylation (DA) by ^1H NMR spectroscopy.....	224
4.2.8	Relative viscosity of chitin in NaOH	224
4.3	Results and discussion	225
4.3.1	Mechanochemical depolymerization/amorphization of α -chitin..	225
4.3.2	Relative estimation of molecular weights (MW) using an ionic liquid (IL)	228
4.3.3	Chitin dissolution studies and preliminary film casting.....	231
4.3.3.1	<i>In 1-ethyl-3-methylimidazolium acetate (EmimAcO)</i>	231
4.3.3.2	<i>In sodium hydroxide (NaOH)</i>	234
4.3.4	Ultrasound assisted heterogeneous deacetylation of α -chitin.....	243
4.3.5	NaOH as a solvent for chitin.....	274
4.4	Conclusions	289
4.5	References.....	292
Chapter 5	Concluding remarks and future directions	299

5.1	References.....	309
Appendix A2	313
Appendix A3	326
Appendix A4	352

List of figures

- Figure 1-1: Beyond irreversible environmental change levels. The inner green shading embodies the proposed safe operating space for nine interconnected planetary systems. The red wedges signify an estimate of our generation's levels of the systems' key variables. Reprinted by permission from Macmillan Publishers Ltd: [NATURE] (Vol 461, 472-475), copyright (2009)..... 1
- Figure 1-2: Green chemistry considerations/skills for satisfaction of modern society's needs. Reproduced from {Green Chem., 2016, **18**, 3914-3934} with permission from The Royal Society of Chemistry..... 6
- Figure 1-3: Potential products from oceanic biomass (excluding fish/shellfish use as meat and direct use of algae as a foodstuff). Reproduced from {Green Chem., 2013, **15**, 860-871} with permission from The Royal Society of Chemistry..... 9
- Figure 1-4: Molecular structure of chitin/chitosan (DP: Degree of Polymerization, DA: Degree of Acetylation)..... 10
- Figure 1-5: Hierarchical microstructure of the cuticle of the lobster *H. americanus* [Reprinted from Acta Materialia, 53, D. Raabe, C. Sachs, P. Romano, The crustacean exoskeleton as an example of a structurally and mechanically graded biological nanocomposite material, 4281-4292, Copyright (2005), with permission from Elsevier]. 12
- Figure 1-6: Difference in intermolecular forces between α -chitin (left) and β -chitin (right). Antiparallel chains in α -chitin have been drawn by a vertical 180° rotation of chain 1. Bold chain label denotes the reducing end direction in the molecule. Chain 3 (green) in α -chitin lies towards the reader; parallel to chain 4 (blue). Hydrogen bonds are in red. Certain hydrogens have been omitted and no other hydrogen bonds (e.g. intramolecular ones) are shown for clarity. Note that pyranose rings preserve the chair conformation. 14
- Figure 1-7: Intermolecular bifurcated hydrogen bond (in red) between parallel chains in α -chitin. Chain numbering is according to Figure 1-6 (based on Petrov et al.).⁸⁶ The hydroxymethyl conformation, which does not favour the bifurcated hydrogen bond, is visualized in green. 16
- Figure 1-8: Categories of valuable products from chitin (or chitinous waste). 17
- Figure 1-9: Enhancement of maize seed germination and seedling growth (root/shoot length, number of roots) by Cu-chitosan nanoparticles (NPs). Seeds were immersed for 4 h in deionized water (control), bulk chitosan (BCH) (0.01%), CuSO₄ (0.01%), and Cu-chitosan NPs at 0.01, 0.04, 0.08, 0.12, and 0.16% w/v and data were recorded after 10 days of growth in a dark room (w/daily watering). Reprinted with permission from Saharan, V.; Kumaraswamy, R. V.; Choudhary, R. C.; Kumari, S.; Pal, A.; Raliya, R.; Biswas, P. Cu-Chitosan Nanoparticle Mediated Sustainable Approach to Enhance Seedling Growth in Maize by Mobilizing Reserved Food. *J. Agric. Food Chem.* **2016**, *64*, (31), 6148-6155. . Copyright (2016) American Chemical Society. 22

- Figure 1–10: Layer by layer (LBL) assembly to fabricate chitosan-based films. Reprinted in part with permission from Wang, H.; Qian, J.; Ding, F. Emerging Chitosan-Based Films for Food Packaging Applications. *J. Agric. Food Chem.* **2018**, *66*, (2), 395-413. Copyright (2018) American Chemical Society.27
- Figure 1–11: Polysaccharide microfibril structures in plant cell walls. Crystalline cellulose is shown in blue, and hemicellulose in orange. Lignin structures are not illustrated for clarity. Source: Office of Biological and Environmental Research of the U.S. Department of Energy Office of Science (science.energy.gov/ber/). Retrieved from <https://public.ornl.gov/site/gallery/>.29
- Figure 1–12: Disruption of solvent-solvent interactions towards solute solubilization. Reproduced from {Otto, S. The role of solvent cohesion in nonpolar solvation. *Chem. Sci.* **2013**, *4*, (7), 2953-2959} with permission of The Royal Society of Chemistry.....38
- Figure 2-1: Scheme of crystalline and amorphous regions in idealized fibers of linear polysaccharides like cellulose and chitin. Void in between the horizontal chains in the crystalline region can be imagined as the zone where the hydrogen bonding of Figures 1–6 and 1–7 form the *bc* and *ac* sheets respectively. Reproduced from {*Nanoscale*, 2012, **4**, 3274} with permission of The Royal Society of Chemistry. (<http://dx.doi.org/10.1039/C2NR30260H>).....65
- Figure 2-2: Milling motion of the reaction vessel in a SPEX 8000M mixer/mill (in blue arrows). The shaft-arm is fixed perpendicular to the clamp which holds the (silver) vial. Used with the permission of SPEX SamplePrep from <https://www.spexsampleprep.com/8000M-mixermill>.71
- Figure 2-3: Four of the most widely used milling modes. Schematics to the right of the mill illustrate the milling media's motion. (A) SPEX 8000M mixer/mill (65 mL), (B) planetary mill (250 mL), (C) attritor (4 L), (D) rolling ball mill (hundreds of L). Reproduced from {*Faraday Discuss.*, 2014, **170**, 223-233} with permission of The Royal Society of Chemistry. <http://dx.doi.org/10.1039/C4FD00007B>.....74
- Figure 2-4: X-ray diffraction (XRD) pattern of native α -chitin with its characteristic reflections.81
- Figure 2-5: The *ab* projection of α -chitin's lattice illustrating the (110) (black lines), (020) (green lines), (100) (pink lines), (010) (orange lines) planes within a proposed 19 chain crystallite. The orthorhombic unit cell is drawn in black lines in the bottom left (distance between 010 lines is 18.85 Å, and in between (100) lines is 4.75 Å). *ac*-Sheet direction is shown in red, and *bc*-sheet direction is shown in blue. Adapted by permission from [Springer Customer Service Centre GmbH]: [Springer Nature] [Journal of Biosciences] [Atkins, E. J Biosci (1985) 8:375 (Conformations in polysaccharides and complex carbohydrates, Edward Atkins)], [Copyright] (1985), doi: 10.1007/BF02703990.82
- Figure 2-6: XRD patterns of untreated (black signal) and milled α -chitin with 2 × 0.5" balls for 30 (red), 60 (green), 90 (blue) and 120 (pink) min. Temperature of the inner surface of the vial did not exceed 40 °C.....84

Figure 2-7: XRD patterns of untreated (black signal) and milled α -chitin with $16 \times 0.25''$ balls for 30 (red), 60 (green), 90 (blue) and 120 (pink) min. Temperature of the inner surface of the vial did not exceed 41°C	85
Figure 2-8: Crystallinity Index (CrI)% of α -chitin over milling time when processed with $2 \times 0.5''$ (blue) and $16 \times 0.25''$ (red) balls.....	86
Figure 2-9: Overlay of XRD patterns (no separation) of 4 (red), 3 (green), 2 (blue) and 1 (pink) g α -chitin milled with $2 \times 0.5''$ balls for 90 min. Dotted lines mark the intensities: 1835 (red), 1547 (green), 1493 (blue), and 1407 (pink) at 19.20° ; 741 (red), 715 (green), 720 (blue), and 756 (pink) at 16.00° ; 872 (red), 709 (green), 644 (blue), 540 (pink) at 9.28°	89
Figure 2-10: Overlay of XRD patterns (no separation) of 4 (red), 3 (green), 2 (blue) and 1 (pink) g α -chitin milled with $16 \times 0.25''$ balls for 90 min. Dotted lines mark the intensities: 1488 (red), 1507 (green), 1250 (blue), 1196 (pink) at 19.20° ; 686 (red), 787 (green), 836 (blue), 826 (pink) at 16.00° ; 678 (red), 698 (green), 560 (blue), 512 (pink) at 9.28°	89
Figure 2-11: Crystallinity Index (CrI)% over α -chitin mixing load when milled for 90 min with $2 \times 0.5''$ (blue) and $16 \times 0.25''$ (red) balls. Inset reads the same data on a balls to chitin mass ratio (BtC) x-axis.....	91
Figure 2-12: Intensity ratio for reflections (110)/(020) over balls to chitin (BtC) mass ratio for milling with $2 \times 0.5''$ (blue) and $16 \times 0.25''$ (red) balls for 90 min. Inset reads the same data on an α -chitin mixing load (g) x-axis.....	94
Figure 2-13: Scanning electron microscopy (SEM) micrographs of untreated (a – 2 mm scale, b – 500 μm scale) and ball milled α -chitin with $16 \times 0.25''$ balls (8.2 BtC) for 45 (c – 500 μm scale) and 105 (d – 500 μm scale) min. Regions I and II are shown in separate SEMs of 50 and 300 μm scale respectively in Figure A2–10.	95
Figure 2-14: ATR FT-IR spectra of native (black signal) and milled α -chitin with $16 \times 0.25''$ balls for 60 (blue) and 120 (red) min (8.2 BtC). The inset shows the hydrogenic stretching region of $3700\text{--}3000\text{ cm}^{-1}$ in more detail.....	99
Figure 2-15: $1670\text{--}1500\text{ cm}^{-1}$ region of infrared spectra of native (black signal) and milled α -chitin with $16 \times 0.25''$ balls for 30 (green), 60 (blue), 90 (pink) and 120 (red) min (8.2 BtC). 1652 and 1621 cm^{-1} bands are characteristic of the α -chitin sample in this thesis.....	102
Figure 2-16: FT-IR data ($1621\text{ cm}^{-1}/1652\text{ cm}^{-1}$ peak ratio) for milled α -chitin with $16 \times 0.25''$ balls (8.2 BtC). Indicatively, the triplicate measurement for the 60 min sample gave a ratio of 0.790 ± 0.011 , which can be reproduced from the average signal in Figure 2–15 ($0.0652 / 0.0824$ is approx. 0.791).	105
Figure 2-17: FT-IR data ($1558\text{ cm}^{-1}/1541\text{ cm}^{-1}$ peak ratio) for milled α -chitin with $16 \times 0.25''$ balls (8.2 BtC). Indicatively, the triplicate measurement for the 60 min sample gave a ratio of 0.961 ± 0.012 , which can be reproduced from the average signal in Figure 2–15 ($0.0778 / 0.0810$ is approx. 0.960).	105

Figure 2-18: Hypothetical mechanical force distribution (orange dotted arrows) through α -chitin's $N^1-H \cdots O7^2$ intermolecular hydrogen bond and backbone structure during ball milling. Note that the $O6^1-H \cdots O7^2$ hydrogen bond of Figure 1-7 is broken here and that opposite force vectors apply to all covalent and non-covalent bonds.....	108
Figure 2-19: FT-IR data ($1154\text{ cm}^{-1}/2875\text{ cm}^{-1}$ peak ratio) for milled α -chitin with $16 \times 0.25''$ balls (8.2 BtC). Figure A2-16 shows the relevant absorbance intensities for the 60 min sample ($0.0353 / 0.0265 = 1.332$).....	111
Figure 2-20: FT-IR data ($1552\text{ cm}^{-1}/2875\text{ cm}^{-1}$ peak ratio) and degree of acetylation (DA%) for milled α -chitin with $16 \times 0.25''$ balls (8.2 BtC). Figure A2-16 shows the relevant absorbance intensities for the 60 min sample ($0.0726 / 0.0265 = 2.740$).	111
Figure 2-21: Solubility % of α -chitin at pH 2.9 (red) and 7.0 (blue) when ball milled with $16 \times 0.25''$ balls. * Solubility values for 0 min milling time correspond to α -chitin ball milled for 3 min with ca. 18% packing (reduced particle size was easier to weigh). When the flakes of native α -chitin were tested standard deviations for the solubility triplicates were large (at pH 7.0: 6.29 ± 1.39 , and at pH 2.9: 6.47 ± 2.16).	120
Figure 3-1: Proposed mechanistic considerations towards mechanocatalytic activation of the glycosidic linkage in cellobiose/cellulose. Reprinted from <i>Catalysis Today</i> , 234, F. Schüth, R. Rinaldi, N. Meine, M. Kåldström, J. Hilgert, M.D. Kaufman Rechulski, Mechanocatalytic depolymerization of cellulose and raw biomass and downstream processing of the products, 24-30, Copyright (2014), with permission from Elsevier.	139
Figure 3-2: Solubility % of pre-milled α -chitin using $2 \times 0.5''$ balls for 30-60-90 min (step 1) when milled with kaolinite (1:1 g:g) by $2 \times 0.5''$ balls for 60 min (step 2) (blue bars in pH 7.0 and red in pH 2.9). Green bars show the predicted average solubility values (pH 7.0) for just step 1.....	151
Figure 3-3: Solubility % of α -chitin when milled by $16 \times 0.25''$ (turquoise/orange) and $2 \times 0.5''$ (blue/red) balls without (2:0 g:g) and with kaolinite (1:1 g:g) for 240 min (turquoise/blue bars in pH 7.0 and orange/red in pH 2.9).....	153
Figure 3-4: XRD patterns of α -chitin (2 g) milled with $1 \times 0.5'' / 72 \times 0.25''$ balls for 15 (black), 30 (red), 60 (orange), 90 (blue), and 120 (green) min (16.5% packing / 40.2 BtC). Dotted lines mark the intensities: 2251 (red), 1469 (blue) at 19.20° ; 1899 (red), 1176 (blue) at 16.00° . CrI values are: 33.5% [$(2251 - 1899) \times 100 / 1051$] for red signal, and 27.4% [$(1469 - 1176) \times 100 / 1069$] for blue. The intensities of all data have been offset relative to the 120 min sample by whole multiples of 200 a.u.	155
Figure 3-5: Crystallinity Index (CrI)% of α -chitin over milling time (min) when processed with $1 \times 0.5'' / 72 \times 0.25''$ balls (16.5% packing / 40.2 BtC; blue data) and with $16 \times 0.25''$ balls (3.3% packing / 8.2 BtC; red data).	155
Figure 3-6: Solubility % of α -chitin when ball milled with $68-70 \times 0.25'' / 2 \times 0.5''$ balls (17.5 % packing); BtC 42.8 at pH 7.0 (blue), 2.9 (red), and 85.6 at pH 7.0 (green). .	158

Figure 3-7: Colour development in ball milled and water-soluble α -chitin products when processed with 68-70 \times 0.25" / 2 \times 0.5" balls (17.5% packing / 42.8 BtC) for 0-2-4-8 h.	158
Figure 3-8: 1600–1100 cm^{-1} region of infrared spectra of milled α -chitin with 68-70 \times 0.25" / 2 \times 0.5" balls (17.5% packing / 85.6 BtC) for 1 (green), 2 (blue), 4 (pink) and 6 (red) h. Insets show the reference band (3000–2800 cm^{-1}) and glycosidic linkage (1169–1135 cm^{-1}) regions. Orange dotted lines highlight the intensities for reproduction of the ratios which probe depolymerization and deacetylation for the 4 h sample (the bands at 2874, 1548, and 1154 cm^{-1} absorb 0.0291, 0.0688, and 0.0272 respectively).	161
Figure 3-9: FT-IR data (1548 cm^{-1} / 2874 cm^{-1} peak ratio) and degree of acetylation (DA%) for milled α -chitin with 68-70 \times 0.25" / 2 \times 0.5" balls (17.5% packing / 85.6 BtC) plotted in green data (inset table records the exact values and standard deviations). Blue data is for the 16 \times 0.25" balls system (3.3% packing / 8.2 BtC) plotted in detail in Figure 2–20.	162
Figure 3-10: FT-IR data (1154 cm^{-1} / 2874 cm^{-1} peak ratio) for milled α -chitin with 68-70 \times 0.25" / 2 \times 0.5" balls (17.5% packing / 85.6 BtC) plotted in green data (inset table records the exact values and standard deviations). Blue data is for the 16 \times 0.25" balls system (3.3% packing / 8.2 BtC) plotted in detail in Figure 2–19.	162
Figure 3-11: 1700–1100 cm^{-1} region of infrared spectra of high MW chitosan (green), as well as milled with 42.8 (blue) and 85.6 (red) BtC [68 \times 0.25" / 2 \times 0.5" balls (17.5% packing)] for 30 min. Insets show the reference band (3000–2800 cm^{-1}) and glycosidic linkage (1167–1135 cm^{-1}) regions. Orange dotted lines highlight the intensities for reproduction of the ratios which probe depolymerization and deacetylation for the 42.8 BtC sample (the bands at 2866, 1552, and 1151 cm^{-1} absorb 0.0331, 0.0192, and 0.0259 respectively).	165
Figure 3-12: Proposed mechanistic considerations towards mechanochemical depolymerization of α -chitin. Elementary α -chitin fibril volumes trapped in between colliding balls are subjected to disruption of intermolecular hydrogen bonds and homolytic cleavage of glycosidic linkages through force distribution (orange dotted arrows).	170
Figure 3-13: Levulinic acid yields (wt.%) produced from native and ball milled chitosan high-MW (green bars) and α -chitin (blue bars) via microwave assisted conversion (for analytical data see Table A3–2). Ball milling was with 17.5% packing/42.8 BtC for 4, 5, 8 h.	173
Figure 3-14: Solubility % of α -chitin at pH 7.0 (blue) and 2.9 (red) when ball milled with 68-70 \times 0.25" / 2 \times 0.5" balls (17.5% packing, BtP 42.8) and kaolinite (1:1 g:g). The 2 h milled sample was not tested in replicates in pH 2.9.	175
Figure 3-15: UV-Vis spectra of initial reaction mixtures between equal volumes of a standard glucose solution and DNS reagents of 0.702 (red), 0.351 (orange), 0.176 (green), and 0.088 (blue) mM 3,5-dinitrosalicylic acid. Inset reads more detail in the 500–520 nm region.	183

- Figure 3-16: UV-Vis spectra of duplicate measurements of 1:20 (orange-red) and 1:40 (turquoise-green) dilutions of the most concentrated and intensely-coloured water-soluble products of Section 3.3.4 ($88.07 \pm 3.53\%$ from 7 h ball milling). The DNS reagent of 0.088 mM 3,5-dinitrosalicylic acid diluted with equal volume of a standard glucose solution (blue) is overlaid for comparison purposes. Inset reads more detail in the 500-550 nm region. Intensity of the 1:40 dilution at 540 nm is 0.042 ± 0.011 186
- Figure 3-17: Glucose calibration curves for DNS assays with reagent A [red; 0.088 mM 3,5-dinitrosalicylic acid, 0.4079 M NaOH (pH 13.61), 0.766 M tartaric acid disodium salt dihydrate, 17.0 mM phenol] and reagent B [blue; 0.088 mM 3,5-dinitrosalicylic acid, 0.3997 M NaOH (pH 13.60), 1.063 M tartaric acid disodium salt dihydrate, 21.6 mM phenol] obtained by 5 min microwave treatments at 100 °C [volumes of DNS reagent and glucose solution were equal (1500 μ L)]. Assay of reagent C [green; 44 mM 3,5-dinitrosalicylic acid, 0.4 M NaOH (pH 13.60), 1.063 M Rochelle salt] was obtained by Saqib and Whitney in a similar way (volumes of DNS reagent and glucose solution were 4 and 1 mL respectively). The $y = \alpha x + \beta$ equations correspond to x values (glucose concentrations) in mM. Secondary horizontal axis reads glucose concentrations in g/L. UV-Vis spectra for reagent's B assay are shown on Figure A3-22. 189
- Figure 3-18: UV-Vis spectra of 2.5 (red), 8.3 (green), and 11.4 (blue) g/L ball milled α -chitin products after 1500 μ L of their corresponding diluted aliquots [0.18 (red), 0.21 (green), and 0.24 (blue) g/L] were treated by microwaves for 5 min at 100 °C with 1500 μ L DNS reagent B [0.088 mM 3,5-dinitrosalicylic acid, 0.3997 M NaOH (pH 13.60), 1.063 M tartaric acid disodium salt dihydrate, 21.6 mM phenol]. Inset focuses on the 530-550 nm region and includes the corresponding signals before the application of microwave irradiation (orange below 0.010 for 0.18 g/L sample, lighter green at 0.020 for 0.21 g/L and lighter blue at 0.030 for 0.24 g/L). 191
- Figure 3-19: *N*-acetyl-D-glucosamine (NAG) calibration curve for the Schales assay. The $y = \alpha x + \beta$ equation corresponds to x values (NAG concentrations) in μ M. Secondary horizontal axis reads NAG concentrations in g/L. UV-Vis spectra for the assay are shown on Figure A3-24. 193
- Figure 3-20: UV-Vis spectra of 2000 μ L Schales reagent when mixed with 1500 μ L of 15 (pink), 20 (red), 25 (orange), 30 (green), 35 (blue), 47 (purple) times diluted intensely-coloured water-soluble products of Section 3.3.4 ($75.77 \pm 1.25\%$ from 6 h ball milling). Inset plots the absorbances at 420 nm against the dilution factor [the value for the 15-fold dilution (0.396) was excluded as it deviated significantly from the linear equation reported (R^2 was ca. 0.91)]. 194
- Figure 3-21: UV-Vis spectra of 2.5 (light blue), 8.3 (green), and 11.4 (orange) g/L ball milled α -chitin products after 1500 μ L of their corresponding 65-fold dilutions [0.039 (darker blue), 0.128 (green), and 0.176 (red) g/L; signals for initial reaction mixtures absorb above 0.78 at 420 nm] were treated by microwaves for 10 min at 100 °C with 2000 μ L Schales reagent. Pink dotted line with transparency marks the absorbance level at 0.78. 196

Figure 3-22: Representative reaction scheme for the formation of chitin-GTMA derivatives.	199
Figure 3-23: MALDI-TOF mass spectra of soluble products from ball milling α -chitin with 68-70 \times 0.25" / 2 \times 0.5" balls (17.5 % packing) and kaolinite (1:1 g:g, BtP 42.8) for 0.5 h (A), 2 h (B) and 6 h (C). Insets show spectra focused at m/z 300-340 without subtracting average spectra for the blank derivatization reaction. Peak height at m/z 303.2 for internal standard can be compared to the monomer (GlcNAc) peak height at m/z 337.2. Table A3-3 records the corresponding detailed peak lists.	201
Figure 3-24: Analyte (monomer to pentamer) to internal standard (IS) peak height ratios for GTMA derivatives of α -chitin oligomers generated by milling (kaolinite, 2 \times 0.5" /68-70 \times 0.25" balls) for 0.5, 2, 4, 6 h. Data were obtained by MALDI-TOF-MS.	204
Figure 3-25: Calibration curves for GlcNAc (blue) and (GlcNAc) ₂ (red) prepared by GTMA derivatization and MALDI-TOF MS. Error bars arise from quintuplicate acquisitions among spots. Representative spectra are available in Figures A3- 29 and A3-30.	206
Figure 4-1: Main experimental considerations towards α -chitin film casting. Steps of film fabrication via the solution casting technique (solvent evaporation can be preceded by an anti-solvent treatment step) and chain entanglement for increasing polymer concentration. Molecular weight, degree of acetylation and crystallinity of α -chitin influence all phases of the process in chorus. Adapted from Suntornnond, R., An, J., Yeong, W. Y. and Chua, C. K. (2015), Biodegradable Polymeric Films and Membranes Processing and Forming for Tissue Engineering. Macromol. Mater. Eng., 300: 858-877. doi:10.1002/mame.201500028 by permission from John Wiley and Sons. © 2015 WILEY-VCH Verlag GmbH & Co. KGaA, Weinheim	220
Figure 4-2: Infrared spectra of native (red), high MW (green), medium MW (blue), and low MW (orange) α -chitin (ball milling conditions and FT-IR ratios are recorded in Table 4-1). Data acquired at MUN.	227
Figure 4-3: Relative viscosities of chitin samples at 0.2070 \pm 0.0052 wt.% in EmimAcO. Dissolution process included microwave treatment. Error bars in native, high MW, and medium MW data are 0.24, 0.37, and 0.06 respectively arising from duplicate for native α -chitin and triplicate for the ball milled samples suspension preparations (0.2068 \pm 0.0002 wt.% native α -chitin, 0.2027 \pm 0.0078 wt.% high MW, 0.2097 \pm 0.0001 wt.% medium MW).....	231
Figure 4-4: Color comparison and appearance of EmimAcO (vial far left) and viscous suspensions of high MW α -chitin [triplicate mass preparation at 0.2 wt.% after sonication bath (60-80 °C) and stirring at ca. 100 °C] and native α -chitin (vial far right; 2.0 wt.% preparation after more than 4 days of stirring at 100-110 °C) in EmimAcO.	233
Figure 4-5: Stages of the polymer (black chains)-solvent (red circles) interface towards dissolution (a: contact, b: swelling, c: disentanglement, d: initial dissolution step,	

e: final dissolution step). Reprinted by permission from [Springer Nature Customer Service Centre GmbH]: [Springer Vienna] [The European Polysaccharide Network of Excellence (EPNOE)] by [Navard P., Wendler F., Meister F., Bercea M., Budtova T.] [COPYRIGHT] (2012).	235
Figure 4-6: Freezing point (°C) of aqueous sodium hydroxide (NaOH) solutions (0-50 wt.%). Data based on Pickering, S. U. LXI.-The hydrates of sodium, potassium, and lithium hydroxides. <i>J. Chem. Soc., Trans.</i> 1893 , 63, (0), 890-909.	238
Figure 4-7: Medium MW α -chitin back in white suspension (vial on the left) after its transparent solution (0.35 wt.% in 18.1 wt.% NaOH) was left at room temperature for a week. Vial on the right shows an undissolved native α -chitin particle (next to the magnetic stir bar in the) in transparent NaOH solution (0.43 wt.% preparation in 21.7 wt.% NaOH) after one freeze-thaw cycle.	239
Figure 4-8: Snapshot of increasing viscosity (from left to right) for 0.41, 0.73, 1.43, 2.69 wt.% practical grade (PG) chitin samples in 20 wt.% NaOH.	240
Figure 4-9: Practical grade (PG) chitin films after their freeze-drying process. Concentrations from left to right are: 1.59, 1.95, and 4.37 wt.%.	243
Figure 4-10: Infrared spectra (triplicate acquisition) of deacetylation product 4-1 (76 min sonication of native α -chitin). Inset table records the absorbance ratios which probe depolymerization (1.088 ± 0.088) and deacetylation (1.071 ± 0.052). .	245
Figure 4-11: NMR spectra of deacetylation product 4-1 (76 min sonication of native α -chitin; 4.4 mg/mL in 2 wt.% DCl). Inset table records the integration details [DA is 32.1% (= 600 / 18.7088)]. Inset spectra shows the 1.70-2.00 ppm region.	246
Figure 4-12: Infrared spectra of deacetylation products 4-1 (red) and 4-2 (green).	247
Figure 4-13: NMR spectra of deacetylation product 4-2 (76 min sonication of high MW α -chitin; 4.3 mg/mL in 2 wt.% DCl). Inset table records the integration details [DA is 19.8% (= 600 / 30.26)]. Inset spectra shows the 1.75-2.10 ppm region.	248
Figure 4-14: Infrared spectra of deacetylation products 4-4 (red) and 4-5 (green).	249
Figure 4-15: NMR spectra of deacetylation product 4-4 (4.3 mg/mL in 2 wt.% DCl). Inset table records the integration details [DA is 50.7% (= 600 / 11.83)]. Inset spectra shows the 1.75-2.05 ppm region in more detail.	250
Figure 4-16: NMR spectra of deacetylation product 4-5 (4.3 mg/mL in 2 wt.% DCl). Inset table records the integration details [DA is 54.8% (= 600 / 10.95)].	250
Figure 4-17: NMR spectra of deacetylation product 4-6 (5.2 mg/mL in 20 wt.% DCl). Inset table records the integration details [DA is 55.0% (= 600 / 10.91)].	251
Figure 4-18: Infrared spectra of deacetylation products 4-7 (red), 4-6 (blue) and 4-1 (green). Inset table records the intensity ratios for the glycosidic linkage and amide II.	252
Figure 4-19: NMR spectra of deacetylation product 4-7 (4.4 mg/mL in 20 wt. % DCl). Inset spectra shows the 2.05-2.27 ppm region [DA is 53.3% (= 600 / 11.26)].	256

Figure 4-20: NMR spectra of deacetylation product 4–8 (5.5 mg/mL in 20 wt.% DCI). Inset spectra shows the 2.06-2.54 ppm region in more detail.	256
Figure 4-21: NMR spectra for deacetylation product 4–10 (5.0 mg/mL in 20 wt.% DCI). Inset spectra shows the 2.10-2.60 ppm region in more detail.	256
Figure 4-22: Snapshot of 4.4 mg/mL α -chitin samples from Table 4–1 [native (GM3 173 K), high (GM3 173 L)-medium (GM3 173 M)-low (GM3 173 N) MW] in 20 wt.% DCI after overnight stirring at 70 °C.	262
Figure 4-23: NMR spectra of native α -chitin (4.4 mg/mL in 20 wt.% DCI); DA is 89.4%. ...	262
Figure 4-24: NMR spectra of high MW chitin (4.4 mg/mL in 20 wt.% DCI); DA is 91.2%. ..	263
Figure 4-25: NMR spectra of medium MW chitin (4.4 mg/mL in 20 wt.% DCI); DA is 92.0%.	263
Figure 4-26: NMR spectra of low MW chitin (4.4 mg/mL in 20 wt.% DCI); DA is 96.4%. ...	263
Figure 4-27: NMR spectra of high MW α -chitin (10.1 mg/mL in 20 wt.% DCI); DA is 90.9%.	265
Figure 4-28: NMR spectra of high MW chitin (14.3 mg/mL in 20 wt.% DCI); DA is 88.7%.	265
Figure 4-29: Solid-state CP/MAS ^{13}C NMR spectra of native α -chitin milled with 16 \times 0.25" balls (8.2 BtC) for 5 (red, code: 8/5), 45 (green, code: 8/45) and 105 (blue, code: 8/105) min.	268
Figure 4-30: Solid-state CP/MAS ^{13}C NMR spectra of Sigma's PG chitin (red) milled with 67 \times 0.25" balls for 10 (13.4 BtC, green, code: 13/10) and 30 (33.5 BtC, blue, code: 33/30) min.	269
Figure 4-31: Degree of acetylation (DA%) of milled PG chitin samples 13/10 (blue, 13.4 BtC for 10 min) and 33/30 (red, 33.5 BtC for 30 min) for MestreNova's (v.10.0.2) GSD peak broadness optimization values (0.10–0.29).	273
Figure 4-32: Relative viscosities (kinematic) of milled PG chitin (60 min with 67 BtC/14% packing) in 9.70, 19.40, and 29.11 wt.% NaOH solutions. Dissolution involved freezing temperatures (<-28 °C).	276
Figure 4-33: Undissolved residue of milled PG chitin (60 min with 67 BtC/14% packing; 41.6% CrI) in 9.70, 19.40, 29.11, and 38.81 wt.% NaOH (from left to right). Dissolution involved freezing temperatures (<-28 °C). Red circles on the 9.70 wt.% NaOH tube (far left) highlight small pieces of undissolved residue.	276
Figure 4-34: Infrared spectra of native (red), 13/10 (orange), 22/30 (green), 33/30 (pink), and 67/60 (blue) PG chitin (ball milling conditions and FT-IR ratios are recorded in Table 4–4).	278
Figure 4-35: X-ray diffraction patterns of native (red) PG chitin and milled with 67 \times 0.25" balls (14.0 % packing); 13.4 BtC for 10 min (orange), 22.3 BtC for 30 min (green), and 67.0 BtC for 60 min (blue). Inset table records the crystallinity indices (CrI%). The intensities of 22/30 (green), 13/10 (orange), and native PG chitin (red) signals have been offset by 200, 500, and 700 a.u. respectively.	280

- Figure 4-36: Relative viscosities (kinematic) of milled 13/10 (orange), 22/30 (green), 33/30 (pink), 67/60 (blue) PG chitin samples in 19.00 wt.% NaOH as a function of concentration (wt.%). Inset table records the exact data, inset graph highlights the polynomial fits along with their equations and R-squared values. Data were obtained by freezing at $-28\text{ }^{\circ}\text{C}$282
- Figure 4-37: Films of ~ 4.7 wt.% 13/10 chitin produced by dissolution in 19.00 wt.% NaOH; thermally-dried (a) and freeze-dried (b).286
- Figure 4-38: Infrared spectra of 13/10 chitin (blue), freeze-dried film (green), and thermally-dried film (red). Inset highlights the $1100\text{--}1300\text{ cm}^{-1}$ region including the signal of the thermally-dried film before its drying and after its washing treatment (pink dotted).288

List of tables

Table 2-1: Crystallinity Index (CrI) reduction percentages reported in literature for cellulose and chitin ball milling.....	68
Table 3-1: Conversion of % solubility (pH 7.0) of ball milled α -chitin products (Figure 3–14) to solubility in g/L based on the actual mass (g) which was solubilized in 7.5 mL water.	180
Table 3-2: Reducing sugars approximation [glucose equivalents (g/L)] in water-soluble α -chitin species generated upon optimized ball milling conditions. Absorbance values (Figure 3–18) were translated into glucose equivalents by DNS reagent's B calibration curve ($y = 0.1979 x - 0.126$), which was assumed to be linear beyond 0.96–1.48 mM.	192
Table 3-3: Reducing sugars approximation [NAG equivalents (g/L)] in water-soluble α -chitin species generated upon optimized ball milling conditions. Absorbance values (Figure 3–21) were translated into NAG equivalents by Schales reagent calibration curve ($y = - 0.0018 x + 0.899$).....	196
Table 3-4: Concentrations (mM) measured by MALDI-TOF MS and yields (wt.%) ^a of GlcNAc and (GlcNAc) ₂ when α -chitin was ball milled with 2 × 0.5" /68–70 × 0.25" balls and kaolinite.	206
Table 4-1: Mechanochemical conditions and FT-IR data for the α -chitin sample set prepared for dissolution studies. ^[a] Spectra shown in Figure 4–2.	226
Table 4-2: Deacetylation experiments on various chitin samples and results (DA%). Results are of preliminary nature.	254
Table 4-3: DA values of the PG-chitin sample for the various global spectral deconvolution (GSD) peak optimization parameters of MestreNova v. 11.	267
Table 4-4: Mechanochemical conditions and FT-IR data for the practical grade (PG) chitin sample set prepared for dissolution studies with 19.00 wt.% NaOH. Spectra shown in Figure 4–34.	277

List of abbreviations

ATR FT-IR: Attenuated total reflectance Fourier transform infrared

AU: Arbitrary unit(s)

BtC: Balls to chitin mass ratio / BtP: Balls to powder mass ratio

CAS: Chemical abstract service

CP/MAS: Cross polarization/Magic angle spinning

CrI: Crystallinity index

CSCT: Centre for Sustainable Chemical Technologies

DA: Degree of acetylation

DD: Degree of deacetylation

DFT: Density functional theory

DHB: 2,5-dihydroxybenzoic acid

DMSO: Dimethyl sulfoxide

DNS: 3,5-dinitrosalicylic acid

DP: Degree of polymerization

EmimAcO: 1-ethyl-3-methylimidazolium acetate

EtOAc: Ethyl acetate

EtOH: Ethanol

GC-MS: Gas chromatography mass spectrometry

Glc: Glucose

Glc-d7: Deuterated glucose

Glc-eq: Glucose equivalents

GlcNAc: *N*-acetyl-D-glucosamine

GlcNH₂: D-glucosamine

GPC: Gel permeation chromatography

GSD: Global spectral deconvolution
GTMA: Glycidyltrimethylammonium
HA: Hexanoic acid
HB: Hydrogen bond(s) or Hydrogen bonding
HPLC: High performance liquid chromatography
IL: Ionic liquid(s)
IS: Internal standard
IUPAC: International Union of Pure and Applied Chemistry
L/G: Lorentzian/Gaussian
LA: Levulinic acid
LAG: Liquid assisted grinding
MALDI-TOF MS: Matrix assisted laser desorption Time of flight Mass spectrometry
MUN: Memorial University of Newfoundland
MW: Molecular weight
NAG: *N*-acetyl-D-glucosamine
NAG-eq: *N*-acetyl-D-glucosamine equivalents
NMR: Nuclear magnetic resonance
PEG/PEO: Polyethylene glycol/Polyethylene oxide
PG: Practical grade
Rpm: revolutions per minute
RSD: Relative standard deviation
S/N: Signal to noise
SEC: Size exclusion chromatography
SEM: Scanning electron microscopy
UV/Vis: Ultraviolet visible
XRD: X-ray diffraction

Chapter 1 Introduction

1.1 Irreversible environmental changes and societal timescales

The way in which our human societies choose to manage risk and uncertainty has resulted in three out of the nine Earth-system processes to exceed their irreversible change levels (Figure 1-1).¹

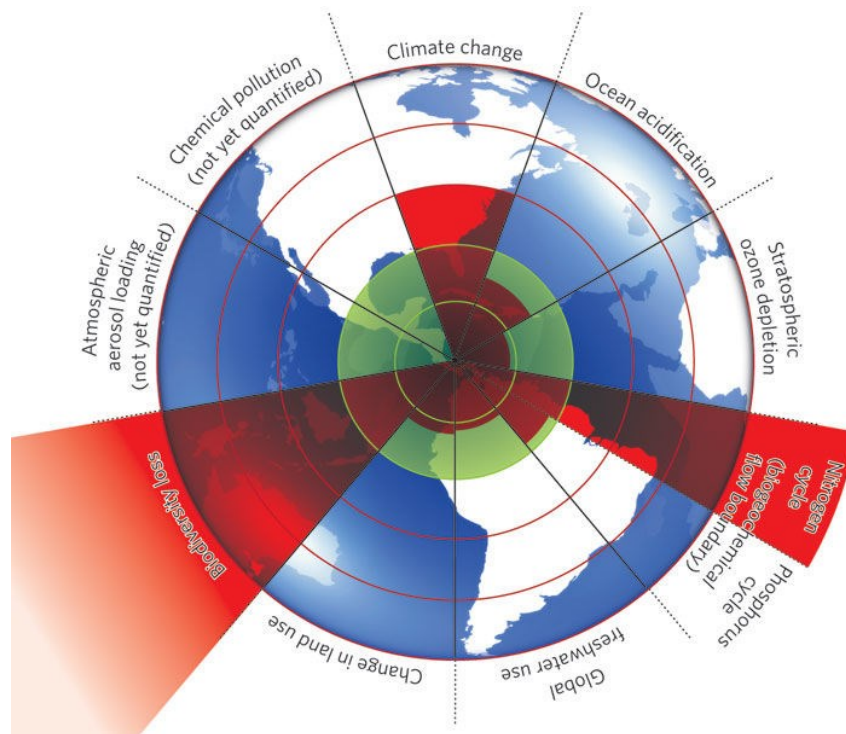


Figure 1-1: Beyond irreversible environmental change levels. The inner green shading embodies the proposed safe operating space for nine interconnected planetary systems. The red wedges signify an estimate of our generation's levels of the systems' key variables. Reprinted by permission from Macmillan Publishers Ltd: [NATURE] (Vol 461, 472-475), copyright (2009).

With key variables for rate of biodiversity loss (species extinction), interference with the nitrogen cycle (rate of atmospheric N_2 removal), and climate change

[atmospheric carbon dioxide (CO₂) concentration] starting to go beyond their critical values after the 1960s,² the resilience of the rest of the planet's subsystems/operations (e.g. freshwater use, ocean acidification) is severely compromised.³ One of the main reasons for the current situation is our increasing dependence on fossil resources fostered within a "growth at all costs" economic model.^{1,4} Fossil feedstocks (natural gas, petroleum, and coal) form over geological timescales,⁵ which are relevant when considering interactions at the ecosystem (hundreds of centuries) or/and ecosphere (thousands of centuries) level.⁶ However, global total CO₂ emissions from fossil fuel use increased over 500-fold within the last three centuries,⁷ entering the 350 ppm zone of uncertainty.¹ At the same time, recent literature estimates that some of them (fossil resources) will peak within the next few generations.⁹ Considering this historical turning point, along with the proposed non-linear (spiral) nature of an organism's biological time,¹⁰ and the United Nations (UN) scenarios on world population distribution,¹¹ the more crucial questions raised are more relevant to *Homo sapiens*' ability to survive on the planet (societal reproduction/health) rather than to the survival of the planet itself (environmental health).ⁱⁱ

ⁱ That atmospheric CO₂ concentration is the proposed critical value for the zone of uncertainty (350–450 ppm) of one of the two control variables suggested by the Planetary Boundary (PB) framework, to which the Earth-system process of climate change is particularly sensitive (the other one is the more stringent "radiative forcing") (3). In May 2018, the value was recorded at 411 ppm (8).

ⁱⁱ Just as individual organisms have their unique biology, so do societies [see some of the articles of "Biology of Societies" Special Issue of *Current Biology* (2007)](12,13). Hence, societal characteristics unfold in their own biological time (maybe not spirally)(14,15).

1.2 Green Chemistry

Darwinian, economic and societal dimensions of evolution have been interwoven for many centuries by alchemy^{16,17} and chemistry,^{18,19} via invented materials and their manufacturing processes. This progress, which is grounded on innovation and systematic work at the molecular level, was refined by pioneering green chemists in the 1980s; who responded to sustainability challenges like waste prevention and hazard minimization at the industrial scale.^{20,21}

That dynamic is now formulated by "The Twelve Principles of Green Chemistry", which were introduced in 1998 by Paul Anastas and John Warner.²² These principles approach the aforementioned human health and environmental problems holistically, and are meant to be complemented by "The Twelve Principles of Green Engineering".²³ They are summarized briefly below:

1. **Prevention.** Waste prevention is better than treatment or clean up.
2. **Atom Economy.** Synthesis should maximize the incorporation of all starting materials used in the process into the final product.
3. **Less Hazardous Synthesis.** Synthesis should use and generate substances that pose little or no toxicity to human health and the environment.
4. **Safer Chemicals.** Chemical products should be designed to preserve efficacy of the function while reducing toxicity.

5. **Safer Solvents and Auxiliaries.** The use of auxiliary substances (e.g. solvents, separation agents etc.) should be made minimized and innocuous.
6. **Energy Efficiency.** Energy requirements of chemical processes should be recognized for their environmental and economic impacts and should be minimized. If possible, synthetic methods should be conducted at ambient temperature and pressure.
7. **Renewable Feedstocks.** A raw material or feedstock should be renewable rather than depleting whenever technically and economically practicable.
8. **Reduce Derivatives.** Unnecessary derivatization (use of blocking groups, protection / deprotection, temporary modification of physical and chemical processes) should be minimized or avoided if possible, because such steps require additional reagents and can generate waste.
9. **Catalysis.** Catalytic reagents (as selective as possible) are superior to stoichiometric reagents.
10. **Degradation.** Chemical products should be designed so that at the end of their function they break down into innocuous degradation products and do not persist in the environment.
11. **Real-Time Analysis for Pollution Prevention.** Analytical methodologies need to be further developed to allow for real-time, in-process monitoring and control prior to the formation of hazardous substances.

12. **Inherently Safer Chemistry for Accident Prevention.** Substances and the form of a substance used in a chemical process should be chosen to minimize the potential for chemical accidents, including releases, explosions and fires.

Significant advances both in academia and industry have been attributed to the twelve principles of green chemistry,²⁴⁻²⁶ however these rules were not meant to be twelve independent commandments but rather an integrated cohesive system of design. Ultimate standards of sustainability can only be obtained if all twelve principles are applied in a scaled-up process,²⁷ but in most cases today this would be unfeasible on economic grounds (e.g. the cost of renewable routes to chemicals are typically more expensive than petrochemical routes).

Moreover, green chemistry and technology in general cannot achieve the target of sustainability alone. The right socio-political conditions are needed to ensure investments in green chemistry and engineering. Some of those are:²⁸

- Appraisalment by society and public acceptance. A demand for new greener products and benign processes throughout the life-cycle of the product.
- Reasonable and sustainable legislation that does not inhibit the application of greener innovation and protects the future generations' needs.
- Convenient market conditions. That implies financial motives to increase research and access to finance for novel applications.

There is a growing body of literature at the interface of natural and social sciences with respect to the above interdependent conditions.²⁹⁻³⁹ Regardless of the academic debate there,ⁱⁱⁱ my hypothesis is that, within a circular economy mindset,⁴⁰ sustainability can only be evaluated on a case by case basis, as opposed to a planetary one.^{41,42} With that sense of responsibility, companies and organizations can take advantage of the scientific/technical or other skills and make a difference; building trust relationships with local communities (Figure 1–2).^{43 iv}

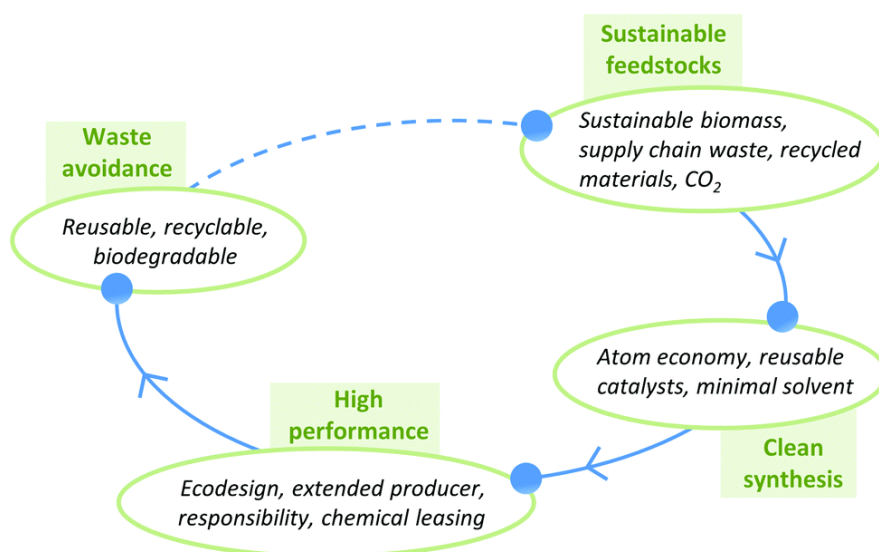


Figure 1–2: Green chemistry considerations/skills for satisfaction of modern society's needs. Reproduced from {Green Chem., 2016, 18, 3914-3934} with permission from The Royal Society of Chemistry.

ⁱⁱⁱ Despite the visionary perspectives, discussion on those is beyond the scope of this thesis.

^{iv} In Section 1.5, we will see how an experienced scientist [Sir John (Kappa) W. Cornforth] perceives the distinction between “making a difference” and “making debate”.

1.3 Renewable resources, food waste and biorefineries

The seventh of the principles of green chemistry was envisioned in the very first issues of the homonym journal back in 1999 through a 2040 horizon scenario regarding the feasibility of a plant-based chemical industry. Making clear assumptions on world population and crop yield improvement, the authors traced the real core of the sustainability challenge in its socio-political nature (the right location to produce the right crop).⁴⁴ As mankind entered the current century when petroleum feedstocks are estimated to meet just decades of global production,⁴⁵ renewable energy paradigms (solar, wind, and biomass) are positioning the concept of sustainability more firmly in the public mind worldwide.⁴⁶ Presently, 10 to 12% of the gross primary energy demand on a global basis is satisfied by biomass (referring to all organic materials of biogenic, non-fossil character including matter living and growing in nature as well as waste materials resulting from both living matter and organic matter that is already dead).⁴⁷

Regardless of how fast this new mentality is being adopted by the market, science has already laid solid foundations for valorisation of alternative feedstocks (as opposed to conventional fossil raw materials) with a new paradigm: the biorefinery concept.⁴⁸ Similar to a petrochemical refinery, the biorefinery of the future will be an integrated facility which will typically be expected to work on a strategic site and on a small scale, alongside the crops and farmland where the feedstocks are grown to offset the economies of scale generated by their giant petrochemical

predecessors. It will convert a variety of bio-feedstocks into power, heat, chemicals and other valuable materials maximizing the value of the biomass and minimizing waste.⁴⁹⁻⁵¹

More specific, food supply chain waste is seen as a resource for production of fuels and chemicals, because almost 15% of the population of the developing countries is estimated to be undernourished,⁵² and also due to the high per-capita food waste generated in the industrialized world (95–115 kg/year).⁵³ A good example of how food waste can fit in the biorefinery concept is the development of a microwave-assisted approach to valorise orange peel residues into a range of valuable products (from chemicals like D-limonene and α -terpineol to polysaccharides like pectin to a novel and most unique form of mesoporous cellulose).⁵⁴

Considering competition for land use with respect to food production and habitats for humans and wildlife, it is worth citing here that researchers are now looking at the oceans for valuable feedstocks. In that context, waste streams from fish processing and algae can provide a wide range of products including lipids, pigments, minerals, and biopolymers such as proteins, cellulose, chitin and their subsequent units (Figure 1–3).^{55,56}

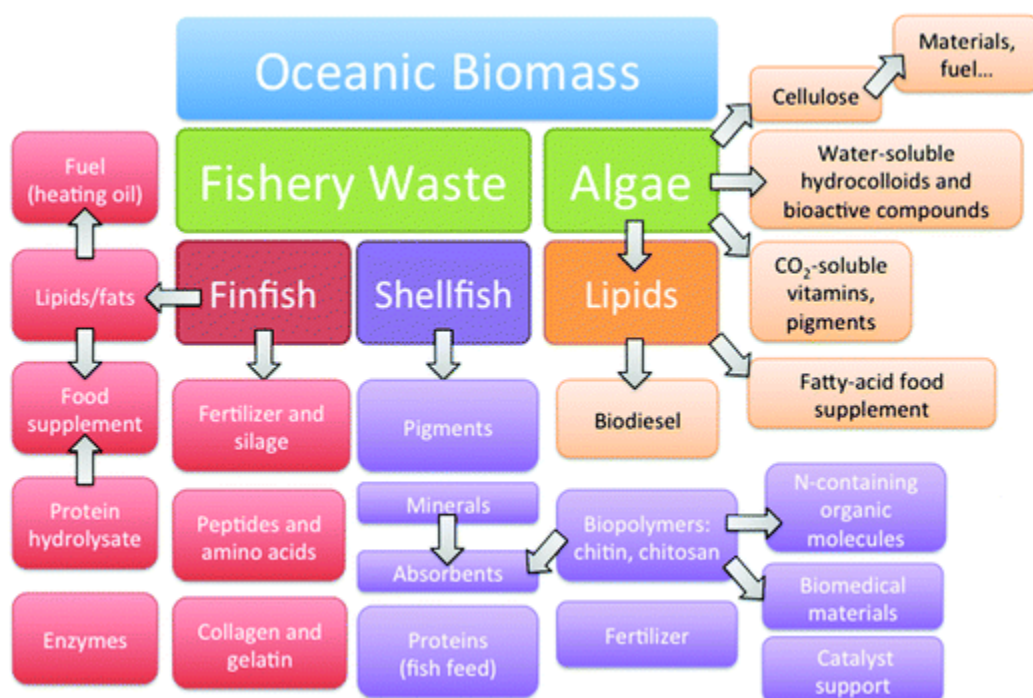


Figure 1–3: Potential products from oceanic biomass (excluding fish/shellfish use as meat and direct use of algae as a foodstuff). Reproduced from {Green Chem., 2013, 15, 860-871} with permission from The Royal Society of Chemistry.

1.4 Chitin

Chitin, a structural polymer of *N*-acetyl-D-glucosamine, is the most copious of the polysaccharides in the marine environment and highly abundant on the planet, with bio-production reaching billions of tons every year. As it contains C, H, O and N, its synthesis and degradation interacts with both carbon and nitrogen cycles.⁵⁷ It constitutes 20–30% of the shells of crustaceans which account for at least 50% of the fished harvest.^{58,59} Global yearly production of decapods (shrimps, crabs and lobsters) reaches over 14 million tonnes, arising mostly (ca. 80%) from Asia.⁶⁰ Hence, over a million tonnes of chitin are produced annually in the world and are

currently mostly discarded.^v This waste stream could satisfy demands for many substances including biologically-active materials,^{61,62} nanomaterials and fibres,^{63,64} and nitrogen-containing platform molecules.⁶⁵

A relatively high Degree of Deacetylation (DD) [reverse of Degree of Acetylation (DA)] gives chitin a chitosan character, but a rigid nomenclature between the two has not been established.⁶⁶ Typical DA values for native (unprocessed, non-modified) chitins are in the range of 90–95%.⁶⁷ Figure 1–4 demonstrates the molecular structure of chitin/chitosan (from now on called chitin).

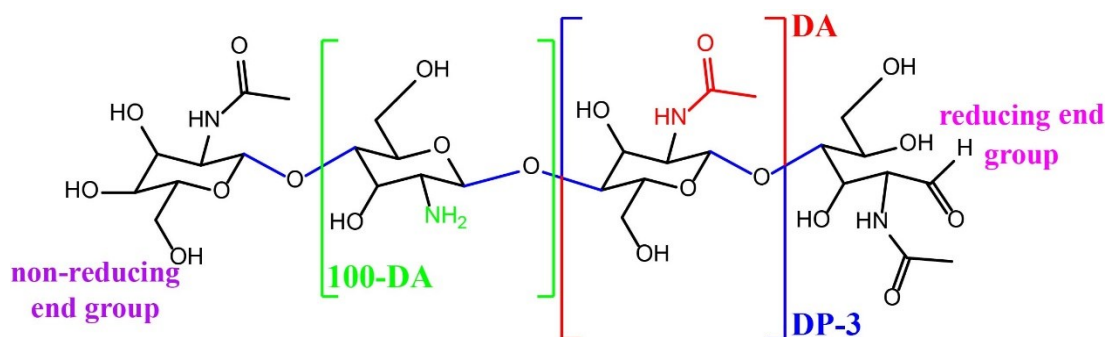


Figure 1–4: Molecular structure of chitin/chitosan (DP: Degree of Polymerization, DA: Degree of Acetylation).

Each sugar unit [either 2-acetamido-2-deoxy-β-D-glucopyranose (221 g/mol) or 2-amino-2-deoxy-β-D-glucopyranose (179 g/mol)] is joined to the next through an equatorial β-(1→4) acetal bond (glycosidic linkage or bridge). This means that the chitin molecule is linear and unbranched, just like cellulose. Experienced researchers estimate chitin's average molecular weight (MW) in vivo to be in the

^v $14 \cdot 10^6$ tonnes crustaceans \times 50% (\rightarrow shell) \times 20% (\rightarrow chitin) $\approx 1.4 \cdot 10^6$ tonnes chitin. Out of that estimated quantity, only 10,000 tonnes per year are utilized globally (55).

order of 1 MDa [$\div 221 = DP >4,500$].⁶⁸ For comparison, cellulose's DP is approximated to 10,000 for wood and 15,000 for native cotton.⁶⁹ However, isolates of chitin (commercial or non-commercial) have probably lower MW values (0.5–1.0 MDa, DP 2,250–4,500) and a wide range of polydispersity values because of the harsh conditions the biopolymer experiences during deproteination, demineralization and depigmentation of crustacean shells.^{68,70} Studies have reported average MWs for chitins of more than 2.0 MDa (data was obtained viscometrically).^{71,72} vi

Just like in cellulose, chitin chains are packed into partially crystalline fibers (embedded in amorphous domains) via a network of inter- and intra- molecular hydrogen bonds.^{69,73} This is likely to occur in analogy to crystallization of cellulose in immature cotton boll, which goes forward via formation of specific intra- and inter-chain hydrogen bonds.⁷⁴ The diameter of elementary nanofibrils is approximated to 2–5 nm (formed by 18–25 molecules),⁷⁵ while recent literature has reported chitin nanofibrils of 25 nm thickness and 400–500 nm length.^{76,77} Figure 1–5 illustrates the hierarchical microstructure of the cuticle of the lobster *H. americanus*.

^{vi} However, considering both the very long polymer chain lengths as well as the sensitive solvent systems used, one should be naturally critical regarding the reproducibility of these data.

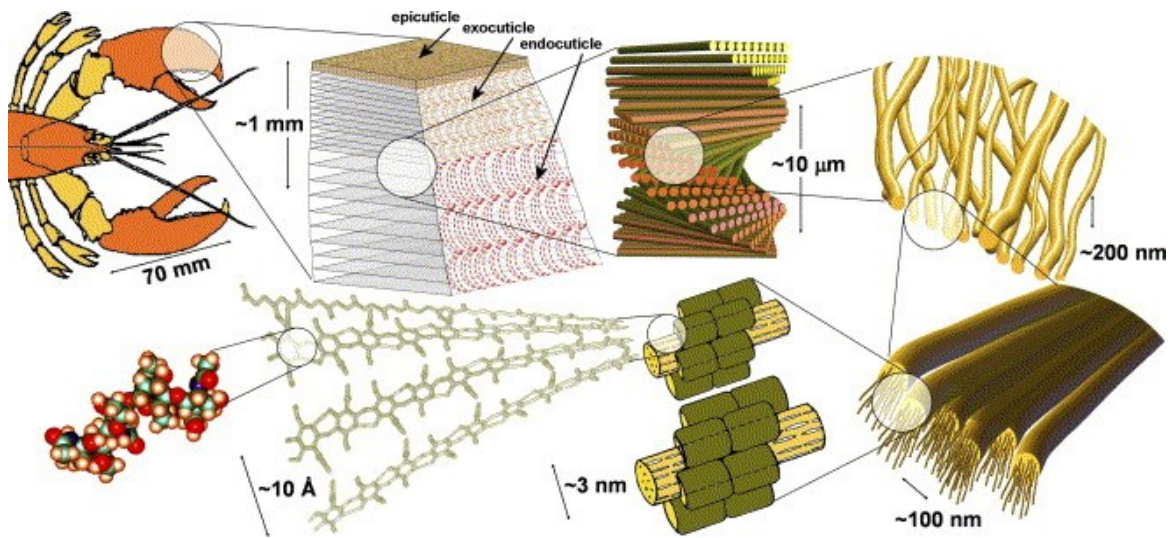


Figure 1-5: Hierarchical microstructure of the cuticle of the lobster *H. americanus* [Reprinted from *Acta Materialia*, 53, D. Raabe, C. Sachs, P. Romano, The crustacean exoskeleton as an example of a structurally and mechanically graded biological nanocomposite material, 4281-4292, Copyright (2005), with permission from Elsevier].

In nature, chitin exists in three polymorphic forms (also called allomorphs) α -, β -, and γ -,⁷⁸ usually in association with proteins^{79,80} depending on the source. The most abundant form is α -chitin, found in decapod (shrimp, crab, lobster) cuticles and fungal cell walls. The rarer β -chitin is synthesized in squid pens and diatoms, and γ -chitin can be found in squid and cuttlefish stomach lining.^{81,82} What distinguishes these different forms is the arrangement of chains in the crystalline domains of a nanofibril (c -axis is the literature convention for the fibre axis). α -Chitin is formed by antiparallel chains on the bc -plane, β -chitin is comprised of parallel chains,⁸³ and the γ polymorph is hypothesized as a variant of α and β polymorphs.^{78,84} ^{vii}

^{vii} A variant form can be considered as a mixture (or combination) of two forms. Comparative diagrams of the three types of chitin have been proposed (67,78).

Antiparallel chains have alternating reducing and non-reducing ends at each edge of a bc -plane [(1→4) acetal bonds of neighboring bc -plane chains are in opposite directions along the fibre axis], just like DNA strands.^{viii} This difference in the orientation of the molecules results in stronger intermolecular forces for α -chitin. Figure 1–6 visualizes the three strongest intermolecular hydrogen bonds which contribute to bc sheet formation [between chain 1 (black) and chain 4 (blue)] in α -chitin,⁸⁶ and the weak polar interaction between the C8¹-H and the O6⁴ in β -chitin (anhydrous)^{87,88}.^{ix} O6^{4'}-H··O6^{1'} lies in the ab -plane (O6^{1'} in Figure 1–6 should be imagined coming towards the reader) with a calculated length of approximately 2.30 Å. C8⁴-H··O3¹ (~2.49 Å) and C8¹-H··O3³ (~2.56 Å) are weaker hydrogen bonds which also lie on the ab plane. Most probably, these bonds do not occur simultaneously but alternate along the chain axis; stabilizing further the crystal's conformation.⁸⁶ Apart from that, both α - and β -chitins form molecular sheets in the ac -plane through hydrophobic interactions of the pyranose rings and interchain hydrogen bonds.^{89,90} The absence of a strong hydrogen bonding network in the b -axis of β -chitin results in swelling of the biopolymer in small molecules, among which are water and methanol.⁹¹

^{viii} A chain's C1→C4 direction can be thought as either up (↑) or down (↓) along the c -axis. Hence, α -chitin's neighbouring bc -plane chains are ↑↓, β -chitin's ↑↑, and γ -chitin's possibly ↑↓↓ (85).

^{ix} Labelling conventions: O6 refers to the oxygen of the primary alcohol, C8 refers to the carbon of the methyl group of the acetyl group, superscripts denote the number of chain according to Petrov et al. (86) and the prime symbol (') refers to the neighboring sugar unit within a chain.

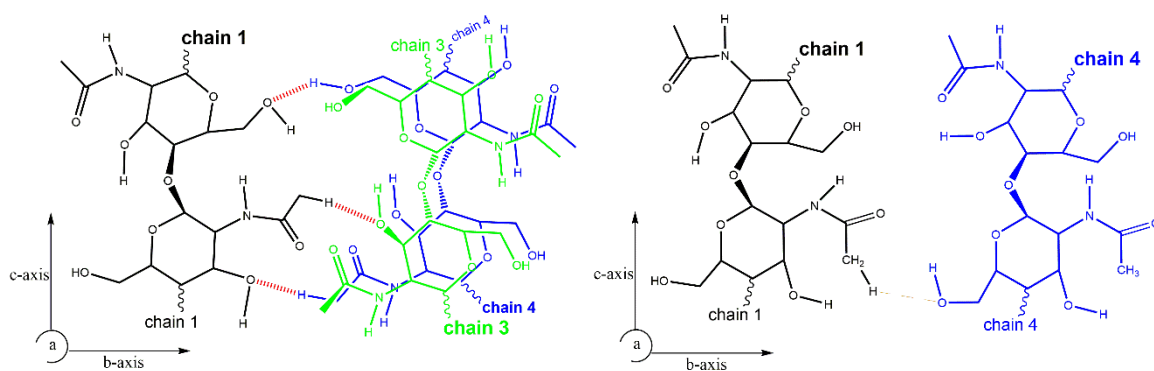


Figure 1-6: Difference in intermolecular forces between α -chitin (left) and β -chitin (right). Antiparallel chains in α -chitin have been drawn by a vertical 180° rotation of chain 1. Bold chain label denotes the reducing end direction in the molecule. Chain 3 (green) in α -chitin lies towards the reader; parallel to chain 4 (blue). Hydrogen bonds are in red. Certain hydrogens have been omitted and no other hydrogen bonds (e.g. intramolecular ones) are shown for clarity. Note that pyranose rings preserve the chair conformation.

Since the late 1970s, a statistical mixture of more than two conformations of the primary alcohol (i.e. hydroxymethyl) group has been realized to give rise to diverse patterns of hydrogen bonding in α -chitin.^{86,92,93} Two recent independent computational studies^{86,94} agree that six out of seven hydroxymethyl groups (86%) take one of the two conformations proposed by the experimental study of Sikorski et al.⁹³ The possible combinations of those two most probable hydroxymethyl conformations within the chains of α -chitin's modelled unit cell give differences of not more than 0.4 kcal/mol (<2 kJ/mol) for computed total energies of the polysaccharide's crystal conformations according to both studies.^{86,94} When compared to the at least 10.4 kcal/mol difference between modes of hydrogen bonding in cellulose I β [one of the two polymorphs of natural cellulose (found in

cotton and wood)],⁹⁵ it is clear that α -chitin slowly unravels an astonishingly flexible molecular structure.

The most stable of the intermolecular hydrogen bonds in α -chitin are $N^1-H \cdots O7^2$ (~ 1.97 Å lying along the a -axis) and $O6^{1'}-H \cdots O7^2$ (~ 2.04 Å lying along the ac plane);⁸⁶ visualized in Figure 1–7 (O7 refers to the carbonyl's oxygen, and O6^{1'} has the conformation in black). This so called bifurcated hydrogen bond is the primary force for crystal packing along the a -axis; forming sheets on the ac plane.^{86,94,96} More specifically, in dispersion-corrected density-functional theory (DFT-D) simulations reported in 2016, an energetic cooperativity effect during ac -sheet formation was claimed. A minimum of 12 kcal/mol (50 kJ/mol) extra stabilization for the ac sheet was observed when compared with the stabilization energy of just two chains in the ac plane (calculations were based on a zero energy for the isolated chain including its intramolecular hydrogen bonds). Depending on the primary alcohol's conformation the stabilization of two parallel chains in the ac -plane ranges from approximately 12 to 24 kcal/mol (50 to 100 kJ/mol).⁹⁴ In view of methodology differences, these figures can be considered as complementary to the 25–30 kcal/mol of free energy to decrystallize an edge chain from an ac -sheet surface which was calculated via molecular dynamics simulations by Beckham and Crowley in 2011.⁹⁶ Again, depending on the hydroxymethyl's conformation, the maximum for the aforementioned ac -sheet extra stabilization is more than 24 kcal/mol (100 kJ/mol). Finally, considering the hydrogen bonding network that forms the bc -sheet,

the overall stabilization for the α -chitin crystal (again relative to the constituent isolated chains) rises above 60 kcal/mol (250 kJ/mol).⁹⁴

Regardless of the computational challenges in α -chitin crystal thermodynamics, the fact that the carbonyl can serve as an acceptor for two hydrogen bonds at the same time (as shown in Figure 1–7), gives rise to the historically observable splitting of the amide I band in between 1620 and 1660 cm^{-1} in α -chitin's FT-IR spectra.⁹⁷⁻¹⁰⁰ The lower frequency vibration has been attributed to the $\text{C}=\text{O}^2$ group hydrogen bonding with $\text{N}^1\text{-H}$ and $\text{O6}^1\text{-H}$, and the vibration at the higher frequency to the $\text{C}=\text{O}^2$ group hydrogen bonding with $\text{N}^1\text{-H}$ exclusively (that is when the hydroxymethyl group has the conformation shown in green in Figure 1–7, which allows a 1.90 Å intramolecular hydrogen bond with O7^1).⁸⁶

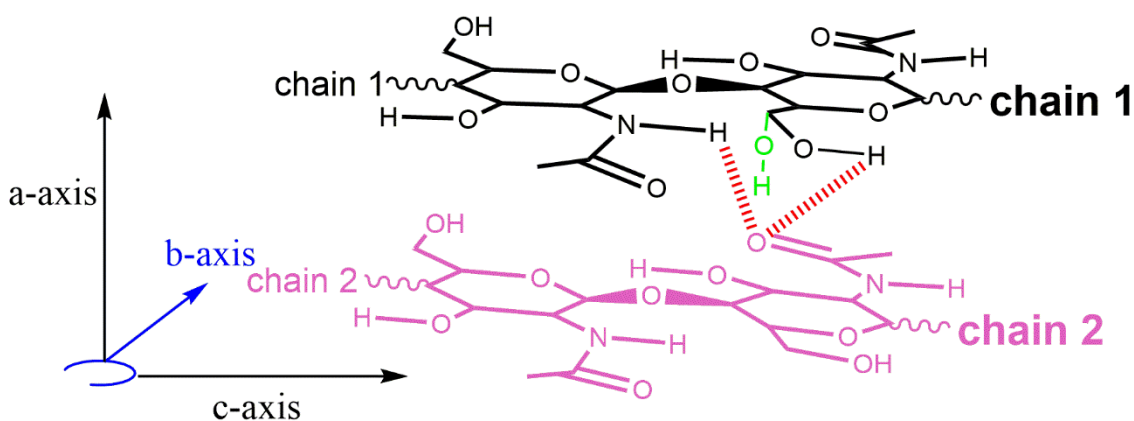


Figure 1–7: Intermolecular bifurcated hydrogen bond (in red) between parallel chains in α -chitin. Chain numbering is according to Figure 1–6 (based on Petrov et al.).⁸⁶ The hydroxymethyl conformation, which does not favour the bifurcated hydrogen bond, is visualized in green.

1.5 Valuable products from chitin

In September 1992, Chemistry Nobel prize winner Sir John (Kappa) W. Cornforth gave the Sir Robert Price Lecture, titled 'The Trouble with Synthesis'. It is quite probable that he was the first scientist¹⁰¹ that spoke publicly about the problem in chemical production (or 'construction' or 'synthesis' to use some of the words that he used) of rejecting the help (or competition) from other organisms, and letting chemical production be directed solely by the human mind. He stressed that "as time goes on the value of a chemical paper tends to reside more and more in what was actually done and made, not in why it was done."¹⁰² With a perspective of that pristine clarity, research groups around the world have demonstrated several valuable products from chitin (or chitinous waste e.g. crustacean shells), which for the purposes of this thesis are being grouped in six categories (Figure 1–8).

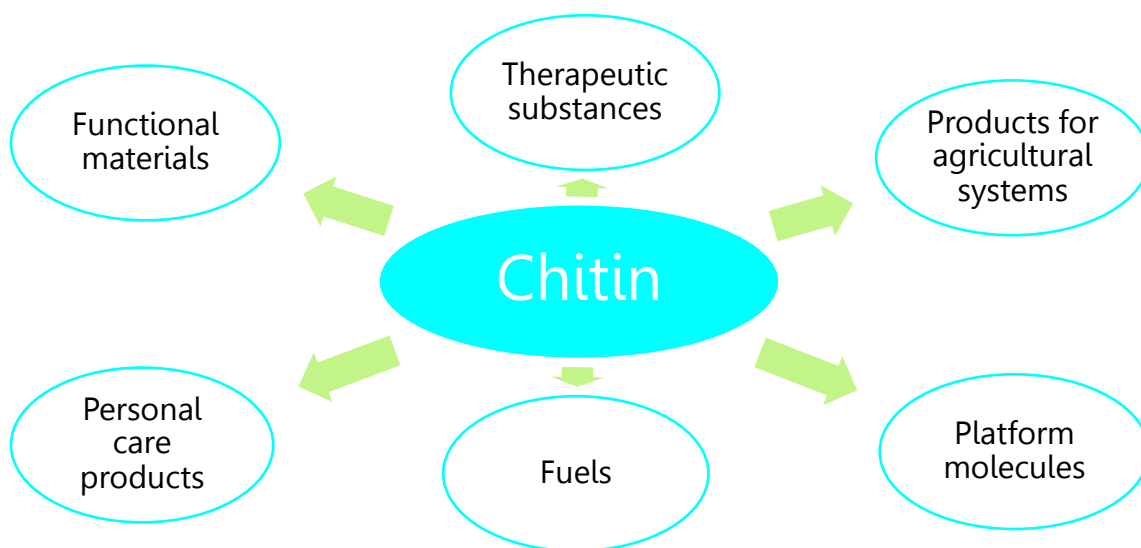


Figure 1–8: Categories of valuable products from chitin (or chitinous waste).

1.5.1 Therapeutic substances

In the past two decades, a plethora of books and reviews have highlighted the therapeutic value of chitin and its derivatives, either by keeping track of the variety of biological activities of these molecules (antioxidative, antihypertensive etc.)¹⁰³⁻¹⁰⁶ or by exploring the numerous forms that they can be processed into, with the scope of being applied in arenas like drug delivery, tissue engineering, gene therapy and wound healing (gels, films, nanoparticles etc.).^{104,106-108} Among the most recently reviewed properties are the anticancer and anti-inflammatory ones, where chitin (often soluble in formulations of MW <46 kDa and usually with high degrees of deacetylation) has exhibited both in vitro and in vivo therapeutic activities on several types of problematic cells/models (including the human liver cancer cell line HepG2).¹⁰⁹ Regarding higher MW chitosans, one of the most fascinating properties is their ability to capture cholesterol and fat in the digestive system (hypocholesterolemic effects).¹⁰⁵ When in vitro experiments were conducted in which the gastric environment was mimicked, 1 g of a 2100 kDa chitosan (DD >90% / high density) managed to bind 821 ± 21 mg cholesterol and up to 27.5 ± 2.3 g oil (soybean).¹¹⁰ A possible explanation is that the polycationic chains of the polysaccharide (stomach pH is ca. 2) form emulsion complexes and micelles with the negative charges of triglycerides and cholesterol particles/droplets. As the species transfer into the neutral/alkaline environment of the duodenum (intestine), their charges are lost, resulting in their precipitation (with the fatty molecules entrapped probably due to hydrophobic interactions with the sugar ring

surfaces).^{105,106,110} The beneficial effect is that lipid substances are prevented from being absorbed by the organ and from entering the blood stream. That way chitin can contribute to a lower risk of atherosclerotic diseases, as well as offsetting the side effects and economic costs of relevant conventional drugs (e.g. statins).^x

1.5.2 Products for agricultural systems

Development of chitin technologies has been recently reviewed for agricultural production-consumption systems through a systematic patent analysis. The study revealed an exponential growth in the number of patents from 1990 until 2005, reflecting the market pull for chitin-based products.^{xi} Applications were distributed in four sectors: food, crop management, veterinary healthcare, and agri-machinery. Reference to all of them far exceeds the scope of this thesis. Hence, I will focus to just crop management which showed the highest citation velocity (forward to backward citations ratio)^{xii, 112}

Regarding plant protection, chitin (often soluble in formulations with DA <65% and MW <120 kDa) has exhibited pesticidal properties on several types of crops like food (e.g. pea, rice, wheat), economic (e.g. tobacco, rapeseed), vegetable (e.g.

^x That function of the marine polysaccharide can also be considered of a nutraceutical character. In fact, a seventh category of valuable substances from chitin could have been discussed based on the literature of carbohydrates as functional foods (111).

^{xi} Interestingly, the typical trend of building a fence around the patent (with owners self-citing in backward citations) was not observed.

^{xii} A high citation velocity is a novelty indicator for the technology demonstrating that it does not comprise an improvement over the current technology. Moreover, it suggests a rich potential for advantageous market value.

cucumber, tomato), and fruits (e.g. grape, apple).¹¹³ Indicatively, Falcon et al. showed that chitosans of different molecular weights (from 300 kDa to oligomers) and degrees of acetylation (from 37% to 1%) presented distinct effects against the oomycete *Phytophthora parasitica nicotianae* (Ppn), a pathogen which is responsible for the worldwide damaging soilborne tobacco disease known as Black shank.¹¹⁴ When the activity of 300 kDa/1% DA and 127 kDa/37% DA chitosan solutions (pH ca. 5.5) was tested in vitro on three strains of *P. parasitica* (one very aggressive, one moderately aggressive, and one tobacco non-host), no correlation among strain aggressiveness and antipathogenic activity of the formulations was observed [the longer and highly deacetylated molecules presented absolute inhibition of all strains at two concentration levels (500 and 1000 mg/L)]. Here, the polycationic character of free amine groups of chitosan in acidic environment is hypothesized of forming polyelectrolyte complexes with the negative charge of carboxyl groups existing in the cell walls of the oomycete. The highest anti-Ppn activity though was associated with chito-oligomers (DA <37% and DP possibly centered around 6–8), which are more likely to exert their beneficial properties from within the cell. This result is of particular relevance to the research presented in this thesis, as chito-oligomers can be produced via mechanocatalytic reactions of chitin (see Chapter 3).

The superior performance of oligomers was confirmed with in vivo tests in which a 46% and 59% plant protection was observed from seed coating and foliar spraying

experiments respectively. The results of the latter set of experiments (leaves spraying) correlate with glucanase activity which is associated with degradation of the cell walls of fungi. With the application of the chitosan solutions taking place before exposure to the pathogen, the authors claim that plant protection is systemically induced using these treatments rather than the consequence of direct antifungal activity.¹¹⁴ Apart from an incentive for more preventive cultivation management, this approach offers a realistic alternative solution to the problem of Ppn resistance to conventional pesticides (e.g. metalaxyl).¹¹⁵

With respect to production enhancement, chitosan (usually soluble in acidic formulations with DA <25% and MW <100 kDa) improved plant growth in terms of seed germination, chlorophyll content, seedling development and uptake of mineral nutrients in various crops (e.g. soybean, cotton, wheat, cabbage etc.).¹¹⁶ Depending on the target crop and the preferred method of application (soil enrichment, foliar spraying, seed coating, hydroponic supplement), chitosan can promote plant growth in nanoforms as well.¹¹⁷ An elegant example is the enhancement of maize seedling growth (Figure 1-9) by 150 nm Cu-chitosan nanoparticles in neutral pH [20% DA/low MW (from Sigma-Aldrich) chitosan was cross-linked with tripolyphosphate anions and copper cations were entrapped into the nanostructure].¹¹⁸

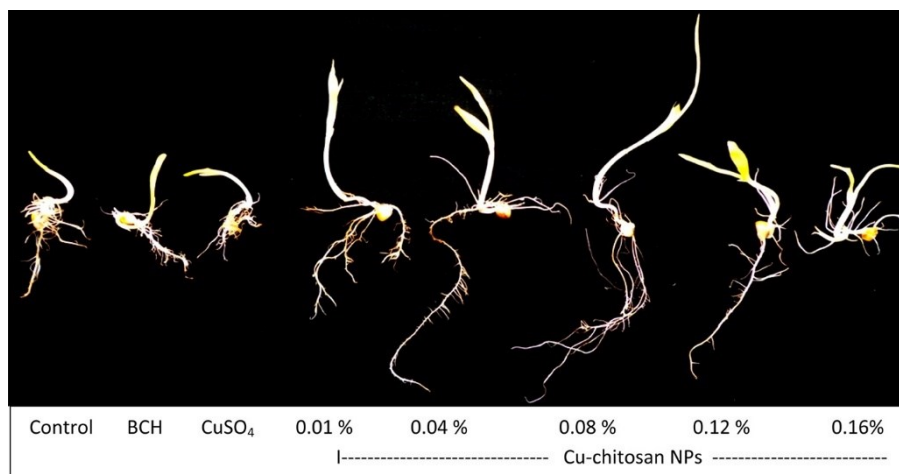


Figure 1-9: Enhancement of maize seed germination and seedling growth (root/shoot length, number of roots) by Cu-chitosan nanoparticles (NPs). Seeds were immersed for 4 h in deionized water (control), bulk chitosan (BCH) (0.01%), CuSO_4 (0.01%), and Cu-chitosan NPs at 0.01, 0.04, 0.08, 0.12, and 0.16% w/v and data were recorded after 10 days of growth in a dark room (w/daily watering). Reprinted with permission from Saharan, V.; Kumaraswamy, R. V.; Choudhary, R. C.; Kumari, S.; Pal, A.; Raliya, R.; Biswas, P. Cu-Chitosan Nanoparticle Mediated Sustainable Approach to Enhance Seedling Growth in Maize by Mobilizing Reserved Food. *J. Agric. Food Chem.* **2016**, *64*, (31), 6148-6155. . Copyright (2016) American Chemical Society.

1.5.3 Platform molecules

Considering certain analytical remarks regarding the definition of a platform molecule, chitin's monomer and dimer can easily be included in this category (and even higher MW derivatives with respect to the term "sugar platform").¹¹⁹ However, for the sake of this thesis section I will briefly cover selected products from the ring opening of chitin/chitosan monosaccharides ($\text{C}_5\text{-C}_8$ molecules). The yields of a furan which contains the nitrogen atom [3-acetamido-5-acetylfuran (3A5AF)] have been optimized from both chitin and *N*-acetyl-D-glucosamine.⁶⁵ The platform has been

recently shown to provide a sustainable basis^{xiii} for the total synthesis of proximicin A, a promising anticancer agent.¹²⁰ Pyrazines which among other interesting properties exhibit biological activity¹²¹ have been produced from pyrolytic processes along with other nitrogen-containing aromatic heterocyclics (pyridines, pyrroles).¹²² Finally, moderate to good yields of 5-HMF and levulinic acid have been reported from various chitinous feedstocks mainly via microwave methods.^{123,124}

1.5.4 Fuels

As part of the efforts for conversion of abundant types of biomass into fuels (mainly via saccharification-fermentation),¹²⁵ pretreated chitin (primarily with acid) has been recently processed with a zygomycota from the kingdom of fungi (*Mucor*), and certain strains have exhibited promising ethanol production.¹²⁶ Likewise, hydrogen evolution from bacterial fermentation of chitin and crustacean shells has been reported.¹²⁷ Ultimately, advances in the field of energy production from chitin are expected to be influenced critically by our understanding of the various parameters which direct the activity of chitinases (the enzymes that hydrolyze chitin).¹²⁸

1.5.5 Personal care products

Chitin can perform its beneficial function when applied in various body sites such as skin, hair, gums and teeth as a component of complex personal care products.

^{xiii} Including avoidance of the toxic and explosive properties of diphenylphosphoryl azide (DPPA).

The polysaccharide's structural characteristics (mainly crystallinity, molecular weight, degree of acetylation, and their distribution) give rise to a wide range of properties which are relevant to the cosmetics industry. Typically for skin care products, the polymer's molecular weight can regulate a formulation's viscosity and moisture absorption capacity.¹²⁹ For example, the viscosity of a vitamin E-containing cream (15% oil phase) increased approx. 20% with doubling of the molecular weight (from 1.2 to 2.4×10^6 Da) of a chitosan (DA ca. 17%) sample (0.5 wt.% of the cream).¹³⁰ Also, chitin nanofibrils have been reported to form nanoparticles together with the well known anti-dandruff agents zinc pyrithione and pyrithione olamine improving their performance in hair treatment.¹³¹ In another intriguing study, substitution of the primary alcohol group (-C6-OH) of chitin samples (DA >35%, MW in between 142 and 248 kDa) with a carboxymethyl group (-C6-O-CH₂COOH, degree of substitution >80%) led to moisture-absorption and moisture-retention abilities which are equivalent to those of hyaluronic acid.¹³² With the latter molecule of concern in the cosmetics industry due to its high cost, chitin derivatives can enrich the toolbox of skin care specialists by offering versatile complementary solutions as moisturizing agents.

Moving on to oral hygiene products, a number of studies have revealed that chitosan samples of DA values lower than 50% and molecular weights up to 1400 kDa have exhibited activity against several bacterial strains (including *Streptococcus mutans*) which are associated with dental plaque formation, dental

caries and gingivitis. Therefore, these molecules have been incorporated in real formulations like tooth pastes/gels and mouthwashes.¹²⁹ In one example, chitosan gels lowered the concentrations of the established anti-*S. mutans* agent chlorhexidine gluconate, which presents various side effects like tooth staining and alteration of tongue sensitivity.¹³³ Further studies towards that direction will clarify if the increased formulation viscosity (due to higher MW chitosans) contributes to a beneficial release of the active ingredients in the periodontal pocket in a prolonged fashion.

1.5.6 Functional materials

The variety of forms which chitin can take (fibers of different size, microspheres, hydro/aero-gels, films/membranes, nanocrystal particles),^{134,135} make it a versatile functional material with numerous applications like wastewater treatment,¹³⁶ packaging,¹³⁷ strengthening of rubber blends,¹³⁸ adhesiveness,¹³⁹ separation membranes,¹⁴⁰ papermaking,¹⁴¹ and organocatalysis.⁵⁹ Regarding wastewater treatment, chitosan-based materials showed competitive adsorption properties for dyes, heavy^{59,136} and precious metals.¹⁴² With the number of commercial dyes lying in the order of hundreds of thousands (many of them being of certain toxicity),¹³⁶ a variety of robust adsorbents would offer alternative options to wastewater treatment plants. In that context, the chains of a 125 kDa/13% DA chitosan proved to be competitive to activated carbon with an average maximum sorption capacity for 1 l

anionic dyes of ca. 680 $\mu\text{mol/g}$.¹⁴³ ^{xiv} Derivatives of that same chitosan revealed also sorption capacities for both Pt and Pd in the order of several hundreds of mg/g .¹⁴⁴ Thinking mechanistically, in the typically low pH values of wastewaters, platinum group metals are usually in an anionic complex form, and it has been hypothesized that they interact electrostatically with the protonated amino groups of the polysaccharide chains.¹⁴⁵

With respect to packaging applications, chitosan and its derivatives have been reported to form functional films (mainly antimicrobial and antioxidant) either by themselves or when blended with inorganic materials (e.g. silver nanoparticles, ZnO), synthetic polymers (e.g. polyethylene, polylactic acid), proteins (e.g. caseinate, gelatin), and polysaccharides (e.g. cellulose, pectin). Principally, chains of various molecular weights dissolve in dilute acid solutions in concentrations usually in the range of 1.5–2.0 wt.%, and strong films are fabricated via a variety of methods like direct casting, coating, dipping or immersing, layer-by-layer assembly (Figure 1–10), and extrusion.¹³⁷ Indicatively, when a 1.5 wt.% medium-MW/15–25% DA chitosan (Sigma-Aldrich) film was prepared by Hosseini et al., the measured tensile strength and elongation at break were 28 ± 6 MPa and $24 \pm 8\%$ respectively. When gelatin was added into the film-forming solution, tensile strength decreased gradually and elongation at break increased accordingly.¹⁴⁶ This means

^{xiv} The average performance of activated carbon for that same set of dyes did not exceed 470 $\mu\text{mol/g}$. However, a possible advantage of activated carbon is that it functions independently of the pH.

that the lost strength of the pure chitosan film has been transformed into a flexibility gain with the addition of gelatin. A similar effect was observed also by Leceta et al. when they blended chitosan and glycerol. Their 1.0 wt.% high-MW/<25% DA chitosan (Sigma-Aldrich) film showed a 62 ± 3 MPa tensile strength and a $6 \pm 1\%$ elongation at break. With the addition of 30% wt. glycerol, the film became more brittle with tensile strength dropping to 32 ± 6 MPa, while the plasticity increased with the elongation at break reaching $31 \pm 2\%$.¹⁴⁷ These indicative results exhibit a promising potential for commercialization of chitin films in the packaging arena, which so far has been dominated by petroleum-derived materials.

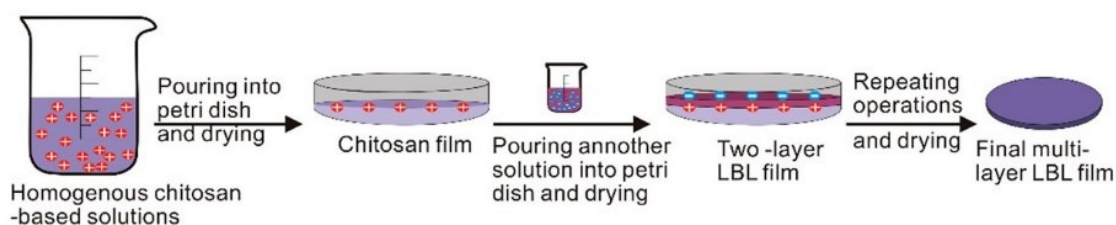


Figure 1–10: Layer by layer (LBL) assembly to fabricate chitosan-based films. Reprinted in part with permission from Wang, H.; Qian, J.; Ding, F. Emerging Chitosan-Based Films for Food Packaging Applications. *J. Agric. Food Chem.* **2018**, *66*, (2), 395–413. Copyright (2018) American Chemical Society.

Concluding, the selected literature of this section gives only a feel of the diverse properties that extended ranges of molecular weights (from >1000 kDa to oligomers) and degrees of acetylation (from 65% to 1%) display either as individual components or as parts of a whole product. It can comprise a starting point for the reader to investigate further as well as to consider whether some of those chitin applications are required in large quantities (e.g. agrochemical formulations, fuels,

certain industrial functional materials). All of them however can satisfy the needs of an increasingly complex society, while at the same time mitigate reliance on fossil resources. Although in most cases (if not all), these natural-polysaccharide-based substances are expected to be readily degraded and hence align with the 10th of “The Twelve Principles of Green Chemistry” (the one aiming for “innocuous degradation products”), the need to carefully consider all phases of their whole-product life cycle (production/multiple uses/disposal) should not be underrated.^{148,149} ^{xv} All in all, the rich diversity offered by chitin products can help scientists gain the necessary societal trust, as well as a better understanding between different disciplines. That will potentially revive the increasingly rare culture of cross-fertilization of ideas and unveil Kappa’s “lovely paradox” of making a difference.¹⁵⁰

1.6 Natural polysaccharides and valorization methods

With cellulose (glucans)^{151,152} and hemicellulose (xylans, mixed linkage β -glucans, xyloglucans, and mannans)¹⁵³ comprising more than 60 wt.% of the above ground biomass,^{154,155} the acetal group of polysaccharides represents the most widely distributed chemical functionality on the planet.^{xvi} These molecules are mainly

^{xv} For example, the pesticidal properties of a chitin formulation on a crop may prove not to be fitting to a community’s crop rotation plan.

^{xvi} Data regarding the composition of 93 varieties of biomass (mostly woody and herbaceous/agricultural) have been reviewed with mean wt.% values for cellulose, hemicellulose, and lignin being: 44.4%, 31.2%, 24.4% respectively (dry ash-free basis and normalized to 100.0%) (156).

sourced in plant cell walls, which are composite materials.^{157,158} Their simplified general structure is shown in Figure 1–11. Basically, cellulose microfibrils are implanted in a hemicellulose matrix, and this polysaccharide network is permeated and protected by lignin, which provides extra rigidity and strength.^{157,158} Molecular interactions between the three polymeric substances are both non-covalent and covalent, which gives rise to the recalcitrance of lignocellulosic biomass.¹⁵⁷

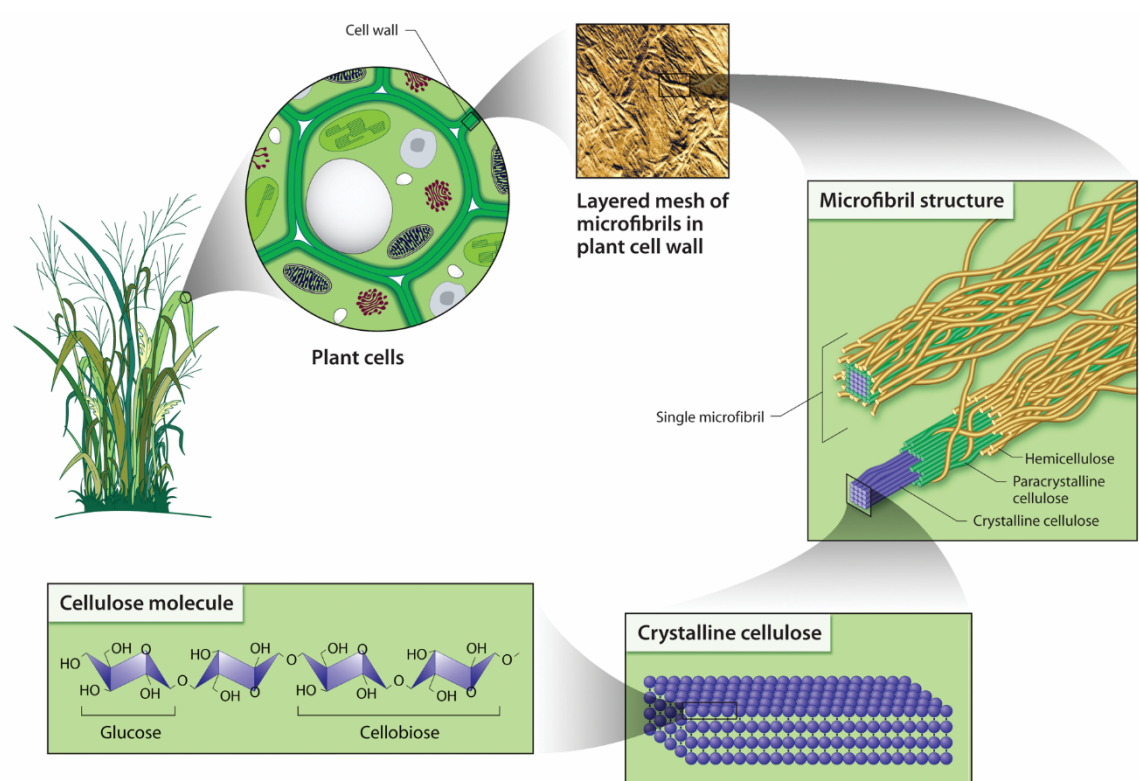


Figure 1–11: Polysaccharide microfibril structures in plant cell walls. Crystalline cellulose is shown in blue, and hemicellulose in orange. Lignin structures are not illustrated for clarity. Source: Office of Biological and Environmental Research of the U.S. Department of Energy Office of Science (science.energy.gov/ber/). Retrieved from <https://public.oml.gov/site/gallery/>.

With fuel production as the primary force driving the shorter-term advances of multi-product lignocellulose biorefineries,¹⁵⁹ pretreatment methods which simultaneously delignify and amorphize cellulose have opened the way to obtain fermentable sugars (mainly glucose) in few steps.¹⁶⁰ An elegant example is the combination of mechanical and alkaline pretreatments. When *Miscanthus* stems were milled to ca. 1000, 220, and 17 μm particles (step 1), and then incubated in 12% NaOH (3.3 M) at 70 °C for 4 h (step 2), mean lignin removal was approximately 69% (soluble fraction).¹⁶¹ When the residual cellulosic solids were subjected to enzymatic hydrolysis (pH 4.8, 45 °C, 72 h), glucan hydrolysis maximums (glucose yield) increased from 37.8% (1000 μm) to 48.1% (220 μm) to 56.0% (17 μm).^{xvii} These results exhibit that both mechanical and alkaline pretreatment steps are important for a concurrent delignification and cellulose amorphization. Hence, when the two were combined in one step (dry biomass was charged in an extruder and NaOH solution was injected downstream the reverse screw element), lignin removal increased to 77% and glucan hydrolysis was measured at 49.7% (comparable performance in a single step instead of two).

Now, alkaline treatment is also the traditional method for deproteination of recalcitrant crustacean shells.^{xviii} Sodium and potassium hydroxide are routinely

^{xvii} Lignin content was not removed in the control experiment (water) of step 2. Glucose yield for the non-NaOH-treated 22 μm sample did not exceed ca. 17%.

^{xviii} Unlike lignocellulose, which is part of the cell, the exoskeleton of crustaceans is an extracellular matrix (cuticle) composed of protein coated chitin fibers which are decorated or enclosed by a mineral phase (mainly calcium carbonate existing mostly as Mg-calcite and amorphous CaCO_3) (162,163).

used at concentrations 0.1–2.5 M and temperatures up to 100 °C to retrieve the protein fraction of crustacean cuticles (soluble) in up to 72 h.^{58,59,164-166} With subsequent acidic demineralization,^{xix} chitin can be recovered in a relatively straightforward way and in good purity. However, the generation of large volumes of strong acid/base aqueous waste (possibly requiring neutralization) comprises a challenging problem. Regarding deproteination, with ca. 20 mL NaOH solution needed per g of shell,^{164,165} the ca. 39,000 t/year of shellfish waste produced in Newfoundland¹⁶⁸ would have required $780 \cdot 10^6$ L of NaOH solution. Hence, local communities would need to consider recycling facilities for quantities in that order of magnitude. Moreover, possible degradation of the protein content is an issue which should not be neglected when dealing with strong bases.⁵⁸

As discussed in Section 1.5, valuable products from the most abundant of the marine polysaccharides can be of molecular weights up to the order of MDa and of a wide range of degrees of acetylation. Hence, one should be critical to methods that aim for complete depolymerization and oligomers, as those limit the diversity of possible products that chitin can offer to a sustainable biorefinery. The usual biological activities of chitin oligomers, as well as the potential platform molecules and fuels produced from intense depolymerization might not necessarily worth the additional energy cost from adjunct treatments (e.g. steam explosion, microwave,

^{xix} CaCO_3 solubilizes to CaCl_2 with HCl at concentrations lower than 1 M, ambient temperatures, and short times (164,165). Also, a decoloration process often involves bleaching of β -carotene derivatives (carotenoids), which are bound to the polysaccharide (167).

ultrasonication, gamma irradiation) proposed on top of acidic or enzymatic hydrolyses (essential treatment).

Depending on the native sample, the traditional acidic hydrolysis of chitin goes forward with concentrated strong acids (usually 3–12 M HCl) at elevated temperatures (20–90 °C) and up to 7 h. The major disadvantages of this process are the creation of large volumes of concentrated acidic waste streams, as well as the requirement for special labor (e.g. protection from vapours) and robust equipment (e.g. corrosive resistant).¹⁶⁹ It is estimated that 1 g of chitin needs at least 40 mL of HCl solution.^{170,171} The ca. 3,900 tons of chitin produced from shellfish waste yearly in Newfoundland would have required $156 \cdot 10^6$ L of concentrated HCl solution. Possible basic solutions for neutralization and inevitable salt formation are issues that need to be addressed. Similarly to the deproteination phase discussed above, this method necessitates strategic design in terms of recycling acid/base quantities at the local level.¹⁷²

On the other hand, chitinases work under mild conditions, however they are expensive,^{xx} and they usually need long times (days), buffers and some sort of biomass pre-treatment.^{173,174} Therefore, if on top of those disadvantages one adds the probable separation steps required for the pretreated chitin (e.g. with microwaves) to enter the essential hydrolysis step (acidic or enzymatic),¹⁶⁹ then the benefits from the anticipated intensification (yields of oligomers) might need to be

^{xx} Often, cocktails of enzymes are needed.

of substantial value. Interestingly, acidic conditions have been reported to produce chitin nanofibers (in some cases with the help of mechanical treatment), however those methods need to clarify if possible deacetylation (at pH values <4.5) favors the formation of stable suspensions.¹⁷⁵

Aiming to valorize higher molecular weights via fiber spinning, the Rogers group dissolved 0.38, 0.62 and 1.4 wt.% of Sigma's practical grade (PG) chitin (product # C7170) in 1-ethyl-3-methylimidazolium chloride, 1-butyl-3-methylimidazolium chloride, and 1-ethyl-3-methylimidazolium acetate respectively while stirring at 100 °C for 19 h. Here it is hypothesized that the acetate's stronger basicity than that of the chloride provides the anionic part of the ionic liquid (IL) with a better ability to disrupt the polysaccharide's hydrogen bonding network and establish a new one between the solvent and the solute. The solvent's power achieved 73.5% shrimp shell solubilization via a short microwave treatment with 94% recovery of the chitin content (higher MW).¹⁷⁶ ^{xxi} In analogy to the lignocellulose treatment discussed above, the ionic liquid's performance comprises an attractive feature for an ocean based biorefinery. The acetate's higher than 0.5 Kamlet-Taft β value was also highlighted as the key dissolution parameter when the ionic liquid with tris (2-hydroxyethyl) methylammonium as a cation managed to dissolve 0.1 wt.% of a chitin sample from Wako Pure Chemical Industries Ltd at room temperature after addition of ethylenediamine.¹⁷⁷

^{xxi} Assumptions were made regarding the dissolution of the shrimp shell's components.

Now, considering the emergence of a market which demands non-shellfish derived chitin (from sources like fungi, insects, and squid-pen),^{178 xxii} academic and industrial research groups can take advantage of a versatile toolbox of modern solvent systems, which apart from ionic liquids offers *N,N*-Dimethylacetamide/LiCl (DMAc/LiCl), CaCl₂/methanol, deep eutectic solvents, highly polar fluorinated solvents, organic salt aqueous solutions, alkali/urea aqueous solutions, and supercritical fluids.^{179,180 xxiii} Most of these options are either organic or aqueous solutions of salts. A special case is that of deep eutectic solvents (DES), which has gained an appreciable dynamic in the past 15 years.¹⁸¹⁻¹⁸³ DES are fluids with a lower melting point compared to those of their two individual components [a halide salt (hydrogen bond acceptor) and a hydrogen bond donor (e.g. urea, amides, carboxylic acids)].¹⁸⁴ When applied in an α -chitin sample with a DP ca. 2000–4000, 9.0 wt.% was dissolved in choline chloride/thiourea [optimized molar ratio (OMR) 1:2], 6.0 wt.% in choline chloride/urea (OMR 1:2), and 5.0 wt.% in betaine hydrochloride/urea (OMR 1:4) with the help of heating at 100 °C for 6, 10, and 10 h respectively.¹⁸⁵

Although mechanistic studies in DES dissolution have not progressed as much as in ionic liquids (IL), interactions of electrostatic nature between the solvent's ions and the hydroxyl and amide groups of chitin are expected to influence the solvation

^{xxii} In parallel to shellfish waste (mainly shrimp, crab and lobster) discussed so far; possibly for the manufacturing of medical grade chitin.

^{xxiii} Here, the reader might enjoy Kappa's "cockroach story" in "The Trouble with Synthesis" paper (102).

performance of DES. Considering the relatively good hydrogen bond donor abilities of ureas, the cation-anion combination in the hydrogen bond acceptor should make a difference. Nevertheless, with the high temperatures (>90 °C) and stirring times (>6 h) reported in most IL and DES dissolution experiments,^{xxiv} a kinetic instead of a thermodynamic control might be more crucial. With a critical perspective on the mechanism of cellulose dissolution, Lindman et al. have highlighted the importance of the neglected amphiphilic character of cellulose and the role of hydrophobic interactions^{xxv} in balance with hydrogen bonding and van den Waals interactions.¹⁸⁶

Therefore, all three of those intermolecular forces are expected to contribute to the free energy (i.e. Gibbs) barrier associated with decrystallization/solvation of an edge chain from an *ac*-sheet surface of an α -chitin fibril (25–30 kcal/mol, see Section 1.4). Approximating the process, the system's Gibbs energy before a solute A (e.g. chitin) and a solvent B (e.g. ionic liquid) are mixed is: $G_i = n_A\mu_A + n_B\mu_B$, where μ_J is the chemical potential of substance J, and n_J is the amount of substance (number of moles). After they are mixed, the chemical potentials of the two components will change, hence the system's Gibbs energy will become: $G_f = n_A\mu'_A + n_B\mu'_B$. Thus, the

^{xxiv} In addition, shorter dissolution times were recorded when non-conventional ways of heating were applied to IL and DES suspensions of chitin (microwaves, ultrasonication) (176,185).

^{xxv} These are due to the axial position of the glucopyranose's ring C-H hydrogens (methines) and their stacking in between polysaccharide chains. Molecular dynamics on small oligomers (DP 1–4) calculated a significantly higher contribution from hydrophobic stacking than from hydrogen bonding (89). The situation however is expected to be more balanced in polysaccharides.

change in Gibbs energy for the system's mixing (*Gibbs energy of mixing*, $\Delta_{\text{mix}}G$) will be: $\Delta_{\text{mix}}G = G_f - G_i$; a function of terms from both the solute (e.g. chitin) and the solvent (e.g. ionic liquid).^{187 xxvi} Fundamentally, if $\Delta_{\text{mix}}G$ is negative for a certain composition (n_A/n_A+n_B), then the two components mix spontaneously; as it approximately happened for tris (2-hydroxyethyl) methylammonium acetate (component B1) and 0.1 wt.% chitin (component A) at room temperature after addition of ethylenediamine (component B2).¹⁷⁷ However, in most of the other cases of ionic liquids (IL) and deep eutectic solvents (DES) discussed above, the high temperatures (>90 °C), which resulted in less than 10 wt.% chitin solubilization, suggest processes which are far from being characterized as truly spontaneous.

With our recent comprehension of hydrophobic interactions at the molecular level, it is not unreasonable to hypothesize that the thermal energy provided by experimentalists is to partially disrupt solvent-solvent interactions in order to create cavity-like conditions, which will favour solvent-solute interactions, allow for solute accommodation, and finally lead to its irreversible solvation (Figure 1–12).¹⁸⁸ Nevertheless, considering the cost of heating ILs and DES for long times, their life cycle issues (complex syntheses, toxicity & biodegradability),^{189,190} and the need to recycle/purify large volumes of liquids,^{184 xxvii} alternative methods that generate

^{xxvi} For two liquids that form an ideal solution, the Gibbs energy of mixing is: $\Delta_{\text{mix}}G = nRT\{x_A \ln x_A + x_B \ln x_B\}$, x_j is the mole fraction of component J (187).

^{xxvii} Most of the solvent systems reviewed do not exceed 10 wt.% solubilization of chitin (179). Hence, a biorefinery's facilities which might be aiming to solubilize 1,000 kg chitin per day would need at least 9,000 kg of solvent. If the scientific community manages to understand and establish solubility minimums of characterized chitins, then a myriad

high-energy microenvironments such as microwaves, ultrasound, and ball milling are promising and complementary tools for the transformation of chitin and biomass.¹⁹⁵ With the mechanochemical treatment of ball milling in particular, processes go forward in the absence of solvent. Therefore, the ΔG for chitin solubilization/decrystallization would lose the term of the solvent's chemical potential and simplify to: $\Delta_{\text{process}}G = \Delta H_{\text{chitin}} - T\Delta S_{\text{chitin}}$. From this equation it is clear that the spontaneity of the mechanochemical process (driven by an increasing system entropy) is dependent only on chitin's molecular weight and intermolecular forces (hydrogen bonding, hydrophobic and van der Waals interactions) which are reflected in the enthalpy term.^{186,187,196} Regardless of the sign of ΔG that chitin ball milling will reveal, the mechanochemistry approach undertaken for the polysaccharide's valorization in this thesis questions "the ingrained belief that solvents are necessary",^{197 xxviii} and aligns with the fifth principle of green chemistry; the challenge of solvent minimization.¹⁹⁸

modification reactions like deacetylation, acylation, and graft copolymerization can be genuinely useful exercises for chemists and offer sustainable value to some of the products discussed in Section 1.5 (191-194).

^{xxviii} John Cornforth's point of view on stereotyped procedures is briefly discussed in "The trouble with synthesis" paper (102).

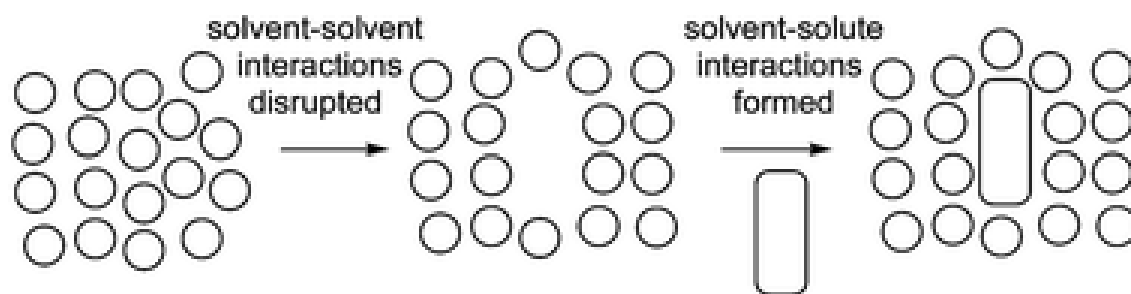


Figure 1–12: Disruption of solvent-solvent interactions towards solute solubilization. Reproduced from {Otto, S. The role of solvent cohesion in nonpolar solvation. *Chem. Sci.* **2013**, *4*, (7), 2953-2959} with permission of The Royal Society of Chemistry.

1.7 Mechanochemistry

'Mechanochemistry' is defined as transformations of solids imposed by absorption of mechanical energy. It has been accepted that these grinding reactions go forward mainly because the reactants' contact surface area increases with particle size reduction and the subsequent more intimate mix. Grinding comprises manual methods (mortar and pestle) and non-manual methods like ball milling, or extrusion. Acceleration and even enabling of mechanochemical reactions between solids can be induced by small amounts of added liquid giving rise to the term 'liquid assisted grinding' (LAG).¹⁹⁹ The volume of the liquid additive should not exceed 1 μL per mg of solid reactants. For additions of more than 1 $\mu\text{L}/\text{mg}$, reactivity is expected to be influenced by the solubility of the reactants.²⁰⁰

Mechanistic models for mechanochemical processes depend primarily on the type of material that undergoes a transformation. For inorganic materials (e.g. metals and metal oxides), hot spot theory and magma-plasma model are the ones most

extensively discussed in literature. The basis of hot spot theory lies originally on frictional processes between two surfaces which slide against each other. Steep rising of local (within approximately $1 \mu\text{m}^2$) temperatures to above $1000 \text{ }^\circ\text{C}$ for short periods ($10^{-3} - 10^{-4} \text{ s}$) are related with plastic deformations which are caused by small protuberances. Instead of lateral frictional processes, the idea of direct impacts gave rise to the magma-plasma model. The generation of local temperatures greater than $10,000 \text{ }^\circ\text{C}$ are considered for impact points, related with transient plasmas and the expulsion of energetic species among which free electrons.¹⁹⁹

The key sites of reactivity in molecular organic and metal-organic mechanochemical reactions are unlikely to be hot spots and magma-plasma sites. If that was the case, widespread decomposition would have been anticipated. Since such processes are not observed, it is hypothesized that these phenomena are probably too fast and/or too localized to explain molecular organic reactions. However, as the localized energy disperses, they might have an influence on general heating.¹⁹⁹

Considering the statistical nature of the mechanochemical process, and as the milling media (usually ball) collides against reactants on the side of the vessel,²⁰¹ it is the temperatures, pressures and processes taking place over larger areas (ca. 1 mm^2) that seem most relevant to reactions of molecular reactants.¹⁹⁹ The transformations of molecular crystals, which are generally softer and more mobile

on molecular scales, are explained by three models: (i) molecular migration across surfaces, potentially facilitated via gas phase diffusion, (ii) emergence of a liquid phase, and (iii) covalent bond rupture/formation through an amorphous phase.^{199,202} Molecules only loosely occupied in their lattices are associated with the first, possibly owing to their notable vapour pressures (e.g. *p*-benzoquinone).²⁰² The liquefaction process applies to cases of low melting point reactants or reaction mixtures which may constitute eutectic systems. The genesis of this fluid phase can affect solid-solid contacts in a variety of ways.²⁰³ A plethora of reaction types (from catalytic ones like aldol condensations and oligomerization of benzylic compounds, to noncatalytic ones like Baeyer - Villiger oxidations and condensation of amines and aldehydes to yield azomethines) proceed via a "*liquid or melt phase*", which provides a zone of mobility for successful reactant collisions.²⁰⁴ Finally, the third model is dedicated to the mapping of molecules which are relatively tightly bound together via strong intermolecular forces but whose reactivity is greater when they pass via an amorphous phase. A relatively recent example is the cocrystallization of piracetam with citric acid.²⁰⁵ Even though the experimental studies mentioned above are entirely representative of the three distinct mechanistic models for intermediate phases, one can not rule out possible cases of mechanochemical reactions being influenced by several of the three in chorus.²⁰²

In principle, the application of mechanical force to activate bonds is advantageous as its vectorial nature gives experimentalists the freedom to have better reaction

control compared to the traditional thermochemical approaches. With force analysis tools developed by theoreticians, mechanochemists can study thermodynamic questions such as “Which bonds, angles, and torsions of the molecule are particularly stressed and why?” and “What are the force distribution patterns in the hydrogen bonds of β -sheets of stress-bearing proteins?”. Moreover, quantum chemical methods (e.g. Bell theory) approximate kinetic effects like the alteration of a reaction's activation energy when an external force is applied.²⁰⁶ Computational methods have started to also predict the equilibrium composition of grinding reactions. Although the Day group has presented some successful results on metathesis reactions between aromatic disulfides, accuracy in sampling of conformational space is needed throughout the identification of global minima for lattice energy of possible observable molecular crystal structures.²⁰⁷ These fascinating elements from the field of quantum mechanochemistry, which are generally unknown to experimental workers, fulfil our needs for designing reactions that yield a desired product (among which stress-responsive materials) as well as for ridding ourselves of excess use of mechanical force in academic and industrial laboratories.²⁰⁶

Until that kind of “order” is imposed in the optimization of ball milling syntheses, rules of thumb will keep training the senses and the unbiased thinking of mechanochemists.²⁰⁶ These are based on the manipulation of several practical

parameters, which have to be investigated in order to scale-up a process, and can be grouped into three categories.²⁰⁸

- Chemical parameters
- Technological parameters
- Process parameters

Chemical parameters summarize all those variables which are directly linked to the chemical transformation taking place in the chamber of the ball mill, which include: the type of chemical reaction, the presence of catalysts or additives, the reagent ratio, and the presence of low amounts of liquid(s) in case of LAG. Technological parameters that should be considered include: the type of ball mill, the milling material, the number of milling balls, the size of milling balls, and the filling degree of the milling chamber. Process parameters are useful for controlling the energy entry during the process and include: operating frequency [revolutions per minute (rpm)], reaction time, temperature.²⁰⁸

1.8 Summary, research objectives and thesis structure

Summing up, in Section 1.5, selected chitin applications which represent only a small fraction of a vast literature were discussed. Essentially, the valuable products from the most abundant of the marine polysaccharides revealed a rich diversity which ranges from therapeutic substances, products for agricultural systems and fuels, to platform molecules, personal care products and functional materials.

Furthermore, the most effective methods for chitin's sustainable valorization were assessed in Section 1.6, and analogies to those for lignocellulose and shellfish waste were highlighted. On the other hand, in footnote (v) the reader might have noticed the percentage of chitin utilization today: less than 1%. How does this come about? How is it possible that this inheritable wealth for both science and society is being used in such low quantity? The key to the answer lies in how poorly systematic the scientific literature is with respect to a factor which has been generally underestimated: polysaccharide crystallinity.¹⁸⁶

In an initial step to fill in that research gap, it should be noted that a mapping of α -chitin's intermolecular hydrogen bonding network was attempted in Section 1.4 through published molecular dynamics simulations and the way that they perceive its crystal packing and elementary fibril structure. With that sense of direction, the technological parameters of a ball mill are presented in detail in Chapter 2, so that some of them be used systematically to determine how the applied mechanical force influences α -chitin's intermolecular hydrogen bonding network and crystallinity both qualitatively and quantitatively. The working hypothesis here is that the more intense the ball mill's process and technological parameters are, the more amorphous and soluble chitin will be. Therefore, a key objective of this thesis was to correlate powder X-ray diffraction (XRD), scanning electron microscopy (SEM), Fourier-transform infrared spectroscopy (FT-IR), and solubility data for sets of chitin samples created by specific ball milling procedures. Considering the

reactivity remarks for mechanochemical processes (see Section 1.7), the key questions to answer here are “Can α -chitin be amorphized in a controlled way?”, and if yes “Is that amorphization a result of the disruption of the intermolecular hydrogen bonding network alone or of covalent bonds as well?”.

Depending on the results of Chapter 2, ball milling parameters were adjusted in Chapter 3 aiming for efficient conversion of α -chitin to water-soluble products. The working hypothesis here is the same as for Chapter 2, and in order to test it, solubility, colorimetry, matrix assisted laser desorption (MALDI) mass spectrometry (MS), and size exclusion chromatography (SEC) data were associated both qualitatively and quantitatively. The objective for that part of the thesis was to answer critical questions like: “Can mechanochemical conversion of α -chitin to water-soluble products be optimized in terms of yield?”, and if yes “What is the composition of the optimized water-soluble products?”.

In Chapter 4, a set of chitins of different MW is created by ball milling in order to select the solvent system which is more effective in dissolving a certain concentration/MW combination and produce films with good mechanical properties. The working hypothesis is that higher molecular weight polysaccharides are harder to dissolve, but they usually yield better mechanical properties when they solidify as films. So as to investigate this, experimental results from XRD, FT-IR, solubility tests in an ionic liquid, and alkali aqueous solutions, and simple film casting were evaluated. The objective in this chapter was to answer the

following crucial questions: “Which solvent system performs better in dissolving ball milled α -chitin?” and “What are the critical concentrations of certain ball milled samples that yield films with acceptable mechanical properties?”.

Finally, Chapter 5 realizes the comprehensive conclusions of the thesis, with a perspective on the main advantages and limitations of the chitin ball milling system, as well as ideas on complementary valorization methods for future investigation.

1.9 References

1. Rockström, J.; Steffen, W.; Noone, K.; Persson, Å; Chapin, F. S.; Lambin, E. F.; Lenton, T. M.; Scheffer, M.; Folke, C.; Schellnhuber, H. J.; Nykvist, B.; De Wit, C. A.; Hughes, T.; Van Der Leeuw, S.; Rodhe, H.; Sörlin, S.; Snyder, P. K.; Costanza, R.; Svedin, U.; Falkenmark, M.; Karlberg, L.; Corell, R. W.; Fabry, V. J.; Hansen, J.; Walker, B.; Liverman, D.; Richardson, K.; Crutzen, P.; Foley, J. A. A safe operating space for humanity. *Nature* **2009**, *461*, (7263), 472-475.
2. Rockström, J.; Steffen, W.; Noone, K.; Persson, A.; Chapin III, F. S.; Lambin, E.; Lenton, T. M.; Scheffer, M.; Folke, C.; Schellnhuber, H. J.; Nykvist, B.; de Wit, C. A.; Hughes, T.; van der Leeuw, S.; Rodhe, H.; Sörlin, S.; Snyder, P. K.; Costanza, R.; Svedin, U.; Falkenmark, M.; Karlberg, L.; Corell, R. W.; Fabry, V. J.; Hansen, J.; Walker, B.; Liverman, D.; Richardson, K.; Crutzen, P.; Foley, J. Planetary boundaries: Exploring the safe operating space for humanity. *Ecol. Soc.* **2009**, *14*, (2), article 32.
3. Steffen, W.; Richardson, K.; Rockström, J.; Cornell, S. E.; Fetzer, I.; Bennett, E. M.; Biggs, R.; Carpenter, S. R.; De Vries, W.; De Wit, C. A.; Folke, C.; Gerten, D.; Heinke, J.; Mace, G. M.; Persson, L. M.; Ramanathan, V.; Reyers, B.; Sörlin, S. Planetary boundaries: Guiding human development on a changing planet. *Science* **2015**, *347*, (6223), article 1259855.
4. Costanza, R.; Atkins, P. W. B.; Bolton, M.; Cork, S.; Grigg, N. J.; Kasser, T.; Kubiszewski, I. Overcoming societal addictions: What can we learn from individual therapies? *Ecol. Econ.* **2017**, *131*, 543-550.
5. Berner, R. A. The long-term carbon cycle, fossil fuels and atmospheric composition. *Nature* **2003**, *426*, (6964), 323-326.

6. Jørgensen, S. E.; Jordán, F. Introduction. In *Models of the Ecological Hierarchy: from molecules to the ecosphere*, 25; 1st ed.; Jordán, F. and Jørgensen, S. E., Eds. ; Elsevier: Oxford, UK, 2012; pp xxiii-xxxi.
7. Andres, R. J.; Fielding, D. J.; Marland, G.; Boden, T. A.; Kumar, N.; Kearney, A. T. Carbon dioxide emissions from fossil-fuel use, 1751-1950. *Telus B* **1999**, *51*, (4), 759-765.
8. NOAA (National Oceanic and Atmospheric Administration) , Earth System Research Laboratory (ESRL) Global Monitoring Division - Global Greenhouse Gas Reference Network, 2018, <https://www.esrl.noaa.gov/gmd/ccgg/trends/>, (accessed 6/23, 2018).
9. Maggio, G.; Cacciola, G. When will oil, natural gas, and coal peak? *Fuel* **2012**, *98*, 111-123.
10. Bailly, F.; Longo, G.; Montevil, M. A 2-dimensional geometry for biological time. *Prog. Biophys. Mol. Biol.* **2011**, *106*, (3), 474-484.
11. United Nations , World Population Prospects - Population Division - United Nations, 2018, <https://esa.un.org/unpd/wpp/>, (accessed 6/23, 2018).
12. Frank, S. A. All of life is social. *Curr. Biol.* **2007**, *17*, (16), R648-R650.
13. Leadbeater, E.; Chittka, L. Social Learning in Insects - From Miniature Brains to Consensus Building. *Curr. Biol.* **2007**, *17*, (16), R703-R713.
14. Helm, B.; Ben-Shlomo, R.; Sheriff, M. J.; Hut, R. A.; Foster, R.; Barnes, B. M.; Dominoni, D. Annual rhythms that underlie phenology: Biological time-keeping meets environmental change. *Proc. R. Soc. B Biol. Sci.* **2013**, *280*, (1765), article 20130016.
15. Longo, G.; Perret, N. Rhythms, retention and protention: philosophical reflections on geometrical schemata for biological time. In *Building Theories*, 41; Springer International Publishing: Cham, Switzerland, 2018; pp 245-259.
16. Oppenheim, A. L. Mesopotamia in the early history of alchemy. *Revue d'assyriologie et d'archéologie orientale* **1966**, *60*, (1), 29-45.
17. Habashi, F. The age of alchemy: History of chemistry, metallurgy, and civilisation. *Interdisciplinary Sci. Rev.* **1998**, *23*, (4), 348-361.
18. Williams, R. J. P. A chemical systems approach to evolution. *Dalton Trans.* **2007**, (10), 991-1001.
19. Hajdu, S. I. A note from history: Two pioneering chemists, three hundred years apart. *Ann. Clin. Lab. Sci.* **2005**, *35*, (1), 105-107.

20. Sheldon, R. Catalytic Oxidations in Organic Synthesis. *Bull. Soc. Chim. Belg.* **1985**, *94*, (9), 651-670.
21. Clark, J. H.; Kybett, A. P.; Macquarrie, D. J.; Barlow, S. J.; Landon, P. Montmorillonite supported transition metal salts as Friedel-Crafts alkylation catalysts. *J. Chem. Soc., Chem. Commun.* **1989**, (18), 1353-1354.
22. Anastas, P. T.; Warner, J. C. *Green Chemistry: Theory and Practice*; Oxford University Press: New York, 1998.
23. Tang, S. Y.; Bourne, R. A.; Poliakoff, M.; Smith, R. L. The 24 Principles of Green Engineering and Green Chemistry: "IMPROVEMENTS PRODUCTIVELY". *Green Chem.* **2008**, *10*, (3), 268-269.
24. Lipshutz, B. H., Ed. Green Chemistry (special issue). *Aldrichim. Acta* **2015**, *48*, (1), 3.
25. Constable, D. J. C.; Dunn, P. J.; Hayler, J. D.; Humphrey, G. R.; Leazer Jr., J. L.; Linderman, R. J.; Lorenz, K.; Manley, J.; Pearlman, B. A.; Wells, A.; Zaks, A.; Zhang, T. Y. Key green chemistry research areas - A perspective from pharmaceutical manufacturers. *Green Chem.* **2007**, *9*, (5), 411-420.
26. Henderson, R. K.; Jiménez-González, C.; Constable, D. J. C.; Alston, S. R.; Inglis, G. G. A.; Fisher, G.; Sherwood, J.; Binks, S. P.; Curzons, A. D. Expanding GSK's solvent selection guide - Embedding sustainability into solvent selection starting at medicinal chemistry. *Green Chem.* **2011**, *13*, (4), 854-862.
27. Anastas, P.; Eghbali, N. Green chemistry: Principles and practice. *Chem. Soc. Rev.* **2010**, *39*, (1), 301-312.
28. Jenck, J. F.; Agterberg, F.; Droescher, M. J. Products and processes for a sustainable chemical industry: A review of achievements and prospects. *Green Chem.* **2004**, *6*, (11), 544-556.
29. Paloniemi, R.; Apostolopoulou, E.; Cent, J.; Bormpoudakis, D.; Scott, A.; Grodzinska-Jurczak, M.; Tzanopoulos, J.; Koivulehto, M.; Pietrzyk-Kaszynska, A.; Pantis, J. D. Public Participation and Environmental Justice in Biodiversity Governance in Finland, Greece, Poland and the UK. *Environ. Policy Gov.* **2015**, *25*, (5), 330-342.
30. Wittmayer, J. M.; Schöpke, N.; van Steenberg, F.; Omann, I. Making sense of sustainability transitions locally: how action research contributes to addressing societal challenges. *Crit. Policy Stud.* **2014**, *8*, (4), 465-485.
31. Hawkins, R. The trouble with innovation: Why cleaning up the environment is going to be a lot more challenging than we think. *Can. Public Policy* **2016**, *42*, (1), S46-S53.

32. Raveaud, G. L'économie face à ses pulsions de mort. *L'Évolution Psychiatrique* **2016**, *81*, 847-854.
33. Maris, B. Economists, experts and politicians. *Innovations* **2003**, *17*, (1), 9-27.
34. Debord, G. L. sections XIII - XIV. In *Comments on the society of the spectacle*, Verso: London; New York, 1990; pp 34-43.
35. Strauss, C. R.; Scott, J. L. The future rewritten. *Chem. Ind.* **2001**, (19), 610-613.
36. Ingre-Khans, E.; Ågerstrand, M.; Beronius, A.; Rudén, C. Transparency of chemical risk assessment data under REACH. *Environ. Sci. Process. Impacts* **2016**, *18*, (12), 1508-1518.
37. Balmer, J. M. T.; Fukukawa, K.; Gray, E. R. The nature and management of ethical corporate identity: A commentary on corporate identity, corporate social responsibility and ethics. *J. Bus. Ethics* **2007**, *76*, (1), 7-15.
38. Deslandes, G. The care-of-self ethic with continual reference to Socrates: Towards ethical self-management. *Bus. Ethics* **2012**, *21*, (4), 325-338.
39. Szerszynski, B. The Post-ecologist condition: Irony as symptom and cure. *Environmental Politics* **2007**, *16*, (2), 337-355.
40. Clark, J. H.; Farmer, T. J.; Herrero-Davila, L.; Sherwood, J. Circular economy design considerations for research and process development in the chemical sciences. *Green Chem.* **2016**, *18*, (14), 3914-3934.
41. BBC Radio 4 Today , Lovelock: 'We can't save the planet', http://news.bbc.co.uk/today/hi/today/newsid_8594000/8594561.stm, (accessed 09/01, 2017).
42. Lovelock, J. A geophysicologist's thoughts on geoengineering. *Philos. Trans. R. Soc. A Math. Phys. Eng. Sci.* **2008**, *366*, (1882), 3883-3890.
43. Zeleny, M. High technology and barriers to innovation: From globalization to relocalization. *Int. J. Inf. Technol. Decis. Mak.* **2012**, *11*, (2), 441-456.
44. Okkerse, C.; Van Bekkum, H. From fossil to green. *Green Chem.* **1999**, *1*, (2), 107-114.
45. BP , Statistical Review of World Energy, Oil Reserves-to-production (R/P) ratios, <http://www.bp.com/en/global/corporate/energy-economics/statistical-review-of-world-energy/oil/oil-reserves.html>, (accessed 09/01, 2017).

46. Li, H.; Jenkins-Smith, H. C.; Silva, C. L.; Berrens, R. P.; Herron, K. G. Public support for reducing US reliance on fossil fuels: Investigating household willingness-to-pay for energy research and development. *Ecol. Econ.* **2009**, *68*, (3), 731-742.
47. Kaltschmitt, M.; Thran, D. Biomass-based Green Energy Generation. In *Sustainable Solutions for Modern Economies*, 1st ed.; Royal Society of Chemistry: Cambridge, UK, 2009; pp 86-124.
48. Cherubini, F. The biorefinery concept: Using biomass instead of oil for producing energy and chemicals. *Energy Convers. Manage.* **2010**, *51*, (7), 1412-1421.
49. Brehmer, B.; Boom, R. M.; Sanders, J. Maximum fossil fuel feedstock replacement potential of petrochemicals via biorefineries. *Chem. Eng. Res. Design* **2009**, *87*, (9), 1103-1119.
50. Sadhukhan, J.; Ng, K. S.; Hernandez, E. M. *Biorefineries and Chemical Processes: Design, Integration and Sustainability Analysis*; Wiley: Hoboken, NJ, 2014.
51. Wertz, J., Bédué, O. *Lignocellulosic Biorefineries*; EPFL Press: Lausanne, 2013.
52. Food and Agriculture Organization of the United Nations (FAO), International Fund for Agricultural Development (IFAD) and World Food Programme (WFP). *The State of Food Insecurity in the World 2012. Economic growth is necessary but not sufficient to accelerate reduction of hunger and malnutrition*. Food and Agriculture Organization of the United Nations: Rome, Italy, 2012; 8-14.
53. J. Gustavsson, C. Cederberg, U. Sonesson and R. van Otterdijk. *Global Food Losses and Food Waste. Extend, Causes and Prevention*. Food and agriculture organization of the United Nations: Rome, Italy, 2011; 4-9.
54. Lin, C. S. K.; Pfaltzgraff, L. A.; Herrero-Davila, L.; Mubofu, E. B.; Abderrahim, S.; Clark, J. H.; Koutinas, A. A.; Kopsahelis, N.; Stamatelatos, K.; Dickson, F.; Thankappan, S.; Mohamed, Z.; Brocklesby, R.; Luque, R. Food waste as a valuable resource for the production of chemicals, materials and fuels. Current situation and global perspective. *Energy Environ. Sci.* **2013**, *6*, (2), 426-464.
55. Yan, N.; Chen, X. Sustainability: Don't waste seafood waste. *Nature* **2015**, *524*, (7564), 155-157.
56. Kerton, F. M.; Liu, Y.; Omari, K. W.; Hawboldt, K. Green chemistry and the ocean-based biorefinery. *Green Chem.* **2013**, *15*, (4), 860-871.
57. Beier, S.; Bertilsson, S. Bacterial chitin degradation-mechanisms and ecophysiological strategies. *Front. Microbiol.* **2013**, *4*, article 149.

58. Kaur, S.; Dhillon, G. S. Recent trends in biological extraction of chitin from marine shell wastes: A review. *Crit. Rev. Biotechnol.* **2015**, *35*, (1), 44-61.
59. Li, B.; Mu, X. Recent Progress in the Utilization of Chitin/Chitosan for Chemicals and Materials. In *Fuels, Chemicals and Materials from the Oceans and Aquatic Sources*, 1st ed.; Kerton, F. M. and Yan, N., Eds.; John Wiley & Sons, Ltd: Hoboken, NJ, 2017; pp 151-187.
60. Food and Agriculture Organization of the United Nations, Global Production Statistics 1950-2013 (online database), <http://www.fao.org/fishery/statistics/global-production/query/en>, (accessed 6/24, 2018).
61. Azuma, K.; Osaki, T.; Minami, S.; Okamoto, Y. Anticancer and Anti-Inflammatory Properties of Chitin and Chitosan Oligosaccharides. *J. Funct. Biomater.* **2015**, *6*, (1), 33-49.
62. Ngo, D.; Lee, S.; Kim, M.; Kim, S. Production of chitin oligosaccharides with different molecular weights and their antioxidant effect in RAW 264.7 cells. *J. Funct. Foods* **2009**, *1*, (2), 188-198.
63. Barber, P. S.; Kelley, S. P.; Griggs, C. S.; Wallace, S.; Rogers, R. D. Surface modification of ionic liquid-spun chitin fibers for the extraction of uranium from seawater: Seeking the strength of chitin and the chemical functionality of chitosan. *Green Chem.* **2014**, *16*, (4), 1828-1836.
64. Salaberria, A. M.; Labidi, J.; Fernandes, S. C. M. Different routes to turn chitin into stunning nano-objects. *Eur. Polym. J.* **2015**, *68*, 503-515.
65. Chen, X.; Liu, Y.; Kerton, F. M.; Yan, N. Conversion of chitin and N-acetyl-d-glucosamine into a N-containing furan derivative in ionic liquids. *RSC Adv.* **2015**, *5*, (26), 20073-20080.
66. Kumirska, J.; Czerwicka, M.; Kaczyński, Z.; Bychowska, A.; Brzozowski, K.; Thöming, J.; Stepnowski, P. Application of spectroscopic methods for structural analysis of chitin and chitosan. *Mar. Drugs* **2010**, *8*, (5), 1567-1636.
67. Maniukiewicz, W. X-Ray Diffraction Studies of Chitin, Chitosan and Their Derivatives. In *Chitin, Chitosan, Oligosaccharides and Their Derivatives*, CRC Press: 2010; pp 83-94.
68. Muzzarelli, R. A. A.; Muzzarelli, C. Native and Modified Chitins in the Biosphere. *ACS Symp. Ser.* **1998**, *707*, 148-162.
69. O'Sullivan, A. C. Cellulose: The structure slowly unravels. *Cellulose* **1997**, *4*, (3), 173-207.

70. Jang, M. -.; Kong, B. -.; Jeong, Y. -.; Lee, C. H.; Nah, J. -. Physicochemical characterization of α -chitin, β -chitin, and γ -chitin separated from natural resources. *J. Polym. Sci. Part A* **2004**, *42*, (14), 3423-3432.
71. Einbu, A.; Naess, S. N.; Elgsaeter, A.; Vårum, K. M. Solution properties of chitin in alkali. *Biomacromolecules* **2004**, *5*, (5), 2048-2054.
72. Susana Cortizo, M.; Berghoff, C. F.; Alessandrini, J. L. Characterization of chitin from *Illex argentinus* squid pen. *Carbohydr. Polym.* **2008**, *74*, (1), 10-15.
73. Pillai, C. K. S.; Paul, W.; Sharma, C. P. Chitin and chitosan polymers: Chemistry, solubility and fiber formation. *Prog. Polym. Sci.* **2009**, *34*, (7), 641-678.
74. Matsuda, Y.; Kowsaka, K.; Okajima, K.; Kamide, K. Structural change of cellulose contained in immature cotton boll during its growth. *Polym. Int.* **1992**, *27*, (4), 347-351.
75. Muzzarelli, R. A. A. Chitin Nanostructures in Living Organisms. In *Chitin: Formation and Diagenesis*, Gupta, N. S., Ed. ; Springer Netherlands: Dordrecht, 2011; pp 1-34.
76. Dobrovol'skaya, I. P.; Kasatkin, I. A.; Yudin, V. E.; Ivan'kova, E. M.; Elokhovskii, V. Y. Supramolecular structure of chitin nanofibrils. *Polym. Sci. Ser. A* **2015**, *57*, (1), 52-57.
77. Yudin, V. E.; Dobrovolskaya, I. P.; Neelov, I. M.; Dresvyanina, E. N.; Popryadukhin, P. V.; Ivan'kova, E. M.; Elokhovskii, V. Y.; Kasatkin, I. A.; Okrugin, B. M.; Morganti, P. Wet spinning of fibers made of chitosan and chitin nanofibrils. *Carbohydr. Polym.* **2014**, *108*, (1), 176-182.
78. Rudall, K. M. *The Chitin/Protein Complexes of Insect Cuticles*; Advances in Insect Physiology; Academic Press: London, 1963.
79. Atkins, E. Conformations in polysaccharides and complex carbohydrates. *J. Biosci.* **1985**, *8*, (1-2), 375-387.
80. Giraud-Guille, M. -. Fine structure of the chitin-protein system in the crab cuticle. *Tissue Cell* **1984**, *16*, (1), 75-92.
81. Habibi, Y.; Lucia, L. A. Chitin Nanofibers as Building Blocks for Advanced Materials. In *Polysaccharide Building Blocks: A Sustainable Approach to the Development of Renewable Biomaterials*, John Wiley and Sons: 2012; pp 227-245.
82. Bruck, W.; Slater, J.; Carney, B. Chitin and Chitosan from Marine Organisms. In *Chitin, Chitosan, Oligosaccharides and Their Derivatives*, CRC Press: 2010; pp 11-23.

83. Ogawa, Y.; Lee, C. M.; Nishiyama, Y.; Kim, S. H. Absence of sum frequency generation in support of orthorhombic symmetry of α -chitin. *Macromolecules* **2016**, *49*, (18), 7025-7031.
84. Rinaudo, M. Chitin and chitosan: Properties and applications. *Prog. Polym. Sci.* **2006**, *31*, (7), 603-632.
85. Rudall, K. M.; Kenchington, W. The chitin system. *Biol. Rev. Camb. Philos. Soc.* **1973**, *48*, (4), 597-636.
86. Petrov, M.; Lymperakis, L.; Friák, M.; Neugebauer, J. Ab Initio Based conformational study of the crystalline α -chitin. *Biopolymers* **2013**, *99*, 22-34.
87. Sawada, D.; Nishiyama, Y.; Langan, P.; Forsyth, V. T.; Kimura, S.; Wada, M. Direct determination of the hydrogen bonding arrangement in anhydrous β -chitin by neutron fiber diffraction. *Biomacromolecules* **2012**, *13*, (1), 288-291.
88. Nishiyama, Y.; Noishiki, Y.; Wada, M. X-ray structure of anhydrous β -chitin at 1 Å resolution. *Macromolecules* **2011**, *44*, (4), 950-957.
89. Medronho, B.; Lindman, B. Competing forces during cellulose dissolution: From solvents to mechanisms. *Curr. Opin. Colloid Interface Sci.* **2014**, *19*, (1), 32-40.
90. Ogawa, Y.; Kimura, S.; Saito, Y.; Wada, M. Infrared study on deuteration of highly-crystalline chitin. *Carbohydr. Polym.* **2012**, *90*, (1), 650-657.
91. Saito, Y.; Okano, T.; Gaill, F.; Chanzy, H.; Putaux, J. -. Structural data on the intra-crystalline swelling of β -chitin. *Int. J. Biol. Macromol.* **2000**, *28*, (1), 81-88.
92. Minke, R.; Blackwell, J. The structure of α -chitin. *J. Mol. Biol.* **1978**, *120*, (2), 167-181.
93. Sikorski, P.; Hori, R.; Wada, M. Revisit of α -chitin crystal structure using high resolution X-ray diffraction data. *Biomacromolecules* **2009**, *10*, (5), 1100-1105.
94. Deringer, V. L.; Englert, U.; Dronskowski, R. Nature, strength, and cooperativity of the hydrogen-bonding network in α -chitin. *Biomacromolecules* **2016**, *17*, (3), 996-1003.
95. Nishiyama, Y.; Johnson, G. P.; French, A. D.; Forsyth, V. T.; Langan, P. Neutron crystallography, molecular dynamics, and quantum mechanics studies of the nature of hydrogen bonding in cellulose I β . *Biomacromolecules* **2008**, *9*, (11), 3133-3140.
96. Beckham, G. T.; Crowley, M. F. Examination of the α -chitin structure and decrystallization thermodynamics at the nanoscale. *J. Phys. Chem. B* **2011**, *115*, (15), 4516-4522.

97. Darmon, S. E.; Rudall, K. M. Infra-red and X-ray studies of chitin. *Discuss. Faraday Soc.* **1950**, *9*, 251-260.
98. Pearson, F. G.; Marchessault, R. H.; Liang, C. Y. Infrared spectra of crystalline polysaccharides. V. Chitin. *J. Polym. Sci.* **1960**, *43*, (141), 101-116.
99. Focher, B.; Naggi, A.; Torri, G.; Cosani, A.; Terbojevich, M. Structural differences between chitin polymorphs and their precipitates from solutions-evidence from CP-MAS ¹³C-NMR, FT-IR and FT-Raman spectroscopy. *Carbohydr. Polym.* **1992**, *17*, (2), 97-102.
100. Cárdenas, G.; Cabrera, G.; Taboada, E.; Miranda, S. P. Chitin characterization by SEM, FTIR, XRD, and ¹³C cross polarization/mass angle spinning NMR. *J. Appl. Polym. Sci.* **2004**, *93*, (4), 1876-1885.
101. *Carbohydrate Chemistry: Proven Synthetic Methods*; Kováč, P., Ed.; CRC Press, Taylor & Francis Group: Boca Raton, FL, 2012.
102. Cornforth, J. W. The trouble with synthesis. *Aust. J. Chem.* **1993**, *46*, (2), 157-170.
103. Various authors. Biological activities of chitin and chitosan derivatives. In *Chitin, Chitosan, Oligosaccharides, and Their Derivatives: Biological Activities and Applications*. Chapman and Hall/CRC: Baton Rouge, 2010; pp 195-294.
104. Sarmento, B.; Das Neves, J. *Chitosan-Based Systems for Biopharmaceuticals: Delivery, Targeting and Polymer Therapeutics*; John Wiley and Sons: Hoboken, NJ, 2012.
105. Xia, W.; Liu, P.; Zhang, J.; Chen, J. Biological activities of chitosan and chitooligosaccharides. *Food Hydrocolloids* **2011**, *25*, (2), 170-179.
106. Kumirska, J.; Weinhold, M. X.; Thöming, J.; Stepnowski, P. Biomedical activity of chitin/chitosan based materials- influence of physicochemical properties apart from molecular weight and degree of N-Acetylation. *Polymers* **2011**, *3*, (4), 1875-1901.
107. Various authors. Biomedical applications of chitin and chitosan derivatives. In *Chitin, Chitosan, Oligosaccharides, and Their Derivatives: Biological Activities and Applications*. Chapman and Hall/CRC: Baton Rouge, 2010; pp 295-480.
108. Anitha, A.; Sowmya, S.; Kumar, P. T. S.; Deepthi, S.; Chennazhi, K. P.; Ehrlich, H.; Tsurkan, M.; Jayakumar, R. Chitin and chitosan in selected biomedical applications. *Prog. Polym. Sci.* **2014**, *39*, (9), 1644-1667.
109. Azuma, K.; Osaki, T.; Minami, S.; Okamoto, Y. Anticancer and anti-inflammatory properties of chitin and chitosan oligosaccharides. *J. Funct. Biomater.* **2015**, *6*, (1), 33-49.

110. Panith, N.; Wichaphon, J.; Lertsiri, S.; Niamsiri, N. Effect of physical and physicochemical characteristics of chitosan on fat-binding capacities under in vitro gastrointestinal conditions. *LWT - Food Sci. Technol.* **2016**, *71*, 25-32.
111. Muzzarelli, R. A. A.; Muzzarelli, C. Chitosan as a Dietary Supplement and a Food Technology Agent. In *Functional food carbohydrates*, Boca Raton : CRC Press: Boca Raton, 2006; pp 215-247.
112. Kalpana Sastry, R.; Shrivastava, A.; Venkateshwarlu, G. Assessment of current trends in R&D of chitin-based technologies in agricultural production-consumption systems using patent analytics. *J. Intellect. Prop. Rights* **2015**, *20*, (1), 19-38.
113. Yin, H.; Du, Y. Mechanism and Application of Chitin/Chitosan and Their Derivatives in Plant Protection. In *Chitin, Chitosan, Oligosaccharides and Their Derivatives : Biological Activities and Applications*, Kim, S. -K, Ed. ; CRC Press: Baton Rouge, 2010; pp 605-617.
114. Falcón, A. B.; Cabrera, J. C.; Costales, D.; Ramírez, M. A.; Cabrera, G.; Toledo, V.; Martínez-Télez, M. A. The effect of size and acetylation degree of chitosan derivatives on tobacco plant protection against *Phytophthora parasitica nicotianae*. *World J. Microbiol. Biotechnol.* **2008**, *24*, (1), 103-112.
115. Van Jaarsveld, E.; Wingfield, M. J.; Drenth, A. Effect of metalaxyl resistance and cultivar resistance on control of *Phytophthora nicotianae* in tobacco. *Plant Dis.* **2002**, *86*, (4), 362-366.
116. Dzung, N. A. Enhancing Crop Production with Chitosan and Its Derivatives. In *Chitin, Chitosan, Oligosaccharides and Their Derivatives : Biological Activities and Applications*, Kim, S. -K, Ed. ; CRC Press: Baton Rouge, 2010; pp 619-631.
117. Kumaraswamy, R. V.; Kumari, S.; Choudhary, R. C.; Pal, A.; Raliya, R.; Biswas, P.; Saharan, V. Engineered chitosan based nanomaterials: Bioactivities, mechanisms and perspectives in plant protection and growth. *Int. J. Biol. Macromol.* **2018**, *113*, 494-506.
118. Saharan, V.; Kumaraswamy, R. V.; Choudhary, R. C.; Kumari, S.; Pal, A.; Raliya, R.; Biswas, P. Cu-Chitosan Nanoparticle Mediated Sustainable Approach to Enhance Seedling Growth in Maize by Mobilizing Reserved Food. *J. Agric. Food Chem.* **2016**, *64*, (31), 6148-6155.
119. Farmer, T. J.; Mascal, M. Platform Molecules. In *Introduction to Chemicals from Biomass*, 2nd ed.; Wiley: 2015; pp 89-155.
120. Sadiq, A. D.; Chen, X.; Yan, N.; Sperry, J. Towards the Shell Biorefinery: Sustainable Synthesis of the Anticancer Alkaloid Proximicin A from Chitin. *ChemSusChem* **2018**, *11*, (3), 532-535.

121. Doležal, M. Biologically active pyrazines of natural and synthetic origin. *Chem. Listy* **2006**, *100*, (11), 959-966.
122. Zeng, L.; Qin, C.; Wang, L.; Li, W. Volatile compounds formed from the pyrolysis of chitosan. *Carbohydr. Polym.* **2011**, *83*, (4), 1553-1557.
123. Omari, K. W.; Besaw, J. E.; Kerton, F. M. Hydrolysis of chitosan to yield levulinic acid and 5-hydroxymethylfurfural in water under microwave irradiation. *Green Chem.* **2012**, *14*, (5), 1480-1487.
124. Mika, L. T.; Cséfalvay, E. Conversion of carbohydrates to chemicals. In *Advanced Green Chemistry: Part 1: Greener Organic Reactions and Processes*, World Scientific Publishing Co.: 2017; pp 19-76.
125. Hasunuma, T.; Kondo, A. Consolidated bioprocessing and simultaneous saccharification and fermentation of lignocellulose to ethanol with thermotolerant yeast strains. *Process Biochem.* **2012**, *47*, (9), 1287-1294.
126. Inokuma, K.; Takano, M.; Hoshino, K. Direct ethanol production from N-acetylglucosamine and chitin substrates by *Mucor* species. *Biochem. Eng. J.* **2013**, *72*, 24-32.
127. Evyernie, D.; Morimoto, K.; Karita, S.; Kimura, T.; Sakka, K.; Ohmiya, K. Conversion of chitinous wastes to hydrogen gas by *Clostridium paraputrificum* M-21. *J. Biosci. Bioeng.* **2001**, *91*, (4), 339-343.
128. Stoykov, Y. M.; Pavlov, A. I.; Krastanov, A. I. Chitinase biotechnology: Production, purification, and application. *Eng. Life Sci.* **2016**, *15*, (1), 30-38.
129. Aranaz, I.; Acosta, N.; Civera, C.; Elorza, B.; Mingo, J.; Castro, C.; Gandía, M. L.; Caballero, A. H. Cosmetics and cosmeceutical applications of chitin, chitosan and their derivatives. *Polymers* **2018**, *10*, (2), article 213.
130. Chen, R. H.; Heh, R. S. Skin hydration effects, physico-chemical properties and vitamin E release ratio of vital moisture creams containing water-soluble chitosans. *Int. J. Cosmet. Sci.* **2000**, *22*, (5), 349-360.
131. Morganti, P. Green ingredients in cosmetic dermatology. Molecular aspects of ingredients and carriers. *J. Appl. Cosmetol.* **2016**, *34*, (1-2), 59-73.
132. Chen, L.; Du, Y.; Wu, H.; Xiao, L. Relationship between molecular structure and moisture-retention ability of carboxymethyl chitin and chitosan. *J. Appl. Polym. Sci.* **2002**, *83*, (6), 1233-1241.

133. İkinci, G.; Senel, S.; Akincibay, H.; Kas, S.; Ercis, S.; Wilson, C. G.; Hincal, A. A. Effect of chitosan on a periodontal pathogen *Porphyromonas gingivalis*. *Int. J. Pharm.* **2002**, *235*, (1-2), 121-127.
134. Duan, B.; Huang, Y.; Lu, A.; Zhang, L. Recent advances in chitin based materials constructed via physical methods. *Prog. Polym. Sci.* **2018**, *82*, 1-33.
135. Lin, N.; Huang, J.; Dufresne, A. Preparation, properties and applications of polysaccharide nanocrystals in advanced functional nanomaterials: a review. *Nanoscale* **2012**, *4*, (11), 3274-3294.
136. Sudha, P. N. Chitin/Chitosan and Derivatives for Wastewater Treatment. In *Chitin, Chitosan, Oligosaccharides and Their Derivatives : Biological Activities and Applications*, Kim, S. -K, Ed. ; Chapman and Hall/CRC: Baton Rouge, 2010; pp 561-585.
137. Wang, H.; Qian, J.; Ding, F. Emerging Chitosan-Based Films for Food Packaging Applications. *J. Agric. Food Chem.* **2018**, *66*, (2), 395-413.
138. Qiu, J.; Wang, J. Chitin in rubber based blends and micro composites. In *Rubber Based Bionanocomposites*, 56; Visakh, P. M., Ed. ; Springer International Publishing: Cham, Switzerland, 2017; pp 71-107.
139. Patel, A. K. Chitosan: Emergence as potent candidate for green adhesive market. *Biochem. Eng. J.* **2015**, *102*, 74-81.
140. Uragami, T. Separation Membranes from Chitin and Chitosan Derivatives. In *Chitin, Chitosan, Oligosaccharides and Their Derivatives : Biological Activities and Applications*, Kim, S-K, Ed. ; Chapman and Hall/CRC: Baton Rouge, 2010; pp 481-506.
141. Song, Z.; Li, G.; Guan, F.; Liu, W. Application of chitin/chitosan and their derivatives in the papermaking industry. *Polymers* **2018**, *10*, (4), article 389.
142. Dodson, J. R.; Parker, H. L.; García, A. M.; Hicken, A.; Asemave, K.; Farmer, T. J.; He, H.; Clark, J. H.; Hunt, A. J. Bio-derived materials as a green route for precious & critical metal recovery and re-use. *Green Chem.* **2015**, *17*, (4), 1951-1965.
143. Guibal, E.; McCarrick, P.; Tobin, J. M. Comparison of the sorption of anionic dyes on activated carbon and chitosan derivatives from dilute solutions. *Sep. Sci. Technol.* **2003**, *38*, (12-13), 3049-3073.
144. Chassary, P.; Vincent, T.; Sanchez Marcano, J.; MacAskie, L. E.; Guibal, E. Palladium and platinum recovery from bicomponent mixtures using chitosan derivatives. *Hydrometallurgy* **2005**, *76*, (1-2), 131-147.

145. Mack, C.; Wilhelmi, B.; Duncan, J. R.; Burgess, J. E. Biosorption of precious metals. *Biotechnol. Adv.* **2007**, *25*, (3), 264-271.
146. Fakhreddin Hosseini, S.; Rezaei, M.; Zandi, M.; Ghavi, F. F. Preparation and functional properties of fish gelatin-chitosan blend edible films. *Food Chem.* **2013**, *136*, (3-4), 1490-1495.
147. Leceta, I.; Guerrero, P.; Ibarburu, I.; Dueñas, M. T.; De La Caba, K. Characterization and antimicrobial analysis of chitosan-based films. *J. Food Eng.* **2013**, *116*, (4), 889-899.
148. Scott, J. L.; Lee, J. Appropriate lifetimes, fitting deaths. *Green Chem.* **2016**, *18*, (23), 6157-6159.
149. Minetola, P.; Evers, D. R. Additive manufacturing as a driver for the sustainability of short-lifecycle customized products: The case study of mobile case covers; International Conference on Sustainable Design and Manufacturing 2017, Howlett, R. J., Campana, G., Cimatti, B. and Setchi, R., Eds.; Springer: Cham, 2017; Vol. 68, pp 766-775.
150. Cornforth, J. W. Scientists as citizens. *Aust. J. Chem.* **1993**, *46*, (3), 265-275.
151. Lazaridou, A.; Biliaderis, C. G. Molecular aspects of cereal β -glucan functionality: Physical properties, technological applications and physiological effects. *J. Cereal Sci.* **2007**, *46*, (2), 101-118.
152. Ramawat, K. G.; Mérillon, J. -, Eds. *Polysaccharides: Bioactivity and biotechnology*; Springer International Publishing: Cham, Switzerland, 2015.
153. Ebringerová, A.; Hromádková, Z.; Heinze, T. Hemicellulose. *Adv. Polym. Sci.* **2005**, *186*, 1-67.
154. Cherubini, F.; Strømman, A. H. Principles of biorefining. In *Biofuels*, Elsevier Inc.: 2011; pp 3-24.
155. Morais, A. R. C.; Lukasik, R. M. Direct Hydrolysis of Biomass Polymers using High-pressure CO₂ and CO₂-H₂O Mixtures. In *High Pressure Technologies in Biomass Conversion*, Lukasik R.M., Ed. ; Royal Society of Chemistry: Cambridge, UK, 2017; pp 83-114.
156. Vassilev, S. V.; Baxter, D.; Andersen, L. K.; Vassileva, C. G.; Morgan, T. J. An overview of the organic and inorganic phase composition of biomass. *Fuel* **2012**, *94*, 1-33.
157. Harris, P. J.; Stone, B. A. Chemistry and Molecular Organization of Plant Cell Walls. In *Biomass Recalcitrance: Deconstructing the Plant Cell Wall for Bioenergy*, Blackwell Publishing Ltd.: 2009; pp 61-93.

158. Marriott, P. E.; Gómez, L. D.; Mcqueen-Mason, S. J. Unlocking the potential of lignocellulosic biomass through plant science. *New Phytol.* **2016**, *209*, (4), 1366-1381.
159. Zhang, Y. -. P. Reviving the carbohydrate economy via multi-product lignocellulose biorefineries. *J. Ind. Microbiol. Biotechnol.* **2008**, *35*, (5), 367-375.
160. Wertz, J., Bédué, O. Pretreatments of Lignocellulosic Biomass. In *Lignocellulosic Biorefineries*, EPFL Press: New York, 2013; pp 299-350.
161. De Vrije, T.; De Haas, G.; Tan, G. B.; Keijsers, E. R. P.; Claassen, P. A. M. Pretreatment of Miscanthus for hydrogen production by Thermotoga elfii. *Int. J. Hydrogen Energy* **2002**, *27*, (11-12), 1381-1390.
162. Fabritius, H. -.; Ziegler, A.; Friák, M.; Nikolov, S.; Huber, J.; Seidl, B. H. M.; Ruangchai, S.; Alagboso, F. I.; Karsten, S.; Lu, J.; Janus, A. M.; Petrov, M.; Zhu, L. -.; Hemzalová, P.; Hild, S.; Raabe, D.; Neugebauer, J. Functional adaptation of crustacean exoskeletal elements through structural and compositional diversity: A combined experimental and theoretical study. *Bioinspir. Biomimetics* **2016**, *11*, (5), article 055006.
163. Moussian, B. The apical plasma membrane of chitin-synthesizing epithelia. *Insect Sci.* **2013**, *20*, (2), 139-146.
164. Shahidi, F.; Synowiecki, J. Isolation and Characterization of Nutrients and Value-Added Products from Snow Crab (*Chionoecetes Opilio*) and Shrimp (*Pandalus Borealis*) Processing Discards. *J. Agric. Food Chem.* **1991**, *39*, (8), 1527-1532.
165. Percot, A.; Viton, C.; Domard, A. Optimization of chitin extraction from shrimp shells. *Biomacromolecules* **2003**, *4*, (1), 12-18.
166. Chen, X.; Yang, H.; Yan, N. Shell Biorefinery: Dream or Reality? *Chem. Eur. J.* **2016**, *22*, (38), 13402-13421.
167. Yeul, V. S.; Rayalu, S. S. Unprecedented Chitin and Chitosan: A Chemical Overview. *J. Polym. Environ.* **2013**, *21*, (2), 606-614.
168. Kerton, F. M.; Liu, Y.; Omari, K. W.; Hawboldt, K. Green chemistry and the ocean-based biorefinery. *Green Chem.* **2013**, *15*, (4), 860-871.
169. Abidin, M. Z.; Junqueira-Gonçalves, M. P.; Khutoryanskiy, V. V.; Niranjana, K. Intensifying chitin hydrolysis by adjunct treatments – an overview. *J. Chem. Technol. Biotechnol.* **2017**, *92*, (11), 2787-2798.
170. Kazami, N.; Sakaguchi, M.; Mizutani, D.; Masuda, T.; Wakita, S.; Oyama, F.; Kawakita, M.; Sugahara, Y. A simple procedure for preparing chitin oligomers through acetone

- precipitation after hydrolysis in concentrated hydrochloric acid. *Carbohydr. Polym.* **2015**, *132*, 304-310.
171. Einbu, A.; Vårum, K. M. Characterization of chitin and its hydrolysis to GlcNAc and GlcN. *Biomacromolecules* **2008**, *9*, (7), 1870-1875.
172. Egbendewe-Mondzozo, A.; Swinton, S. M.; Bals, B. D.; Dale, B. E. Can Dispersed Biomass Processing Protect the Environment and Cover the Bottom Line for Biofuel? *Environ. Sci. Technol.* **2013**, *47*, (3), 1695-1703.
173. Banerjee, G.; Scott-Craig, J. S.; Walton, J. D. Improving enzymes for biomass conversion: A basic research perspective. *Bioenergy Res.* **2010**, *3*, (1), 82-92.
174. Zhang, A.; Gao, C.; Wang, J.; Chen, K.; Ouyang, P. An efficient enzymatic production of N-acetyl-d-glucosamine from crude chitin powders. *Green Chem.* **2016**, *18*, (7), 2147-2154.
175. Zhang, X.; Rolandi, M. Engineering strategies for chitin nanofibers. *J. Mater. Chem. B* **2017**, *5*, (14), 2547-2559.
176. Qin, Y.; Lu, X.; Sun, N.; Rogers, R. D. Dissolution or extraction of crustacean shells using ionic liquids to obtain high molecular weight purified chitin and direct production of chitin films and fibers. *Green Chem.* **2010**, *12*, (6), 968-971.
177. Shimo, M.; Abe, M.; Ohno, H. Functional Comparison of Polar Ionic Liquids and Onium Hydroxides for Chitin Dissolution and Deacetylation to Chitosan. *ACS Sustainable Chem. Eng.* **2016**, *4*, (7), 3722-3727.
178. Jardine, A.; Sayed, S. Challenges in the valorisation of chitinous biomass within the biorefinery concept. *Curr. Opin. Green Sustain. Chem.* **2016**, *2*, 34-39.
179. Duan, B.; Huang, Y.; Lu, A.; Zhang, L. Recent advances in chitin based materials constructed via physical methods. *Prog. Polym. Sci.* **2018**, *82*, 1-33.
180. Farrán, A.; Cai, C.; Sandoval, M.; Xu, Y.; Liu, J.; Hernáiz, M. J.; Linhardt, R. J. Green Solvents in Carbohydrate Chemistry: From Raw Materials to Fine Chemicals. *Chem. Rev.* **2015**, *115*, (14), 6811-6853.
181. Abbott, A. P.; Boothby, D.; Capper, G.; Davies, D. L.; Rasheed, R. K. Deep Eutectic Solvents formed between choline chloride and carboxylic acids: Versatile alternatives to ionic liquids. *J. Am. Chem. Soc.* **2004**, *126*, (29), 9142-9147.
182. Yang, Z.; Wen, Q. Deep eutectic solvents as a new reaction medium for biotransformations. In *Ionic Liquid-Based Surfactant Science: Formulation, Characterization, and Applications*, Paul, B. K. and Moulik, S. P., Eds. ; Wiley: Toronto, 2015; pp 517-531.

183. Zhang, Q.; De Oliveira Vigier, K.; Royer, S.; Jérôme, F. Deep eutectic solvents: Syntheses, properties and applications. *Chem. Soc. Rev.* **2012**, *41*, (21), 7108-7146.
184. Vigier, K. D. O., Dr.; Chatel, G., Dr.; Jérôme, F. Contribution of deep eutectic solvents for biomass processing: Opportunities, challenges, and limitations. *ChemCatChem* **2015**, *7*, (8), 1250-1260.
185. Sharma, M.; Mukesh, C.; Mondal, D.; Prasad, K. Dissolution of a-chitin in deep eutectic solvents. *RSC Adv.* **2013**, *3*, (39), 18149-18155.
186. Lindman, B.; Karlström, G.; Stigsson, L. On the mechanism of dissolution of cellulose. *J. Mol. Liq.* **2010**, *156*, (1), 76-81.
187. Atkins, P. W.; De Paula, J. Simple mixtures. In *Physical Chemistry*, 8th ed.; Oxford University Press: Great Britain, 2006; pp 136-173.
188. Otto, S. The role of solvent cohesion in nonpolar solvation. *Chem. Sci.* **2013**, *4*, (7), 2953-2959.
189. Zhang, Y.; Bakshi, B. R.; Demessie, E. S. Life cycle assessment of an ionic liquid versus molecular solvents and their applications. *Environ. Sci. Technol.* **2008**, *42*, (5), 1724-1730.
190. Wood, N.; Stephens, G. Accelerating the discovery of biocompatible ionic liquids. *Phys. Chem. Chem. Phys.* **2010**, *12*, (8), 1670-1674.
191. Kurita, K. Controlled functionalization of the polysaccharide chitin. *Prog. Polym. Sci.* **2001**, *26*, (9), 1921-1971.
192. Harish Prashanth, K. V.; Tharanathan, R. N. Chitin/chitosan: modifications and their unlimited application potential-an overview. *Trends Food Sci. Technol.* **2007**, *18*, (3), 117-131.
193. Mourya, V. K.; Inamdar, N. N. Chitosan-modifications and applications: Opportunities galore. *React. Funct. Polym.* **2008**, *68*, (6), 1013-1051.
194. Khan, F. I.; Rahman, S.; Queen, A.; Ahamad, S.; Ali, S.; Kim, J.; Hassan, M. I. Implications of molecular diversity of chitin and its derivatives. *Appl. Microbiol. Biotechnol.* **2017**, *101*, (9), 3513-3536.
195. Tabasso, S.; Carnaroglio, D.; Calcio Gaudino, E.; Cravotto, G. Microwave, ultrasound and ball mill procedures for bio-waste valorisation. *Green Chem.* **2015**, *17*, (2), 684-693.
196. Miller-Chou, B. A.; Koenig, J. L. A review of polymer dissolution. *Prog. Polym. Sci.* **2003**, *28*, (8), 1223-1270.

197. Leahy, K.; Mack, A. M.; Mack, J. An EcoScale comparison of mechanochemistry and solution based reactions. In *Green Technologies for the Environment*, 1186; Obare, S.O., Luque, R., Eds. ; American Chemical Society: Washington, D.C., 2014; pp 129-137.
198. Kerton, F. M.; Marriott, R. *Alternative Solvents for Green Chemistry*; The Royal Society of Chemistry: Cambridge, UK, 2013.
199. James, S. L.; Adams, C. J.; Bolm, C.; Braga, D.; Collier, P.; Friic, T.; Grepioni, F.; Harris, K. D. M.; Hyett, G.; Jones, W.; Krebs, A.; Mack, J.; Maini, L.; Orpen, A. G.; Parkin, I. P.; Shearouse, W. C.; Steed, J. W.; Waddell, D. C. Mechanochemistry: Opportunities for new and cleaner synthesis. *Chem. Soc. Rev.* **2012**, *41*, (1), 413-447.
200. Do, J. -.; Frišćic, T. Mechanochemistry: A Force of Synthesis. *ACS Cent. Sci.* **2017**, *3*, (1), 13-19.
201. Fischer, F.; Fendel, N.; Greiser, S.; Rademann, K.; Emmerling, F. Impact Is Important - Systematic Investigation of the Influence of Milling Balls in Mechanochemical Reactions. *Org. Process Res. Dev.* **2017**, *21*, (4), 655-659.
202. Frišćic, T.; Jones, W. Recent advances in understanding the mechanism of cocrystal formation via grinding. *Cryst. Growth Des.* **2009**, *9*, (3), 1621-1637.
203. Boldyreva, E. Mechanochemistry of inorganic and organic systems: What is similar, what is different? *Chem. Soc. Rev.* **2013**, *42*, (18), 7719-7738.
204. Rothenberg, G.; Downie, A. P.; Raston, C. L.; Scott, J. L. Understanding solid/solid organic reactions. *J. Am. Chem. Soc.* **2001**, *123*, (36), 8701-8708.
205. Rehder, S.; Klukkert, M.; Löbmann, K. A. M.; Strachan, C. J.; Sakmann, A.; Gordon, K.; Rades, T.; Leopold, C. S. Investigation of the formation process of two piracetam cocrystals during grinding. *Pharmaceutics* **2011**, *3*, (4), 706-722.
206. Stauch, T.; Dreuw, A. Advances in Quantum Mechanochemistry: Electronic Structure Methods and Force Analysis. *Chem. Rev.* **2016**, *116*, (22), 14137-14180.
207. Bygrave, P. J.; Case, D. H.; Day, G. M. Is the equilibrium composition of mechanochemical reactions predictable using computational chemistry? *Faraday Discuss.* **2014**, *170*, 41-57.
208. Stolle, A.; Schmidt, R.; Jacob, K. Scale-up of organic reactions in ball mills: Process intensification with regard to energy efficiency and economy of scale. *Faraday Discuss.* **2014**, *170*, 267-286.

Chapter 2 Mechanochemical amorphization of α -chitin

2.1 Introduction

2.1.1 Mechanical force and organic macromolecules

The study of force sensing by cells has now evolved into a dynamic discipline within the area of molecular biology.¹ In that context, lipid-bilayer/embedded-protein systems in membranes have been examined for their ability to sense osmotic force; the cell's way to "measure" the concentration of the universal biochemistry solvent. Thus, it has been argued that sensing of force can be considered a "solvent sense", in contrast to "solute senses" which, for example, allow nutrients to enter the cell by lock-and-key interactions.^{2,3} When a cell experiences an environment of low water availability ("hyperosmotic stress"), it loses its own, and the aforementioned systems (equipped with the protein "mechanosensitive channels") respond to the reduced turgor pressure/force.^{2,4,5} Now, if that mechanobiology narrative is taken to its extreme (a cell in absolute drought conditions), one can surely imagine that the consequences at the cellular level offer a familiar source of inspiration to the scientists who describe molecular transformations in ball mills by the term "solvent-free".^{xxix}

Regardless of hierarchical level analogies, the challenges with respect to the ways in which mechanical stress can induce chemical changes in organic

^{xxix} The responses of bone cells on mechanical forces comprise another fascinating source of motivation to researchers who develop self-healing materials (6).

macromolecules have become accepted by certain researchers as soon as proof of covalent bond scission by force was reported for a highly branched synthetic polymer more than 10 years ago.⁷ Questions addressing the core issue of the possibility of directing forces towards certain bonds of complex organic macromolecular structures have started being openly raised. It was only more recently, with advances in molecular dynamics simulations that polymeric systems have started being examined in depth for possible deformations by external forces.⁸ In particular, stress-bearing proteins (e.g. in spider silk) were some of the first structures studied in detail in this way. Just like in all other major classes of biopolymers (carbohydrates and nucleic acids), the development of their mechanical properties is critically dependent on their hydrogen bonding network, the understanding of which requires a combination of computational and experimental methods.

In 2010, force distribution analysis (FDA) was employed to estimate the optimal length of β -sheets, which are abundant in tertiary and quaternary structure of stress-bearing proteins. The average β -sheet strands comprise four or five amino acids, whereas in proteins of spider dragline silk they are twice that length. The strands can be networked with hydrogen bonds (HB) formed between two adjacent peptide bonds (hence one hydrogen bond per residue).⁸⁻¹⁰ FDA revealed that when a central strand was pulled, the force propagating along its length was deflected vertically towards the two neighboring strands (an upper one and a lower one if the

central strand is visualized horizontally) through the hydrogen bonds. The two hydrogen bonds (first pair) closest to the point of applied force (one with the upper and one with the lower strand) managed to carry a load of 80 pN each, the second and third pair 20–30 pN per HB, the fourth about 10 pN per HB, and then forces leveled off to zero around the eighth residue.¹⁰ These figures for the forces that single hydrogen bonds can take up (before their rupture) fall into the strength range (up to 148 pN) which has been reported when forces for biologically related processes were reviewed.³ This is an example of how intermolecular forces in structures of biopolymers can direct applied mechanical stress according to their natural architectural design.

Hence, on the basis of these existing simulations it is reasonable to hypothesize that the hydrogen bonding forces that form the sheets of chitin (see Section 1.4 and reference 11)¹¹ will distribute the applied force from the collisions with the milling media in their own natural way and protect the biopolymer's covalent bonds from the possibility of rupturing. In general, the hydrogen bonding network that is being created in natural polysaccharide biosynthesis results in crystalline and amorphous regions within the material's fiber/nanocrystal.¹²⁻¹⁵ Figure 2–1 shows a proposed simplified two-dimensional scheme of crystalline and amorphous regions in idealized fibers of linear polysaccharides like cellulose and chitin.

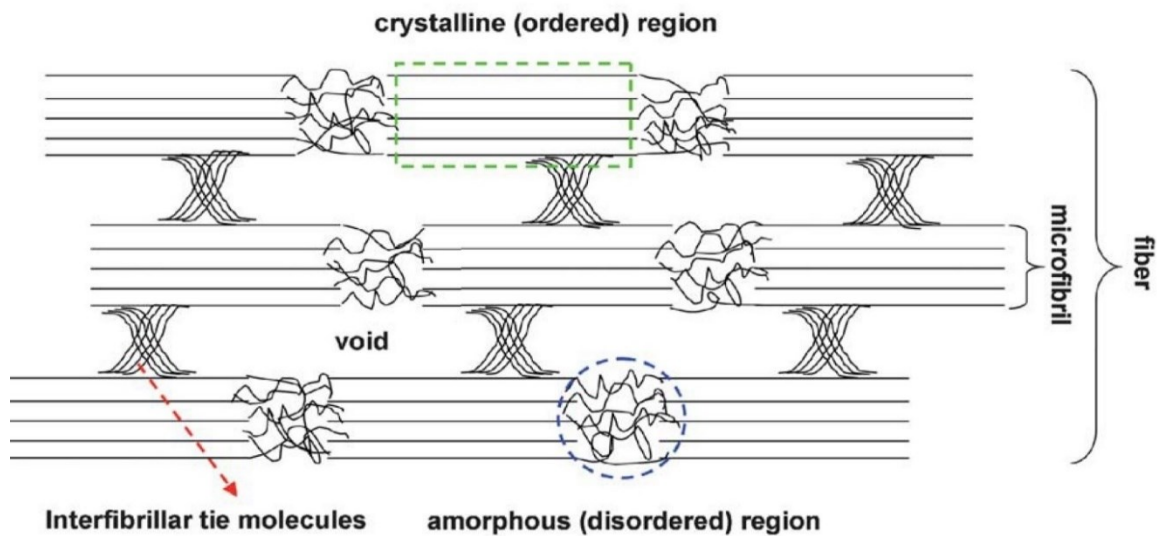


Figure 2-1: Scheme of crystalline and amorphous regions in idealized fibers of linear polysaccharides like cellulose and chitin. Void in between the horizontal chains in the crystalline region can be imagined as the zone where the hydrogen bonding of Figures 1–6 and 1–7 form the *bc* and *ac* sheets respectively. Reproduced from {*Nanoscale*, 2012, 4, 3274} with permission of The Royal Society of Chemistry. (<http://dx.doi.org/10.1039/C2NR30260H>)

2.1.2 Reduction of polysaccharide crystallinity via ball milling

X-ray diffraction (XRD) is a powerful technique that can determine the relative proportions of the crystalline and amorphous components in cellulose fibers. This has been known since the 1940s and gave rise to the concept of crystallinity.¹² Building on that momentum, in 1959 Segal et al. proposed the "Crystallinity Index" (CrI) as an empirical method to calculate the crystalline fraction in cellulose samples. According to that work, cellulose's CrI is the difference between the maximum intensity of the (002) lattice diffraction and the intensity of the amorphous scatter expressed as a percentage of the former.¹⁶

Considering the interest in producing energy from cellulosic materials, it is important to note that this method, which is based on peak height measurements, serves as an approximation of the crystalline fraction allowing a first level of comparison of cellulose as well as other biomass samples.¹⁷ In 2010, a literature review of about 80 journal articles which presented crystallinity measurements for commercial samples of cellulose revealed that 70–85% of the results were obtained using the peak height method (also referred to as Segal CrI method). The rest of the 15–30% was roughly evenly distributed between XRD deconvolution, XRD amorphous subtraction, and solid-state ¹³C NMR methods. When Park et al. measured eight commercial samples of cellulose with all four of the aforementioned methods, they found that the order of the crystallinity values was the same for all four methods (average values ranged from 81 to 57%) with the Segal method giving $25 \pm 3\%$ higher crystallinity values compared to the average of the other three methods (e.g. Sigmacell-20 cellulose from Sigma-Aldrich gave a crystallinity of 84.8% with the Segal CrI method while the average from the other three methods was 61.3%; the standard deviation of triplicate measurements didn't exceed 2.2% in any of the four methods).¹⁸ This demonstrates the usefulness (primarily in terms of precision) of the long time used peak height method. However, with our current knowledge of polymorphic forms of cellulose, the accuracy limitations of the Segal CrI method are being increasingly debated.^{19,20} As cellulose is not the main focus of this thesis, further discussion of this debate is beyond the scope of the current work.

With ball milling producing some of the cellulose samples in those early XRD investigations more than 70 years ago,¹² it is only natural to wonder if certain mechanochemical conditions can amorphize linear polysaccharides in a controlled way. A survey of the primary literature reveals lack of systematic studies regarding amorphization of polysaccharides. In most cases, researchers achieve certain amorphization results of cellulose or chitin for a limited set of milling times without investigating technological parameters as the vessel and ball material, the filling degree of the vessel with balls (packing), the number of balls per mass of substrate. In some studies, a CrI is not even calculated and overlays of XRD signals are presented as evidence of amorphization. Moreover, in many cases, the polysaccharide samples processed are not characterized by degree of polymerization (DP), nor viscosity, nor particle size, nor by degree of acetylation (DA) for chitin. Hence, the reader can have an indication of the range of some basic ball milling parameters along with the reported Crystallinity Index (CrI)% reduction percentages (therefore independent of the calculation method) for cellulose and chitin from selected independent studies in Table 2–1 (information is not meant to be exhaustive):^{xxx}

^{xxx} On 17/1/2018, the 8 references of Table 2–1 had received a total of 258 citations in SCOPUS database (Elsevier B.V.). Among those, 22 were review articles, 13 book chapters and 1 book (36 documents in total). When the term “mill*” was searched in the abstracts of those 36 documents, no results were obtained. When the term “mechanochemi*” was searched, only one result was obtained (chapter “Mechanical Pretreatment” in the book “Biomass Fractionation Technologies for a Lignocellulosic Feedstock Based Biorefinery”) (21). Although Lomovsky *et al.* produced an excellent review of the different types of milling devices for biomass processing, they haven't

Table 2-1: Crystallinity Index (CrI) reduction percentages reported in literature for cellulose and chitin ball milling.

	Polysaccharide	Technological parameters	Operation frequency (rpm)	Milling time (h)	Crystallinity Index (CrI) reduction (%)
1	Cellulose [Sigma-Aldrich (product no. C6663)]	ZrO ₂ balls/polypropylene vessel - 35% packing	60	144	33
2	Cellulose [DP 1010, Hubei Xiangtai Cellulose Co., Ltd.]	Steel vessel – 33% packing	375	2	17
3	Cellulose [DP 237 after processing]	Steel vessel – 25% packing	375	2	69
4	Cellulose	ZrO ₂ balls/ceramic vessel - 20% packing	60	96	83
5	Cellulose (microcrystalline, Avicel PH-101, particle size 50 μm, Sigma-Aldrich)	Ceramic vessel & balls	300	24	89
6	Chitin (Crab, 3mm flakes, Yaizu Suisankagaku Industry)	ZrO ₂ vessel/chromium steel balls - 9% packing - 690 balls/g chitin	800	0.5	56
7	Chitin (Crab, 2mm flakes, Yaizu Suisankagaku Industry)	ZrO ₂ balls - possibly 0.65 balls/g chitin	800	0.5	57
8	Chitin (Sigma-Aldrich)	ZrO ₂ vessel & balls - 28% packing - 24 balls/g chitin	700	2	100

References for Table 2–1 entries are: 1,²⁵ 2,²⁶ 3,²⁷ 4,²⁸ 5,²⁹ 6,³⁰ 7,³¹ 8.³² If the packing degree is not mentioned explicitly, the author has calculated it based on the reported balls' masses and accepted density values of the material of the balls.

corelated them with results for Crystallinity Index reductions. SCOPUS is one of the non-negligible databases for searching the scientific literature providing results which partially overlap with the coverages of Web of Science (Clarivate Analytics) and SciFinder [Chemical Abstracts Service (CAS)] (22-24).

Although it is challenging to draw conclusions from this table as in addition to the reasons mentioned above, the different types of ball milling equipment are certainly not easily compared due to the different types of motions (hence forces developed during collisions), certain trends can be extrapolated, and help raise questions. When comparing entries 2 and 3, which have the same operating frequencies, milling times, and similar technological parameters, the significantly higher CrI reduction for entry 3 (69% vs 17%) can be attributed to the almost 4 times lower degree of polymerization of the milled cellulose sample. Assuming the DP value of microcrystalline cellulose in entry 5 is not more than double that in entry 3 (DP 237), and that the speeds and technological parameters of the two processes create similar forces, the 20 units greater CrI reduction is most probably justified by the 12 times longer milling time. The longer milling time and probably the more intense milling for entry 8 compared to entries 6 and 7 (assuming that a 100rpm difference in operating frequencies is relatively small) can partly explain the more than 40 units greater CrI reduction reported for chitin in the study of Aida et al. Finally, when one compares the systems in entries 1 and 4, which have the same operating frequencies and material for the balls, it is not unreasonable to hypothesize that the much lower crystallinity reduction achieved with higher packing and in a longer milling time in entry 1 can be ascribed to the much lower hardness of the polypropylene vessel compared to the ceramic one in entry 4. One can conclude that the polysaccharide amorphization levels reported in Table 2-1 have covered a broad range (from as low as 17–33% to as high as 89–100%) with wide variation

in milling times due to the numerous options of technological parameters. However, these experimental results confirm the intuitive expectation that high operating frequencies (>700 rpm) achieve high amorphization levels in short milling times (<2 hours) especially when harder milling materials are used (both vessels and balls).

2.1.3 Ball milling essentials and collision frequency

In this study, SPEX 8000M mixer/mill, the most well-known laboratory scale vibration (or shaker) mill with a fixed high operating frequency (approx. 1080 rpm, 18 Hz, or 113 rad/s) was selectively investigated for its mechanochemical performance.³³⁻³⁶ The milling motion of the cylindrical vial, which is clamped horizontally along its height, couples back-and-forth swings with short lateral movements, each end of the vial drawing one of the lobes of a figure-8 (Figure 2-2).³³ A swing is a 15° rotation around a cartesian vertical axis (it can be visualized as left-right movement in the plane of the screen/paper), and a lateral movement is a 15° rotation around the shaft-arm axis (it can be visualized as the left flat base of the cylinder coming towards the reader, and at the same time, the right flat base fading away from the reader, or vice versa). Both motions occur at 18 Hz, with their lengths being comparable to the vial's dimensions.^{33,37}

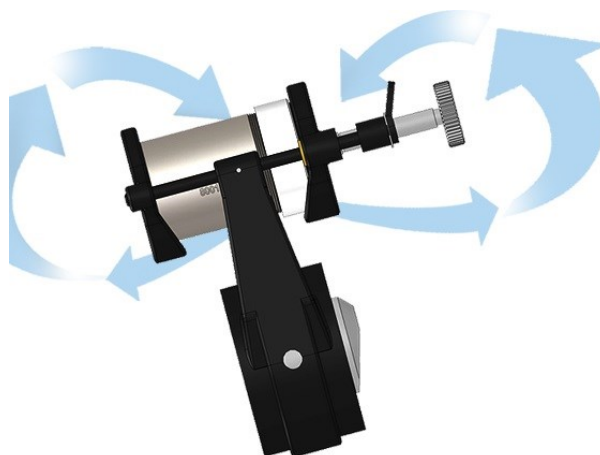


Figure 2-2: Milling motion of the reaction vessel in a SPEX 8000M mixer/mill (in blue arrows). The shaft-arm is fixed perpendicular to the clamp which holds the (silver) vial. Used with the permission of SPEX SamplePrep from <https://www.spexsampleprep.com/8000M-mixermill>.

The motion of one 12.6 mm (approx. half inch diameter) ball (with specific weight equivalent to steel) in a 65.8 mL vial (3.8 cm internal diameter, 5.8 cm internal height) has been simulated for the SPEX's clamp motion using the discrete element method (DEM) from Concas et al.³⁷ The generated collisions result in highly disordered motion of the ball with an average impact velocity of 4.17 ± 1.46 m/s. After the first 34 s (transient period), the system functions in a "stationary milling regime" producing approx. 142 impacts per second, with the sphere spinning approx. 80 times per second. The clear majority of the collisions (approx. 54%) take place at a tangential direction (at an angle in between 80 and 90° if 0° is set for the head-on collision) mostly on the cylindrical surface. The average impact energy has been calculated at 0.093 J per collision. More than 45% of the impacts occur with a restitution coefficient (the ratio between the ball velocity before and after collision)

of 0.95–1.00 (the calculated system average is 0.94), which is indicative of a small amount of energy (~6%) being lost in heating the vial or deforming the milling media. Varying the operating frequency reveals a proportional linear response of impact velocity, impact frequency, impact energy, and spin velocity [e.g. if rpm is elevated from 1080 to 1296 (20% rise), the impact frequency will increase from 142 to 170/s (approx. 20%)]. Interestingly, impact energy was found to have a more sensitive response than the rest, with a 49% increase in J/hit corresponding to a 20% rise in operating frequency (rpm).³⁷ The packing of the vial in this study was 1.6%.

Building on the study by Concas et al., Prasad and Theuerkauf employed DEM to explore the relationship between number of collisions and force per impact for SPEX 8000M steel-equivalent systems with higher packings.³⁵ Keeping the packing constant (13.6%) in a 43.1 mL vial (3.8 cm internal diameter, 3.8 cm internal height), they varied the number and diameter of balls using 832×2.38 mm, 351×3.17 mm, 104×4.76 mm, 44×6.35 mm, 13×9.52 mm, 6×12.7 mm. The results showed that the force per impact was inversely proportional to the number of collisions per second per ball, with the rate of decrease of the former being roughly in the same order of magnitude as the rate of increase of the latter. The median contact force for the 6×12.7 mm system was approx. 40 N arising from approx. 100 collisions/s/ball, while the 832×2.38 mm system reached around 530 collisions/s/ball with only 2 N median contact force.³⁵ The number of collisions/s/ball for six half inch balls from Prasad and Theuerkauf is surprisingly low compared to the 142 for one half inch

ball from Concas et al., especially with that significant difference in packing (or vice versa). However, this can be attributed to differences in the DEM softwares used, and possibly to the shorter cylindrical shape of the vial. What is important is that together these two studies give a feel of the frequency of collisions in the selected ball mill.

In 2012, Dreizin and Santhanam reported a 22% packing SPEX 8000 steel system (2.64 cm diameter/5.24 cm height vial, approx. 14×9.5 mm balls) in which collision forces reached as high as 1000 N. However, according to their DEM histogram, these high energy impacts are a minority, as more than 75% of the total collisions do not exceed 100 N. Their computations show that these less-than-100-N impacts represent approx. 30% of the energy transferred to the milled powder. Total energy, which was used to reinforce nanocomposite powders, was found to be 2.3 and 2.7 times higher than a 350 rpm - 3% packing planetary and a 400 rpm – 90% packing attritor system respectively. Although, that indicative result afforded shorter milling times for the SPEX system, it stresses the imperative need for further comparative studies among different milling modes as the packing and operating frequencies of those three milling devices were very different. This study also offers further insight on the magnitude of forces developed in the selected SPEX system used throughout this thesis.³⁸ Figure 2–3 illustrates four of the most widely used milling modes at different scales. The reader can have a feel of the advantages and

disadvantages of these technologies as well as the considerations regarding transferring processes from one to the other from some recent reviews.^{21,34,39}

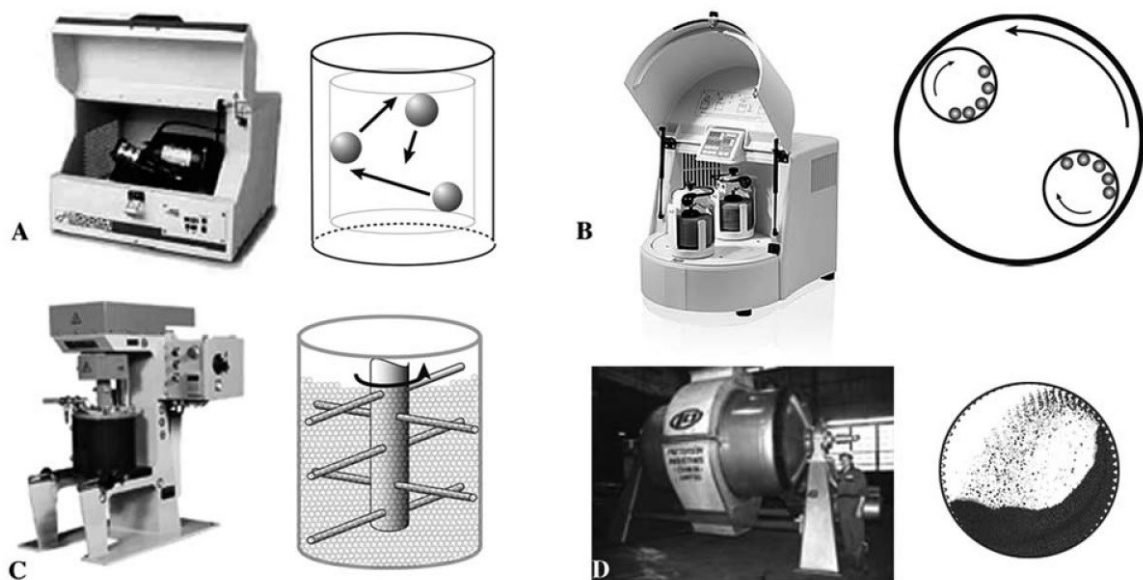


Figure 2-3: Four of the most widely used milling modes. Schematics to the right of the mill illustrate the milling media's motion. (A) SPEX 8000M mixer/mill (65 mL), (B) planetary mill (250 mL), (C) attritor (4 L), (D) rolling ball mill (hundreds of L). Reproduced from {*Faraday Discuss.*, 2014, **170**, 223-233} with permission of The Royal Society of Chemistry. <http://dx.doi.org/10.1039/C4FD00007B>

2.1.4 Amorphization-solubilization of polysaccharides via collisional forces

Regarding cellulose transformation, the Blair group reported no appreciable solubilization when 2 g of microcrystalline cellulose was milled with 3×12.7 mm steel balls in a 65 mL steel vial using the 1080 rpm of a SPEX 8000D mixer/mill (5% packing, balls to cellulose mass ratio 12.5).⁴⁰ This is not exactly in line with Meine et al. who have reported approx. 5% solubilization of α -cellulose (DP 2200) when milling for 5 hours with a 800 rpm planetary device using a 19.8 balls to cellulose

mass ratio and 21% packing.⁴¹ While exploring the mechanochemistry toolbox, scale up studies were performed with the attrition technology, and it was observed that when a relatively small pilot-scale mill was used (charged with 1 kg of a 1:1 cellulose:catalyst mixture), a long induction period (associated with amorphization) preceded substantial conversion rates (during the first 4 hours, soluble saccharides did not exceed 4%, while in the next 4, they reached close to 50%).^{40,42} More specifically, when using a 700 rpm system with 6 mm balls, they calculated approx. 4000 collisions of greater than 150 N per minute per kg for a tank of approx. 1.4 L. When they moved to a 160 L tank (keeping the same balls to cellulose mass ratio and presumably with the same packing) the number of collisions of greater than 150 N per minute per kg increased to nearly 60000 (15-fold).⁴³ This valuable for the growing community of mechanochemists information echoes with the increased average ball velocities for increased vial length reported by Prasad and Theuerkauf for SPEX 8000M systems and opens the way for further scale up studies on different kinds of ball mills.³⁵ More importantly for chitin transformation, a critical debate has been started on decoupling amorphization from hydrolysis possibly by using different milling modes.⁴³

Regardless of the strategies that are being developed for scaled up processes, control of intermolecular forces via ball milling has been reported by Fischer et al., who in addition to all the technological parameters discussed above have experimented with vial/balls differential densities.⁴⁴ Using a Perspex vial

[poly(methyl methacrylate) density is 1.2 g/mL], steel balls, and a 50 Hz (3000 rpm) vibrational mill, they managed to disrupt the hydrogen bonding in imidazole and felodipine [ethyl methyl 4-(2,3-dichlorophenyl)-2,6-dimethyl-1,4-dihydro-3,5-pyridinedicarboxylate] without breaking covalent bonds, and form a cocrystal with one of the imidazole N-H hydrogen bonding to the ethyl ester of a felodipine molecule, and the other one to the N-H of the dihydropyridine ring of a second felodipine molecule (XRD, Raman, solid-state NMR characterization). Keeping a constant packing, they realized that the more energetic impacts of 2×10 mm balls gave 8.6 times higher reaction rates than the more frequent ones of the 16×5 mm system (cocrystallization rates k were 0.24 vs 0.028 min^{-1} respectively with satisfactory standard deviations).⁴⁴ This result suggests that despite the high operating frequency (3000 rpm), force development during collisions of the steel balls with the acrylic vial was limited (possibly to the pico-newton level) due to their differential densities. As intermolecular forces are a critical component in the structure of chitin, studies such as this one are important to keep in mind.

2.1.5 Methodological approach to the problem

Considering the 1080 rpm of the ball mill used as well as the mm-scale particles of native α -chitin, the mechanochemical potential of stainless-steel vial and balls was explored, as their high density would possibly allow for a certain impact-force/impact-frequency combination to irreversibly overcome likely stress-distribution/polymorphism phenomena originating from a minimum mixing load of

α -chitin's hydrogen bonding network. Based on the hypothesis that a more milled sample might exhibit increased solubility,⁴¹ a minimum polysaccharide mass of two g was milled as a compromise of the required amount to monitor runs of certain milling times with several characterization methods [powder XRD (~0.25 g) for amorphization, ATR FT-IR (triplicates), solubility tests (~1.35 g for triplicates in neutral and acidic pH), SEM for particle size], and having comparable balls to polysaccharide mass ratio and packing degree with the SPEX cellulose studies of the Blair group [we investigate the milling time effect with a balls to chitin (BtC) ratio of 8.2 instead of 12.5 and a packing of approx. 3.3% instead of 5%]^{40, xxxi}. As mentioned in Section 1.8, the key questions to answer here are "Can α -chitin be amorphized in a controlled way (possibly dependent on milling time)?", and if yes "Is that amorphization a result of the disruption of the intermolecular hydrogen bonding network alone or of covalent bonds as well?".

2.2 Experimental

2.2.1 Materials

α -Chitin, which was isolated from snow crab, was provided by ChitinWorks LLC (1-2 mm flakes of approx. 0.30 g/mL,^{xxxii} moisture content determined gravimetrically at 5.5 wt.%). Full details on residual protein and mineral (ash) content were not provided. Chitosan high molecular weight (MW) [Degree of Deacetylation (DD) 75–

^{xxxix} The latter values of each pair correspond to those used in the work of the Blair group.

^{xxxii} For comparison, microcrystalline cellulose from Aldrich (Product #: 435236) of 51 μm particle size has a bulk density of 0.6 g/mL.

85%] was purchased from Sigma Aldrich (Product #: 419419, Brookfield viscosity 800–2000 cP). Glacial acetic acid was purchased from Fisher Scientific.

2.2.2 Mechanochemical treatment of α -chitin

Milling experiments were conducted using a SPEX SamplePrep 8000M mixer/mill. A hardened 440C stainless steel vial with a volume of 65 mL (1.5" int. diameter \times 2.25" deep) was charged with 2.00 g α -chitin unless otherwise stated. Stainless steel balls (estimated density 7.8 g/mL) were used with diameters of half inch (0.5" or 12.7 mm) and quarter inch (0.25" or 6.4 mm). Milling times reported herein refer to the time the vial was shaken at 1080 cycles per minute (18 Hz). The temperature of the outer surface of the vial was monitored with a thermocouple immediately after the end of milling cycles and did not exceed 60 °C in any case. This is in accordance with previous studies using the same mixer/mill (steel equipment) that reports plateaus for maximum temperatures throughout milling times dependent on the packing degree of the vial.⁴⁵ In representative experiments, the vial containing α -chitin was weighed at room temperature before and after milling and no appreciable mass loss was realized within the range of the standard deviation of the balance.

2.2.3 Gravimetric analysis to determine the mass of soluble products (sample solubility%)

Approximately 250 mg of milled sample was vortex mixed in 7.5 mL of either distilled water (pH 7.0) or 0.1 M acetic acid (pH 2.9) for one minute. A compact solid

was achieved via centrifugation at 5000 rpm for 30 min and soluble products were separated with a pipet. The residue was dried overnight (70 °C) and weighed. Solubility for the samples from milling α -chitin was calculated by subtracting the mass of the undissolved residue from 250 mg (the sample taken from the mill) and reported as a weight percentage. Each sample was analyzed in triplicate.

2.2.4 X-ray diffraction (XRD)

X-ray diffraction data were obtained using a Rigaku Ultima IV X-ray diffractometer with copper radiation operating at 40 kV and 44 mA. X-ray diffraction patterns were acquired from 5 to 40° 2θ with a sampling width of 0.02°. The crystallinity index (CrI%) was calculated using the equation $CrI = [(I_{110} - I_{am})/I_{110}] \times 100$, where I_{110} is the maximum intensity at 19.20° (2θ), and I_{am} is the intensity for the amorphous region at 16.00° (2θ).⁴⁶

2.2.5 Fourier transform infrared (FT-IR) spectroscopy

The FT-IR spectra of samples were recorded using a Bruker ALPHA spectrometer with a platinum diamond ATR module. After a background measurement taken against air, the sample covered the whole surface of the ATR crystal, and a fixed pressure was applied on it with the clamp to obtain satisfactory contact with the diamond. A total of 24 interferograms (scans) with a 4 cm^{-1} resolution were signal-averaged and stored for each measurement; the wavenumber region investigated was 4000 to 400 cm^{-1} . The intensity of the selected absorption bands was determined by the baseline correction method suggested by the OPUS software

package of the instrument. Each sample was measured in triplicate, spectra were exported in an ASCII file (approx. wavenumber difference 2.04 cm^{-1}) using the vendor's software, imported to Microsoft Excel, averaged for presentation, and plotted with a 0.25 pt smoothed line.

2.3 Results and Discussion

2.3.1 X-ray diffraction of native α -chitin

Figure 2–4 shows the X-ray diffraction pattern of native α -chitin. Maximum intensities for crystalline reflections were observed at the following 2θ values: 9.28° , 19.20° , and 23.14° .^{xxxiii} Using Bragg's law, these correspond to d spacings of 9.52, 4.62, and 3.84 \AA respectively, which in turn are in close agreement with the values published before 1985 for (020), (110), and (130) reflections observed with X-ray diffraction for lobster chitin⁴⁷ and with electron diffraction for crab chitin.⁴⁸ The intensity ratio of the two strongest peaks [(110) and (020)] is 2.6 in Figure 2–4 (characteristic of the native α -chitin sample), and it is in close agreement with reported signals for crangon chitin flakes (2.7),⁴⁶ shrimp chitin (2.6),⁴⁹ and in between reported signals for crab α -chitin (2.2),⁵⁰ (3.3).⁵¹ There have been a few groups that reported XRD patterns with a ratio lower than 1.0,^{52–54} something which gives a feel of the diversity of the natural source of chitin. It should be noted though

^{xxxiii} Bragg 2θ (2θ) values are reported to two decimal places in this work (as acquired by the XRD method). The values extracted from referenced literature are to the accuracy reported therein.

that the ratio is probably affected to an extent by the isolation process used to obtain the chitin from the shell.

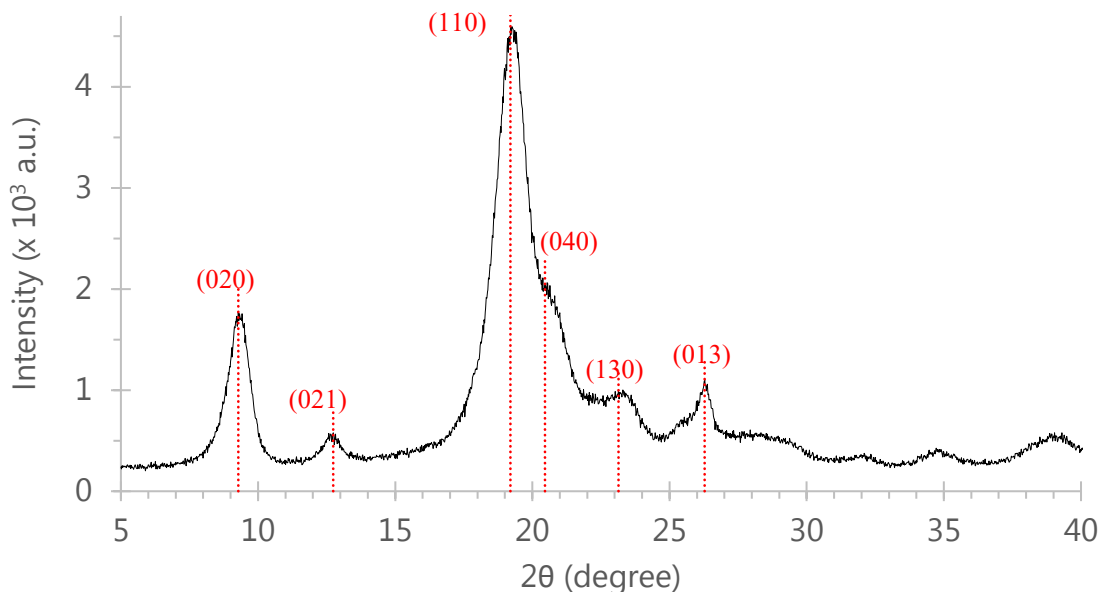


Figure 2-4: X-ray diffraction (XRD) pattern of native α -chitin with its characteristic reflections.

The geometries of the constructive interferences of reflections (110) and (020) have been visualized within a proposed 19 chain crystallite in Figure 2-5.⁵⁵ This *ab* plane stacking can be hypothesized to be originating from the already explained hydrogen bonding in the *a*-direction (creating the *ac*-sheets, see Figure 1-7) as well as in the *b*-direction (creating the *bc*-sheets, see Figure 1-6). It is reasonable hence to expect that the former intermolecular interactions (including the bifurcated hydrogen bond) are the main contributors to the rise of the (020) reflection, while the latter of the (110) reflection. With the stabilization that the *ac*-sheets offer to the

crystal being at least 3 times higher than that from the *bc*-sheets (Figure 6 in reference 11 shows the computed interchain energies for 3 representative models of α -chitin's unit cell; *bc*-sheet energies do not exceed 54 kJ/mol while *ac*-sheet ones rise to at least 150 kJ/mol),¹¹ the (110)/(020) intensity ratio can safely be considered as a reflection of the strength of the α (alpha) character of the polysaccharide.

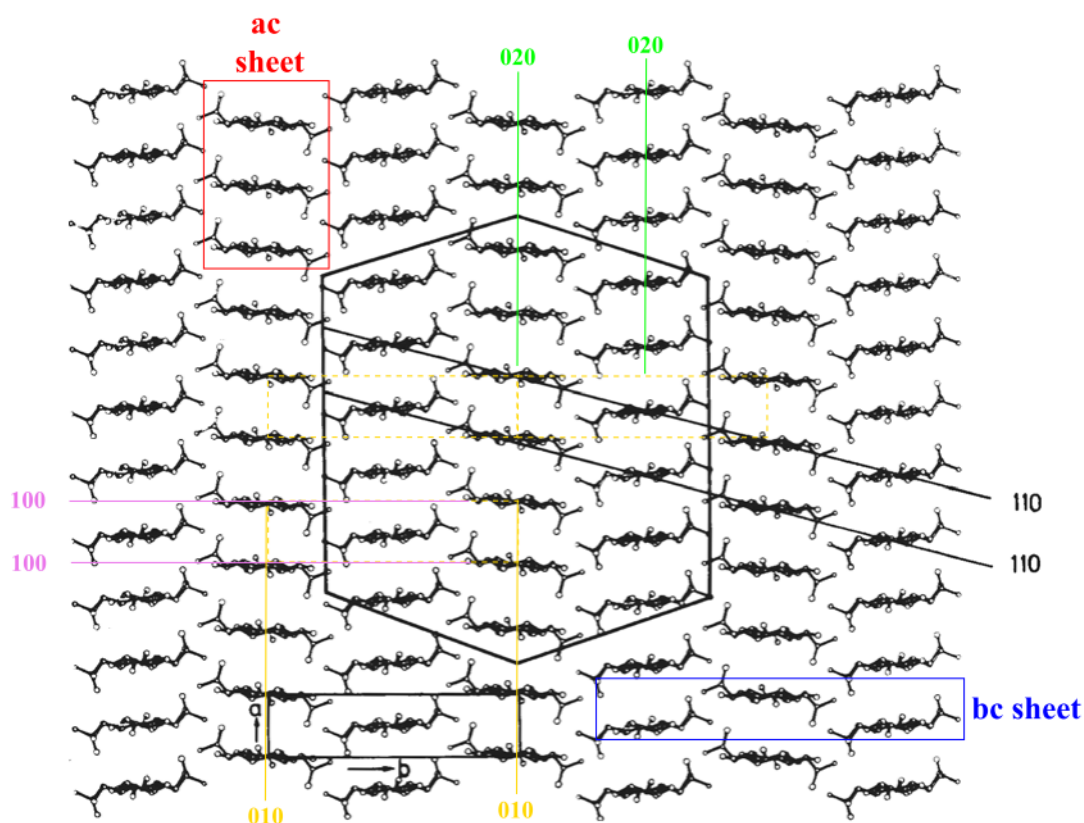


Figure 2-5: The *ab* projection of α -chitin's lattice illustrating the (110) (black lines), (020) (green lines), (100) (pink lines), (010) (orange lines) planes within a proposed 19 chain crystallite. The orthorhombic unit cell is drawn in black lines in the bottom left (distance between 010 lines is 18.85 Å, and in between (100) lines is 4.75 Å). *ac*-Sheet direction is shown in red, and *bc*-sheet direction is shown in blue. Adapted by permission from [Springer Customer Service Centre GmbH]: [Springer Nature] [Journal of Biosciences] [Atkins, E. J Biosci (1985) 8:375 (Conformations in polysaccharides and complex carbohydrates, Edward Atkins)], [Copyright] (1985), doi: 10.1007/BF02703990.

The aforementioned three peaks along with a shoulder [possibly (040)] on the (110) peak (at 20.46° in Figure 2–4), and the claimed (013)⁴⁷ reflection (at 26.28°) have been also observed (with reasonable experimental deviations on the second decimal of 2θ) for α-chitins from different decapod species in the first half of the 2000s.^{49,56,57} In 2003, Jaworska et al.⁴⁹ observed also a peak at 12.55° (7.05 Å), arising from the (021) reflection,⁴⁷ in a chitin sample from shrimp. This reflection exhibits a maximum at 12.74° (6.94 Å) in the pattern of the native α-chitin sample, and it has been also recently observed at 12.71° in samples of crab and shrimp chitin.⁵⁸ β-Chitin has been observed to have a simpler XRD spectra with mainly two peaks. Values of 7.77°, and 9.1° for the one at lower 2θ, and 19.81°, and 20.3° for the one at higher 2θ have been reported in two of the above studies.^{50,56} Chitosan has been reported to have two major peaks [one above 10.0° (10.8°)^{59,60} and the other above 20.0° (20.4°)^{59,60} 2θ].⁶¹

2.3.2 Effect of the milling ball diameter on crystallinity

X-ray diffraction data for α-chitin processed with 2 × 0.5" and 16 × 0.25" balls for increasing milling time are shown in Figures 2–6 and 2–7 respectively. Each of the six reflections of native α-chitin in Figure 2–4 (black signal in Figures 2–6 and 2–7) decreased in intensity with increasing milling time. Their maximum intensities remained at the same 2θ values indicating that the bulk of the ball milled material has kept its α-chitin characteristics (see Figures A2–1 and A2–2). The 2.60 (4600/1770) ratio of the two strongest peaks [(110) and (020)] in native chitin

dropped to 2.43 (1460/600) with the $2 \times 0.5''$ balls (7% reduction) and to 2.08 (1153/554) with the $16 \times 0.25''$ balls (20% reduction) for the 120 min samples. This is a sign that the α character of the ball milled chitin is decreasing with both sets of balls, with the $0.25''$ balls being more effective most probably because of the doubling of the surface area available for collisions. Nevertheless, with a ratio higher than 2.0, the a-direction stabilization remains appreciably stronger than the stabilization in the b-direction; sustaining the polysaccharide's α (alpha) character.

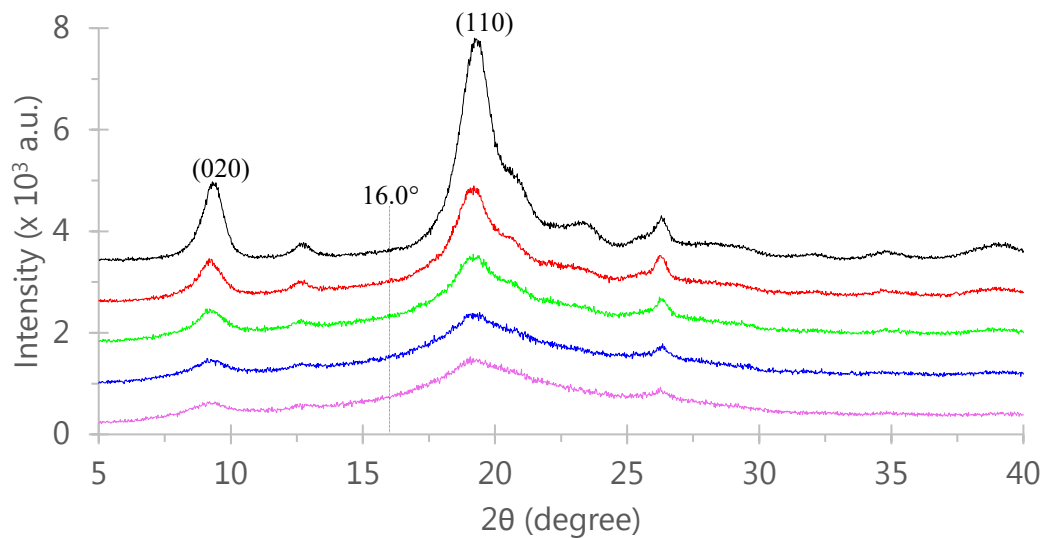


Figure 2-6: XRD patterns of untreated (black signal) and milled α -chitin with $2 \times 0.5''$ balls for 30 (red), 60 (green), 90 (blue) and 120 (pink) min. Temperature of the inner surface of the vial did not exceed 40°C .

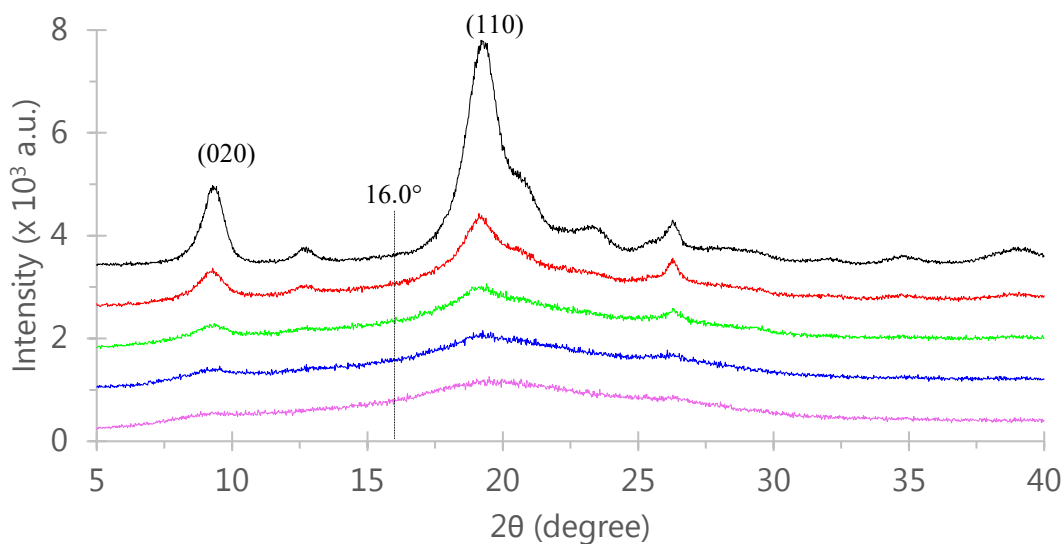


Figure 2-7: XRD patterns of untreated (black signal) and milled α -chitin with $16 \times 0.25''$ balls for 30 (red), 60 (green), 90 (blue) and 120 (pink) min. Temperature of the inner surface of the vial did not exceed 41°C .

Considering the empirical nature of the Segal method to assess crystallinity in polysaccharides (see Section 2.1.2), the selection of the 2θ values which will represent the crystalline and amorphous components of chitin's crystal can be based on a historical continuum. In 1990, Focher et al. were probably the first to apply Segal's CrI equation to an α -chitin sample selecting the (110) reflection as the crystalline diffraction (at $19^\circ 2\theta$), and the diffuse halo at $16^\circ 2\theta$ as the scatter that reflects most meaningfully the amorphous component.⁴⁶ From then, several groups have used the same values to approximate chitin crystallinity.^{49,52,62-65} However, in 2010, when Kumirska et al. reviewed X-ray diffraction methods for chitin and chitosan characterization, they have highlighted a few studies which have used $12.6^\circ 2\theta$ to represent the amorphous content without mentioning any $16^\circ 2\theta$

literature.⁶¹ Indeed, 12.6° 2θ has been used in two more investigations; without proper caution though, as those native chitin signals have weak but non-negligible crystalline diffractions at that angle.^{32,57}

Figure A2-3 focuses on the 11.0° to 17.0° 2θ region of Figure 2-7. The signals for 30 (red), 60 (green), 90 (blue) min progress throughout the region in that order of relative increasing intensities except from in between 12.2° and 13.0° where the red and green signals merge with the higher intensities of the blue signal. Characteristically, the blue signal reaches a spike of 696 at 12.74° [2θ value for native chitin's (021) reflection]. This clearly shows that 16.00° is a more meaningful representation of the amorphous portion of α -chitin samples among the values proposed in the literature. Therefore, the crystallinity indices (CrI) are calculated using that value and plotted for both sets of experiments in Figure 2-8.

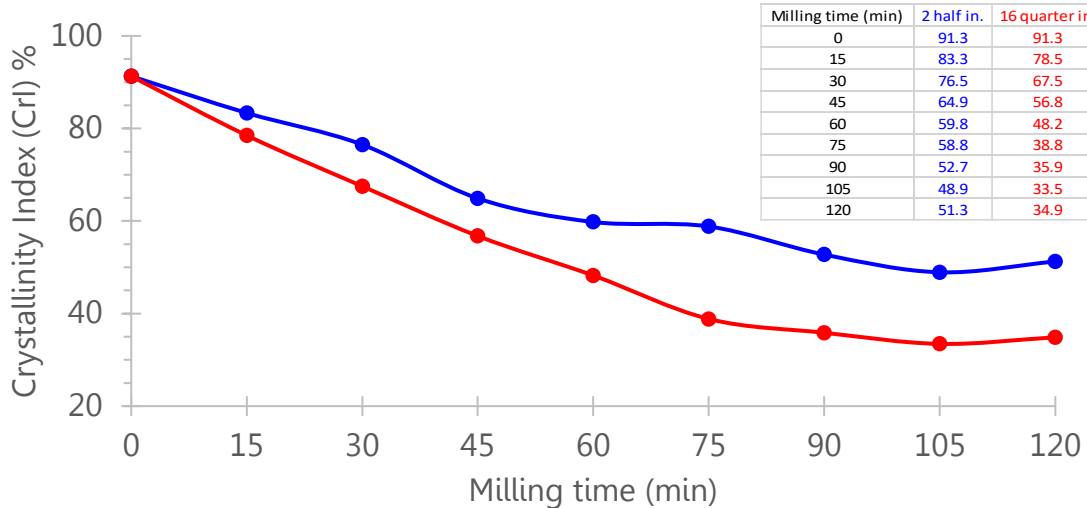


Figure 2-8: Crystallinity Index (CrI)% of α -chitin over milling time when processed with $2 \times 0.5''$ (blue) and $16 \times 0.25''$ (red) balls.

In both cases, the crystallinity of α -chitin is gradually reduced from 91.3% to 51.3% with the 0.5" balls and to 34.9% with the 0.25" balls.^{xxxiv} Figure A2-5 provides sufficient detail of the 15° to 20° 2 θ region for the 30, 60, 90 min signals of Figure 2-7 to allow reproduction of the calculations. Although the 2 \times 0.5" balls offer higher energy collisions due to their higher mass, the 16 \times 0.25" balls are more effective from the first 15 minutes probably due to the higher frequency of collisions that they offer. Interestingly, their productivity compared to the 2 \times 0.5" balls is fully realized after 45 min and until 75 min when the ball mill process begins to level off, and at 120 min – a 34.9% CrI plateau is achieved. This reduction in CrI of 62% lags behind compared to the 100% reduction observed by others (Table 2-1/entry 8),³² probably because of the lower packing - number of balls/g chitin in the milling system (28% - 24 vs 3% - 8), and therefore lower number of collisions; differences though in chitin DP cannot be excluded. In 30 min the CrI resulting from milling with the 16 \times 0.25" balls is 67.5% representing a 26% reduction. When that value is compared with the 56% reduction in Table 2-1/entry-6,³⁰ the three-fold higher

^{xxxiv} Figure A2-4 shows a representative trial line that was taken as background on the XRD signal of the sample milled for 90 min with 16 \times 0.25" balls. The line was drawn by JADE software [Materials Data, Inc. (MDI)] when from the proposed points the ones at 5.0°, 5.8°, 34.0°, and 39.9° 2 θ were kept by the investigator. When that background was removed from the XRDs of the samples of the 16 \times 0.25" balls set, the decreasing trend was the same as Figure 2-8 except that the crystallinity index (CrI%) values were 10.2 \pm 2.1 higher (e.g. the 78.5% of the 15 min sample was calculated at 87.1% and the 35.9% of the 90 min sample was found at 50.0%). Since the Segal method has been reported to give 25 \pm 3% higher crystallinity values than the average of other three methods (see Section 2.1.2) and no other study of those in Table 2-1 has assessed background removal, the method was hypothesized to overestimate CrI and it was considered unnecessary.

packing can be speculated as the cause for the doubling of the amorphization effect (if all other variables are considered similar).

The precision of the XRD technique was investigated by repeating the measurement on two samples prepared in the same way. The overlaid signals for the 15 and 105 min samples ($2 \times 0.5''$ balls) in Figures A2–6 and A2–7 show that CrI values were $84.1 \pm 1.0\%$ and $51.2 \pm 3.2\%$, and the intensity ratios for the (110)/(020) reflections were 2.53 ± 0.16 (RSD 6.3%) and 2.26 ± 0.04 (RSD 1.8%) respectively.

2.3.3 Effect of chitin mixing load on crystallinity

A critical parameter for scale-up of chitin ball milling is the amount of polysaccharide (mixing load) that undergoes the process. To maximize that, a basic study of the balls-to-chitin mass ratio (BtC) for the steel ball mill system was considered essential. X-ray diffraction data for increasing loads of α -chitin (1, 2, 3, 4 g) processed for 90 min with $2 \times 0.5''$ and $16 \times 0.25''$ balls are shown in Figures 2–9 and 2–10 respectively. The charged loads (g) correspond to approximately 16.5, 8.2, 5.5, 4.1 balls-to-chitin mass ratios (BtC) respectively [the actual volume of $2 \times 0.5''$ balls is 2.14 mL and 2.08 mL for the $16 \times 0.25''$ system (<3% relative difference)]. The diffractogram presented focus on the region related to crystallinity calculation (from 8° to $20^\circ 2\theta$), as the rest of the signal was not expected to differ significantly from the blue signals in Figures 2–6 and 2–7; indeed, reflections (040), (031), and (130) subsided with decreasing chitin load.

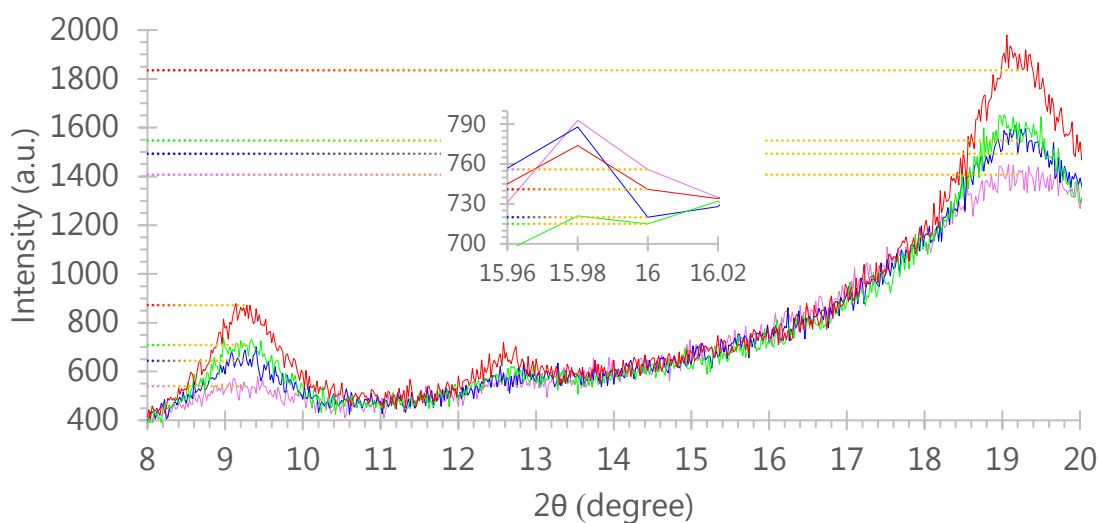


Figure 2-9: Overlay of XRD patterns (no separation) of 4 (red), 3 (green), 2 (blue) and 1 (pink) g α -chitin milled with $2 \times 0.5''$ balls for 90 min. Dotted lines mark the intensities: 1835 (red), 1547 (green), 1493 (blue), and 1407 (pink) at 19.20° ; 741 (red), 715 (green), 720 (blue), and 756 (pink) at 16.00° ; 872 (red), 709 (green), 644 (blue), 540 (pink) at 9.28° .

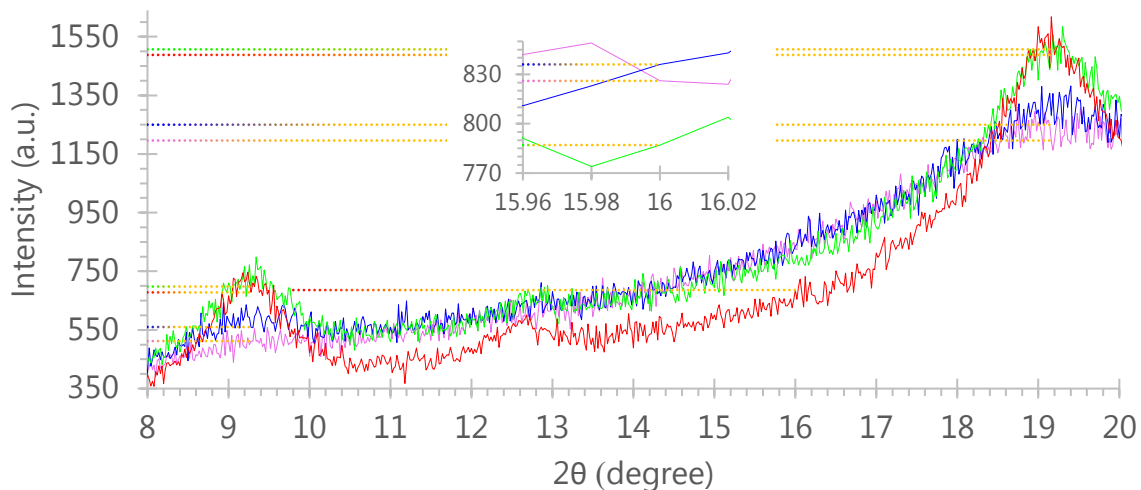


Figure 2-10: Overlay of XRD patterns (no separation) of 4 (red), 3 (green), 2 (blue) and 1 (pink) g α -chitin milled with $16 \times 0.25''$ balls for 90 min. Dotted lines mark the intensities: 1488 (red), 1507 (green), 1250 (blue), 1196 (pink) at 19.20° ; 686 (red), 787 (green), 836 (blue), 826 (pink) at 16.00° ; 678 (red), 698 (green), 560 (blue), 512 (pink) at 9.28° .

Figure 2-11 shows the CrI values decreasing in both sets of samples with decreasing chitin load, something which was expected, as the greater the mass that shares a fixed number of collisions (and amount of energy), the more crystalline that mass will remain at the end of a fixed process time. The mechanochemical potential of the $2 \times 0.5''$ balls system lowers the crystallinity of 1 g to 46.3% [49% reduction from native chitin's CrI (91.3%)] while when an identical process was performed with 4 g chitin the CrI was reduced to 59.6%. The latter 35% reduction is at the same level as when 2 g were milled for 60 min. Hence, doubling the chitin load does not necessarily mean that the $2 \times 0.5''$ balls require twice as much time to achieve a similar amorphization effect. The increased impact frequency of the $16 \times 0.25''$ steel balls system managed to amorphize 4 g of native chitin to a CrI level of 53.9% (41% reduction), while when colliding with 1 g of chitin crystallinity was decreased to 30.9% (66% reduction).

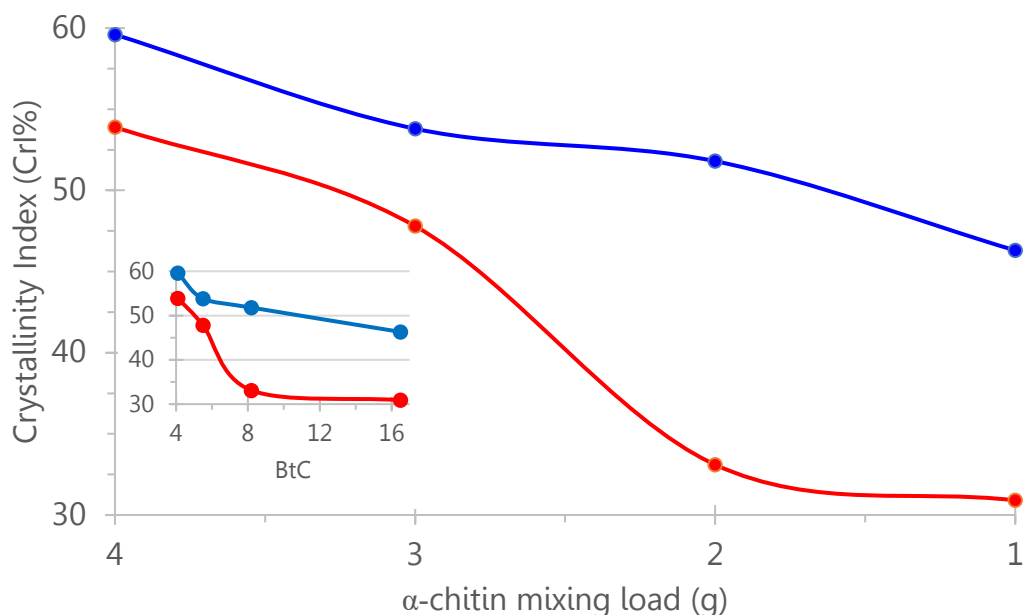


Figure 2-11: Crystallinity Index (CrI)% over α -chitin mixing load when milled for 90 min with 2 x 0.5" (blue) and 16 x 0.25" (red) balls. Inset reads the same data on a balls to chitin mass ratio (BtC) x-axis.

The latter reduction percentage can be compared to the 56% reported by Osada et al. in 2013 (Table 2-1/entry 6)³⁰ on the basis that the 3-fold higher milling time here is compensated by the 3-fold higher packing. The additional 10% higher reduction in our system may result from a greater rate of shaking/mixing, 1080 rpm compared to 800 rpm (assuming that their converge mill produces similar impacts with the shaker mill here). However, the amorphization level reported by Osada et al. was obtained using a much larger amount of steel balls per gram of chitin compared to the current study: 690 x 0.2" (5 mm diameter) Note: (a 5 mm sphere occupies 0.065 mL, which weighs approx. 0.5 g of steel; they reported usage of 704 g of chromium steel balls for 2 g of chitin).³⁰ That high number of balls raises

questions about the effectiveness of smaller balls, especially with entry 7 (Table 2–1) achieving an equivalent result (57% CrI reduction) with $0.65 \times 0.39''$ (10 mm diameter) zirconia (5.9 g/mL density) balls per g of chitin using again a converge mill.^{xxxv} Indeed, a bigger balls system [$24 \times 0.39''$ (10 mm diameter) per g of chitin] used by Aida et al.³² managed to achieve absolute chitin amorphization. With ZrO_2 balls used, that system's balls-to-chitin mass ratio was 74.1, which is 4.6 times higher than the 16.1 mass ratio used in this thesis that revealed a 66% reduction in crystallinity with $16 \times 0.25''$ steel balls. That high BtC number might have compensated for the lower zirconia density (5.9 vs 7.8 g/mL), the lower operating frequency (700 vs 1080 rpm), and a possible milder force for collisions in a planetary mill (rotational motion) compared to the shaker mill in this thesis.

Figure 2–11 clearly shows that if the $16 \times 0.25''$ system would have kept the same amorphization potential it had with an imaginary 1.5 g chitin load, it would have managed to lower the crystallinity of 4 g to 37.5% (59% reduction). However, the CrI achieved was only 53.9% (41% reduction). The phenomenon is more evident when considering it in terms of balls-to-chitin mass ratio (BtC) instead of chitin mixing load (g) (see inset of Figure 2–11). The straight blue line from 5.5 to 16.5 BtC reveals that the 5.5 BtC mass ratio (3 g chitin mixing load) milled with the $2 \times 0.5''$

^{xxxv} That is assuming their $\sim 2000 \mu\text{m}$ chitin particles are of similar density to ours, their 20 g must have occupied approx. 68 mL, which means they've used 6.8 mL of the aforementioned 0.524 mL balls, hence 13 balls for 20 g chitin; if a dm^3 (L) scale vessel was used for entry 7, the estimated packing does not exceed 2% (31).

system experiences the same amorphization dynamic as the 1 g chitin mixing load (16.5 BtC). This means that even though the higher volume balls offer less frequent collisions with chitin, the higher force collision offered from their higher mass (8.3 g for each 0.5" ball vs 1.0 g for each 0.25" ball in our case) will probably be necessary when researchers aim to maximize the amount of polysaccharide milled to a required amorphization level. The higher collision frequency might prove complementary to the higher forces in cases where the chitin load charged in the vessel has a flaky texture (from its shell isolation phase) and exhibits a relatively low density (e.g. 0.3 g/mL like with the chitin in this thesis), hence the ball mill process will have to start with vials containing a relatively high chitin filling degree.

Figure 2–12 shows the intensity ratio for reflections (110)/(020) (strength of α character) over balls to chitin (BtC) mass ratio for milling with $2 \times 0.5''$ (blue) and $16 \times 0.25''$ (red) balls for 90 min. The $16 \times 0.25''$ balls system is more effective in lowering the α character (from 2.60 to 2.34) when the balls to chitin (BtC) ratio is at its highest value (16.5). It is noted that the $2 \times 0.5''$ balls do not make a difference in the α character during milling as their 2.61 ratio lies within the method's 0.16 standard deviation.^{xxxvi} However, as the BtC ratio drops (chitin mixing load

^{xxxvi} The precision of ball milling (investigator bias, native chitin's homogeneity, mixer/mill's motor performance) was investigated by repeating the run of two samples. The overlaid signals for the 90 min milling/8.2 BtC samples in Figures A2–8 ($16 \times 0.25''$ balls) and A2–9 ($2 \times 0.5''$ balls) show that CrI values were $34.5 \pm 1.9\%$ and $52.3 \pm 0.7\%$, and the intensity ratios for the (110)/(020) reflections were 2.12 ± 0.16 and 2.29 ± 0.04 respectively. Since these deviations (average for CrI is $\pm 1.3\%$) do not exceed the ones of the characterization technique (average for CrI is $\pm 2.1\%$, see Section 2.3.2), the reproducibility of ball milling

increases), the bigger balls become more productive, and with a BtC of 4.1 they manage to lower α character to 2.10, which falls within XRD's precision for the value of the $16 \times 0.25''$ system (2.19). This 19% α character reduction $[(2.60 - 2.10) \times 100 / 2.60]$ on 4 g in 90 min is equivalent to the effect that the $16 \times 0.25''$ system can achieve on 2 g in 120 min. That result can prove of significance when designing scaled up processes in the future, as it can help to better direct chitin's diverse functionalities to the different valuable product categories (see Section 1.5).

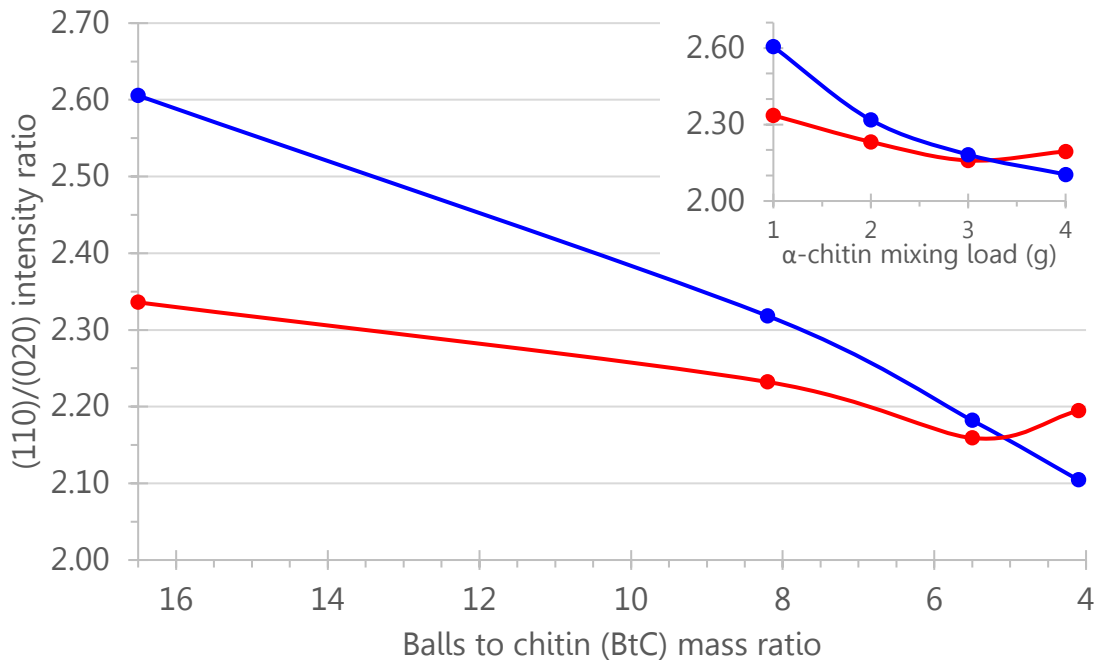


Figure 2-12: Intensity ratio for reflections (110)/(020) over balls to chitin (BtC) mass ratio for milling with $2 \times 0.5''$ (blue) and $16 \times 0.25''$ (red) balls for 90 min. Inset reads the same data on an α -chitin mixing load (g) x-axis.

can be considered acceptable with the overall method producing representative samples $[\pm 2.5 \text{ CrI units } (= \sqrt{1.3^2 + 2.1^2})]$ (66).

2.3.4 Effect of milling time on particle size and morphology

An approximation of the particle size distribution of the native and ball milled samples is presented in scanning electron microscopy (SEM) images of 2-mm and 500- μm scale in Figure 2–13. These micrographs illustrate that ball milling with $16 \times 0.25''$ balls (BtC 8.2) for 45 min reduces the size of α -chitin particles from ca. $>500 \mu\text{m}$ (flakes in Figure 2–13a,b) to ca. $<100 \mu\text{m}$ (CrI 56.8%) (Figure 2–13c). Milling for 105 min (Figure 2–13d) does not induce a significant further reduction in the average diameter of the particles. These results are comparable with those of entries 6 and 7 of Table 2–1, in which 30 min grinding (of $>2000 \mu\text{m}$ particles) produced approx. $22 \mu\text{m}$ chitin particles (CrI 40%) in both cases.^{30,31}

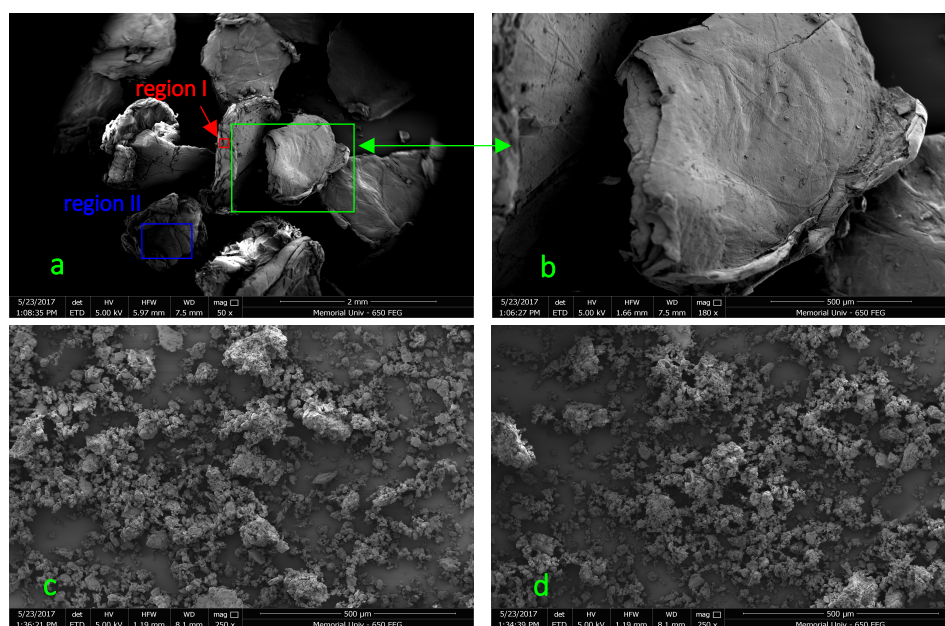


Figure 2-13: Scanning electron microscopy (SEM) micrographs of untreated (a – 2 mm scale, b – 500 μm scale) and ball milled α -chitin with $16 \times 0.25''$ balls (8.2 BtC) for 45 (c – 500 μm scale) and 105 (d – 500 μm scale) min. Regions I and II are shown in separate SEMs of 50 and 300 μm scale respectively in Figure A2–10.

A notable change in the morphology of native α -chitin upon ball milling is observed when closely inspecting the smoothness of certain edges of the particles. Regions I (in red) and II (in blue) of Figure 2-13a, which are from two separate particles of native α -chitin, are illustrated in Figure A2-10 in 50 and 300 μm scale respectively. The pink circles and the orange diamonds highlight smooth surfaces and rough edges respectively in native α -chitin particles. The zoomed area of region I (in red) allows inspection of statistically significant fibrils,^{xxxvii} which merge into wider smooth surfaces. The fibrils' lengths vary from a few to several micrometers while their width is less than a micrometer. The red bar which makes prominent the width of one of the longest and widest fibrils is estimated to approximately 300 nm. Structures in the nanometer scale are also observed in the zoomed-in section of region II (thin sheets). These observed features have probably been influenced to an extent by the shell isolation steps followed by ChitinWorks (deproteination, demineralization, drying). Unfortunately, technical limitations with the SEM instrument did not allow observation at the nanometer level. However, future researchers can expect morphologies for chitin's fibril similar to those reported by the Dobrovolskaya group.^{68,69} The enthusiast reader of the electronic copy is encouraged to magnify the page of the images of Figure A2-11 to more than 300%

^{xxxvii} The term "fibril" (or equivalently macrofibril for biological structures) refers to diameters of less than a micrometer, while "nanofibril" to less than 100 nm (67).

(avoiding the pixilation effect) to have a feel of the absence of rough edges in the samples of ball milled chitin.

The observed changes in morphology and particle size are a direct consequence of the forces developed during collisions between steel surfaces and the sheets (*ac* and *bc*) of the fibril terminals (appearing either as smooth or rough particle surfaces). The lack of covalent bonds connecting chitin sheets allows the reader to briefly use an analogy between the median contact force in the ball mill and the failure force needed to disrupt a cluster of hydrogen bonds in amyloid fibrils of different lengths.⁷⁰ Paparcone and Buehler have emphasized that a minimum failure force of 175 ± 125 pN is necessary for a 986 nm amyloid fibril to deviate from its elastic deformation regime and fail. Longer than ca. 1 μ m fibrils are expected to defect independently of their length, while the failure mechanism of shorter ones has been explained to be length dependent (the shorter the fibril the greater the failure force).⁷⁰ Hence, it is not unreasonable to assume that particle size reduction during ball milling proceeds with the smoothing of those rough edges (also thought as fibril thinning) as well as with nanometer-scale crack generation on the smooth surfaces of the particles (both due to disruption of the hydrogen bonding network in both a and b directions). A comparison of a more “wrinkled” surface of a smaller particle with the relatively wider “smooth” surfaces of a bigger particle in any of the micrographs of Figure A2–11 is in support of the aforementioned hypothesis.

2.3.5 FT-IR investigation into molecular origins of changes in crystallinity

2.3.5.1 Qualitative analysis and weakening of α -chitin's hydrogen bonding network

From the XRD data collected and their interpretation, it is evident that the increased collision frequency of the $16 \times 0.25''$ balls system decreases crystallinity of α -chitin faster than the $2 \times 0.5''$ balls. Hence, we investigated the possibility of correlating the CrI behavior of the smaller balls system in Figure 2–8 with the bifurcated hydrogen bond, which is the most stable of the intermolecular hydrogen bonds, critical to the decrystallization of α -chitin, and visible with FT-IR spectroscopy (see Section 1.4).^{71,72}

Figure 2–14 shows the changes in the FT-IR spectra of native α -chitin milled with $16 \times 0.25''$ balls for 60 and 120 min (8.2 BtC). The spectra exhibit the characteristic strong and sharp absorption bands for chitin at the skeletal frequencies region of $1000\text{--}1200\text{ cm}^{-1}$ (C-O and C-O-C stretching vibrations),^{73,74} ca. 1560 cm^{-1} (N-H in-plane bending & C-N stretch – termed amide II),^{75,76} and ca. 1630 cm^{-1} (C=O stretch – termed amide I)^{75,76,61}. The lower signal intensity for native α -chitin (black) is due to the flaky texture of the sample which limits contact with the diamond ATR surface. The same effect is also evident in the spectrums of entry 6 and 7 of Table 2–1.^{30,31}

The O-H stretching bands at 3473 and 3428 cm^{-1} have been attributed to hydrogen bonded O6-H and O3-H respectively.⁷⁷⁻⁷⁹ Their 45 cm^{-1} difference is in close agreement with 33 ,⁷⁷ 36 ,³⁰ and 40 ⁷⁸ cm^{-1} for crab chitin, 31 ,⁵⁷ 33 ,⁸⁰ and 35 ⁸¹ cm^{-1} for

shrimp/prawn chitin, and 48 cm^{-1} for *Phaeocystis globosa* (a genus of algae) α -chitin.⁸² Native α -chitin's band at 3256 cm^{-1} has been associated with the hydrogen bonded N–H stretch for solid state monosubstituted amides,^{83,84} and has been termed amide A.⁸⁵ Its frequency is adjacent with those reported for various α -chitin samples (3264 ,⁷⁷ 3265 ,^{78,82} 3266 ,⁸⁶ 3268 ,⁵⁷ 3269 ,⁸¹ and ca. 3250 ³¹ cm^{-1}). Based on the structure proposed by Sikorski et al., it is not unreasonable to assume that hydrogen bonded primary alcohols contribute to the rise of the amide A band.^{30,79,80}

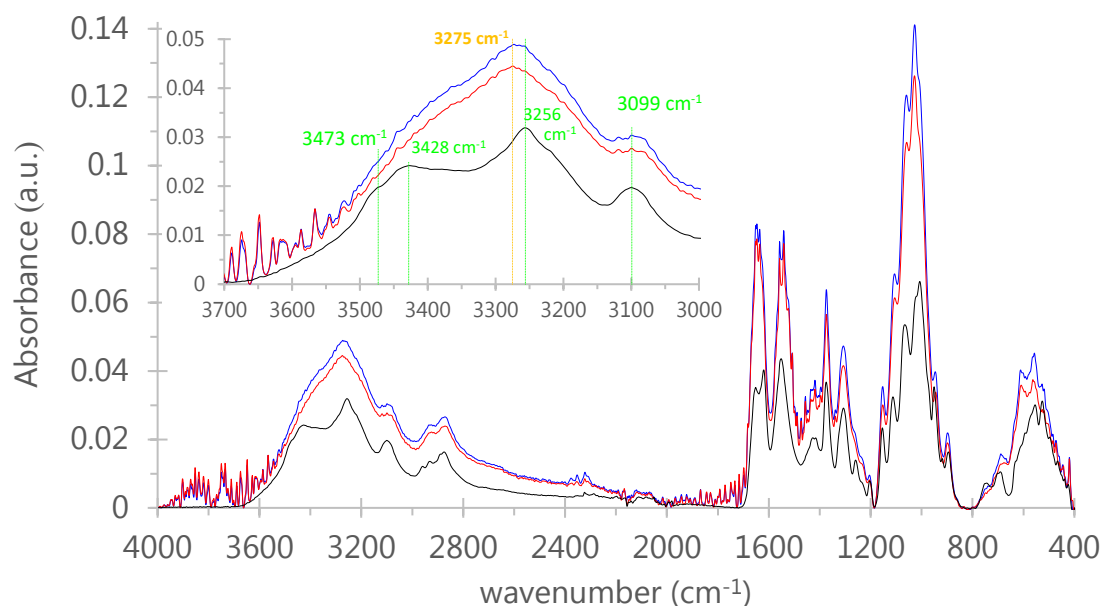


Figure 2-14: ATR FT-IR spectra of native (black signal) and milled α -chitin with $16 \times 0.25''$ balls for 60 (blue) and 120 (red) min (8.2 BtC). The inset shows the hydrogenic stretching region of $3700\text{--}3000\text{ cm}^{-1}$ in more detail.

The weaker band at 3099 cm^{-1} has been attributed to the Fermi resonance between the N-H stretch and the perturbed first overtone of amide II,⁸⁷ and has been termed amide B^{85, xxxviii}. The frequency of amide B is in line with those observed for various α -chitin samples (ca. 3085,³¹ 3106,^{57,89} ca. 3108,^{30,78,81} and 3100^{82,86} cm^{-1}). As can be seen in the inset of Figure 2–14, ball milling for 60 and 120 min (blue and red signal respectively) does not change the frequency of amide B and increases the frequency of the amide A band to 3273 and 3275 cm^{-1} respectively. This shift (ca. 18 cm^{-1}) of amide A to higher frequencies upon grinding is also visible (on close inspection) in the spectra of entry 6 of Table 2–1 and is indicative of a statistically (or energetically) less significant involvement of N-H in hydrogen bonding {mostly in the a-direction [associated with the (020) XRD peak] through the bifurcated HB}. Moreover, the hydrogen bonded O6-H and O3-H bands have become broader with milling and merge with the Amide A band (similarly to the spectra of entry 6 of Table 2–1). This suggests that interchain hydrogen bonding in the b-direction [partly reflected in the (110) XRD peak] through the aforementioned hydroxyl groups (check Figure 1–6) is also weakening upon ball milling.

With this evidence for weakening of the hydrogen bonding network in α -chitin, increasing moisture uptake is expected to occur with increasing milling time. Indeed, gravimetric analysis experiments for ball milled samples that will follow in

^{xxxviii} The consideration of the possibility of the partial origin of amide A and amide B bands from vibrational self-trapping is beyond the scope of this study (88).

later chapters indicate that native chitin's 5.5 wt.% moisture [possibly partly on the water density "hot spot" zone offered by the (100) interface (b-direction)]⁹⁰ is expected to rise above 6.0 wt.%, but not to exceed ca. 6.7 wt.% (approx. 20% increase) for the 3.3% packing set studied here. Researchers in the future might hypothesize that the reduced intermolecular hydrogen bonding involvement of the polysaccharide's side chains allows increasing hydrogen-bonded clusters of water to be adsorbed onto certain surfaces of α -chitin's lattice.⁹¹ Anyhow, these low water content values (orders of magnitude lower compared to a concentrated protein aqueous solution ca. 10 mg/mL), along with the fact that molar absorptivities of strong bands of biopolymers are orders of magnitude higher than those of water bands (e.g. protein amide I band lies in the range of 300–1000 M⁻¹ cm⁻¹ while water's O-H bend at 1643.5 cm⁻¹ is 21.8 M⁻¹ cm⁻¹),⁹² suggest that a quantitative analysis of the FT-IR spectra using the peak height ratio method^{93,94} will be minimally affected by water interferences. Nevertheless, considering the broad absorption of water's O-H stretch in the hydrogenic region (see water's IR spectrum in Figure A2-12), which is roughly 5 times more intense than the sharp O-H bend ca. 1640 cm⁻¹,^{92,95} the region of amide I and II was selectively investigated without drying the samples.

2.3.5.2 Quantitative analysis and a force distribution hypothesis

Figure 2-15 presents the amide I and II bands in more detail. Amide I of native α -chitin splits at 1652 and 1621 cm⁻¹, and amide II mode is at 1552 cm⁻¹. This 31 cm⁻¹ difference for the amide I doublet is characteristic for the source of crab α -chitin

from ChitinWorks LLC, and its value is adjacent with all three α -chitin entries of Table 1 (33,^{30,32} ca. 32³¹ cm^{-1}), as well as with numerous other α -chitin studies (33,^{57,77,79,96} 34,⁷⁸ 35,^{82,97} 36,^{80,86} 37⁸¹ cm^{-1}). Although in several of those cases researchers were clearly stating that the lower frequency peak of the C=O stretch is due to a doubly hydrogen bonded oxygen and the higher one to a singly one, none of them has even attempted to calculate their peak height ratios. It is only fair to highlight at this point that α -chitin's unit cell proposal from Minke and Blackwell in 1978⁴⁷ has contributed significantly in confirming the hydrogen bonding regime of amide I, which has been a matter of debate for the most abundant of the marine polysaccharides since the 1950s.^{77,79}

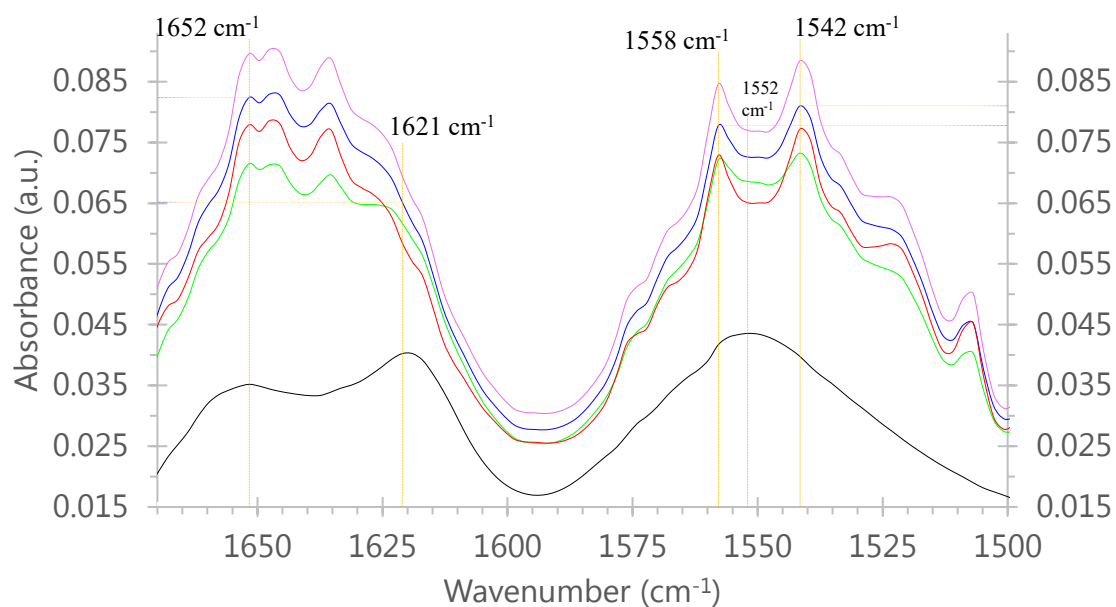


Figure 2-15: 1670–1500 cm^{-1} region of infrared spectra of native (black signal) and milled α -chitin with $16 \times 0.25''$ balls for 30 (green), 60 (blue), 90 (pink) and 120 (red) min (8.2 BtC). 1652 and 1621 cm^{-1} bands are characteristic of the α -chitin sample in this thesis.

Regardless of the pace of chitin research so far, and as discussed in Chapter 1, the lower frequency vibration has been attributed to the $C=O^2$ group hydrogen bonding with N^1-H and $O6^1-H$, while the vibration at the higher frequency to the $C=O^2$ group hydrogen bonding with N^1-H exclusively. Figure 2–16 shows the ratio between the absorbance intensities at 1621 and 1652 cm^{-1} . A 33% decrease in this ratio (from 1.146 to 0.766) with no error bar overlap is observed for the first 75 min of ball milling, something which according to Beer's law reveals a declining relative number of doubly hydrogen-bonded amide groups. This implies a weakening of the intermolecular hydrogen bonding network by statistically breaking the weaker of the two of the bifurcated's hydrogen bonds ($O6^1-H \cdots O^2=C$). That means that the degrees of freedom for the primary alcohol are raised, while at the same time the stronger $N^1-H \cdots O7^2$ is theoretically sustained; keeping the chains connected along the a-direction. Considering the clear amorphization and particle size reduction results from the XRD and SEM methods though, these FT-IR data (amide I split ratio) allow future researchers to form new hypotheses regarding force distribution in chitinous materials. Since a logical systematic retention of the $N^1-H \cdots O7^2$ is being monitored, it is not unreasonable to assume that the median contact force applied from the 16 balls is being directed to an extent through deformation of the covalent bonds of the *N*-acetyl and hydroxymethyl groups to the chains' backbone; possibly deforming the pyranose rings. Figure A2–13 gives a feel of the types of molecular transformations studied with force spectroscopy techniques like atomic force microscopy (AFM) or magnetic tweezers,⁹⁸⁻¹⁰⁰ and is used at this point to encourage

the consideration of a length-force continuum for the mechanochemical treatment applied to chitin.

Going back to experimental results, the clear change in the amide I band upon ball milling with $16 \times 0.25''$ balls (8.2 BtC system) is reflected in the amide II band as shown in Figure 2-15. This is something that might make sense intuitively since the two bands represent the delocalization of nitrogen's lone pair and the partial charges on both sides of carbon (plus for nitrogen and minus for oxygen). Figure 2-17 studies the ratio between the heights of the strongest components of amide II band (1558 and 1541 cm^{-1}). A steady 9% downward trend (from 1.051 to 0.954) is observed for the higher frequency for the same as amide I milling-time interval (0-75 min) with no error bar overlap in between samples of 0-15-60 min. Mysteriously for future mechanochemistry enthusiasts, none of the three α -chitin studies of Table 2-1 show a clear separation between the two most intense amide II contributors, which are 17 cm^{-1} apart in Figure 2-15.

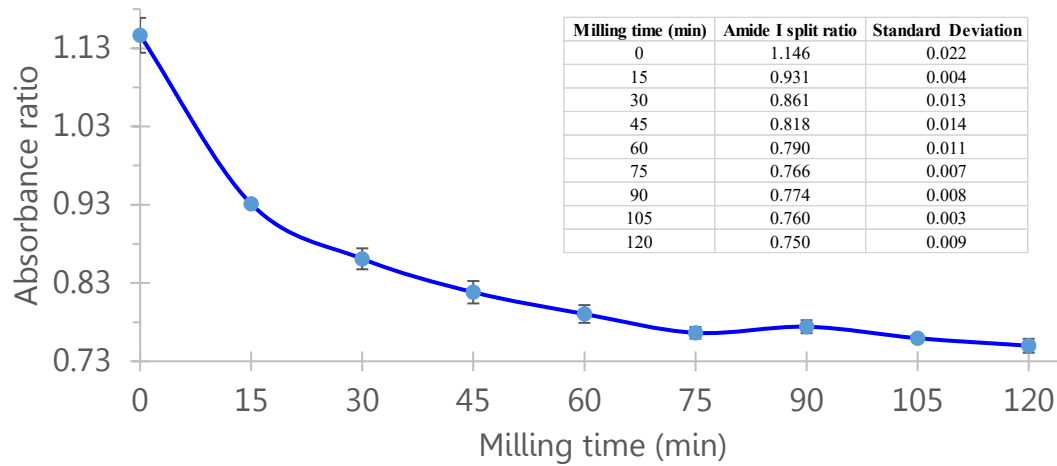


Figure 2-16: FT-IR data ($1621\text{ cm}^{-1}/1652\text{ cm}^{-1}$ peak ratio) for milled α -chitin with $16 \times 0.25''$ balls (8.2 BtC). Indicatively, the triplicate measurement for the 60 min sample gave a ratio of 0.790 ± 0.011 , which can be reproduced from the average signal in Figure 2–15 ($0.0652 / 0.0824$ is approx. 0.791).

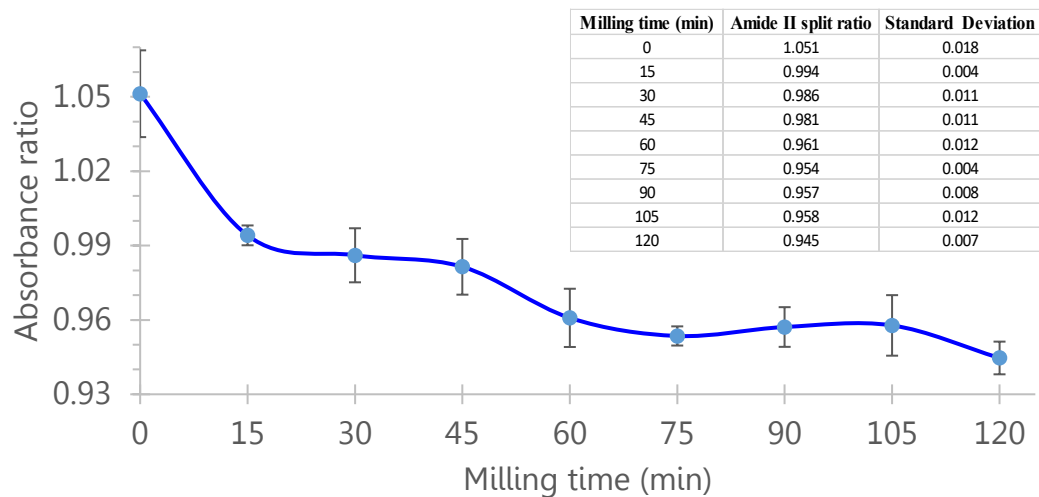


Figure 2-17: FT-IR data ($1558\text{ cm}^{-1}/1541\text{ cm}^{-1}$ peak ratio) for milled α -chitin with $16 \times 0.25''$ balls (8.2 BtC). Indicatively, the triplicate measurement for the 60 min sample gave a ratio of 0.961 ± 0.012 , which can be reproduced from the average signal in Figure 2–15 ($0.0778 / 0.0810$ is approx. 0.960).

A systematic literature survey unveils that this parallel behavior of the two amide bands can be explained on the basis of the two-dimensional (2D) FT-IR study of α -chitin from Yamaguchi et al.⁷⁸ Their analysis of synchronous 2D correlation spectra (obtained at a wide temperature range) disclosed consistent positive cross-peaks between the higher frequency component of the amide II region (1581 cm^{-1} for their hydrolyzed crab chitin samples) and the lower frequency contributor of amide I (1619 cm^{-1} respectively), as well as between the lower frequency component of amide II (1538 cm^{-1}) and high frequency of amide I (1648 cm^{-1}). To the best of my knowledge this is the only sensible evidence in primary literature correlating the two amide bands in α -chitin, something which highlights the shared origin of the associated vibrational modes.

Therefore, by analogy, it is safe to assign the bands at 1621 and 1558 cm^{-1} for the α -chitin samples in this work to the bifurcated hydrogen bonded amide group, and the ones at 1652 and 1542 cm^{-1} to the singly hydrogen bonded mode (as discussed in Chapter 1). Oxygen's higher electronegativity than nitrogen's, as well as the non-negligible contribution of the N-H in-plane bending to the amide II mode explain the reduced abatement (9%) (and the corresponding error bar overlap between 30–45 and 60–75 min samples) of the $1558/1541\text{ cm}^{-1}/\text{cm}^{-1}$ ratio compared to that of $1621/1652\text{ cm}^{-1}/\text{cm}^{-1}$ (33%) (with complete absence of error bar overlap). This parallel behavior of amide I and II is an indication that the attachment of the *N*-acetyl group in chitin's backbone is retained, as if the amino content was increasing upon

ball milling, the hydrogen bonding possibility of the carbonyl group would have significantly decreased and Figure 2-17 wouldn't have had that mild reduction of the $1558\text{ cm}^{-1}/1541\text{ cm}^{-1}$ peak ratio between the samples of 15-30-45 min.

After 75 min, both amide I and II split ratios enter a plateau phase. These are in line with the behavior of the corresponding crystallinity index in Figure 2-8. Figure A2-14 shows an 84% change in slopes of the CrI behavior before and after 75 min milling time $[(0.5976 - 0.0955) \cdot 100\% / 0.5976 \text{ equals } 84.0\%]$. The plot demonstrates that if the crystallinity index would have kept decreasing with the same rate as it was from 45 to 75 min, it would have reached as low as 20.0% in 107 min (green dotted line). However, it was limited to ca. 33.5%. Figure A2-15 shows a 77% change in slopes of the $1621/1652\text{ cm}^{-1}/\text{cm}^{-1}$ absorbance ratio before and after 75 min milling time $[(0.0017 - 0.0004) \cdot 100\% / 0.0017 \text{ equals } 76.5\%]$. The difference between 84 and 77% in the change of the slopes is objectively small (<10%), and unlikely to be coincidental.

Therefore, since the reduction in hydrogen bonding for $\text{O6}^1\text{-H} \cdots \text{O}=\text{C}$ is significantly diminished after 75 min of ball milling (77%), and the *N*-acetyl arm seems to be remaining intact, it is only natural to hypothesize that the average impact energy (ca. 0.093 J per collision) transferred to a chitin nanofibril is being "heterogeneously" directed (through the N-C2 bond) to the pyranose unit. That would mean that the angle deformations of the covalent bonds of the sugar rings are likely to distribute the energy from the hit with the steel surfaces in between the

anomeric centers (through puckering conformation interconversion pathways),¹⁰¹ and ultimately to the glycosidic linkages (Figure 2–18).^{xxxix}

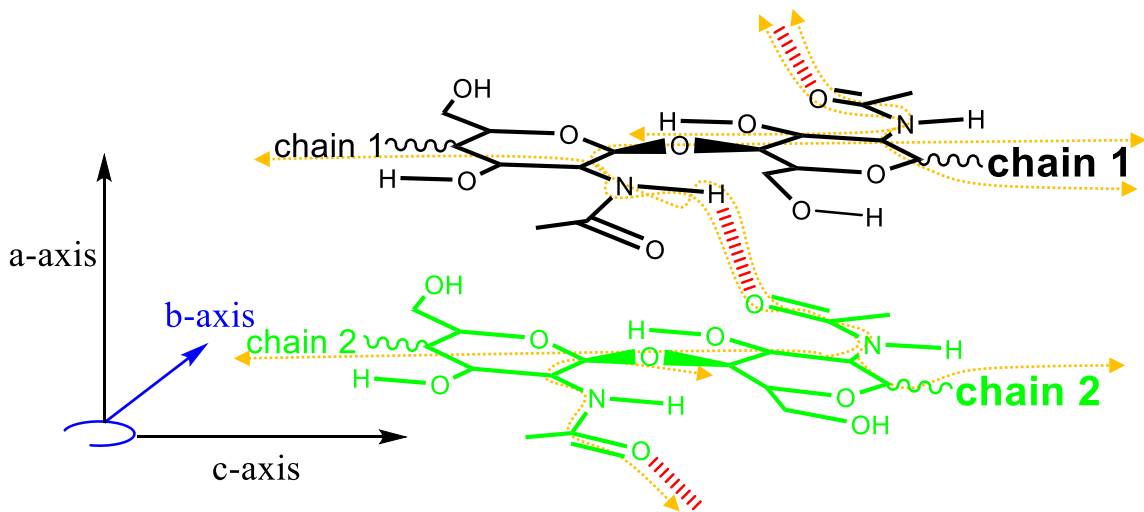


Figure 2-18: Hypothetical mechanical force distribution (orange dotted arrows) through α -chitin's $N^1\text{-H}\cdots O7^2$ intermolecular hydrogen bond and backbone structure during ball milling. Note that the $O6^1\text{-H}\cdots O7^2$ hydrogen bond of Figure 1–7 is broken here and that opposite force vectors apply to all covalent and non-covalent bonds.

Indeed, Figure 2–19 shows the $1154\text{ cm}^{-1}/2875\text{ cm}^{-1}$ absorbance ratio decreasing steadily during 120 min of ball milling (from 1.44 to 1.25) with no error bar overlap between 15, 30, 60, and 120 min.^{xi} This comprises direct evidence of depolymerization as the 1154 cm^{-1} band has long been attributed to the antisymmetric C-O-C stretch connecting two sugar units,^{61,77} and the most intense C-H stretch band (at 2884 cm^{-1} in recent literature, at 2875 cm^{-1} in spectra here) has been eased from possible associations with the multitudes of the carbon-hydrogen

^{xxxix} Without computational simulations this is still a hypothesis at this stage.

^{xi} FT-IR spectra are shown in Figure A2–16.

vibrational modes (e.g. CH₂, CH₃), and tentatively assigned to the methine groups (C-H bonds of the ring carbons).⁸² At the same time, researchers can now have less doubts in using the same band as reference for studying the possibility of amide hydrolysis.

Figure 2–20 reveals that the 1552 cm⁻¹/2875 cm⁻¹ absorbance ratios of all samples remain constant (2.746 ± 0.036 , RSD is 1.3%) with all error bars overlapping. This is clear confirmation of the parallel-amide-I/amide-II-behavior hypothesis regarding lack of deacetylation, as native chitin's 1552 cm⁻¹ band presents an absorbance minimum for the ball milled samples in between the frequencies of their two main modes of amide II (doubly and singly hydrogen bonded). The work of the Iwakura group on the use of the 1550 cm⁻¹/2878 cm⁻¹ IR peak ratio for the determination of the degree of acetylation (DA),¹⁰² which has been appreciated by Van de Velde and Kiekens,¹⁰³ allows a meaningful calculation of DA values for all the samples. The inset table in Figure 2–20 discloses that when the ratio is multiplied by the coefficient offered from Sannan et al. (35.46),¹⁰² native chitin's $95.0 \pm 5.6\%$ DA remains within its triplicates' standard deviation for all 8 ball milled samples ($97.7 \pm 1.0\%$). The 5.6% standard deviation of native α -chitin is at the same level as that reported for commercial chitosans from Sigma Aldrich. The aforementioned IR method for DA determination was selected after trial and error efforts with linear relationships of various absorbance ratios proposed by the relevant review prepared by Kasaai.¹⁰⁴ Indicatively, when the ratios are plugged into $A_{1560}/A_{2875} = 0.2$

+ 0.0125 · DA ($R^2 = 0.99$),¹⁰⁴ the obtained DA values are higher than 200%, something which does not make sense by chitin's definition. When the amide III/CH₃ absorbance ratio was used, the highlighted equation for the entire DA range ($A_{1320}/A_{1420} = 0.3822 + 0.03133 \cdot DA$)¹⁰⁴ gave acetylation values in the core of the chitosan character range (26–33%), which intuitively is not consistent with the relative heights of the amide I and II bands against the ones of the hydrogenic region (notice IR spectra that will follow in later chapters) nor with the observed 2θ values in the XRD signals.^{59,61} When the amide-I / O-H absorbance ratio was used in $DA = (A_{1655} / A_{3450}) \cdot 100 / 1.33$ and $DA = (A_{1655} / A_{3450}) \cdot 115$,¹⁰⁴ both sets of DA values for the samples produced from milling with 16 × 0.25" balls were significantly and consistently higher than 100%.^{xii} Therefore, the work in this thesis is in agreement with that of the Iwakura group viz-a-viz the most suitable bands and frequencies to measure towards DA determination.^{xiii}

^{xii} Considerations of possible limitations of the selected (and rejected) method(s) pertain to a deeper discussion regarding FT-IR variables for quantitative analysis, which is beyond the scope of this work. It is worth noting though that the selected method is part of a comprehensive series of studies on chitin (including on solubility and deacetylation kinetics) conducted in the 1970s at Seikei University, Tokyo, Japan (105-110). The university's dedication to the material's diversity potential until recent times can certainly constitute a source of inspiration for future researchers of the polysaccharide toolbox (111-113).

^{xiii} The use of the 1552 / 2878 cm⁻¹ / cm⁻¹ has been claimed to interfere to a limited extent (ca. ±3 DA% units) with water absorption (114). However, that hypothesis is subject to interferometer and other experimental parameters, the discussion of which is beyond the scope of this thesis.

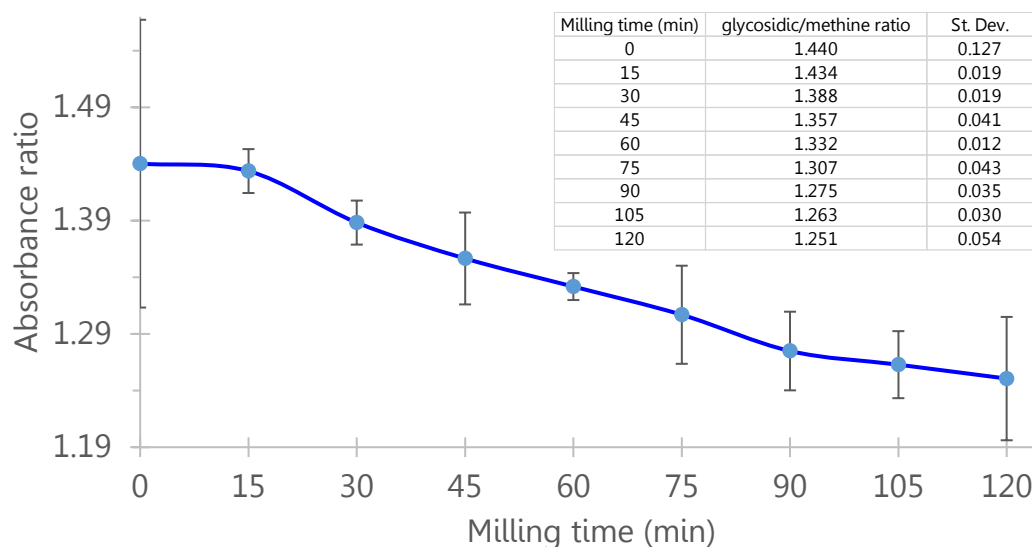


Figure 2-19: FT-IR data ($1154\text{ cm}^{-1}/2875\text{ cm}^{-1}$ peak ratio) for milled α -chitin with $16 \times 0.25''$ balls (8.2 BtC). Figure A2-16 shows the relevant absorbance intensities for the 60 min sample ($0.0353 / 0.0265 = 1.332$).

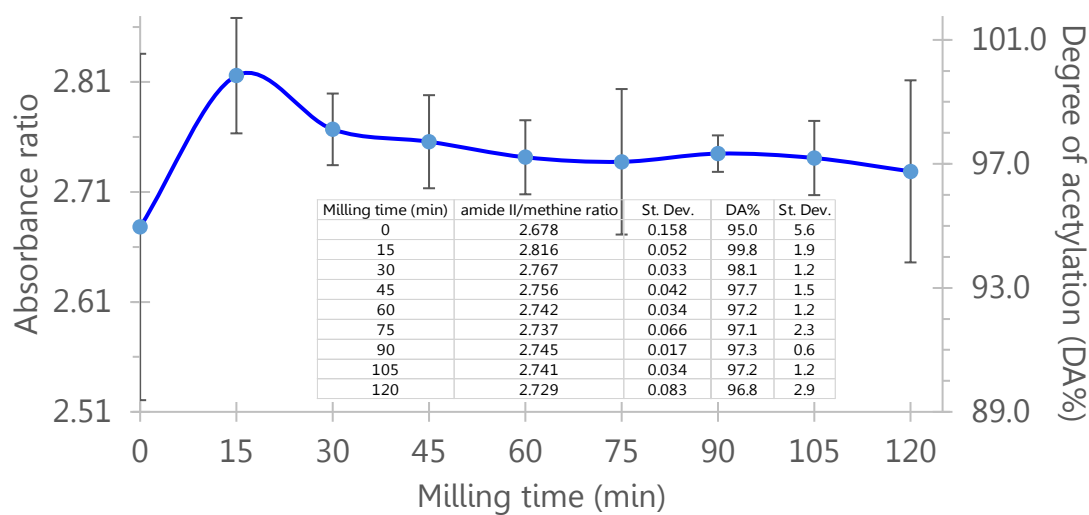


Figure 2-20: FT-IR data ($1552\text{ cm}^{-1}/2875\text{ cm}^{-1}$ peak ratio) and degree of acetylation (DA%) for milled α -chitin with $16 \times 0.25''$ balls (8.2 BtC). Figure A2-16 shows the relevant absorbance intensities for the 60 min sample ($0.0726 / 0.0265 = 2.740$).

2.3.5.3 Comparison with literature data

Unfortunately, none of the prior ball-milling studies of chitin (Table 2–1) attempted to investigate the possibility of amide hydrolysis upon ball milling using their obtained FT-IR spectra. Only a few qualitative results were presented with minimal discussion despite the fact that the 2008 review by Kasaai offers extensive coverage of the quantitative analysis potential of the infrared region of the electromagnetic spectrum.¹⁰⁴ Furthermore, and mysteriously for future mechanochemists, none of those groups have used any of the plethora of methods offered for DA approximation (including solution or solid-state NMR, titrimetric approaches, UV/Vis light).^{61,115,116} In contrast, and regardless of the quality of the reported results, it is worth citing that in 2012 Zhang et al. have attempted to correlate FT Raman with NMR spectroscopy for chitin DA determination.¹¹⁷ Stimulatingly for future green chemistry researchers, Aida et al. focused on reporting acetic acid yields (among other platform molecules of which none was nitrogen-containing) after a very high temperature water treatment (400 °C; in sequence to the initial ball milling step). Characterization of their possible chitosan by-product though was tactfully ignored (FT-IR and SEM observations), despite the fact that they have highlighted the material's medical applications (high value).³²

Similarly to the gaps in chitin literature, and paradoxically for the more studied polysaccharide of cellulose, a lack of characterization of its most idiosyncratic covalent bond (glycosidic linkage) applies for all five entries of Table 2–1. In entry

1, Zhao et al. have attributed the observed CrI reduction (and subsequent increase in hydrolysis rates) to just decreased intermolecular hydrogen bonding (CP/MAS ^{13}C solid-state NMR data on C4 peak areas between 79 and 92 ppm are associated with crystalline and non-crystalline fractions, not bonding regime of anomeric carbons).²⁵ A similar XRD/ ^{13}C solid-state NMR interpretation of amorphization is adopted also by Komanoya et al. (entry 4). Even though the authors highlight the importance of cellulose depolymerization as the rate-determining step towards mixtures of monosaccharides (sorbitol and mannitol), they take for granted that a noble metal catalyst is necessary to hydrolyze the glycosidic linkages.^{28,118} That approach might raise questions in the future on the basis of the twelve principles of green chemistry and elemental sustainability;¹¹⁹ much more with the ground that earth-abundant metal catalysis and organocatalysis are gaining in general.¹²⁰ Entry 5 by Wang et al. works with FT-IR peak height ratios, but only to track molecular changes of crystalline and amorphous (ball milled) cellulose during their pyrolytic treatment (temperatures $>240\text{ }^\circ\text{C}$).²⁹

It is only with entries 2 and 3 that a reduction in degree of polymerization (DP) is measured. In the latter study of Hu et al. (from 2014), kinematic viscosity measurements in copper ethylene diamine solution revealed that the 69% crystallinity reduction (CrI drops from 78.5 to 24.1%) of entry's 3 DP-237-cellulose (originating from 120 min of 375 rpm ball milling with 25% packing of a steel vessel) corresponds to a 46% decrease in DP (the 2 h milling sample has chains of ca. 128

glucose units).²⁷ Applying the same viscometric method, Zhang et al. tested a similar ball mill system (with 33% packing this time) and in their 2015 paper reported that the 1010 DP untreated cellulose (CrI 85.3%) was steadily degraded to ca. 645 DP (CrI 70.7%) after 2 h milling, representing a ca. 36% drop in the average length of the chains (entry 2).²⁶ Considering that both ball milling processes started from similar crystallinities (and equivalent packing), the fact that depolymerization of the longer chains of entry 2 lagged behind that of the shorter ones of entry 3 might be an indication of force propagation along the chains through deformation of all covalent bonds.

Likewise, the three chitin studies of Table 2–1 barely manage to qualitatively reference the glycosidic linkage. The only evidence for rupture of the bond under mechanochemical conditions is offered by Osada et al., who have used a gel permeation chromatography method (GPC), and reported a mean molecular weight (\overline{MW}) reduction of their chitin sample (from >760 kDa for untreated) to 407 kDa for the 10 min (68% CrI), and to 267 kDa for the 30 min (40% CrI) milling sample.³⁰ This reduction of CrI by 28 units arising from 20 min ball milling with the system of entry 6 of Table 2–1 (9% packing, 690 balls/g chitin) corresponds to a 34% reduction in \overline{MW} (from 407 to 267 kDa). That result from the Totani-Nikaido group can be compared with the 6% reduction in glycosidic linkage content in this thesis (1154 cm^{-1} /2875 cm^{-1} peak ratio drops from 1.388 to 1.307) for the 30-to-75 min milling period (45 min) of the 16 \times 0.25 balls system (see Figure 2–8), since the

CrI reduction is equivalent (from 67.5 to 38.8%). The almost 6 times faster depolymerization of entry 6 might be attributed to the higher BtC-ratio and packing (resulting intuitively in higher collision frequency), but also to a higher \overline{MW} chitin used in this work. The latter reason would probably result in the mean contact force to spend more of the milling time distributing along the chains.^{xiii} From a mechanochemistry point of view, it is worth mentioning that the process of the Totani-Nikaido group [Ichinoseki National College of Technology (Japan)] took place in a newly developed converge mill (comparable to the rotational motion of a planetary mill), which had a fixed guide vane inside the milling chamber. That unique characteristic might have intensified the mean impact force (compared to those in a regular planetary mill of the same operating frequency) which along with the high impact frequency offered from the 690 balls to chitin (BtC) mass ratio might have resulted in the reported interesting depolymerization rate (assuming lack of deacetylation).

2.3.6 Effect of milling on the solubility of α -chitin in water

To investigate the extent to which the observed reduction in glycosidic linkage content (and subsequent amorphization) corresponds to an increase in aqueous solubility, the ball-milled samples prepared with $16 \times 0.25''$ balls were subjected to solubility tests in water and dilute acetic acid (0.1 M/pH 2.9). The latter test

^{xiii} One can imagine a hypothetical situation of ball milling α -chitin's pentamer (MW = 1034 g/mol); the chains would have lost their hydrogen bonding network and glycosidic bonds a lot sooner than a chitin of MW in the order of MDa.

conditions were based on a proposal by G.A.F. Roberts¹²¹ and Kumirska et al.⁶¹ regarding chitin/chitosan classification (the latter being soluble in the acidity of that environment while the former not). The suspension was prepared at a concentration adjacent to the only chitin/water solubility test of Table 2-1 (entry's 8 ca. 33 mg/mL),³² which is roughly 3 times higher than that of the cellulose solubility tests by Meine et al.⁴¹ During initial experimentation, suspensions were stirred for 2 hours as suggested by Aida et al., but after 30 and 3 min tests the relative standard deviations (RSD%) for solubilities were realized not greater than 10%, hence a 1 min high speed vortex was found adequate (see data in Table A2-1). Since there was no clear trend observed in primary literature regarding the separation method for polysaccharide solubility tests in water (indicatively see the experimental procedures of the ball milling studies of Hick et al.⁴⁰ and Meine et al.⁴¹), centrifugation was selected because it was found more practical for triplicate tests compared to filtration.^{xliv}

^{xliv} The reader who might expect that the solubility of polysaccharides is a "hot" research area for the scientific (and in particular the chemistry) community will surely be disappointed (if not puzzled) by the relevant literature. When the terms "*saccharide*" (covering e.g. cyclomaltooligosaccharides) together with "solubility" were searched in the titles of articles available in SCOPUS, only 60 results were returned on 21/3/2018. With the breadth of information that the database covers, that poor figure is characteristic of the all-time lack of interest for the problems associated with the topic. Out of those 60 documents, only one review was identified, which focused on medical applications of polysaccharides rather than a fundamental understanding of their structure-solubility relationship (Title: Review on: Importance and methods of reduction of water solubility and swelling of natural polysaccharide polymer for colon specific drug delivery system) (122). It is at least a mystery that the "chemistry" term of "solubility" finds such lack of application to a class of compounds mentioned in surely more than 60 academic organic chemistry textbooks throughout the curriculums of the world (developed or not). That unfortunate situation might be related with an excessive focus on intellectualistic synthesis

In water, solubility increased steadily from 5.9% for native α -chitin ($t = 0$) to 11.0% for the $t = 120$ min sample with no error bar overlap between all samples presented in Figure 2–21. The almost doubling of the solubility lags to the 10-fold increase (from 3 to 35%) achieved by Aida et al. That can be justified by the significantly higher packing (28 vs 3%), as well as BtC mass ratio (24 vs 8) used in that study. MALDI-TOF MS evidence from that study (entry 8) suggests that the solubility can be attributed to chito-oligomers with $m/z < 2000$ (although results should be interpreted with caution as no experimental procedure was presented for the analytical method).³² The solubility of native α -chitin (5.9%) is mainly due to the significant moisture content (originally 5.5%) removal in the undissolved residue (see Section 2.2.3). Minor contributions to solubility can be attributed to the rotation speed limits of the regular centrifuge used, which at those particular suspension concentrations (>25 mg/mL) did not manage to pellet possible lower MW chitin, residual oligo-peptides and other impurities originating from the demineralization-deproteination-decoloration of the crab sample from ChitinWorks LLC. Considering the dimensions of the equipment (the radius from the rotor center to the bottom of the tube was not more than ca.15 cm), the 5000-rpm applied is estimated to have not exceeded a relative centrifugal force (RCF) of ca. $4200 \times g$.^{xiv}

(see the Cornforth perspective in the Introduction chapter), a permanent hypothermia of “solvent sense” (see mechanobiology narrative in Section 2.1.1), and the vicious circle of reproducibility problems which they create (123).

^{xiv} $RCF = 11.18 \times r \times \omega^2 / 10^5$, r : distance from the axis of rotation (cm), ω : rotation speed [revolutions per minute (rpm)] (124).

That value is lower than the $6650 \times g$ used for chitosan purification by Moura et al.,¹²⁵ and much lower than the $29,220 \times g$ used for the cellulose solubility tests by Meine et al.^{41, xlv} A contribution from residual minerals (or other impurities from shell isolation) to the soluble fraction should not be ignored in the future as the infrared signals showed some absorbance ca. 1430 cm^{-1} , which is characteristic for CaCO_3 .¹²⁶

In acid, solubility followed the same increasing trend only with higher values (an average of 0.83 solubility % units), which can be attributed to calcium acetate formation as well as the $2.3 \pm 1.0\%$ average degree of deacetylation of the set's samples (protonation of the amino groups leads to solvation of the chains).¹²⁷ Considering the higher differences of the 60-90-120 min samples (compared to 0 and 30 min), future researchers should set up experiments taking into account studies which report the possibility of protonation of the amide group of chitin/chitosan at pH values below 3.5.¹²⁸ As a reference experiment, a high-molecular-weight chitosan sample (DD 75–85%) was ball milled with $2 \times 0.5'' / 68\text{--}70 \times 0.25''$ balls for 4 h and resulted in a solubility of $98.0 \pm 0.9\%$ at pH 2.9 and $26.3 \pm 1.2\%$ at pH 7.0. This emphasizes the significant differences in solubility between chitin (i.e., acetylated biopolymer) and chitosan (i.e., deacetylated biopolymer) at acidic pHs and acts to confirm that the milled chitin has not increased

^{xlv} Future researchers might consider relative centrifugal forces (RCF) higher than $60,000 \times g$ (ultracentrifugation), which is a powerful method to study macromolecular structures in solution (124).

in solubility due to deacetylation. What is most important though is that the samples become clearly more soluble with increasing milling time, hence the FT-IR observation of loss of glycosidic linkages is complemented by a macroscopic confirmation.

Figure A2-17 shows UV-Vis spectra of the soluble products.^{xlvii} Peaks at ca. 273, ca. 292, and ca. 306 nm grow taller with increasing milling time, while absorbances of all signals fade out when they approach the visible region. In the violet region (380–435 nm), the products of 120 min milling present higher absorbances than the ones of the 30 min sample, producing the pale yellow-green color in the right vial of the photo in the inset. These results are likely due to Maillard-type reactions that occur between the amine groups and the reducing sugars formed to yield a range of intensely-pigmented substances (from small molecules like pyrazines to polymeric ones like melanoidins).

X-ray diffraction patterns of the insoluble residue from the pH 7.0 solubility tests are shown in Figure A2-18. Diffraction peaks at 2θ values are identical to those for α -chitin. The CrI values of this insoluble, residual material follow a decreasing trend ranging from 83.2% ($t = 30$ min) to 76.1% ($t = 120$ min) when compared to ca. 90% for untreated chitin. On the other hand, if one considers the crystallinity behavior of the whole ball milled sample (both water-soluble and water-insoluble fractions)

^{xlvii} UV-Vis spectra were acquired using an Ocean Optics USB4000 spectrometer at 420 nm. Integration time was 5000 μ sec, and signals were the average of 50 scans.

reported in Figure 2–8, it is evident that the shorter chains of α -chitin formed new hydrogen bonds after the solubility test, and recrystallized. Interestingly, the more depolymerized the sample, the higher the recrystallization effect. The sample of 120 min increased by 41.2 CrI units (from 34.9 to 76.1), that of 90 min by 40.2 (from 35.9 to 76.1), the one of 60 min by 31.5 (from 48.2 to 79.7), and 30 min milled chitin by 15.7 (from 67.5 to 83.2). Considering the range of useful products discussed in Section 1.5, that result might function as extra motivation for mechanochemists to design more efficient processes, as a more established market for water-soluble chitin products can drive a less developed one for water-insoluble ones (or vice versa).

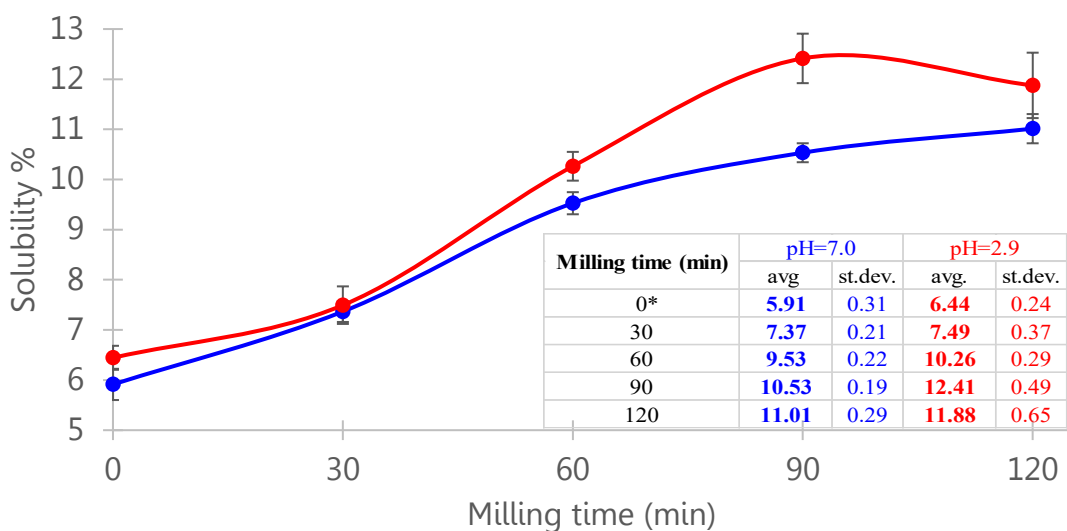


Figure 2-21: Solubility % of α -chitin at pH 2.9 (red) and 7.0 (blue) when ball milled with 16 \times 0.25" balls. * Solubility values for 0 min milling time correspond to α -chitin ball milled for 3 min with ca. 18% packing (reduced particle size was easier to weigh). When the flakes of native α -chitin were tested standard deviations for the solubility triplicates were large (at pH 7.0: 6.29 ± 1.39 , and at pH 2.9: 6.47 ± 2.16).

2.4 Conclusions

In this chapter, a rational selection of technological and process parameters of ball milling was undertaken in order to amorphize α -chitin in a controlled way. Using powder XRD, an 8.2 balls to chitin (BtC) mass ratio - 3.3% packing - steel vial/balls SPEX SamplePrep 8000M system was found to systematically amorphize the polysaccharide, which originally possessed a 91% crystallinity index (CrI). This way, a consistent crystallinity reduction was observed in regular milling time intervals (an average of 6.0 CrI units every 15 min) with good precision (± 2.5 CrI units). The higher collision frequency of 16 quarter-inch balls was more effective than the higher energy collisions of the 2 half-inch system in 120 min total milling time with the CrI reaching a plateau of ca. 35% in the former case while ca. 51% in the latter. Moreover, the effect of chitin mixing load [balls to chitin mass ratio (BtC)] was studied for both systems with results confirming that higher BtC ratios produce greater amorphization. The intensity ratio for XRD reflections (110)/(020) was rationalized as an experimental indicator for strength of α character for chitin [hydrogen bonding in the a -direction (creating the ac -sheets) in the extended structure] and was found to reduce with decreasing BtC mass ratio.

Particle size and morphology were studied with SEM. Ball milling was shown to reduce α -chitin particles from ca. $>500 \mu\text{m}$ to ca. $<100 \mu\text{m}$, smooth the rough edges of the particles and wrinkle (potentially defect or crack) the smooth surfaces of the native polysaccharide sample. A detailed FT-IR analysis revealed α -chitin's

qualitative characteristics. Several indications observed in the hydrogenic region revealed weakening of the hydrogen bonding network upon ball milling. These changes were quantified in the region of amide I and amide II vibrations (1670–1500 cm^{-1}). The ratio between absorbance intensities at 1621 and 1652 cm^{-1} decreased by 33% in the first 75 min of milling suggesting a declining relative number of doubly hydrogen-bonded amide groups. The behaviour of amide I peak was associated with that of amide II and was also found to correlate well with the corresponding gradual reduction of the crystallinity index (CrI%). All that experimental evidence raised the hypothesis that the average contact force applied to a chitin nanofibril during collisions is being directed from the hydrogen bonding region to the pyranose unit. That hypothesis was supported by direct evidence of depolymerization which was observed via a steady decline of the 1154 cm^{-1} /2875 cm^{-1} absorbance ratio during the whole period of 120 min ball milling. At the same time, degree of acetylation (DA) remained unchanged during ball milling ($97.7 \pm 1.1\%$) providing additional proof of *N*-acetyl's role in force distribution within α -chitin's nanofibril. Solubility tests have correlated the aforementioned depolymerization/amorphization evidence with an increase in aqueous solubility. All these interpreted results were discussed alongside the relevant literature and were found to fill in a significant gap in the area of chitin amorphization. Apart from comprising the basis of the following chapters, the work here offers a simple, rapid, and semiquantitative method for designing mechanochemical systems within the

scope of producing chitins (and other renewable resources) for a range of high-value applications like drug delivery and tissue engineering.^{129,130}

2.5 References

1. Vogel, V.; Sheetz, M. Local force and geometry sensing regulate cell functions. *Nat. Rev. Mol. Cell Biol.* **2006**, *7*, (4), 265-275.
2. Kung, C. A possible unifying principle for mechanosensation. *Nature* **2005**, *436*, (7051), 647-654.
3. Anishkin, A.; Loukin, S. H.; Teng, J.; Kung, C. Feeling the hidden mechanical forces in lipid bilayer is an original sense. *Proc. Natl. Acad. Sci. U. S. A.* **2014**, *111*, (22), 7898-7905.
4. Feng, W.; Lindner, H.; Robbins li, N. E.; Dinneny, J. R. Growing out of stress: The role of cell- and organ-scale growth control in plant water-stress responses. *Plant Cell* **2016**, *28*, (8), 1769-1782.
5. Haswell, E. S.; Verslues, P. E. The ongoing search for the molecular basis of plant osmosensing. *J. Gen. Physiol.* **2015**, *145*, (5), 389-394.
6. Chidanguro, T.; Weng, W.; Simon, Y. C. Chapter 1: Mechanochemistry: Inspiration from Biology. In *Mechanochemistry in Materials*, 1st ed.; Simon Y.C. and Craig S.L. ; Royal Society of Chemistry: Cambridge, UK, 2018; pp 1-35.
7. Granick, S.; Sung, C. B. Physical chemistry: Stressed molecules break down. *Nature* **2006**, *440*, (7081), 160-161.
8. Stauch, T.; Dreuw, A. Advances in Quantum Mechanochemistry: Electronic Structure Methods and Force Analysis. *Chem. Rev.* **2016**, *116*, (22), 14137-14180.
9. Cheng, P. -.; Pham, J. D.; Nowick, J. S. The supramolecular chemistry of β -sheets. *J. Am. Chem. Soc.* **2013**, *135*, (15), 5477-5492.
10. Xiao, S.; Stacklies, W.; Debes, C.; Gräter, F. Force distribution determines optimal length of β -sheet crystals for mechanical robustness. *Soft Matter* **2011**, *7*, (4), 1308-1311.
11. Deringer, V. L.; Englert, U.; Dronskowski, R. Nature, strength, and cooperativity of the hydrogen-bonding network in α -chitin. *Biomacromolecules* **2016**, *17*, (3), 996-1003.

12. Hermans, P. H.; Weidinger, A. Quantitative x-ray investigations on the crystallinity of cellulose fibers. A background analysis. *J. Appl. Phys.* **1948**, *19*, (5), 491-506.
13. Lin, N.; Huang, J.; Dufresne, A. Preparation, properties and applications of polysaccharide nanocrystals in advanced functional nanomaterials: a review. *Nanoscale* **2012**, *4*, (11), 3274-3294.
14. Salmon, S.; Hudson, S. M. Crystal Morphology, Biosynthesis, and Physical Assembly of Cellulose, Chitin, and Chitosan. *Journal of Macromolecular Science, Part C* **1997**, *37*, (2), 199-276.
15. Sugiyama, J.; Boisset, C.; Hashimoto, M.; Watanabe, T. Molecular directionality of β -chitin biosynthesis. *J. Mol. Biol.* **1999**, *286*, (1), 247-255.
16. Segal, L.; Creely, J. J.; Martin, A. E., Jr.; Conrad, C. M. An Empirical Method for Estimating the Degree of Crystallinity of Native Cellulose Using the X-Ray Diffractometer. *Text. Res. J.* **1959**, *29*, (10), 786-794.
17. Xu, F.; Shi, Y. -.; Wang, D. X-ray scattering studies of lignocellulosic biomass: A review. *Carbohydr. Polym.* **2013**, *94*, (2), 904-917.
18. Park, S.; Baker, J. O.; Himmel, M. E.; Parilla, P. A.; Johnson, D. K. Cellulose crystallinity index: Measurement techniques and their impact on interpreting cellulase performance. *Biotechnol. Biofuels* **2010**, *3*, article 10.
19. De Figueiredo, L. P.; Ferreira, F. F. The Rietveld Method as a Tool to Quantify the Amorphous Amount of Microcrystalline Cellulose. *J. Pharm. Sci.* **2014**, *103*, (5), 1394-1399.
20. French, A. D.; Santiago Cintrón, M. Cellulose polymorphy, crystallite size, and the Segal Crystallinity Index. *Cellulose* **2013**, *20*, (1), 583-588.
21. Lomovsky, O.; Bychkov, A.; Lomovsky, I. Mechanical Pretreatment. In *Biomass Fractionation Technologies for a Lignocellulosic Feedstock Based Biorefinery*, Elsevier Inc.: 2016; pp 23-55.
22. Zibareva, I. V. A review of information resources on nanoscience, nanotechnology, and nanomaterials. *Sci. Global Secur. Tech. Inf. Process.* **2015**, *42*, (2), 93-111.
23. Badia, G. Identifying "best bets" for searching in chemical engineering: Comparing database content and performance for information retrieval. *J. Doc.* **2018**, *74*, (1), 80-98.
24. Niel, G.; Boyrie, F.; Virieux, D. Chemical bibliographic databases: The influence of term indexing policies on topic searches. *New J. Chem.* **2015**, *39*, (11), 8807-8817.

25. Zhao, H.; Kwak, J. H.; Wang, Y.; Franz, J. A.; White, J. M.; Holladay, J. E. Effects of crystallinity on dilute acid hydrolysis of cellulose by cellulose ball-milling study. *Energy Fuels* **2006**, *20*, (2), 807-811.
26. Zhang, Y.; Li, Q.; Su, J.; Lin, Y.; Huang, Z.; Lu, Y.; Sun, G.; Yang, M.; Huang, A.; Hu, H.; Zhu, Y. A green and efficient technology for the degradation of cellulosic materials: Structure changes and enhanced enzymatic hydrolysis of natural cellulose pretreated by synergistic interaction of mechanical activation and metal salt. *Bioresour. Technol.* **2015**, *177*, 176-181.
27. Hu, H.; Zhang, Y.; Liu, X.; Huang, Z.; Chen, Y.; Yang, M.; Qin, X.; Feng, Z. Structural changes and enhanced accessibility of natural cellulose pretreated by mechanical activation. *Polym. Bull.* **2014**, *71*, (2), 453-464.
28. Komanoya, T.; Kobayashi, H.; Hara, K.; Chun, W. -.; Fukuoka, A. Kinetic study of catalytic conversion of cellulose to sugar alcohols under low-pressure hydrogen. *ChemCatChem* **2014**, *6*, (1), 230-236.
29. Wang, Z.; Pecha, B.; Westerhof, R. J. M.; Kersten, S. R. A.; Li, C. -.; McDonald, A. G.; Garcia-Perez, M. Effect of cellulose crystallinity on solid/liquid phase reactions responsible for the formation of carbonaceous residues during pyrolysis. *Ind. Eng. Chem. Res.* **2014**, *53*, (8), 2940-2955.
30. Osada, M.; Miura, C.; Nakagawa, Y. S.; Kaihara, M.; Nikaido, M.; Totani, K. Effects of supercritical water and mechanochemical grinding treatments on physicochemical properties of chitin. *Carbohydr. Polym.* **2013**, *92*, (2), 1573-1578.
31. Nakagawa, Y. S.; Eijsink, V. G. H.; Totani, K.; Vaaje-Kolstad, G. Conversion of α -chitin substrates with varying particle size and crystallinity reveals substrate preferences of the chitinases and lytic polysaccharide monooxygenase of *Serratia marcescens*. *J. Agric. Food Chem.* **2013**, *61*, (46), 11061-11066.
32. Aida, T. M.; Oshima, K.; Abe, C.; Maruta, R.; Iguchi, M.; Watanabe, M.; Smith Jr., R. L. Dissolution of mechanically milled chitin in high temperature water. *Carbohydr. Polym.* **2014**, *106*, (1), 172-178.
33. SPEX SamplePrep , 8000M Mixer/Mill® High-Energy Ball Mill, <https://www.spexsampleprep.com/8000M-mixermill>, (accessed 02/06, 2018).
34. Stolle, A. Technical implications of organic syntheses in ball mills. In *Ball Milling Towards Green Synthesis: Applications, Projects, Challenges*, 1st ed.; Ranu B. and Stolle A. ; Royal Society of Chemistry: Cambridge, UK, 2015; pp 241-276.
35. Prasad, D. V. N.; Theuerkauf, J. Effect of grinding media size and chamber length on grinding in a spex mixer mill. *Chem. Eng. Technol.* **2009**, *32*, (7), 1102-1106.

36. Chen, W.; Schoenitz, M.; Ward, T. S.; Dave, R. N.; Dreizin, E. L. Numerical simulation of mechanical alloying in a shaker mill by discrete element method. *KONA Powder Part. J.* **2005**, *23*, (March), 152-162.
37. Concas, A.; Lai, N.; Pisu, M.; Cao, G. Modelling of comminution processes in Spex Mixer/Mill. *Chem. Eng. Sci.* **2006**, *61*, (11), 3746-3760.
38. Santhanam, P. R.; Dreizin, E. L. Predicting conditions for scaled-up manufacturing of materials prepared by ball milling. *Powder Technol.* **2012**, *221*, 403-411.
39. Dreizin, E. L.; Schoenitz, M. Mechanochemically prepared reactive and energetic materials: a review. *J. Mater. Sci.* **2017**, *52*, (20), 11789-11809.
40. Hick, S. M.; Griebel, C.; Restrepo, D. T.; Truitt, J. H.; Buker, E. J.; Bylda, C.; Blair, R. G. Mechanocatalysis for biomass-derived chemicals and fuels. *Green Chem.* **2010**, *12*, (3), 468-474.
41. Meine, N.; Rinaldi, R.; Schüth, F. Solvent-Free catalytic depolymerization of cellulose to water-soluble oligosaccharides. *ChemSusChem* **2012**, *5*, (8), 1449-1454.
42. Blair, R. G.; Chagoya, K.; Biltek, S.; Jackson, S.; Sinclair, A.; Taraboletti, A.; Restrepo, D. T. The scalability in the mechanochemical syntheses of edge functionalized graphene materials and biomass-derived chemicals. *Faraday Discuss.* **2014**, *170*, 223-233.
43. Maini; Halasz; Takacs; James; Belenguer; Frišćic; Jones; Stolle; Boldyreva; Blair; Galembeck; Suslick; Margoutidis; Mack; Jörres; Nagapudi; Beyer; Brekalo; Lamaty; Irikura; Khripin; Hamilton; Zhang Mechanistic understanding, catalysis and scaling up of mechanochemistry: General discussion. *Faraday Discuss.* **2014**, *170*, 287-310.
44. Fischer, F.; Fendel, N.; Greiser, S.; Rademann, K.; Emmerling, F. Impact Is Important - Systematic Investigation of the Influence of Milling Balls in Mechanochemical Reactions. *Org. Process Res. Dev.* **2017**, *21*, (4), 655-659.
45. Takacs, L.; McHenry, J. S. Temperature of the milling balls in shaker and planetary mills. *J. Mater. Sci.* **2006**, *41*, (16), 5246-5249.
46. Focher, B.; Beltrame, P. L.; Naggi, A.; Torri, G. Alkaline N-deacetylation of chitin enhanced by flash treatments. Reaction kinetics and structure modifications. *Carbohydr. Polym.* **1990**, *12*, (4), 405-418.
47. Minke, R.; Blackwell, J. The structure of α -chitin. *J. Mol. Biol.* **1978**, *120*, (2), 167-181.
48. Paralikar, K. M.; Balasubramanya, R. H. Electron diffraction study of alpha -chitin. *J. Polym. Sci. Polym. Lett. Ed.* **1984**, *22*, (10), 543-546.

49. Jaworska, M.; Sakurai, K.; Gaudon, P.; Guibal, E. Influence of chitosan characteristics on polymer properties. I: Crystallographic properties. *Polym. Int.* **2003**, *52*, (2), 198-205.
50. Jang, M. -.; Kong, B. -.; Jeong, Y. -.; Lee, C. H.; Nah, J. -. Physicochemical characterization of α -chitin, β -chitin, and γ -chitin separated from natural resources. *J. Polym. Sci. Part A* **2004**, *42*, (14), 3423-3432.
51. Nakagawa, Y. S.; Oyama, Y.; Kon, N.; Nikaido, M.; Tanno, K.; Kogawa, J.; Inomata, S.; Masui, A.; Yamamura, A.; Kawaguchi, M.; Matahira, Y.; Totani, K. Development of innovative technologies to decrease the environmental burdens associated with using chitin as a biomass resource: Mechanochemical grinding and enzymatic degradation. *Carbohydr. Polym.* **2011**, *83*, (4), 1843-1849.
52. Zhang, Y.; Xue, C.; Li, Z.; Zhang, Y.; Fu, X. Preparation of half-deacetylated chitosan by forced penetration and its properties. *Carbohydr. Polym.* **2006**, *65*, (3), 229-234.
53. Zhang, Y.; Xue, C.; Xue, Y.; Gao, R.; Zhang, X. Determination of the degree of deacetylation of chitin and chitosan by X-ray powder diffraction. *Carbohydr. Res.* **2005**, *340*, (11), 1914-1917.
54. Hajji, S.; Younes, I.; Ghorbel-Bellaaj, O.; Hajji, R.; Rinaudo, M.; Nasri, M.; Jellouli, K. Structural differences between chitin and chitosan extracted from three different marine sources. *Int. J. Biol. Macromol.* **2014**, *65*, 298-306.
55. Atkins, E. Conformations in polysaccharides and complex carbohydrates. *J. Biosci.* **1985**, *8*, (1-2), 375-387.
56. Cho, Y. -.; Jang, J.; Park, C. R.; Ko, S. -. Preparation and solubility in acid and water of partially deacetylated chitins. *Biomacromolecules* **2000**, *1*, (4), 609-614.
57. Cárdenas, G.; Cabrera, G.; Taboada, E.; Miranda, S. P. Chitin characterization by SEM, FTIR, XRD, and ^{13}C cross polarization/mass angle spinning NMR. *J. Appl. Polym. Sci.* **2004**, *93*, (4), 1876-1885.
58. Hajji, S.; Younes, I.; Ghorbel-Bellaaj, O.; Hajji, R.; Rinaudo, M.; Nasri, M.; Jellouli, K. Structural differences between chitin and chitosan extracted from three different marine sources. *Int. J. Biol. Macromol.* **2014**, *65*, 298-306.
59. Zhang, W.; Zhang, J.; Xia, W. Effect of ball-milling treatment on physicochemical and structural properties of chitosan. *Int. J. Food Prop.* **2014**, *17*, (1), 26-37.
60. Cervera, M. F.; Heinämäki, J.; Räsänen, M.; Maunu, S. L.; Karjalainen, M.; Acosta, O. M. N.; Colarte, A. I.; Yliruusi, J. Solid-state characterization of chitosans derived from lobster chitin. *Carbohydr. Polym.* **2004**, *58*, (4), 401-408.

61. Kumirska, J.; Czerwicka, M.; Kaczyński, Z.; Bychowska, A.; Brzozowski, K.; Thöming, J.; Stepnowski, P. Application of spectroscopic methods for structural analysis of chitin and chitosan. *Mar. Drugs* **2010**, *8*, (5), 1567-1636.
62. Liu, T.; Li, B.; Zheng, X.; Liang, S.; Song, X.; Zhu, B.; Kennedy, J. F.; Xia, J. Effects of freezing on the condensed state structure of chitin in alkaline solution. *Carbohydr. Polym.* **2010**, *82*, (3), 753-760.
63. Osada, M.; Miura, C.; Nakagawa, Y. S.; Kaihara, M.; Nikaido, M.; Totani, K. Effect of sub- and supercritical water pretreatment on enzymatic degradation of chitin. *Carbohydr. Polym.* **2012**, *88*, (1), 308-312.
64. Zhang, H.; Jin, Y.; Deng, Y.; Wang, D.; Zhao, Y. Production of chitin from shrimp shell powders using *Serratia marcescens* B742 and *Lactobacillus plantarum* ATCC 8014 successive two-step fermentation. *Carbohydr. Res.* **2012**, *362*, 13-20.
65. Kaya, M.; Baran, T.; Mentés, A.; Asaroglu, M.; Sezen, G.; Tozak, K. O. Extraction and Characterization of α -Chitin and Chitosan from Six Different Aquatic Invertebrates. *Food Biophys.* **2014**, *9*, (2), 145-157.
66. Harris, D. C. Sample Preparation. In *Quantitative Chemical Analysis*, 7th ed.; W. H. Freeman and Company: New York, 2007; pp 644-663.
67. Chinga-Carrasco, G. Cellulose fibres, nanofibrils and microfibrils: The morphological sequence of MFC components from a plant physiology and fibre technology point of view. *Nanoscale Res. Lett.* **2011**, *6*, 1-7.
68. Yudin, V. E.; Dobrovolskaya, I. P.; Neelov, I. M.; Dresvyanina, E. N.; Popryadukhin, P. V.; Ivan'kova, E. M.; Elokhovskii, V. Y.; Kasatkin, I. A.; Okrugin, B. M.; Morganti, P. Wet spinning of fibers made of chitosan and chitin nanofibrils. *Carbohydr. Polym.* **2014**, *108*, (1), 176-182.
69. Dobrovol'skaya, I. P.; Kasatkin, I. A.; Yudin, V. E.; Ivan'kova, E. M.; Elokhovskii, V. Y. Supramolecular structure of chitin nanofibrils. *Polym. Sci. Ser. A* **2015**, *57*, (1), 52-57.
70. Paparcone, R.; Buehler, M. J. Failure of A β (1-40) amyloid fibrils under tensile loading. *Biomaterials* **2011**, *32*, (13), 3367-3374.
71. Beckham, G. T.; Crowley, M. F. Examination of the α -chitin structure and decrystallization thermodynamics at the nanoscale. *J. Phys. Chem. B* **2011**, *115*, (15), 4516-4522.
72. Petrov, M.; Lymperakis, L.; Friák, M.; Neugebauer, J. Ab Initio Based conformational study of the crystalline α -chitin. *Biopolymers* **2013**, *99*, 22-34.

73. Zeiss, H. H.; Tsutsui, M. The Carbon-Oxygen Absorption Band in the Infrared Spectra of Alcohols. *J. Am. Chem. Soc.* **1953**, *75*, (4), 897-900.
74. Colthup, N. B.; Daly, L. H.; Wiberley, S. E. Chapter 10 - ethers, alcohols, and phenols. In *Introduction to Infrared and Raman Spectroscopy*, 3rd ed.; Academic Press: San Diego, 1990; pp 327-337.
75. Fraser, R. D.; Price, W. C. Infra-red dichroism and protein structure. *Nature* **1952**, *170*, (4325), 490-491.
76. Miyazawa, T.; Shimanouchi, T.; Muzushima, S. -. Normal vibrations of *N*-methylacetamide. *J. Chem. Phys.* **1958**, *29*, (3), 611-616.
77. Pearson, F. G.; Marchessault, R. H.; Liang, C. Y. Infrared spectra of crystalline polysaccharides. V. Chitin. *J. Polym. Sci.* **1960**, *43*, (141), 101-116.
78. Yamaguchi, Y.; Nge, T. T.; Takemura, A.; Hori, N.; Ono, H. Characterization of uniaxially aligned chitin film by 2D FT-IR spectroscopy. *Biomacromolecules* **2005**, *6*, (4), 1941-1947.
79. Sikorski, P.; Hori, R.; Wada, M. Revisit of α -chitin crystal structure using high resolution X-ray diffraction data. *Biomacromolecules* **2009**, *10*, (5), 1100-1105.
80. Lu, Y.; Sun, Q.; She, X.; Xia, Y.; Liu, Y.; Li, J.; Yang, D. Fabrication and characterisation of α -chitin nanofibers and highly transparent chitin films by pulsed ultrasonication. *Carbohydr. Polym.* **2013**, *98*, (2), 1497-1504.
81. Focher, B.; Naggi, A.; Torri, G.; Cosani, A.; Terbojevich, M. Structural differences between chitin polymorphs and their precipitates from solutions-evidence from CP-MAS ^{13}C -NMR, FT-IR and FT-Raman spectroscopy. *Carbohydr. Polym.* **1992**, *17*, (2), 97-102.
82. Ogawa, Y.; Lee, C. M.; Nishiyama, Y.; Kim, S. H. Absence of sum frequency generation in support of orthorhombic symmetry of α -chitin. *Macromolecules* **2016**, *49*, (18), 7025-7031.
83. Sutherland, G. B. B. M. Infrared Analysis of the Structure of Amino Acids, Polypeptides and Proteins. *Adv. Protein Chem.* **1952**, *7*, 291-318.
84. Colthup, N. B.; Daly, L. H.; Wiberley, S. E. Chapter 9 - Carbonyl compounds. In *Introduction to Infrared and Raman Spectroscopy*, 3rd ed.; Academic Press: San Diego, 1990; pp 289-325.
85. Miyazawa, T. Infrared Studies of the Conformations of Polypeptides and Proteins. In *Aspects of Protein Structure: Proceedings of a Symposium held in Madras 14-18*

January 1963 and organized by the University of Madras, Ramachandran, G. N. ; Academic Press: London, New York, 1963; pp 257.

86. Naumann, D.; Barnickel, G.; Bradaczek, H.; Labischinski, H.; Giesbrecht, P. Infrared Spectroscopy, a Tool for Probing Bacterial Peptidoglycan: Potentialities of Infrared Spectroscopy for Cell Wall Analytical Studies and Rejection of Models Based on Crystalline Chitin. *Eur. J. Biochem.* **1982**, *125*, (3), 505-515.
87. Miyazawa, T. The characteristic band of secondary amides at 3100 cm⁻¹. *J. Mol. Spectrosc.* **1960**, *4*, (1), 168-172.
88. Edler, J.; Hamm, P. Spectral response of crystalline acetanilide and N-methylacetamide: Vibrational self-trapping in hydrogen-bonded crystals. *Phys. Rev. B Condens. Matter Mater. Phys.* **2004**, *69*, (21), 214301-1-214301-8.
89. Pearson, F. G.; Marchessault, R. H.; Liang, C. Y. Infrared spectra of crystalline polysaccharides. V. Chitin. *J. Polym. Sci.* **1960**, *43*, (141), 101-116.
90. Brown, A. H.; Walsh, T. R. Elucidating the influence of polymorph-dependent interfacial solvent structuring at chitin surfaces. *Carbohydr. Polym.* **2016**, *151*, 916-925.
91. Brovchenko, I.; Oleinikova, A. 7 - Water in low-hydrated biosystems. In *Interfacial and Confined Water*, 1st ed.; Elsevier: Amsterdam, 2008; pp 165-214.
92. Venyaminov, S. Y.; Prendergast, F. G. Water (H₂O and D₂O) Molar Absorptivity in the 1000–4000 cm⁻¹ Range and Quantitative Infrared Spectroscopy of Aqueous Solutions. *Anal. Biochem.* **1997**, *248*, 234-245.
93. Larkin, P. Chapter 3 - Instrumentation and Sampling Methods. In *Infrared and Raman Spectroscopy*, 1st ed.; Elsevier: Oxford, 2011; pp 27-54.
94. Colthup, N. B.; Daly, L. H.; Wiberley, S. E. Chapter 2 - IR experimental considerations. In *Introduction to Infrared and Raman Spectroscopy*, 3rd ed.; Academic Press: San Diego, 1990; pp 75-107.
95. Max, J. -.; Chapados, C. Isotope effects in liquid water by infrared spectroscopy. III. H₂O and D₂O spectra from 6000 to 0 cm⁻¹. *J. Chem. Phys.* **2009**, *131*, (18), article 184505.
96. Gow, N. A. R.; Gooday, G. W.; Russell, J. D.; Wilson, M. J. Infrared and X-ray diffraction data on chitins of variable structure. *Carbohydr. Res.* **1987**, *165*, (1), 105-110.
97. Rinaudo, M. Chitin and chitosan: Properties and applications. *Prog. Polym. Sci.* **2006**, *31*, (7), 603-632.

98. Clausen-Schaumann, H.; Seitz, M.; Krautbauer, R.; Gaub, H. E. Force spectroscopy with single bio-molecules. *Curr. Opin. Chem. Biol.* **2000**, *4*, 524-530.
99. Beyer, M. K.; Clausen-Schaumann, H. Mechanochemistry: The mechanical activation of covalent bonds. *Chem. Rev.* **2005**, *105*, (8), 2921-2948.
100. Caruso, M. M.; Davis, D. A.; Shen, Q.; Odom, S. A.; Sottos, N. R.; White, S. R.; Moore, J. S. Mechanically-induced chemical changes in polymeric materials. *Chem. Rev.* **2009**, *109*, (11), 5755-5798.
101. Mayes, H. B.; Broadbelt, L. J.; Beckham, G. T. How sugars pucker: Electronic structure calculations map the kinetic landscape of five biologically paramount monosaccharides and their implications for enzymatic catalysis. *J. Am. Chem. Soc.* **2014**, *136*, (3), 1008-1022.
102. Sannan, T.; Kurita, K.; Ogura, K.; Iwakura, Y. Studies on chitin: 7. I.r. spectroscopic determination of degree of deacetylation. *Polymer* **1978**, *19*, 458-459.
103. Van De Velde, K.; Kiekens, P. Structure analysis and degree of substitution of chitin, chitosan and dibutylchitin by FT-IR spectroscopy and solid state ¹³C NMR. *Carbohydr. Polym.* **2004**, *58*, (4), 409-416.
104. Kasaai, M. R. A review of several reported procedures to determine the degree of N-acetylation for chitin and chitosan using infrared spectroscopy. *Carbohydr. Polym.* **2008**, *71*, (4), 497-508.
105. Sannan, T.; Kurita, K.; Iwakura, Y. Studies on chitin, 1. Solubility change by alkaline treatment and film casting. *Die Makromolekulare Chemie* **1975**, *176*, (4), 1191-1195.
106. Sannan, T.; Kurita, K.; Iwakura, Y. Studies on chitin, 2. Effect of deacetylation on solubility. *Die Makromolekulare Chemie* **1976**, *177*, (12), 3589-3600.
107. Kurita, K.; Sannan, T.; Iwakura, Y. Studies on chitin, 3. Preparation of pure chitin, poly(N-acetyl-D-glucosamine), from the water-soluble chitin. *Die Makromolekulare Chemie* **1977**, *178*, (9), 2595-2602.
108. Kurita, K.; Sannan, T.; Iwakura, Y. Studies on chitin, 4. Evidence for formation of block and random copolymers of N-acetyl-D-glucosamine and D-glucosamine by hetero- and homogeneous hydrolyses. *Die Makromolekulare Chemie* **1977**, *178*, (12), 3197-3202.
109. Sannan, T.; Kurita, K.; Iwakura, Y. Studies on Chitin. V. Kinetics of Deacetylation Reaction. *Polym. J.* **1977**, *9*, 649.
110. Kurita, K.; Sannan, T.; Iwakura, Y. Studies on chitin. VI. Binding of metal cations. *J. Appl. Polym. Sci.* **1979**, *23*, (2), 511-515.

111. Kurita, K. Controlled functionalization of the polysaccharide chitin. *Prog. Polym. Sci.* **2001**, *26*, (9), 1921-1971.
112. Kurita, K. Chitin and chitosan: Functional biopolymers from marine crustaceans. *Mar. Biotechnol.* **2006**, *8*, (3), 203-226.
113. Ishimaru, M.; Nagatsuka, M.; Masubuchi, A.; Okazaki, J. -; Kurita, K. Cellulose-chitin hybrids: Synthesis of branched amino polysaccharides by regioselective introduction of (N-acetyl)-d-glucosamine branches into cellulose. *Polym. Bull.* **2014**, *71*, (2), 301-313.
114. Beil, S.; Schamberger, A.; Naumann, W.; MacHill, S.; Van Pée, K. -. Determination of the degree of N-acetylation (DA) of chitin and chitosan in the presence of water by first derivative ATR FTIR spectroscopy. *Carbohydr. Polym.* **2012**, *87*, (1), 117-122.
115. Czechowska-Biskup, R.; Jarosinska, D.; Rokita, B.; Ulanski, P.; Rosiak, J. M. Determination of degree of deacetylation of chitosan - Comparison of methods. *Prog. Chem. Appl. Chitin Deriv.* **2012**, *XVII*, 5-20.
116. Khan, T. A.; Peh, K. K.; Ch'ng, H. S. Reporting degree of deacetylation values of chitosan: The influence of analytical methods. *J. Pharm. Pharm. Sci.* **2002**, *5*, (3), 205-212.
117. Zhang, K.; Geissler, A.; Fischer, S.; Brendler, E.; Bäücker, E. Solid-state spectroscopic characterization of α -chitins deacetylated in homogeneous solutions. *J. Phys. Chem. B* **2012**, *116*, (15), 4584-4592.
118. Kobayashi, H.; Ito, Y.; Komanoya, T.; Hosaka, Y.; Dhepe, P. L.; Kasai, K.; Hara, K.; Fukuoka, A. Synthesis of sugar alcohols by hydrolytic hydrogenation of cellulose over supported metal catalysts. *Green Chem.* **2011**, *13*, (2), 326-333.
119. Hunt, A. J. The importance of elemental sustainability and critical element recovery for the pharmaceutical industry. In *Green and Sustainable Medicinal Chemistry: Methods, Tools and Strategies for the 21st Century Pharmaceutical Industry*, Jones, L. C., Sneddon, H. F., Summerton, L., Clark, J. H., Eds. ; Royal Society of Chemistry: Cambridge, UK, 2016; pp 54-62.
120. Constable, D. J. C. Reaction: Sustainable Catalysis without Metals. *Chem* **2017**, *2*, 446-447.
121. Roberts, G. A. F. Thirty Years of Progress in Chitin and Chitosan. *Progress in the Chemistry and Application of Chitin and its Derivatives* **2008**, *XIII*, 7-15.
122. Patil, A. D.; Patil, S. V.; Salunkhe, K. S.; Chaudhari, S. R. Review on: Importance and methods of reduction of water solubility and swelling of natural polysaccharide

- polymer for colon specific drug delivery system. *Res. J. Pharm. Technol.* **2013**, *6*, (5), 447-453.
123. Baker, M. Reproducibility: Check your chemistry. *Nature* **2017**, *548*, (7668), 485-488.
124. Frei, M. Centrifugation basics. *Sigma-Aldrich Biofiles* **2011**, *6*, (5), 4-5.
125. Moura, C. M. D.; Moura, J. M. D.; Soares, N. M.; Pinto, L. A. D. A. Evaluation of molar weight and deacetylation degree of chitosan during chitin deacetylation reaction: Used to produce biofilm. *Chem. Eng. Process. : Process Intensif.* **2011**, *50*, (4), 351-355.
126. Miller, F. A.; Wilkins, C. H. Infrared Spectra and Characteristic Frequencies of Inorganic Ions. *Anal. Chem.* **1952**, *24*, (8), 1253-1294.
127. Sogias, I. A.; Khutoryanskiy, V. V.; Williams, A. C. Exploring the factors affecting the solubility of chitosan in water. *Macromol. Chem. Phys.* **2010**, *211*, (4), 426-433.
128. Roberts, G. A. F. Chemical Behaviour of Chitin and Chitosan. In *Chitin Chemistry*, 1st ed.; Macmillan Press Ltd: London, 1992; pp 203-273.
129. Shen, X.; Shamshina, J. L.; Berton, P.; Gurau, G.; Rogers, R. D. Hydrogels based on cellulose and chitin: Fabrication, properties, and applications. *Green Chem.* **2015**, *18*, (1), 53-75.
130. Courtenay, J. C.; Johns, M. A.; Galembeck, F.; Deneke, C.; Lanzoni, E. M.; Costa, C. A.; Scott, J. L.; Sharma, R. I. Surface modified cellulose scaffolds for tissue engineering. *Cellulose* **2017**, *24*, (1), 253-267.

Chapter 3 Mechanochemical conversion of α -chitin to oligomers of *N*-acetyl-D-glucosamine

3.1 Introduction

3.1.1 Relevant ball milling methods in polysaccharide literature

Aiming for water soluble depolymerization products, Hick et al. were the first who systematically explored ball milling parameters for polysaccharide transformations.¹ The researchers tried different solid catalysts [1:1 mixture with microcrystalline cellulose, which typically has a DP of not more than 400²] using a shaker mill (5% packing of the vial, 3 balls per g of cellulose, run at 1060 rpm), an attrition mill (41% packing, 29 balls per g of cellulose, 350 rpm), and a rolling mill (23% packing, 25 balls per g of cellulose, 100 rpm). All three vial-balls systems were made from steel (assumed of equivalent hardness) and were estimated to give 9-10 impacts every 10 s with the forces developed in the rolling mill being an order of magnitude less than the other two (approx. 100 N vs. 1000 N). Despite the high percentages of packing, the attrition and rolling mills gave non-appreciable conversions of microcrystalline cellulose into water soluble products, hence the results presented for the efficiencies of more than ten solid catalysts were obtained with the relatively high-energy shaker mill (SPEX 8000D Mixer/Mill). Materials with high surface acidities like kaolinite ($\text{Al}_2\text{Si}_2\text{O}_7 \cdot 2\text{H}_2\text{O}$), alumina super acid, aluminium phosphate (AlPO_4), alumina (Al_2O_3), Y-type zeolite, and bentonite ($\text{Al}_2\text{Si}_4\text{O}_{11} \cdot \text{H}_2\text{O}$) presented satisfactory catalytic performance with kaolinite reaching as high as

approx. 65% soluble products in 2 h. Solids like talc [$\text{H}_2\text{Mg}_3(\text{SiO}_3)_4$], vermiculite [$(\text{MgFe,Al})_3(\text{Al,Si})_4\text{O}_{10}(\text{OH})_2 \cdot 4\text{H}_2\text{O}$], quartz (SiO_2), and silicon carbide (SiC), which are of low acidity, did not exceed 30% solubilization in the same milling time. The efficiency of the milling process was not affected by the catalyst hardness.^{1xlviii}

The observed effectiveness of kaolinite has been attributed to its layered structure.¹

This natural clay is a hydrated aluminosilicate comprised of layers of octahedrally $\text{Al}(\text{OH})_4$ sheets covalently bound to tetrahedrally SiO_4 sheets in a 1:1 ratio.^{1,3} When protons from the hydroxyl groups of the $\text{Al}(\text{OH})_4$ sheet form hydrogen bonds with open Si–O–Si sites the layers are bound together to form the particles of kaolinite.^{1,3}

The aluminium-containing sheet in bentonite, which is structurally similar to kaolinite, is covalently bonded above and below with a silicon-containing sheet in a 2:1 configuration. Hence, the active sites are not so free to interact with cellulose, explaining partly why bentonite did not exceed 20% cellulose solubilization in the same milling time.¹

Further advances in mechanically assisted depolymerization of cellulose appeared after 2012 with Meine et al., who managed to fully convert α -cellulose into water-soluble products (oligosaccharides) in 2 h.⁴ The quantitative yields were obtained when α -cellulose (DP 2200) was impregnated with strong acids like HCl and H_2SO_4 (0.61 and 0.44 mmol per g of substrate respectively), and ball milled in a planetary

^{xlviii} Based on the results and discussion of Hick et al., the possibility of kaolinite (and other solid acid catalysts) to assist the amorphization/depolymerization of polysaccharides in a physical way is considered negligible.

steel system [21% packing, 5 balls (total mass $5 \times 3.95 = 19.75$ g) per g of acid-impregnated cellulose, 800 rpm].⁴ This successful approach of acidulated cellulose was also applied by Shrotri et al.⁵ Their group found that complete solubility of Sigma-Aldrich's Sigmacell 20 microcrystalline cellulose (DP approx. 200) was achieved with 0.25 mmol H₂SO₄/g impregnation, and ball milling in a planetary system (10 g of balls per g of acidulated substrate, 300 rpm) for 10 h. An average degree of polymerization of 6–9 for those soluble oligomers was determined. Interestingly, during the milling process, α -(1→6) linkages were formed (branched oligomers) which explain the higher solubility of larger oligosaccharides and suggest repolymerization of cellulose monomers.⁵

3.1.2 Mechanistic considerations

In all the above systems, cellulose gave very low yields of water-soluble products when ball milled by itself (without the presence of the acidic material). Indicatively, Meine et al. reported only 10% solubilization after a 10 h treatment in their relatively high speed and high packing planetary system.⁴ These experimental observations imply the necessity for strong acids (either in the liquid or solid state) to hydrolyze the glycosidic bond. Indeed, a density-functional theory (DFT) study on cellobiose (assumed analogous to cellulose) has realised that the basicity of the glycosidic oxygen (especially for the axial position of the lone pairs) is generally lacking compared to the surrounding hydroxyl and pyranic oxygens.⁶ Calculations for the relative Gibbs energy of protonation on both of the cellobiose conformers that

randomly occur in the most common polymorph of native cellulose (I_{β}) (as well as on two hypothetical conformers that were generated with rotations of the hydroxymethyl group of the most common of the two “native” conformers) have clearly demonstrated that the primary alcohol group in particular is the most basic of all sites.^{xlix} Moreover, when an explicit water molecule was present, the proton from the protonated cellobiose site was always dissociating and binding to water.

These computational insights highlight the requirement for strong acids in cellulose depolymerization, with which the selective protonation of the hydroxyl sites can be surmount. In mechanistic terms, Loerbroks et al. realized that when the most common of the two “native” cellobiose conformers gets its glycosidic oxygen [O(1)] protonated axially, a cooperativity of the exo-anomeric ($n_{O(1)} \rightarrow \sigma^*_{C(1)O(5)}$)⁷ and endo-anomeric ($n_{O(5)} \rightarrow \sigma^*_{C(1)O(1)}$) effect (mitigation of the exo-anomeric effect and enhancement of the endo-anomeric effect) is responsible for an approximate 7% elongation of the C(1)-O(1) bond [(C1) is the anomeric carbon], and to favourable bond dissociation. In addition, it has been calculated that the 8.5 kcal/mol stabilization that the intramolecular O(5) \cdots HO(3') hydrogen bond offers to that “native” conformer drops to 0.8 kcal/mol. Overall, and using solvation models as

^{xlix} With the liberation of the primary alcohol group from its natural constraints (hydrogen bonding regime) during ball milling (observed amide I split IR ratio decrease in Figure 2–16), competition for protons in our ball milled chitin samples is expected to slow down hydrolysis in acidic conditions.

well, the authors found that the protonation accounts for about 90% of the approximately 31 kcal mol^{-1} activation energy of cellobiose hydrolysis.^{6,8}

However, the above computational analysis results do not mean that acid impregnation alone can lead to appreciable levels of hydrolysis. When cellulose was left to impregnate with H_2SO_4 for 7 days, its solubility reached only 8%.⁹ Moreover, a darkening of the acid impregnated cellulose has been observed over time, providing evidence for carbonization instead of depolymerization.⁸ Indeed, the remaining 10% for the activation of the glycosidic linkage (approx. 3.0 kcal/mol) has been attributed to necessary conformational changes of one of the pyranic rings of cellobiose (from chair to half-chair) which further enhance an endo-anomeric charge transfer.^{6,8} That structural distortion of the protonated conformer results also in the complete loss of the aforementioned 0.8 kcal/mol stabilization from the $\text{O}(5) \cdots \text{HO}(3')$ hydrogen bond, resulting in a more favourable cleavage of the $\text{C}(1)\text{-O}(1)$ bond.⁶ Figure 3-1 illustrates the most important mechanistic considerations proposed towards the mechanocatalytic cellobiose/cellulose hydrolysis.

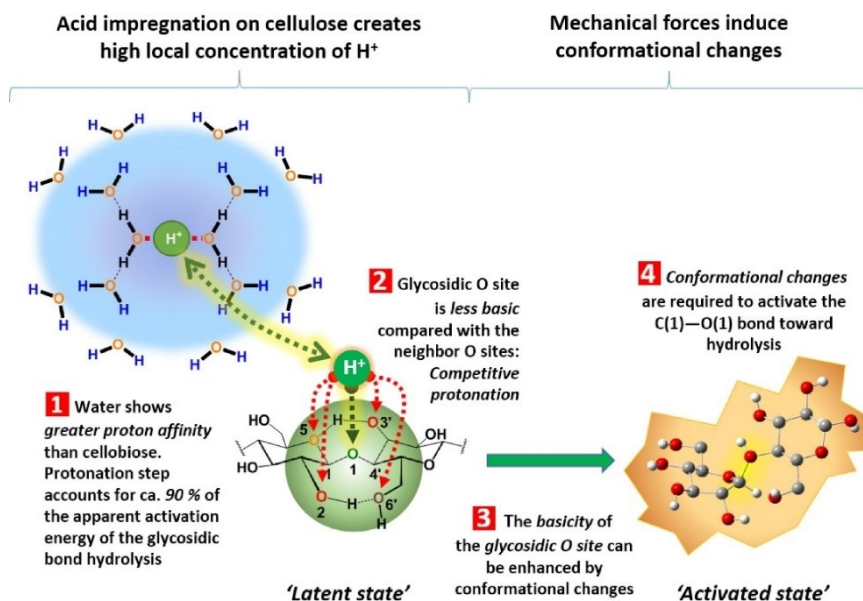


Figure 3-1: Proposed mechanistic considerations towards mechanochemical activation of the glycosidic linkage in cellobiose/cellulose. Reprinted from *Catalysis Today*, 234, F. Schüth, R. Rinaldi, N. Meine, M. Kåldström, J. Hilgert, M.D. Kaufman Rechulski, Mechanochemical depolymerization of cellulose and raw biomass and downstream processing of the products, 24-30, Copyright (2014), with permission from Elsevier.

3.1.3 Summary and methodological approach to the problem

One can conclude that, although literature provides a molecular mechanism which justifies the experimental trend for the use of acidic media during mechanochemical depolymerization of cellulose, on the other hand it underestimates the factor of collision frequency. By ignoring the effects of vial-packing and balls-to-cellulose mass ratio, the above studies devalue the potential of their ball mills' operating frequencies towards the necessary pyranic ring conformational changes. As we now know from Chapter 2 that the higher collision frequency of the 0.25"-balls/3%-packing/8.2-BtC system is more effective for chitin amorphization-depolymerization than that of 0.5" balls, the collision frequency was selectively increased by

concurrently raising the packing and BtC values to ca. 18% and 42.8 respectively. Having established a proportional relationship between water soluble products and loss of glycosidic linkages (see Sections 2.3.5.2 and 2.3.6), the ball mill's depolymerization performance was evaluated based on the former. Likewise, the effect of kaolinite on α -chitin's solubility was investigated as well as the depolymerization effect on the microwave production of levulinic acid (LA). Depending on the optimum ball milling conditions, water soluble products from α -chitin were analysed colorimetrically, as well as with MALDI-TOF MS and SEC.

3.2 Experimental

3.2.1 Materials

α -Chitin, which was isolated from snow crab, was provided by ChitinWorks LLC (1-2 mm flakes of approx. 0.30 g/mL, moisture content determined gravimetrically at 5.5 wt.%). Chitosan high molecular weight (MW) [CAS: 9012-76-4, Vendor's product #: 419419, DD>75%, Brookfield viscosity 800–2000 cP], 3,5-dinitrosalicylic acid, glycidyltrimethylammonium chloride (GTMA) ($\geq 90\%$), 2,5-dihydroxybenzoic acid (DHB) (98%) were purchased from Sigma Aldrich. *N*-acetyl-D-glucosamine (GlcNAc) 98% was purchased from AK Scientific, Inc. *N, N'* diacetylchitobiose (GlcNAc)₂ and oligosaccharides were purchased from Toronto Research Chemicals Inc. Deuterated glucose (1,2,3,4,5,6,6-D7, 97–98%) (Glc-d7) was purchased from Cambridge Isotope Laboratories, Inc. Kaolinite (sample No.5, API project 49, Lamar Pit, Bath, South Carolina) was purchased from Ward's Natural

Science.¹ Acetic acid was purchased from Fisher Scientific. NaOH and potassium ferricyanide (III) [K₃Fe(CN)₆] were purchased from BDH Chemicals Ltd. Sodium carbonate monohydrate Na₂CO₃·H₂O was purchased from Merck. Methanol was supplied by ACP Chemicals Inc. All chemicals were used as received.

3.2.2 Mechanochemical treatment of α -chitin

Performed as in Chapter 2, with the addition of milling experiments where 1.00 g of α -chitin was charged along with 1.00 g of kaolinite.

3.2.3 Gravimetric analysis to determine the mass of soluble products (sample solubility %)

Performed as in Chapter 2, with the addition of: Solubility for the samples from milling α -chitin with kaolinite was calculated by subtracting the mass of the undissolved residue from 250 mg and reported as a weight percentage of half of the weight of the milled sample, as kaolinite accounts for 50% w/w of the original sample. Each sample was analyzed in triplicate.

3.2.4 X-ray diffraction (XRD) and Fourier transform infrared (FT-IR) spectroscopy

Performed as in Chapter 2.

¹ Possible composition of the sample can be found from the "Crustal Geophysics and Geochemistry Science Center", which is part of the United States Geological Survey (USGS).

https://crustal.usgs.gov/speclab/data/HTMLmetadata/Kaolinite_CM5_BECKb_AREF.html

3.2.5 Chitin conversion to levulinic acid (LA)

Approximately 100.0 mg chitinous sample (native or milled, standard deviation for a set of 8 experiments was ca. 6.0%) was charged along with 89.1 ± 11.5 mg $\text{SnCl}_4 \cdot 5 \text{H}_2\text{O}$ (0.254 ± 0.033 mmol, RSD ca. 13%), 4.0 mL deionized H_2O , and a magnetic stir bar in a microwave vial (2–5 mL) according to literature.¹⁰ The mixture was set at 190 °C in a Biotage Initiator 2.5 microwave synthesizer and left to react for 30 min at very high absorption level.ⁱⁱ A 250 μL room temperature aliquot of the reaction mixture was withdrawn and poured into 2 mL of ethyl acetate (EtOAc). A fixed volume of hexanoic acid was added to all eight reaction mixtures as an internal standard (1.82 μL). Levulinic (LA) and hexanoic (HA) acids were extracted by high-speed vortex for 30 sec and centrifugation at 1500 rpm for 2 min. The organic (upper) phase was pipetted out and the residual reaction mixture underwent the above extraction process two more times with fresh EtOAc (3 \times 2 mL in total). The combined extracts were evaporated with a Buchi Rotavap and the dried residue was reconstituted in 1000 μL EtOAc for analysis with GC-MS according to Omari et al.¹⁰ Representative gas chromatograms with the retention times and mass spectra of HA and LA are shown in Figures A3–1 and A3–2 respectively. A calibration curve for LA yields from 100 mg of chitinous samples (Figure A3–3) was constructed

ⁱⁱ In accordance to the relevant paper, the actual pressure was monitored and found stable for most of the reaction time (from the 8th to the 30th minute) at ca. 20 bar. According to the vendor's manual, that pressure value for water corresponds to 205 °C (11). For reference, when 5.0 mL of water were tested on 14/1/2015 at a set temperature of 200 °C, the pressure was recorded at 21 bar which is close to the instrument's functional limit. Default stirring is at 600 rpm.

based on standard solutions prepared according to the data of Table A3–1 (HA was integrated from 3.81 to 4.22 min and LA from 4.38 to 4.88 min).

3.2.6 Colorimetric approximation of reducing ends of soluble products

3.2.6.1 Dinitrosalicylic acid (DNS) method

This was performed in a similar way to methods reported in the literature.^{12,13} The DNS reagent was prepared by dissolving 0.2503 g 3,5-dinitrosalicylic acid (MW 228.12 g/mol) in 25.0 mL distilled water (1% or 43.9 mM) with the aid of a warm tap water bath. Approximately 0.80 g NaOH, 8.8–12.2 g L-tartaric acid disodium salt dihydrate (CAS 6106-24-7; MW 230.08 g/mol),ⁱⁱⁱ and 80–100 mg phenol were added in a 50.0 mL volumetric flask and the components were dissolved in ca. 42 mL distilled water with the aid of warm tap water bath.ⁱⁱⁱⁱ 100 μ L of the 1% 3,5-dinitrosalicylic acid solution was transferred into the flask, which was then made up to the mark with distilled water. The DNS reagent was kept in darkness during sets of experiments that were undertaken over several weeks.

An aliquot of the water-soluble products (pH 7.0) created as per Section 3.2.3 was diluted in order to bring the visual absorbance of the solution of the ball-milled samples in close proximity to that of the DNS reagent. 1500 μ L of the DNS reagent were vortex-mixed with 1500 μ L of the diluted soluble product (or standard

ⁱⁱⁱ The substance was the most economic and readily available analog to Rochelle salt (potassium sodium tartrate tetrahydrate; MW 282.1 g/mol).

ⁱⁱⁱⁱ Exact concentrations are reported in the corresponding Results and Discussion section according to optimization experiments.

monosaccharide) solution. This mixture was heated under microwave irradiation (Biotage instrument) at 100 °C for 5 min (high absorption) and then cooled to room temperature. The colour intensity of the mixture was measured using an Ocean Optics USB4000 spectrometer at 540 nm. Integration time was 5000 μ sec, and signals were the average of 50 scans. Calibration curves were prepared using Glc and GlcNAc for quantification.

3.2.6.2 Schales' method

This was performed in a similar way to methods reported in the literature.¹⁴ Schales' reagent was prepared by dissolving 0.0500 g potassium ferricyanide ($K_3Fe(CN)_6$) and 6.2009 g sodium carbonate monohydrate $Na_2CO_3 \cdot H_2O$ in 100.0 mL distilled water. The solution was transferred to a dark glass container and was kept in a cabinet. An aliquot of the water-soluble products isolated above (385 μ L, pH 7.0) was diluted to 25.0 mL to approximate the visual absorbance of the initial solution of the ball-milled samples compared with that of *N*-acetyl-D-glucosamine (GlcNAc). 2000 μ L of Schales' reagent was vortex mixed with 1500 μ L of the diluted soluble product (or GlcNAc) solution. This mixture was heated under microwave irradiation (Biotage instrument) at 100 °C for 10 min and then cooled to room temperature. The colour intensity of the mixture was measured using an Ocean Optics USB4000 spectrometer at 420 nm. Experiments were also performed using GlcNAc for comparison.

3.2.7 Derivatization of soluble products, GlcNAc and (GlcNAc)₂ for quantification using MALDI-TOF MS analysis

Derivatization of the soluble products formed by dissolution at pH 7.0 was carried out using a procedure reported by Gouw et al. with minor modifications.¹⁵ Deuterated glucose (Glc-d7) was used as an internal standard. A 1000 μL aliquot of the soluble products solution (water for blank) was added to 1000 μL of a 7.0 mM Glc-d7 solution (20.0 mg in 1500 μL H₂O, the internal standard). 60.0 μL 1M NaOH and 8.00 μL glycidyltrimethylammonium chloride (GTMA) were added to that solution. The resulting mixture was vortex mixed, heated at 60–65 °C for 2 h and stored in a fridge until analyzed. Calibration curves for quantifying GlcNAc and (GlcNAc)₂ using MALDI-TOF MS, were constructed by diluting a 35.62 mM (197.0 mg GlcNAc in 25 mL H₂O) and a 3.9 mM (8.2 mg (GlcNAc)₂ in 15 mL H₂O) respectively. The volumes of the above solutions were in the range of 15–1800 μL and they were diluted to volumes of 20 mL for GlcNAc and 1300 μL for (GlcNAc)₂. Details of the MALDI-TOF MS experiments follows below.

3.2.8 MALDI-TOF instrumentation and mass spectra processing

900 μL of a 10 mg/mL 2,5-dihydroxybenzoic acid (DHB) solution (2:1 v/v methanol:water) were mixed with 100 μL of the derivatized soluble products solution and 0.75 μL of this mixture was spotted onto the MALDI target plate. The samples were dried at ambient temperature and the plate was loaded into a 4800 MALDI TOF/TOF analyzer (AB Sciex). Spectra were acquired automatically (multiple positions on the sample spot) in reflectron positive method from 100 to

1200 Da (focus mass 550) using 400 total shots per spectrum. The machine was equipped with a Nd:YAG laser of 355 nm with a firing rate of 200 Hz. Laser intensity was fixed to 76%. Peaks were detected (min S/N = 3) with no baseline subtraction or smoothing and the intensity of the base peak in all spectra was found within the range of 1000 to 65000 counts. Spectra were exported in a simple ASCII file (approx. m/z difference 0.00615) using the vendor's Data Explorer software and imported to the open source multifunctional mass spectrometry software mMass.⁵ Relevant peaks were labelled and their native intensities (no baseline correction) and resolutions were revealed. Spectra (at least 4 among spots) for the derivatives of the soluble products and for the blank were averaged using the relevant command in mMass (Figure A3-4). In all cases, the m/z standard deviation was below 0.050 (Figure A3-5). The average spectrum for the blank derivatization reaction (Figure A3-6) has been subtracted from the average spectrum of the soluble products derivatives using the relevant command in mMass for clarity of presentation. Finally, analyte to internal standard (Glc-d7) peak height ratios were calculated from the labelled spectra for quantification purposes.

3.2.9 Size Exclusion Chromatography (SEC) analyses

SEC was performed at 35 °C on a Viscotek VE 2001 GPCMax equipped with a Viscotek VE 3580 RI detector and phenomenex aqueous columns (PolySep-GFC-P 2000, PolySep-GFC-P 4000 and guard). Samples were prepared at a concentration of approximately 2 mg/mL and left to equilibrate for 18 h. Prior to analysis, samples

were filtered using 0.2 μM syringe filters. 100 μL of sample was injected, and samples were eluted using HPLC grade water (with 0.05% w/v NaN_3) at a flow rate of 0.30 mL/min. Nine PEG/PEO standards (Agilent Easivial) were used to prepare a calibration curve, in the molecular weight range of 106 to 130 000 Da. NAG, *N,N*-diacetylchitobiose (NAG_2) and three chitooligosaccharide standards (Toronto Research Chemicals) were analyzed and their retention volumes recorded for comparison with unknown chitin-derived samples. Under the same conditions, samples of aqueous (pH 7.0) soluble portions of chitin were analyzed. Data were processed using OmniSEC software.

3.3 Results and discussion

3.3.1 Effect of kaolinite on α -chitin's amorphization/solubility

In preliminary investigations, powder X-ray diffraction (XRD) was assessed as a method for evaluating the amorphization of chitin in the presence of kaolinite. Figure A3–7 shows the XRD pattern of kaolinite (red signal) exhibiting peaks at the following 2θ : 12.3 (strong and sharp), 19.9, 20.3, 21.3, 24.8 (strong and sharp), 37.7, 38.5, 39.2, and 62.3. These values are in good agreement with those characteristic for the structure of kaolinite.¹⁶ When the signal is overlaid with that of native α -chitin (light blue signal with transparency), the possibility of chitin's (110) reflection at 19.2 overlapping with kaolinite's (020) peak at 19.9 raises questions regarding an uncomplicated crystallinity index calculation as presented in Chapter 2. Indeed, Figure A3–8 shows significant changes for the pattern of a 1:1 chitin:kaolinite

mixture (green signal). α -Chitin's (110) reflection at 19.20 shifts to 19.48 with its intensity reduced by 66% (from 4603 in Figure 2–4 to 1544). At the same time, kaolinite's (020) peak appears more than 80% intensified (from 850 to 1544) at 19.48 maintaining its ($1\bar{1}0$) reflection at 19.92 (0.38 shift). This masking of reflections is also evident on chitin's (020) peak at 9.28 and on kaolinite's (001) peak at 12.32. In the former case, the polysaccharide shifts to 9.50 (from 9.28) with its intensity reduced by 61% (from 1773 to 689) when mixed with kaolinite, and by 76% (from 1773 to 431) when 0.5 g of that mixture was mortared (with a pestle) for 4 min. In the latter case, the main kaolinite signal shifts to 12.46 (from 12.32) with its intensity reduced by 34% (from 1805 to 1186) when mixed with kaolinite, and by 21% (from 1805 to 1417) when 0.5 g of that mixture was mortared (with a pestle) for 4 min respectively. Taken into account these complications of the materials' crystalline fractions, as well as the 60% reduction of chitin's amorphous halo at 16.00 (from 401 to 159), assessment of chitin's crystallinity during mechanochemical treatment with kaolinite was consider a task which is beyond the scope of this thesis.^{liv} Figure A3–10 in the Appendix gives a feel of the changes for the pattern of the 1:1 chitin:kaolinite mixture (pink signal) when milled with $2 \times 0.5''$ balls (8.2 balls-to-powder mass ratio) for 30 (green signal) and 90 (red signal) min. All of the mixture's peaks decrease in intensity with increased milling time with α -chitin's masked (110) reflection at 19.48 appearing to shift to 20.02. The region around 16.00, which can

^{liv} In addition, future researchers should also consider a new peak arising for the mixture at $44.3^\circ 2\theta$ (see Figure A3–9).

be considered representative for chitin's amorphous fraction appears more intense with increased milling time something which makes sense intuitively.

Due to these limitations of powder X-ray diffraction (XRD) on solid mixture analysis in this case, a relationship between crystallinity index and solubility is proposed to assess the depolymerization efficiency of kaolinite in relation to that of the ball mill's 3% packing. Figure A3-11 correlates the crystallinity index data of the 16 × 0.25" balls sample set from Figure 2-8 with the corresponding average solubility values from Figure 2-21. Considering the approximate character of a relationship like that, the resulting equation (Solubility % = -0.0856 · CrI + 13.533) presents a reasonable linearity ($R^2 = 0.9843$) for milling times up to 90 min. Hence, it can be used to translate the crystallinity indices for the 2 × 0.5" balls set (76.5, 59.8, and 52.7% in Figure 2-8) into predicted solubility values (pH 7.0) for those samples (green bars in Figure 3-2 are 6.98, 8.41, and 9.02% respectively). The 2.04 solubility-units increase arising from 60 min ball milling (from 6.98% for the 30 min sample to 9.02% for the 90 min sample) represents a 29.2% rise, which is the result of the work of the 2 × 0.5" balls / 8.2 balls-to-powder mass ratio system on native α -chitin.

Now, when those pre-milled samples were milled in 1:1 mass ratio with kaolinite for 60 min (2 × 0.5" balls / 8.2 balls-to-powder mass ratio),^{lv} α -chitin solubility increased

^{lv} When 2 g kaolinite were ball milled by themselves with 2 × 0.5" / 68-70 × 0.25" balls for 60 min the material (turned from white to grey) was completely insoluble in both neutral and acidic pH values (conditions were similar to those for chitin solubility tests, the dry mass after the tests was ca. 1.8 ± 1.6 % heavier than before the tests).

to $14.5 \pm 0.3\%$ (blue bars in Figure 3–2).^{lvi} The 5.61 solubility-units rise which resulted from 60 min ball milling (from 9.02 to 14.63% for the 90 min pre-milled sample) represents a 62.2% increase produced from the cooperation of the $2 \times 0.5''$ balls / 8.2 balls-to-powder mass ratio system with kaolinite. When comparing the 62.2% rise observed from a 60 min SPEX-8000 process with kaolinite with the 29.2% without it, one can hypothesize that the natural clay at least doubles the depolymerization efficiency of the ball milling process. If the reader considers the 7.24 solubility-units elevation for the 30 min pre-milled sample (from 6.98 to 14.22%), then the 103.7% solubility increase denotes a 3.6 times more efficient process resulting from the use of kaolinite. These results confirm the significant role of acidity offered by the clay's layers as explained in Section 3.1.

^{lvi} Solubility in pH 2.9 was slightly higher as expected (red bars in Figure 3–2 are at $18.1 \pm 0.5\%$).

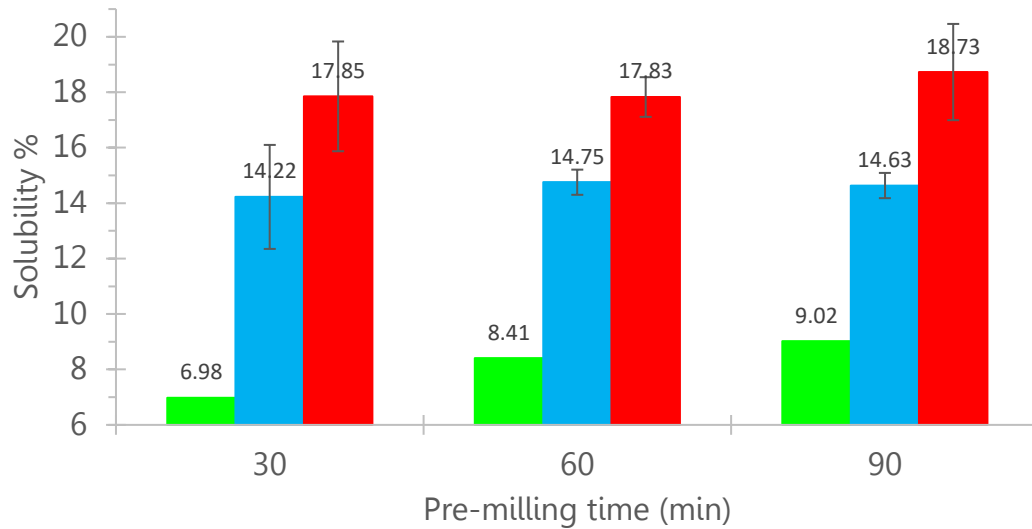


Figure 3-2: Solubility % of pre-milled α -chitin using $2 \times 0.5''$ balls for 30-60-90 min (step 1) when milled with kaolinite (1:1 g:g) by $2 \times 0.5''$ balls for 60 min (step 2) (blue bars in pH 7.0 and red in pH 2.9). Green bars show the predicted average solubility values (pH 7.0) for just step 1.^{lvii}

With kaolinite producing ca. $14.5 \pm 0.3\%$ soluble products in 60 min ($2 \times 0.5''$ balls / 8.2 balls-to-powder mass ratio), one would expect that increasing milling time would increase the solubility of α -chitin by the same factor. Figure 3-3 shows that when milling time was quadrupled ($4 \times 60 = 240$ min), solubility did not exceed $31.5 \pm 1.5\%$, a value which is appreciably lower than the expected ca. 58% (4×14.5). The higher collision frequency system of the $0.25''$ balls gave water-soluble products at the same levels ($30.9 \pm 0.3\%$), which were 3 times those without kaolinite. This result can be associated with the observed amorphization and delamination of kaolinite upon grinding,¹⁷ which exposes their surface protons to

^{lvii} Predicted average solubility values for milling with $2 \times 0.5''$ balls were obtained by applying the corresponding CrI values (Figure 2-8) to the equation of Figure A3-11.

chitin's deformed glycosidic linkages. That catalytic activity of the clay on chitin (ca. 31% solubility in 4 h) is significantly lower than that on microcrystalline cellulose reported by the Blair group (>40% in 1 h).¹ That difference might be partly attributed to a possibly higher \overline{MW} polysaccharide in this study, something which provides an additional reason to explore the effects of increased collision frequency.

Now, the $10.1 \pm 0.6\%$ solubility resulting from 240 min collisions of the $16 \times 0.25''$ balls presents a puzzling hysteresis viz-a-viz performance when compared with the $11.01 \pm 0.3\%$ maximum achieved in 120 min (see Figure 2–21). The $13.2 \pm 0.3\%$ obtained from the higher force per impact of the $2 \times 0.5''$ system can be considered as a more productive depolymerization process, however it still lags behind when compared with the 8.4% solubility expected from the first 60 min of ball milling (see Figure 3–2). In summary, although kaolinite definitely provides a significant improvement to the yields of water-soluble products, the factor of collision frequency certainly requires further exploration in order to maximize ball milling efficiency in a SPEX-8000 mixer/mill and likely other mechanochemical systems too.

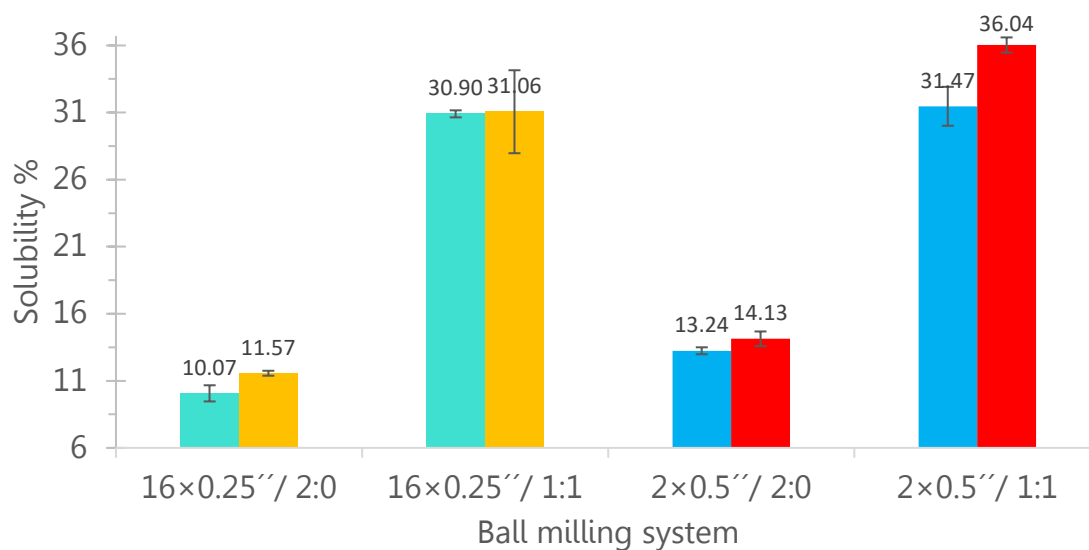


Figure 3-3: Solubility % of α -chitin when milled by 16 \times 0.25" (turquoise/orange) and 2 \times 0.5" (blue/red) balls without (2:0 g:g) and with kaolinite (1:1 g:g) for 240 min (turquoise/blue bars in pH 7.0 and orange/red in pH 2.9).

3.3.2 Effect of increased packing and balls-to-chitin (BtC) ratios (intense ball milling) on α -chitin

3.3.2.1 Fast amorphization

X-ray diffraction (XRD) data for α -chitin (2 g) processed with 1 \times 0.5" and 72 \times 0.25" balls for milling times between 15 and 120 min are shown in Figure 3–4 [packing and BtC were quintupled ($5 \times 3.3\% = 16.5\%$, and $5 \times 8.2 \approx 40.2$)]. It is important to note that temperature of the outer surface of the vial was monitored with a thermocouple and did not exceed 50 °C in any case (ca. 10 °C increase from the 3.3% packing experiments). Figure 3–5 shows the CrI values of α -chitin over milling time (min) when processed with 1 \times 0.5" / 72 \times 0.25" balls. Almost half of the polysaccharide's crystallinity (48%) is lost in the first 15 min, a result which took the

less intensive $16 \times 0.25''$ system approximately 60 min. In the next 15 min, the 16.5% packing system brings α -chitin's CrI down to 33.5%, which is at the same level as the 120 min plateau of the more efficient of the 3.3% packing systems (see Figure 2–8). This crystallinity behaviour indicates at least a three-fold decrease in milling time and can be associated with the increased collision frequency of the higher-packing/higher-BtC system. This intensive ball milling manages to amorphize the polysaccharide to a CrI as low as 25.9% after 75 min of total processing time, where the crystallinity of the material exhibits an interesting resistance for times up to 120 min. The reader is reminded here that the average standard deviation of CrI values is ± 2.5 units (see footnote xxxvi) with a maximum of ± 3.2 units arising from just the precision of the XRD technique (see last paragraph of Section 2.3.2). Therefore, the “oscillating” trend in Figure 3–5 highlights the need for reproduction of this set of experiments. The plateau for the crystallinity index at $26.7 \pm 0.9\%$ possibly correlates with the $25 \pm 3\%$ higher crystallinity values that the Segal method gives for cellulose samples when compared to the average of three other methods¹⁸ (see Section 2.1.2). The above explanation implies the possibility that the CrI for those four samples (observed at $26.7 \pm 0.9\%$) are actually close to zero. That would mean that achieving absolute amorphous α -chitin is possible in less than 2 h with the intense ball milling conditions described here (16.5% packing / 40.2 BtC). However, future researchers should consider the possibility of reagglomeration and coalescence phenomena taking place during mechanochemical processes.¹⁹⁻²¹

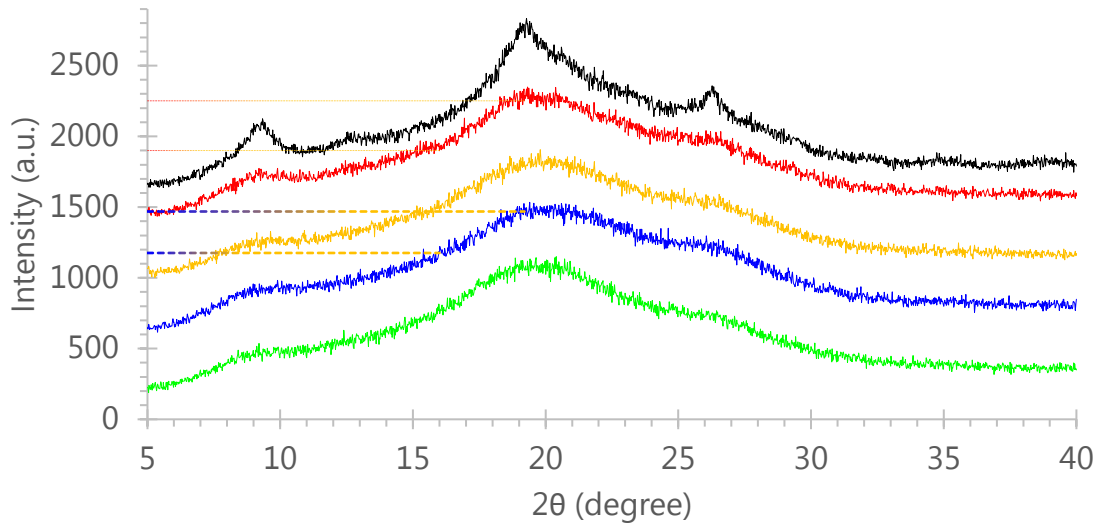


Figure 3-4: XRD patterns of α -chitin (2 g) milled with $1 \times 0.5'' / 72 \times 0.25''$ balls for 15 (black), 30 (red), 60 (orange), 90 (blue), and 120 (green) min (16.5% packing / 40.2 BtC). Dotted lines mark the intensities: 2251 (red), 1469 (blue) at 19.20° ; 1899 (red), 1176 (blue) at 16.00° . CrI values are: 33.5% $[(2251 - 1899) \times 100 / 1051]$ for red signal, and 27.4% $[(1469 - 1176) \times 100 / 1069]$ for blue. The intensities of all data have been offset relative to the 120 min sample by whole multiples of 200 a.u.

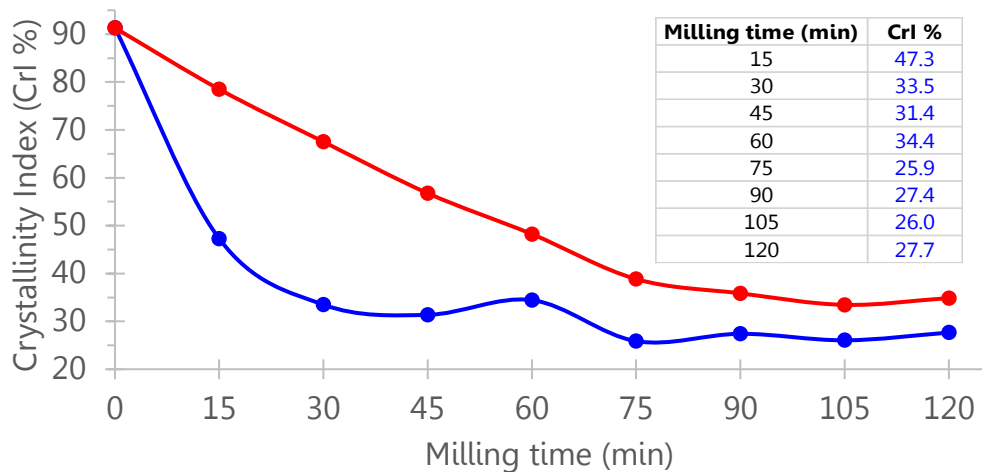


Figure 3-5: Crystallinity Index (CrI)% of α -chitin over milling time (min) when processed with $1 \times 0.5'' / 72 \times 0.25''$ balls (16.5% packing / 40.2 BtC; blue data) and with $16 \times 0.25''$ balls (3.3% packing / 8.2 BtC; red data).

Wanting to record potentially useful information regarding likely polymorphism phenomena for the crystalline fraction, Figure A3–12 presents the intensity ratio for reflections (110)/(020) (possibly reflecting strength of α -character) over milling time (min) for the 16.5% (green data) as well as the two 3.3% packing systems discussed in Chapter 2. It is interesting to notice that the trends for the two 0.25" balls systems (green and red data) are the same for the first 75 min (ratio drops in the first 30 min, raises in the next 30, and drops again for the 75-min sample). The higher BtC system exhibits a wider range of values for the ratio [from 1.84 (30 min) to 2.60 (60 min) vs from 2.02 (30 min) to 2.24 (60 min) for the 8.2 BtC one] suggesting a more dynamic ball milling process (something which intuitively makes sense).^{lviii} Moreover, in none of the samples did the ratio increase above 2.76, which is the sum of the value for native α -chitin (2.60) and the maximum standard deviation (0.16). These analog trends for the three systems might be meaningful only when contrasted with a hypothetical continuous decline of the ratio with increased milling time (the reader can imagine no "ups and downs").^{lix}

3.3.2.2 *Fast solubilization*

From the XRD data collected and their interpretation, it is evident that the increased collision frequency of the 16.5% packing/40.2 BtC system amorphizes α -chitin

^{lviii} The reader is reminded that standard deviation for the (110)/(020) ratio from duplicate XRD measurements of two samples did not exceed 0.16 (see Section 2.3.2).

^{lix} The data set is presented here in order to create a record for a future researcher to further investigate possible polymorphism phenomena. Thinking in entropy terms, α -character should have been decreasing with increasing milling time.

(possibly to absolute levels) faster than the 3.3% packing/8.2 BtC systems. Therefore, solubilities of samples which were milled with $68\text{--}70 \times 0.25'' / 2 \times 0.5''$ balls [hence slightly higher packing (17.5%)] were explored in an attempt to maximize them.^{lx} Figure 3–6 reveals that the 42.8 BtC system gave $19.3 \pm 0.6\%$ soluble products in 2 h (blue data in pH 7.0), while the 85.6 BtC one achieved the same levels ($19.6 \pm 1.6\%$) in 1 h. These results along with the ones for double the milling time (4 h and 2 h points for 42.8 and 85.6 BtC respectively) imply the possibility of a proportional relationship between balls-to-chitin mass ratio (BtC) and milling time (the higher the BtC, the less milling time required for a desired solubilization result). Overall, both systems exhibit a logarithmic growth with solubilities for the 42.8 BtC plateauing ca. 36% after 6 h milling, while the ones of the 85.6 one reaching as high as $45.5 \pm 0.8\%$.^{lxi} ^{lxii} Figure 3–7 shows the development of color in both ball milled (from white to darker shades of grey) and water-soluble soluble (from colorless to darker shades of orange-brown) products. Similarly to Section 2.3.6, pigmentation is hypothesized to arise from Maillard-type reactions.

^{lx} The addition of a second 0.5'' ball probably raised the frequency of higher impact collisions as a maximum of 63–65 °C was measured when a thermocouple came in contact with the balls and inner walls of the vial immediately after milling for hours.

^{lxi} Water soluble products were slightly increased in pH 2.9 (1.6 ± 0.9 solubility units) just as expected (red data are for BtC 42.8).

^{lxii} Figure A3–13 shows the X-ray diffraction patterns of the insoluble residue from the pH 7.0 solubility tests. Crystallinity indices are in between 74 and 82%; at similar levels as those of the $16 \times 0.25''$ balls set (see Figure A2–18).

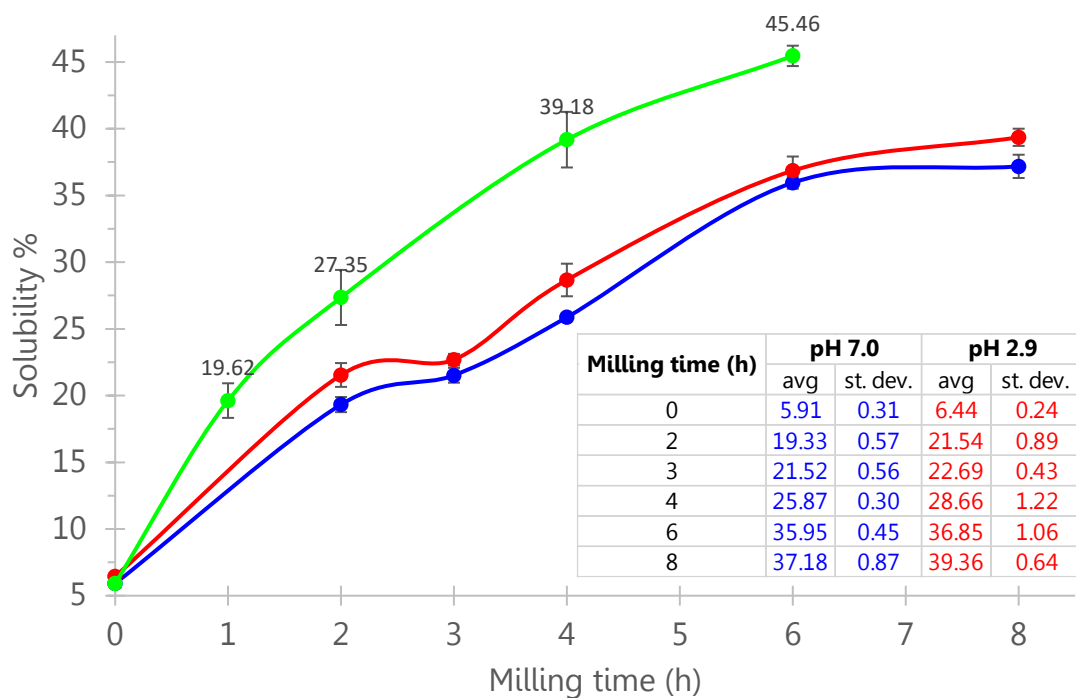


Figure 3-6: Solubility % of α -chitin when ball milled with 68-70 \times 0.25" / 2 \times 0.5" balls (17.5 % packing); BtC 42.8 at pH 7.0 (blue), 2.9 (red), and 85.6 at pH 7.0 (green).

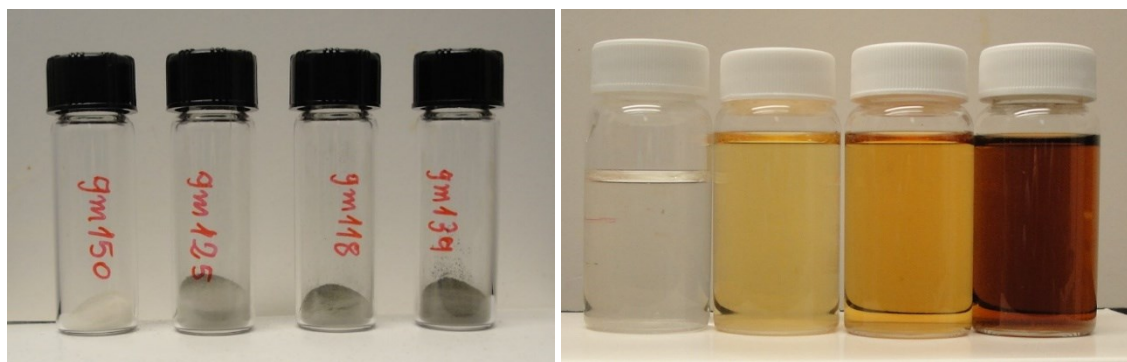


Figure 3-7: Colour development in ball milled and water-soluble α -chitin products when processed with 68-70 \times 0.25" / 2 \times 0.5" balls (17.5% packing / 42.8 BtC) for 0-2-4-8 h.

3.3.2.3 Fast and deep depolymerization, deacetylation trend, and a liquid assisted grinding (LAG) test

Figure 3–8 shows the FT-IR spectra of milled α -chitin with $68\text{-}70 \times 0.25'' / 2 \times 0.5''$ balls (17.5% packing / 85.6 BtC) for 60 (green), 120 (blue), 240 (pink) and 360 (red) min (green data of Figure 3–6). The main qualitative difference with the spectra of the samples milled with $16 \times 0.25''$ (see Figure A2–16) is that the signals of intense milling here are evidently smoother in the $1600\text{--}1400 \text{ cm}^{-1}$ region. More specifically, the amide II band does not exhibit its two components (1558 and 1541 cm^{-1}) associated with the doubly and singly hydrogen bonded *N*-acetyl group. Its maximum absorbance is at 1548 cm^{-1} and its ratio with the methine group (2874 cm^{-1}) is plotted in Figure 3–9. The first 60 min of milling reveal a decrease of the degree of acetylation (DA) to $85.4 \pm 0.8\%$ from $95.0 \pm 5.6\%$ for native α -chitin. After that, the DA remains stable at $84.4 \pm 0.9\%$ until 360 min milling.^{lxiii} Looking at the chain backbone, the glycosidic linkage reveals a 24.7% drop (from 1.440 to 1.084) in the first 60 min (Figure 3–10), which is at least 3-fold that of the 3.3% packing/8.2 BtC system [7.5% (from 1.440 to 1.332)]. After that, the rate of DP reduction slows ca. 6.6 times to a linear decline of $y = -0.0009 \cdot x + 1.1473$ ($R^2=0.9891$; y is the FT-IR ratio and x is milling time in min) until 360 min where the absorbance ratio is 58%

^{lxiii} The amide I split ratio ($1621 \text{ cm}^{-1} / 1652 \text{ cm}^{-1}$) followed the same trend as the $1548 \text{ cm}^{-1} / 2874 \text{ cm}^{-1}$ peak ratio dropping at 0.845 for the 1 h sample (from 1.146), reaching as low as 0.820 for the 2 h sample and then rising at 0.875 and 0.915 for the 4 and 6 h samples respectively (average standard deviation was 0.007). That behaviour is in parallel lines to that for the 3.3% packing/8.2 BtC system (see Figure 2–16) only with ca. 0.062 higher ratio values.

of its “native” level (from 1.440 to 0.836). Comparing the FT-IR data with those from Figure 3–6, it is clear that solubility is inversely proportional to glycosidic linkage content in analogy to the lower collision frequency system in Chapter 2. More specifically, the FT-IR ratio probing depolymerization is in a linear relationship with solubility from 2 to 6 h milling time [$y = -81.237 x + 114.01$ ($R^2 = 0.9894$; y is the solubility % and x is the $1154 \text{ cm}^{-1} / 2874 \text{ cm}^{-1}$ ratio); see green data in Figure 3–6]. This allows prediction of α -chitin solubility properties by manipulating the BtC ratio and acquiring FT-IR spectra, something which is applied in Chapter 4. Finally, the spectra reveal that concurrent controlled deacetylation is possible to a low extent (ca. 10%) with higher collision frequency systems.

Liquid assisted grinding (LAG) was tested by adding 180 μL deionized water (0.01 mol) in the 85.6 BtC system (hence 0.18 $\mu\text{L}/\text{mg}$) and milling for 2 hours.^{lxiv} After some treatment with mortar/pestle and drying, FT-IR measurements revealed a ratio for the glycosidic linkage content of 1.21 ± 0.03 . This value is clearly higher than 1.06 ± 0.05 obtained with dry milling (see Figure 3–10), therefore one can hypothesize that liquid water does not assist depolymerization of α -chitin. It might be a challenge for future researchers to clarify whether the adsorbed moisture (5.5 wt.%) of α -chitin favours depolymerization (i.e. experiment with absolute dry mass).

^{lxiv} After the milling cycle, the mass had some crystal chunks and did not stick on the inner steel walls of the vial as with usual dry milling.

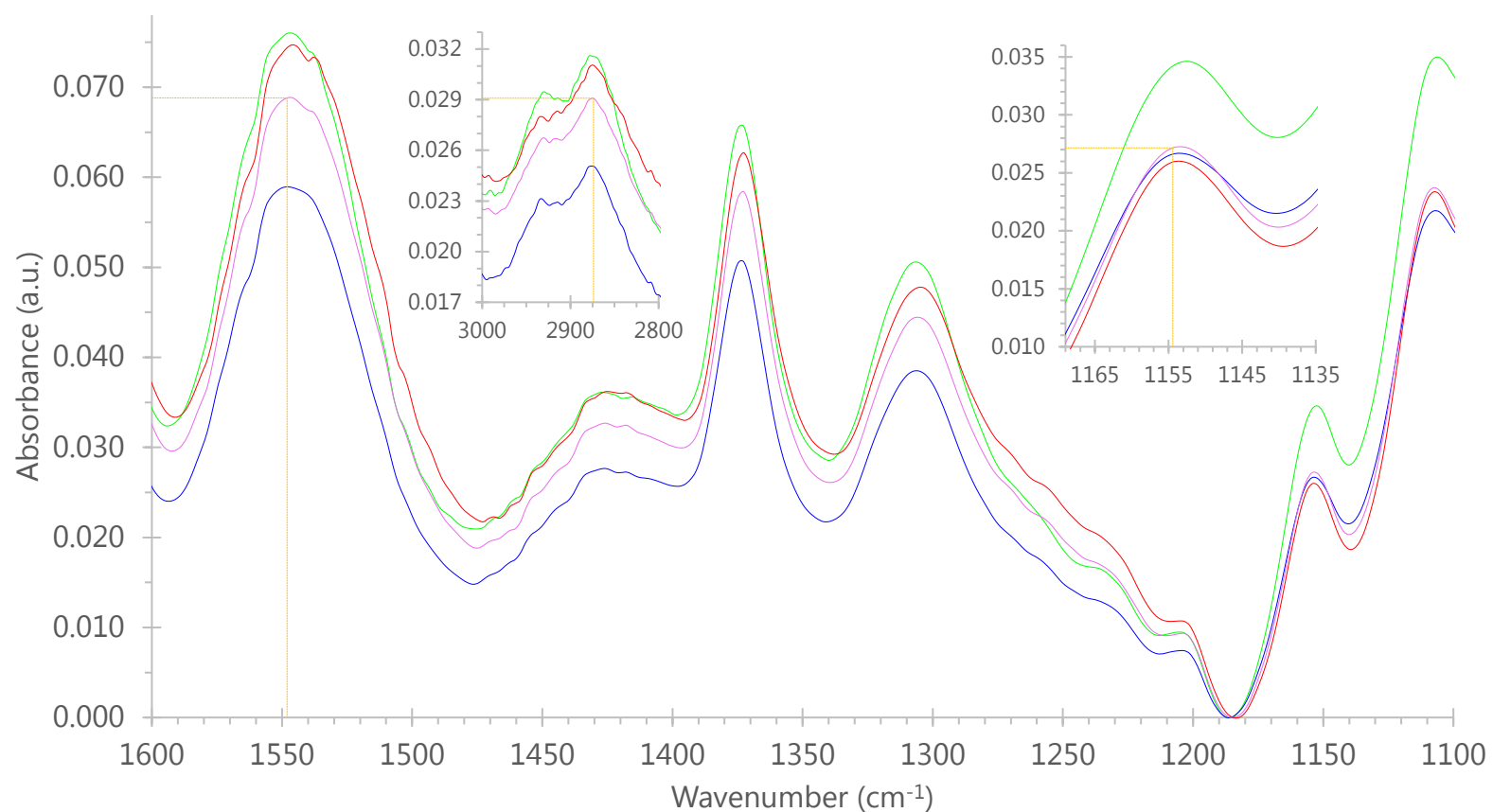


Figure 3-8: 1600–1100 cm^{-1} region of infrared spectra of milled α -chitin with 68-70 \times 0.25" / 2 \times 0.5" balls (17.5% packing / 85.6 BtC) for 1 (green), 2 (blue), 4 (pink) and 6 (red) h. Insets show the reference band (3000–2800 cm^{-1}) and glycosidic linkage (1169–1135 cm^{-1}) regions. Orange dotted lines highlight the intensities for reproduction of the ratios which probe depolymerization and deacetylation for the 4 h sample (the bands at 2874, 1548, and 1154 cm^{-1} absorb 0.0291, 0.0688, and 0.0272 respectively).

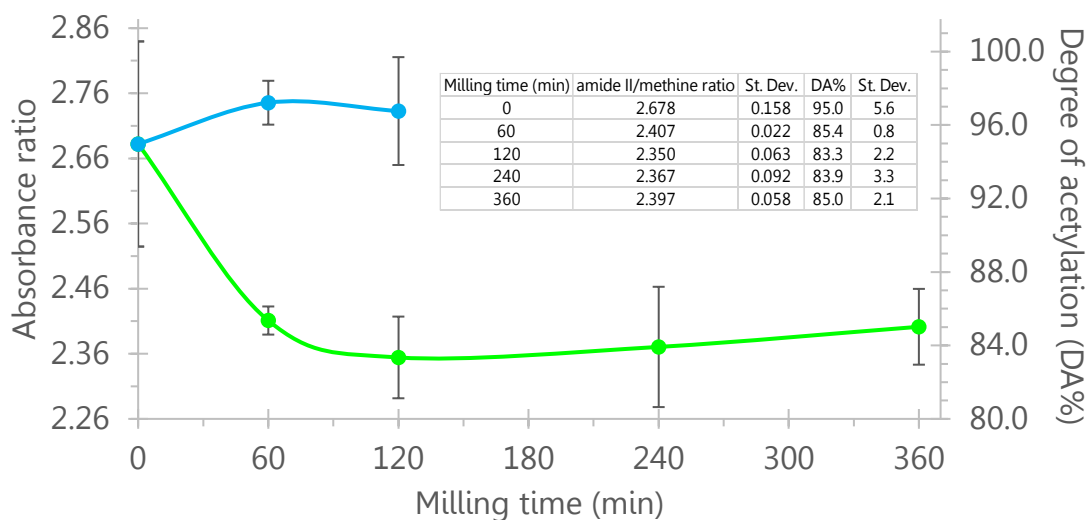


Figure 3-9: FT-IR data ($1548\text{ cm}^{-1} / 2874\text{ cm}^{-1}$ peak ratio) and degree of acetylation (DA%) for milled α -chitin with $68\text{-}70 \times 0.25'' / 2 \times 0.5''$ balls (17.5% packing / 85.6 BtC) plotted in green data (inset table records the exact values and standard deviations). Blue data is for the $16 \times 0.25''$ balls system (3.3% packing / 8.2 BtC) plotted in detail in Figure 2-20.

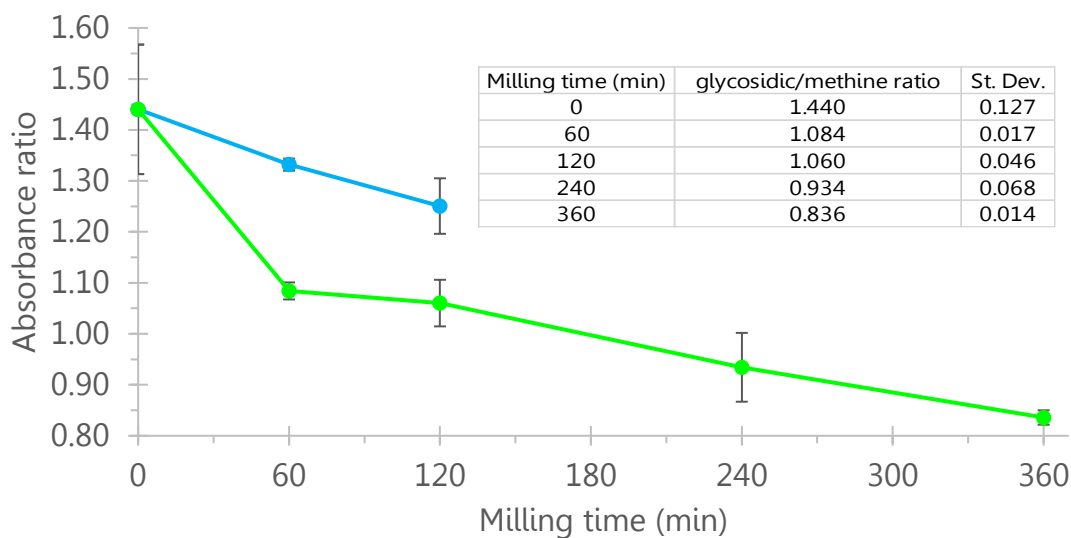


Figure 3-10: FT-IR data ($1154\text{ cm}^{-1} / 2874\text{ cm}^{-1}$ peak ratio) for milled α -chitin with $68\text{-}70 \times 0.25'' / 2 \times 0.5''$ balls (17.5% packing / 85.6 BtC) plotted in green data (inset table records the exact values and standard deviations). Blue data is for the $16 \times 0.25''$ balls system (3.3% packing / 8.2 BtC) plotted in detail in Figure 2-19.

3.3.2.4 Depolymerization of chitosan

Figure 3–11 shows the FT-IR spectra of high MW chitosan (green), as well as milled with 42.8 (blue) and 85.6 (red) BtC [68 × 0.25" / 2 × 0.5" balls (17.5% packing)] for 30 min. The main qualitative differences with the α-chitin spectra of Figure 3–8 are: the reduced absorbances of all three amide bands in the region 1700-1300 cm⁻¹, the rise of a relatively strong shoulder of amide II at 1589 cm⁻¹ (likely NH₂ deformation),²²⁻²⁴ the shifting of the carbon-hydrogen vibrations to lower frequencies (e.g. α-chitin's alkyl stretch at 2931 cm⁻¹ appears at 2916 cm⁻¹ in chitosan), the absence of amide B, and the shifting of amide A to higher frequencies (hydrogenic region is not shown to narrow the presentation of data). The most intense of the C-H bands appears at 2866 cm⁻¹, which is 8-9 cm⁻¹ lower than α-chitin's reference band.^{lxv} Using that vibration as a reference, the DA of the unmilled sample was 20.9 ± 0.6% (1552/2866 cm⁻¹/cm⁻¹ ratio is 0.589 ± 0.018), which is within the range given by its supplier (DD>75%). The DA values for the 42.8 and 85.6 BtC milled samples were 20.6 ± 0.4% (IR ratio 0.580 ± 0.012) and 21.2 ± 0.1% (IR ratio 0.599 ± 0.003) respectively, which practically means that deacetylation did not occur during the 30 min of both high collision frequency conditions. On the other hand, depolymerization was clearly observed with the 1151/2866 cm⁻¹/cm⁻¹ ratio dropping from 0.869 ± 0.037 for the unmilled sample, to 0.782 ± 0.027 for 42.8 BtC, to 0.738 ± 0.004 for 85.6 BtC. The latter ball milling performance represents a ca.

^{lxv} Compared to α-chitin, the weaker hydrogen bonding network of chitosan possibly allows different conformations to the carbon-hydrogen bonds.

15.0% DP reduction from the untreated chitosan, which is slightly higher than the 12.4% expected for the 85.6 BtC system of α -chitin (predicted IR ratio is 1.26; see 0-60 min slope of Figure 3-10). This can be attributed to the stronger hydrogen bonding network of the acetylated polysaccharide and allows a hypothesis of comparable molecular weights.^{lxvi} The reduced collision frequency of the 42.8 BtC system achieved an approximate 10.0% depolymerization of Sigma's high MW chitosan. That performance might be comparable with the 33.5% CrI of α -chitin produced from 30 min milling with 1 × 0.5" / 72 × 0.25" balls (16.5% packing / 40.2 BtC; see Figure 3-5).

^{lxvi} The higher 1154 cm⁻¹/2874 cm⁻¹ ratio for native α -chitin (1.44 vs. 0.87) does not necessarily mean that its glycosidic linkage content is proportionally higher to that of unmilled high-MW chitosan. Figure A3-14 shows a NAG₅ FT-IR spectra with a 1154 cm⁻¹/2874 cm⁻¹ ratio of 2.40. Signals of NAG, NAG₂, and α -chitin are overlaid for comparison.

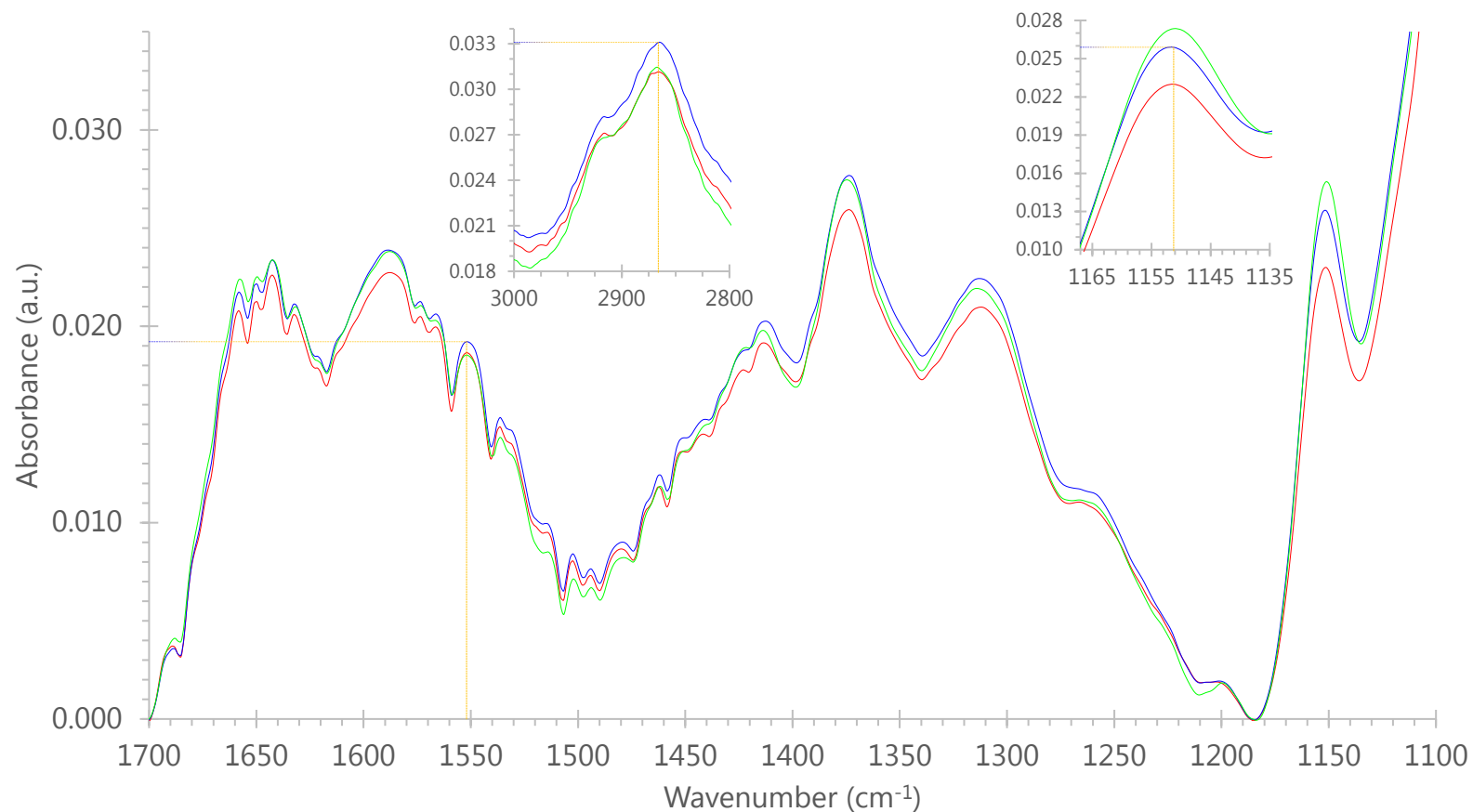


Figure 3-11: 1700–1100 cm⁻¹ region of infrared spectra of high MW chitosan (green), as well as milled with 42.8 (blue) and 85.6 (red) BtC [68 × 0.25" / 2 × 0.5" balls (17.5% packing)] for 30 min. Insets show the reference band (3000–2800 cm⁻¹) and glycosidic linkage (1167–1135 cm⁻¹) regions. Orange dotted lines highlight the intensities for reproduction of the ratios which probe depolymerization and deacetylation for the 42.8 BtC sample (the bands at 2866, 1552, and 1151 cm⁻¹ absorb 0.0331, 0.0192, and 0.0259 respectively).

3.3.2.5 A hypothesis on α -chitin molecular weight (MW)

When high MW chitosan from Aldrich [Brookfield viscosity 800–2000 cP (or mPa·s in SI), DD>75%) was milled with 68–70 × 0.25" / 2 × 0.5" balls for 4 h (BtC 42.8), a solubility of 26.3 ± 1.2% in pH 7.0 (same level as α -chitin), and 98.0 ± 0.9% in pH 2.9 was measured. The latter result underlines the significant differences in solubility between chitin and chitosan in acidic environments and can serve as indication of the possible negligible deacetylation of chitin under the intense ball milling conditions described. The former comprises preliminary experimental evidence of possibly comparable molecular weight ranges between native α -chitin used in this thesis and Aldrich's high-MW chitosan. Although it is accepted that a higher viscosity measurement arises from a higher MW polymer, to the best of my knowledge, literature lacks a review of a relationship between Brookfield viscosity measurements and average MW for chitin/chitosan. However, a few chitosan studies have reported the following results: 14 mPa·s corresponds to 87 kDa,²⁵ 100 mPa·s to 119 kDa,²⁶ 200 mPa·s to 300 kDa,²⁶ 461 mPa·s to 532 kDa,²⁵ >400 mPa·s to 570 kDa,²⁷ which are in better mutual agreement compared to 128 kDa from 6 mPa·s,²⁸ 400 kDa from 10 mPa·s,²⁹ and 1239 kDa from 289 mPa·s,²⁸ that are possibly overestimating the average MW of their polysaccharide samples. Considering the above literature results, it is not unreasonable for Sigma Aldrich's 800–2000 mPa·s Brookfield viscosity measurements to correspond to molecules of approximately 980–2400 kDa. On the basis of the almost identical solubility of α -chitin in neutral pH

rising from 4 h intense ball milling ($25.9 \pm 0.3\%$ vs $26.3 \pm 1.2\%$ for high-MW chitosan), as well as the weaker hydrogen bonding network for the deacetylated chains, it is not irrational to expect that the molecular weights of the native α -chitin sample from ChitinWorks do not exceed 2400 kDa.^{lxvii} Further studies would be needed to support this conclusion and this is challenging given the generally insoluble nature of α -chitin. One could imagine that ionic liquids, which have the potential to dissolve chitin,³⁰ would possibly be useful in obtained MW data [see work from the Moores group (<https://doi.org/10.26434/chemrxiv.7312070.v3>)].

3.3.2.6 Proposed mechanistic considerations

Regardless of the challenges in the field of chitin MW estimation, what matters primarily in this set of experiments is that water-soluble product yields have been significantly and systematically improved from those in Chapter 2. The higher packing and BtC ratios have resulted in higher collision frequencies than those of the $16 \times 0.25''$ system, which in turn have statistically increased glycosidic bond rupture [observed as a 0.38 drop (from 1.44 to 1.06) of the $1154 \text{ cm}^{-1}/2874 \text{ cm}^{-1}$ absorbance ratio in 2 h milling, see Figure 3–10].^{lxviii} Electron spin resonance (ESR) spectra of ball milled chitin and chitosan acquired by Sasai et al. confirmed the

^{lxvii} That rationale can provide a starting point for the formation of future hypotheses regarding chitin MW determinations.

^{lxviii} A future challenge for researchers can be the study of the $1154 \text{ cm}^{-1}/2875 \text{ cm}^{-1}$ FT-IR absorbance ratio for α -chitin samples with CrI values below 30% (hence possibly totally amorphous) and solubilities higher than ca. 20% as achieved in this section with packing and BtC values higher than 16.5% and 40 respectively.

expected homolytic cleavage of covalent bonds (possibly including the glycosidic ones) during this mechanochemical process.³¹ When chitin particles (finer than ca. 63–75 μm) were milled in a 60 Hz stainless steel system of 5.9 BtC, radical concentration reached a maximum (ca. $5.2 \cdot 10^{17}$ spin numbers/g) after 30 min of collisions and decreased by approximately 15% after 90 min milling (a >80% DD chitosan exhibited a similar behaviour). Computer simulations of the ESR spectra revealed four spectral components, one of which was hypothesized to result from glycosidic bond scission (observed as a single broad-line spectrum)^{lxix} and the other three from subsequent hydrogen abstraction from the ring carbons.³¹ Although this challenging task, which requires significant computational efforts,³² did not provide a definite assignment of the single broad-line spectrum to a C_1 centered radical, it certainly provides a strong reference for future researchers of polysaccharide mechanochemistry as the aforementioned unpaired electron system was stable enough to be identified experimentally in radiated disaccharide crystals (sucrose).³³

Now, given that particle size reduction was clearly demonstrated for the systematic amorphization experiments (from >500 μm to <100 μm , see Section 2.3.4), it is logical to hypothesize that the higher collision frequency of this set reduces the average particle size via simultaneous disruption of intermolecular hydrogen

^{lxix} Intriguingly, this component was the major one for chitosan ball milling and the second-major one for chitin.

bonding and homolytic glycosidic linkage cleavage (see Figure 3–10). As discussed in Section 2.1.3, collisions of steel surfaces in the SPEX system are to a good approximation perfectly elastic (restitution coefficient 0.95-1.00),³⁴ hence the Hertz theory of impact has been applied to explain the essentials of the ball deformation geometry,³⁵ as well as to determine the impact duration, pressure, and deformed volume.³⁶ Maurice and Courtney³⁶ have found that when a half inch stainless steel ball collides with 3.9 m/s on a curved surface of the same material (e.g. the vial's inner walls or another ball) in a SPEX system, the impact duration (total time of ball compression and subsequent relaxation) is ca. 31 μ s, the Hertz radius is 620 μ m,^{lxx} and the maximum pressure is 3.30 GPa.^{lxxi} One can imagine that as the first nanoseconds of the steel-chitin contact increase, the radius of the stressed area increases too. A fraction of the α -chitin particle gets trapped in between colliding media and eventually is subjected to plastic deformation, which will potentially result in fragmentation of the particle.^{lxxii} The phenomenon is likely to proceed via crack initiation and propagation,²⁰ which can be hypothesized to involve force distribution (discussed in Section 2.3.5.2) in elementary α -chitin fibril

^{lxx} The area of the contacting surfaces between a 0.5" steel ball and a particle of native α -chitin is illustrated approximately on Figure A3–15.

^{lxxi} For comparison, the contact time of a colliding steel ball in a Fritsch Pulverisette 7 (P7) planetary ball mill (relative impact velocity of 4.5 m/s) was calculated at 39 μ s, the Hertz radius at 670 μ m, and the maximum pressure at 6.3 GPa (37).

^{lxxii} Collision modeling has proposed three stages for a collision. The first stage where the deformation of both ball and powder is within an elastic regime and its duration is very short compared to the total collision time. The second is that of the plastic deformation of the powder, and the third one is considered again elastic with stress distribution beyond the Hertz radius (20).

volumes. Ultimately, after compression and relaxation (hence past the microseconds of the collision), statistical rupture of intermolecular hydrogen bonds and glycosidic linkages is the outcome which is reflected in the results of the solubility tests, XRD diffractograms and FT-IR spectra presented in this thesis (Figure 3–12).

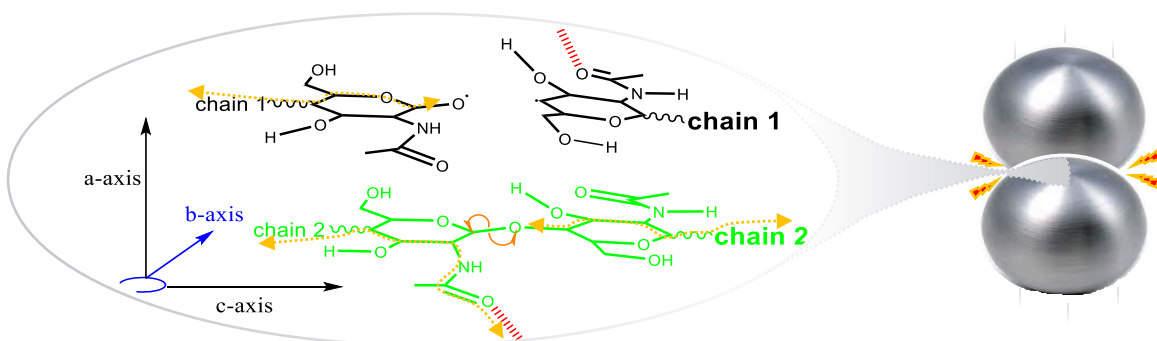


Figure 3-12: Proposed mechanistic considerations towards mechanochemical depolymerization of α -chitin. Elementary α -chitin fibril volumes trapped in between colliding balls are subjected to disruption of intermolecular hydrogen bonds and homolytic cleavage of glycosidic linkages through force distribution (orange dotted arrows).

3.3.3 Effect of intense ball milling on α -chitin's conversion to levulinic acid (LA)

Previous studies in the group have shown that the reactivity of α -chitin towards acid-catalyzed hydrolysis under microwave irradiation and aqueous conditions to yield levulinic acid (LA) was limited to ca. 12.3 ± 0.7 wt.% (average of 3 α -chitin samples). These low levels^{lxxiii} were hypothesized to arise from the crystalline and insoluble nature of the native sample of the biopolymer. Having demonstrated the significant

^{lxxiii} Compared to 32.0 wt.% LA from glucosamine hydrochloride and 24.6 ± 0.6 wt.% from the three chitosan samples of Sigma-Aldrich (low-medium-high MW).

decrease in the crystallinity index (below 30% in 75 min) and increase in solubility (above 35% in 6 h) achieved by increased collision frequency (see Section 3.3.2), LA yields were assessed for chitinous samples which were produced using increasing milling times with the 17.5% packing/42.8 BtC system.

Firstly, a feel of the GC-MS method precision was obtained by running triplicates for each sample.^{lxxiv} The average RSD value for triplicate LA/HA peak area ratios of 8 samples ($3 \times 8 = 24$ injections) was 0.97%, which is three times lower compared with the average RSD for the duplicate injections of the four standard LA solutions used to prepare the calibration curve (3.12%, see Table A3-1). The highest one was 2.94% (LA/HA peak area ratio for an extract of the 5 h milled α -chitin reaction mixture was 0.300 ± 0.009).^{lxxv} This means that the standard deviation in LA yield of a GC-MS injection did not exceed ± 1.9 wt.% (with the average being ± 1.4 wt.%). Secondly, the precision of the extraction step was tested with duplicates on three reaction mixtures (native α -chitin and milled for 5 and 8 h). Figures A3-16 and A3-17 show the two chromatograms for the duplicate extraction of a unique 8 h milled α -chitin reaction mixture, which presented the highest RSD (12.4% based on triplicate GC-MS injections). The first one exhibits a 17.2 wt.% LA yield, and the second a 20.0 wt.% (hence the average is 18.6 ± 2.0 wt.%). Overall, the LA/HA ratio's standard deviation for the three (reaction mixture) duplicate extractions was

^{lxxiv} "Sample" refers to a unique extract of a unique microwaved reaction mixture, which was injected in the GC-MS system.

^{lxxv} The 0.300 ± 0.009 peak area ratio corresponds to 23.9 ± 1.9 wt.% LA (see Figure A3-3).

± 0.012 , hence each extraction carried an average error of ± 2.1 wt.% LA. Cumulatively, the overall standard deviation (from extraction and injection together) for LA yield from a unique microwave reaction mixture was ± 2.5 wt.% ($= \sqrt{1.4^2 + 2.1^2}$).^{lxxvi}

Figure 3–13 shows that the three yields of LA from ball milled α -chitin (18.1 ± 2.8 wt.%) did not exceed the levels of the standard deviation of the triplicate microwave runs for the native sample (16.9 ± 2.5 wt.%).^{lxxvi} Taking into account the significant solubility differences of those α -chitin samples (see Figure 3–6), the data of this set of six aqueous microwave reactions (blue bars in Figure 3–13) provides sufficient evidence of the fact that the ball milling performance of the 17.5% packing/42.8 BtC system does not give rise to an increase in LA yield.^{lxxvii} This puzzling result seems to be confirmed from the chitosan experiments (green bars), the yields of which are in acceptable consistency with the published ones (see introductory paragraph of this section).^{lxxviii} Considering the LA yields of 24.6 ± 3.5 wt.% from 4 h milled high-MW chitosan and 20.0 ± 3.5 wt.% from 5 h milled α -chitin, it is not unreasonable to expect a comparable molecular weight for the acetylated chains.^{lxxix} Although the

^{lxxvi} Overall standard deviation for LA yield from a random MW-run (so anyone of the green or blue bars in Figure 3–13) is ± 3.5 wt.% ($= \sqrt{2.5^2 + 2.5^2}$) (38).

^{lxxvii} With α -chitin solubility quadrupling from 4 h intense ball milling, LA yields were expected to be at least doubled ($2 \times 16.9 = 33.8$ wt.%).

^{lxxviii} The aqueous aliquots (after extraction) were observed to be of increasing darkness according to the following reaction-mixture sequence: α -chitin (native), chitosan high-MW, α -chitin 4 h milled.

^{lxxix} The reader is reminded here of the close proximity of the solubilities of ball milled high-MW chitosan and α -chitin in pH 7.0 (see Section 3.3.2.5).

results of this set of experiments are somewhat disappointing, efforts to maximize the yields of water soluble products from α -chitin by mechanochemical means were still pursued, as *N*-acetyl-D-glucosamine and chito-oligosaccharides would also be highly desirable products.

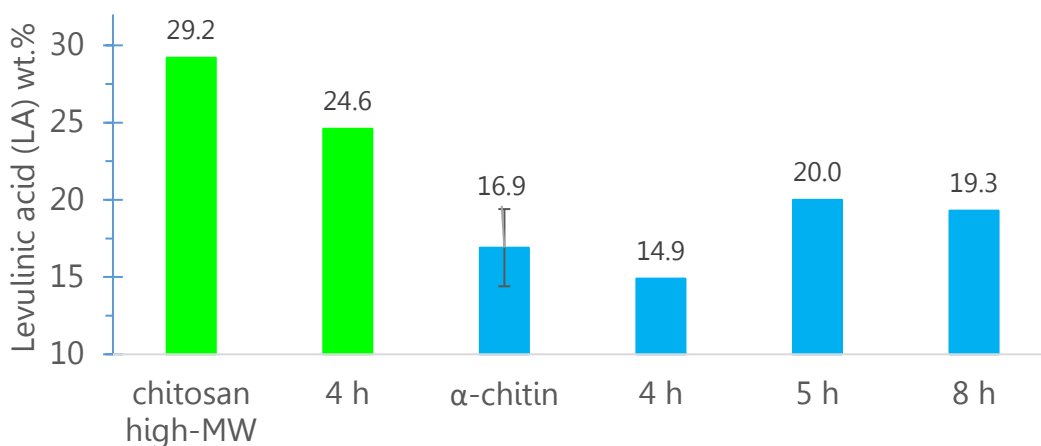


Figure 3-13: Levulinic acid yields (wt.%) produced from native and ball milled chitosan high-MW (green bars) and α -chitin (blue bars) via microwave assisted conversion (for analytical data see Table A3-2). Ball milling was with 17.5% packing/42.8 BtC for 4, 5, 8 h.

3.3.4 Effect of the combination of intense ball milling and kaolinite on α -chitin solubility

After achieving systematically positive results with regards to produce α -chitin-derived water-soluble species (in the region below 50%) using kaolinite and intense ball milling, it was only natural to combine the two into a set of solubilization experiments. Figure 3-14 shows the solubility values of α -chitin over milling time (h) when processed with $2 \times 0.5'' / 68-70 \times 0.25''$ balls and kaolinite (1:1 g:g; BtP 42.8). In the first two hours, the system reveals a more active process than that

without kaolinite achieving the production of $50.3 \pm 2.5\%$ water-soluble species (84% increase from the 27.3% solubility produced using the 85.6 BtC system).^{lxxx} After that, its productivity starts to level out entering a logarithmic phase where it reaches $73.7 \pm 2.8\%$ soluble α -chitin in 4 h milling.^{lxxxi} That value represents a 1.9 times higher solubility than when ball milled without kaolinite (39.2% in Figure 3–6), which signifies the system's optimum performance time ($75.8 \pm 1.2\%$ soluble products were obtained at 6 h corresponding to a 1.7-fold rise from 45.5%). Wanting to test a lower packing/BtC value, the 1:1 α -chitin:kaolinite mixture was milled with $1 \times 0.5'' / 48 \times 0.25''$ balls for 90 min. The sample's solubility in pH 7.0 was $27.91 \pm 1.36\%$, which is clearly lower than the ca. 39.1% expected with $2 \times 0.5'' / 68 \times 0.25''$ balls for 90 min [the neutral solubility values of 0, 0.5, 2 h milling runs fall into a straight line with $y = 22.247 \cdot x + 5.7733$ and $R^2 = 0.9999$ (y is solubility % and x is milling time in h)]. These data form a solid basis for future kinetic studies. The average solubility difference between pH 7.0 and 2.9 for the 2-4-6 h milling experiments is $11.6 \pm 0.2\%$ (RSD 1.5%). When comparing that value with the $1.6 \pm 0.9\%$ solubility difference between the two pHs for intense ball milling without kaolinite (ca. 7-fold increase, see red/blue data Figure 3–6), the significant difference (10.0% solubility units) along with the very low relative standard

^{lxxx} Comparison is made in terms of the mass of water soluble products (mg) produced from 1000 mg α -chitin (hence the reader should recall the solubility values of the 85.6 BtC set in Figure 3–6 and not the ones with 42.8 BtC).

^{lxxxi} The reproducibility of ball milling for this set of experiments was tested when the 2 and 4 h runs were repeated; sample solubilities in pH 7.0 were $49.40 \pm 2.14\%$ and $67.67 \pm 0.17\%$ respectively. Therefore, 4 h of ball milling generally gives $70.7 \pm 4.3\%$ solubility.

deviation (1.5%) is likely indicative for possibly new types of reactions (perhaps including deacetylation) occurring during the process with kaolinite. At 7 h, the increase of water soluble products stops, hence further increases in milling time were considered beyond the scope of this work. That fact coincides with an increase in the difference between solubilities for the two pHs (from $11.6 \pm 0.2\%$ to 13.9%), and this might suggest of a change in reactivity during that phase of the milling process, but this would require further investigation to be unequivocal.^{lxxxii}

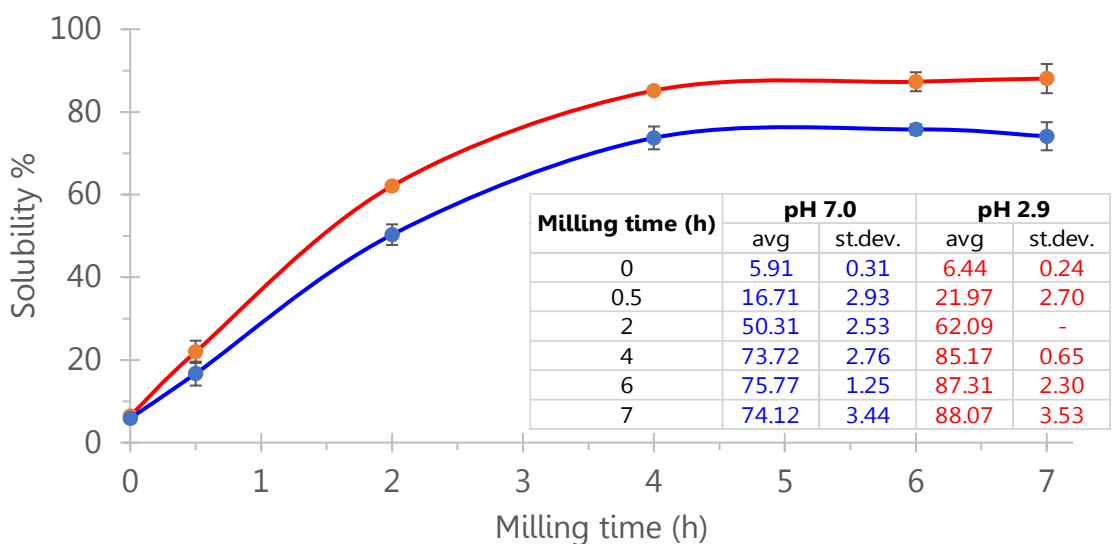


Figure 3-14: Solubility % of α -chitin at pH 7.0 (blue) and 2.9 (red) when ball milled with 68-70 \times 0.25" / 2 \times 0.5" balls (17.5% packing, BtP 42.8) and kaolinite (1:1 g:g). The 2 h milled sample was not tested in replicates in pH 2.9.

^{lxxxii} All samples of water-soluble species of Figure 3-14 were kept in the fridge for further analysis. When the ones milled for 4 h ($73.7 \pm 2.8\%$ at pH 7.0 and $85.2 \pm 0.7\%$ at 2.9) were examined a month after their generation, a visible suspension was observed. When vortexed for 10 s the particles got smaller and the solution appeared more homogeneous. When the sample was left for some time (e.g. 30 min) particles settled down at the bottom of the vial. The samples milled for 2 h ($50.3 \pm 2.5\%$ at pH 7.0 and 62.1% at 2.9) were clear with no visible solid mass.

XRD data for the set of experiments here is given in Figure A3–18, where the patterns of α -chitin (red), and kaolinite (green) when milled with $68\text{-}70 \times 0.25'' / 2 \times 0.5''$ balls [17.5% packing, 85.6 balls-to-powder (BtP) mass ratio] for 4 h, as well as of a 1:1 α -chitin:kaolinite mixture (blue) milled with 42.8 BtP (same packing) for the same time are overlaid. α -Chitin has a 33.5% CrI [(553-368) \times 100% / 553] and two new peaks upon milling; one at 43.72° , and another at 44.64° 2θ , which is tall and sharp. This is indicative of possible new reactions without the effect of kaolinite. The intensities of kaolinite do not exceed 160 (a.u.), which when compared with those of the signal in Figure A3–7 reveal a loss of the clay's native structure (with inevitable delamination). Their 1:1 ball milled mixture exhibits the same masked characteristics shown in Figure A3–10 only with lower intensities (20.0° 2θ region is >750 in the low BtP system while <400 for the set in this section).

An analog slope change observed for the pH 7.0 solubility curve (blue data in Figure 3–14) at 2 h milling time (from linear to logarithmic) has been reported by the Blair group in the work which is discussed in Section 3.1.1.^{lxxxiii} When ball milling 1:1 cellulose:kaolinite mixtures in their 5%-packing steel SPEX system (BtP 12.5), the researchers have systematically^{lxxxiii} measured a change in the solubility curve slope around 1.1 h milling time (solubility at that point was ca. 45%).^{lxxxiv} Taking into

^{lxxxiii} A set of five (conditioned) kaolinites was studied.

^{lxxxiv} The next point reported is at 1.5 h where water soluble products were measured at ca. 60%. This ca. 15 solubility units (%) increase from about 25 min milling comprises a small but not negligible hysteresis compared to the 45 (%) in the first 60 min of the experiment (1).

account that the mixer/mill equipment in between the two studies is exactly the same (operating frequency, vial material and dimensions) the doubling of the time for the change of slopes for α -chitin water-soluble products can surely be attributed to the significantly stronger hydrogen bonding network and probably to a polysaccharide of higher \overline{MW} in this thesis.^{lxxxv} The analogies between the two studies extend even further as both solubilization curves fade out logarithmically to a plateau of ca. 76% with α -chitin reaching it in 6 h and microcrystalline cellulose in 3 h.

Given the aforementioned discussion of the results in this section as well as of that in Section 3.1, the significant improvement in α -chitin solubility with the use of kaolinite in the ball mill process is assumed to be originating from a protonation of the glycosidic oxygen [O(1)]. With the delamination of kaolinite upon grinding, its active specific surface area (ca. 852 m²/g)¹ is likely to offer its protons to the surfaces of α -chitin particles. However, as it has been hypothesized in Section 3.3.2.6, glycosidic oxygens are likely to be in a statistical decline in the collision's trapped volume (which is plastically deformed) due to homolytic cleavage of glycosidic linkages and the several possibilities for subsequent hydrogen abstraction from pyranic carbon atoms. Hence, the stages of collision in which the protons of kaolinite are more likely to protonate glycosidic oxygens of α -chitin (and other

^{lxxxv} As mentioned in Section 3.1.1, microcrystalline cellulose used from the Blair group does not exceed a DP of 400 (2). That value corresponds to a ca. 72 kDa MW (400×180), which falls in the range of Sigma Aldrich's low-MW chitosan [Brookfield viscosity <300 cP which is approximated to not exceed ca. 400 kDa (see Section 3.3.2.5)].

polysaccharides) are either the first or the third where the collision's regime is elastic,²⁰ and stress distribution is more likely to break just hydrogen bonds and statistically expose glycosidic oxygens to the protons of kaolinite.^{lxxxvi} That perspective might be complementing the "end-only" kinetics of the Blair group, as one does not limit the other.¹ Finally, the logarithmic phase and 76% plateau of Figure 3–14 can be attributed to a particle size reduction limit which has been observed for cellulose ball milling.⁹ This empirical explanation is likely to be traced to reagglomeration and coalescence phenomena taking place during mechanochemical processes.¹⁹⁻²¹

Reusability of the milled catalyst was tested by milling 2 g kaolinite with 68 × 0.25" / 2 × 0.5" balls for 3 h and then mixing 1 g of that delaminated clay with 1 g α-chitin and milling with the same packing for 1 h. Solubility of the polysaccharide was found at 21.9 ± 0.7%, while according to $y = 22.247x + 5.7733$ [see page 174 (page 199 of the thesis' pdf)] a 1 h milling with native kaolinite would have produced 28.0% water-soluble products. This difference between the two yields represents a 78.2% reusability, which is a promising advantage of the clay considering the intense pre-milling it has been subjected to.

To check for potential volatile, relatively-non-polar platform molecules formed from ring opening of *N*-acetyl-D-glucosamine, a small set of extraction experiments was

^{lxxxvi} The aforementioned hypothesis does not exclude an O(1) protonation from kaolinite during the second (plastic deformation) stage.

conducted on both ball-milled and water-soluble samples produced in this section. When 250 μL of the water-soluble samples generated after 2 and 4 h of ball milling (of both pHs) were processed with 5 mL solvent (either ethyl acetate or chloroform),^{lxxxvii} the abundances of chromatograms produced with the same GC-MS method as in Section 3.2.5 were below 7000 (only noise detected). The same negative result was obtained also when ca. 200 mg of the 2 h ball-milled^{lxxxviii} sample underwent the aforementioned extraction process.^{lxxxix}

3.3.5 Colorimetric approximation of reducing ends of soluble products

From the solubility data collected and their interpretation, it is evident that the combination of intense ball milling and kaolinite (17.5% packing/BtP 42.8 and 1:1 g:g chitin:kaolinite) provides optimized conditions for the mechanochemical conversion of α -chitin to water-soluble products. Since yields of fermentable reducing sugars comprise an indicative criterion for the effectiveness of a polysaccharide valorization method,^{39,40} the reducing potential of the pH 7.0 soluble species generated in Section 3.3.4 was of extensive scope to investigate. Reducing ends of chitin molecules (Figure 1–4) arise from the hemiacetal tautomeric equilibrium between the open-ring aldehyde (and its hydrate) form (acyclic) and

^{lxxxvii} Extraction process was similar to that reported for levulinic acid (LA) (vortex at room temperature-centrifugation-evaporation-reconstitution).

^{lxxxviii} With 17.5% packing, BtP 42.8.

^{lxxxix} Future investigations might focus on using different solvents and maybe at higher temperatures.

the various cyclic forms (mainly α and β anomers of the pyranose).^{41,42 xc} The most convenient and communicative methods to measure concentrations of reducing sugars in depolymerized polysaccharide samples are colorimetric assays,^{44,45} with more than five oxidizing agents reported in literature.⁴⁶⁻⁴⁸ All these assays attain similar qualitative results but vary in their detection limits, sensitivity, linear quantification range and operating conditions (temperature and pH).⁴⁸ Most of them express the concentration of reducing sugar molecules (analytes) usually in g/L, hence in Table 3-1, a conversion of the % solubilities of Figure 3-14 to solubilities in g/L provides the basis for further analysis. The methods most studied over the past decades have been the Nelson-Somogyi (NS), and the 3,5-dinitrosalicylic acid (DNS).⁴⁹⁻⁵¹ The latter was selected as a starting point since it has been applied often in the field of cellulose hydrolysis.⁵²⁻⁵⁴

Table 3-1: Conversion of % solubility (pH 7.0) of ball milled α -chitin products (Figure 3-14) to solubility in g/L based on the actual mass (g) which was solubilized in 7.5 mL water.

Milling time (h)	Solubility %		Soluble mass (g)		Solubility (g/L)	
	avg	st. dev.	avg	st. dev.	avg	st. dev.
0.5	16.71	2.93	0.0189	0.0023	2.5	0.3
2	50.31	2.53	0.0623	0.0082	8.3	1.1
4	73.72	2.76	0.0989	0.0218	13.2	2.9
6	75.77	1.25	0.0857	0.0079	11.4	1.0
7	74.12	3.44	0.0854	0.0103	11.4	1.4

^{xc} The proportion of the acyclic forms for various aldohexoses has been found to not exceed 1% (43).

3.3.5.1 Dinitrosalicylic acid (DNS) method

The 3,5-dinitrosalicylic acid (DNS) assay was first presented by Sumner and Graham in 1921 to measure reducing sugars in the urine.⁵⁵ The basis of the method lies on the concurrent oxidation of functional sugar groups and the reduction of DNS (yellow compound) to 3-amino-5-nitrosalicylic acid (orange compound) when alkaline conditions and heat are applied. Although the pure form of the latter molecule has an absorption maximum at 458 nm, reproducible measurements for the assay are obtained for wavelengths above 520 nm.⁵⁶ The oxidizing reagent was subsequently advanced by the addition of Rochelle salt (sodium potassium tartrate), phenol and sodium bisulfite, which protect from dissolved oxygen, enhance and stabilize the reaction color respectively. The concentrations of all the components of the DNS reagent were optimized by Miller in 1959 on the basis of maximum color development at 575 nm upon 5 min reactions with equal volumes of glucose solutions in a boiling water bath. In summary they are: 44 mM DNS, 0.25 M NaOH, 0.18 M Rochelle salt,^{xci} 21 mM phenol, and 4.0 mM Na₂SO₃. The reagent could quantify reducing sugars up to 0.2 g/L.¹² In 1987, as part of the efforts for standardizing protocols for the measurement of cellulase activities, the International Union of Pure and Applied Chemistry (IUPAC) has modified the aforementioned concentrations on the basis of 25–40% sugar-sample/DNS-reagent volume ratio and readings at 540 nm to: 33 mM DNS, 0.35 M NaOH, 0.77 M Rochelle salt, 61 mM

^{xci} Addition of the Rochelle salt to the reaction mixture is suggested by Miller immediately after color development and before its cooling due to interference with bisulfite's role.

phenol, and 31.0 mM Na₂S₂O₅.^{xcii} The reagent here could quantify reducing sugars up to 5 g/L (possibly up to 10 g/L).¹³

In preliminary experiments, a 44 mM DNS reagent was prepared in approximation to the Miller method (in the absence of Rochelle salt and phenol) and reacted accordingly (ca. 93 °C oil bath) with equal volumes of standard solutions of *N*-acetyl-D-glucosamine (NAG) in the range of 1.3 to 14.7 g/L.^{xciii} After ca. 3 min of heating, a yellow to orange color change was observed for the >8.0 g/L NAG solutions, which was qualitative confirmation of the method even at concentrations much higher than those designed for. However, when UV-Vis spectra were acquired, all signals were saturated with their intensities in the targeted wavelength region (below 600 nm) being higher than the spectrometer's 0.0–1.5 (AU) linear dynamic range.

Therefore, it was realized that the concentration of 3,5-dinitrosalicylic acid had to be lowered. Figure 3–15 shows the UV-Vis spectra of initial reaction mixtures^{xciv} between equal volumes of a standard glucose solution and DNS reagents of 0.702 (red), 0.351 (orange), 0.176 (green), and 0.088 (blue) mM 3,5-dinitrosalicylic acid. It is clear that the 44 mM 3,5-dinitrosalicylic acid of the Miller method has to be diluted at least 250 times to have a smooth peak at ca. 371 nm. Moreover, in order

^{xcii} Just as in the Miller method, reaction mixtures developed the color of the product upon 5 min heating in 100 °C.

^{xciii} The total reaction mixture volume was 4000 µL.

^{xciv} Initial reaction mixture means before the application of heating.

to have the least absorbance possible in the region higher than 500 nm [e.g. below 0.010 (AU)], it is suggested to dilute 500 times (blue data are for 0.088 mM 3,5-dinitrosalicylic acid in the DNS reagent).

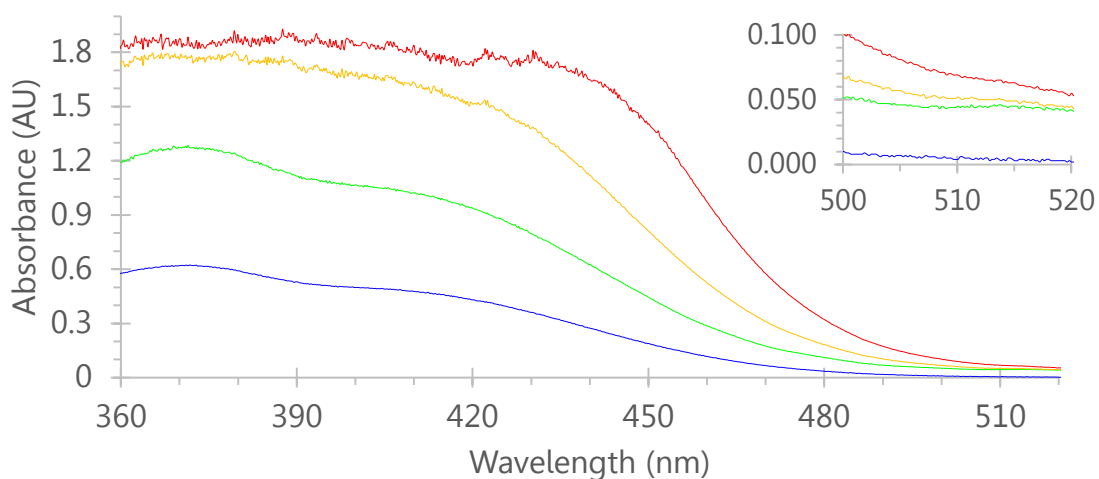


Figure 3-15: UV-Vis spectra of initial reaction mixtures between equal volumes of a standard glucose solution and DNS reagents of 0.702 (red), 0.351 (orange), 0.176 (green), and 0.088 (blue) mM 3,5-dinitrosalicylic acid. Inset reads more detail in the 500–520 nm region.

Although both IUPAC and Miller DNS reagents are intensely alkaline, they are not exactly at the same level. In the former case a 0.35 M NaOH solution offers a pH of 13.60, while in the latter the concentration of 0.25 M brings the oxidizing reagent to a pH of 13.40. Figure A3–19 shows UV-Vis spectra of 1500 μL of a 1.86 mM glucose solution after being reacted upon microwave irradiation for 5 min at 100 $^{\circ}\text{C}$ with 1500 μL IUPAC-like DNS reagents [0.088 mM 3,5-dinitrosalicylic acid, ca. 0.9 M tartaric acid disodium salt dihydrate, 62 mM phenol, 32 mM $\text{Na}_2\text{S}_2\text{O}_5$] of the

following pH values: 12.80 (blue), 13.24 (green), and 13.60 (red).^{xcv} When comparing the intensities of this small set of signals at 540 nm, it is clear that a pH difference in the order of 0.20 units (from 13.40 to 13.60) corresponds to a ca. 0.055 difference in absorbance (from 0.121 to 0.176), which represents a significant increase (45%) in 3-amino-5-nitrosalicylic acid production. Therefore, a pH of 13.60 was selected for further studies as it would provide a sensitive response to reducing sugar concentrations.

Both IUPAC and Miller DNS reagents use sulfite substances ($\text{Na}_2\text{S}_2\text{O}_5$ and Na_2SO_3 respectively) in order to stabilize the color developed in the presence of phenol (presumably by scavenging dissolved oxygen). However, more recent DNS assays seem to find them unnecessary.⁵⁷⁻⁵⁹ In order to investigate the effect of that component, IUPAC-like and sulfite-free DNS reagents were reacted with two levels of glucose concentration. Figure A3–20 shows UV-Vis spectra of 1500 μL of 1.86 (blue/red) and 0.93 (turquoise/orange) mM glucose solutions after being reacted upon microwave irradiation for 5 min at 100 °C with 1500 μL IUPAC-like [blue/turquoise; 0.088 mM 3,5-dinitrosalicylic acid, 0.40 M NaOH, ca. 0.9 M tartaric acid disodium salt dihydrate, 62 mM phenol, 32 mM $\text{Na}_2\text{S}_2\text{O}_5$] and sulfite-free [red/orange; 0.088 mM 3,5-dinitrosalicylic acid, 0.39 M NaOH, 0.77 M tartaric acid disodium salt dihydrate, 18 mM phenol] DNS reagents. The clearly higher absorbances at 540 nm of the sulfite-free assays at both levels of glucose

^{xcv} Heating in an oil bath was found inefficient when switching to test tubes of thicker glass.

concentration led to the exclusion of that component from further experimentation. Likewise, Figure A3–21 exhibits enhanced absorbance at 540 nm for phenol-containing DNS reagent; therefore that component was included in the following assays.^{xcvi}

As shown in Figure 3–7, water soluble products contained intensely coloured species. Therefore, dilution was considered necessary in order to bring the above 520 nm analyte absorbance to levels which are comparable to those of the selected DNS reagent (0.088 mM 3,5-dinitrosalicylic acid) in the reaction mixture [e.g. at least below 0.100 (AU)]. Figure 3–16 exhibits the UV-Vis spectra of duplicate measurements of 1:20 (orange-red) and 1:40 (turquoise-green) dilutions of the most concentrated and intensely-coloured water-soluble products of Figure 3–14 ($88.07 \pm 3.53\%$ or 13.1 ± 1.9 g/L from 7 h ball milling).^{xcvii} Considering the instrument's precision, the 520 nm absorbance of the 1:20 dilution (0.66 g/L) is found below 0.100 and that of the 1:40 (0.33 g/L) below 0.060. Hence, in order to quantify the reducing sugars into monomeric equivalents, glucose and *N*-acetyl-D-glucosamine calibration curves aimed at concentrations below 0.33 g/L.

^{xcvi} Future researchers might try and avoid the use of toxic phenol by optimizing the other components of the DNS assay or/and considering less hazardous substitutes proposed like cysteine (60).

^{xcvii} The actual soluble mass of the 7 h milled sample in 7.5 mL of pH 2.9 was 97.9 ± 14.0 mg, which corresponds to a solubility of 13.1 ± 1.9 g/L.

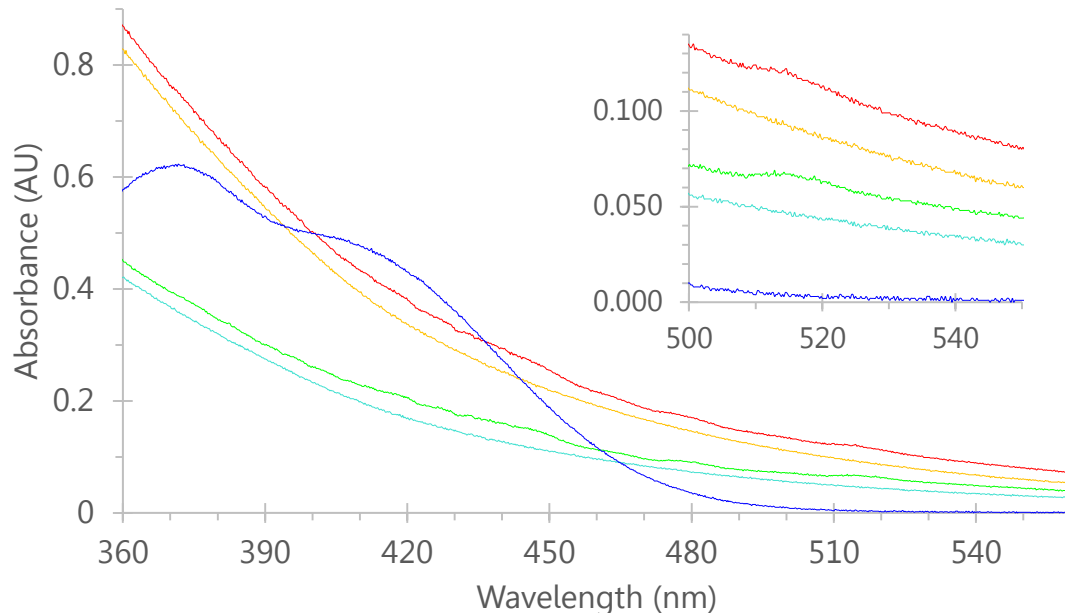


Figure 3-16: UV-Vis spectra of duplicate measurements of 1:20 (orange-red) and 1:40 (turquoise-green) dilutions of the most concentrated and intensely-coloured water-soluble products of Section 3.3.4 ($88.07 \pm 3.53\%$ from 7 h ball milling). The DNS reagent of 0.088 mM 3,5-dinitrosalicylic acid diluted with equal volume of a standard glucose solution (blue) is overlaid for comparison purposes. Inset reads more detail in the 500-550 nm region. Intensity of the 1:40 dilution at 540 nm is 0.042 ± 0.011 .

Figure 3-17 shows three glucose calibration curves for three DNS assays. The red one is with DNS reagent A [0.088 mM 3,5-dinitrosalicylic acid, 0.4079 M NaOH (pH 13.61), 0.766 M tartaric acid disodium salt dihydrate (MW 230.1 g/mol), 17.0 mM phenol] and the blue one is with DNS reagent B [0.088 mM 3,5-dinitrosalicylic acid, 0.3997 M NaOH (pH 13.60), 1.063 M tartaric acid disodium salt dihydrate (MW 230.1 g/mol), 21.6 mM phenol]. Data for both were obtained by 5 min microwave runs at

100 °C between equal volumes of DNS reagent and glucose solution (1500 μL).^{xcviii} The green one was obtained by Saqib and Whitney when 4 mL of DNS reagent C [44 mM 3,5-dinitrosalicylic acid, 0.4 M NaOH (pH 13.60), 1.063 M Rochelle salt (MW 282.1 g/mol)] reacted with 1 mL glucose solution upon 5 min heating in a boiling water bath.⁵⁸ Although DNS reagents A (red) and B (blue) revealed very good linearity for the concentration ranges presented, their response to glucose was less sensitive to reagent C (green) (slopes are evidently lower than 0.2359).^{xcix} Moreover, the quantification limits for DNS reagents A and B are clearly higher (> 0.50 mM) than that of reagent C (<0.20 mM). These differences between the assay of reagent C and the other two can be attributed to the 2000 times higher 3,5-dinitrosalicylic acid to glucose molar ratio in the former case.^{c ci} With more nitro groups around the open-ring aldehydes of glucose, it is reasonable for the assay of reagent C to produce higher concentrations of 3-amino-5-nitrosalicylic acid compared to those of reagents A and B. The slightly higher slope (sensitivity i.e. resolution) and quantification limit of reagent's B assay compared to that of reagent

^{xcviii} UV-Vis spectra for the calibration curve of reagent's B assay can be consulted in Figure A3-22.

^{xcix} The $y = \alpha x + \beta$ equations correspond to x values (glucose concentrations) in mM.

^c On the basis of the 1.00 mM glucose reaction mixture, the 3,5-dinitrosalicylic acid to glucose molar ratio for the assay of reagent B is 0.088 (0.088 mM/mM \times 1 $\mu\text{L}/\mu\text{L}$), and for the assay of reagent C 176 (44 mM/mM \times 4 $\mu\text{L}/\mu\text{L}$). Hence, reagent C initiates all reactions of its calibration with 2000 times (176 \div 0.088) higher 3,5-dinitrosalicylic acid to glucose molar ratio.

^{ci} That is assuming that the amounts of thermal energy transferred to the reaction mixture and UV-Vis detector responses are equal. Moreover, the assumption should include negligible effects of Rochelle salts and phenol.

A can be attributed to its higher concentrations of tartaric acid disodium salt dihydrate [39% (from 0.766 to 1.063 M)] and phenol [27% (from 17.0 to 21.6 mM)].^{cii}

Figure A3–23 exhibits the UV-Vis spectra of standard *N*-acetyl-D-glucosamine (NAG) solutions of 0.594 (orange), 0.927 (green), 1.224 (blue), 1.484 (red) mM after being reacted upon microwave irradiation for 5 min at 100 °C with DNS reagent A.

Unlike the results with glucose (red data in Figure 3–17), and despite the stronger absorbances below 1.00 mM, the signals revealed a lack of linearity for the concentration range 0.59–1.22 mM ($y = 0.1589x + 0.0026$, $R^2 = 0.8833$).^{ciii}

Considering also the scarcity of DNS assays, which might quantify reducing sugars from chitin into *N*-acetyl-D-glucosamine equivalents, DNS reagent B was applied to ball milled α -chitin products with the scope to obtain an approximation of their reducing potential in glucose equivalents.

^{cii} pH values of all three DNS reagents were the same (ca. 13.60).

^{ciii} A loss of linearity to lower absorbance values was also observed for glucose concentrations higher than 1.50 mM, which might be the reason why Saqib and Whitney have not experimented with higher concentrations (58).

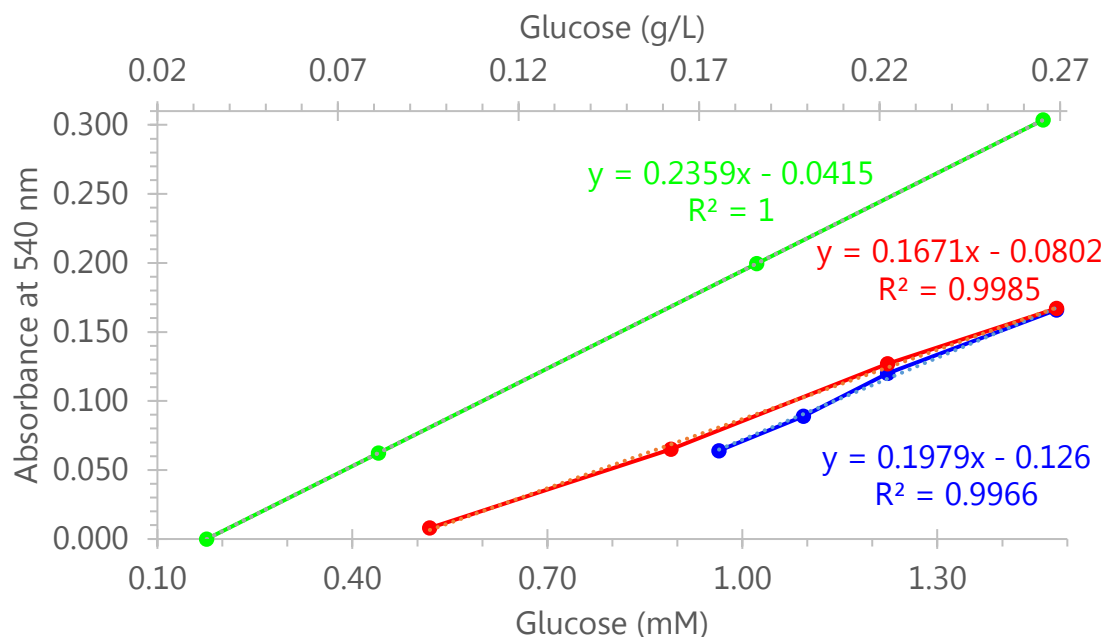


Figure 3-17: Glucose calibration curves for DNS assays with reagent A [red; 0.088 mM 3,5-dinitrosalicylic acid, 0.4079 M NaOH (pH 13.61), 0.766 M tartaric acid disodium salt dihydrate, 17.0 mM phenol] and reagent B [blue; 0.088 mM 3,5-dinitrosalicylic acid, 0.3997 M NaOH (pH 13.60), 1.063 M tartaric acid disodium salt dihydrate, 21.6 mM phenol] obtained by 5 min microwave treatments at 100 °C [volumes of DNS reagent and glucose solution were equal (1500 μ L)]. Assay of reagent C [green; 44 mM 3,5-dinitrosalicylic acid, 0.4 M NaOH (pH 13.60), 1.063 M Rochelle salt] was obtained by Saqib and Whitney in a similar way (volumes of DNS reagent and glucose solution were 4 and 1 mL respectively). The $y = \alpha x + \beta$ equations correspond to x values (glucose concentrations) in mM. Secondary horizontal axis reads glucose concentrations in g/L. UV-Vis spectra for reagent's B assay are shown on Figure A3-22.

Figure 3-18 illustrates UV-Vis spectra of 2.5 (red), 8.3 (green), and 11.4 (blue) g/L ball milled α -chitin products after 1500 μ L of their corresponding diluted aliquots [0.18 (red), 0.21 (green), and 0.24 (blue) g/L] were treated by microwaves for 5 min at 100 °C with 1500 μ L DNS reagent B [0.088 mM 3,5-dinitrosalicylic acid, 0.3997 M NaOH (pH 13.60), 1.063 M tartaric acid disodium salt dihydrate, 21.6 mM

phenol]. When comparing the intensities at 540 nm before and after the reaction, it is clear that the species from the samples of 6 and 2 h milling give positive proof for reducing sugar oxidation, while the ones from 0.5 h not. Based on the corresponding glucose calibration curve (reagent B), Table 3–2 approximates the concentration of reducing sugars in the ball milled samples in glucose equivalents (Glc-eq in g/L). With the standard deviation of absorbances at 540 nm expected to not exceed 0.011 (see Figure 3–16), potential reducing species from the 0.5 h milling sample (0.002 ± 0.011) coincide with the hypothesized quantification limit of the calibration curve (0.62 mM). More importantly, however, the absorbance elevations originating from the redox reaction (final – initial reaction mixture) of the 2 (0.031) and 6 ($0.054 - 0.031 = 0.023$) h milling samples exceed the standard deviation for the set of UV-Vis measurements in this section (0.011). Hence, the corresponding 0.79 and 0.91 mM measured glucose equivalents (0.14 and 0.16 g/L respectively) can be extrapolated to glucose equivalents (g/L) before their dilution. The more than 230% Glc-eq increase (from 1.6 to 5.7 g/L) for the 0.5 to 2 h milling samples, and the ca. 36% Glc-eq increase (from 5.7 to 7.7 g/L) for the 2 to 6 h ones are in line with the corresponding solubility growths of those samples (2.5-8.3-11.4 g/L; see Table 3–1). Therefore, it is meaningful to consider the percentage of soluble species that those Glc-eq concentrations correspond to. With the deviations in between the 63-69-68% for the set of samples studied with DNS reagent B being so small ($66 \pm 3\%$), it is only reasonable to assume that glucose equivalents offer an acceptable approximation of reducing sugar quantification of the ball milled

samples in this chapter. However, the remaining ca. 34% can be hypothesized to arise from a different response of *N*-acetyl-D-glucosamine (or/and potential chitin oligomers) to DNS reagents; and since a lack of linearity was observed when a calibration curve for NAG was attempted, another colorimetric method was pursued.^{civ}

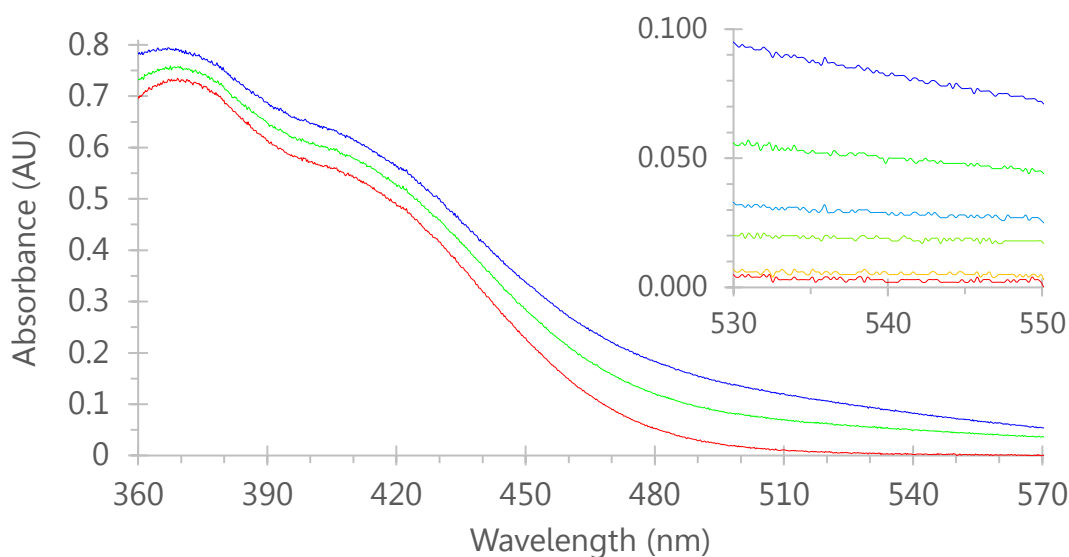


Figure 3-18: UV-Vis spectra of 2.5 (red), 8.3 (green), and 11.4 (blue) g/L ball milled α -chitin products after 1500 μ L of their corresponding diluted aliquots [0.18 (red), 0.21 (green), and 0.24 (blue) g/L] were treated by microwaves for 5 min at 100 $^{\circ}$ C with 1500 μ L DNS reagent B [0.088 mM 3,5-dinitrosalicylic acid, 0.3997 M NaOH (pH 13.60), 1.063 M tartaric acid disodium salt dihydrate, 21.6 mM phenol]. Inset focuses on the 530–550 nm region and includes the corresponding signals before the application of microwave irradiation (orange below 0.010 for 0.18 g/L sample, lighter green at 0.020 for 0.21 g/L and lighter blue at 0.030 for 0.24 g/L).

^{civ} In addition, when the rest of the visible spectrum was examined, it was observed that the samples of 2 and 6 h milling exhibited their maximum absorbance (of final – initial reaction mixture) at ca. 471 nm [their intensities reached 0.059 (vs 0.031) and 0.097 (vs 0.054) respectively]. Hence, a quantification of reducing sugars at 540 nm might prove not fitting for water-soluble products of chitin ball milling.

Table 3-2: Reducing sugars approximation [glucose equivalents (g/L)] in water-soluble α -chitin species generated upon optimized ball milling conditions. Absorbance values (Figure 3–18) were translated into glucose equivalents by DNS reagent's B calibration curve ($y = 0.1979 x - 0.126$), which was assumed to be linear beyond 0.96–1.48 mM.

Measured quantity by DNS assay		Milling time (h)		
		0.5	2	6
Absorbance at 540 nm	final	0.002	0.050	0.082
	initial	0.005	0.019	0.028
	final - initial	-0.003	0.031	0.054
Diluted glucose equivalents	mM	0.62	0.79	0.91
	g/L	0.11	0.14	0.16
Dilution factor		14	40	47
Glucose equivalents	g/L	1.6	5.7	7.7
	% of soluble species	63	69	68

3.3.5.2 Schales' method

The Schales assay was invented by Selma and Otto Schales in 1945 as a result of their efforts to determine glucose in blood with a colorimetric procedure that would not require strict conditions and formation of a new color. The method is based on the disappearance of ferricyanide (yellow) upon its reduction by the acyclic forms of aldohexoses in strongly alkaline conditions.⁶¹ In 1971, Imoto and Yagishita developed a practical Schales reagent (0.5 g/L $K_3Fe(CN)_6$, 0.5 M Na_2CO_3), which provided reproducible measurements of *N*-acetyl-D-glucosamine (NAG) with 15 min heating of 1.3/1.0 v/v Schales-reagent/sugar solution ratio.¹⁴

Figure 3–19 shows the *N*-acetyl-D-glucosamine calibration curve prepared for the method (the corresponding UV-Vis spectra are on Figure A3–24). The data show

good linearity, and they are in good agreement with that of Eijssink and Horn.^{62 cv} Just as in the DNS method, dilution of the analyte was considered necessary to bring its 420 nm absorbance to levels which are comparable to those of the Schales reagent in the initial reaction mixture (ca. 0.91). Figure 3–20 exhibits the UV-Vis spectra of 2000 μL Schales reagent when mixed with 1500 μL of 15 (pink), 20 (red), 25 (orange), 30 (green), 35 (blue), 47 (purple) fold dilutions of intensely-coloured water-soluble products of Section 3.3.4 ($75.77 \pm 1.25\%$ from 6 h ball milling). The inset reveals a linear function between the absorbances at 420 nm (y) and the dilution factor (x): $y = 0.0082 x + 0.3823$. Using that equation, it was calculated that a ca. 0.91 absorbance for the initial reaction mixture would require a dilution factor for the 6 h ball milled soluble products of 65.

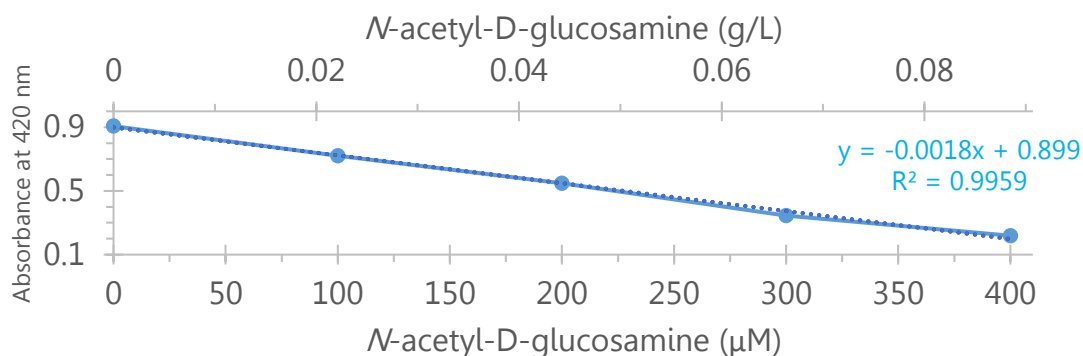


Figure 3-19: *N*-acetyl-D-glucosamine (NAG) calibration curve for the Schales assay. The $y = \alpha x + \beta$ equation corresponds to x values (NAG concentrations) in μM . Secondary horizontal axis reads NAG concentrations in g/L. UV-Vis spectra for the assay are shown on Figure A3–24.

^{cv} The 5 min shorter heating time in this study can be hypothesized to result from the efficiency of the microwave process.

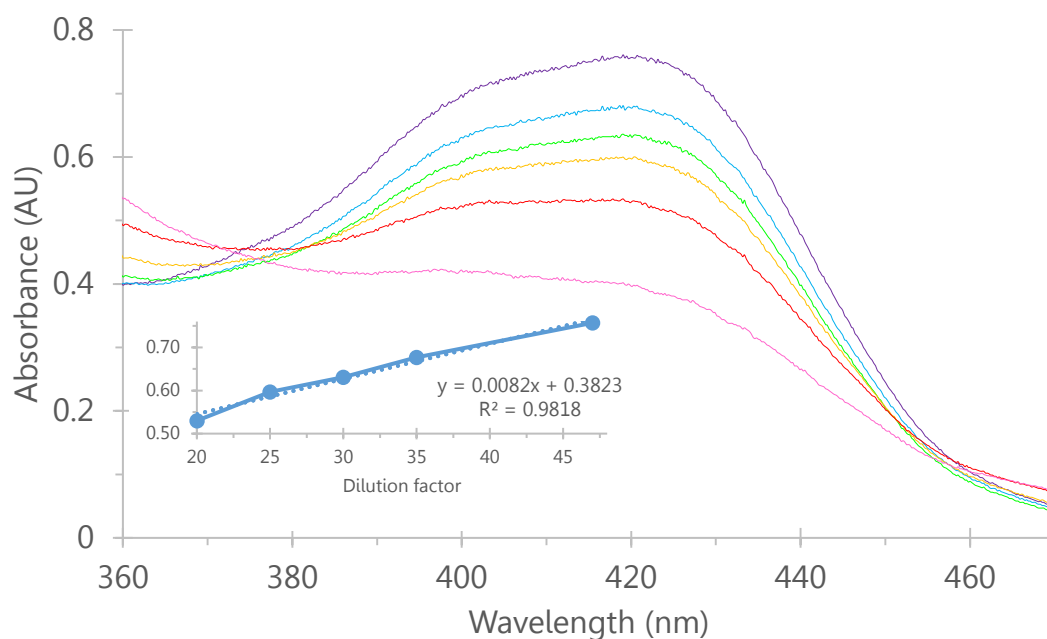


Figure 3-20: UV-Vis spectra of 2000 μL Schales reagent when mixed with 1500 μL of 15 (pink), 20 (red), 25 (orange), 30 (green), 35 (blue), 47 (purple) times diluted intensely-coloured water-soluble products of Section 3.3.4 ($75.77 \pm 1.25\%$ from 6 h ball milling). Inset plots the absorbances at 420 nm against the dilution factor [the value for the 15-fold dilution (0.396) was excluded as it deviated significantly from the linear equation reported (R^2 was ca. 0.91)].

Figure 3-21 shows the UV-Vis spectra of 2.5 (light blue), 8.3 (green), and 11.4 (orange) g/L ball milled α -chitin products after 1500 μL of their corresponding 65-fold dilutions [0.039 (darker blue), 0.128 (green), and 0.176 (red) g/L; signals for initial reaction mixtures absorb above 0.78 at 420 nm] were treated by microwaves for 10 min at 100 $^\circ\text{C}$ with 2000 μL Schales reagent. When comparing the intensities at 420 nm before and after the reaction, it is clear that the species from all three samples give positive proof for reducing sugar oxidation. Based on the corresponding *N*-acetyl-D-glucosamine calibration curve, Table 3-3 approximates the concentration of reducing sugars in the ball milled samples in monomer

equivalents (NAG-eq in g/L). Just like in the DNS assay, ferricyanide disappearance originating from the redox reaction (initial - final reaction mixture) of the 0.5 (0.102), 2 (0.340) and 6 (0.566) h milling samples increases with increasing milling time. Hence, the corresponding 73, 235, 371 μM measured NAG equivalents (0.017, 0.053, 0.084 g/L respectively) can be extrapolated to NAG equivalents (g/L) before their dilution. The 220% NAG-eq increase (from 1.1 to 3.5 g/L) for the 0.5 to 2 h milling samples, and the 58% NAG-eq increase (from 3.5 to 5.5 g/L) for the 2 to 6 h ones are in line with the corresponding solubility growths of those samples (2.5-8.3-11.4 g/L; see Table 3-1). Therefore, it is meaningful to consider the percentage of soluble species that those NAG-eq concentrations correspond to. With the deviations in between the 43-42-48% for the set of samples studied with Schales reagent being so small ($44 \pm 3\%$), it is only reasonable to assume that NAG equivalents offer an acceptable approximation of reducing sugar quantification of the ball milled samples in this chapter. However, the remaining ca. 56% can be hypothesized to arise from a different response of chitin oligomers to Schales reagent.

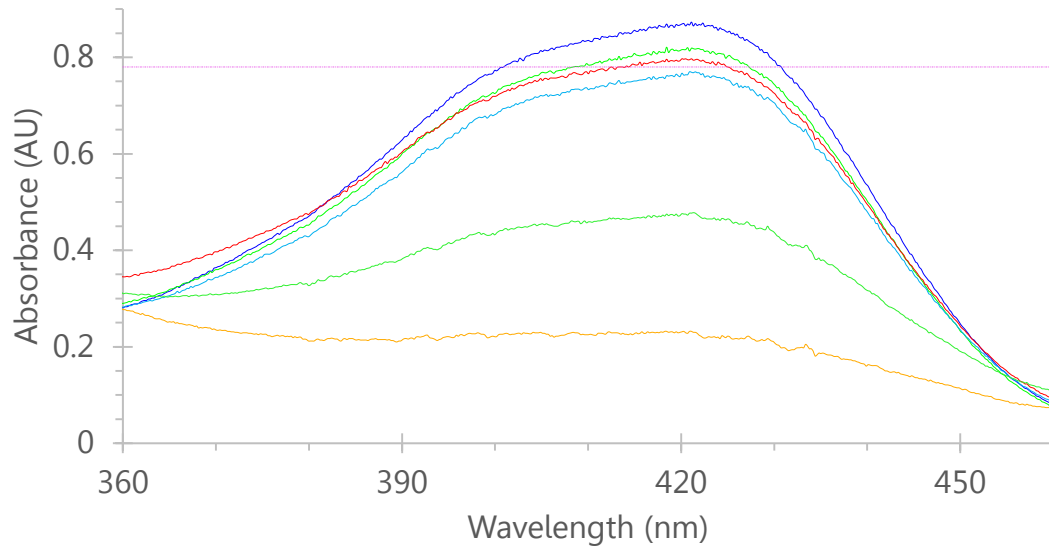


Figure 3-21: UV-Vis spectra of 2.5 (light blue), 8.3 (green), and 11.4 (orange) g/L ball milled α -chitin products after 1500 μ L of their corresponding 65-fold dilutions [0.039 (darker blue), 0.128 (green), and 0.176 (red) g/L; signals for initial reaction mixtures absorb above 0.78 at 420 nm] were treated by microwaves for 10 min at 100 °C with 2000 μ L Schales reagent. Pink dotted line with transparency marks the absorbance level at 0.78.

Table 3-3: Reducing sugars approximation [NAG equivalents (g/L)] in water-soluble α -chitin species generated upon optimized ball milling conditions. Absorbance values (Figure 3–21) were translated into NAG equivalents by Schales reagent calibration curve ($y = - 0.0018 \cdot x + 0.899$).

Measured quantity by Schales assay		Milling time (h)		
		0.5	2	6
Absorbance at 420 nm	final	0.767	0.476	0.231
	initial	0.869	0.816	0.797
	Initial - final	0.102	0.340	0.566
Diluted NAG equivalents	μ M	73	235	371
	g/L	0.017	0.053	0.084
Dilution factor		65	65	65
NAG equivalents	g/L	1.1	3.5	5.5
	% soluble species	43	42	48

What is important for the results of Section 3.3.5 is not the determination of concentrations of reducing sugars as both of the colorimetric methods used display differential behaviours towards different degrees of polymerization (DP),^{58,62} rather that they responded in a consistent way to the increases of solubility for increasing milling time. Since the unknown variability in molecular weights could have led traditional separation techniques (chromatography, electrophoresis, analytical centrifugation) to characterization problems (broad peaks/bands),⁶³ a mass spectrometry (MS) approach was undertaken to determine the composition of the water-soluble products of the optimized ball-milling process.

3.3.6 Mass spectrometry analysis of soluble products with matrix assisted laser desorption ionization (MALDI)

Due to their negligible vapor pressure and complex structures (involving various non-covalent interactions), mass spectrometry analysis of biopolymers (proteins, nucleic acids, saccharides) has started developing only in the 1980s with the introduction of ion desorption techniques [fast atom bombardment (FAB), electrospray ionization mass spectrometry (ESI MS), and matrix-assisted laser desorption–ionization (MALDI)].⁶⁴ Unlike proteins, for which peptide bond scission is likely to lead to relatively defined fragmentation patterns, carbohydrates undergo more complex fragmentations due to cleavages of glycosidic linkages as well as bonds between several stereogenic centres comprising the rings.⁶⁵⁻⁶⁷ The influence of the nature of the parent ion on fragmentation is significant with positively charged analytes receiving more attention.⁶⁸ Besides those with amino groups (e.g.

chitosan), saccharide molecules are neutral and therefore their basicity potential is low for attraction of protons. Even when they do protonate, those species decompose much faster than adducts with metal cations (mainly from group I), which consequently are of more use for qualitative analysis.^{66,67} ^{cvi} Ionization efficiencies have been reported to vary with molecule size and desorption method with MALDI demonstrating good reproducibility on quantitative analysis of oligosaccharide mixtures.^{67,69} However, by introducing a charge-tag (derivatization), stronger intensities and independency of metal adducts can be gained regardless of the analyte concentration.⁶⁷

Therefore, at Memorial University, a method has been developed for analyzing sugars using MALDI-TOF MS.⁷⁰ The process reduces the need for time- and solvent-intensive chromatographic separations, which is desirable in greener analytical method development.⁷¹ Applying the procedure to water-soluble milled products, oligomers of GlcNAc with degrees of polymerization (DP) between 1 and 5 were detected as their derivatives using glycidyltrimethylammonium chloride GTMA. Figure 3–22 shows a representative reaction scheme for the formation of the derivatives on the primary alcohols of chitin molecules.^{cvi} The quaternary ammonium tag offers increased sensitivity towards carbohydrate analytes.¹⁵

^{cvi} It has been hypothesized that complexation of the cation occurs via the participation of multiple oxygen lone pairs (67).

^{cvi} The primary alcohol is the most reactive/nucleophilic site for both steric and electronic reasons (72,73).

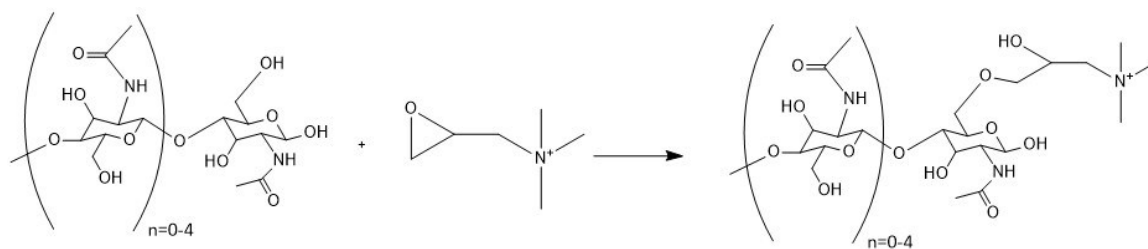


Figure 3-22: Representative reaction scheme for the formation of chitin-GTMA derivatives.

3.3.6.1 Qualitative analysis

Figure 3-23 shows MALDI-TOF mass spectra of the soluble products from ball milling α -chitin with $68\text{-}70 \times 0.25'' / 2 \times 0.5''$ balls (17.5% packing, BtP 42.8) and kaolinite (1:1 g:g) for 0.5 h (A), 2 h (B) and 6 h (C). In all spectra, the intensities of the derivative species in decreasing order are: dimer (m/z 540.3), monomer (m/z 337.2), trimer (m/z 743.4), tetramer (m/z 946.5), and pentamer (m/z 1149.6).^{cviii cix cx}

As expected based on the previously described colorimetry/solubility data, the intensities of the peaks assigned to the dimer and monomer increase with increasing milling time. The intensities of the corresponding dehydrated fragments ($[\text{ion} - \text{H}_2\text{O}]^+$, m/z 319.2, 522.3, 725.4, 928.5, 1131.6) decrease with oligomer size.

^{cviii} Representative data regarding the m/z precision are given in Figures A3-4 and A3-5. The standard deviation for the set of samples analyzed did not exceed 82.5 ppm [± 0.021 for the (GlcNAc)₅ derivative peak (average m/z among 7 spots was 1149.609) of the 6 h milled sample], which provides a very good level of certainty for the first decimal. Figure A3-25 shows the structures and exact masses of the analytes (monomer to pentamer).

^{cix} For details on m/z accuracy see Appendix A3.1.

^{cx} If the average spectrum for the blank derivatization reaction (Figure A3-6) was not subtracted from the ones for the analyzed samples, the intensities of the GTMA peaks (m/z 116.1, 134.1), which in general were at least 6 times higher than those for the analytes, would not have allowed the relative heights of the five analytes to be highlighted (spectra for the samples would have appeared like in Figure A3-28).

GlcNAc is known to dehydrate under catalytic and noncatalytic conditions to form Chromogen I^{74,75} (which with the quaternary ammonium tag used here would appear at m/z 319.2), and we propose that the other dehydrated fragments observed are formed in a similar way. The protonated fragments of the derivatives (m/z 338.2, 541.3, 744.4, 947.5, 1150.6) were also observed but were much weaker than their parent peaks [over 8 times less intense for the monomer (Figure A3–29), 5 times for the dimer (Figure A3–27), 3 times for the trimer, 2.5 times for the tetramer and 2 times for the pentamer]. Underivatized oligomers (m/z 221.2, 424.4, 627.6, 830.8, and 1034.0) were not detected. This is not surprising as the derivatization method can lead to a 2000-fold increase in sensitivity.¹⁵ The peaks at m/z 133.1 and 229.2 likely arise from degradation of GlcNAc in the ionization process as they were observed in spectra of GlcNAc standards (although in lower proportions; see inset tables with peak lists in Figure A3–29). Other minor peaks (m/z 429.2, 547.3, 565.3, 632.2, 835.4) were not assigned and could come from degradation products (either formed within the mass spectrometer or during the ball-milling processes).

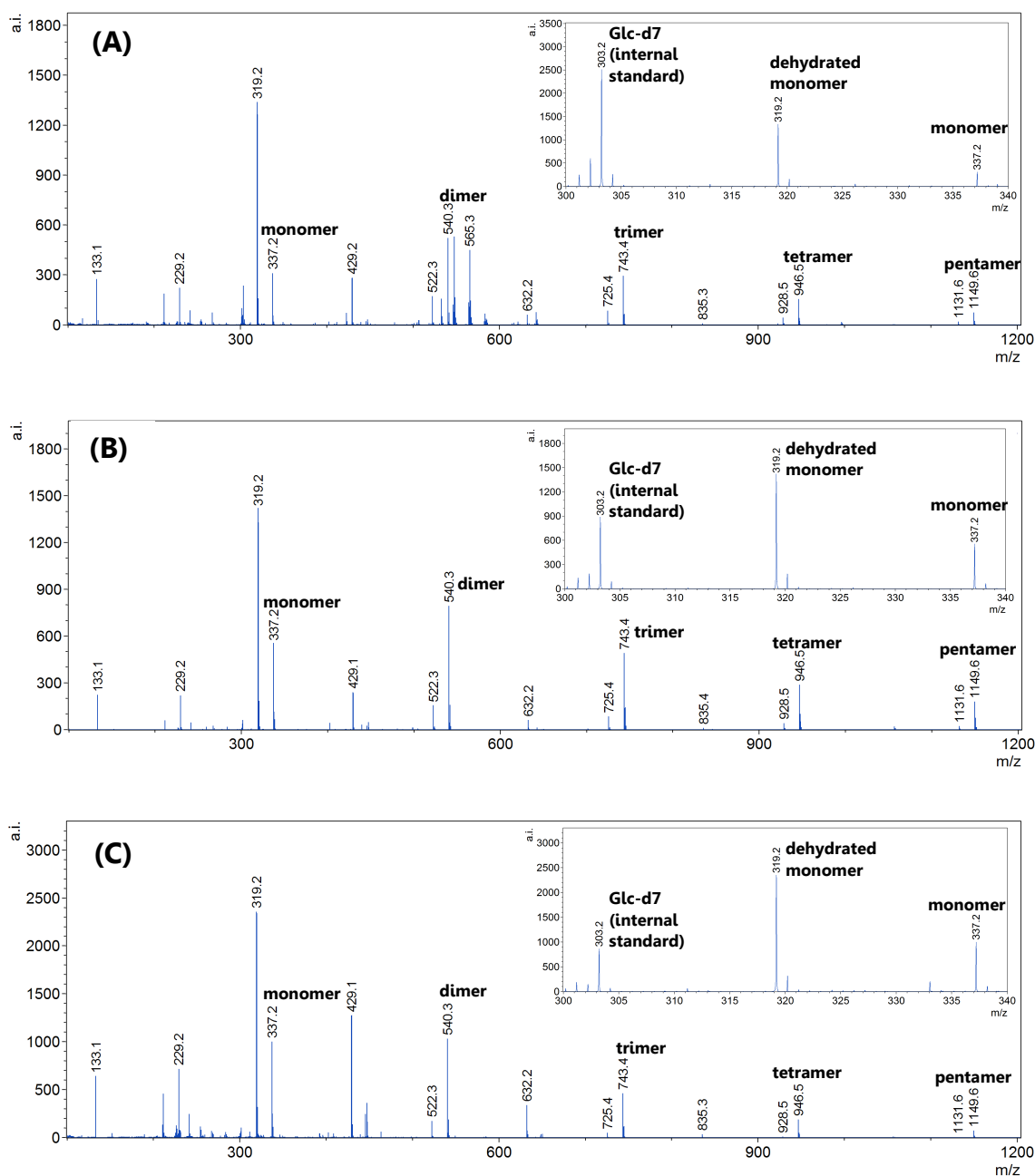


Figure 3-23: MALDI-TOF mass spectra of soluble products from ball milling α -chitin with $68-70 \times 0.25'' / 2 \times 0.5''$ balls (17.5 % packing) and kaolinite (1:1 g:g, BtP 42.8) for 0.5 h (A), 2 h (B) and 6 h (C). Insets show spectra focused at m/z 300-340 without subtracting average spectra for the blank derivatization reaction. Peak height at m/z 303.2 for internal standard can be compared to the monomer (GlcNAc) peak height at m/z 337.2. Table A3-3 records the corresponding detailed peak lists.

3.3.6.2 Quantitative analysis

Isotopically labeled glucose (glucose-d7) was selected as an appropriate internal standard (IS) as it is expected that the ionization efficiencies of the GlcNAc oligomers will be proportional to its ionization. Furthermore, the IS's competitive reaction with the derivatizing agent allowed quantitative analysis of our analytes. Figure 3–24 shows the analyte to IS peak height ratios for samples ball milled for 0.5, 2, 4, 6 h. An increase in height ratio and therefore concentration for GlcNAc and (GlcNAc)₂ is evident for the samples as milling time increases from 0.5 to 6 h, which correlates to the corresponding solubility/colorimetry data increase. For the 0.5 to 2 h and 2 to 6 h milling intervals, the elevations of [GlcNAc] based on its peak height ratio with IS were 408% (from 0.12 to 0.61) and 87% (from 0.61 to 1.14) respectively. The ratio of the two percentages ($408 / 87 = 4.7$) is near with the corresponding ratio for NAG-eq. elevations given by the Schales method ($220 / 58 = 3.8$). For the dimer and trimer, the corresponding ratios between the two phases of ball milling (0.5 to 2 h and 2 to 6 h) are 8.1 (305/38; analyte/IS ratio changes from 0.21 to 0.85 to 1.17) and 82.9 (325 / 4; likewise, from 0.12 to 0.51 to 0.53) respectively. This increasing trend for this ratio, which goes even further for the tetramer and pentamer, is characteristic for the specific parameters of the ball milling system used (SPEX 8000M, steel vial/balls, 17.5% packing, 1:1 α -chitin:kaolinite, 42.8 BtP) and is expected to differ with mechanochemical variations. The consideration of that data might provide future researchers with a basis to form new hypotheses regarding kinetics of polysaccharide ball milling.

The trimer, tetramer, and pentamer peak height ratios also rise initially (0.5 to 2 h) but level out after longer milling times. The tetramer and pentamer reveal an evident decrease from 4 to 6 h. This suggests that these oligomers likely break up to form GlcNAc and (GlcNAc)₂ upon longer milling times. For the 0.5 and 2 h samples, the analyte/IS peak height ratios of *m/z* 295.2, 498.3, 701.3, and 904.4 which correspond to the derivatives of the deacetylated sugars of GlcNH₂, GlcNAc–GlcNH₂, GlcNAc–GlcNAc–GlcNH₂, and GlcNAc–GlcNAc–GlcNAc–GlcNH₂ respectively, were found to be less than 10% of the pentamer ratio (indicative data can be found in the peak lists of the samples' average spectra in Table A3–3). For the 6 h sample, the analyte/IS peak height ratios of *m/z* 295.2 (DA 0%), 498.3 (DA 50%), 701.3 (DA 67%), and 904.4 (DA 75%) were 21, 17, 10, and 2% of the acetylated pentamer (DA 100%) ratio respectively. Although these values are generally higher than those for the 0.5 and 2 h samples, their contribution to average oligomer DA is still miniscule considering those of the acetylated ones. Therefore, the significantly higher solubilities of ball milled α-chitin in pH 2.9 (see Section 3.3.4) can be hypothesized to arise from reactions that do not include deacetylation. Even with higher BtC and a solid acid catalyst in the system, these results complement the IR data suggesting that deacetylation is minimal under the ball milling conditions explored. However, future researchers should consider the possibility of color development (see Figure 3–7) through deacetylation and subsequent reactions of the amino group.

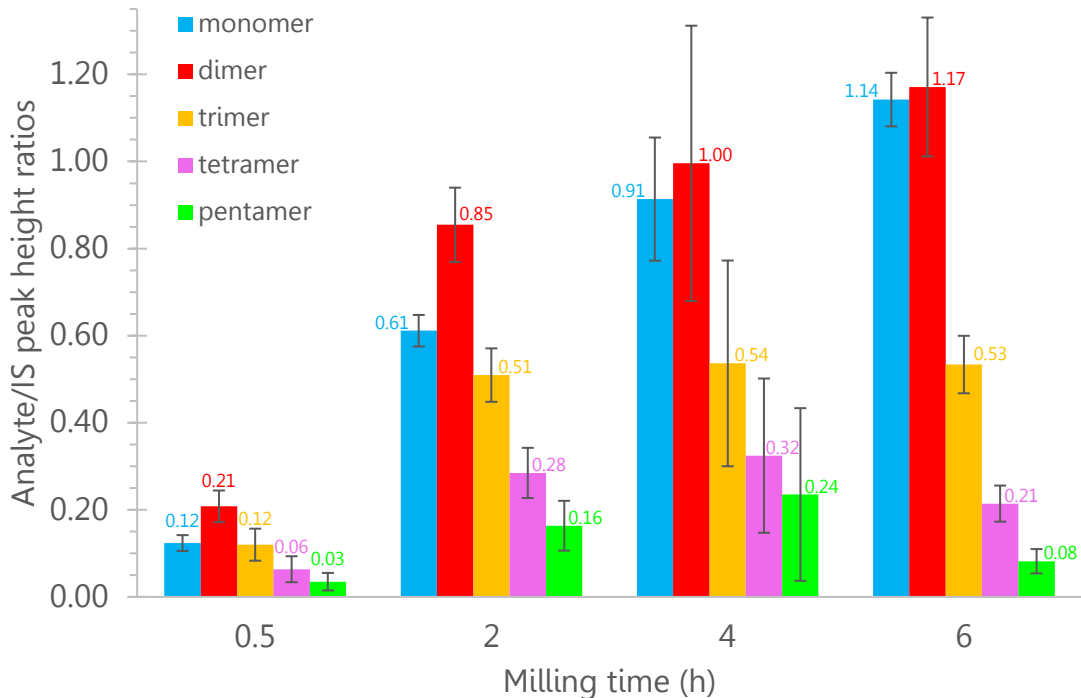


Figure 3-24: Analyte (monomer to pentamer) to internal standard (IS) peak height ratios for GTMA derivatives of α -chitin oligomers generated by milling (kaolinite, $2 \times 0.5''$ / $68-70 \times 0.25''$ balls) for 0.5, 2, 4, 6 h. Data were obtained by MALDI-TOF-MS.

Figure 3–25 shows the calibration curves for GlcNAc and $(\text{GlcNAc})_2$ with correlation coefficients (R^2) greater than 0.996 (representative spectra shown in Figures A3–29 and A3–30).^{cxix} ^{cxii} Using these, analysis of the spectra allows the calculation of concentrations (mM) and yields from ball milling α -chitin with $2 \times 0.5''$ / $68-70 \times 0.25''$ balls and kaolinite (Table 3–4). The 4 h yields for GlcNAc (3.4 wt.%) and

^{cxix} When a 3.80 mM point was attempted for the calibration curve of GlcNAc, the analyte/IS ratio (1.44 ± 0.13) lowered the linearity to $R^2 = 0.9867$, hence data were excluded.

^{cxii} Calibration curves based on the dehydrated derivative-monomer peak (and its summation with its parent) were considered, however linearities (R^2) of the ratios with the IS (and its dehydrated fragment) ranged between 0.90 and 0.96. Presentation of that data is beyond the scope of the thesis.

(GlcNAc)₂ (2.8 wt.%) are comparable to 3 h yields for Glc (4.3 wt.%) and (Glc)₂ (3.5 wt.%) from sulfuric acid impregnated cellulose by Dornath et al.⁷⁶ The slightly lower values and longer milling time needed for GlcNAc and (GlcNAc)₂ production can be a reflection of the greater degree of hydrogen bonding present in α-chitin compared with cellulose, the higher MW and possibly to the different ball milling conditions used. Microcrystalline cellulose used by Dornath et al. had a DP of 215. Considering the hypothesis in Section 3.3.2.5 regarding the MW of α-chitin in this study, the 4 h yields for GlcNAc and (GlcNAc)₂ can be considered to be produced from a competitive depolymerization process. Mysteriously, the technological parameters of the ball milling process of Dornath et al. are not available to compare with the work here.⁷⁶ Using a 500-rpm planetary ball mill (Fritsch, Pulverisette), alumina balls and a BtC ratio ca. 20 in a 6 h process, Yabushita et al. achieved an interesting composition of oligomer yields from sulfuric acid impregnated chitin (assumed of a certain alpha character).⁷⁷ The fully acetylated trimer [(GlcNAc)₃] revealed the highest yield with 11% and the lowest recorded was for GlcNAc (4.7%). Unfortunately, no calibration curve or preparation of standard solutions are mentioned.⁷⁷ When a calibration curve for the oligosaccharide standard (GlcNAc)₅ was attempted (Figure A3–31), the correlation coefficient was unfortunately not acceptable ($R^2 < 0.95$). However, one can approximate that the concentrations of the pentamer in our samples are less than 0.60 mM [pentamer peak height ratio does not exceed 0.44 (= 0.24 + 0.20) in the 4 h sample]. Although the yields of GlcNAc, (GlcNAc)₂, and related oligosaccharides are low, they can be improved in the future

by combining a range of pretreatment, chemical, and biochemical approaches, e.g., liquid assisted grinding before treatment with an enzyme cocktail.

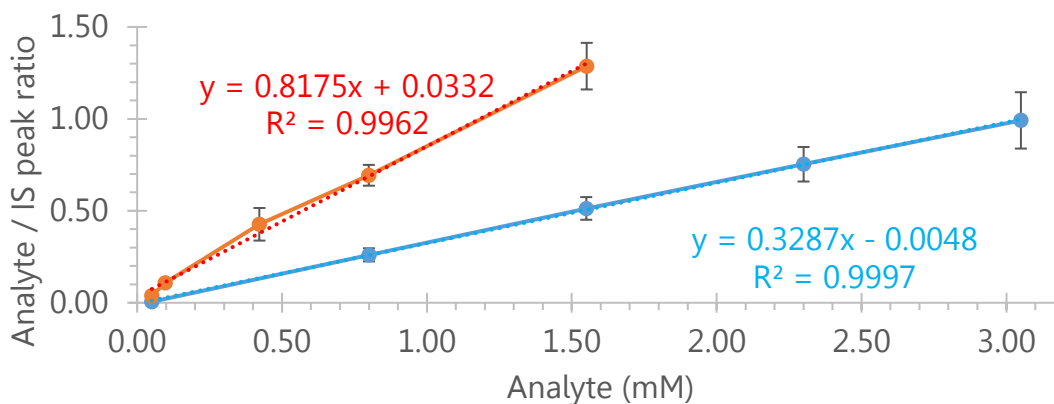


Figure 3-25: Calibration curves for GlcNAc (blue) and (GlcNAc)₂ (red) prepared by GTMA derivatization and MALDI-TOF MS. Error bars arise from quintuplicate acquisitions among spots. Representative spectra are available in Figures A3–29 and A3–30.

Table 3-4: Concentrations (mM) measured by MALDI-TOF MS and yields (wt.%)^a of GlcNAc and (GlcNAc)₂ when α-chitin was ball milled with 2 × 0.5" /68–70 × 0.25" balls and kaolinite.

milling time (h)	GlcNAc		(GlcNAc) ₂	
	concentration (mM)	Yield %	concentration (mM)	Yield %
0.5	0.39 ± 0.07	0.6	0.21 ± 0.01	0.6
2	1.87 ± 0.12	2.5	1.00 ± 0.06	2.6
4	2.79 ± 0.44	3.4	1.18 ± 0.35	2.8
6	3.49 ^b ± 0.20	5.1	1.39 ± 0.15	3.9

^a Yield % calculated on a mass basis (see Table A3–4).

^b Determined by derivatizing a 1:10 diluted sample of the soluble products.

3.3.7 Size Exclusion Chromatography (SEC) analysis of soluble products

Results from the mass spectrometric analysis provided evidence for the mechanochemical production of chito-oligosaccharides in the DP range 1-5. As the application of that procedure was new in general, we wanted to complement the data set with a chromatographic method. SEC was performed on standard samples of NAG, (NAG)₂, (NAG)₄, (NAG)₅ and (NAG)₆. M_n values for these were obtained via conventional calibration against PEG/PEO standards and compared with their real M_f . SEC data consistently gave higher than anticipated M_n values (Table A3-5), the expected narrow dispersities (M_w/M_n) and retention volumes of between 16.32 mL for (NAG)₆ (our highest M_f standard) and 19.22 mL for NAG (our lowest M_f standard). In contrast, the chromatograms for the mixtures of water soluble compounds generated by milling chitin with kaolinite showed broad multimodal traces (Figure A3-32). The chromatograms spanned retention volumes of 13–23 mL and calculated dispersities were between 4 and 6. In agreement with the mass spectrometric data, the most intense peak corresponded to (NAG)₂. However, products with larger retention volumes than NAG (possibly low molecular weight organic dehydration products) and smaller retention volumes than (NAG)₆ were also observed. The chromatograms for samples ground for 4 to 6 h were nearly identical and this is in agreement with the mass spectra. Furthermore, the overlapping nature of the peaks compared with the standards suggests that the oligosaccharide mixtures are heterogeneous in nature.

3.4 Conclusions

In this chapter, a thorough investigation of the effects of kaolinite and packing/balls-to-chitin (BtC) ratios (intense ball milling) was undertaken in order to optimize the yield of water-soluble products from α -chitin. Using solubility tests, a 1:1 w/w α -chitin:kaolinite mix milled with 8.2 BtP - 3.3% packing for 1 h was found to at least double the depolymerization efficiency of the system; confirming the significant role of acidity offered by the clay's layers. However, the solid catalyst's performance did not produce the expected increase in yields for longer milling times (4 h), hence the factor of collision frequency was investigated by concurrently raising the packing and BtC values higher than 16% and 40 respectively. This way, the crystallinity of the polysaccharide was observed to gradually decrease over a 3-fold shorter milling time compared with the 8.2 BtC - 3.3% packing system. At the same time, solubility reached 36 and 45% after 6 h milling with 43 and 86 BtC respectively confirming that a higher BtC will result in higher yields of water-soluble products. FT-IR data from both α -chitin and high-MW chitosan ball milling confirmed that solubility is inversely proportional to glycosidic linkage content in analogy to the lower collision frequency system of Chapter 2. Evidence for deacetylation suggests that it only occurs in the first 60 min of α -chitin milling, when it decreases to $85.4 \pm 0.8\%$ from $95.0 \pm 5.6\%$ for the native chains. These data provide the basis of my hypothesis that the α -chitin in this study and Aldrich's high-MW chitosan (approximated between 980 and 2400 kDa) have comparable

molecular weights (MW). Moreover, the data led to a new question for future research: “Do the increased levels of glycosidic bond rupture originate from plastic deformation of α -chitin particles during collisions in the ball mill?”. A possible computational contribution on polysaccharide ball milling might help to approach the answer.

The combination of increased collision frequency along with the presence of the solid catalyst provided optimum mechanochemical conditions for efficient conversion of α -chitin into water-soluble products. In the first 2 h of milling, the system achieved $50.3 \pm 2.5\%$ water-soluble species increasing significantly the kinetics compared with the process without kaolinite. This improved depolymerization reaction is hypothesized to originate from protonation of glycosidic oxygens during the elastic phases of collisions when covalent bonds of pyranic rings are subjected to conformational changes. After that point, and in parallel to literature cellulose studies, the system started leveling out reaching a plateau of ca. 76% solubility in 6 h probably due to reagglomeration and coalescence phenomena known to occur in ball milling.

The composition of the optimum yields of α -chitin water-soluble products (2.5, 8.3, 11.4 g/L for 0.5, 2, 6 h milling respectively) was first assessed with a colorimetric approximation of reducing ends. Both dinitrosalicylic acid (DNS) and Schales assays responded in a consistent way to the solubility increases of the two phases of ball milling [232% increase (from 2.5 to 8.3 g/L) for the depolymerization/particle-

reduction phase and 37% increase (from 8.3 to 11.4 g/L) for the depolymerization/reagglomeration phase]. The DNS reagent gave 230 and 36% increases in glucose equivalents (Glc-eq) for the two phases of the process respectively, while Schales reagent revealed 220 and 58% increases in *N*-acetyl-D-glucosamine equivalents (NAG-eq). The differential behaviour of both assays towards different degrees of polymerization led to a mass spectrometric study of the water-soluble species. The application of a MALDI-TOF-MS method developed at Memorial University revealed oligomers of NAG with degrees of polymerization (DP) of 1 to 5. Relative quantification using an internal standard showed that the bigger oligomers (pentamer, tetramer, trimer) depolymerize with increasing milling time (increasing trends for the monomer and dimer concentrations were recorded accordingly). Deacetylated oligomers were found at minimal to negligible levels complementing the FT-IR data obtained for ball milling without kaolinite. *N*-acetyl-D-glucosamine (NAG) and *N,N'*-diacetylchitobiose (NAG₂) were obtained in yields of 5.1 and 3.9 wt.%, respectively, within 6 h, which is comparable with yields of glucose and cellobiose from literature cellulose ball milling. These data agreed with chromatographic observations (SEC analysis), which showed broad dispersities (\mathcal{D}) for the ball milled samples (\mathcal{D} 4-6) in contrast to narrow ones for NAG-oligomer standards (\mathcal{D} 1.00–1.04).

In brief, milling α -chitin with $2 \times 0.5'' / 68\text{--}70 \times 0.25''$ balls (17.5% packing) and kaolinite (1:1 g:g; BtP 42.8) revealed the most efficient mechanochemical conditions

for the production of chitin oligomers with the system's optimum performance time being in between 2 and 4 h (>80% increase in solubility afforded by the use of the solid acid catalyst). Elementary α -chitin fibril volumes trapped in between colliding balls are subjected to disruption of intermolecular hydrogen bonds and homolytic cleavage of glycosidic linkages through force distribution (see Figure 3–12) and the improved depolymerization reaction is hypothesized to originate from protonation of glycosidic oxygens during the elastic phases of collisions when covalent bonds of pyranic rings are subjected to conformational changes.

3.5 References

1. Hick, S. M.; Griebel, C.; Restrepo, D. T.; Truitt, J. H.; Buker, E. J.; Bylda, C.; Blair, R. G. Mechanocatalysis for biomass-derived chemicals and fuels. *Green Chem.* **2010**, *12*, (3), 468-474.
2. Trache, D.; Hussin, M. H.; Hui Chuin, C. T.; Sabar, S.; Fazita, M. R. N.; Taiwo, O. F. A.; Hassan, T. M.; Haafiz, M. K. M. Microcrystalline cellulose: Isolation, characterization and bio-composites application—A review. *Int. J. Biol. Macromol.* **2016**, *93*, 789-804.
3. Alaba, P. A.; Sani, Y. M.; Ashri, W. D. Kaolinite properties and advances for solid acid and basic catalyst synthesis. *RSC Adv.* **2015**, *5*, (122), 101127-101147.
4. Meine, N.; Rinaldi, R.; Schüth, F. Solvent-Free catalytic depolymerization of cellulose to water-soluble oligosaccharides. *ChemSusChem* **2012**, *5*, (8), 1449-1454.
5. Shrotri, A.; Lambert, L. K.; Tanksale, A.; Beltramini, J. Mechanical depolymerisation of acidulated cellulose: Understanding the solubility of high molecular weight oligomers. *Green Chem.* **2013**, *15*, (10), 2761-2768.
6. Loerbroks, C.; Rinaldi, R.; Thiel, W. The electronic nature of the 1,4- β -glycosidic bond and its chemical environment: DFT insights into cellulose chemistry. *Chem. - Eur. J.* **2013**, *19*, (48), 16282-16294.
7. Alonso, E. R.; Peña, I.; Cabezas, C.; Alonso, J. L. Structural expression of exo-anomeric effect. *J. Phys. Chem. Lett.* **2016**, *7*, (5), 845-850.

8. Schüth, F.; Rinaldi, R.; Meine, N.; Källdström, M.; Hilgert, J.; Rechulski, M. D. K. Mechanocatalytic depolymerization of cellulose and raw biomass and downstream processing of the products. *Catal. Today* **2014**, *234*, 24-30.
9. Schmidt, R.; Fuhrmann, S.; Wondraczek, L.; Stolle, A. Influence of reaction parameters on the depolymerization of H₂SO₄-impregnated cellulose in planetary ball mills. *Powder Technol.* **2016**, *288*, 123-131.
10. Omari, K. W.; Besaw, J. E.; Kerton, F. M. Hydrolysis of chitosan to yield levulinic acid and 5-hydroxymethylfurfural in water under microwave irradiation. *Green Chem.* **2012**, *14*, (5), 1480-1487.
11. Biotage , Initiator 2.5 - Getting started guide, 2010, http://biotage.com/literature/download/initiator_2.5_getting_started_guide_red.pdf?ref=http%3A%2F%2Fbiotage.com%2Fliterature%2Fsearch%2F11%2F50%3Fq%3D, (accessed 4/28, 2018).
12. Miller, G. L. Use of dinitrosalicylic acid reagent for determination of reducing sugar. *Anal. Chem.* **1959**, *31*, (3), 426-428.
13. Ghose, T. K. Measurement of cellulase activities. *Pure Appl. Chem.* **1987**, *59*, (2), 257-268.
14. Imoto, T.; Yagishita, K. A Simple Activity Measurement of Lysozyme. *Agric. Biol. Chem.* **1971**, *35*, (7), 1154-1156.
15. Gouw, J. W.; Burgers, P. C.; Trikoupis, M. A.; Terlouw, J. K. Derivatization of small oligosaccharides prior to analysis by matrix-assisted laser desorption/ionization using glycidyltrimethylammonium chloride and Girard's reagent T. *Rapid Commun. Mass Spectrom.* **2002**, *16*, (10), 905-912.
16. Fialips, C. -; Petit, S.; Decarreau, A.; Beaufort, D. Influence of synthesis pH on kaolinite 'crystallinity' and surface properties. *Clays Clay Miner.* **2000**, *48*, (2), 173-184.
17. Yariv, S.; Lapidés, I. The effect of mechanochemical treatments on clay minerals and the mechanochemical adsorption of organic materials onto clay minerals. *J. Mater. Synth. Process.* **2000**, *8*, (3-4), 223-233.
18. Park, S.; Baker, J. O.; Himmel, M. E.; Parilla, P. A.; Johnson, D. K. Cellulose crystallinity index: Measurement techniques and their impact on interpreting cellulase performance. *Biotechnol. Biofuels* **2010**, *3*, article 10.
19. Fadda, S.; Cincotti, A.; Concas, A.; Pisu, M.; Cao, G. Modelling breakage and reagglomeration during fine dry grinding in ball milling devices. *Powder Technol.* **2009**, *194*, (3), 207-216.

20. Maurice, D.; Courtney, T. H. Modeling of mechanical alloying: Part I. deformation, coalescence, and fragmentation mechanisms. *Metall. Mater. Trans. A* **1994**, *25*, (1), 147-158.
21. Knieke, C.; Sommer, M.; Peukert, W. Identifying the apparent and true grinding limit. *Powder Technol.* **2009**, *195*, (1), 25-30.
22. Colthup, N. B.; Daly, L. H.; Wiberley, S. E. Amines, C=N, and N=O compounds. In *Introduction to infrared and Raman spectroscopy*, 3rd ed.; Academic Press: San Diego, 1990; pp 339-354.
23. Kasaai, M. R. A review of several reported procedures to determine the degree of N-acetylation for chitin and chitosan using infrared spectroscopy. *Carbohydr. Polym.* **2008**, *71*, (4), 497-508.
24. Dimzon, I. K. D.; Knepper, T. P. Degree of deacetylation of chitosan by infrared spectroscopy and partial least squares. *Int. J. Biol. Macromol.* **2015**, *72*, 939-945.
25. Jumaa, M.; Furkert, F. H.; Müller, B. W. A new lipid emulsion formulation with high antimicrobial efficacy using chitosan. *Eur. J. Pharm. Biopharm.* **2002**, *53*, (1), 115-123.
26. Kim, K. W.; Min, B. J.; Kim, Y. -; Kimmel, R. M.; Cooksey, K.; Park, S. I. Antimicrobial activity against foodborne pathogens of chitosan biopolymer films of different molecular weights. *LWT - Food Sci. Technol.* **2011**, *44*, (2), 565-569.
27. Arias-Moscoso, J. L.; Soto-Valdez, H.; Plascencia-Jatomea, M.; Vidal-Quintanar, R. -; Rouzaud-Sández, O.; Ezquerro-Brauer, J. M. Composites of chitosan with acid-soluble collagen from jumbo squid (*Dosidicus gigas*) by-products. *Polym. Int.* **2011**, *60*, (6), 924-931.
28. Kleekayai, T.; Suntornsuk, W. Production and characterization of chitosan obtained from *Rhizopus oryzae* grown on potato chip processing waste. *World J. Microbiol. Biotechnol.* **2011**, *27*, (5), 1145-1154.
29. Waldeck, J.; Daum, G.; Bisping, B.; Meinhardt, F. Isolation and molecular characterization of chitinase-deficient *Bacillus licheniformis* strains capable of deproteinization of shrimp shell waste to obtain highly viscous chitin. *Appl. Environ. Microbiol.* **2006**, *72*, (12), 7879-7885.
30. Qin, Y.; Lu, X.; Sun, N.; Rogers, R. D. Dissolution or extraction of crustacean shells using ionic liquids to obtain high molecular weight purified chitin and direct production of chitin films and fibers. *Green Chem.* **2010**, *12*, (6), 968-971.

31. Sasai, Y.; Yamauchi, Y.; Kondo, S.; Kuzuya, M. Nature of mechanoradical formation of substituted celluloses as studied by electron spin resonance. *Chem. Pharm. Bull.* **2004**, *52*, (3), 339-344.
32. Vrielinck, H.; De Cooman, H.; Callens, F.; Sagstuen, E. Radiation chemistry of solid-state carbohydrates using EMR. In *Applications of EPR in Radiation Research*, 1st ed.; Lund, A., Shiotani, M., Eds. ; Springer International Publishing: Cham, Switzerland, 2014; pp 189-254.
33. De Cooman, H.; Pauwels, E.; Vrielinck, H.; Sagstuen, E.; Callens, F.; Waroquier, M. Identification and Conformational Study of Stable Radiation-Induced Defects in Sucrose Single Crystals using Density Functional Theory Calculations of Electron Magnetic Resonance Parameters. *J. Phys. Chem. B* **2008**, *112*, (24), 7298-7307.
34. Concas, A.; Lai, N.; Pisu, M.; Cao, G. Modelling of comminution processes in Spex Mixer/Mill. *Chem. Eng. Sci.* **2006**, *61*, (11), 3746-3760.
35. Leroy, B. Collision between two balls accompanied by deformation: A qualitative approach to Hertz's theory. *Am. J. Phys.* **1985**, *53*, (4), 346-349.
36. Maurice, D. R.; Courtney, T. H. The physics of mechanical alloying: A first report. *Metall. Trans. A* **1990**, *21*, (1), 289-303.
37. Alkebro, J.; Bégin-Colin, S.; Mocellin, A.; Warren, R. Modeling high-energy ball milling in the alumina-yttria system. *J. Solid State Chem.* **2002**, *164*, (1), 88-97.
38. Harris, D. C. Sample Preparation. In *Quantitative Chemical Analysis*, 7th ed.; W. H. Freeman and Company: New York, 2007; pp 644-663.
39. Loow, Y. -.; Wu, T. Y.; Jahim, J. M.; Mohammad, A. W.; Teoh, W. H. Typical conversion of lignocellulosic biomass into reducing sugars using dilute acid hydrolysis and alkaline pretreatment. *Cellulose* **2016**, *23*, (3), 1491-1520.
40. Sun, Y.; Cheng, J. Hydrolysis of lignocellulosic materials for ethanol production: A review. *Bioresour. Technol.* **2002**, *83*, (1), 1-11.
41. Clayden, J.; Greeves, N.; Warren, S.; Wothers, P. Nucleophilic addition to the carbonyl group. In *Organic chemistry*, 1st ed.; Oxford University Press: Oxford ; New York, 2001; pp 135-150.
42. Angyal, S. J. The composition of reducing sugars in solution: Current aspects. In *Advances in Carbohydrate Chemistry and Biochemistry*, 49; Horton, D., Ed. ; Academic Press: London, 1991; pp 19-35.

43. Zhu, Y.; Zajicek, J.; Serianni, A. S. Acyclic forms of [1-¹³C]aldohexoses in aqueous solution: Quantitation by ¹³C NMR and deuterium isotope effects on tautomeric equilibria. *J. Org. Chem.* **2001**, *66*, (19), 6244-6251.
44. Schwald, W.; Chan, M.; Breuil, C.; Saddler, J. N. Comparison of HPLC and colorimetric methods for measuring cellulolytic activity. *Appl. Microbiol. Biotechnol.* **1988**, *28*, (4-5), 398-403.
45. Courtin, C. M.; Van Den Broeck, H.; Delcour, J. A. Determination of reducing end sugar residues in oligo- and polysaccharides by gas-liquid chromatography. *J. Chromatogr. A* **2000**, *866*, (1), 97-104.
46. Kormelink, F. J. M.; van de Vis, J. W.; Leeuwen, M. -; Voragen, A. G. J. Comparison of different reducing sugar assays in relation to their application to glycanase tests. *Top. Catal.* **1991**, *4*, (6), 481-487.
47. Deng, S. P.; Tabatabai, M. A. Colorimetric determination of reducing sugars in soils. *Soil Biol. Biochem.* **1994**, *26*, (4), 473-477.
48. Kongruang, S.; Han, M. J.; Breton, C. I. G.; Penner, M. H. Quantitative analysis of cellulose-reducing ends. *Appl. Biochem. Biotechnol. Part A Enzyme Eng. Biotechnol.* **2004**, *113*, (1-3), 213-231.
49. Breuil, C.; Saddler, J. N. Comparison of the 3,5-dinitrosalicylic acid and Nelson-Somogyi methods of assaying for reducing sugars and determining cellulase activity. *Enzyme Microb. Technol.* **1985**, *7*, 327-332.
50. Rahman, M. S.; Fernando, S.; Ross, B.; Wu, J.; Qin, W. Endoglucanase (eg) activity assays. In *Cellulases: Methods and Protocols*, 1796; Lubeck, M., Ed. ; Springer: 2018; pp 169-183.
51. McCleary, B. V.; McGeough, P. A Comparison of Polysaccharide Substrates and Reducing Sugar Methods for the Measurement of endo-1,4- β -Xylanase. *Appl. Biochem. Biotechnol.* **2015**, *177*, (5), 1152-1163.
52. Guo, H.; Lian, Y.; Yan, L.; Qi, X.; Smith, R. L. Cellulose-derived superparamagnetic carbonaceous solid acid catalyst for cellulose hydrolysis in an ionic liquid or aqueous reaction system. *Green Chem.* **2013**, *15*, (8), 2167-2174.
53. Li, C.; Wang, Q.; Zhao, Z. K. Acid in ionic liquid: An efficient system for hydrolysis of lignocellulose. *Green Chem.* **2008**, *10*, (2), 177-182.
54. Zhuo, K.; Du, Q.; Bai, G.; Wang, C.; Chen, Y.; Wang, J. Hydrolysis of cellulose catalyzed by novel acidic ionic liquids. *Carbohydr. Polym.* **2015**, *115*, 49-53.

55. Sumner, J. B.; Graham, V. A. Dinitrosalicylic acid: A reagent for the estimation of sugar in normal and diabetic urine. *J. Biol. Chem.* **1921**, *47*, (1), 5-9.
56. Hostettler, F.; Borel, E.; Deuel, H. Über die Reduktion der 3,5-Dinitrosalicylsäure durch Zucker. *Helv. Chim. Acta* **1951**, *34*, (6), 2132-2139.
57. Goncalves, C.; Rodriguez-Jasso, R. M.; Gomes, N.; Teixeira, J. A.; Belo, I. Adaptation of dinitrosalicylic acid method to microtiter plates. *Anal. Methods* **2010**, *2*, (12), 2046-2048.
58. Saqib, A. A. N.; Whitney, P. J. Differential behaviour of the dinitrosalicylic acid (DNS) reagent towards mono- and di-saccharide sugars. *Biomass Bioenergy* **2011**, *35*, (11), 4748-4750.
59. Wood, I. P.; Elliston, A.; Ryden, P.; Bancroft, I.; Roberts, I. N.; Waldron, K. W. Rapid quantification of reducing sugars in biomass hydrolysates: Improving the speed and precision of the dinitrosalicylic acid assay. *Biomass Bioenergy* **2012**, *44*, 117-121.
60. Teixeira, R. S. S.; Da Silva, A. S.; Ferreira-Leitão, V. S.; Da Silva Bon, E. P. Amino acids interference on the quantification of reducing sugars by the 3,5-dinitrosalicylic acid assay mislead carbohydrase activity measurements. *Carbohydr. Res.* **2012**, *363*, 33-37.
61. Schales, O.; Schales, S. S. Simple method for the determination of glucose in blood. *Proceedings of The American Federation for Clinical Research*, 1945; Vol. 2, pp 78.
62. Horn, S. J.; Eijsink, V. G. H. A reliable reducing end assay for chito-oligosaccharides. *Carbohydr. Polym.* **2004**, *56*, (1), 35-39.
63. Kaltashov, I. A.; Eyles, S. J. Overview of Traditional Experimental Arsenal to Study Biomolecular Structure and Dynamics. In *Mass Spectrometry in Structural Biology and Biophysics: Architecture, Dynamics, and Interaction of Biomolecules*. 2nd ed.; John Wiley & Sons, Inc.: Hoboken, New Jersey, 2012; pp 26-51.
64. Kaltashov, I. A.; Eyles, S. J. Overview of Biological Mass Spectrometry. In *Mass Spectrometry in Structural Biology and Biophysics: Architecture, Dynamics, and Interaction of Biomolecules*. 2nd ed.; John Wiley & Sons, Inc.: Hoboken, New Jersey, 2012; pp 52-88.
65. Kaltashov, I. A.; Eyles, S. J. Other Biopolymers and Synthetic Polymers of Biological Interest. In *Mass Spectrometry in Structural Biology and Biophysics: Architecture, Dynamics, and Interaction of Biomolecules*. 2nd ed.; John Wiley & Sons, Inc.: Hoboken, New Jersey, 2012; pp 212-238.
66. Harvey, D. J. Carbohydrate Analysis by ESI and MALDI. In *Electrospray and MALDI Mass Spectrometry: Fundamentals, Instrumentation, Practicalities, and Biological*

Applications. 2nd ed.; Cole, R. B., Ed. ; John Wiley & Sons, Incorporated: Hoboken, 2009; pp 723-769.

67. Mischnick, P. Mass spectrometric characterization of oligo- and polysaccharides and their derivatives. *Adv. Polym. Sci.* **2012**, *248*, 105-174.
68. Trombotto, S.; Ladaviere, C.; Delolme, F.; Domard, A. Chemical preparation and structural characterization of a homogeneous series of chitin/chitosan oligomers. *Biomacromolecules* **2008**, *9*, (7), 1731-1738.
69. Zaia, J. Mass spectrometry of oligosaccharides. *Mass Spectrom. Rev.* **2004**, *23*, (3), 161-227.
70. Parsons, V. H. Analysis of bio-derived platform chemicals in ionic liquid media by desorption/ionization mass spectrometry. M.S. Thesis, Memorial University of Newfoundland, St. John's, Newfoundland and Labrador, 2015.
71. Young, J. L.; Raynie, D. E. Replacement of hazardous solvents and reagents in analytical chemistry. In *Challenges in Green Analytical Chemistry*, de la Guardia, M. and Garrigues, S., Eds. ; Royal Society of Chemistry: Cambridge, UK, 2011; pp 44-62.
72. Miljković, M. Relative Reactivity of Hydroxyl Groups in Monosaccharides. In *Carbohydrates: Synthesis, Mechanisms, and Stereoelectronic Effects*, Springer: New York, 2009; pp 113-142.
73. Pedersen, C. M.; Olsen, J.; Brka, A. B.; Bols, M. Quantifying the electronic effects of carbohydrate hydroxy groups by using aminosugar models. *Chem. Eur. J.* **2011**, *17*, (25), 7080-7086.
74. Osada, M.; Kikuta, K.; Yoshida, K.; Totani, K.; Ogata, M.; Usui, T. Non-catalytic synthesis of Chromogen I and III from N-acetyl-d-glucosamine in high-temperature water. *Green Chem.* **2013**, *15*, (10), 2960-2966.
75. Zheng, X. -.; Peng, J. -.; Livera, M. M. V. S.; Luo, Y.; Wang, Y. -.; Kong, X. -.; Long, L. -.; Zheng, Z.; Zheng, L. -. Selective Formation of Chromogen i from N-Acetyl-D-glucosamine upon Lanthanide Coordination. *Inorg. Chem.* **2017**, *56*, (1), 110-113.
76. Dornath, P.; Cho, H. J.; Paulsen, A.; Dauenhauer, P.; Fan, W. Efficient mechano-catalytic depolymerization of crystalline cellulose by formation of branched glucan chains. *Green Chem.* **2015**, *17*, (2), 769-775.
77. Yabushita, M.; Kobayashi, H.; Kuroki, K.; Ito, S.; Fukuoka, A. Catalytic Depolymerization of Chitin with Retention of N-Acetyl Group. *ChemSusChem* **2015**, *8*, (22), 3760-3763.

Chapter 4 α -Chitin dissolution studies towards film casting

4.1 Introduction and methodological approach to the problem

Natural and synthetic polymer scaffold fabrication (hydrogels or films e.g. for tissue engineering) is based in two main approaches: polymer melt and polymer solubilization.¹ Regarding those made from polysaccharides, the majority is based on the dissolution of cellulosic or chitinous material into a solvent system followed by various fabrication techniques [casting (with or without porogens), gas foaming (e.g. using CO₂), electrospinning etc.].^{1,2} Polar solvents (e.g. LiCl/DMAc, NMMO), ionic liquids (e.g. [C₂mim][OAc]), deep eutectic solvents (e.g. ChCl/urea) and alkali aqueous systems (e.g. alkali/urea) have been reported to lead to dissolution of the matrix (different types of cellulose, wood pulp or chitin at concentrations that usually do not exceed 12.5 wt.%) and production of hydrogels (via various gelation procedures like cast, mold, coagulate). However, most of those processes do not report the molecular weight (MW) of the polysaccharides used.^{2,3} Yet, in polymer chemistry MW is a critical parameter for the reproducibility of scaffolds, since it controls crucial physical properties; from rheology (including viscoelasticity) through to mechanics (such as tensile strength). In general, higher MW polymers are harder to dissolve as changes in entropy upon dissolution are less favourable; however, the resulting materials usually have better mechanical properties.⁴

In this chapter, studies on a set of chitins with a similar degree of acetylation (DA) but of 3 different MWs (high, medium, low) are described. These were performed to test which solvent system would be most effective in dissolving a certain concentration-MW combination and produce scaffolds (after appropriate gelation) with acceptable mechanical properties.^{cxiii} In cases where polymer concentration is greater than $1/[\eta]$ by a factor of approximately 10 ($[\eta]$: intrinsic viscosity), chain entanglements start to influence their dynamics and rheology. For high-MW polymers, that concentration is generally ca. 10 mg/mL,⁶ and of course the phenomenon enhances with increasing molecular weight.⁴ Formation of new hydrogen bonding networks and intensification of intermolecular interactions in general is expected to lead to gelation and even phase separation.^{3,7,8} In parallel, chitin's flexibility is inversely proportional to its degree of acetylation (DA),^{9,10} and since flexible polymers have higher solubility than stiff ones,¹¹ the DA is considered equally important with MW for the production of chitinous scaffolds with tunable properties. Therefore, the above set of chitins served, at the same time, as a basis for a set of deacetylation reactions that aimed for two levels of DA (high e.g. 65% and low e.g. 15%) for the high and low MW samples and a medium DA (e.g. 40%) for the medium MW sample. Using the optimum concentration-MW-solvent-system

^{cxiii} Initial experiments were designed and conducted in collaboration with the Scott group of the Centre for Sustainable Chemical Technologies (CSCT) of the University of Bath (UK) within the framework of a 3-month Royal Society of Chemistry (RSC) Researcher Mobility Grant. Future work on that direction can involve reactive printing of the scaffold's surface for cell attachment enhancement (5).

combinations, the effect of DA on the mechanical (and other) properties of the resulting scaffolds can be investigated in the future. Figure 4–1 illustrates the most important experimental considerations towards α -chitin film fabrication.

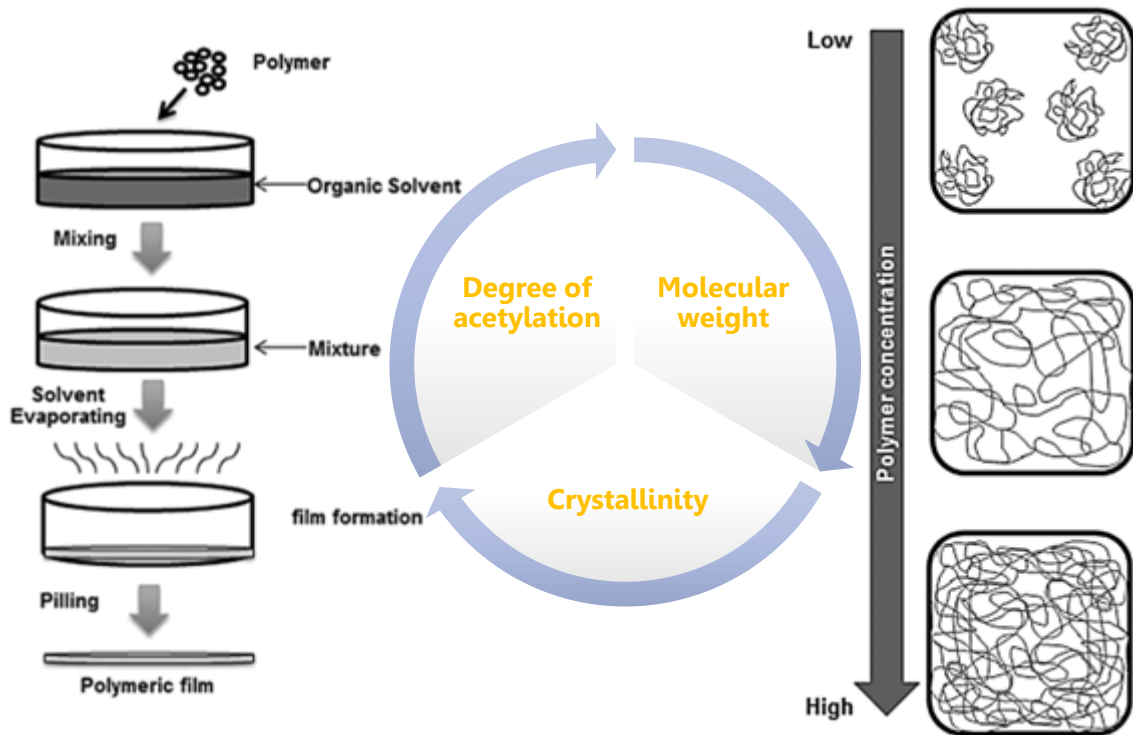


Figure 4-1: Main experimental considerations towards α -chitin film casting. Steps of film fabrication via the solution casting technique (solvent evaporation can be preceded by an anti-solvent treatment step) and chain entanglement for increasing polymer concentration. Molecular weight, degree of acetylation and crystallinity of α -chitin influence all phases of the process in chorus. Adapted from Suntornnond, R., An, J., Yeong, W. Y. and Chua, C. K. (2015), *Biodegradable Polymeric Films and Membranes Processing and Forming for Tissue Engineering*. *Macromol. Mater. Eng.*, 300: 858-877. doi:[10.1002/mame.201500028](https://doi.org/10.1002/mame.201500028) by permission from John Wiley and Sons. © 2015 WILEY-VCH Verlag GmbH & Co. KGaA, Weinheim

4.2 Experimental

4.2.1 Mechanochemical treatment of α -chitin

This was performed as previously described in Chapters 2 and 3.

4.2.2 X-ray diffraction (XRD)

This was performed as previously described in Chapters 2 and 3.

4.2.3 Fourier transform infrared (FT-IR) spectroscopy

Some FT-IR spectra were acquired at Memorial University of Newfoundland (MUN) as previously described in Chapters 2 and 3. Other spectra were acquired on a Spectrum 100 spectrometer with a diamond/ZnSe ATR module (PerkinElmer) at CSCT (University of Bath). A total of 24 scans with a 4 cm^{-1} resolution were signal-averaged and stored for each measurement; the wavenumber region investigated ranged from 4000 to 650 cm^{-1} . The intensities of the selected absorption bands were determined by the baseline correction method on the basis of the vendor's software package of the instrument. Each sample was measured in triplicate and spectra were averaged for presentation. Reproducibility of measurements taken at CSCT are subject to the variable force applied to the sample (anvil force gauge was taken care to be at least 110).

4.2.4 Relative viscosity of chitin in 1-ethyl-3-methylimidazolium acetate

This was performed according to literature methods with minor modifications.¹² 25.48 ± 0.28 mg of dry chitinous sample was mixed with 12.2779 ± 0.3506 g of 1-

ethyl-3-methylimidazolium acetate (EmimAcO) in a 30 mL glass vial [average chitin concentration for 12 suspension preparations was 0.2076 ± 0.0046 wt.% (RSD 2.2%)]. The capped mixture was heated in a domestic microwave oven (800W) using 3-5 s pulses at full power. Between each pulse, the vial was removed, the mixture was stirred vigorously and then replaced in the microwave. After at least 100 pulses (and oil bath treatment at 100 °C for some samples), complete dissolution was monitored optically. Kinematic viscosity measurements were conducted in a 35.0 ± 1.0 °C water bath (>20 L)^{cxiv} using a Cannon-Fenske Routine viscometer (size 200 No. N637, Cannon Instrument Co.) with a calibration constant of $0.1009 \text{ mm}^2/\text{s}^2$ (cSt/s) (approximate charge volume was 7.1 mL).^{cxv} The duplicate average efflux time of EmimAcO was 646.53 ± 0.04 s. Relative viscosity values for the samples are the average of two measurements with the average standard deviation being 2.08 s.^{cxvi}

4.2.5 Chitin dissolution studies and preliminary film casting

These are described along within the Results and Discussion section as they required a trial and error approach.

^{cxiv} Temperature fluctuations of a 3 L water bath exceeded 1.0 °C.

^{cxv} Before each measurement, the charged sample was left to equilibrate thermally for ca. 15 min and visible bubbles were taken care to be released from the liquid mass.

^{cxvi} Viscometer was washed with acetone in between charging of samples, and the second measurement of the sample was conducted by pushing the volume of the first measurement to the appropriate level.

4.2.6 Ultrasound assisted heterogeneous deacetylation of α -chitin

Sonication experiments were conducted using a QSonica Q500 ultrasonic processor (output frequency 20 kHz). The probe was a standard 13 mm and the microtip had a diameter of 6 mm suitable for processing volumes of 5 to 50 mL. 2.041 \pm 0.014 g of chitin sample (RSD 0.7%) were charged in a 30 mL cylindrical glass vial and 25.0 mL of NaOH 40.0 wt.% was added along with a magnetic stir bar. This 1:12.5 w/v (or ca. 5 wt.%) concentration is relatively high compared to 1:22.7 w/v¹³ and 1:20.0 w/v¹⁴ used in the literature for α -chitin, but lower than the 1:10 w/v for β -chitin.¹⁵ ^{cxvii} The vial was clamped inside the sound enclosure booth and the tip was immersed to a depth that was at least 1.5 times the tip diameter. The setting for the amplitude was in the functional range (between 20 and 50%). Pulses of 4 s ON / 7 s OFF of 20-25 % amplitude were found to keep the 25-30 mL reaction mixture temperature relatively stable at 60.0 \pm 1.0 °C. Sonication time reported refers to the time which the tip was vibrating during the aforementioned 11 s pulse, while at the same time the reaction mixture was under constant magnetic stirring on an ordinary hotplate (with no additional heating) and its temperature was monitored with a thermocouple.

^{cxvii} Considering the available glassware (30 mL vials), the concentration used herein was convenient for the purpose of these preliminary experiments.

4.2.7 Determination of degree of acetylation (DA) by ¹H NMR spectroscopy

The samples were dispersed at 4 to 5 mg/mL in either 2 wt.% or 20 wt.% DCl in D₂O and achieved dissolution (visually clear) when stirred vigorously at 70 °C overnight. Samples were filtered through cotton wool and solution-state ¹H NMR experiments were performed using a 500 MHz Bruker Avance III spectrometer (5 mm PABBO BB- probe). Quantitative spectra were recorded at 25 °C with a 10 μs pulse, a repetition delay of 5 s and 64 scans accumulated.^{cxviii} Spectra were processed with Topspin 2.1 (Bruker BioSpin GmbH). The DA value for each sample was calculated using the following equation:

$$DA\% = 100 * \frac{\frac{I(CH3)}{3}}{\frac{I(H2 + H3 + H4 + H5 + H6)}{6}}$$

Where I(CH₃) is the integral value for the methyl group of the *N*-acetyl group at ca. 1.8 ppm (corresponding to 3 protons of acetylated units only), and I(H₂+H₃+H₄+H₅+H₆) is the integral value for the signals of the H₂ to H₆ protons between 2.8 and 4.2 ppm (corresponding to 6 protons of all units).¹⁶

4.2.8 Relative viscosity of chitin in NaOH

93.0 ± 0.2 mg of 67/60 chitin^{cxix} was mixed with 18.6791 ± 0.1026 g NaOH solution (9.70, 19.40, 29.11, 38.81 wt.%) in a 20 mL glass vial [average chitin concentration

^{cxviii} The software used in CSCT was Topspin 2.1 (Bruker). Tuning and shimming were always conducted before data acquisition with final B0 stdDev < 0.5 Hz.

^{cxix} That is PG chitin milled with 67 BtC/14% packing for 60 min.

for 4 suspension preparations was 0.4954 ± 0.0031 wt.% (RSD 0.6%)]. The capped mixture was stirred for ~ 2 h at ca. -14 °C with a magnetic stir bar, and then placed in dry ice until frozen (~ 30 min). When thawed and stirred, stir bars were removed and samples were charged into 15 mL centrifuge tubes (VWR, poly-propylene). After centrifugation at 7500 rpm for 10 min, solution was decanted. Kinematic viscosity measurements were conducted at room temperature using an Ubbelohde type viscometer (size 1, No. C193, Cannon Instrument Co.) with a calibration constant of ca. $0.01 \text{ mm}^2/\text{s}^2$ (cSt/s) (approximate charge volume was 11 mL). The duplicate average efflux times of the 9.70, 19.40, 29.11 wt.% NaOH solutions were 125.0 ± 0.2 , 259.0 ± 1.4 , 710.0 ± 1.4 s respectively. Relative viscosity values for the samples are the average of two measurements with the average standard deviation being 2.8 s.

4.3 Results and discussion

4.3.1 Mechanochemical depolymerization/amorphization of α -chitin

In Chapters 2 and 3, a systematic study of α -chitin's transformation in a mechanochemical system (ball mill) was carried out demonstrating the potential of varying the vial's packing degree and size of milling media. Therefore, a set of three α -chitin samples was produced from native α -chitin for which the ball milling parameters and resulting FT-IR data are shown on Table 4-1 (spectra shown on Figure 4-2).

Table 4-1: Mechanochemical conditions and FT-IR data for the α -chitin sample set prepared for dissolution studies.^[a] Spectra shown in Figure 4-2.

<u>Measured quantity</u>	<u>α-chitin sample</u>			
	native	high MW	medium MW	low MW
mixing load (g)	-	2.00	2.00	1.00
# of 0.25" balls	-	24	32	68
BtC ratio	-	12.0	16.0	68.0
packing %		5.0	6.6	14.0
milling time (min)	-	10	25	60
glycosidic linkage	1.423	1.316	1.194	1.116
FT-IR ratio	± 0.080	± 0.063	± 0.024	± 0.051
amide II	2.736	2.503	2.366	2.349
FT-IR ratio	± 0.116	± 0.131	± 0.037	± 0.090
DA%^[b]	97.0 \pm 4.1	88.8 \pm 4.6	83.9 \pm 1.3	83.3 \pm 3.2
amide I split	1.133	1.017	0.903	0.840
FT-IR ratio	± 0.013	± 0.005	± 0.001	± 0.009
CrI %	91.3	83.6 ^[c]	74.1 ^[c]	62.2 ^[c]

[a] The minimum quantity prepared for each sample was at least 6 g to ensure sufficient mass for multiple production/analysis. Therefore, several milling batches were undertaken for each sample. Triplicate FT-IR spectra were acquired on vortex-mixed ball milled batches.

[b] Calculated by the Sannan method.¹⁷

[c] Crystallinity Index (CrI%) is an approximation obtained from its relationship with the amide I split FT-IR ratio when data from 3.3% packing/8.2 BtC ball milling were correlated (see Figures 2-8 and 2-16).

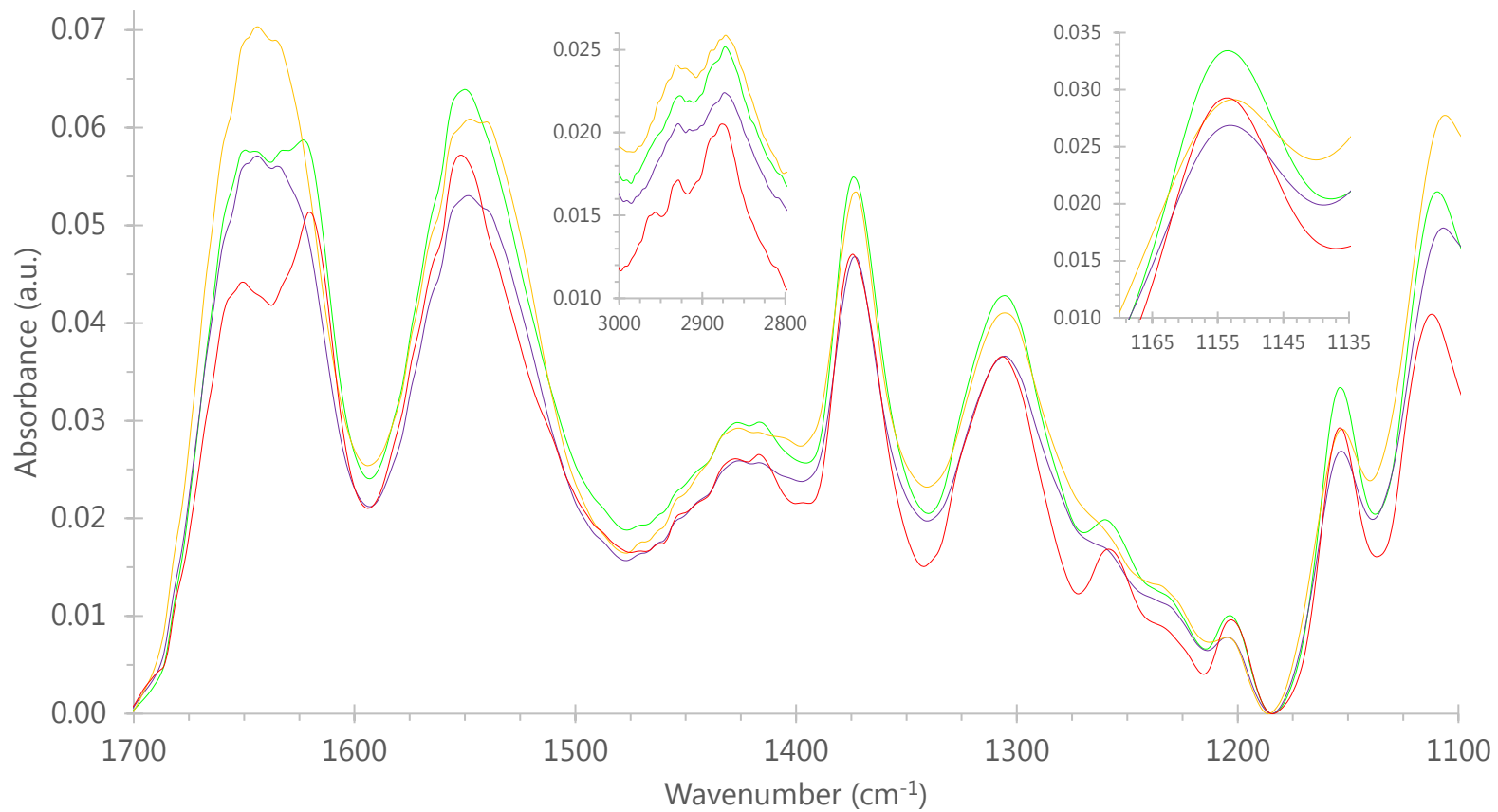


Figure 4-2: Infrared spectra of native (red), high MW (green), medium MW (blue), and low MW (orange) α-chitin (ball milling conditions and FT-IR ratios are recorded in Table 4-1). Data acquired at MUN.

FT-IR data are similar to those of Section 3.3.2.3 (see Figures 3–8 to 3–10) with degree of acetylation dropping to $88.8 \pm 4.6\%$ for the high MW and then remaining relatively stable at ca. 83.6% for the more milled samples. Glycosidic linkage content revealed clear differences with no error bar overlap (Figure A4–1).^{cxx} Based on the amide I split ratio, crystallinity was found to decrease with decreasing molecular weight. Therefore, the sample set provided a solid basis for dissolution studies with common solvents used in film casting.^{cxxi}

4.3.2 Relative estimation of molecular weights (MW) using an ionic liquid (IL)

In order to see if the above set of solid-state data on native and ball milled α -chitin will be reflected in a solution property, relative viscosities were measured in 1-ethyl-3-methylimidazolium acetate [EmimAcO]. The milled set of chitins was expanded with Sigma's practical grade (PG) chitin, a darker colored chitin donated to MUN (ChitinWorks), and two samples from CSCT (one of flaky texture and one of fine particles). As dry samples were required, they were vacuum dried (ca. 50 mbar) at 105 °C for 14 h and the samples' moisture contents were determined gravimetrically with an analytical balance that measures 2 decimals of the milligram (see Figure A4–2). The moisture content values ranged from 5.48 wt.% for native α -chitin to 8.29 wt.% for Sigma's practical grade (PG) chitin which were at similar

^{cxx} The 1.116 ± 0.051 FT-IR ratio for glycosidic linkage content of the low MW sample is comparable with the 1.084 ± 0.017 obtained from 60 min milling with 68-70×0.25"/2×0.5" balls (17.5% packing / 85.6 BtC; see Figure 3–10).

^{cxxi} After this point, experimental work was performed in the University of Bath.

levels with literature.¹² Moisture content of ball milled samples increased with decreasing MW; from 6.01 wt.% for high MW α -chitin to an average of 6.65 wt.% for the medium and low MW samples. Thermogravimetric analysis (TGA) was conducted on the high MW milled α -chitin. Moisture content was determined as 5.74 wt.% in a ca. 21 min run (Figure A4–3) revealing a 3.2% RSD with the value obtained from the overnight drying gravimetric analysis. Decomposition of the sample (possibly including depolymerization and deacetylation) started above 240 °C (Figure A4–4) in close agreement with literature.^{18,19}

Figure 4–3 compares the relative viscosities of the ball milled samples among each other as well as with native α -chitin and Sigma's practical grade chitin. A decrease in viscosity with decreasing MW with no overlap between the error bars for the triplicate mass preparation of high and medium MW was observed (from 2.94 ± 0.37 to 2.08 ± 0.06). Moreover, the viscosity of the low MW (1.08) sample is significantly lower than the deviation for the medium MW. Low MW chitin produced a clear solution in about 100 microwave pulses while the medium MW required around 150. These data suggest that the three ball milled samples are of clearly different molecular weights reflecting the FT-IR data in Section 4.3.1. The darker colored chitin (ChitinWorks), and the two chitin samples from CSCT (flakes and fine powder) had relative viscosities of 4.40 (0.2097 wt.%), 5.14 (0.2093 wt.%) and 8.56

(0.2097 wt.%) respectively.^{cxixii} Native α -chitin, high MW and the fine powder sample from CSCT needed more pulses of the microwave treatment than the rest of the samples, and they were also left stirring in an oil bath at >70 °C. Although, the high MW and fine powder suspensions afforded clear solutions after some hours, native α -chitin sample had some visible particulates, so it was left at 110 °C for ca. 36 h. After this treatment, the solution appeared clear, hence the measurement was taken. However, the lower relative viscosity than that of the high MW sample (2.67 ± 0.24 vs 2.94 ± 0.37) might be attributed to persistent crystalline domains^{cxixiii} not easily spotted with the human eye as well as to possible increased intermolecular interactions between the chains upon cooling to room temperature. Both of these factors would decrease the soluble polymer concentration, hence limiting the preparation's viscosity. The higher degree of acetylation (DA) of native α -chitin compared to the high MW sample (97.0% vs 88.8%) is hypothesized to favour reformation of hydrogen bonds which might have been temporarily broken at 110 °C.^{cxixiv} Finally, Sigma's practical grade chitin viscosity is higher than the one measured by Qin et al. (2.40 vs 2.02^{12}) but probably within experimental error

^{cxixii} Replicates of kinematic viscosity measurements for these three samples were not conducted as the samples were not included in experimental design but also because efflux times were too long (exceeded 47 min).

^{cxixiii} Thin crystalline particulates (e.g. chitin nanofibers) not being dissolved.

^{cxixiv} One can also hypothesize that the chitin samples from CSCT and the darker colored chitin which revealed relative viscosities higher than 4.40 are possibly of lower than 89% DA.

(assuming the batches produced from the company are of a certain reproducibility and also considering deviations due to suspension preparation/dissolution steps).

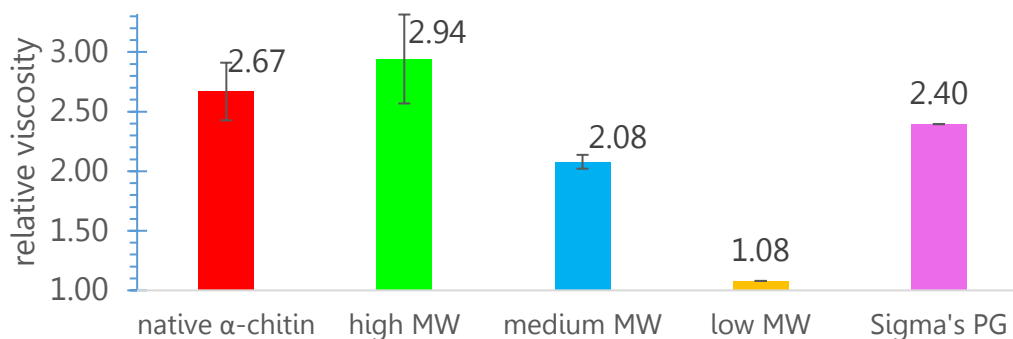


Figure 4-3: Relative viscosities of chitin samples at 0.2070 ± 0.0052 wt.% in EmimAcO. Dissolution process included microwave treatment. Error bars in native, high MW, and medium MW data are 0.24, 0.37, and 0.06 respectively arising from duplicate for native α -chitin and triplicate for the ball milled samples suspension preparations (0.2068 ± 0.0002 wt.% native α -chitin, 0.2027 ± 0.0078 wt.% high MW, 0.2097 ± 0.0001 wt.% medium MW).

4.3.3 Chitin dissolution studies and preliminary film casting

4.3.3.1 In 1-ethyl-3-methylimidazolium acetate (EmimAcO)

Before conducting the above microwave study, a triplicate mass preparation of high MW α -chitin in 1-ethyl-3-methylimidazolium acetate (EmimAcO) was attempted at a similar concentration level (ca. 0.2 wt.%) using a roller table at room temperature. After 5 days, only suspended particulate matter was observed, so the preparations were placed in a 60 °C sonication bath (100% power, frequency 37 kHz) for several hours in order to try and assist the dissolution process. However, visible particles were still observed. When the temperature was increased to 80 °C, particles were still visible after 2 h. As no dissolution was achieved, the vials were placed in a >100

°C oil bath with vigorous stirring. After overnight treatment, two of the three preparations appeared as clear solutions (samples labelled GM3 28 V2C and GM3 28 V1C, Figure 4–4), however particulate matter was still visible in the third preparation (sample GM3 28 V3C, Figure 4–4).^{xxxv} The progression of these experiments confirm that microwave heating (see Section 4.3.2) is superior to other methods in assisting chitinous materials to dissolve in EmimAcO, but also that kinetic control of the dissolution process is important (as hypothesized in Section 1.6).

At the same time, trials of native α -chitin with EmimAcO at the 2 wt.% level were attempted since that was the aim towards film casting.^{xxxvi} A concentration of 2.14 wt.% native α -chitin in the IL underwent the same thermal treatments as the 0.2 wt.% high MW suspensions above with visible particulate matter observed in every step. Therefore, the sample was placed in a 100 °C oil bath with vigorous stirring. After more than 4 days at 100–110 °C, the preparation still contained particulate matter [temperature was not set over 110 °C as there might be a stability issue for the ionic liquid.(or/and the polysaccharide) at the timescale of days]. Upon cooling, the mixture was very viscous, and its color was dark red-brown (Figure 4–4).

^{xxxv} The yellow to orange color change can be attributed to reactions originating from impurities in the supplied ionic liquid.

^{xxxvi} Researchers at CSCT knew from experience that cellulose film casting occurs at a minimum concentration of ca. 1.0 wt.%. The reader might also remember from Section 1.5.6, that chitin films with acceptable mechanical properties are usually casted from 1.5–2.0 wt.% solutions.

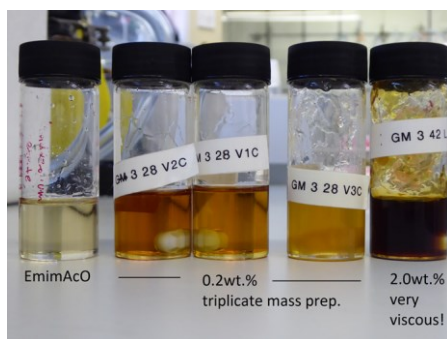


Figure 4-4: Color comparison and appearance of EmimAcO (vial far left) and viscous suspensions of high MW α -chitin [triplicate mass preparation at 0.2 wt.% after sonication bath (60–80 °C) and stirring at ca. 100 °C] and native α -chitin (vial far right; 2.0 wt.% preparation after more than 4 days of stirring at 100–110 °C) in EmimAcO.

During this set of experiments, it was noticed that literature reports a 6 wt.% solubility of α -chitin (crab, $n = 35$ cp) in BmimAcO at 110 °C.²⁰ However, the Brookfield viscosity reported seems to be low; based on the fact that Sigma-Aldrich gives a range of 20–200 (or 300) cp for low MW chitosan which corresponds to 50,000–190,000 Da. For further reference, viscosity 200–800 cp is medium MW and 800–2000 cp is high MW (see also Sections 3.3.2.5 and 3.3.4). It is not unreasonable therefore to assume that dissolution at the 6% level might have been possible with the low MW α -chitin of the prepared set.

After the above cumbersome dissolution trials with EmimAcO, it was hypothesized that a less viscous solvent system might allow more efficient dissolution via stronger shear forces. Hence, a 1:1 molar ratio for EmimAcO : DMSO was used to prepare a 1.0 and 2.0 wt.% native α -chitin dispersion (with the polysaccharide being pre-

soaked in DMSO and stirred for 3 hours).^{cxxvii} After overnight stirring at 80 °C, the samples appeared as suspensions with the 2.0 wt.% preparation having more visible particles. Hence, temperature was gradually increased to 100 °C and samples were left to stir for a couple more days. Despite the potential of increased kinetics, no visible dissolution was achieved (see Figure A4–5). During the course of experiments, and after realizing that Sigma's practical grade chitin (PG chitin) is of lower MW than native α -chitin (rel. viscosity 2.40 vs 2.67), suspensions of 0.5 and 1.0 wt.% PG chitin were prepared in 1:1 molar EmimAcO : DMSO (with overnight pre-soaking in DMSO). After 22 h of stirring at 100 °C, both samples had still fine particles suspended so they were not studied further.

4.3.3.2 In sodium hydroxide (NaOH)

In parallel to the preliminary experiments with the aforementioned ionic liquid, dissolution of the high MW α -chitin sample in 10 wt.% NaOH (at 4 °C in a cold room) was attempted to see if MW estimation was possible according to a published viscosity-light scattering study.²² After almost 3 days of stirring, a preparation of 2.28 mg/mL remained as a suspension. Even after filtering with 0.45 μ m syringe filters, dilutions with concentrations below 1.5 mg/mL gave relative viscosity measurements below 1.00 suggesting that the preparation was still a suspension.

^{cxxvii} DMSO has been observed to compete with the acetate as a hydrogen bond acceptor with the anion of the ionic liquid comprising the inner solvation shell of cellulose chains (21).

Thinking mechanistically, when a solvent is brought in contact with a polymer (Figure 4-5a), it penetrates the chain matrix from the more amorphous parts of the fibers, and its diffusion results in swelling of the solid phase (Figure 4-5b). When the concentration of the solvent in the polymer reaches a critical value, disentanglement of the chains begins (Figure 4-5c). The macromolecules of the swollen interphase are then able to move in to the solvent phase (Figure 4-5d), leaving the solvent front to advance into more crystalline parts (Figure 4-5e).²³⁻²⁶ Localized swelling has been observed in cotton fibers by optical microscopy long ago; creating balloon-like structures.²⁷ More specific for this thesis, this ballooning effect has also been reported for cellulose samples in 7.6 % NaOH.²⁸

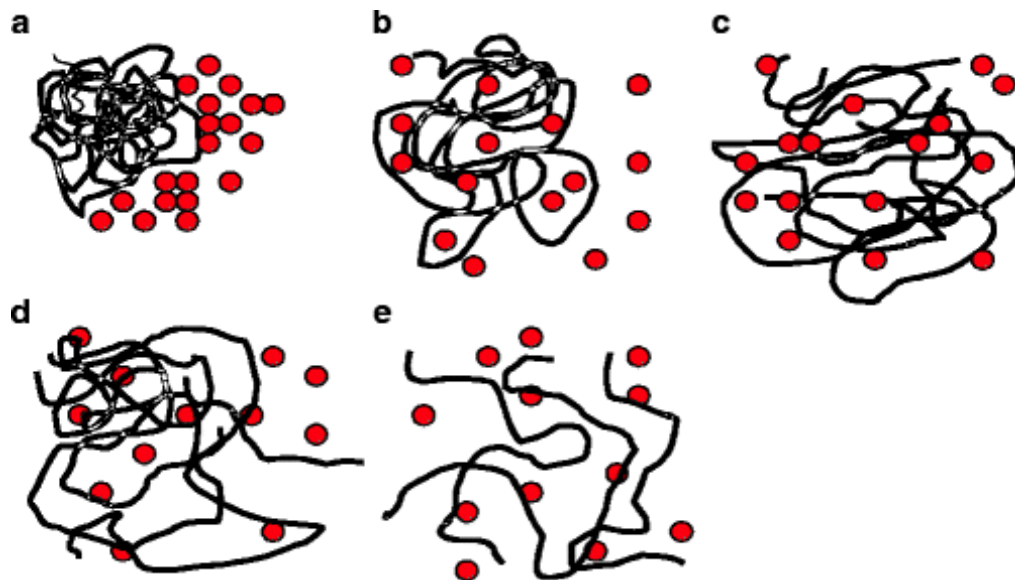


Figure 4-5: Stages of the polymer (black chains)-solvent (red circles) interface towards dissolution (a: contact, b: swelling, c: disentanglement, d: initial dissolution step, e: final dissolution step). Reprinted by permission from [Springer Nature Customer Service Centre GmbH]: [Springer Vienna] [The European Polysaccharide Network of Excellence (EPNOE)] by [Navard P., Wendler F., Meister F., Bercea M., Budtova T.] [COPYRIGHT] (2012).

Looking into relevant literature, Liu et al. observed that chitin^{cxviii} absorbs double its weight in 40 wt.% NaOH solution after one hour soaking at room temperature (100 g chitin absorbed 220 g solvent).^{cxix} Moreover, absorption (i.e. swelling) was found to increase with alkali concentration; soaking for 4 h in 25 wt.% NaOH resulted at ca. 75 g alkali solution absorbed per 100 g chitin, while the performance rose sharply to more than 200 g/100 g chitin in 40 wt.% NaOH.^{cxix cxix} Therefore, it has been hypothesized that as the hydrated ion radius decreases with increasing electrolyte concentration, the hydrated Na⁺ OH⁻ ions are able to better diffuse into the hydrogen bonding network of the polysaccharide chains.³¹ This hypothesis is supported by computations of the binding strength of sodium ions in cellulose of various water contents. Via first-principles density functional theory (DFT), Deshpande et al. concluded that sodium's interaction with cellulose is not influenced so much from coordinate covalent bonds with the lone pairs of the polysaccharide's hydroxyl groups, but more from interaction with the H₂O molecules which are strategically oriented in between them.³² A 0.42 eV difference in binding energies was calculated between cases where sodium interacted with a secondary alcohol in the presence of one (2.74 eV) and two (3.16 eV) water molecules. Binding with

^{cxviii} The sample was of 510 kDa and 89% DA.

^{cxix} Data were obtained by 10,000 rpm centrifugation.

^{cxix} Interestingly, H₂O contributed more than NaOH to the swelling of chitin.

^{cxix} Another study has reported that when five commercially available chitin samples (ca. 80% DA) of a wide range of Brookfield viscosities (from 4 to 1152 cP) had been soaked in room temperature water for 30 min, their weight had increased from 381 to 673% (data were obtained by 25 min centrifugation) (29). The same method has been also applied to non-commercial chitosan samples (30).

the primary alcohol was measured at 3.36 eV in the absence of water, and at 3.52 eV when one water molecule was present.³² For reference, adsorption energies for a single water molecule on different O sites of cellulose I β were computed from 0.26 to 0.41 eV.³³ These computational results support experimental observations of increased ionic conductivity (therefore mobility) with increasing hydration in cellulose,³⁴ and suggest that the interaction between the hydration shell of the ions with the protruding groups of polysaccharides dictates the rate of their diffusion within the hydrogen bonding network.^{32,34} cxxxii

Intriguingly, when Liu et al. soaked chitin for 4 h at reduced temperatures (-18 to -20 °C), absorption in 25 wt.% NaOH increased ca. 10-fold (ca. 750 g/100 g chitin) with the maximum value recorded for 20 wt.% NaOH (>800 g/100 g chitin). Here, the authors hypothesized water expansion upon freezing with subsequent weakening of the intermolecular hydrogen bonding network and decrystallization of the polysaccharide.³¹ However, it is only natural for one to wonder if at the reported temperature (-20 °C) there is actual freezing of the 20 wt.% NaOH solution in particular, as according to caustic soda specialists the freezing point of a ca. 19 wt.% NaOH solution is -28 °C (Figure 4–6).^{cxxxiii}

^{cxxxii} Diffusion coefficients of Na⁺ and OH⁻ in cellulose were both measured in the order of 10^{-9} cm²/s (34,35).

^{cxxxiii} A similar graph for the freezing point of NaOH solutions is available in a handbook from Occidental Petroleum Corporation and OxyChem at: <https://www.oxy.com/OurBusinesses/Chemicals/Products/Documents/CausticSoda/caustic.ic.pdf>. The freezing point minimum there appears to be -28 °C at 19 wt.% NaOH. Complementary data are also available from Avantor® Puritan Products at:

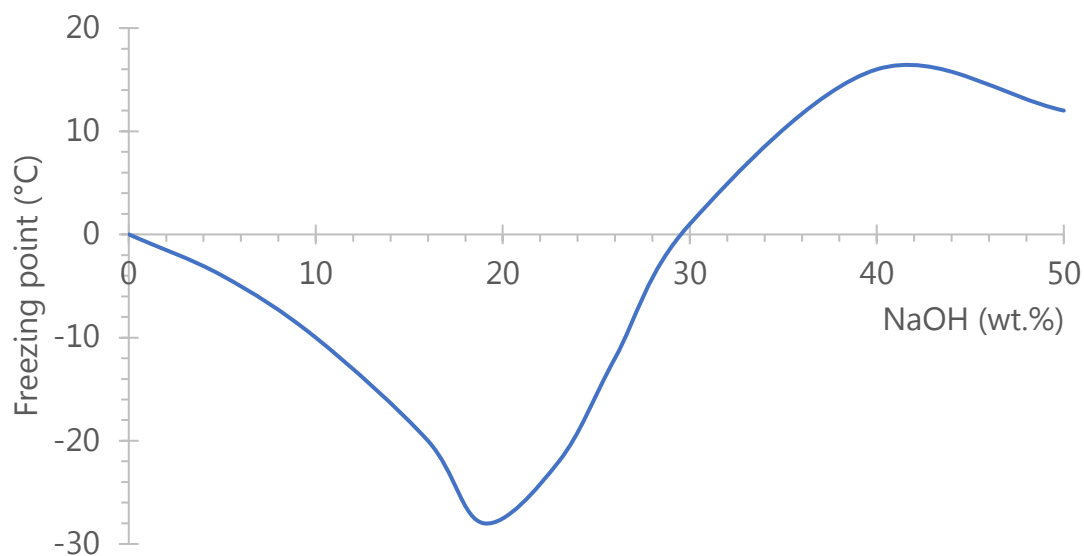


Figure 4-6: Freezing point (°C) of aqueous sodium hydroxide (NaOH) solutions (0-50 wt.%). Data based on Pickering, S. U. LXI.-The hydrates of sodium, potassium, and lithium hydroxides. *J. Chem. Soc. , Trans.* **1893**, *63*, (0), 890-909.

Considering the fact that alkali solutions are reported in several solvent systems for chitin^{37,38} and cellulose,³⁹ the dissolution power of ~20 wt.% NaOH was worth exploring. Hence, 0.35 wt.% of medium MW chitin sample was soaked overnight at -18 °C in 18.1 wt.% NaOH (appeared as a white suspension). When it was placed in a -80 °C freezer for 10 min, the suspension was frozen.^{cxv} When thawed and stirred, the suspension was transparent with no particulates visible to the naked eye. After leaving the solution for about a week at room temperature, chitin came out of solution to yield a suspension once more (Figure 4-7 shows the contrast of

<https://www.puritanproducts.com/resources-support/technical-resources/freezing-point-chart/>. Both of these references are in close agreement with the measurements of Pickering (36).

^{cxv} Total suspension mass was ca. 3.0 g.

transparent solution and white suspension). Going back to alkaline based solvent systems, high MW chitin was subjected to solubility tests using 8:4:88 wt.% NaOH : urea : H₂O solution according to literature.^{40 cxxxv} Suspensions were frozen at -18 °C, however even at a concentration as low as 0.125 mg/mL dissolution was not achieved.

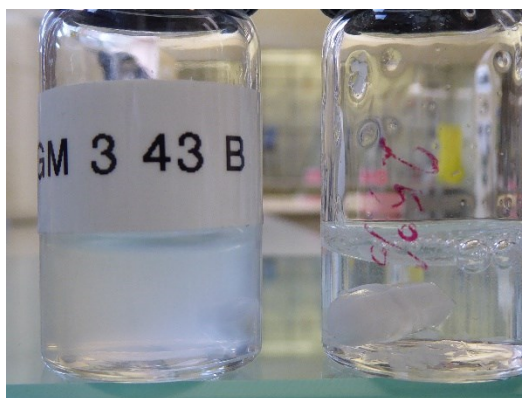


Figure 4-7: Medium MW α -chitin back in white suspension (vial on the left) after its transparent solution (0.35 wt.% in 18.1 wt.% NaOH) was left at room temperature for a week. Vial on the right shows an undissolved native α -chitin particle (next to the magnetic stir bar in the) in transparent NaOH solution (0.43 wt.% preparation in 21.7 wt.% NaOH) after one freeze-thaw cycle.

Comparing the experiments of EmimAcO and NaOH, the freeze-thaw process with ~20 wt.% NaOH seemed to provide a dissolution method with relatively short processing times and less intense work (considering the numerous pulses in the domestic microwave). Hence, it was pursued further with the aim of casting films of Sigma's practical grade (PG) chitin. Concentrations of 0.41, 0.73, 1.43 and 2.69 wt.%

^{cxxxv} In the field of cellulose dissolution by aqueous alkali systems, urea has been hypothesized to weaken the interactions between the hydrophobic surfaces consisted of pyranose hydrogens (41) (see also the Lindman hypothesis in Section 1.6).

of PG chitin were dispersed in 20.0 wt.% NaOH. The samples were stirred for 2 h in an ice bath, and after that they were stirred in a dry ice/acetone bath which was in between -13 and -18 °C. In less than 10 min, the two more concentrated samples became very viscous. After that, all samples underwent 3 freeze-thaw cycles with the use of a -80 °C freezer. Viscosity appeared to increase with increasing concentration, but the 0.41 wt.% sample contained particulates. Figure 4–8 exhibits the increased viscosity of this set, which can also be thought as swelling of the polysaccharide particles.

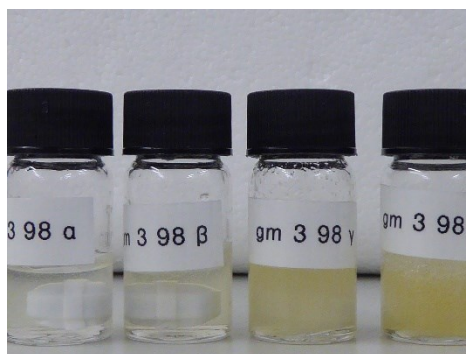


Figure 4-8: Snapshot of increasing viscosity (from left to right) for 0.41, 0.73, 1.43, 2.69 wt.% practical grade (PG) chitin samples in 20 wt.% NaOH.

The last set of experiments provided evidence that 20 wt.% NaOH can be an effective solvent for the more amorphous fractions of chitin particles, but considering all dissolution trials, it is assumed that native α -chitin used in this thesis and Sigma's practical grade chitin have persistent crystalline domains whose dissolution is particularly challenging. These fractions of the polysaccharide's nanofibrils have been claimed to possess an amphiphilic-like structure with

hydrophobic surfaces involving the ring hydrogens, and hydrophilic sections entailing the hydroxyl groups directed towards the sides of the ring.⁴² If future research focuses deeper into that structural aspect, ball milling might receive increasing attention in polysaccharide studies. At the moment though, and at the laboratory scale, filtering that undissolved mass might be the objective for some researchers, however the increased viscosity of the dispersion is expected to push ordinary pumps to their limits.^{cxxxvi}

Regardless of the separation challenges, experimentation with HCl as an anti-solvent was thought worth trying. Therefore, concentrations of 0.46, 1.01, 1.59, 1.95 and 4.37 wt.% of PG chitin were dispersed in 20.0 wt.% NaOH (0.0293 ± 0.0001 mol NaOH in vials of 7 mL). The samples were stirred and went through two consecutive freeze-thaw cycles within 1 h using the -80 °C freezer. Most of the dissolution seemed to happen in the first cycle, and sample viscosity increased with increasing concentration. An exception was the 4.37 wt.% sample which was so viscous after the second cycle that the magnetic stir bar in the vial could not spin. Samples were poured into petri dishes (except the 4.37 wt.% sample which had solidified and had to be warmed), and the magnetic bars were removed. Viscous solutions were spread to cover the whole surface of the petri dish with no visible gaps [except 4.37 wt.% (see Figure A4–6)].

^{cxxxvi} An alternative technique might be ultracentrifugation.

An equimolar, neutralizing 250 mL HCl bath was prepared (0.12 M gives approx. 0.029 mol) and petri dishes were immersed slowly. Viscous solutions detached from the petri dish surface and films started floating. However, with careful manipulation, the films were kept on the petri dish surfaces and placed on the bottom of the bath tank. The 0.46 wt.% sample easily lost its coherence during bath immersion. The rest of the petri dishes were left in their corresponding acid baths overnight. Figure A4–7 shows the appearance of films after being removed from their baths (note: the 1.01 wt.% sample tore apart when it was brought up in the bath's surface). The reader might notice how even the 4.37 wt.% sample (far right in Figure A4–7) covered the whole area of the petri dish. The remaining three samples were washed in a deionized water tank and sample 1.59 wt.% tore apart in some places. After about 20 min, the samples were placed at $-18\text{ }^{\circ}\text{C}$ for about 35 min to be conditioned before freeze drying (they appeared less smooth at this point in processing). Freeze-drying required about 5 h under a 7-mbar vacuum. The film prepared from the 1.59 wt.% sample tore apart even more but the other two were in one piece (although sample 1.95 wt.% can be characterized as fragile with thinner areas and some cracks). The film from the 4.37 wt.% sample was the strongest and happened to develop a smooth and relatively transparent area (as opposed to the white and relatively rough domains in others; Figure 4–9). The piece of film could easily tolerate a fall from the benchtop to the floor with no crack whatsoever. It also had a rigid structure, except from the transparent part, which revealed some flexibility. The latter result along with the breaking of the 1.59 wt.% sample suggest

that the parameters of the freeze-drying process (and probably anti-solvent treatment) affect the entanglement of the chains and the texture of the solidified film. However, it seems that the acetylated chains of PG chitin require a minimum concentration of ca. 2 wt.% for casted films with acceptable mechanical properties.

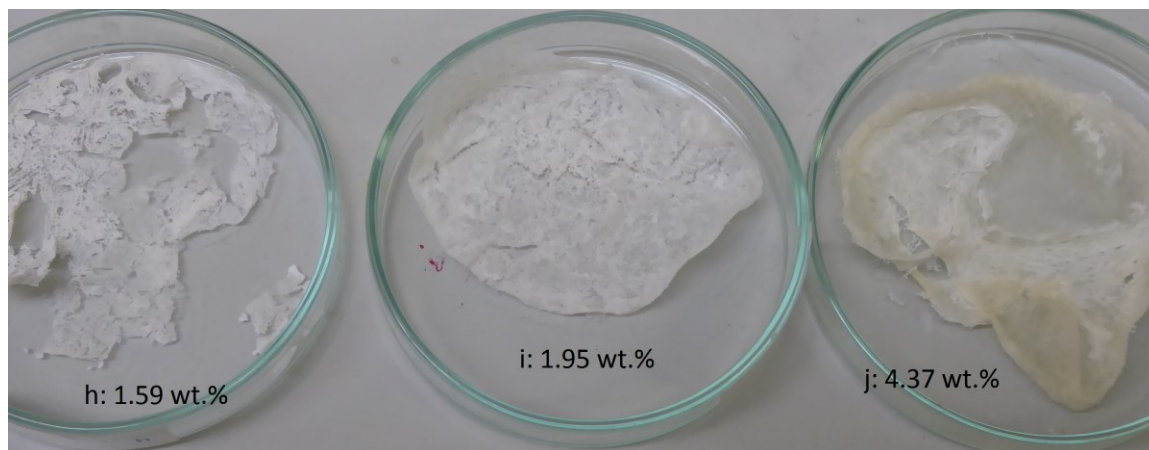


Figure 4-9: Practical grade (PG) chitin films after their freeze-drying process. Concentrations from left to right are: 1.59, 1.95, and 4.37 wt.%.

4.3.4 Ultrasound assisted heterogeneous deacetylation of α -chitin

Chitin's amide groups can be hydrolyzed chemically either with acids or bases.⁴³ Since glycosidic linkages are sensitive to acidic treatment though (as seen in Chapter 3), alkali deacetylation has been preferred by most researchers even before the first spectroscopic investigations of the marine polysaccharide.^{44,45} By means of usually NaOH,^{cxxxvii} both homogeneous and heterogeneous methodologies have been explored using the traditional one-variable-at-a-time

^{cxxxvii} Generally, concentrations higher than 30 wt.% NaOH are applied, which create an excessively alkaline environment. For reference, a ca. 6 wt.% NaOH (1 M) gives a pH of 14.

experimentation.⁴⁶⁻⁴⁸ More recently though, it has been found that among seven variables (number of successive alkali baths, reaction time, reaction temperature, alkali reagent, alkali concentration, atmospheric conditions, use of an oxygen scavenger), temperature is the most significant variable that controls the process.¹⁴

The importance of temperature was also highlighted in a study that explored the deacetylation potential of sonication on β -chitin.¹⁵ It was found that high intensity ultrasound irradiation can yield high molecular weight chitosan (which can lead to preferable mechanical properties for the desired scaffold applications) when deacetylation temperature was controlled at 60 °C.^{cxviii} Therefore, sonication treatments were applied to the α -chitin set from Section 4.3.1 aiming for efficient amide hydrolysis and minimal depolymerization. Having a feel of the deacetylation effect that certain sonication times would give on the native α -chitin sample was considered necessary. Also, the influence of the work up of the reaction mixture^{cxix} as well as the methodology for ¹H NMR measurements of DA were investigated.

The initial trial was performed by sonicating the native sample for 76 min (based on a compromise between two consecutively 50 min processes reported by Fiamingo et al. for a 1:10 w/v β -chitin reaction mixture).¹⁵ After cooling the reaction mixture in an ice bath, 5–6 large particles were observed floating on the reaction mixture's

^{cxviii} The relatively low molecular oxygen conditions that ultrasound irradiation usually creates along with the relatively low temperature (60 °C) are hypothesized to minimize oxidative depolymerization which usually occurs in thermochemical processes (15).

^{cxix} Lowering the pH to 8.5 has been hypothesized to terminate the reaction and “increase the proportion of the insoluble fraction” (49).

surface indicating that they had not mixed with the bulk of it. After their removal, more than 100 mL of 1M HCl were added, the pH was measured with an indicator paper and found to be 8-9. Filtering of the sample was attempted using 0.45 μm filters (Versapor Membrane, PALL), but filtration with the available pumps was very slow. Therefore, the reaction mixture was centrifuged at 5000 rpm and washed with deionized water. After drying at 80 °C overnight, approx. 1.26 g of a flaky textured product with an orange coloration was recovered and mortared to prepare for analysis (product 4-1). FT-IR data for the triplicate measurement of product 4-1 is shown in Figure 4-10. The intensity ratio for the amide II has dropped from 2.736 for native chitin to 1.071 and for the glycosidic linkage from 1.423 to 1.088. These figures suggest extensive deacetylation and little depolymerization.

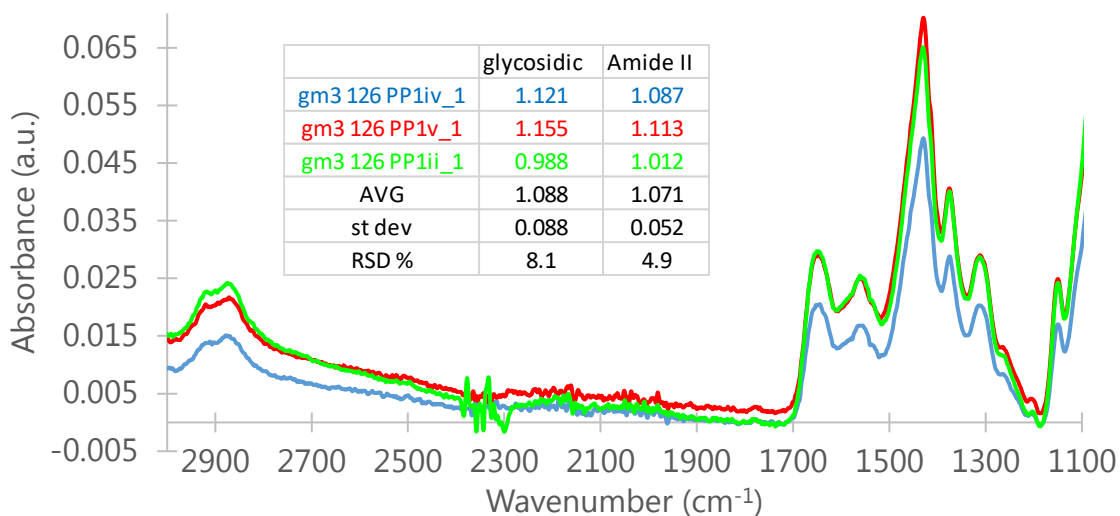


Figure 4-10: Infrared spectra (triplicate acquisition) of deacetylation product 4-1 (76 min sonication of native α -chitin). Inset table records the absorbance ratios which probe depolymerization (1.088 ± 0.088) and deacetylation (1.071 ± 0.052).

Product 4-1 was passed through a mesh and dissolved in 2 wt.% DCl (4.4 mg/mL). NMR data for product 4-1 is shown in Figure 4-11. With the ca. 1.85 ppm resonance assigned to the methyl group of the *N*-acetyl group, the DA value is 32.1%.

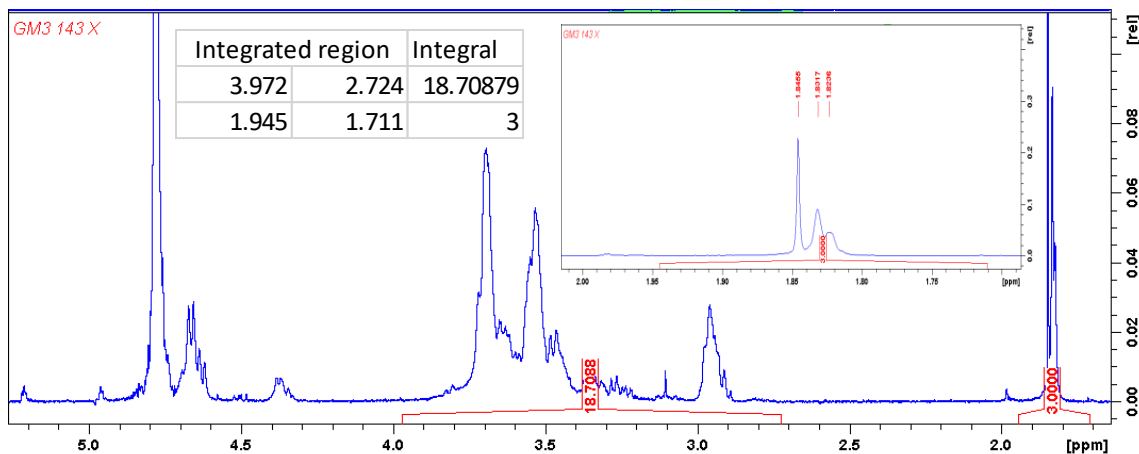


Figure 4-11: NMR spectra of deacetylation product 4-1 (76 min sonication of native α -chitin; 4.4 mg/mL in 2 wt.% DCl). Inset table records the integration details [DA is 32.1% (= 600 / 18.7088)]. Inset spectra shows the 1.70-2.00 ppm region.

The process was tested with another chitin sample by applying the same sonication time to the high MW α -chitin. After approx. 4 min of sonication (10 min real time), the reaction mixture appeared light brown. Upon completion of 76 min sonication, the reaction mixture appeared more viscous than the trial with the native sample and was washed with approx. 50 mL water. This viscosity was decreased when more than 80 mL of 1M HCl were added. When approx. 40 mL of 1.8 M HCl were added, the reaction mixture reached a total volume of approx. 200 mL and was centrifuged/washed/dried as described before for the native sample. The resulting

solid appeared of a darker brown shade (product 4-2). An overlay of FT-IR spectra of products 4-2 and 4-1 is shown in Figure 4-12.

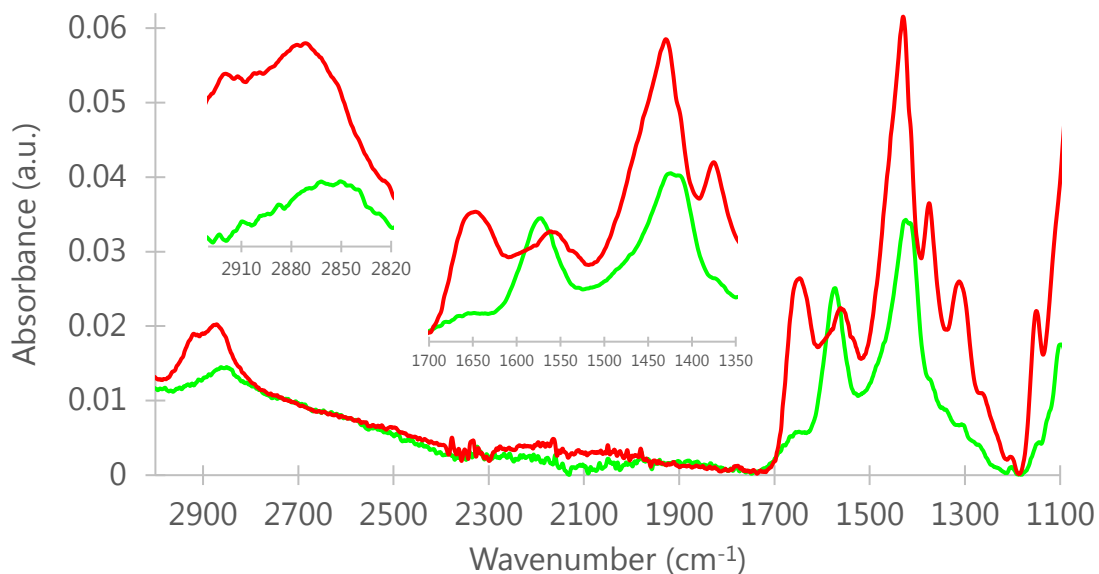


Figure 4-12: Infrared spectra of deacetylation products 4-1 (red) and 4-2 (green).

The signal for product 4-2 is characteristic for a carboxylic acid salt, which gives rise to two bands involving the out-of-phase and in-phase carboxylate stretching vibrations.⁵⁰ The out-of-phase stretching band is observed near 1570 cm^{-1} (1572-1574 cm^{-1} in spectra here) and the in-phase stretching band is observed near 1415 cm^{-1} (a doublet at 1424 and 1414 cm^{-1} in spectra). A possible interpretation is that chitosan has been acidified to such a large extent that it has turned into a chitosan

acetate salt.^{cx1} This might also suggest that the amide stretches (from the acetylated residues in the chains) are masked. One can also observe that the glycosidic linkage stretch is significantly lower compared to the 2875 cm⁻¹ reference band (which has shifted to lower frequencies).

Product 4-2 was dissolved in 2 wt.% DCl (4.3 mg/mL) and NMR data are shown in Figure 4-13. The DA value here is 19.8%. The more deshielded protons appearing around 1.99 ppm (the difference from 1.858 is 0.134 ppm) are potentially from the acetyl group of the chitosan acetate salt.^{51,52} The lower DA value (19.8 vs 32.1%) can be explained by the lower crystallinity of the high MW α -chitin, which facilitates the penetration of NaOH within the entangled chains.

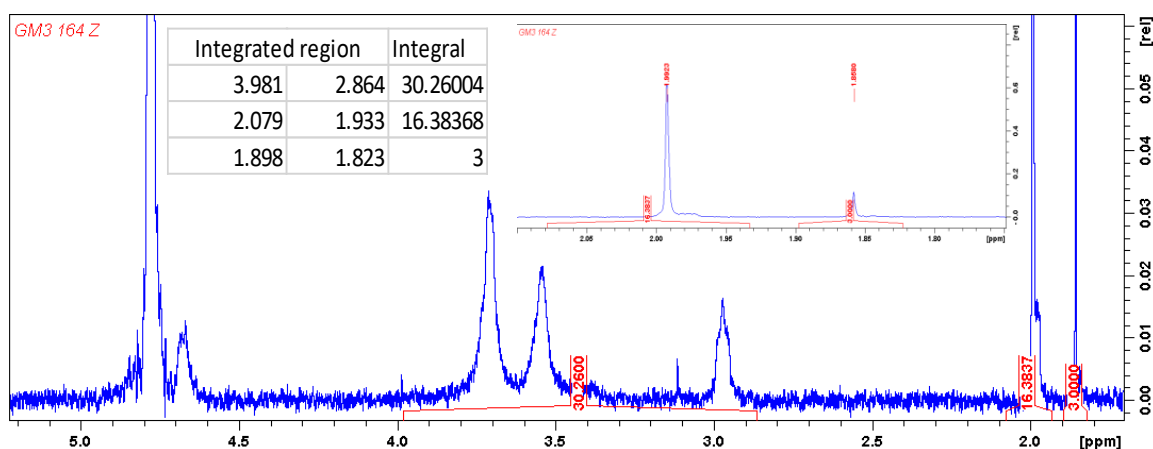


Figure 4-13: NMR spectra of deacetylation product 4-2 (76 min sonication of high MW α -chitin; 4.3 mg/mL in 2 wt.% DCl). Inset table records the integration details [DA is 19.8% (= 600 / 30.26)]. Inset spectra shows the 1.75-2.10 ppm region.

^{cx1} Another explanation might be that the washing was inadequate, and that sodium acetate contaminated the product.

Wanting to lower the work up volumes and also try a potentially faster neutralization step, undiluted HCl was used on the reaction mixture from a 29 min sonication of native α -chitin (product 4-3). It seemed that when 13 mL of 12 M HCl were added, the pH which was measured with a pH electrode did not go below 13.0 immediately. However, the temperature rose significantly to ca. 50 °C, therefore this approach was not pursued further.

Aiming for a shorter (than 76 min) sonication treatment as well as to gain a better understanding of the reproducibility of the whole process, 44 min ultrasound was applied (and no neutralization step) to native α -chitin twice (product 4-4 and product 4-5). The FT-IR spectra of both samples are shown in Figure 4-14. The two spectra are similar to each other and share common features with product 4-2 (carboxylate stretching vibrations, low glycosidic content); assumed to arise from sodium acetate salt formation.

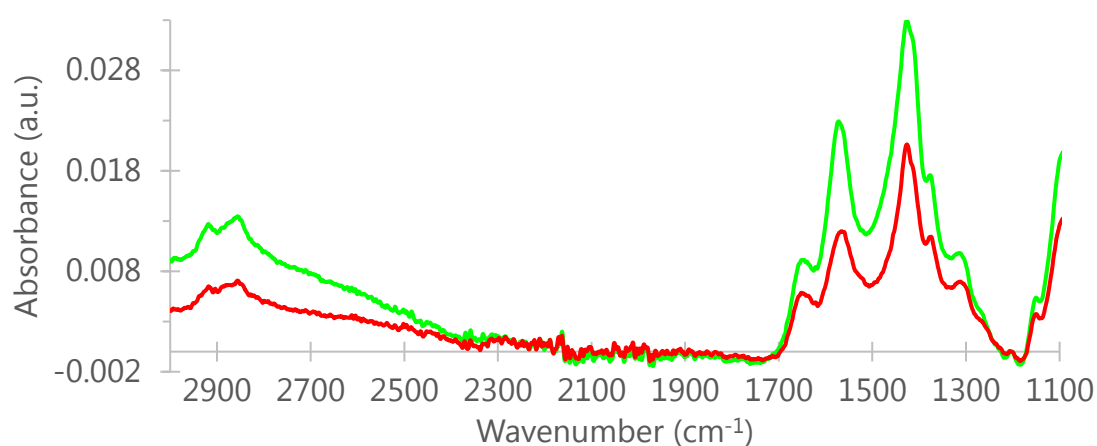


Figure 4-14: Infrared spectra of deacetylation products 4-4 (red) and 4-5 (green).

Products 4–4 and 4–5 were dissolved in 2 wt.% DCl (4.3 mg/mL). The NMR data are shown in Figures 4–15 and 4–16 with the DA values being 50.7% and 54.8% respectively. In line with the FT-IR characterization, the NMR spectra here are also similar to that of product 4–2 (i.e. two acetyl groups are observed) which provides additional evidence for contamination of the biopolymer with acetate salt.

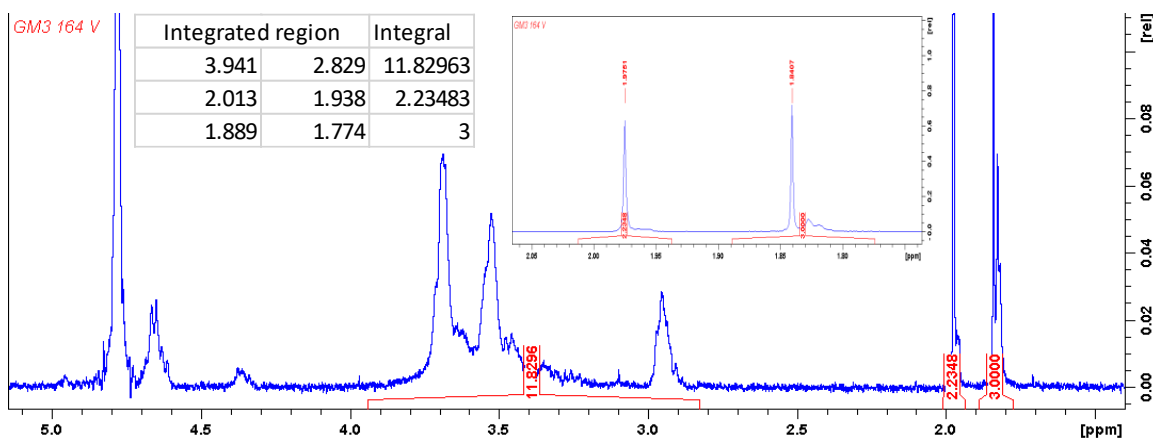


Figure 4-15: NMR spectra of deacetylation product 4–4 (4.3 mg/mL in 2 wt.% DCl). Inset table records the integration details [DA is 50.7 % (= 600 / 11.83)]. Inset spectra shows the 1.75-2.05 ppm region in more detail.

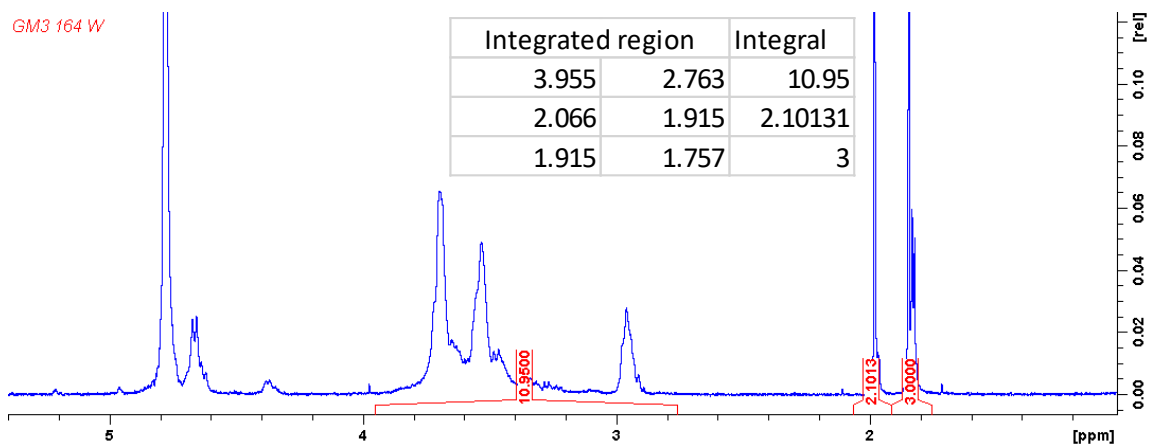


Figure 4-16: NMR spectra of deacetylation product 4–5 (4.3 mg/mL in 2 wt.% DCl). Inset table records the integration details [DA is 54.8 % (= 600 / 10.95)].

Investigations of reduced sonication times were further pursued with 21 min on native α -chitin. Approximately 50 mL of 6 M HCl were added to the reaction mixture and pH was found to be \sim 8.0 using indicator paper. After centrifugation, the reaction mixture was washed several times (in an effort to reduce acetate salt contamination) and was finally freeze-dried (product 4–6). Product 4–6 was dissolved in 20 wt.% DCl (as a higher DA value was expected; 5.2 mg/mL) and NMR data are shown in Figure 4–17 [sodium-3-trimethyl silylpropionate (TMSP-2.2.3.3-D4) was spiked for reference]. The peak for the *N*-acetyl protons appears at 2.1319 ppm, and the region up to 2.27 ppm where possible acetate protons would have been expected is clear. The region of the ring protons though appears less clear (DA is 55.0%).

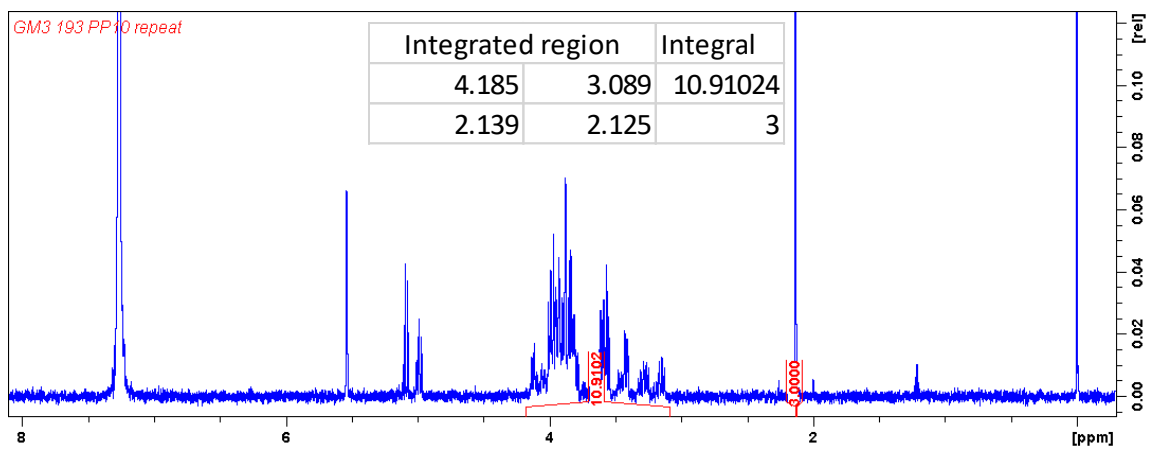


Figure 4-17: NMR spectra of deacetylation product 4–6 (5.2 mg/mL in 20 wt.% DCl). Inset table records the integration details [DA is 55.0 % (= 600 / 10.91)].

After these preliminary experiments, a sonication time of 22 min was applied to the high MW sample (aiming for a high or medium DA value). With the addition of 45 mL of 6M HCl, the reaction mixture appeared very viscous and about 20 mL of water

were added to reduce that viscosity. When the pH was ~ 8.5 , the reaction mixture was diluted up to a total volume of 200 mL. After centrifugation and washing, the residue was thermally dried under vacuum and approx. 1.7 g was recovered (product 4-7). An overlay of FT-IR spectra for products 4-7, 4-6 and 4-1 is shown in Figure 4-18. With the amide II peak appearing ca. 1550 cm^{-1} in all 3 signals and no carboxylate in-phase stretching band near 1415 cm^{-1} for products 4-7 and 4-6, one can calculate amide II intensity ratios in order to have a relative estimation of the DA value.^{cxli}

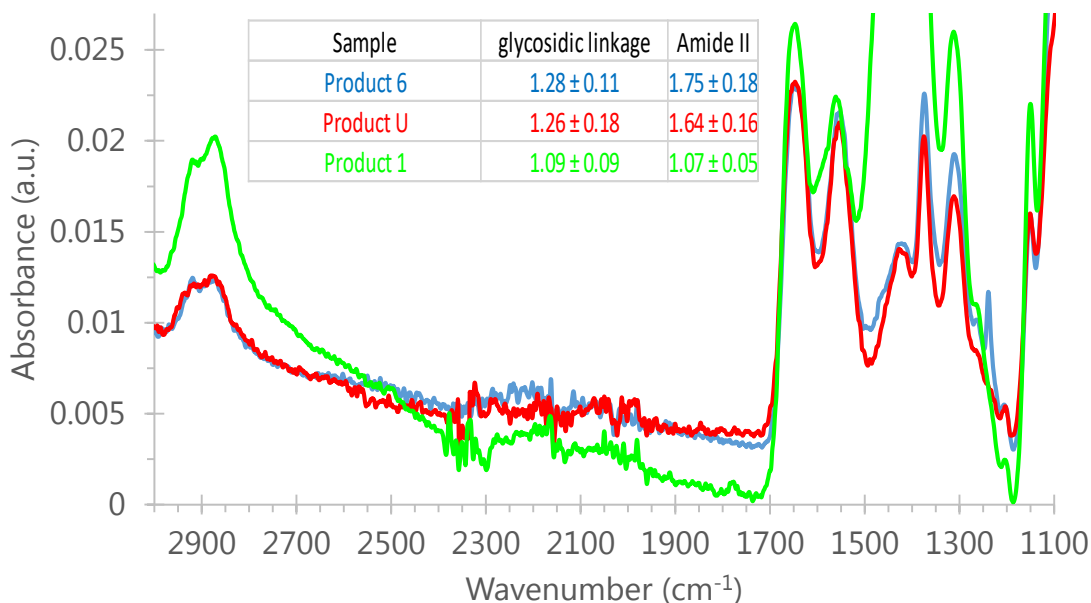


Figure 4-18: Infrared spectra of deacetylation products 4-7 (red), 4-6 (blue) and 4-1 (green). Inset table records the intensity ratios for the glycosidic linkage and amide II.

^{cxli} The band at 1430 cm^{-1} for product 4-1 (see Figure A4-8) raises questions for future research.

The 0.10 difference in the IR ratio for the glycosidic linkage in between native α -chitin and high MW α -chitin (1.42 - 1.32; see Section 4.3.1), gives a 0.11 difference (1.75 - 1.64) in the amide II ratio of the resulting deacetylated product from 22 min sonication. Assuming that an amide II ratio of 1.75 corresponds to a DA value of 55% [from its NMR; 62% using the FT-IR Sannan coefficient] and of 1.07 to a DA value of 32% (as measured above with NMR; 38% with the Sannan method), it is not unreasonable for one to expect that an aimed amide II ratio of 1.50 [from the 0.14 difference from product's 4-7 (high MW) 1.64 ratio which arises from the 0.13 difference of the glycosidic linkage ratio difference between high and medium MW (1.32 - 1.19)] might correspond to an approx. 46% DA value (from 22 min sonication).^{cxlii} Therefore, a 50% DA value was aimed [as a medium DA value for the medium MW chitin sample in the Design of Experiments context (see Section 4.1)] with an 18 min sonication treatment. Table 4-2 presents a record of the deacetylation experiments (4-1 to 4-6) described to this point, as well as those that follow (4-7 to 4-11).

^{cxlii} The higher DA values obtained by FT-IR compared to those from NMR (6 ± 1 DA% units, see Table 4-2) could be due to both NMR and FT-IR acquisition variables.

Table 4-2: Deacetylation experiments on various chitin samples and results (DA%). Results are of preliminary nature.

Product code	Starting chitin	Sonication time (min)	DA%	
			FT-IR	NMR
4-1	native	76	38.0	32.1
4-2	high MW	76	-	19.8
4-3	native	29	-	-
4-4	native	44	-	50.7
4-5	native	44	-	54.8
4-6	native	21	62.0	55.0
4-7	high MW	22	58.2	53.3
4-8	medium MW	18	-	<10
4-9	low MW	22	-	-
4-10	medium MW	9	-	<10
4-11	medium MW	65	-	-

Indeed, a sonication time of 18 min was applied to the medium MW sample (aiming for a medium DA value of 50%). After neutralization (~8.0), centrifugation and washing, the residue was freeze-dried and approx. 0.55 g was recovered (product 4-8). When sonication was applied to the low MW sample (aiming for a low DA value), it was found that the reaction mixture got very viscous after 18 min sonication. As there was little visible diffusion, the treatment was stopped at 22 min. With addition of only 10 mL of 6M HCl, viscosity was completely lost, and the product appeared fully dissolved. After a couple of days, the product was recovered with the addition of EtOH (acetone was also tried and did not lead to any precipitation). The product isolated by centrifugation was thermally dried under vacuum and saved for future analysis (product 4-9).

Wanting to have a better feel for the deacetylation process on the medium MW chitin sample, a sonication time of 9 min was applied (aiming for a high DA value around 75%). The reaction mixture was worked up as for product 4–8 and approx. 0.39 g was recovered (product 4–10). Aiming for a low DA value for the medium MW chitin sample, more than 45 min sonication was applied. At 65 min, the reaction mixture appeared very viscous and ~100 mL of water was added. After the addition of 19 mL of 6M HCl, viscosity was lost (as for product 4–9; the pH was ~9.5). The product was recovered the day after with the use of EtOH (as for product 4–9), and after centrifugation and drying, it was saved for future analysis (product 4–11).

Products 4–7, 4–8, 4–10 were dissolved in 20 wt.% DCl at 4.4, 5.5, 5.0 mg/mL respectively and NMR data are shown in Figures 4–19, 4–20, and 4–21 respectively [sodium-3-trimethyl silylpropionate (TMSP-2.2.3.3-D4) was spiked for reference]. Products 4–8 and 4–10 achieved dissolution with just 20 min stirring at 70 °C. The peak for the *N*-acetyl protons in product 4–7 appears at 2.11 ppm, and no signals for acetate protons were seen in the region up to 2.24 ppm. The DA value is 53.3%.^{cxliii} The DA values for the other two products (which had medium MW chitin as starting material) are unexpectedly low (<10%) by NMR analysis.

^{cxliii} The Sannan method gives a DA of $58.2 \pm 5.7\%$ (amide II ratio in Figure 4–18 was 1.64 ± 0.16).

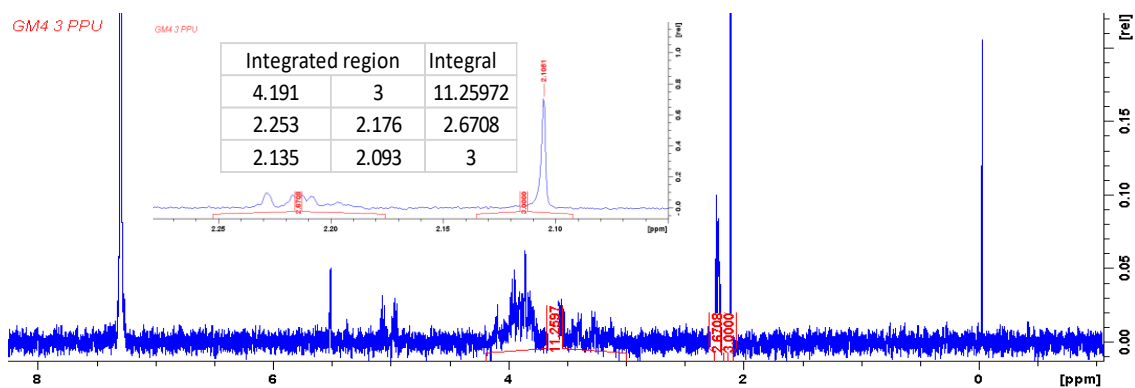


Figure 4-19: NMR spectra of deacetylation product 4-7 (4.4 mg/mL in 20 wt. % DCI). Inset spectra shows the 2.05-2.27 ppm region [DA is 53.3% (= 600 / 11.26)].

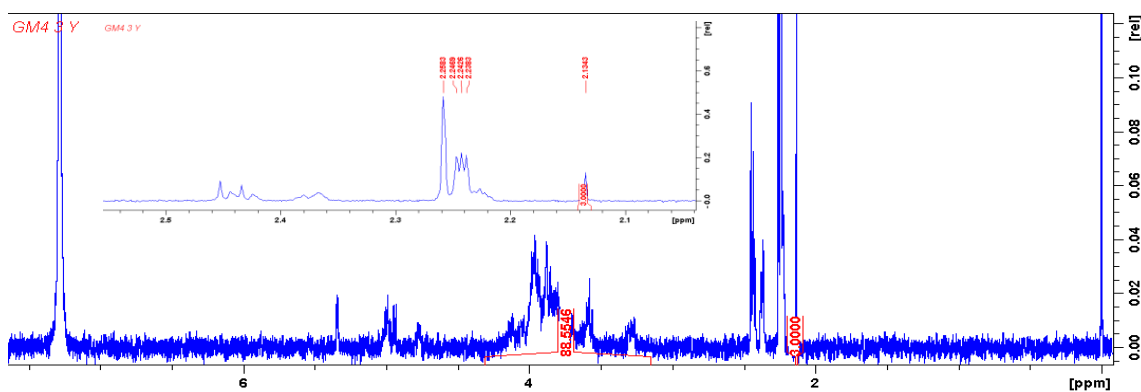


Figure 4-20: NMR spectra of deacetylation product 4-8 (5.5 mg/mL in 20 wt.% DCI). Inset spectra shows the 2.06-2.54 ppm region in more detail.

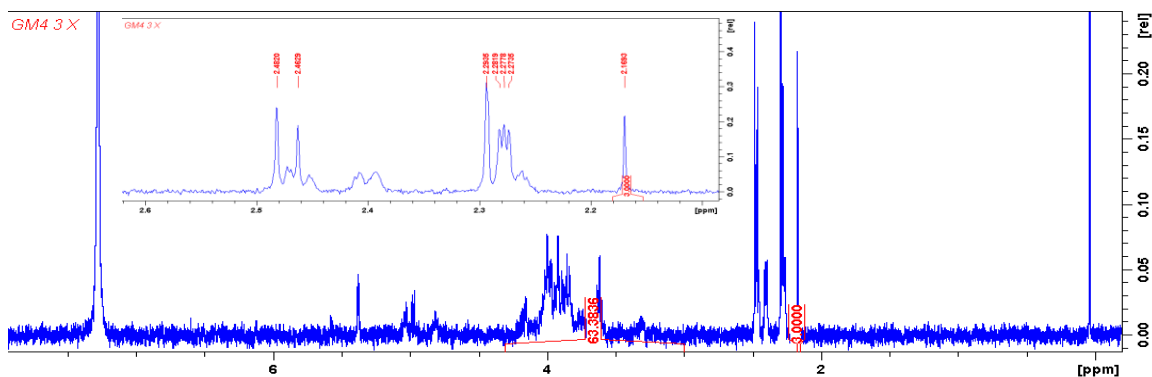


Figure 4-21: NMR spectra for deacetylation product 4-10 (5.0 mg/mL in 20 wt.% DCI). Inset spectra shows the 2.10-2.60 ppm region in more detail.

The set of the above deacetylation experiments provided preliminary evidence that the sonication method applied is able to give predictable results for the higher MW α -chitin samples (native and high MW). Sonication times of 22 and 76 min were found to lower the DA to ca. $57 \pm 4\%$ and $35 \pm 4\%$ respectively^{cxliv} with concurrent depolymerization taking place to a lower extent.^{cxlv} The performance appears more efficient in its initial phase compared to the 37% DA from 50 min sonication of β -chitin observed by Fiamingo et al.¹⁵ However, chitin concentration in the set of deacetylations here was ca. 20% lower, and the exact nature of ultrasound treatment was slightly different.

Based on these results, the lower MW α -chitins of the set (medium and low MW) gave unexpectedly low DA values suggesting that a significant redesign of the deacetylation method is required.^{cxlvi} Moreover, the neutralization process by means of HCl resulted in recoveries below 0.55 g for the deacetylation products of the lower MW chitins,^{cxlvii} which is ca. 1/3 of the recovered masses for the higher

^{cxliv} A more than 3-fold increase in the reaction time ($3 \times 22 = 66$ min) did not seem to have a proportional DA decline, confirming the known leveling off of chitin deacetylation kinetics (53).

^{cxlv} When comparing the initial FT-IR ratios for the glycosidic linkages and amide II (Section 4.3.1) with those of Figure 4–18, the average decreases were 0.18 for the former and 1.17 for the latter. These suggest that the rate of depolymerization was roughly 15% that of deacetylation. A possible mechanistic hypothesis for alkaline depolymerization is through deprotonation of the C8 and subsequent nucleophilic attack on the anomeric C, which seems kinetically demanding.

^{cxlvi} However, the preliminary observations for these reactions confirmed the hypothesis that more amorphous α -chitin samples can give faster deacetylations (assumed to arise from randomly accessed *N*-acetyl groups) (49). Hence, shorter than 18 min sonication times are hypothesized to give lower than 50% DA values.

^{cxlvii} That mass represents less than 30% of the starting chitin (~ 2.0 g).

MW. Therefore, a more systematic study is needed to understand the work-up step (removal of acetate salts). Principally, in the excessively alkaline conditions of the reaction mixture, sodium acetate exists between the neutral deacetylated chains, and separation of the salt and chitinous material requires washing with aqueous solutions. The polysaccharide chains are expected to precipitate during certain centrifugation conditions, however the results suggest that repetitive washings are needed with fresh quantities of aqueous solution to extract all of the sodium acetate. The hypothesis that the lowering of the pH by means of HCl to 8.5 maximizes the recovery of the polysaccharide might be a challenge for future research. Considering a hypothesized tendency of the chains to reentangle upon cooling to room temperature, a neutralization process by HCl might increase the risk for acetic acid and ammonium acetate local entrapment (through competitive diffusion with NaCl within the hydrogen bonding network) and lead to their inevitable precipitation. To the best of my knowledge, literature has not yet experimented systematically with the details of the work-up step.

Focusing on product 4-1, the strong infrared band at 1430 cm^{-1} (see Figure 4A-8) is hypothesized to arise from contamination with an acetate salt (probably that with sodium). Hence, upon arrival to MUN, the sample was subjected to a washing treatment^{cxlviii} and examined with FT-IR. Figures A4-9, A4-10, and A4-11 show the

^{cxlviii} Approximately 400 mg of product 4-1 were stirred with ~10 mL deionized water in a >50 °C water bath for ~20 min. The mixture was treated for another 20 min in a sonic bath and then it was centrifuged at 7500 rpm for 10 min. Supernatant was removed, fresh water was added, and the suspension was left under stirring in a 45 °C water bath overnight.

amide, glycosidic linkage, and carbon-hydrogen infrared regions respectively of standard mixtures of anhydrous sodium acetate with milled α -chitin^{cxlix cl} along with that of product 4-1 before and after its aforementioned washing. The orange colored signals show an increasing intensity of the characteristic CH_3COONa vibrations at 1407, 1562, 2930, and 2999 cm^{-1} with increasing concentration of the salt.^{54 cli} Observing the spectra for product 4-1 (red and green signals) in Figure A4-9, the clear decline of the 1407 cm^{-1} band (in-phase symmetric carboxylate stretch)^{50,55} to the usual absorbance levels of chitin (<0.10 a.u.),^{clii} as well as the emergence of the glycosidic linkage at ca. 1150 cm^{-1} in Figure A4-10^{cliii} indicate that a simple washing treatment can make a difference which can be monitored with infrared spectroscopy.^{cliv} The changes upon washing are also evident in the C-H

The sample was centrifuged at 7700 rpm for 70 min, supernatant was removed, and the insoluble residue was placed in a ~ 55 °C oven under vacuum overnight.

^{cxlix} An α -chitin sample with amide I split, amide II, and glycosidic linkage infrared ratios of 0.764 ± 0.008 , 2.356 ± 0.029 (DA $83.5 \pm 1.0\%$), and 1.264 ± 0.019 respectively was created by milling 1.00 g of dried α -chitin (larger particles were selected through a mesh) with 67 quarter inch balls for 60 min. Crystallinity index (CrI%) was measured by XRD at 34.8%. The higher ratio for the glycosidic linkage obtained here (1.26) compared to that of the low MW sample (1.12; see Table 4-1) is a good basis for future studies of the relationship between chitin particle size and depolymerization efficiency of ball milling.

^{cl} Intimate mixtures of 14, 35, 50, 65, 74 wt. % anhydrous sodium acetate in the milled α -chitin sample were prepared by vortexing totals of ~ 100.0 mg for ~ 60 s in vials of 2 mL volume.

^{cli} The signals for the 14 and 74 wt.% mixtures were in between those for 0 and 35 wt.% the former and 65 and 100 wt.% the latter and are omitted for clarity.

^{clii} Higher absorbance levels in general (compared to those for the polysaccharide) were also observed for chitin's monomer, dimer and pentamer (see Figure A3-14).

^{cliii} The glycosidic linkage stretch is clearly suppressed in chitin mixtures of higher than 74 wt.% CH_3COONa .

^{cliv} The washing steps might not necessarily have to be that long as executed in these preliminary experiment here.

stretching region where chitin's methine group (at $\sim 2870\text{ cm}^{-1}$) confirmed its stronger absorbance compared to the bands above 2910 cm^{-1} (Figure A4-11).

That region of infrared ($3000\text{--}2800\text{ cm}^{-1}$) along with the $1400\text{--}1420\text{ cm}^{-1}$ band might prove reliable probes for effective chitin washing even if ammonium acetate is formed during the neutralization of the deacetylation reaction mixture. Figure A4-12 overlays the FT-IR spectra of ammonium and sodium acetate.^{clv} Ammonium acetate exhibits its expected N-H stretches and bends in the hydrogenic region and above 1600 cm^{-1} respectively. This carboxylate salt shows its in-phase symmetric carboxylate stretch in a slightly lower frequency (1393 cm^{-1}) than that of sodium acetate (1407 cm^{-1}), which is in close agreement with literature along with the rest of the spectrum's peaks.^{56 clvi} Therefore, FT-IR might be used more in the future to study the work-up step of deacetylation reactions.

The amide II and glycosidic linkage infrared ratios^{clvii} for product 4-1 before its washing treatment were 0.580 (DA 20.6%) and 0.129 respectively, while after the aforementioned washing the latter rose significantly to 0.879 (as clearly seen in Figure A4-10) and the former to 0.652 (DA 23.1%). Similar results were obtained for product 4-2; before its washing, amide II and glycosidic linkage ratios were

^{clv} Ammonium acetate was produced by reacting $\sim 100\text{ mL}$ glacial acetic acid (ca. 17.4 M) with $\sim 120\text{ mL}$ NH_4OH (ca. 14.5 M). The reaction mixture was gently heated overnight, and ca. 4.85 g of white crystals were recovered. Residual unreacted reactants are not excluded.

^{clvi} Interestingly, ammonium acetate presents an additional CH_2 wagging vibration at 1148 cm^{-1} compared to sodium acetate (54,56).

^{clvii} Measured at MUN.

0.295 (DA 10.5%) and 0.095 respectively, while after the washing they were measured at 0.486 (DA 17.2%) and 0.679.^{clviii} These results reveal that the glycosidic linkages in both deacetylation products were suppressed by sodium acetate contamination to a similar extent (85.6 ± 0.5%; product 4-1 from 0.879 to 0.129 and product 4-2 from 0.679 to 0.095). But more importantly, the DA values obtained from the FT-IR measurements at MUN (20.6% for product 4-1 and 10.5% for product 4-2) are consistently lower (10.4 ± 1.5 DA% units) than those obtained by solution state ¹H NMR [32.1% for product 4-1 (see Figure 4-11) and 19.8% for product 4-2 (see Figure 4-13)]. Therefore, it was only natural to investigate the DA values that solution state ¹H NMR would give for the starting materials of the aforementioned deacetylations.

Measurements of the DA of the α-chitin set (native and high-medium-low MW from Table 4-1) were attempted. Suspensions of 4.4 mg/mL in 20 wt.% DCl were prepared and subjected to vigorous overnight stirring at 70 °C.^{clix} The native α-chitin sample (labeled K in Figure 4-22) did not dissolve fully (particles were still visible), high MW (labeled L) seemed homogeneous but was somewhat cloudy, medium MW (labeled M) and low MW (labeled N) were transparent. Samples were filtered through cotton wool and NMR data are shown in Figures 4-23, 4-24, 4-25,

^{clviii} Spectra of the washings of the rest of the deacetylation products are not shown for the sake of a shorter thesis.

^{clix} It was observed though that the low MW chitin sample seemed to dissolve in seconds.

and 4–26.^{clx} DA values are within a sensible range (89.4–96.4%), however they increase with decreasing MW. That fact is not consistent with the results obtained from FT-IR (the higher the MW, the higher the DA; see Table 4–1). That puzzling set of results was hypothesized to arise from a low S/N, which in turn might have been originating from the relatively low concentration of the preparations (<5 mg/mL).



Figure 4-22: Snapshot of 4.4 mg/mL α -chitin samples from Table 4–1 [native (GM3 173 K), high (GM3 173 L)-medium (GM3 173 M)-low (GM3 173 N) MW] in 20 wt.% DCI after overnight stirring at 70 °C.

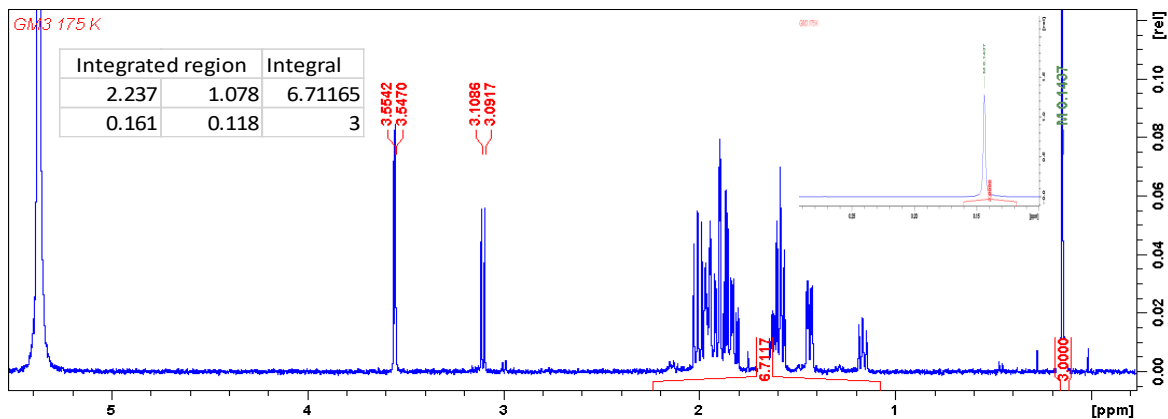


Figure 4-23: NMR spectra of native α -chitin (4.4 mg/mL in 20 wt.% DCI); DA is 89.4%.

^{clx} Experimental work up to this point was conducted in the University of Bath.

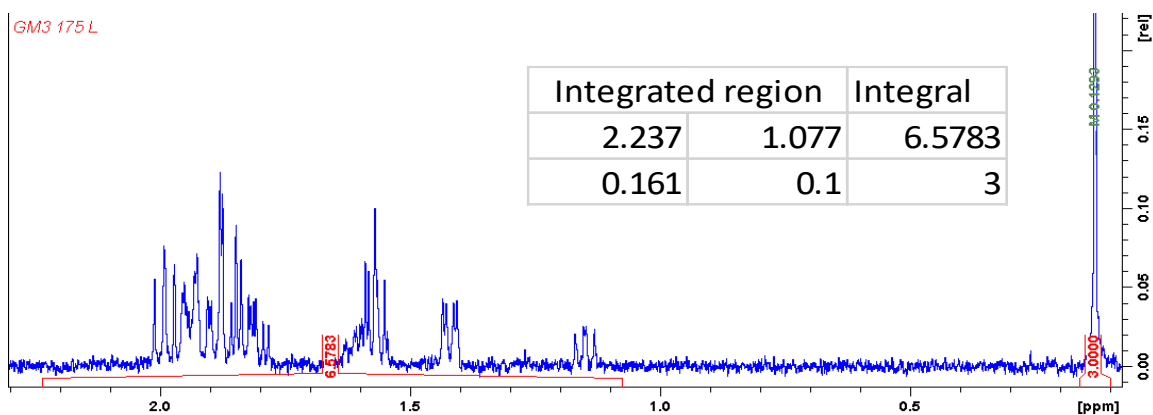


Figure 4-24: NMR spectra of high MW chitin (4.4 mg/mL in 20 wt.% DCI); DA is 91.2%.

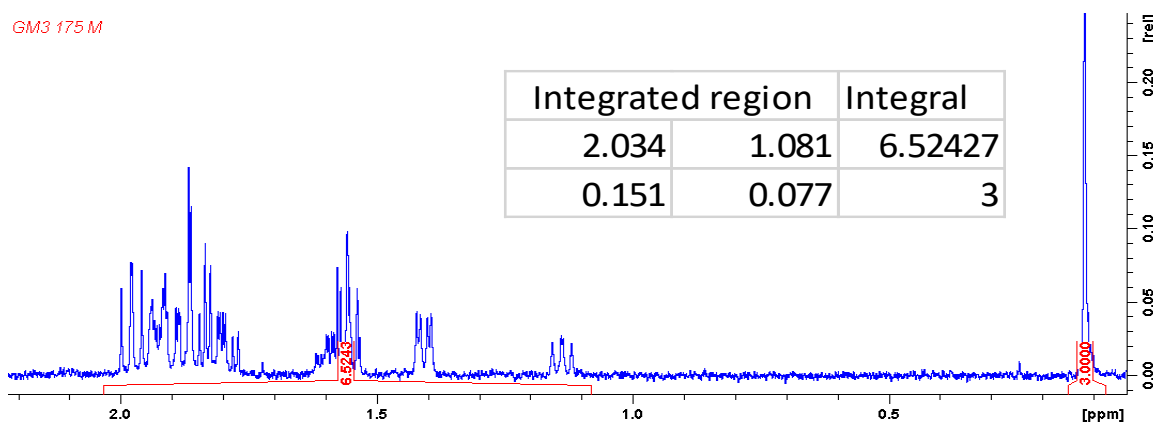


Figure 4-25: NMR spectra of medium MW chitin (4.4 mg/mL in 20 wt.% DCI); DA is 92.0%.

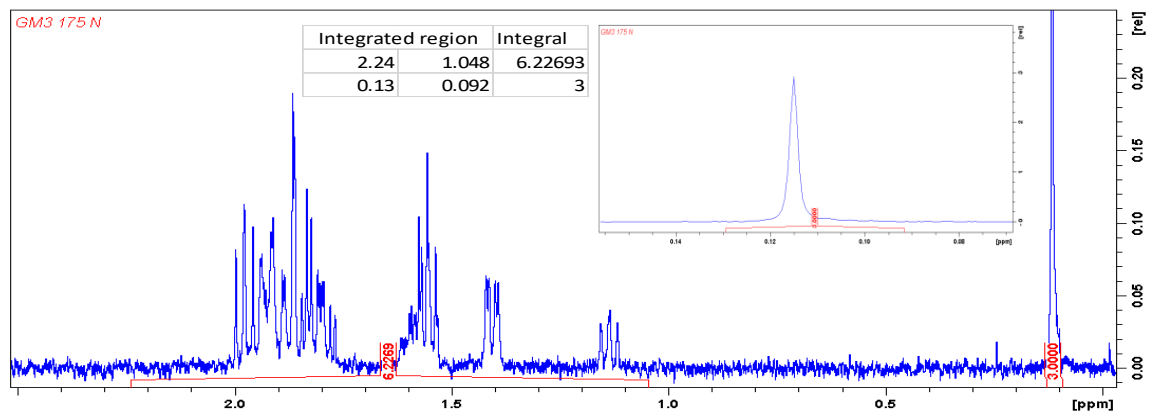


Figure 4-26: NMR spectra of low MW chitin (4.4 mg/mL in 20 wt.% DCI); DA is 96.4%.

Therefore, after returning to MUN from the CSCT (University of Bath), a new sample of high MW chitin was produced using the same ball milling process as Table 4–1 [from bigger particles of native α -chitin though (obtained by mesh)]^{clxi}. This time, 10.1 and 14.3 mg/mL in 20 wt.% DCl suspensions were prepared in order to check the NMR S/N effects as well as the reproducibility of ball milling. After overnight stirring at 70 °C both solutions remained turbid. Samples were filtered through cotton wool and NMR data are shown in Figures 4–27 and 4–28.^{clxii} The S/N ratio appears improved here, and the average DA value ($89.8 \pm 1.6\%$) is in close agreement with that obtained from the lower S/N spectra (91.2%; Figure 4–24). This result enhances the hypothesis made above that solution state ¹H NMR and FT-IR give results which at this high DA range (>80%) can be considered as contradictory. The above observations along with the fact that FT-IR measurements obtained at the CSCT were found to give higher DA values compared to solution state ¹H NMR (6 ± 1 DA% units; see Table 4–2), have led to the search for a third method for DA determination.^{clxiii} Out of the several methods used in literature,⁶⁰⁻⁶²

^{clxi} Similar to the sample described in footnote cl, this sample is hypothesized of a higher than 1.32 infrared ratio for the glycosidic linkage content. DA though is not expected to differ significantly from 88.8% (see Table 4–1).

^{clxii} Data were obtained on January 2017 with the help of NMR specialist David Davidson using Topspin 1.3 on the 500 MHz spectrometer (Bruker AVANCE) at MUN (acquisition parameters were similar as those in Section 4.2.7).

^{clxiii} Moreover, when a milled PG-chitin sample in 20 wt.% DCl was attempted to be measured on July 2017 in MUN, tuning of the 500 MHz NMR was not possible. The high ionic strength of the concentrated strong electrolyte was hypothesized as a formidable barrier for manual tuning attempts. However, there are a few studies where measurements of chitin samples in concentrated DCl have been reported with the use of longer radio frequency pulses (57,58). In principal, advances in the design of pulses for

solid-state NMR was selected for further investigations as after exceptionally analytical studies of experienced researchers, it has been hypothesized to be less biased than solution-state NMR.⁶³

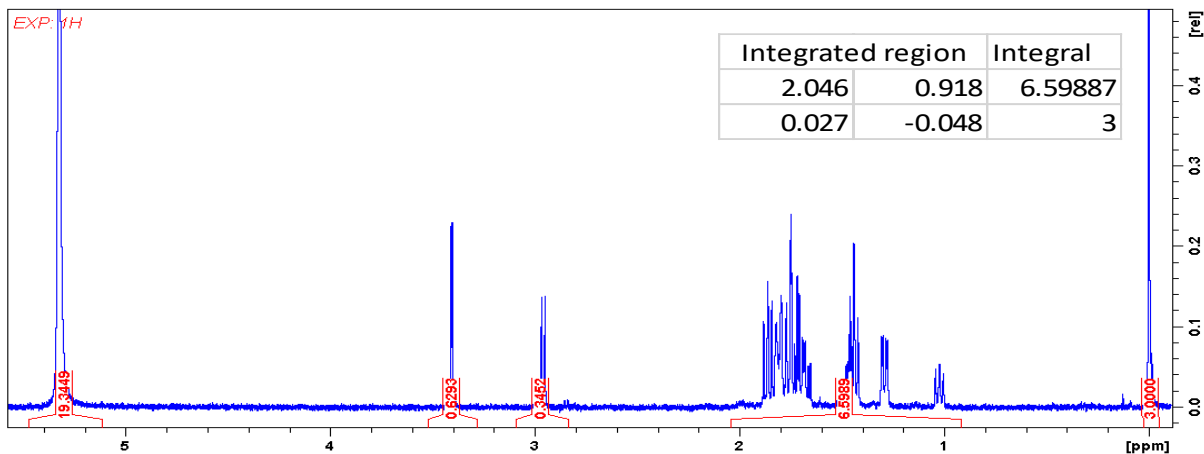


Figure 4-27: NMR spectra of high MW α -chitin (10.1 mg/mL in 20 wt.% DCl); DA is 90.9%.

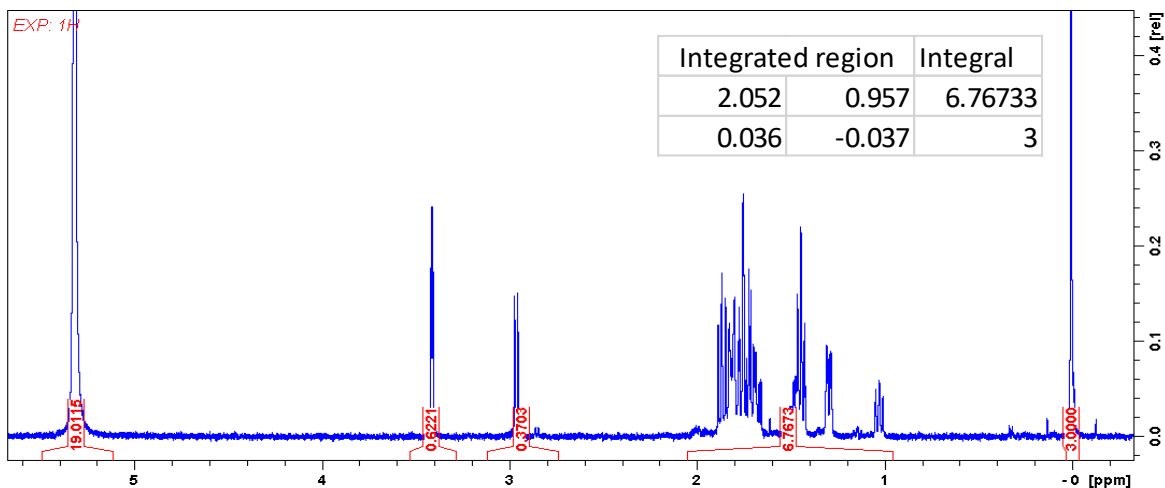


Figure 4-28: NMR spectra of high MW chitin (14.3 mg/mL in 20 wt.% DCl); DA is 88.7%.

general-purpose suppression of the water signal are expected to contribute to new methods which will satisfy some of the diverse demands of biomass research (59).

For solid-state NMR studies, two α -chitin sets were put together; one from native (ChitinWorks) and one from practical grade (PG; Sigma Aldrich). The former was comprised of native α -chitin milled with $16 \times 0.25''$ balls (8.2 BtC) for 5, 45 and 105 min. The latter was comprised of unmilled PG-chitin and milled with $67 \times 0.25''$ balls for 10 (13.4 BtC) and 30 (33.5 BtC) min. Each of the 5 milled samples is coded after BtC/milling-time [e.g. the native α -chitin milled with $16 \times 0.25''$ balls (8.2 BtC) for 45 min is coded 8/45 and the PG-chitin milled with $67 \times 0.25''$ balls (33.5 BtC) for 30 min is coded 33/30]. Generally, the higher the numbers in the code, the more intense the milling. Figures 4–29 and 4–30 show solid-state CP/MAS ^{13}C NMR spectra of the samples of native α -chitin and PG-chitin respectively.^{clxiv} The data are in good qualitative agreement with literature; the *N*-acetyl methyl group appears at ~ 23 ppm and C1 to C6 in between 50–110 ppm.^{64,65} ^{clxv} Moreover, all peaks become broader with increased milling treatment, something which confirms relevant amorphization studies of chitin.⁶⁶ When the standard peak picking algorithm of MestreNova 11 was applied to the spectra, the DA values for the milled samples were up to 120%.^{clxvi} When using GSD (global spectral deconvolution) as the method for peak picking, the DA values of the PG-chitin sample for the various

^{clxiv} Data were acquired using a Bruker AVANCE II 600 MHz spectrometer with a frequency of 150.97 MHz (probe: 3.2 mm MAS ^{13}C - ^1H / ^{15}N B4704/ 00154, magic angle spinning (MAS) rate was at 20 kHz and cross-polarization (CP) was used]. Spectra were recorded with a 22.5 ms acquisition time, 4 μs pulse width, 4 s relaxation delay and 1931 to 2048 accumulated scans at 298 °K.

^{clxv} Carbonyl's resonance (ca. 174 ppm) is excluded from this presentation as it is not involved in DA calculation.

^{clxvi} For details on these conventional integrations see Appendix A4.1.

parameters of the algorithm are recorded in Table 4–3. As seen, the parameter of peak broadness optimization makes a significant difference to the results with values higher than 2.00 (spectrum is deconvoluted on a narrow peak basis) revealing reasonable DAs (below 100.0%).^{clxvii} When the narrow optimization (with refinement level 2) was applied to the 8/5 α -chitin sample of Figure 4–29, the DA was 95.0%, which is in between the expected values (97.0 and 88.8%; see FT-IR data in Table 4–1). These observations confirm the usefulness of a deconvolution tool for a biopolymer like chitin.

Table 4-3: DA values of the PG-chitin sample for the various global spectral deconvolution (GSD) peak optimization parameters of MestreNova v. 11.

Optimized for peaks	Refinement level	
	1	2
Narrow (2.00)	97.8	97.7
Average (1.00)	100.9	100.3
Broad (0.25)	107.4	109.5
Custom ---> 3.00	-	97.7

^{clxvii} Figure A4–13 shows the solid-state CP/MAS ^{13}C NMR spectra of PG chitin. DA obtained with MestreNova 11 GSD peak picking (optimization for narrow peaks, refinement level 2) is 97.7%.

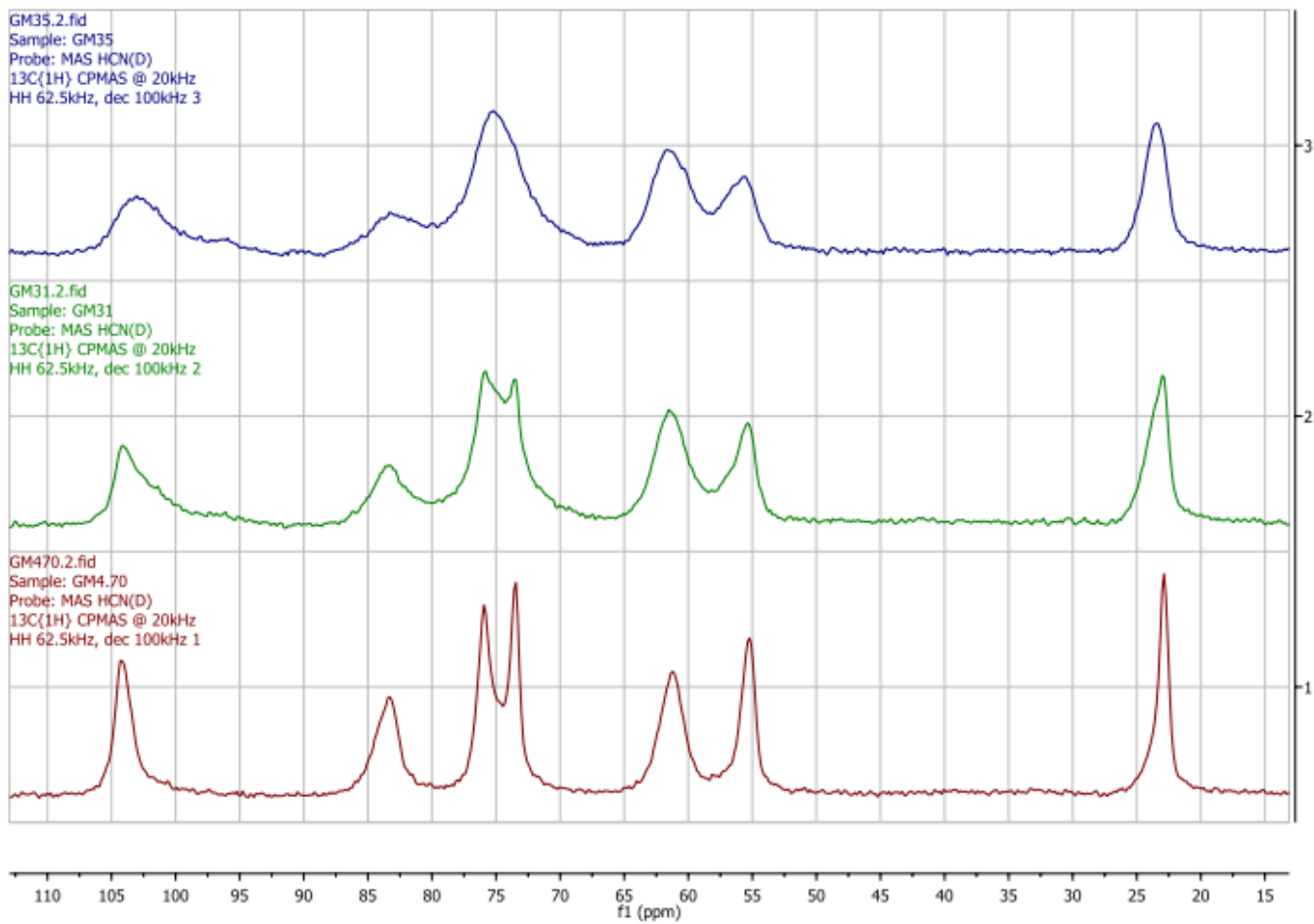


Figure 4-29: Solid-state CP/MAS ^{13}C NMR spectra of native α -chitin milled with $16 \times 0.25''$ balls (8.2 BtC) for 5 (red, code: 8/5), 45 (green, code: 8/45) and 105 (blue, code: 8/105) min.

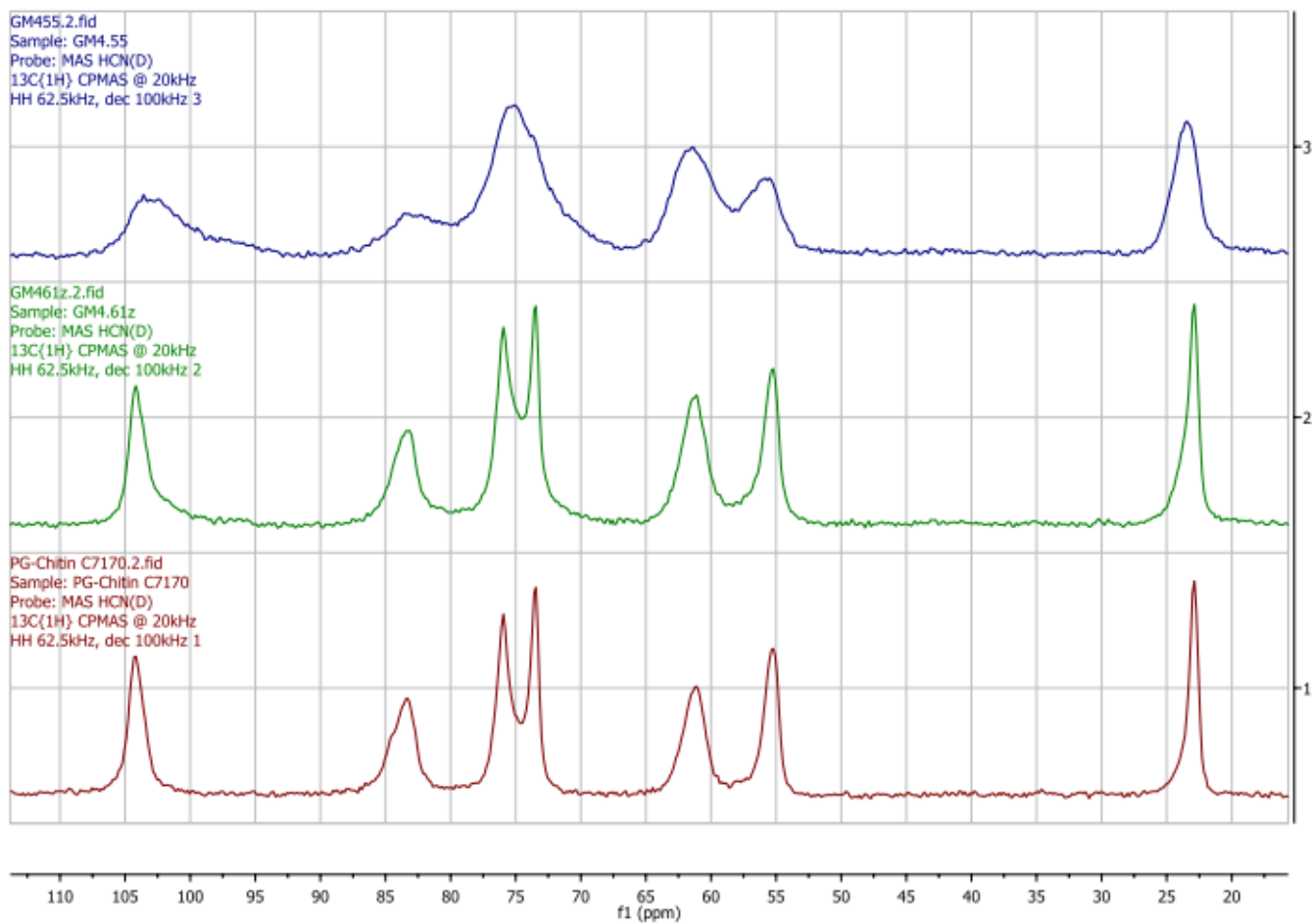


Figure 4-30: Solid-state CP/MAS ^{13}C NMR spectra of Sigma's PG chitin (red) milled with $67 \times 0.25''$ balls for 10 (13.4 BtC, green, code: 13/10) and 30 (33.5 BtC, blue, code: 33/30) min.

However, as C1 peaks (~104 ppm) in samples 8/105 and 33/30 deviate clearly from Lorentzian/Gaussian (L/G) shapes,^{clxviii} line fitting with possible minimization of the residual error^{67,68} was considered a more appropriate approach for DA determination. Figure A4–14 shows the deconvolution and line fitting of the spectra of PG chitin and Table A4–2 records the corresponding peak parameters and DA calculation.^{clxix clxx} With a DA of 92.6% for PG-chitin, one can hypothesize that different versions/methods of the same software produce different results (GSD peak picking of version 11 gave a DA of 97.7%).

Regardless of the aforementioned deviation,^{clxxi} line fittings for the other two samples of Figure 4–30 were investigated with MestreNova v. 10.0.2. It was observed that when the GSD peak broadness optimization value was 0.30 and higher, some of the obtained DA values for sample 13/10 were higher than 100%.^{clxxii} Hence, the line fitting peak parameters for only the first 20 GSD peak broadness optimization values (from 0.10 to 0.29) were recorded for both 13/10 and 33/30. Figure 4–31 shows that the DAs of the more amorphous 33/30 range from 77 to 87% with higher GSD peak

^{clxviii} Line width at half height of the C1 peak of 33/30 (at 102.6 ppm) is approximately 600 Hz (probably the broadest peak in all 6 spectra of Figures 4–29 and 4–30).

^{clxix} MestreNova v. 10.0.2 – 15465 (released on 17/6/2015) had to be used in late July 2017 as v.11 used so far was losing its license.

^{clxx} The selected line fit was observed to be consistent among several fits with GSD peak optimization values in between 1.74 and 3.47. These are relative high values which are meant to optimize the resolution of narrow peaks (see Table 4–3; for more details the reader can consult the corresponding MestreNova manual).

^{clxxi} Which is in reasonable DA ranges.

^{clxxii} This possibly makes sense as it is the lower GSD peak broadness optimization values that are designed for broader peaks.

broadness optimization values giving higher DAs. At the same time, the more crystalline 13/10 exhibits a wider range of DAs (from 74% to 91%) with no particular trend for the software's deconvolution tool. Considering the preliminary and investigative nature of this analysis, these observations are actually sensible as that region of GSD peak broadness optimization values (0.10 – 0.29) is designed to improve the resolution in spectra where broader peaks dominate over narrow ones.^{clxxiii}

When observing the analytical data for the peaks of all 20 different GSD line fittings,^{clxxiv} Lorentzian/Gaussian (L/G) ratio was found to have the highest deviation (RSD%) among all 4 peak parameters by far (ppm, height, width, L/G ratio; ppm changes usually only to the 2nd decimal). For example, in the set of the 20 line fittings of the C4 peak of sample 13/10, the following average parameters were recorded: resonance at 83.51 ± 0.02 ppm (0.03% RSD), height 83357 ± 728 (0.9% RSD), width 356 ± 3 Hz (0.8% RSD), L/G 0.078 ± 0.115 (147% RSD), area 2078411 ± 43939 (2.1 RSD%). Similar figures were obtained for all peaks of the 13/10 sample; RSD values for the L/G parameter were almost always above 80%, while RSDs for the rest (ppm, width, height, area) did not exceed 10% in any case. Sample 33/30

^{clxxiii} To the best of my knowledge, literature on chitin solid state NMR does not report the particulars of DA determination (software used, integration method, possible deconvolution). Moreover, in some cases the DA is measured to only two significant figures (65), and in general, research questions on the possible effects of acquisition parameters have not been raised openly yet (63,64). Therefore, the short investigative analysis here is only to stimulate future research.

^{clxxiv} Recorded in tables like that of Table A4–2.

gave RSDs ca. 12% for the L/G parameter and less than 4% for the rest. The question arising then is: “does it make sense to select the optimum (out of 20) GSD fitting based on the average L/G value for the probe peak (*N*-acetyl methyl at 23.0 ppm)?”. And if yes, “should the fitting (“reading”) error (MestreNova's GSD deviation) arise from +/- 0.01 (or maybe more) for the GSD peak-broadness optimization?”. These questions are somehow rhetorical for this thesis as when they were asked to the research and development (R&D) team of MestreNova, the specialists recommended the line-fitting algorithm of the newer version of the software.^{clxxv} Out of the 20 line fittings (v. 10.0.2), the average L/G value of the *N*-acetyl methyl (probe) peak of the 13/10 sample was 0.28 ± 0.48 . That average value (0.28) was actually the L/G value of the probe peak for 4 consecutive line fittings (GSD peak broadness optimization values 0.26, 0.27, 0.28, 0.29). The average DA of those 4 line fittings was $87.4 \pm 3.1\%$. Applying the same logic to the 33/30 sample, the average L/G value of the *N*-acetyl methyl (probe) peak was 1.34 ± 0.17 . That average value (ca. 1.4) was actually the L/G value of the probe peak for 3 consecutive line fittings (GSD peak broadness optimization values 0.18, 0.19, 0.20). The average DA of those 3 line fittings was $83.2 \pm 1.8\%$. The latter result (obtained by 30 min milling of PG chitin with 33.5 BtC/14% packing) might be comparable with the $83.9 \pm 1.3\%$ of medium MW α -chitin obtained by 25 min milling with 16 BtC/6.6% packing (see Table 4–1).

^{clxxv} Access to version 12 (beta) was kindly provided by MestreNova on August 2017, however further discussion on the obtained results is beyond the scope of this thesis.

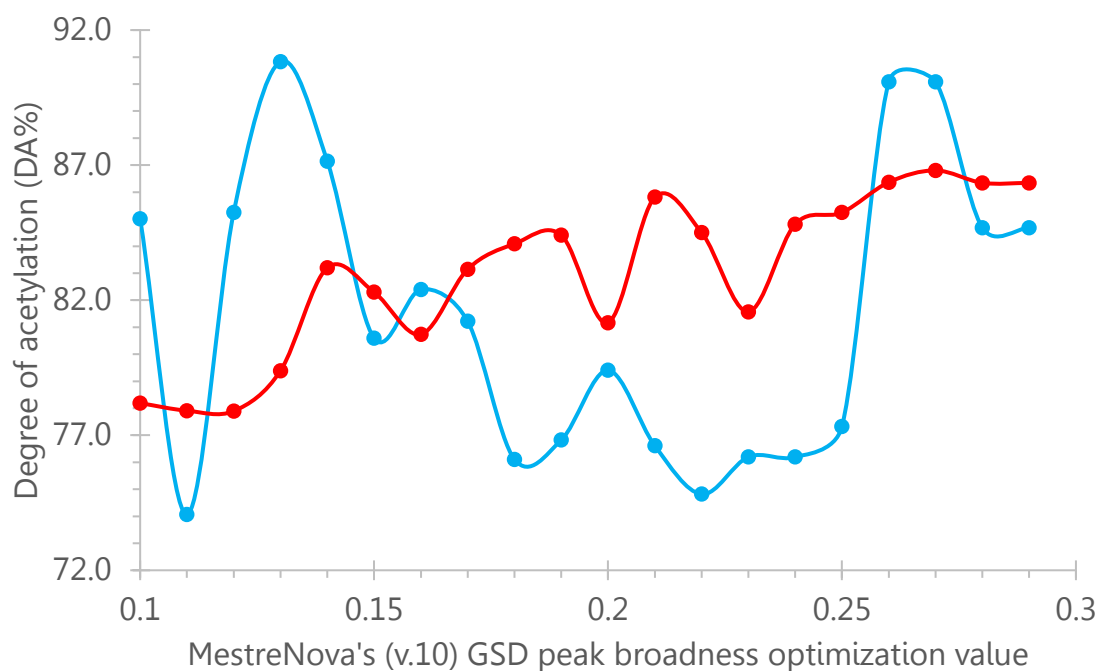


Figure 4-31: Degree of acetylation (DA%) of milled PG chitin samples 13/10 (blue, 13.4 BtC for 10 min) and 33/30 (red, 33.5 BtC for 30 min) for MestreNova's (v.10.0.2) GSD peak broadness optimization values (0.10–0.29).

All in all, the experimental results presented in Section 4.3.4 along with their discussion suggest that controlled deacetylation of α -chitin samples of different MW requires first a method for DA determination which is more reproducible than those currently reported in literature. This probably needs a methodological approach where two (spectroscopic) methods measure a set of chitin samples and a minimum reading error in between the two is defined; as attempted by Zhang et al.⁶⁵ Solid-state NMR and FT-IR can certainly contribute towards that, but a more dedicated

study is desirable to better understand their quantification potential.^{clxxvi clxxvii} Once reliable reading errors are established for the whole DA range, then the work-up step and the separation of acetate salts can be standardized with FT-IR. That will open the way for a more controlled study of the numerous deacetylation parameters. In the end, considering the promising potential of NaOH as solvent for chitin (see Section 4.3.3.2), homogeneous conditions for deacetylation might prove more attractive to future researchers. These are suggested to be combined with a microwave approach as the concentrated alkali is very likely to degrade the metallic surface of a sonication tip.

4.3.5 NaOH as a solvent for chitin

With the dissolving power of ~20 wt.% NaOH being effective in a wide range of concentrations of higher MW chitin samples (Section 4.3.3.2), one might ask how do solvation performances of other concentrations of the electrolyte compare to that of the freezing point minimum. Figures 4–32 and 4–33 show the relative viscosities of 67/60 PG chitin^{clxxviii} in 9.70, 19.40, and 29.11 wt.% NaOH solutions and their corresponding undissolved residues respectively (for experimental procedure see

^{clxxvi} Ball milling with low and high BtC/packing of steel has proved a reliable tool, which can amorphize, depolymerize and deacetylate α -chitin. Hence the created samples can drive the investigation of the abilities of the quantifying algorithms.

^{clxxvii} Solution state NMR might also prove useful in the long term, but more work is necessary to understand the relationship between NMR acquisition parameters, solvent concentration, and chitin MW.

^{clxxviii} PG chitin milled with 67 BtC/14% packing for 60 min is coded 67/60 after BtC/milling time.

Section 4.2.8). The dissolution performance of 19.40 wt.% NaOH was the most effective with relative viscosity reaching 1.180 and no undissolved residue left after centrifugation. The concentration of 9.70 wt.% was a close second with a relative viscosity of 1.156 and miniscule pieces of undissolved residue after centrifugation. The average concentration of the two suspensions prepared was 0.4978 ± 0.0005 wt.% (0.10 % RSD). The RSD in concentrations is ~ 14 times lower than the RSD of the two relative viscosities (1.43% originating from an average relative viscosity value of 1.168 ± 0.017). Therefore, it is safe to conclude that 19.40 wt.% NaOH revealed better solvent properties for low MW chitin compared to 9.70 wt.% NaOH. With a relative viscosity of 1.065, the concentration of 29.11 wt.% NaOH was far below the first two, and that is confirmed from a visibly higher proportion of viscous undissolved mass compared to those for <20 wt.%. The residue of the 38.81 wt.% NaOH is even denser from that of the 29.11 wt.%, and that is evident from its darker orange color.^{clxxix} These results agree with the observations of Chen et al., who have obtained homogeneous chitin solutions only with 20 wt.% NaOH.⁶⁹

^{clxxix} Hence, a measurement of the solution's relative viscosity was found unnecessary.

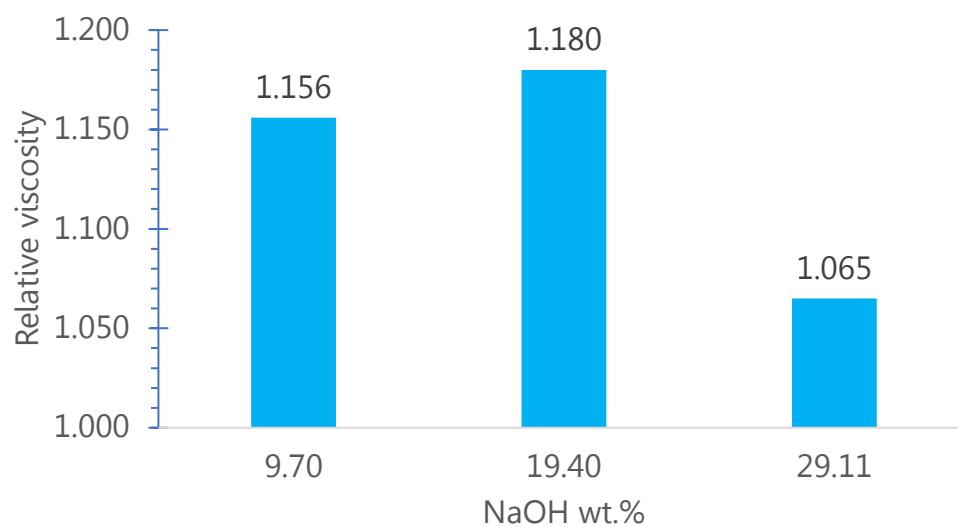


Figure 4-32: Relative viscosities (kinematic) of milled PG chitin (60 min with 67 BtC/14% packing) in 9.70, 19.40, and 29.11 wt.% NaOH solutions. Dissolution involved freezing temperatures (<-28 °C).

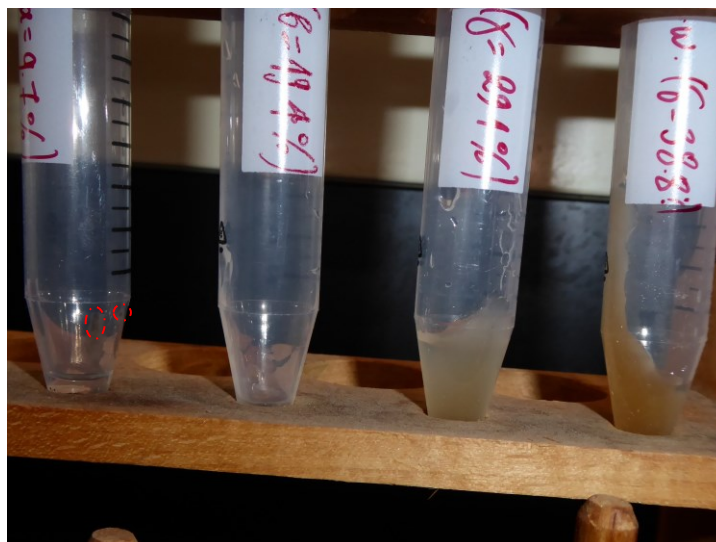


Figure 4-33: Undissolved residue of milled PG chitin (60 min with 67 BtC/14% packing; 41.6% CrI) in 9.70, 19.40, 29.11, and 38.81 wt.% NaOH (from left to right). Dissolution involved freezing temperatures (<-28 °C). Red circles on the 9.70 wt.% NaOH tube (far left) highlight small pieces of undissolved residue.

The questions rising then are: how does relative viscosity in ~20 wt.% NaOH behave for increasing concentrations of the lowest MW chitin sample (67/60), and how does that behavior change for higher-MW/more-crystalline samples of the polysaccharide. To answer those, a set of milled samples from Sigma's PG chitin was created according to parameters in Table 4-4.

Table 4-4: Mechanochemical conditions and FT-IR data for the practical grade (PG) chitin sample set prepared for dissolution studies with 19.00 wt.% NaOH. Spectra shown in Figure 4-34.

Measured quantity	PG chitin sample				
	native	13/10	22/30	33/30	67/60
mixing load (g)	-	5.00	3.00	2.00	1.00
# of 0.25" balls	-	67	67	67	67
BtC ratio	-	13.4	22.3	33.5	67.0
packing %	-	14.0	14.0	14.0	14.0
milling time (min)	-	10	30	30	60
glycosidic linkage	1.742	1.382	1.099	1.031	1.012
FT-IR ratio	± 0.008	± 0.037	± 0.015	± 0.038	± 0.066
amide II	2.967	2.670	2.268	2.260	2.227
FT-IR ratio	± 0.047	± 0.087	± 0.017	± 0.071	± 0.121
DA%^[a]	>100 ^[b]	94.7 ± 3.1	80.4 ± 0.6	80.1 ± 2.5	79.0 ± 4.3
amide I split	1.288	1.115	0.907	0.900	0.854
FT-IR ratio	± 0.020	± 0.023	± 0.021	± 0.013	± 0.016

[a] Calculated by the Sannan method. [b] 105.2 ± 1.7%.

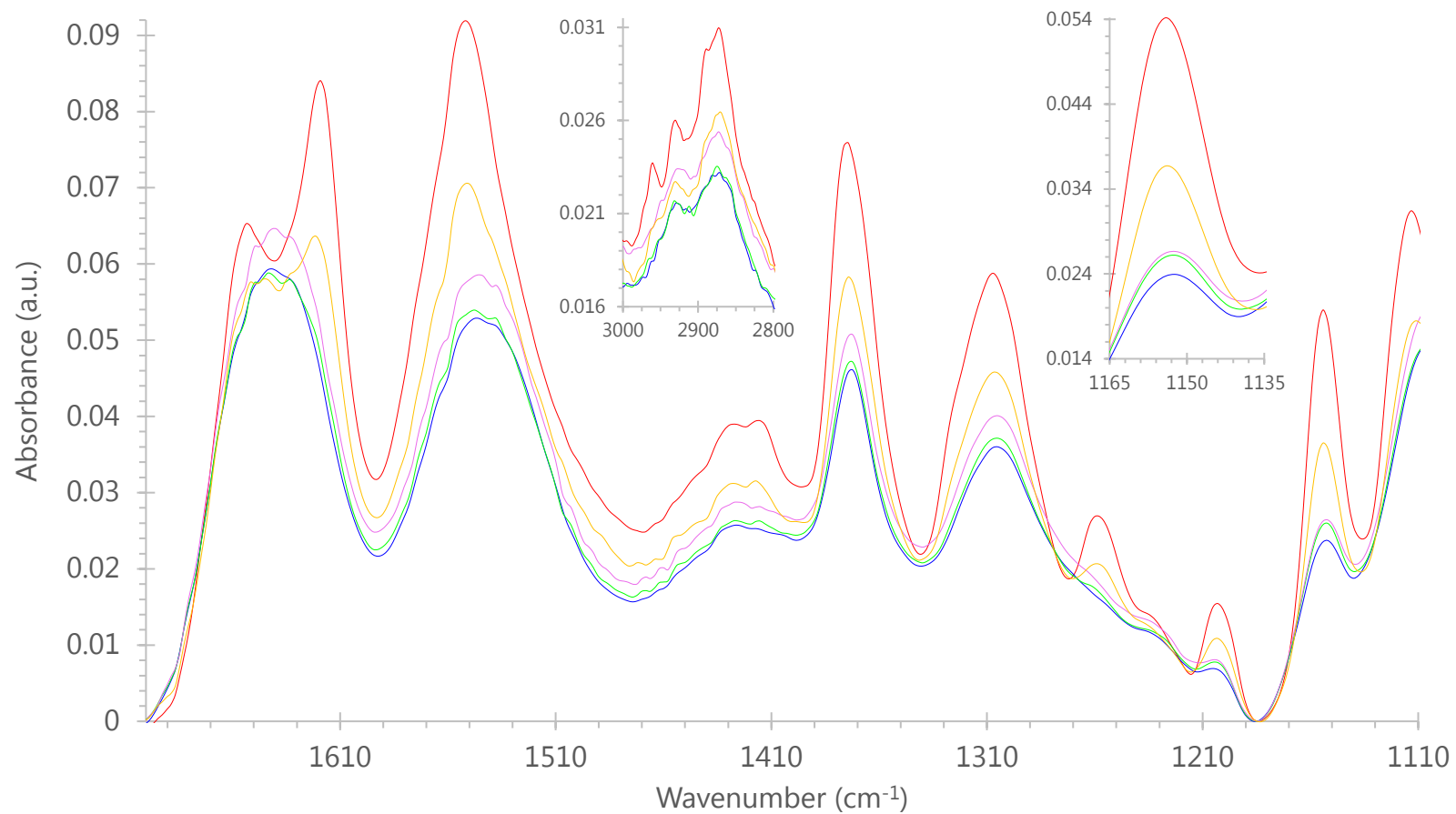


Figure 4-34: Infrared spectra of native (red), 13/10 (orange), 22/30 (green), 33/30 (pink), and 67/60 (blue) PG chitin (ball milling conditions and FT-IR ratios are recorded in Table 4-4).

Infrared data are similar to those of Section 4.3.1 with degree of acetylation (DA) dropping to $80.4 \pm 0.6\%$ for the 22/30 PG chitin and then remaining relatively stable at ca. $79.8 \pm 0.7\%$ for the more milled samples.^{clxxx clxxxi} These results complement the ones obtained for intense ball milling of α -chitin (ChitinWorks) where deacetylation leveled off to $84.4 \pm 1.0\%$ (see Figure 3–9). Glycosidic linkage content revealed a clear decreasing trend (from 1.74 to 1.01; ~42% drop) with error bar overlap only for samples 67/60 and 33/30. The MW reduction is almost double that observed in Table 4–1 (~22%; from 1.42 to 1.12), and it might be due to the significantly larger particle size of native α -chitin compared to that of PG chitin.^{clxxxii} The amide I split ratio was confirmed to decrease (from 1.29 to 0.85) with decreasing molecular weight.^{clxxxiii} Crystallinity decreased from 88.2% for the native sample to ca. 36.5% for the most milled (67/60) (Figure 4–35). Therefore, the sample set provided a solid basis for dissolution studies with 19.00 wt.% NaOH.

^{clxxx} The $80.1 \pm 2.5\%$ DA of sample 33/30 is in close agreement with $83.2 \pm 1.8\%$ obtained by solid-state NMR (see page 272).

^{clxxxi} Native's sample 2.967 ± 0.047 amide II ratio exceeds the upper limit of the Sannan method (~2.8) (17). Hence, a more reliable measurement of that DA is the one obtained by deconvolution of solid-state NMR spectra (97.7%, see Table 4–3).

^{clxxxii} The relationship between particle size, crystallinity and molecular weight of polysaccharides might comprise a challenging research field in the future.

^{clxxxiii} Error bar overlap was observed only for samples 33/30 and 22/30.

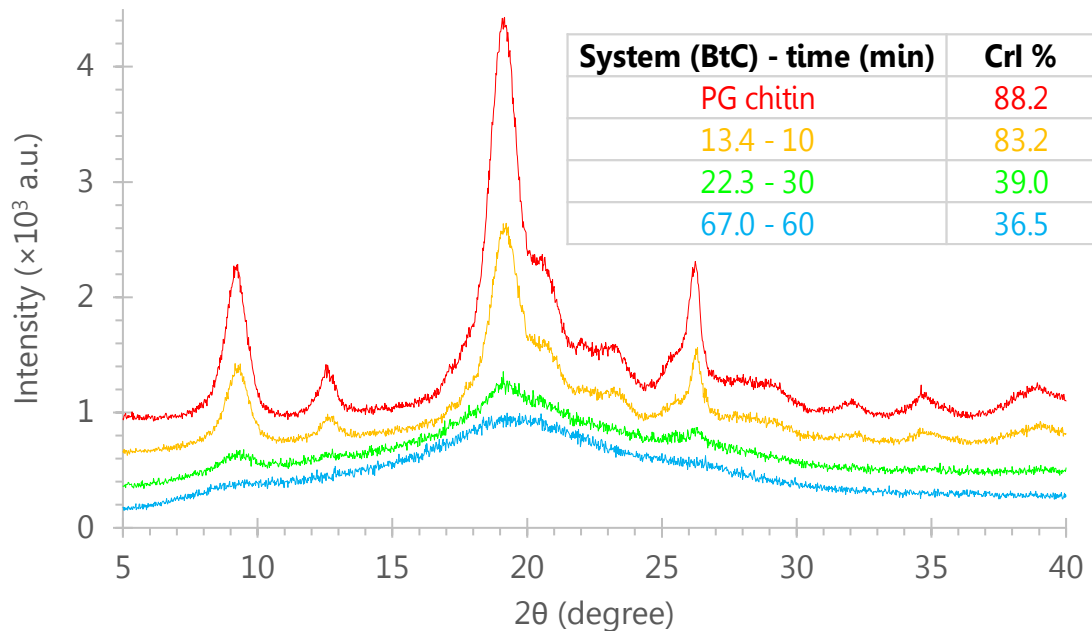


Figure 4-35: X-ray diffraction patterns of native (red) PG chitin and milled with 67×0.25" balls (14.0 % packing); 13.4 BtC for 10 min (orange), 22.3 BtC for 30 min (green), and 67.0 BtC for 60 min (blue). Inset table records the crystallinity indices (CrI%). The intensities of 22/30 (green), 13/10 (orange), and native PG chitin (red) signals have been offset by 200, 500, and 700 a.u. respectively.

Figure 4-36 shows the relative viscosities of milled 13/10, 22/30, 33/30, 67/60 PG chitin samples in 19.00 wt.% NaOH as a function of concentration.^{clxxxiv clxxxv} Relative

^{clxxxiv} Data were obtained according to Section 4.2.8, except that stirring at ca. -14 °C was reduced to 30 min and centrifugation was increased to 7700 rpm. Kinematic viscosity measurements were conducted at room temperature using an Ubbelohde type viscometer (size 1C, No. A622, Cannon Instrument Co.) with a calibration constant of ca. 0.02932 mm²/s² (cSt/s). The duplicate average efflux time of the 19.00 wt.% NaOH solution was 104.0 ± 2.0 s. Relative viscosity values for the samples are the average of two measurements with the average standard deviation being 5.7 s.

^{clxxxv} Figure A4-15 shows snapshots of 0.5, 1.0, 2.0, 4.0 wt.% low MW α-chitin (see Table 4-1) in ~20 wt.% NaOH when frozen and after thawing. These are characteristic of the visual appearance of low MW preparations; the whole volume of the frozen mass was homogeneously white below 1 wt.%, while it turned into darker shades of orange for increasing concentrations.

viscosity of the lowest MW sample (67/60 chitin) increased gradually up to 9.83 at ~9.6 wt.%, while similar viscosity levels were obtained at decreasing polysaccharide concentrations for increasing MW/crystallinity; the 13/10 sample reached 9.73 at ~0.9 wt.% (10-fold analogies for the set). The undissolved residues of the highest (13/10) and lowest (67/60) MW samples were $2.80 \pm 0.28\%$ ^{clxxxvi} and $0.13 \pm 0.11\%$ ^{clxxxvii} respectively.^{clxxxviii} The inset graph underlines the fact that relative viscosities for all samples increase parabolically (not linearly) with increasing concentration. For example, if the 22/30 milled chitin had kept dissolving to the same extent it did up to 0.47 wt.% for up to 1.28 wt.%, the relative viscosity would have only been 4.65 and not 7.52 as it was measured. Moreover, the reader might have already noticed that the relative viscosities of the lowest MW sample (67/60) increase linearly for concentrations up to ~2.3 wt.%. If that trend had remained the same for up to 4.60 wt.%, the relative viscosity of the most intense milled polysaccharide would have been 2.87 and not 3.53 as it was observed.

^{clxxxvi} The 0.36 wt.% 13/10 sample gave 2.6 wt.% undissolved residue after the freeze-thaw/centrifugation process, while the 0.92 wt.% preparation gave 3.0 wt.%.

^{clxxxvii} The 9.63 wt.% 67/60 sample gave 0.3 wt.% undissolved residue after the freeze-thaw/centrifugation process, while the 0.77 wt.% preparation gave 0.1 wt.%.

^{clxxxviii} Undissolved residues were washed twice with ~9 mL deionized water (7700 rpm centrifugation for 10 min was applied) and the clean residue was dried and weighed.

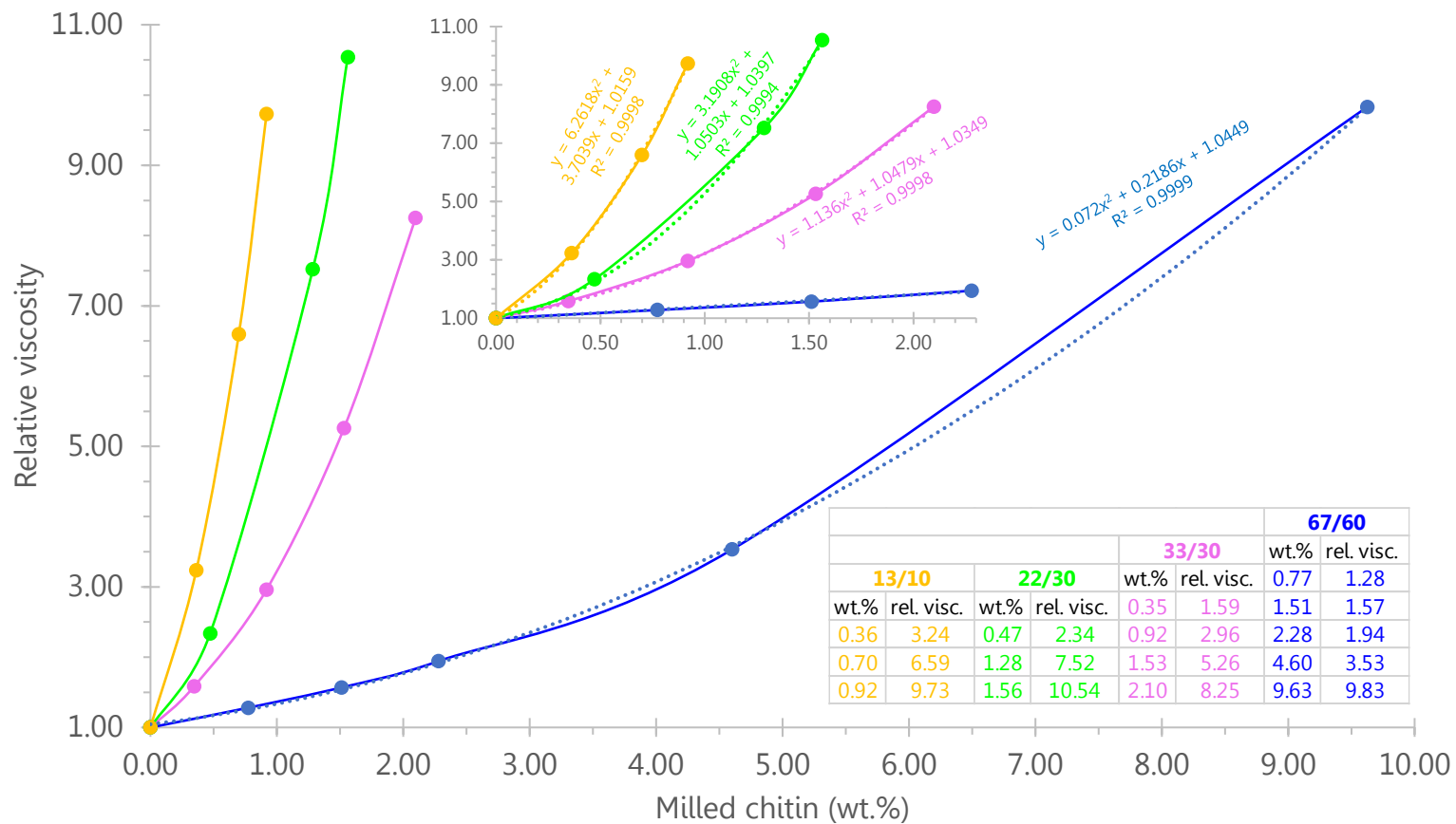


Figure 4-36: Relative viscosities (kinematic) of milled 13/10 (orange), 22/30 (green), 33/30 (pink), 67/60 (blue) PG chitin samples in 19.00 wt.% NaOH as a function of concentration (wt.%). Inset table records the exact data, inset graph highlights the polynomial fits along with their equations and R-squared values. Data were obtained by freezing at $-28\text{ }^{\circ}\text{C}$.

With the same behaviour being observed for the whole range of molecular weights and crystallinities in the set, it is reasonable to hypothesize that the diffusion of the hydrated Na^+ and OH^- is driven into more crystalline fractions of chitin fibrils by the macroscopic stirring at near-freezing temperatures (ca. $-15\text{ }^\circ\text{C}$).^{clxxxix} That hypothesis is supported by vibrational observations of NaOH solutions of various concentrations [from 0.5 to 10 M (4.8–29.5 wt.%)] which suggest that the hydrated OH^- reorients as a whole via local thermal equilibrium.^{71 cxc} At the same time, the possibility of the ca. 19.0 wt.% electrolyte to form heptahydrates upon freezing at ca. $-28\text{ }^\circ\text{C}$ ($\text{NaOH}\cdot 7\text{H}_2\text{O}$)³⁶ provides the ions with a driver to reach a state of definite orientation and minimum entropy. The possible formation of $\text{NaOH}\cdot 7\text{H}_2\text{O}$ crystals in between the polysaccharide chains is expected to statistically disrupt the interactions in both NaOH solution (hydrogen bonding of the hydrated species with their surrounding “bulk” water) and chitin (intermolecular hydrogen bonding and hydrophobic interactions) leading to chain disentanglement.^{cxci cxcii} However, future researchers should take into account various types of alkali hydrates; from

^{clxxxix} Solvent diffusion possibly involves an equilibrium of hydrogen bond breaking and reformation; similar in nature to that observed for cyclodextrins (70).

^{cxc} Several groups have calculated that the hydroxide hydration shell at room temperature comprises of ca. 4.5 water molecules (71).

^{cxci} To the best of my knowledge, mercerization literature has not investigated systematically freezing temperatures; the focus has usually been on alkali concentration and process time (72,73). With the theoretical diversity of polysaccharide samples though, a more systematic investigation of those conditions is of significant scope.

^{cxcii} This hypothesis along with the fact that the freezing point of ca. 19 wt.% NaOH does not exceed a $\sim 55\text{ }^\circ\text{C}$ difference from room temperature might stimulate future research of NaOH systems as solvents for polysaccharides. Considering scaling up, a process like this might be favoured in industrial facilities located in countries where sub-zero temperatures are already part of their productive life (Scandinavia, Canada, Russia).

separated ion pairs with hydrodynamic diameters of 1.5–2 nm to hydrated dipoles of 0.5–0.8 nm.³⁹

Regardless of the mechanistic challenges, the fact that the dissolution of 1.56 wt.% 22/30 chitin gave 1.9 wt.% undissolved residue and that of 2.10 wt.% 33/30 chitin 1.0 wt.% complements the corresponding data for the highest and lowest MWs and suggests that 19.00 wt.% NaOH might require a second freeze-thaw cycle to dissolve the persistent crystalline domains present in high MW chitin samples. Another alternative might be the use of KOH instead of NaOH, as its freeze-thaw properties have been suggested to provide better dissolution performance than NaOH.⁷⁴

Nevertheless, with the solvation properties of 19.00 wt.% NaOH giving results of reasonable reproducibility, the highest-MW/most-crystalline chitin of the set (13/10) was selected for film casting as its properties are near to those of the native PG sample used in Section 4.3.3.2. Two experiments were conducted at the 5% level in order to check for differences in the drying process; one aimed for freeze-drying and another for thermal drying. Suspensions of 4.66 and 4.77 wt.% of 13/10 chitin in 19.00 wt.% NaOH were prepared, subjected to ~30 min stirring in -15 °C and then frozen in dry ice. After thawing, the viscous solutions were poured in petri dishes which were left to stand for ~30 min.^{cxci} Immersion in separate equimolar HCl baths

^{cxci} Using $6.2618x^2 + 3.7039x + 1.0159$ (see Figure 4–36), the relative viscosities of the 4.66 and 4.77 wt.% 13/10 chitin preparations are calculated at ca. 154 and 161 respectively.

resulted in immediate formation of white materials [see Figure A4–16(a)]. This observation provides some evidence of chain entanglement where formation of new hydrogen bonding networks and intensification of intermolecular interactions generally lead to gelation. After 4 h, the films appeared to become thicker (Figure A4–16(b)). The 4.77 wt.% film was washed twice in water baths (deionized), and placed back on the petri dish, which was then surrounded by dry ice overnight (conditioning) and freeze-dried the next day.^{cxciiv} The 4.66 wt.% film was left in its acid bath overnight and then washed in the same way. After that, it was left to dry slowly at 50 °C under vacuum (the process lasted ~30 h).

Figure 4–37 shows that both films were in one piece after their drying process. The 4.66 wt.% sample which was thermally dried [Figure 4–37(a)] shrunk substantially to a radius of ca. 2 cm developing a characteristic curvature. The film was relatively stiff with its surface being smooth, translucent and of an orange shade. The 4.77 wt.% sample which was freeze-dried [Figure 4–37(b)] shrunk to a much lesser extent remaining relatively flat. The film was more flexible than that which was thermally-dried with its surface being rougher and white. Its thickness was comparable to that of 10 sheets of regular printing paper. Although mechanical tests were not conducted, both films were of appreciable minimum strength.^{cxciiv}

^{cxciiv} Freeze-drying was conducted on the facilities of the Biochemistry department of MUN with the kind help of the instrumentation support specialist Craig Skinner.

^{cxciiv} When tension was applied to a piece of the 4.77 wt.% film (by hand gripping at diametrically opposite sites and pulling at opposite directions), the force needed to break

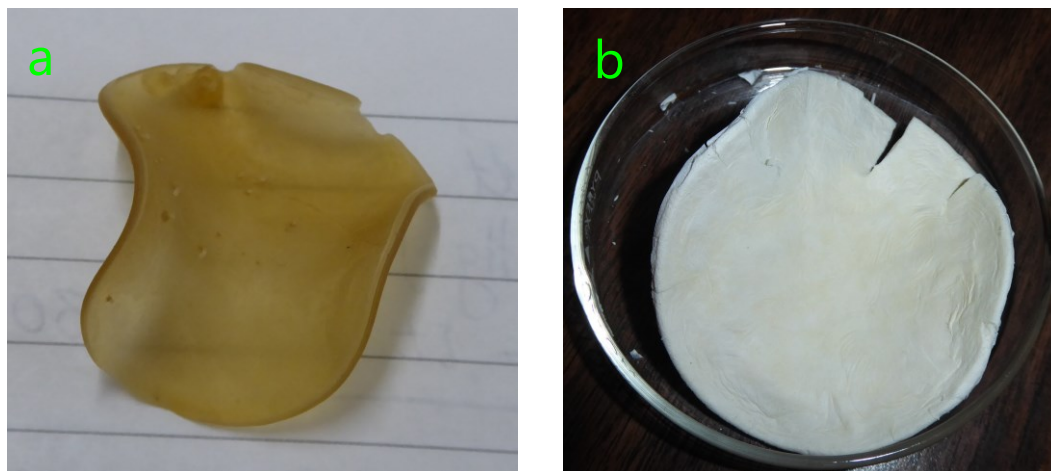


Figure 4-37: Films of ~4.7 wt.% 13/10 chitin produced by dissolution in 19.00 wt.% NaOH; thermally-dried (a) and freeze-dried (b).

Figure 4–38 shows how the infrared spectra of the two films compare to that of 13/10 chitin. The freeze-dried film (green spectrum) exhibits the same bands as those of the milled powder (blue spectrum) only with generally lower intensities. That might be attributed to a limited contact with the ATR diamond surface due to the film's thickness.^{cxvii} The only significant qualitative differences are the puzzling intense bands at 1425 and $\sim 880\text{ cm}^{-1}$ that are generally of negligible absorbance in chitins. Another interesting difference is the significantly higher glycosidic linkage ratio (1.97 ± 0.13) that the freeze-dried film has revealed. With polymerization of the chains being highly unlikely during the dissolution process, future research might consider investigating how the entanglement/gelation process affects the packing

the piece in two was certainly greater than that needed for a sheet of regular printing paper. The freeze-dried film can be thought to resemble certain qualities of paperboard.^{cxvii} The film seemed to have a sheet-like texture. Microscopy examinations are certainly expected to complement FT-IR data in future studies.

of the pyranic rings.^{cxvii} That might also be the reason which makes the amide II ratio appearing slightly increased (2.74 ± 0.21) compared to the sample before the NaOH/HCl treatment (2.67 ± 0.09). Otherwise, the amide I split ratio seems to lie at a reasonable level (1.05 ± 0.01).

The IR spectrum of the thermally-dried film has several qualitative differences with that of the 13/10 chitin. The hydrogenic region showed unexpected bands at ~ 3450 , 2915 , and 2850 cm^{-1} . Moreover, the amide II band is unusually suppressed compared to amide I and the region in between the glycosidic linkage and amide III is paradoxically active. Most probably, these qualitative differences arise from the thermal drying process as the inset spectra highlights the fact that the relatively wet film (just after washing) exhibits the expected chitin signal in that region.

^{cxvii} The carbon-hydrogen vibrations were not only significantly suppressed compared to the glycosidic linkage, but they showed a few qualitative differences as well.

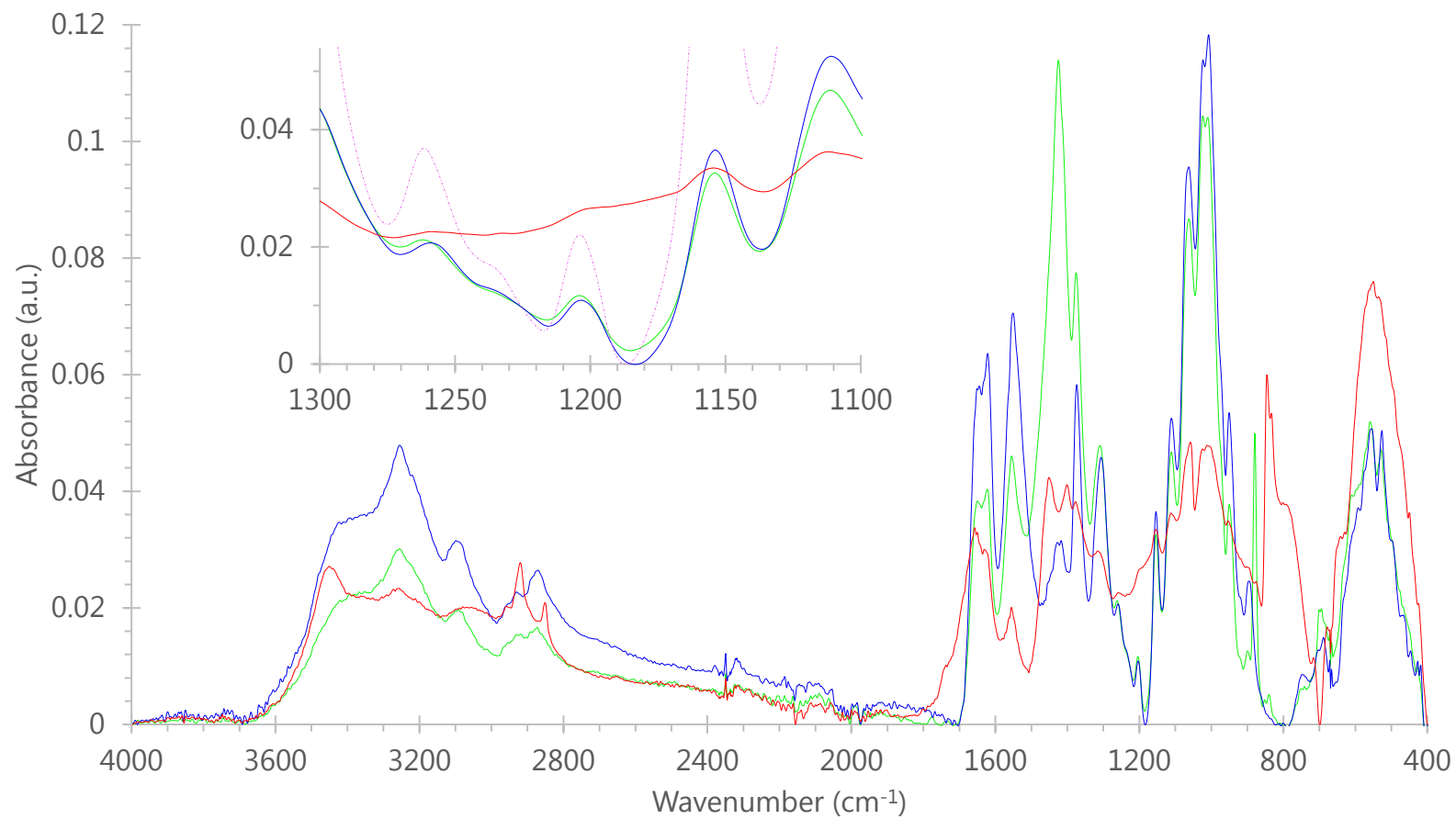


Figure 4-38: Infrared spectra of 13/10 chitin (blue), freeze-dried film (green), and thermally-dried film (red). Inset highlights the 1100–1300 cm⁻¹ region including the signal of the thermally-dried film before its drying and after its washing treatment (pink dotted).

These preliminary results suggest that freeze-drying produces films with more attractive properties than those thermally-dried (size and flexibility); but a more systematic study is needed on the factors that influence film thickness and transparency. With dilute HCl baths providing an effective anti-solvent/gelation treatment and ~19 wt.% NaOH dissolving high MW chitins at the 5 wt.% level, future research can focus on fine-tuning the film properties according to market needs by experimenting with lower MWs and concentrations. That can be done relatively easy using the freeze-thaw process of ~19 wt.% NaOH at $-28\text{ }^{\circ}\text{C}$, which has proven to produce predictable solvation results (relative viscosity/undissolved residue) for a wide range of chitin concentrations (up to ~10 wt.%) and MW/crystallinities (1.01–1.38 glycosidic linkage FT-IR ratio/36–83 % CrI).

4.4 Conclusions

Preliminary results obtained in collaboration with the University of Bath towards film-casting of chitin for applications in biomedical engineering were successful. However, there were many unforeseen challenges and this process was more difficult than initially envisioned. Dissolution experiments of amorphous/depolymerized α -chitin in both an ionic liquid and an alkali aqueous solution were conducted aiming to compare solvent systems for the production of α -chitin films. An approximate concentration of 19 wt.% NaOH was found to dissolve high MW/crystallinity α -chitin in a wide range of concentrations (up to ~5 wt.%) via a freeze-thaw process. The method was proven to be short involving swelling of the

polysaccharide at ca. $-15\text{ }^{\circ}\text{C}$ and then freezing at $-28\text{ }^{\circ}\text{C}$ (total process time $\sim 1\text{ h}$). Overall, and using a neutralizing anti-solvent treatment as well, the process revealed that a minimum around 2 wt.% of higher MW α -chitin is required to obtain films of acceptable mechanical properties. In contrast, a 0.5 wt.% suspension of the same α -chitin was insoluble when EmimAcO : DMSO at $100\text{ }^{\circ}\text{C}$ was used. However, EmimAcO was useful at the 0.2 wt.% level where a relative estimation of α -chitin MWs has revealed that a 0.10 ± 0.03 reduction in the glycosidic linkage FT-IR ratio (produced by ball milling with increasing BtC/packing ratios) corresponds to a 0.93 ± 0.10 reduction in relative viscosity.

Relative viscosities of α -chitin in 19 wt.% NaOH increased parabolically with increasing concentration; the lowest MW sample [1.01 ± 0.07 glycosidic linkage ratio, 36.5 % CrI] reached 9.83 at $\sim 9.6\text{ wt.}\%$, while similar viscosity levels for the highest MW sample (1.38 ± 0.04 glycosidic linkage ratio, 83.2 % CrI) touched 9.73 at $\sim 0.9\text{ wt.}\%$ (10-fold analogies for the set). Furthermore, with the masses of the undissolved residues decreasing for decreasing MW/crystallinity, it was hypothesized that swelling of chitin fibers at $-15\text{ }^{\circ}\text{C}$ and chain disentanglement at $-28\text{ }^{\circ}\text{C}$ go forward via enhanced diffusion of hydrated Na^+ and OH^- ions and formation of $\text{NaOH}\cdot 7\text{H}_2\text{O}$ crystals respectively. With more dedicated studies required for a mechanistic elucidation though, the 1.38 ± 0.04 glycosidic linkage ratio/83.2 % CrI sample was casted as a film at the 5 wt.% level using a dilute HCl bath. The acidic gelation/phase-separation treatment was found practical

producing strong films after only 4 h. Thermal drying resulted in translucent films of reduced size and flexibility, while freeze-drying gave white products with FT-IR data being in close agreement to those of the milled sample. These preliminary casting experiments comprise a starting point for future fine-tuning of chitin films with 2 to 5 wt.% of higher MWs expected to yield acceptable mechanical properties.

At the same time though, and as lower DA values are hypothesized to contribute to higher flexibility of the films, a set of ultrasound assisted heterogeneous deacetylation reactions was performed on a wide range of α -chitin MWs using 40 wt.% NaOH. The experiments showed preliminary evidence that the sonication method applied is able to give predictable results for the higher MW/crystallinities of α -chitin samples. Analysis of solution state ^1H NMR and FT-IR spectra showed that sonication times of 22 and 76 min lowered the DA to $57 \pm 4\%$ and $35 \pm 4\%$ respectively. However, the lower MW α -chitins of the set gave unexpectedly low DA values suggesting that further work is needed. Also, more research is needed on the separation of acetate salts formed upon neutralizing deacetylation reaction mixtures. The initial results obtained here suggest that FT-IR spectroscopy is an effective monitoring technique. With the powerful solvation properties that 19 wt.% NaOH has revealed though, homogeneous deacetylation approaches might prove more efficient in the future both in terms of reaction kinetics and the work-up step. Future research might also focus more on the microwave technology, which has received little attention for chitin deacetylation studies. Last but not least, a method

for DA determination which would be more reproducible than those currently reported in literature is imperative. Solid-state NMR showed a promising potential, however a deeper understanding of peak deconvolution methods is necessary, as chitin samples with lower DAs and crystallinities are expected to give increasingly broader peaks, which generally comprise a serious problem for conventional integration algorithms.

4.5 References

1. Suntornnond, R.; An, J.; Yeong, W. Y.; Chua, C. K. Biodegradable Polymeric Films and Membranes Processing and Forming for Tissue Engineering. *Macromol. Mater. Eng.* **2015**, *300*, (9), 858-877.
2. Takada, A.; Kadokawa, J. -. Fabrication and characterization of polysaccharide ion gels with ionic liquids and their further conversion into value-added sustainable materials. *Biomolecules* **2015**, *5*, (1), 244-262.
3. Shen, X.; Shamshina, J. L.; Berton, P.; Gurau, G.; Rogers, R. D. Hydrogels based on cellulose and chitin: fabrication, properties, and applications. *Green Chem.* **2016**, *18*, (1), 53-75.
4. Ravve, A. Physical Properties and Physical Chemistry of Polymers. In *Principles of Polymer Chemistry*, 3rd ed.; Springer: New York, 2012; pp 17-67.
5. Courtenay, J. C.; Johns, M. A.; Galembeck, F.; Deneke, C.; Lanzoni, E. M.; Costa, C. A.; Scott, J. L.; Sharma, R. I. Surface modified cellulose scaffolds for tissue engineering. *Cellulose* **2017**, *24*, (1), 253-267.
6. Larson, R. G.; Desai, P. S. Modeling the rheology of polymer melts and solutions. *Ann. Rev. Fluid Mech.* **2015**, *47*, 47-65.
7. Burchard, W. Structure formation by polysaccharides in concentrated solution. *Biomacromolecules* **2001**, *2*, (2), 342-353.
8. Isobe, N.; Kimura, S.; Wada, M.; Kuga, S. Mechanism of cellulose gelation from aqueous alkali-urea solution. *Carbohydr. Polym.* **2012**, *89*, 1298-1300.
9. Franca, E. F.; Freitas, L. C. G.; Lins, R. D. Chitosan molecular structure as a function of N-acetylation. *Biopolymers* **2011**, *95*, (7), 448-460.

10. Yu, Z.; Lau, D. Flexibility of backbone fibrils in α -chitin crystals with different degree of acetylation. *Carbohydr. Polym.* **2017**, *174*, 941-947.
11. Lindman, B.; Karlström, G.; Stigsson, L. On the mechanism of dissolution of cellulose. *J. Mol. Liq.* **2010**, *156*, (1), 76-81.
12. Qin, Y.; Lu, X.; Sun, N.; Rogers, R. D. Dissolution or extraction of crustacean shells using ionic liquids to obtain high molecular weight purified chitin and direct production of chitin films and fibers. *Green Chem.* **2010**, *12*, (6), 968-971.
13. Birolli, W. G.; Delezuk, J. A. D. M.; Campana-Filho, S. P. Ultrasound-assisted conversion of α -chitin into chitosan. *Appl. Acoust.* **2016**, *103*, 239-242.
14. Younes, I.; Ghorbel-Bellaaj, O.; Chaabouni, M.; Rinaudo, M.; Souard, F.; Vanhaverbeke, C.; Jellouli, K.; Nasri, M. Use of a fractional factorial design to study the effects of experimental factors on the chitin deacetylation. *Int. J. Biol. Macromol.* **2014**, *70*, 385-390.
15. Fiamingo, A.; Delezuk, J. A. D. M.; Trombotto, S.; David, L.; Campana-Filho, S. P. Extensively deacetylated high molecular weight chitosan from the multistep ultrasound-assisted deacetylation of β -chitin. *Ultrason. Sonochem.* **2016**, *32*, 79-85.
16. Mnatsakanyan, M.; Thevarajah, J. J.; Roi, R. S.; Lauto, A.; Gaborieau, M.; Castignolles, P. Separation of chitosan by degree of acetylation using simple free solution capillary electrophoresis. *Anal. Bioanal. Chem.* **2013**, *405*, (21), 6873-6877.
17. Sannan, T.; Kurita, K.; Ogura, K.; Iwakura, Y. Studies on chitin: 7. I.r. spectroscopic determination of degree of deacetylation. *Polymer* **1978**, *19*, (4), 458-459.
18. Jang, M. -.; Kong, B. -.; Jeong, Y. -.; Lee, C. H.; Nah, J. -. Physicochemical characterization of α -chitin, β -chitin, and γ -chitin separated from natural resources. *J. Polym. Sci. Part A* **2004**, *42*, (14), 3423-3432.
19. Moussout, H.; Ahlafi, H.; Aazza, M.; Bourakhouadar, M. Kinetics and mechanism of the thermal degradation of biopolymers chitin and chitosan using thermogravimetric analysis. *Polym. Degrad. Stab.* **2016**, *130*, 1-9.
20. Wu, Y.; Sasaki, T.; Irie, S.; Sakurai, K. A novel biomass-ionic liquid platform for the utilization of native chitin. *Polymer* **2008**, *49*, (9), 2321-2327.
21. Gale, E.; Wirawan, R. H.; Silveira, R. L.; Pereira, C. S.; Johns, M. A.; Skaf, M. S.; Scott, J. L. Directed discovery of greener cosolvents: New cosolvents for use in ionic liquid based organic electrolyte solutions for cellulose dissolution. *ACS Sustainable Chem. Eng.* **2016**, *4*, (11), 6200-6207.

22. Einbu, A.; Naess, S. N.; Elgsaeter, A.; Vårum, K. M. Solution properties of chitin in alkali. *Biomacromolecules* **2004**, *5*, (5), 2048-2054.
23. Narasimhan, B.; Peppas, N. A. On the importance of chain reptation in models of dissolution of glassy polymers. *Macromolecules* **1996**, *29*, (9), 3283-3291.
24. Navard, P.; Wendler, F.; Meister, F.; Bercea, M.; Budtova, T. Preparation and properties of cellulose solutions. In *The European Polysaccharide Network of Excellence (EPNOE): Research Initiatives and Results*, Springer-Verlag Vienna: 2013; pp 91-152.
25. Chaudemanche, C.; Navard, P. Swelling and dissolution mechanisms of regenerated Lyocell cellulose fibers. *Cellulose* **2011**, *18*, (1), 1-15.
26. Miller-Chou, B. A.; Koenig, J. L. A review of polymer dissolution. *Prog. Polym. Sci.* **2003**, *28*, (8), 1223-1270.
27. Rollins, M. L.; Tripp, V. W. Optical and Electron Microscopic Studies of Cotton Fiber Structure. *Text. Res. J.* **1954**, *24*, (4), 345-357.
28. Cuissinat, C.; Navard, P. Swelling and dissolution of cellulose part II: Free floating cotton and wood fibres in NaOH-water-additives systems. *Macromol. Sympos.* **2006**, *244*, 19-30.
29. Cho, Y. I.; No, H. K.; Meyers, S. P. Physicochemical Characteristics and Functional Properties of Various Commercial Chitin and Chitosan Products. *J. Agric. Food Chem.* **1998**, *46*, (9), 3839-3843.
30. Alishahi, A.; Mirvaghefi, A.; Tehrani, M. R.; Farahmand, H.; Shojaosadati, S. A.; Dorkoosh, F. A.; Elsabee, M. Z. Enhancement and Characterization of Chitosan Extraction from the Wastes of Shrimp Packaging Plants. *J. Polym. Environ.* **2011**, *19*, (3), 776-783.
31. Liu, Y.; Liu, Z.; Pan, W.; Wu, Q. Absorption behaviors and structure changes of chitin in alkali solution. *Carbohydr. Polym.* **2008**, *72*, (2), 235-239.
32. Deshpande, M. D.; Scheicher, R. H.; Ahuja, R.; Pandey, R. Binding Strength of Sodium Ions in Cellulose for Different Water Contents. *J. Phys. Chem. B* **2008**, *112*, (30), 8985-8989.
33. Li, Y.; Lin, M.; Davenport, J. W. Ab Initio Studies of Cellulose I: Crystal Structure, Intermolecular Forces, and Interactions with Water. *J. Phys. Chem. C* **2011**, *115*, (23), 11533-11539.
34. Brohede, U.; Frenning, G.; Strømme, M. Characterization of the drug release process by investigation of its temperature dependence. *J. Pharm. Sci.* **2004**, *93*, (7), 1796-1803.

35. Nilsson, M.; Alderborn, G.; Strømme, M. Water-induced charge transport in tablets of microcrystalline cellulose of varying density: dielectric spectroscopy and transient current measurements. *Chem. Phys.* **2003**, *295*, 159-165.
36. Pickering, S. U. LXI.-The hydrates of sodium, potassium, and lithium hydroxides. *J. Chem. Soc., Trans.* **1893**, *63*, (0), 890-909.
37. Fang, Y.; Zhang, R.; Duan, B.; Liu, M.; Lu, A.; Zhang, L. Recyclable Universal Solvents for Chitin to Chitosan with Various Degrees of Acetylation and Construction of Robust Hydrogels. *ACS Sustainable Chem. Eng.* **2017**, *5*, (3), 2725-2733.
38. Duan, B.; Huang, Y.; Lu, A.; Zhang, L. Recent advances in chitin based materials constructed via physical methods. *Prog. Polym. Sci.* **2018**, *82*, 1-33.
39. Budtova, T.; Navard, P. Cellulose in NaOH-water based solvents: a review. *Cellulose* **2016**, *23*, (1), 5-55.
40. Li, G.; Du, Y.; Tao, Y.; Liu, Y.; Li, S.; Hu, X.; Yang, J. Dilute solution properties of four natural chitin in NaOH/urea aqueous system. *Carbohydr. Polym.* **2010**, *80*, (3), 970-976.
41. Isobe, N.; Noguchi, K.; Nishiyama, Y.; Kimura, S.; Wada, M.; Kuga, S. Role of urea in alkaline dissolution of cellulose. *Cellulose* **2013**, *20*, (1), 97-103.
42. Alves, L. C. H. Cellulose solutions: Dissolution, regeneration, solution structure and molecular interactions. Ph.D. Thesis, Universidade de Coimbra, Coimbra, 2015.
43. Clayden, J.; Greeves, N.; Warren, S.; Wothers, P. Nucleophilic substitution at the carbonyl group. In *Organic chemistry*, 1st ed.; Oxford University Press: Oxford ; New York, 2001; pp 279-304.
44. Meyer, K. H.; Wehrli, H. Comparaison chimique de la chitine et de la cellulose. *HCA* **1937**, *20*, (1), 353-362.
45. Darmon, S. E.; Rudall, K. M. Infra-red and X-ray studies of chitin. *Discuss. Faraday Soc.* **1950**, *9*, 251-260.
46. Kurita, K.; Sannan, T.; Iwakura, Y. Studies on chitin, 4. Evidence for formation of block and random copolymers of N-acetyl-D-glucosamine and D-glucosamine by hetero- and homogeneous hydrolyses. *Die Makromolekulare Chemie* **1977**, *178*, (12), 3197-3202.
47. Chang, K. L. B.; Tsai, G.; Lee, J.; Fu, W. R. Heterogeneous N-deacetylation of chitin in alkaline solution. *Carbohydr. Res.* **1997**, *303*, (3), 327-332.

48. Nemtsev, S. V.; Gamzazade, A. I.; Rogozhin, S. V.; Bykova, V. M.; Bykov, V. P. Deacetylation of chitin under homogeneous conditions. *Appl. Biochem. Microbiol.* **2002**, *38*, (6), 521-526.
49. Lamarque, G.; Viton, C.; Domard, A. Comparative study of the first heterogeneous deacetylation of α - and β -chitins in a multistep process. *Biomacromolecules* **2004**, *5*, (3), 992-1001.
50. Larkin, P. Chapter 6 - IR and Raman Spectra-Structure Correlations: Characteristic Group Frequencies. In *Infrared and Raman Spectroscopy*, 1st ed.; Elsevier: Oxford, 2011; pp 73-115.
51. Hirai, A.; Odani, H.; Nakajima, A. Determination of degree of deacetylation of chitosan by ^1H NMR spectroscopy. *Polym. Bull.* **1991**, *26*, (1), 87-94.
52. Kasaai, M. R. Determination of the degree of N-acetylation for chitin and chitosan by various NMR spectroscopy techniques: A review. *Carbohydr. Polym.* **2010**, *79*, (4), 801-810.
53. Lamarque, G.; Chaussard, G.; Domard, A. Thermodynamic aspects of the heterogeneous deacetylation of β -chitin: Reaction mechanisms. *Biomacromolecules* **2007**, *8*, (6), 1942-1950.
54. Noma, H.; Miwa, Y.; Yokoyama, I.; Machida, K. Infrared and Raman intensity parameters of sodium acetate and their intensity distributions. *J. Mol. Struct.* **1991**, *242*, (C), 207-219.
55. Colthup, N. B.; Daly, L. H.; Wiberley, S. E. Chapter 9 - Carbonyl compounds. In *Introduction to Infrared and Raman Spectroscopy*, 3rd ed.; Academic Press: San Diego, 1990; pp 289-325.
56. Başkan, M. H.; Aydın, M.; Çanakçı, D.; Osmanoglu, Ş Electron paramagnetic resonance and FT-IR spectroscopic studies of DL-2-aminoadipic acid and ammonium acetate powders. *Radiat. Eff. Defects Solids* **2014**, *169*, (3), 256-264.
57. Riemer, T.; Nimptsch, A.; Nimptsch, K.; Schiller, J. Determination of the glycosaminoglycan and collagen contents in tissue samples by high-resolution ^1H NMR spectroscopy after DCl-induced hydrolysis. *Biomacromolecules* **2012**, *13*, (7), 2110-2117.
58. Einbu, A.; Vårum, K. M. Characterization of chitin and its hydrolysis to GlcNAc and GlcN. *Biomacromolecules* **2008**, *9*, (7), 1870-1875.
59. Aguilar, J. A.; Kenwright, S. J. Robust NMR water signal suppression for demanding analytical applications. *Analyst* **2016**, *141*, (1), 236-242.

60. Khan, T. A.; Peh, K. K.; Ch'ng, H. S. Reporting degree of deacetylation values of chitosan: The influence of analytical methods. *J. Pharm. Pharm. Sci.* **2002**, *5*, (3), 205-212.
61. Kumirska, J.; Czerwicka, M.; Kaczyński, Z.; Bychowska, A.; Brzozowski, K.; Thöming, J.; Stepnowski, P. Application of spectroscopic methods for structural analysis of chitin and chitosan. *Mar. Drugs* **2010**, *8*, (5), 1567-1636.
62. Czechowska-Biskup, R.; Jarosinska, D.; Rokita, B.; Ulanski, P.; Rosiak, J. M. Determination of degree of deacetylation of chitosan - Comparison of methods. *Prog. Chem. Appl. Chitin Deriv.* **2012**, *XVII*, 5-20.
63. Thevarajah, J. J.; Bulanadi, J. C.; Wagner, M.; Gaborieau, M.; Castignolles, P. Towards a less biased dissolution of chitosan. *Anal. Chim. Acta* **2016**, *935*, 258-268.
64. Heux, L.; Brugnerotto, J.; Desbrières, J.; Versali, M. -; Rinaudo, M. Solid state NMR for determination of degree of acetylation of chitin and chitosan. *Biomacromolecules* **2000**, *1*, (4), 746-751.
65. Zhang, K.; Geissler, A.; Fischer, S.; Brendler, E.; Bäücker, E. Solid-state spectroscopic characterization of α -chitins deacetylated in homogeneous solutions. *J. Phys. Chem. B* **2012**, *116*, (15), 4584-4592.
66. Kameda, T.; Miyazawa, M.; Ono, H.; Yoshida, M. Hydrogen bonding structure and stability of α -chitin studied by ^{13}C solid-state NMR. *Macromol. Biosci.* **2005**, *5*, (2), 103-106.
67. Reid, L. M.; Wu, G.; Crudden, C. M. Accessible bidentate diol functionality within highly ordered composite periodic mesoporous organosilicas. *New J. Chem.* **2016**, *40*, (7), 6487-6497.
68. Hughes, T. S.; Wilson, H. D.; De Vera, I. M. S.; Kojetin, D. J. Deconvolution of complex 1D NMR spectra using objective model selection. *PLoS ONE* **2015**, *10*, (8),.
69. Chen, C.; Li, D.; Yano, H.; Abe, K. Dissolution and gelation of alpha-chitin nanofibers using a simple NaOH treatment at low temperatures. *Cellulose* **2014**, *21*, (5), 3339-3346.
70. Jana, M.; Bandyopadhyay, S. Hydration properties of α -, β -, and γ -cyclodextrins from molecular dynamics simulations. *J. Phys. Chem. B* **2011**, *115*, (19), 6347-6357.
71. Liu, L.; Hunger, J.; Bakker, H. J. Energy Relaxation Dynamics of the Hydration Complex of Hydroxide. *J. Phys. Chem. A* **2011**, *115*, (51), 14593-14598.

72. Borysiak, S.; Garbarczyk, J. Applying the WAXS method to estimate the supermolecular structure of cellulose fibres after mercerisation. *Fibres Text. East. Eur.* **2003**, *11*, (5), 104-106.
73. Mansikkamäki, P.; Lahtinen, M.; Rissanen, K. Structural changes of cellulose crystallites induced by mercerisation in different solvent systems; determined by powder X-ray diffraction method. *Cellulose* **2005**, *12*, (3), 233-242.
74. Gong, P.; Wang, J.; Liu, B.; Ru, G.; Feng, J. Dissolution of chitin in aqueous KOH. *Cellulose* **2016**, *23*, (3), 1705-1711.

Chapter 5 Concluding remarks and future directions

The work described in this thesis builds on the design of mechanochemical systems which aim to find value in α -chitin. As discussed in Chapter 2, the challenging crystallinity of the most copious of the marine polysaccharides can be reduced in a controlled way via manipulating certain ball milling technological parameters. Using that method, in Chapter 4, a simple and rapid process to fabricate α -chitin films is investigated via mechanochemical amorphization and subsequent dissolution in aqueous NaOH. An optimum concentration of 19 wt.% of the alkali was found to dissolve \sim 5 wt.% high MW/crystallinity α -chitin via a freeze-thaw process at -28 °C and give films of acceptable mechanical properties after a simple gelation treatment with HCl. This route based on XRD/FT-IR characterization of the milled samples has not been reported previously. Practically, it avoids some of the disadvantages of ionic liquids and deep eutectic solvents like the need for a costly recycling/purification treatment, their life cycle issues, the high temperatures, and the long stirring times.¹ However, the reader of Section 4.3.5 might have noticed that the dissolution of \sim 0.9 wt.% high-MW α -chitin gave also \sim 3% undissolved residue. Therefore, it is only natural for one to ask questions like “What are the levels of undissolved mass in the \sim 5 wt.% film?” and “Do they lower or raise the strength of the resulting film?”. Moreover, and considering a recent study where very strong and transparent films of a low MW α -chitin (101 kDa) were obtained via stirring in aqueous KOH/urea solutions at -30 °C,² chemists might wonder if a

freezing step is actually necessary for the dissolution of certain MW-concentration ranges of the polysaccharide.^{cxviii}

Furthermore, the ball-milling/cold-NaOH method is expected to conveniently create homogeneous solutions of predictable viscosities in the 1–10 wt.% range allowing for more efficient and controlled chitin deacetylation. That approach might prove more attractive in the future, as although the sonication method applied to α -chitin suspensions resulted in a favourable deacetylation over depolymerization for the higher MW α -chitins, the DA values obtained from the lower MW chains were not predictable (see Section 4.3.4). It is precisely at that lower MW region though that more controlled and efficient deacetylation processes are required in the near future as the resulting chitosans can be used as high value materials for a range of applications. In addition to the diverse products described in Section 1.5, recent studies show that chitosans (DD 75–85%) of 26 and 109 kDa increase cell attachment of plant α -cellulose scaffolds by up to 3000%,⁴ while derivatives of chains with DD >92% and MWs of 40–150 kDa produced robust shells for capsules with liquefied cores which can be applied in a broad spectrum of fields (from medicine to electronics).⁵

However, with the latter results obtained with commercial chitosan samples, the specific ranges of the reported DA and MW values emphasize the urgent need

^{cxviii} The aforementioned study does not mention freezing of the cold 3.5 M KOH/0.6 M urea solvent, in spite of the fact that a 3.5 M KOH solution (~17 wt.%) has a freezing point ca. –18 °C (3).

within an ocean-based biorefinery to characterize samples both accurately and precisely. Although the DA values measured with FT-IR, solution and solid-state NMR in Chapter 4 have shown to complement each other to some extent, a more dedicated study is needed in the immediate future. The preliminary results from solid-state NMR of ball milled α -chitins indicate that with a better understanding of peak deconvolution options which modern softwares offer, that powerful spectroscopic method can complement FT-IR data towards a less biased and precise DA determination. In order to reach reproducible results for a wide range of MW/crystallinities though, future studies need to accept the challenges that arise from the numerous parameters of the combined steps of the work-up and reaction in aqueous alkali mediums. With separation of acetate salts proving to require laborious washing conditions (perhaps involving multiple centrifugation or filtration steps during purification of chitosans), future scaled-up processes might benefit from the possibility of deacetylation by ball milling. Based on FT-IR and solid-state NMR measurements of several α -chitin sets in Chapters 3 and 4, high balls-to-chitin (BtC) and packing ratios of stainless steel media are hypothesized to deacetylate the polysaccharide to some extent concurrently with its extensive depolymerization/amorphization. If this evidence is reproduced by other chitin ball milling studies in the future, it might confirm that high frequency/impact collisions are capable of liberating the acetyl group in some other form than that of the interfering acetate salts. Recent experimentation with different grinding media

shapes (cylinder, square), operating frequencies and other technological parameters opens the way for fine-tuning a wide range of α -chitin transformations.⁶

Nevertheless, chitin deacetylation by ball milling has already been achieved with the use of a base as a catalyst. When high MW chitin (362 kDa, ~96% DA) was milled with equal amounts of NaOH using a planetary ZrO₂ vial/balls system, low MW chitosan was produced with chains of ~8 kDa and ~73% DD.⁷ Despite the fact that this remarkable result opens the way for the mechanochemical production of low MW chitosan straight from the shells of crustaceans, the study might raise challenging questions in the future regarding the reactants' contact surface area.^{cxix}

Alternatively, the surface basic sites of hydrotalcites, which are readily available and economic solid bases,⁸ are expected to gain increasing attention from the mechanochemistry community in the future.

In my related studies presented in Chapter 3, the active specific surface area of kaolinite led to significant improvements in α -chitin depolymerization. The increased acidity of the system upon milling of the solid catalyst along with the high BtC/packing ratios allowed for $50 \pm 3\%$ water-soluble products in the first 2 h of milling (84% increased productivity than that without kaolinite). This improved depolymerization reaction is in agreement with a reported cellulose ball mill system

^{cxix} NaOH pellets are expected to only deform in the ball mill and not to reduce in size. Moreover, separation of water-soluble low MW chitosan from equal amounts of NaOH is hypothesized to be laborious in a scaled-up process. Liquid-assisted grinding or an impregnation technique might reveal a more sustainable approach for alkali catalyzed deacetylation of chitin.

and is hypothesized to originate from protonation of glycosidic oxygens during the elastic phases of collisions when covalent bonds of pyranic rings are subjected to conformational changes. After 2 h milling, the system entered a phase of leveling out reaching a plateau of ca. 76% solubility in 6 h probably due to coalescence of chitin particles. Colorimetric approximations of reducing ends via the dinitrosalicylic acid (DNS) and Schales assays confirmed the solubility elevations for the two ball milling phases.

The application of a MALDI-TOF-MS method developed in Memorial University showed that water-soluble products contained oligomers of NAG with degrees of polymerization (DP) of 1 to 5. Relative quantification using a derivatization approach revealed that the bigger oligomers (pentamer, tetramer, trimer) lose their glycosidic linkages with increasing milling time (increasing trends for the monomer and dimer concentrations were demonstrated accordingly). Deacetylated oligomers were found at minimal to negligible levels supplementing the FT-IR data obtained for ball milling without kaolinite. *N*-acetyl-D-glucosamine (NAG) and *N,N'*-diacetylchitobiose (NAG₂) reached yields of 5.1 and 3.9 wt.%, respectively, within 6 h, which compare well with yields of glucose and cellobiose from literature cellulose ball milling.⁹ These data agreed with chromatographic observations (SEC analysis), which showed broad dispersities (\mathcal{D}) for the ball milled samples (\mathcal{D} 4–6) in contrast to narrow ones for NAG-oligomer standards (\mathcal{D} 1.00–1.04). Consisting exclusively of acetylated sugar units, these oligomers have been categorized as

homooligomers.¹⁰ Similar mixtures of chitin chains near 1 kDa have been hypothesized to inhibit oxidative stress in live cells and potentially prevent neurodegenerative diseases like Alzheimer's and Parkinson's, however the studies do not specify whether their mass spectra peaks correspond to parent or adduct ions.^{11,12} In general, weaknesses in characterization of chitin oligosaccharides are not unusual in literature and that is reflected in several of the publications which review their biological activities.^{13,14} However, with the commonly beneficial properties that these molecules reveal in critical fields like therapeutics, food additives and plant protection,¹⁴ tandem mass spectrometric techniques¹⁰ as well as synthetic biology approaches¹⁵ are expected to make a lasting difference in the future.

At the same time, and until higher standards of oligomer characterization are established, networks of sea-based biorefineries can take advantage of the diverse functionalities that higher MW chitin chains (>10 kDa) have been shown to possess (see Section 1.5). As discussed in Section 2.3.6, the production of water-soluble chitin species comes along with an inevitable insoluble fraction of higher MW chitin which can comprise an alternative source of molecules for markets such as those of personal care products and functional materials. If a concerted effort is made towards the realisation of the diversity of valuable products from chitin, the results of the low BtC/packing set presented in Chapter 2 can provide a solid basis for more advanced work with ball mills. In this thesis, for the first time a semi-quantitative

correlation has been achieved using IR data where a gradual reduction of α -chitin's crystallinity with an unaffected DA can be seen to correlate with a steady decline of glycosidic linkage content, and the characteristic amide I split. This application of IR spectroscopy might be useful for other researchers using chitin which is after all the most abundant of the marine polysaccharides.

The results in Chapters 2 and 3 demonstrate that with systematic ball milling and detailed product characterization, α -chitin can be amorphized in a controlled way, which involves disruption of the intermolecular hydrogen bonding network and simultaneous depolymerization. However, that methodology contributes only to academic debate at the moment as the shaking mode of the SPEX 8000 system which was used in this thesis is not scalable without significant redesign.¹⁶ Nevertheless, similar magnitude of forces have been shown to develop with the attritor technology which is scalable and revealed a 15-fold increase in the frequency of high energy collisions upon scaling from a 1.4 to a 160 L reactor.^{17,18} Moreover, it is not only the technique of ball milling that induces mechanochemical transformations; continuous flow processes can go forward in twin-screw extruders in multi kg h⁻¹ quantities.¹⁹ In general, future advances in the scalability of mechanochemical approaches will most probably allow companies and biorefineries to start designing high DA chitins of tunable MWs in a lab/pilot scale without the use of concentrated strong acids; avoiding this way the need for special labor and neutralization of acidic waste streams. Although scaling up

mechanochemical processes is not straightforward yet,^{18,20} milling experiments on depolymerization of lignocellulosic biomass suggest a reduction of electrical energy consumption with increase from the hectogram to the kilogram scale.²¹ Therefore, similar technology assessments coupled with industrial implementation studies specifically on α -chitin should be performed in order to expand the field from lab research to feasible realisation of added value products such as excipients in formulations for human use (personal care products, functional packaging etc.). This will signal new support drivers towards the meaningful commercial exploitation of the various abundant chitinous waste streams.

Returning to the here-and-now, one of the things that this thesis did not manage to achieve is a determination of the MWs of the chitin samples used. This is not unusual considering the strong intermolecular forces present within α -chitin samples. Studies in Chapter 3 indicated a MW in the order of 1 MDa for the native α -chitin sample from ChitinWorks. When cold 10 wt.% NaOH was used as a solvent on ball milled samples of significantly lower crystallinity/MW according to a published viscosity/light-scattering study,²² the MW values obtained were not reasonable. Although more systematic attempts should be made with that method as well as those using *N,N*-dimethylacetamide/LiCl,^{23,24} at the same time, the overall assessment of relevant literature suggests that chemists will soon be forced to invent new methods of MW determination of chitin. Based on the understanding of chitin crystal packing and its elementary fibril structure we have obtained during the past

10 years from the concerted studies of high resolution X-ray diffraction data and molecular dynamics simulations,²⁵⁻²⁸ the research groups which work systematically on the versatile toolbox of modern solvent systems are expected to challenge each other with optimum dissolution parameters towards solvation of increasing MWs and crystallinities. Considering the rich diversity of chitin sources and shell isolation processes though, as well as the neglected role of hydrophobic interactions, the scientific community can take advantage of similar ball milling methods and start the investigations of solvents' potentials from lower crystallinities/MWs working their way up to the higher MW samples.

Until higher standards of chitin MW determination reach wider acceptance, mechanochemists might challenge their own specialty by investigating the relationship between particle size, crystallinity, and molecular weight of polysaccharides. As discussed in Chapter 4, the larger particles of native α -chitin showed a significant hysteresis in glycosidic linkage content reduction upon similar ball milling conditions compared to those of practical grade (PG) α -chitin. This allows researchers who use ball mills that operate via shaking modes to raise questions like "To what extent should collision frequency be increased in order for the larger α -chitin particles to achieve an equal depolymerization efficiency to that of the smaller particle system?" and "What are the optimum collision force/frequency combinations for efficient depolymerization of different α -chitin crystallinities?". Considering the hypothesized link between the FT-IR absorbance

ratio of the amide I split and the crystallinity index (CrI %), experimentalists might want to test if that relationship is valid for α -chitin amorphization which does not include concurrent depolymerization (e.g. by using lower operating frequencies or differential vial/balls densities upon ball milling). Moreover, with recent computational methods contributing to a fast discovery of super-hard materials,²⁹ the performances of steel systems here and elsewhere might be significantly improved and make a difference in the functional costs of scaled-up mechanochemical processes.

If one puts the above study next to those that have shed light on chitin's crystal packing and elementary fibril structure, then it is not unreasonable to think of computational chemists as orchestra conductors who raise the mutual understanding and cross-fertilization of ideas of scientists of different disciplines more and more.³⁰ These scientific efforts seem to have already started to find a positive response from societies, who either embrace or question the motto "think globally, act locally"; with questioning considered vital for a better interaction between science and society.³⁰⁻³⁴ For example, "To value the 'waste' of some companies as resources for others" is an element which gains increasing levels of agreement between experts of circular economy and that is encouraging for the industrial symbiosis of small and medium-sized enterprises (SMEs).³⁵ With volumes of produced crustaceans in the EU distributed broadly among both Mediterranean (mainly Spain and Italy) and Northern (mainly Ireland, UK, Denmark, Netherlands)

countries,³⁶ and new public-private partnerships supporting bio-based networks of SMEs at the European level,³⁷ chitin applicability in innovative technologies like 3D-printing³⁸ and others mentioned in Section 1.5 can surely transform the dream of the ocean-based biorefinery into a lasting reality.³⁹⁻⁴¹

5.1 References

1. Wood, N.; Stephens, G. Accelerating the discovery of biocompatible ionic liquids. *Phys. Chem. Chem. Phys.* **2010**, *12*, (8), 1670-1674.
2. Huang, J.; Zhong, Y.; Zhang, L.; Cai, J. Extremely Strong and Transparent Chitin Films: A High-Efficiency, Energy-Saving, and "Green" Route Using an Aqueous KOH/Urea Solution. *Adv. Funct. Mater.* **2017**, *27*, (26), article 1701100.
3. Pickering, S. U. LXI.-The hydrates of sodium, potassium, and lithium hydroxides. *J. Chem. Soc., Trans.* **1893**, *63*, (0), 890-909.
4. Johns, M. A.; Bae, Y.; Guimaraes, F. E. G.; Lanzoni, E. M.; Costa, C. A. R.; Murray, P. M.; Deneke, C.; Galembeck, F.; Scott, J. L.; Sharma, R. I. Predicting ligand-free cell attachment on next-generation cellulose-chitosan hydrogels. *ACS Omega* **2018**, *3*, (1), 937-945.
5. Costa, A. M. S.; Mano, J. F. Solvent-free strategy yields size and shape-uniform capsules. *J. Am. Chem. Soc.* **2017**, *139*, (3), 1057-1060.
6. Yin, Z.; Peng, Y.; Zhu, Z.; Yu, Z.; Li, T. Impact load behavior between different charge and lifter in a laboratory-scale mill. *Mater.* **2017**, *10*, (8), 882.
7. Chen, X.; Yang, H.; Zhong, Z.; Yan, N. Base-catalysed, one-step mechanochemical conversion of chitin and shrimp shells into low molecular weight chitosan. *Green Chem.* **2017**, *19*, (12), 2783-2792.
8. Othman, M. R.; Helwani, Z.; Martunus; Fernando, W. J. N. Synthetic hydrotalcites from different routes and their application as catalysts and gas adsorbents: A review. *Appl. Organomet. Chem.* **2009**, *23*, (9), 235-246.
9. Dornath, P.; Cho, H. J.; Paulsen, A.; Dauenhauer, P.; Fan, W. Efficient mechano-catalytic depolymerization of crystalline cellulose by formation of branched glucan chains. *Green Chem.* **2015**, *17*, (2), 769-775.

10. Haebel, S.; Bahrke, S.; Peter, M. G. Quantitative sequencing of complex mixtures of heterochitooligosaccharides by vMALDI-linear ion trap mass spectrometry. *Anal. Chem.* **2007**, *79*, (15), 5557-5566.
11. Ngo, D. -.; Kim, M. -.; Kim, S. -. Chitin oligosaccharides inhibit oxidative stress in live cells. *Carbohydr. Polym.* **2008**, *74*, (2), 228-234.
12. Oh, S. -.; Vo, T. -.; Ngo, D. -.; Kim, S. -.; Ngo, D. -.; Kim, S. -. Prevention of H₂O₂-induced oxidative stress in murine microglial BV-2 cells by chitin-oligomers. *Process Biochem.* **2016**, *51*, (12), 2170-2175.
13. Kim, S. -.; Rajapakse, N. Enzymatic production and biological activities of chitosan oligosaccharides (COS): A review. *Carbohydr. Polym.* **2005**, *62*, (4), 357-368.
14. Liaqat, F.; Eltem, R. Chitooligosaccharides and their biological activities: A comprehensive review. *Carbohydr. Polym.* **2018**, *184*, 243-259.
15. Naqvi, S.; Moerschbacher, B. M. The cell factory approach toward biotechnological production of high-value chitosan oligomers and their derivatives: an update. *Crit. Rev. Biotechnol.* **2017**, *37*, (1), 11-25.
16. Hick, S. M.; Griebel, C.; Restrepo, D. T.; Truitt, J. H.; Buker, E. J.; Bylda, C.; Blair, R. G. Mechanocatalysis for biomass-derived chemicals and fuels. *Green Chem.* **2010**, *12*, (3), 468-474.
17. Santhanam, P. R.; Dreizin, E. L. Predicting conditions for scaled-up manufacturing of materials prepared by ball milling. *Powder Technol.* **2012**, *221*, 403-411.
18. Maini; Halasz; Takacs; James; Belenguer; Frišćic; Jones; Stolle; Boldyreva; Blair; Galembeck; Suslick; Margoutidis; Mack; Jörres; Nagapudi; Beyer; Brekalo; Lamaty; Irikura; Khripin; Hamilton; Zhang Mechanistic understanding, catalysis and scaling up of mechanochemistry: General discussion. *Faraday Discuss.* **2014**, *170*, 287-310.
19. Crawford, D. E.; Miskimmin, C. K. G.; Albadarin, A. B.; Walker, G.; James, S. L. Organic synthesis by Twin Screw Extrusion (TSE): Continuous, scalable and solvent-free. *Green Chem.* **2017**, *19*, (6), 1507-1518.
20. Blair, R. G.; Chagoya, K.; Biltek, S.; Jackson, S.; Sinclair, A.; Taraboletti, A.; Restrepo, D. T. The scalability in the mechanochemical syntheses of edge functionalized graphene materials and biomass-derived chemicals. *Faraday Discuss.* **2014**, *170*, 223-233.
21. Kaufman Rechulski, M. D.; Käldestrom, M.; Richter, U.; Schüth, F.; Rinaldi, R. Mechanocatalytic Depolymerization of Lignocellulose Performed on Hectogram and Kilogram Scales. *Ind. Eng. Chem. Res.* **2015**, *54*, (16), 4581-4592.

22. Einbu, A.; Naess, S. N.; Elgsaeter, A.; Vårum, K. M. Solution properties of chitin in alkali. *Biomacromolecules* **2004**, *5*, (5), 2048-2054.
23. Terbojevich, M.; Carraro, C.; Cosani, A.; Marsano, E. Solution studies of the chitin-lithium chloride-N,N-di-methylacetamide system. *Carbohydr. Res.* **1988**, *180*, (1), 73-86.
24. Poirier, M.; Charlet, G. Chitin fractionation and characterization in N,N-dimethylacetamide/lithium chloride solvent system. *Carbohydr. Polym.* **2002**, *50*, (4), 363-370.
25. Sikorski, P.; Hori, R.; Wada, M. Revisit of α -chitin crystal structure using high resolution X-ray diffraction data. *Biomacromolecules* **2009**, *10*, (5), 1100-1105.
26. Beckham, G. T.; Crowley, M. F. Examination of the α -chitin structure and decrystallization thermodynamics at the nanoscale. *J. Phys. Chem. B* **2011**, *115*, (15), 4516-4522.
27. Petrov, M.; Lymperakis, L.; Friak, M.; Neugebauer, J. Ab initio based conformational study of the crystalline α -chitin. *Biopolymers* **2013**, *99*, (1), 22-34.
28. Deringer, V. L.; Englert, U.; Dronskowski, R. Nature, strength, and cooperativity of the hydrogen-bonding network in α -chitin. *Biomacromolecules* **2016**, *17*, (3), 996-1003.
29. Mansouri Tehrani, A.; Oliynyk, A. O.; Parry, M.; Rizvi, Z.; Couper, S.; Lin, F.; Miyagi, L.; Sparks, T. D.; Brgoch, J. Machine Learning Directed Search for Ultraincompressible, Superhard Materials. *J. Am. Chem. Soc.* **2018**, *140*, (31), 9844-9853.
30. Cornforth, J. W. Scientists as citizens. *Aust. J. Chem.* **1993**, *46*, (3), 265-275.
31. Breyer, C.; Heinonen, S.; Ruotsalainen, J. New consciousness: A societal and energetic vision for rebalancing humankind within the limits of planet Earth. *Technol. Forecast. Soc. Change* **2017**, *114*, 7-15.
32. Zeleny, M. High technology and barriers to innovation: From globalization to relocalization. *Int. J. Inf. Technol. Decis. Mak.* **2012**, *11*, (2), 441-456.
33. Lopolito, A.; Prosperi, M.; Sisto, R.; De Meo, E. Translating local stakeholders' perception in rural development strategies under uncertainty conditions: An application to the case of the bio-based economy in the area of Foggia (South Italy). *J. Rural Stud.* **2015**, *37*, 61-74.
34. Buckley, P. J.; Pinnegar, J. K.; Painting, S. J.; Terry, G.; Chilvers, J.; Lorenzoni, I.; Gelcich, S.; Duarte, C. M. Ten Thousand Voices on Marine Climate Change in Europe: Different Perceptions among Demographic Groups and Nationalities. *Front. Mar. Sci.* **2017**, *4*, 206.

35. Prieto-Sandoval, V.; Ormazabal, M.; Jaca, C.; Viles, E. Key elements in assessing circular economy implementation in small and medium-sized enterprises. *Bus. Strat. Env.* **2018**, 1-10.
36. Nisticò, R. Aquatic-derived biomaterials for a sustainable future: A European opportunity. *Resources* **2017**, 6, (4), 65.
37. Mengal, P.; Wubbolts, M.; Zika, E.; Ruiz, A.; Brigitta, D.; Pieniadz, A.; Black, S. Bio-based Industries Joint Undertaking: The catalyst for sustainable bio-based economic growth in Europe. *New Biotechnol.* **2018**, 40, 31-39.
38. Mohan, T.; Maver, T.; Štiglic, A. D.; Stana-Kleinschek, K.; Kargl, R. 3D bioprinting of polysaccharides and their derivatives: From characterization to application. In *Fundamental Biomaterials: Polymers*, 1st ed.; Thomas, S., Balakrishnan, P., Sreekala, M.S., Eds.; Elsevier Inc.: Duxford, UK, 2018; pp 105-141.
39. Chen, X.; Yang, H.; Yan, N. Shell Biorefinery: Dream or Reality? *Chem. Eur. J.* **2016**, 22, (38), 13402-13421.
40. Kerton, F. M.; Liu, Y.; Omari, K. W.; Hawboldt, K. Green chemistry and the ocean-based biorefinery. *Green Chem.* **2013**, 15, (4), 860-871.
41. *Fuels, Chemicals and Materials from the Oceans and Aquatic Sources*; Kerton, F. M.; Yan, N., Eds.; John Wiley & Sons: Hoboken, NJ, 2017.

Appendix A2

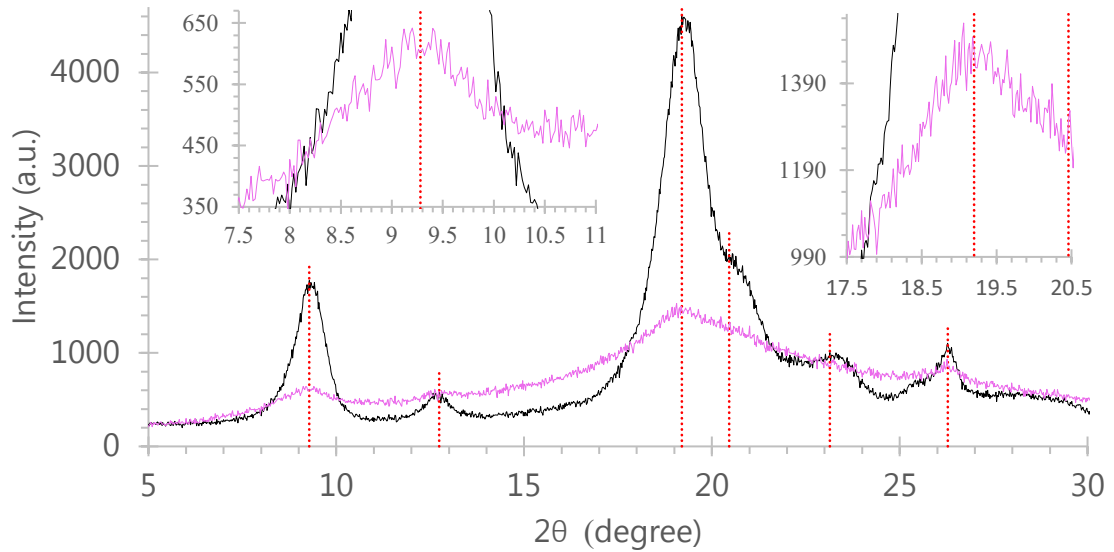


Figure A2– 1: Overlay of XRD signals (with no separation) for native α -chitin (black) and ball milled for 120 min with 2×0.5 " balls (pink). Insets highlight (in red dotted line) the maximum intensity of the pink signal at the same 2θ values as the ones considered for the (020) and (110) reflections of native chitin (9.28° and 19.20° respectively).

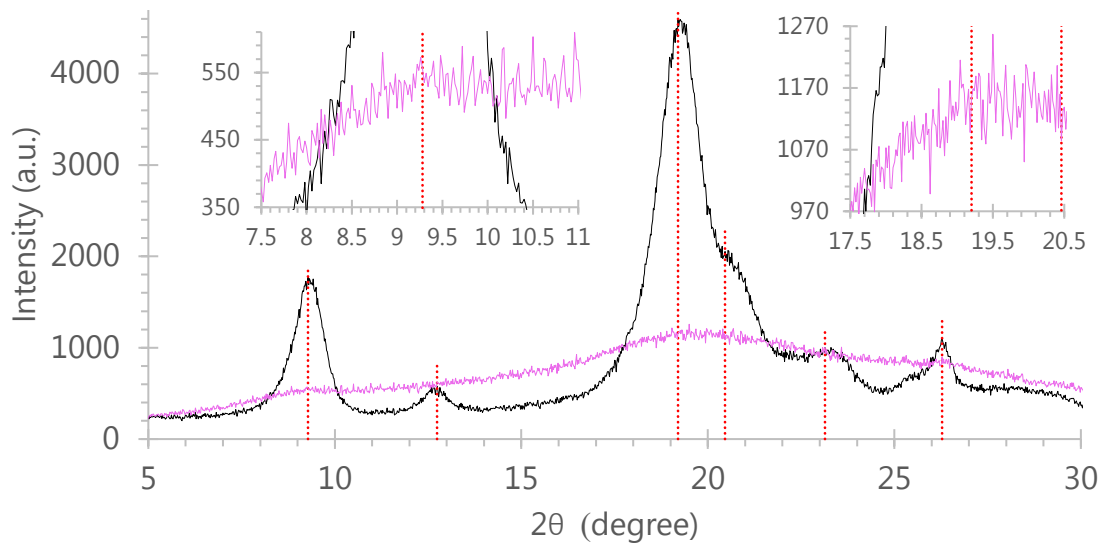


Figure A2– 2: Overlay of XRD signals (with no separation) for native α -chitin (black) and ball milled for 120 min with 16×0.25 " balls (pink).

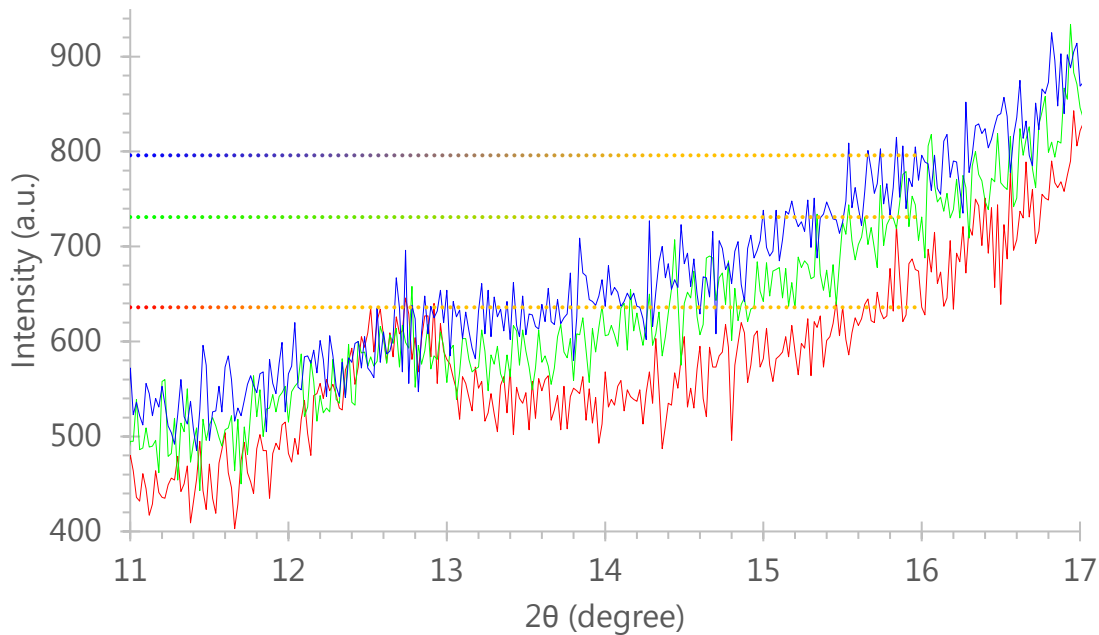


Figure A2– 3: Overlay of XRD signals (no separation) of α -chitin milled for 30 (red), 60 (green), 90 (blue) min with $16 \times 0.25''$ balls. Dotted lines mark the intensities of the amorphous scatter at $16.00^\circ 2\theta$.

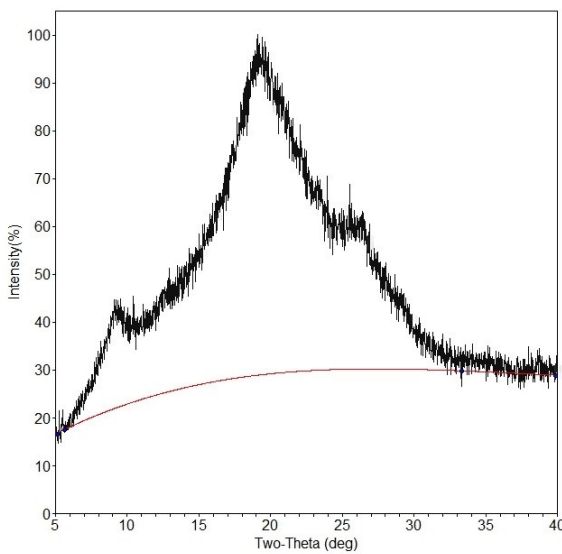


Figure A2– 4: Trial line taken as background on the XRD signal of the α -chitin sample milled for 90 min with $16 \times 0.25''$ balls. The line was drawn by JADE software [Materials Data, Inc. (MDI)] when from the proposed points the ones at 5.0° , 5.8° , 34.0° , and $39.9^\circ 2\theta$ were kept by the investigator.

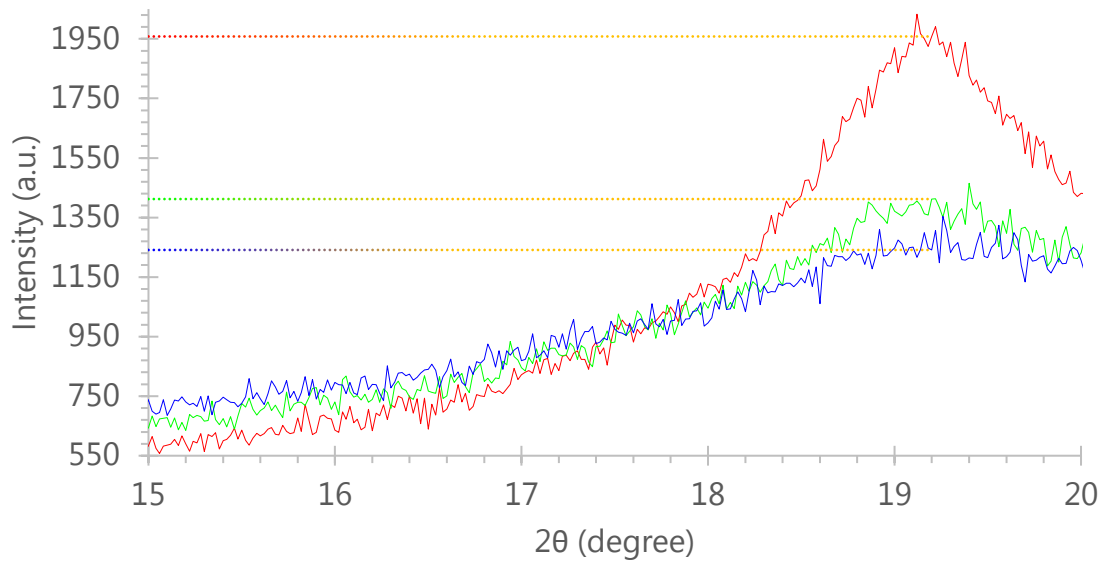


Figure A2– 5: Overlay of XRD signals (no separation) of α -chitin milled for 30 (red), 60 (green), 90 (blue) min with $16 \times 0.25''$ balls. Dotted lines mark the intensities of the crystalline (110) reflection at $19.20^\circ 2\theta$.

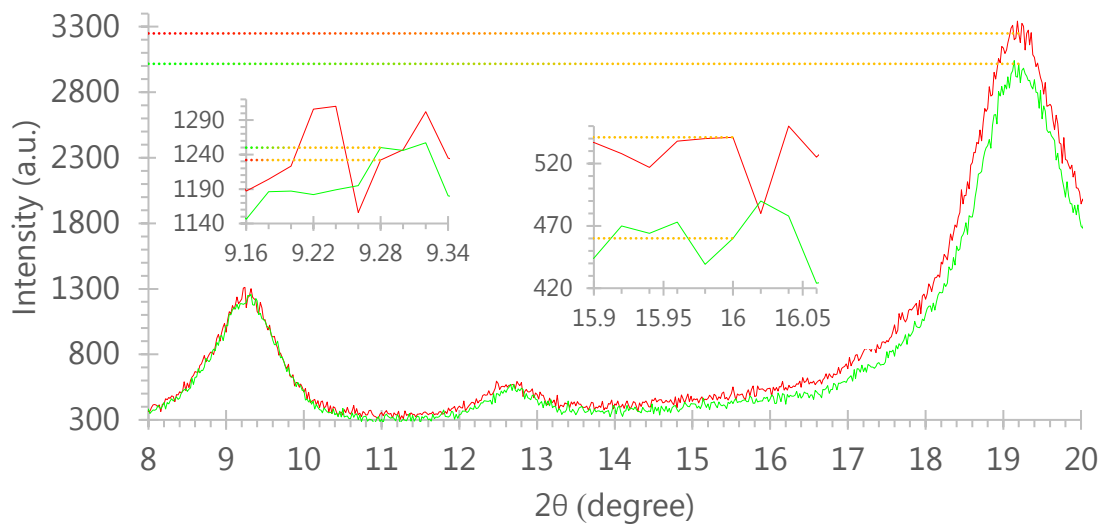


Figure A2– 6: Overlay of XRD signals (no separation) of the sample milled for 15 min with $2 \times 0.5''$ balls. CrI measured on May 2014 (red) is 83.3% $[(3249 - 541) \times 100 / 3249]$, and on December 2014 (green) is 84.8% $[(3017 - 460) \times 100 / 3017]$. The intensity ratios for the (110)/(020) reflections are: 2.64 (3249 / 1232) for the red signal, and 2.41 (3017 / 1250) for the green signal.

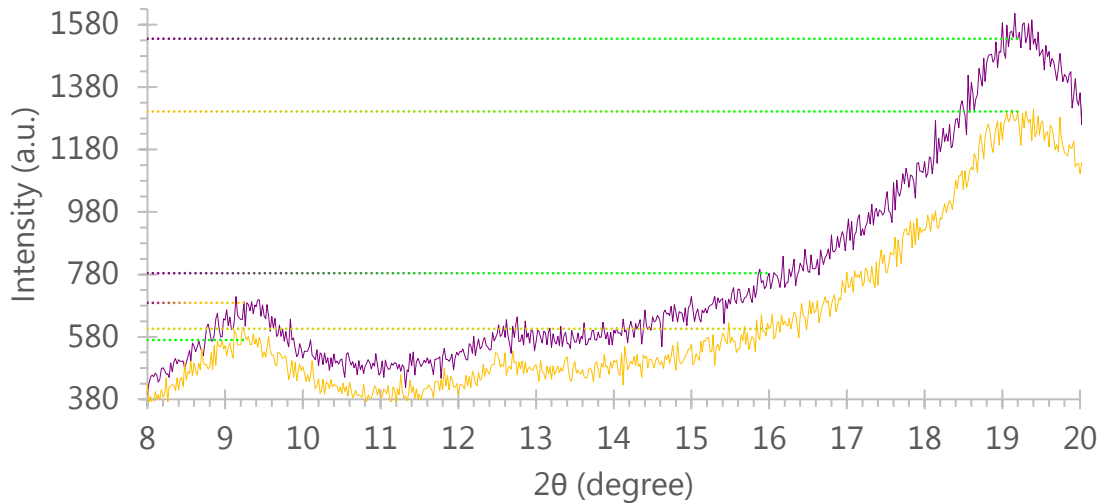


Figure A2– 7: Overlay of XRD signals (no separation) of the sample milled for 105 min with 2×0.5 " balls. CrI measured on May 2014 (purple) is 48.9% $[(1535 - 784) \times 100 / 1535]$, and on December 2014 (orange) is 53.5% $[(1302 - 606) \times 100 / 1302]$. The intensity ratios for the (110)/(020) reflections are: 2.23 (1535 / 689) for the purple signal, and 2.28 (1302 / 570) for the orange signal.

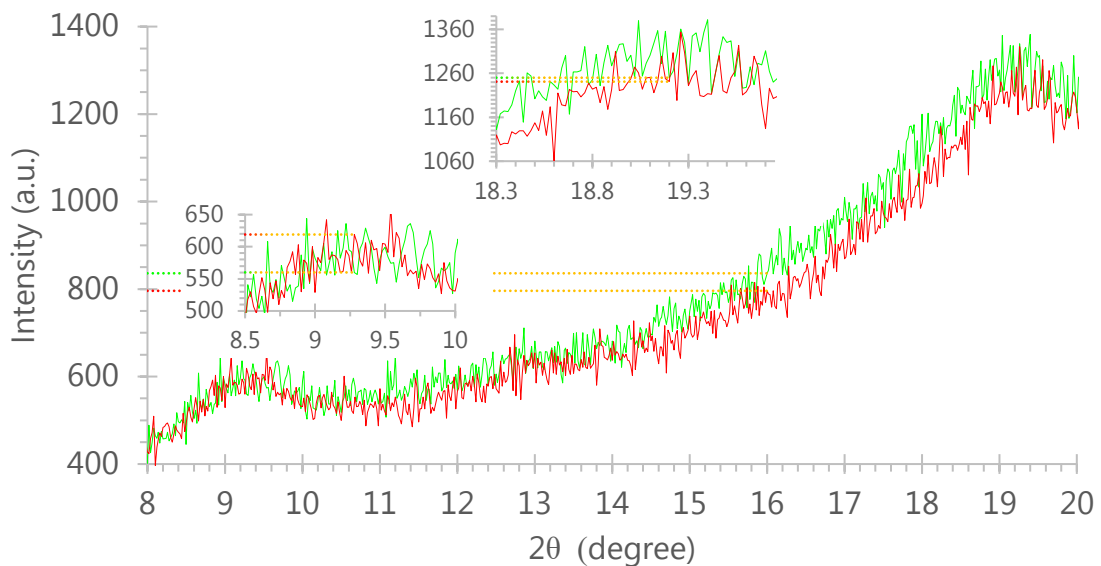


Figure A2– 8: Overlay of XRD signals (no separation) of two samples milled for 90 min with 16×0.25 " balls (BtC: 8.2). CrI is 35.9% $[(1241 - 796) \times 100 / 1241]$ for the red signal, and 33.1% $[(1250 - 836) \times 100 / 1250]$ for the green signal. The intensity ratios for the (110)/(020) reflections are: 2.00 (1241 / 619) for the red signal, and 2.23 (1250 / 560) for the green signal.

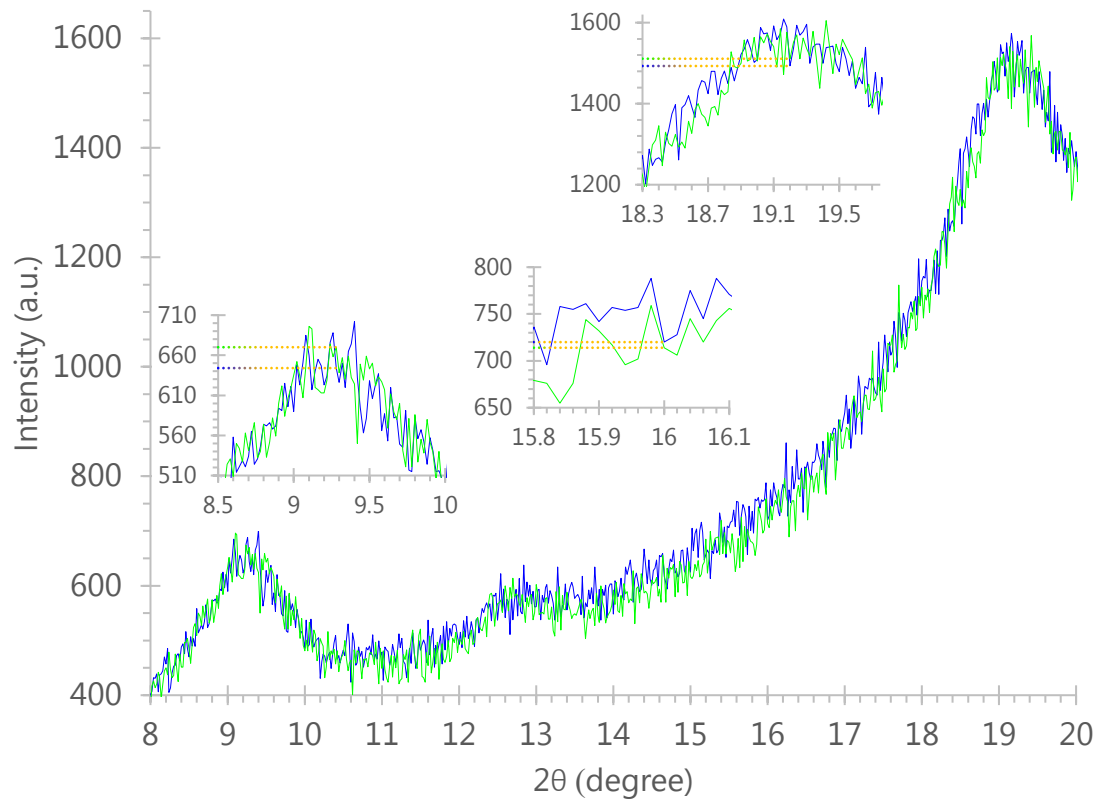


Figure A2– 9: Overlay of XRD signals (no separation) of two samples milled for 90 min with 2×0.5 " balls (BtC: 8.2). CrI is 51.8% $[(1493 - 720) \times 100 / 1493]$ for the blue signal, and 52.7% $[(1511 - 714) \times 100 / 1511]$ for the green signal. The intensity ratios for the (110)/(020) reflections are: 2.32 (1493 / 644) for the blue signal, and 2.26 (1511 / 670) for the green signal.

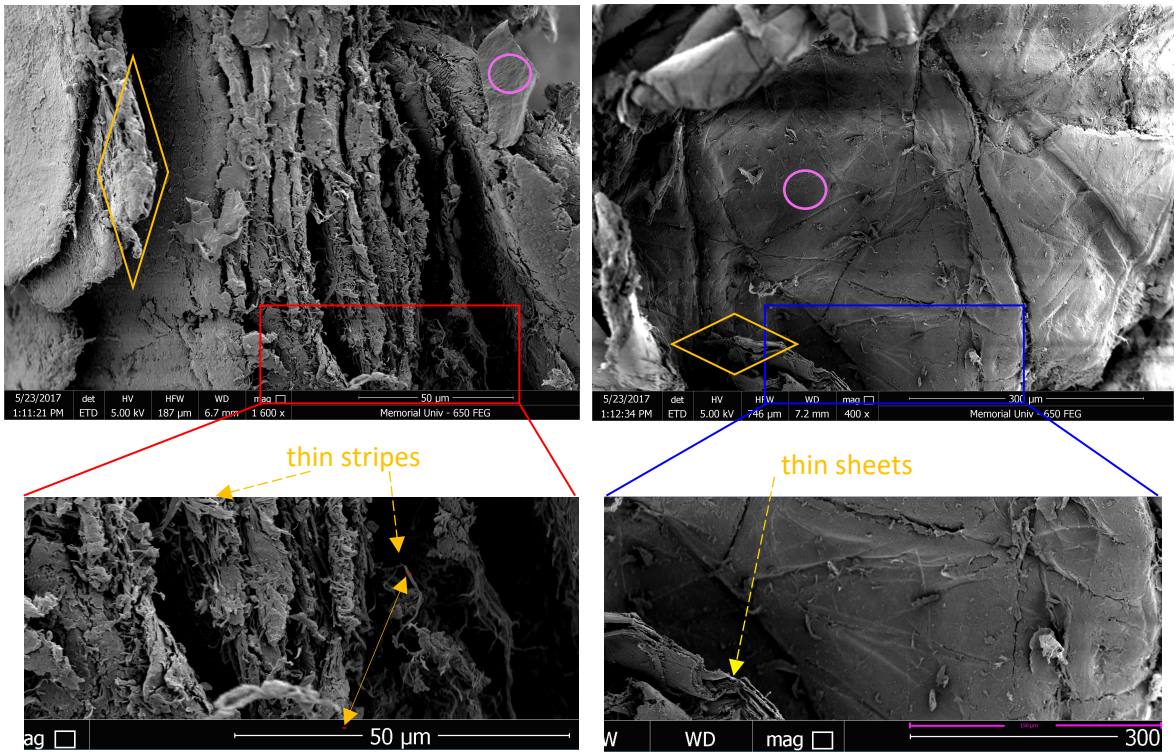


Figure A2– 10: Scanning electron microscopy (SEM) micrographs of native α -chitin. The 50 μm scale on the left corresponds to region I and the 300 μm one on the right to region II of Figure 2–13. All marks in color are discussed in Section 2.3.4.

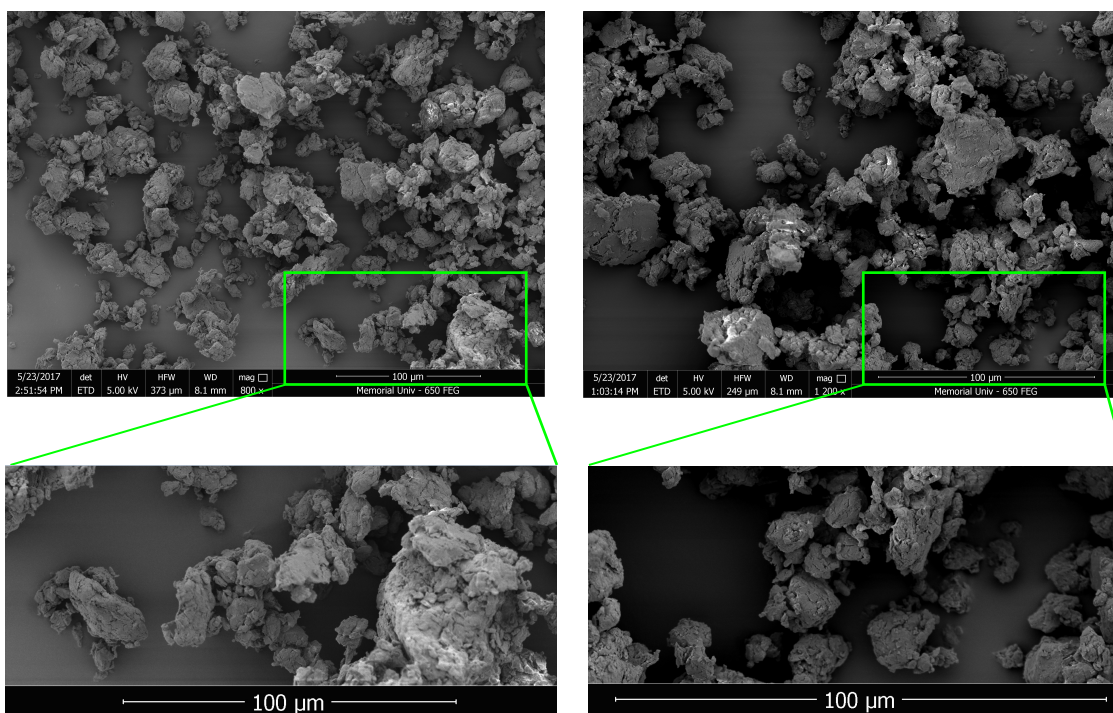


Figure A2- 11: Scanning electron microscopy (SEM) micrographs (100 μm) of ball milled α -chitin with $16 \times 0.25''$ balls for 45 (left) and 105 (right) min.

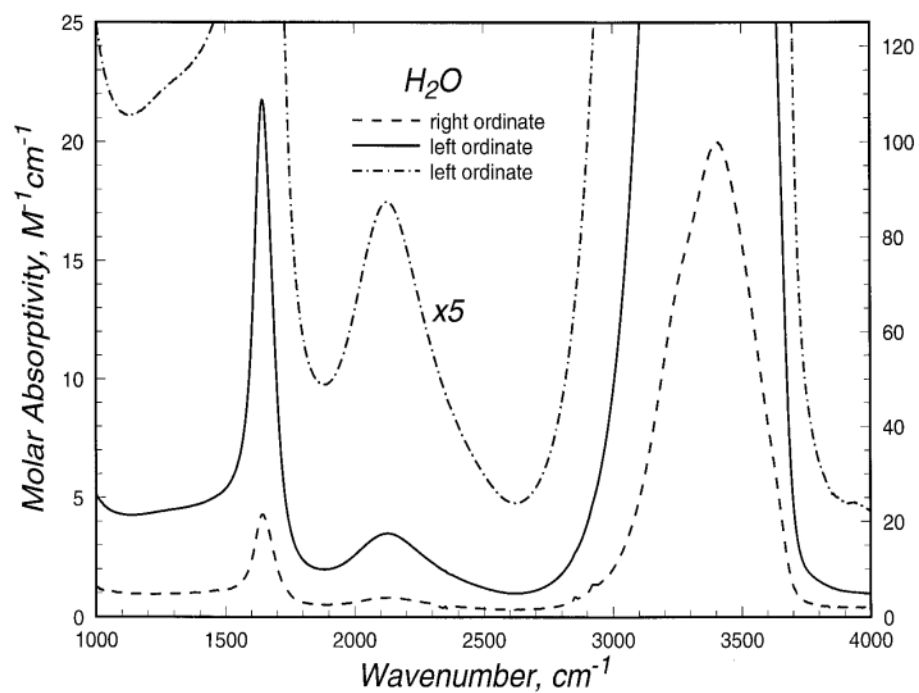


Figure A2- 12: Molar absorptivity of water in the 1000-4000 cm⁻¹ spectral range at 25 °C (ordinate is the left or right y-axis on which the signal's intensities are read). Reprinted from Analytical Biochemistry, Vol. 248, Sergei Yu. Venyaminov, Franklyn G. Prendergast, Water (H₂O and D₂O) Molar Absorptivity in the 1000-4000 cm⁻¹ Range and Quantitative Infrared Spectroscopy of Aqueous Solutions, 234-245, Copyright (1997), with permission from Elsevier.

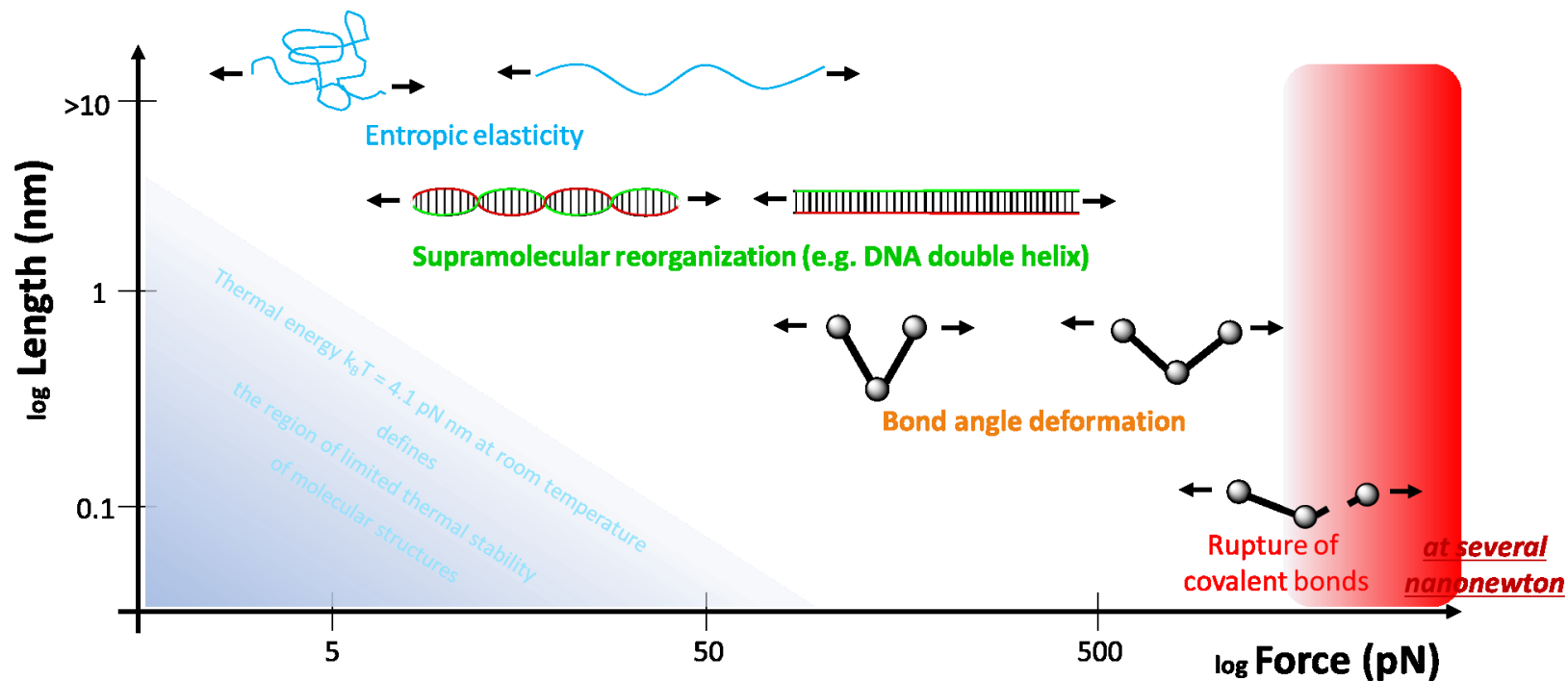


Figure A2– 13: Types of molecular transformations studied with force spectroscopy techniques. Adapted minimally from Current Opinion in Chemical Biology, 4, Hauke Clausen-Schaumann, Markus Seitz, Rupert Krautbauer and Hermann E Gaub, Force spectroscopy with single bio-molecules, 524-530, Copyright (2000), with permission from Elsevier.

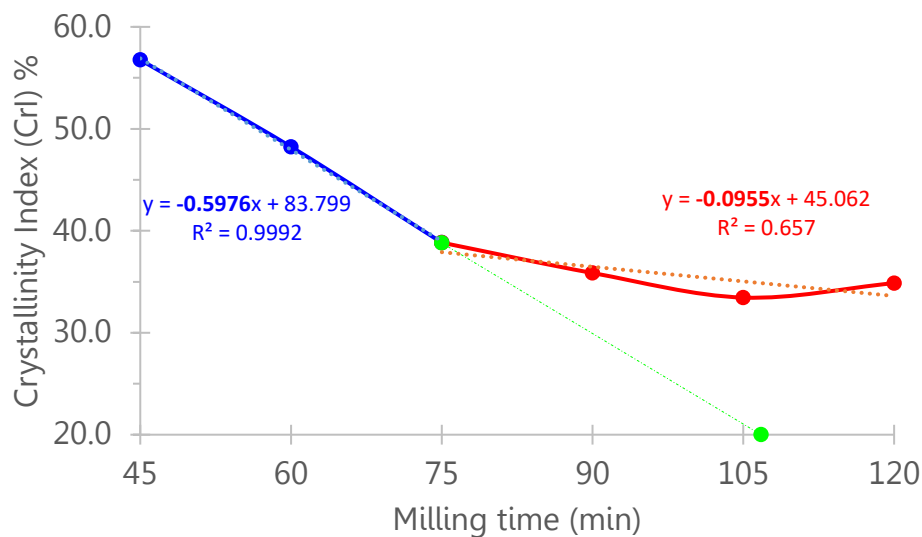


Figure A2- 14: Change in slopes of the crystallinity index (CrI %) before and after 75 min milling time for the 16 × 0.25" balls system $[(0.5976 - 0.0955) \times 100\% / 0.5976$ equals 84.0%].

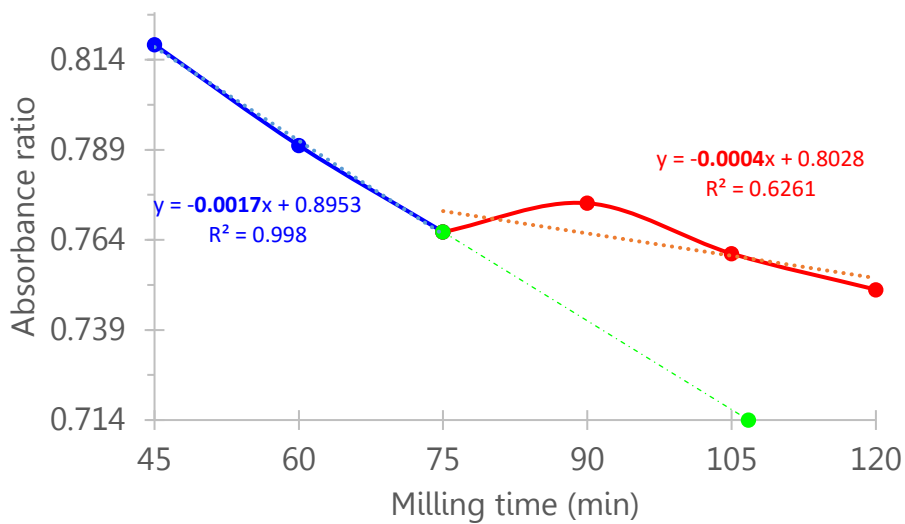


Figure A2- 15: Change in slopes of the 1621/1652 $\text{cm}^{-1}/\text{cm}^{-1}$ FT-IR absorbance ratio before and after 75 min milling time for the 16 × 0.25" balls system $[(0.0017 - 0.0004) \times 100\% / 0.0017$ equals 76.5%].

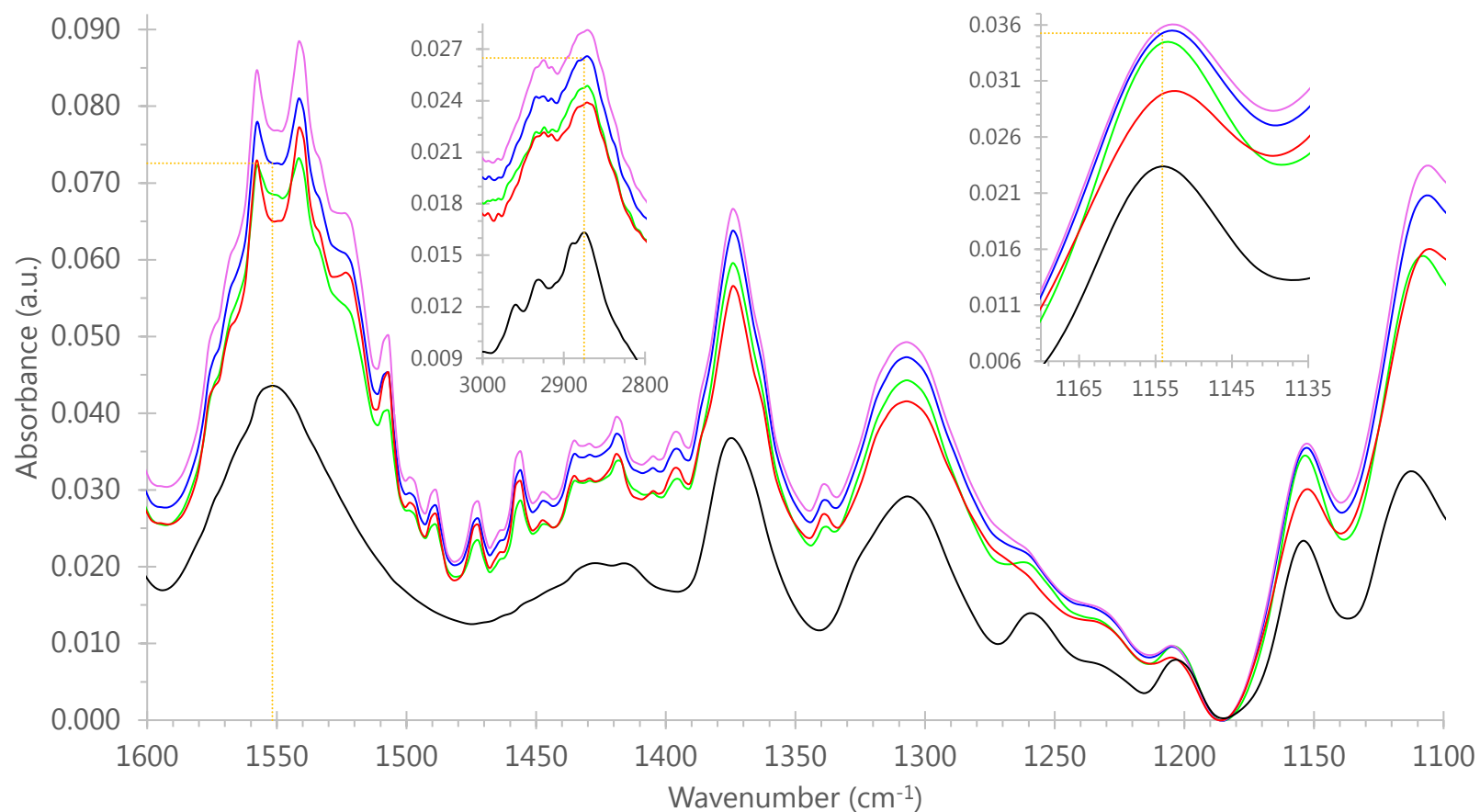


Figure A2– 16: 1600–1100 cm^{-1} region of infrared spectra of native (black signal) and milled α -chitin with $16 \times 0.25''$ balls (8.2 BtC) for 30 (green), 60 (blue), 90 (pink) and 120 (red) min. Insets show the reference band (3000–2800 cm^{-1}) and glycosidic linkage (1170–1135 cm^{-1}) regions. Orange dotted lines highlight the intensities for reproduction of the ratios which probe depolymerization and deacetylation for the 60 min sample (see Figures 2–19 and 2–20).

Table A2– 1: Solubility results of α -chitin samples milled with $2 \times 0.5''/70 \times 0.25''$ balls (17.7% packing) for two distinct milling times (1 and 5 h) [stirring time 120,^{cc} 30, 3 (vortex) min].

Milling time (h)	Stirring time (min)	Solubility %	Average solubility %	St. deviation	RSD %
1	120	12.21	12.23	1.18	9.64
	30	13.42			
	3 (vortex)	11.07			
5	120	29.01	29.16	1.14	3.90
	30	28.10			
	3 (vortex)	30.36			

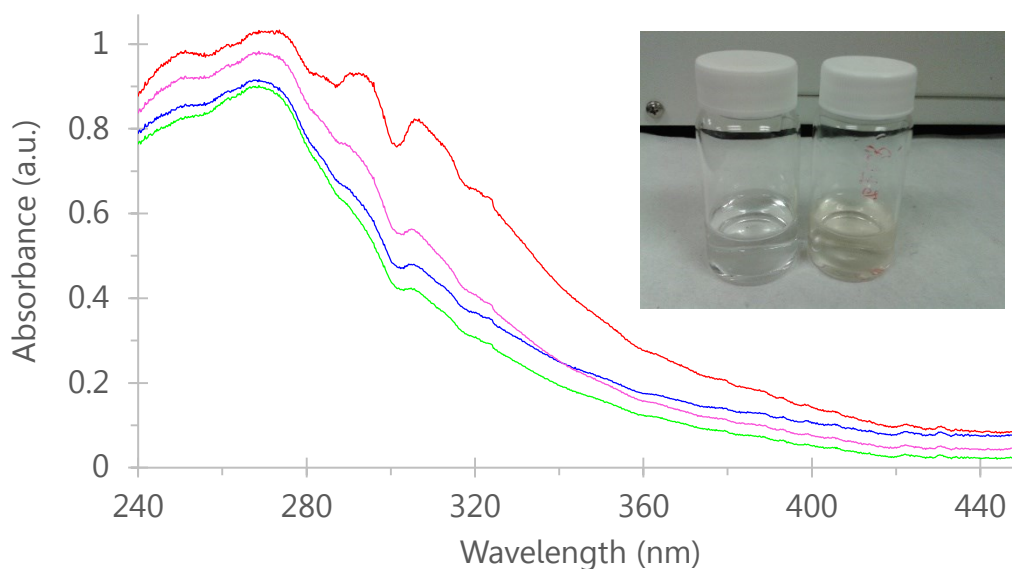


Figure A2– 17: UV-Vis spectra of soluble products of milled α -chitin with $16 \times 0.25''$ balls (8.2 BtC) for 30 (green), 60 (blue), 90 (pink) and 120 (red) min. Inset shows a photo of the color of 0 min (left vial), and 120 min (right vial) soluble products (at pH 7.0).

^{cc} When monitoring the temperature of the stirred mixture (ca. 250 mg chitin in 7.5 mL aqueous solvent), a 5.0 ± 0.8 °C increase (from room temperature) was recorded during the 120 minutes of the test [observed for six α -chitin samples (milled with 17.7% packing for: 3 min, 2-3-4-6-8 h)]. Interestingly, the rise was steeper in the first hour of the test (ca. 3.5 °C). Future researchers might use that experimental evidence to formulate the hypothesis of whether the solvation of chitin (and maybe polysaccharides in general) is an exothermic process.

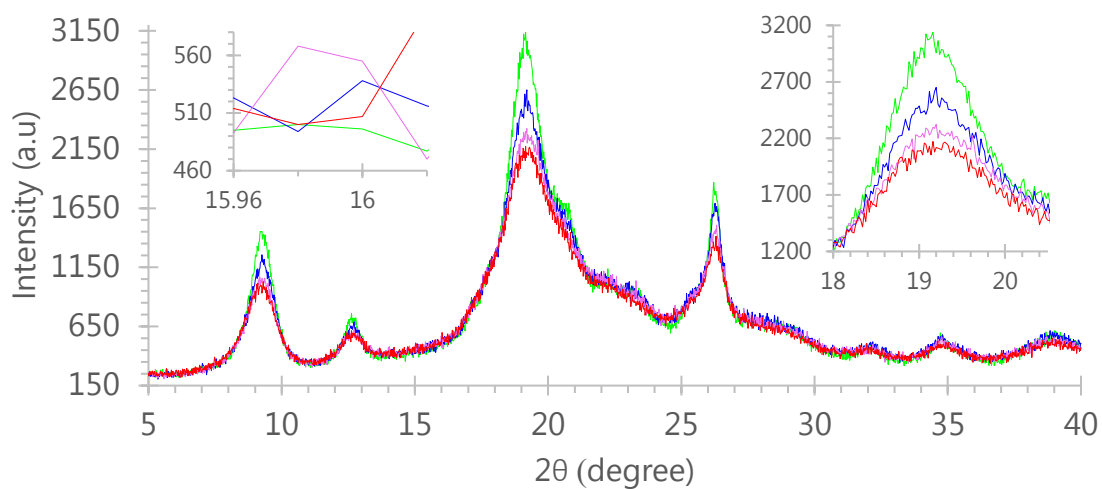


Figure A2– 18: X-ray diffraction patterns (no separation) of the insoluble residue from the pH 7.0 solubility tests of milled α -chitin with $16 \times 0.25''$ balls for 30 (green), 60 (blue), 90 (pink) and 120 (red) min (8.2 BtC). The crystallinity indices are: 83.2% $[(2957 - 496) \times 100 / 2957]$ for $t = 30$ min (green), 79.7% $[(2651 - 538) \times 100 / 2651]$ for $t = 60$ min (blue), 76.12% $[(2324 - 555) \times 100 / 2324]$ for $t = 90$ min (pink), and 76.08% $[(2120 - 507) \times 100 / 2120]$ for $t = 120$ min (red).

Appendix A3

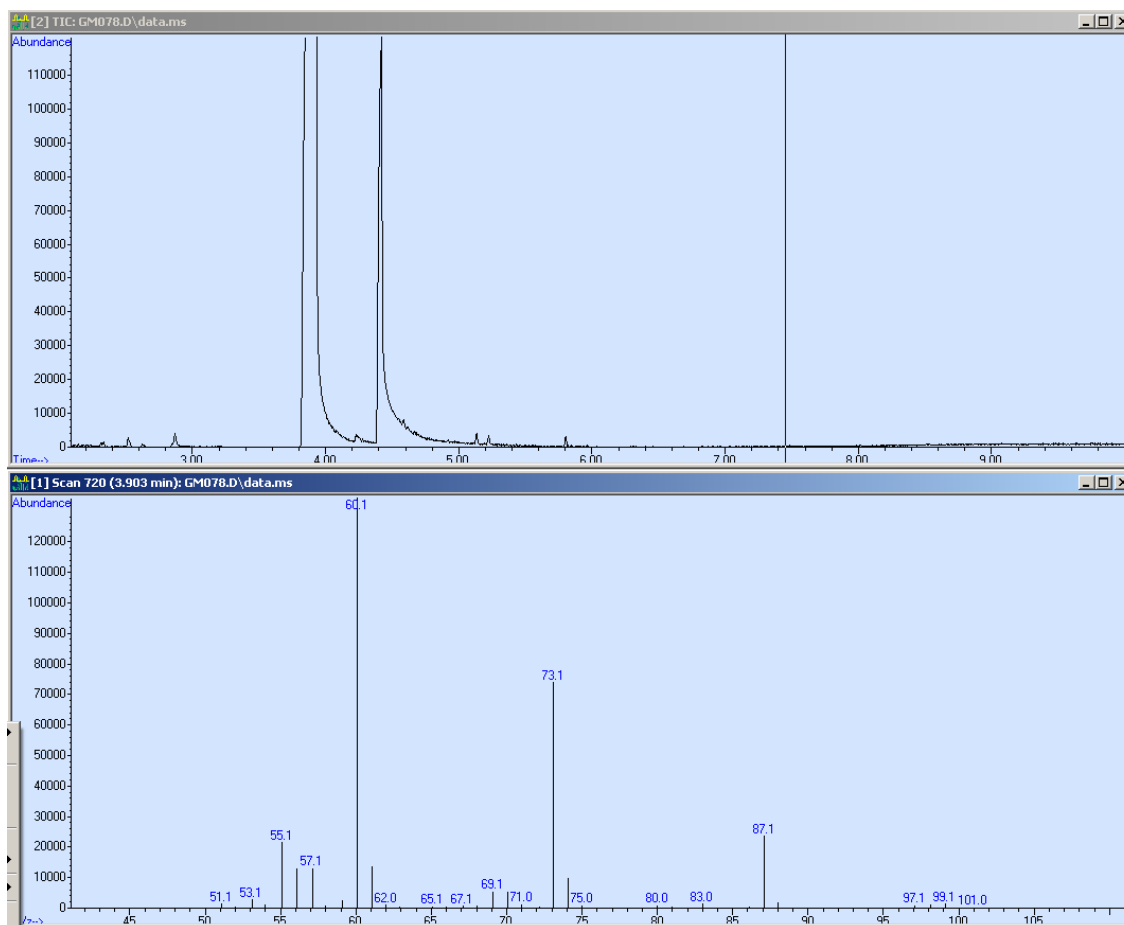


Figure A3- 1: Gas chromatogram of the EtOAc-extracted reaction mixture which was generated when the microwave method was applied to the 8 h milled (17.5% packing/42.8 BtC) α -chitin sample. Mass spectrum of the 3.903 min peak corresponds to hexanoic acid (HA).¹

1. National Institute of Standards and Technology (NIST), NIST Chemistry WebBook,

Standard Reference Database Number 69,

<https://webbook.nist.gov/cgi/cbook.cgi?ID=C142621&Units=SI&Mask=200#Mass->

[Spec](#), (accessed 06/05, 2018).

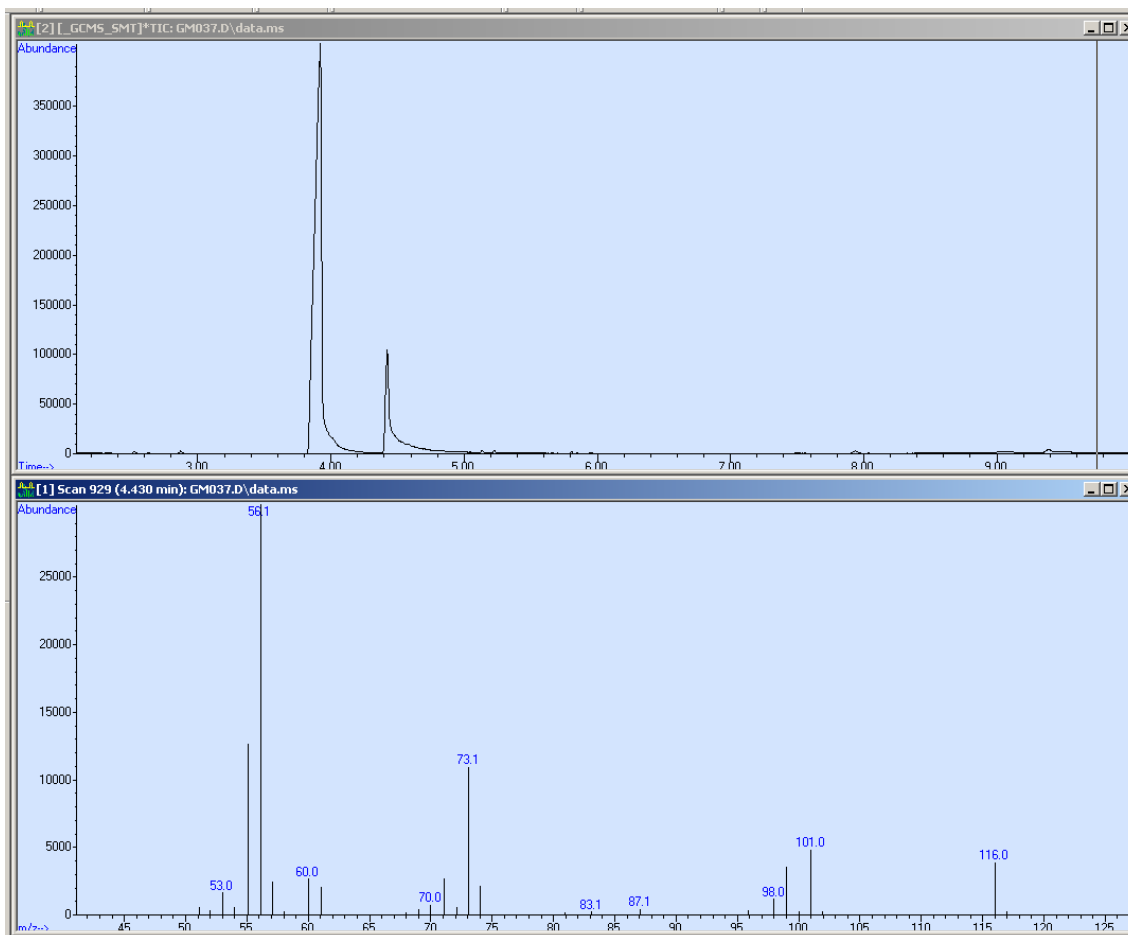


Figure A3– 2: Gas chromatogram of the EtOAc-extracted reaction mixture which was generated when the microwave method was applied to the 5 h milled (17.5% packing/42.8 BtC) α -chitin sample. Mass spectrum of the 4.430 min peak corresponds to levulinic acid (LA).²

2. Omari, K. W.; Besaw, J. E.; Kerton, F. M. Hydrolysis of chitosan to yield levulinic acid and 5-hydroxymethylfurfural in water under microwave irradiation. *Green Chem.* 2012, 14, (5), 1480-1487.

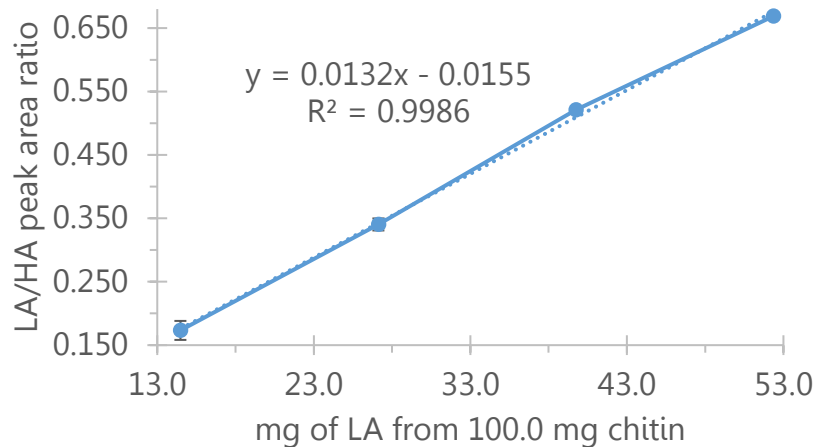


Figure A3– 3: Calibration curve for LA yields from 100 mg of chitinous sample (prepared according to data of Table A3–1).

Table A3– 1: Chromatographic data (peak areas of duplicate injections) for standard solutions of levulinic acid (LA) used to prepare the calibration curve (cc) of Figure A3–3. Standard solution cc1 (0.11 mg/ml LA) was too dilute for the analyte peak to be quantified.

Measured quantity		Solution				
		cc1	cc8	cc15	cc22	cc29
Volume (µl)	EtOAc	10000	10000	10000	10000	10000
	LA	1	8	15	22	29
	HA					
	total	10019	10026.3	10033.3	10040.3	10047.3
Mass (mg)	LA	1.13	9.07	17.01	24.95	32.89
	HA					
Conc. (mg/ml)	LA	0.113	0.905	1.695	2.485	3.273
	HA	1.70	1.70	1.69	1.69	1.69
LA concentration × 16 (mg/100 mg α-chitin)			14.5	27.13	39.76	52.37
Peak area 1	HA	t	17875079	17671883	17805747	18224168
	LA	o	2908113	5896181	9302646	12135719
	ratio	o	0.163	0.334	0.522	0.666
Peak area 2	HA	d	15777171	17143482	18533243	18220970
	LA	i	2900998	5949766	9627943	12244410
	ratio	l	0.184	0.347	0.519	0.672
Average ratio		u	0.173	0.340	0.521	0.669
Standard deviation		e	0.015	0.009	0.002	0.004
RSD %			8.64	2.79	0.40	0.64

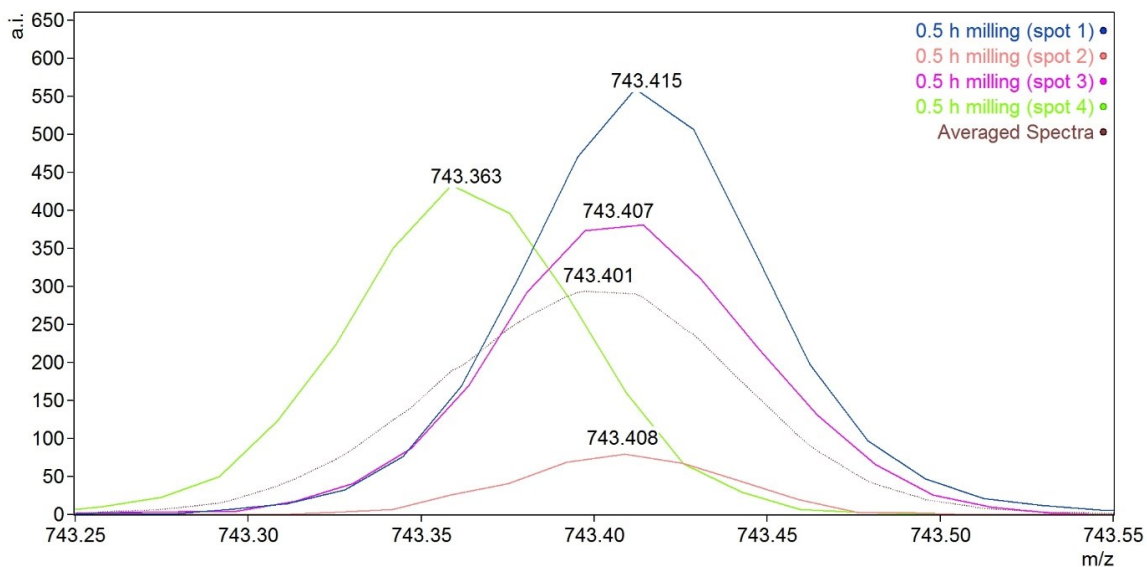


Figure A3- 4: Averaging of the chitin trimer-derivative peak in the 0.5 h milling sample ($2 \times 0.5'' / 68-70 \times 0.25''$ balls, with kaolinite) using the relevant mMass function.

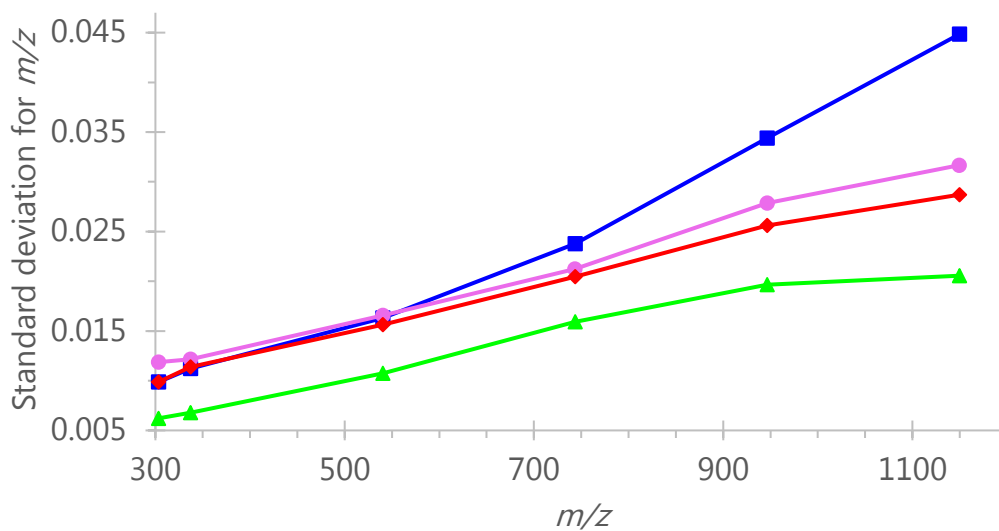


Figure A3- 5: m/z precision for the MALDI-TOF MS method. Number of spectra (among spots) are $n=4$ for 0.5 (blue \square), $n=4$ for 4 (pink \circ), $n=5$ for 2 (red \diamond), $n=7$ for 6 (green Δ) h milling soluble product samples ($2 \times 0.5'' / 68-70 \times 0.25''$ balls, with kaolinite). Exact masses of the analytes are shown in Figure A3-25.

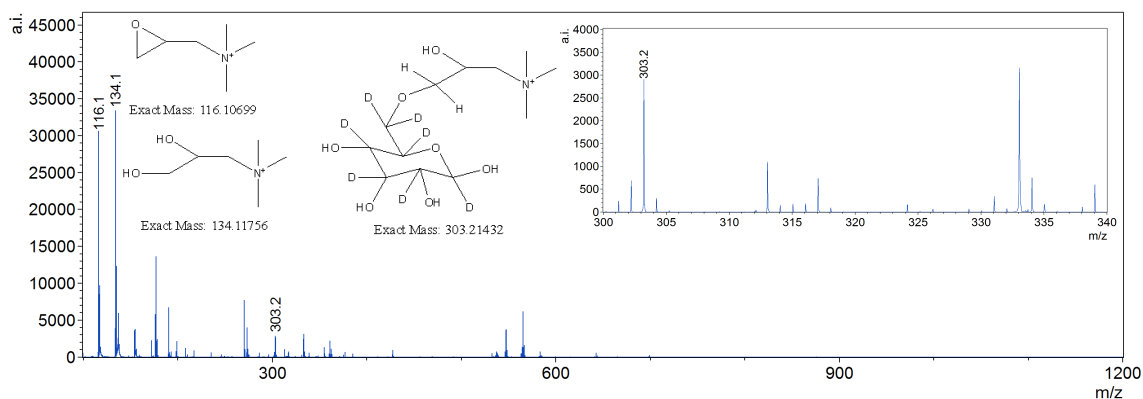


Figure A3– 6: Average MALDI-TOF MS spectra for blank derivatization reaction with structures and exact masses of assigned peaks. Inset focuses on m/z 300–340.

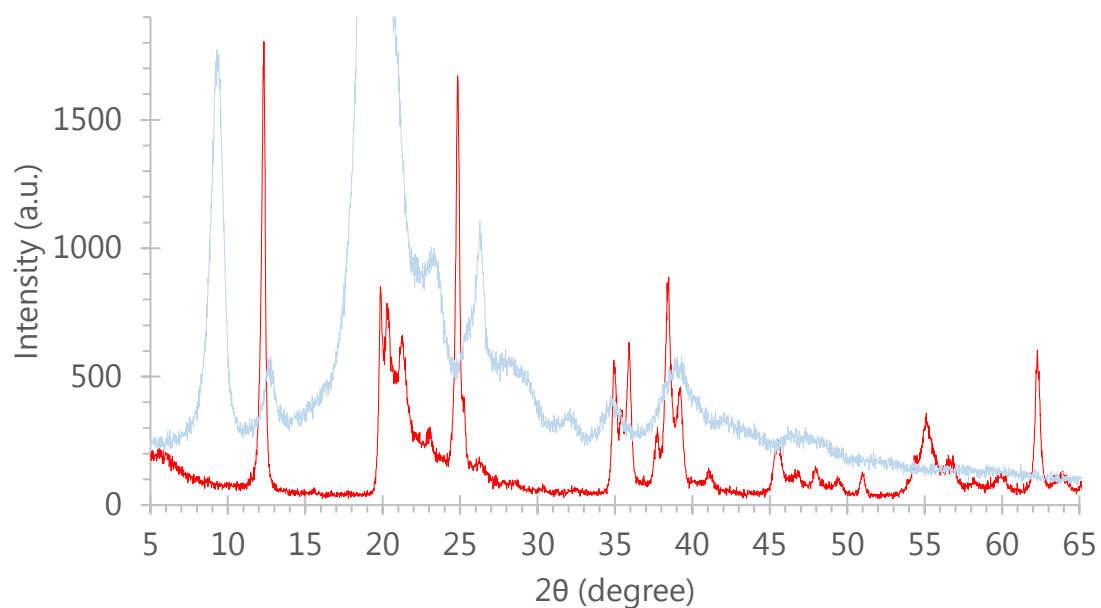


Figure A3– 7: X-ray diffraction (XRD) patterns (from 5 to 65° 2θ) of kaolinite (red signal) and native α -chitin (transparent light blue signal). Kaolinite does not exhibit any significant peaks for 2θ higher than 65°.

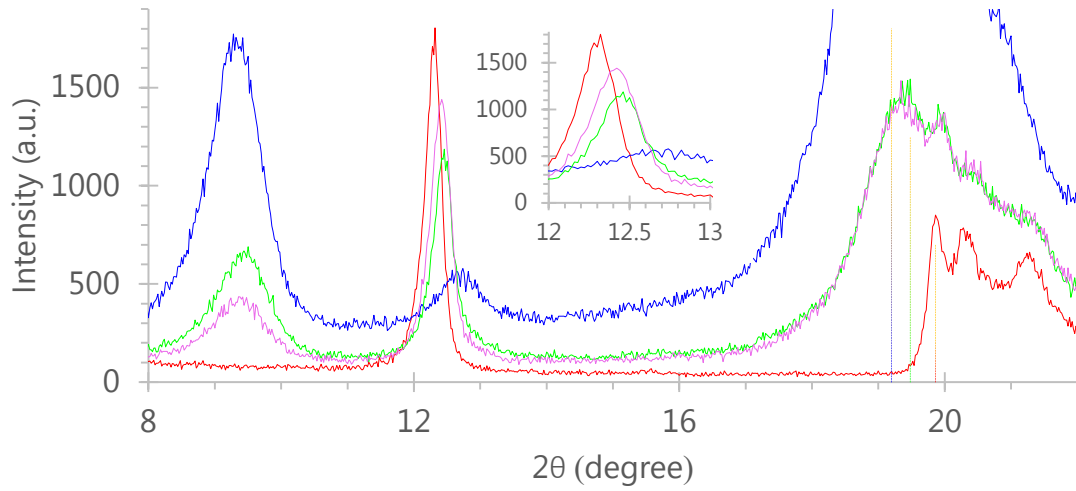


Figure A3– 8: XRD patterns (from 8 to 22° 2θ) of kaolinite (red signal), native α -chitin (blue), 1:1 chitin:kaolinite mixture (green), and 1:1 chitin:kaolinite mixture (0.5g) mortared for 4 min (pink).

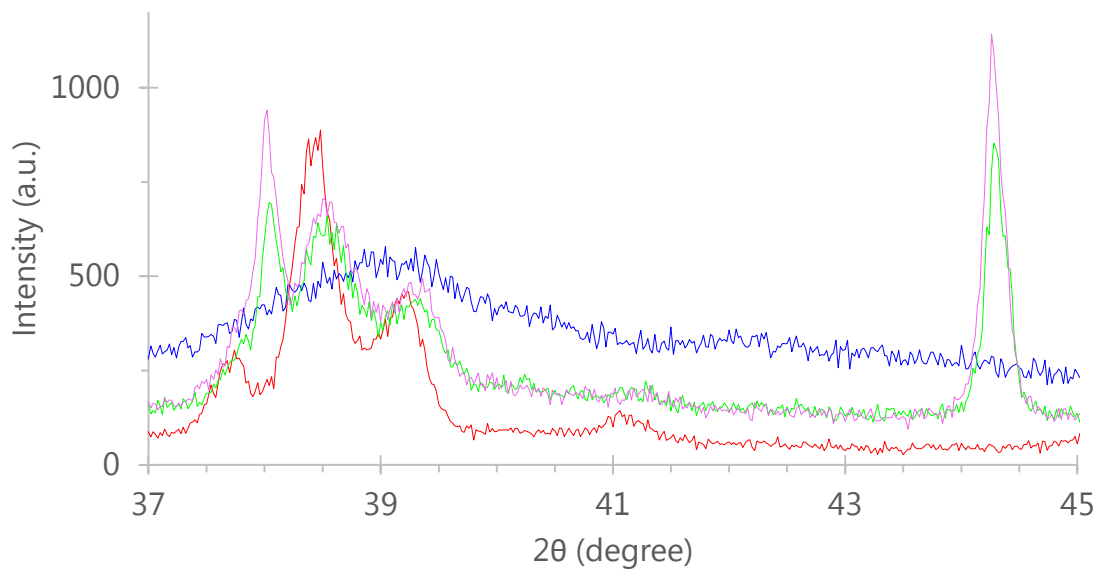


Figure A3– 9: XRD patterns (from 37 to 45° 2θ) of kaolinite (red signal), native α -chitin (blue), 1:1 chitin:kaolinite mixture (green), 1:1 chitin:kaolinite mixture (0.5g) mortared for 4 min (pink).

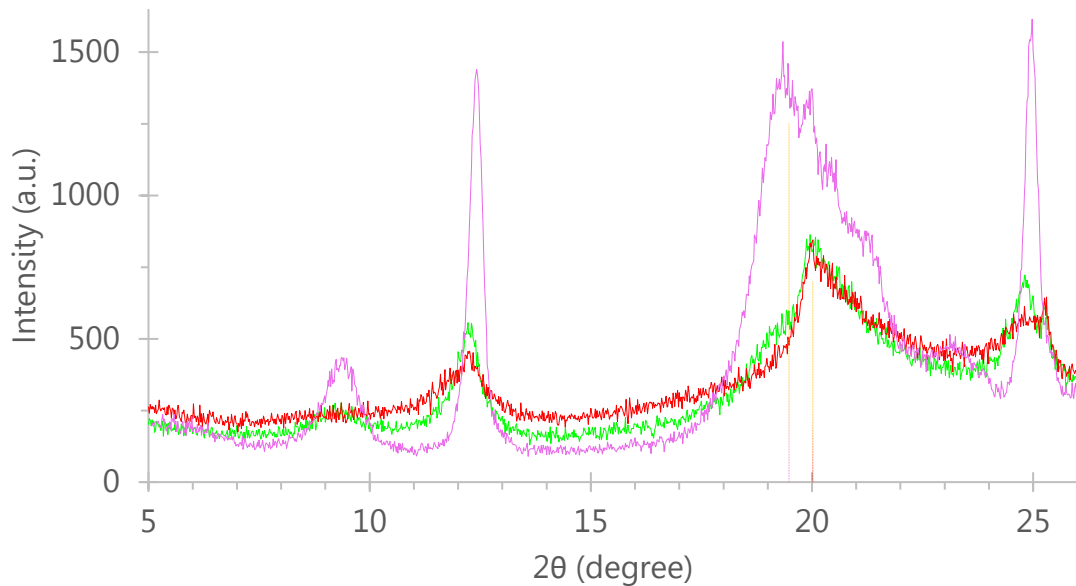


Figure A3– 10: XRD patterns (from 5 to 26° 2θ) of 1:1 chitin:kaolinite mixture (0.5g) mortared for 4 min (pink signal) when milled with 2×0.5" balls (8.2 BtP) for 30 (green) and 90 (red) min.

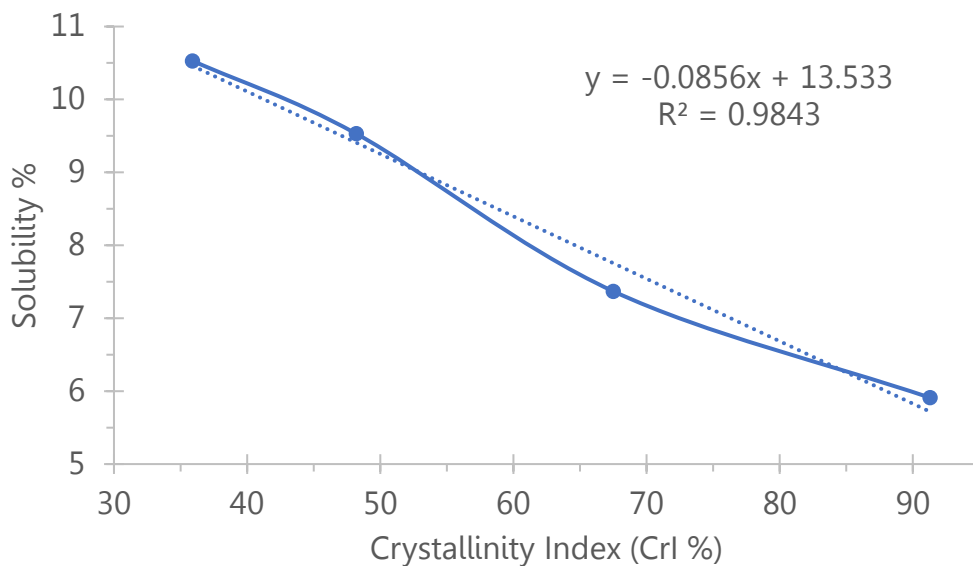


Figure A3– 11: Correlation between crystallinity index (CrI%) and solubility % for α-chitin. Data based on milling with 16×0.25" balls (8.2 BtC, see Chapter 2).

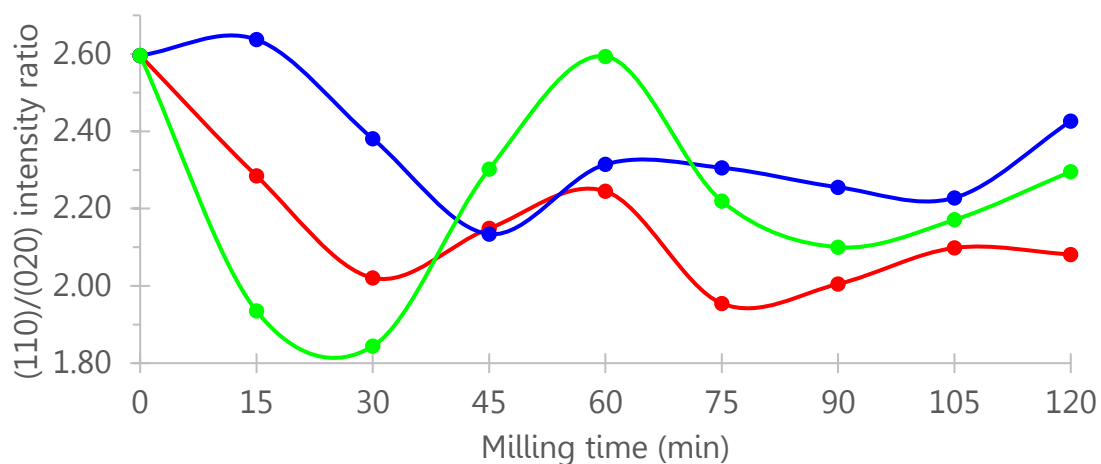


Figure A3- 12: Intensity ratio for reflections (110)/(020) over milling time (min) for 1x0.5\"/>

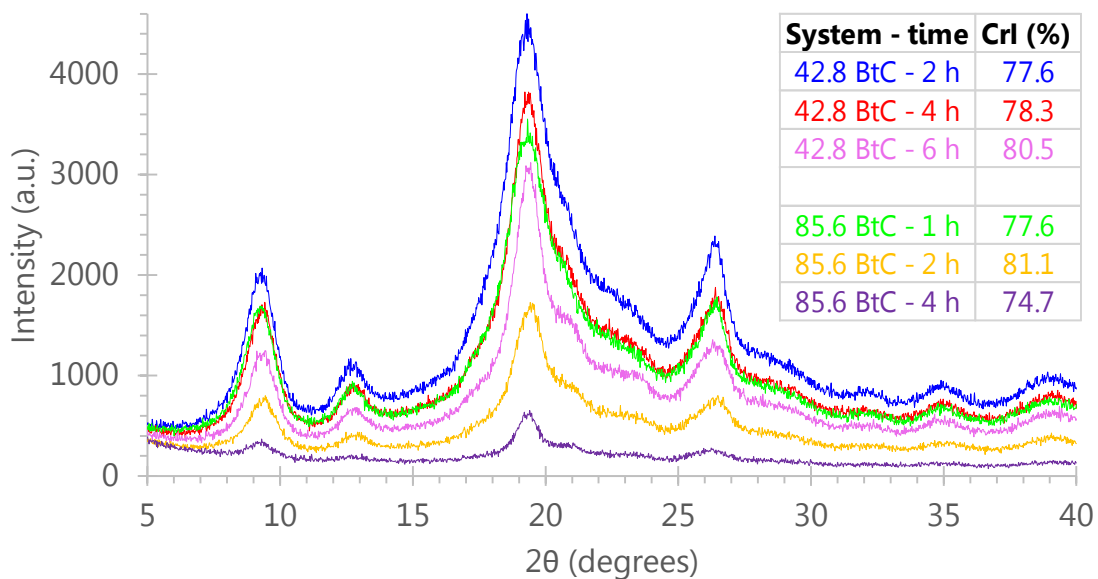


Figure A3- 13: X-ray diffraction patterns (no separation) of the insoluble residue from the pH 7.0 solubility tests of milled α -chitin with 68–70x0.25\"/>

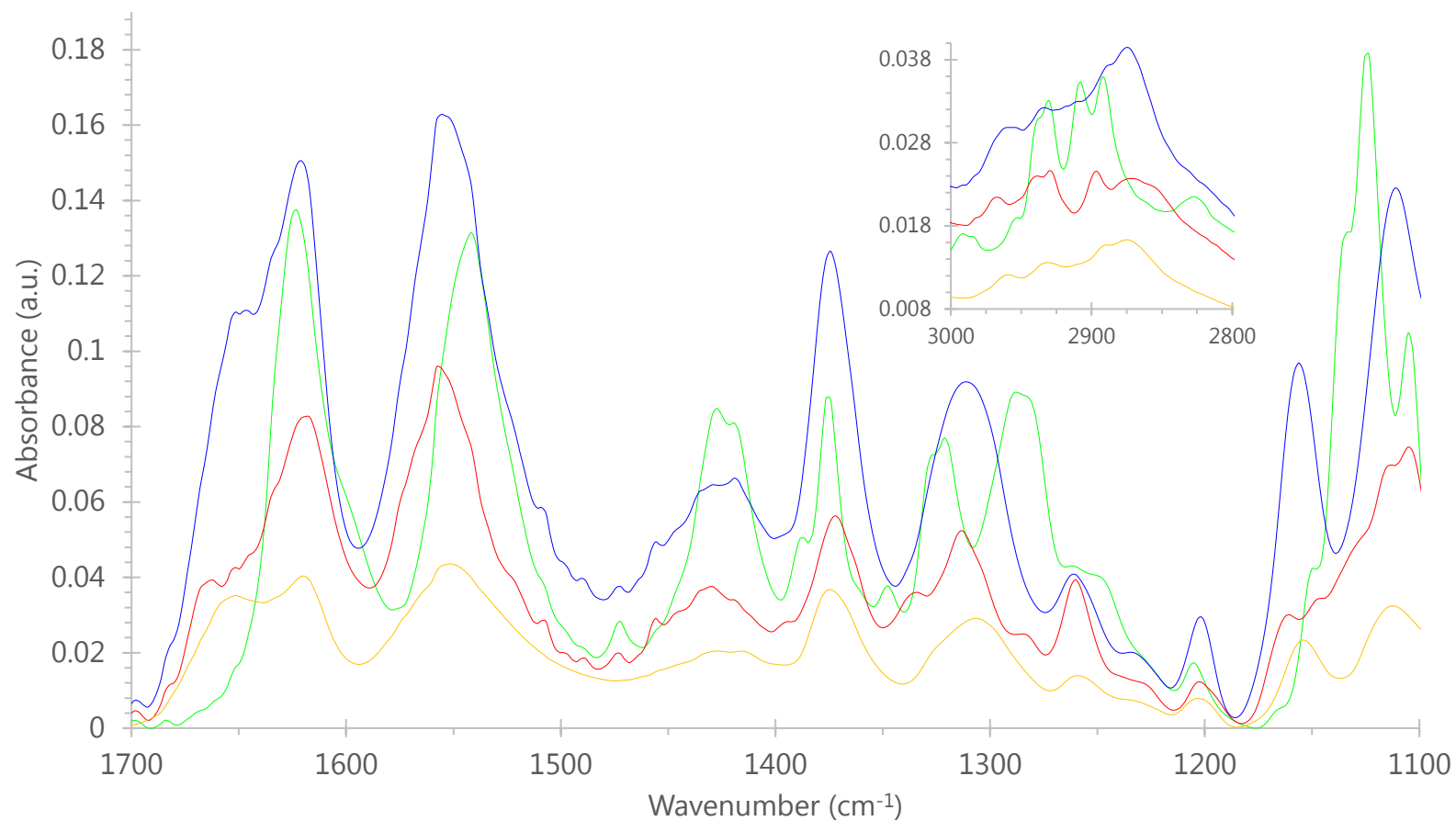


Figure A3– 14: 1700–1100 cm^{-1} region of infrared spectra of native α -chitin (orange), NAG₅ (blue), NAG₂ (red), and NAG (green). Inset shows the carbon-hydrogen region (3000–2800 cm^{-1}) for reference.

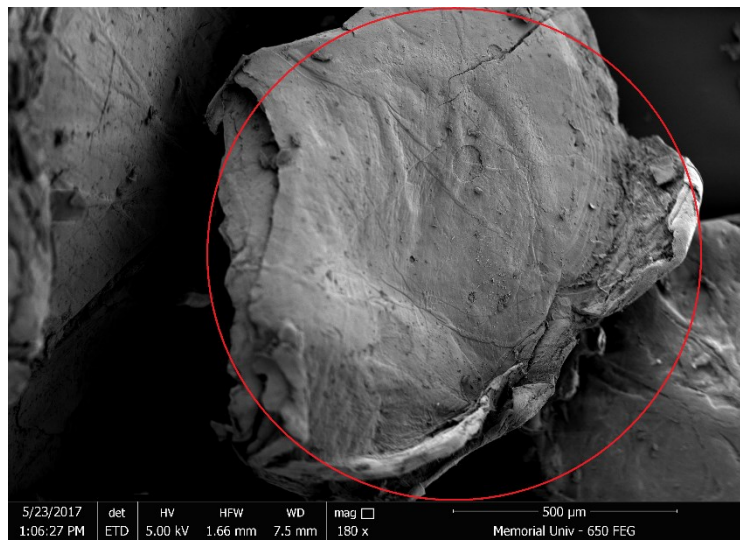


Figure A3– 15: Scanning electron microscopy (SEM) micrograph of native α -chitin particle (500 μ m scale). Red circle approximates the contact surface area (Hertz radius 620 μ m) when impacted from a 0.5" steel ball (3.9 m/s velocity) in a SPEX system.

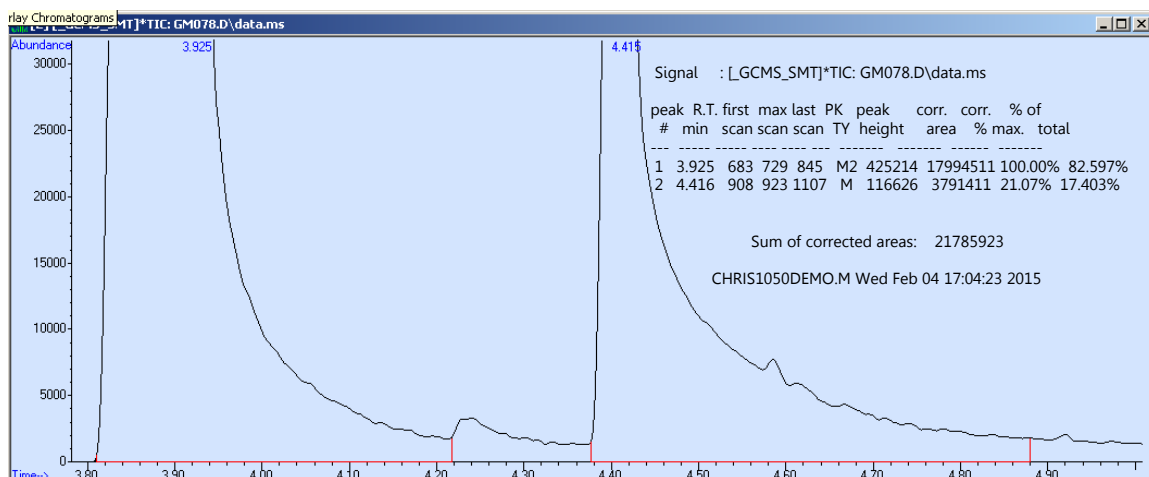


Figure A3– 16: Gas chromatogram of the first (of two) extract of the 8 h milled α -chitin reaction mixture. LA/HA peak area ratio is 0.211 (3791411 / 17994511), which translates to 17.2 wt.% LA from the chitinous sample.

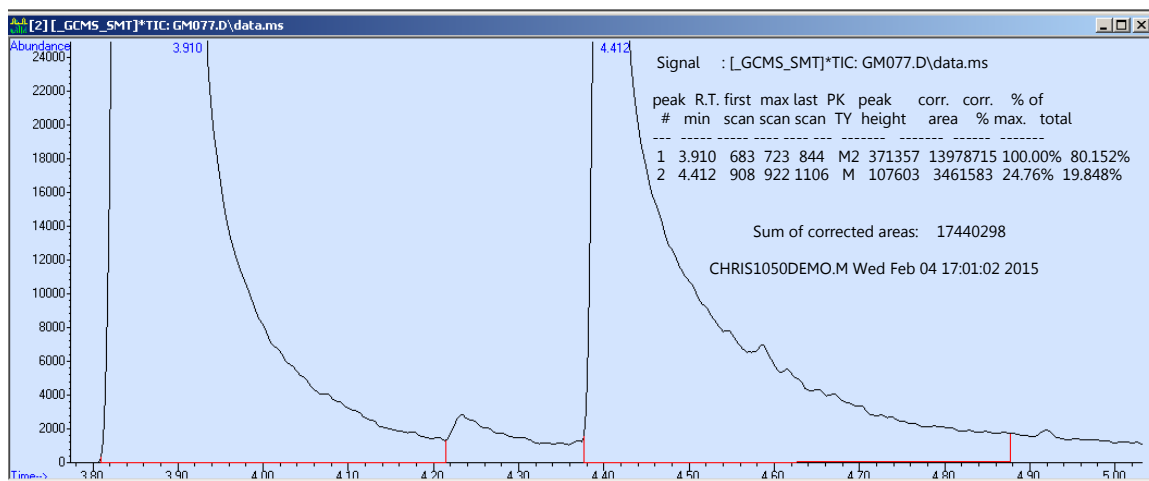


Figure A3– 17: Gas chromatogram of the second (of two) extract of the 8 h milled α -chitin reaction mixture. LA/HA peak area ratio is 0.248 (3461583 / 13978715), which translates to 20.0 wt.% LA from the chitinous sample.

Table A3– 2:Chromatographic results (peak areas) for LA production from 6 chitinous samples (reproducibility of microwave reaction was tested with triplicates on native α -chitin). Yield (mg LA) is obtained by application of the LA/HA peak area ratio to the equation of Figure A3–3, and then corrected with respect to the corresponding chitinous sample mass (corrected yields are plotted in Figure 3–13). Chitosan is Sigma Aldrich's high-MW product.

Measured quantity	Chitosan	Chitosan (4 h)	α -Chitin (i)	α -Chitin (ii)	α -Chitin (iii)	α -Chitin (4 h)	α -Chitin (5 h)	α -Chitin (8 h)
Chitinous sample (g)	0.1001	0.0855	0.0998	0.1015	0.0997	0.1061	0.1000	0.0991
SnCl ₄ 5 H ₂ O (g)	0.0850	0.0853	0.0824	0.0911	0.0836	0.0836	0.0851	0.1168
HA peak area	15679659	16786907	15390049	16367305	17235882	18802425	16156850	16561678
LA peak area	5814915	4396101	3153051	4027362	3031557	3620620	4014384	3914900
LA/HA peak area ratio	0.371	0.262	0.205	0.246	0.176	0.193	0.248	0.236
Yield (mg LA)	29.3	21.0	16.7	19.8	14.5	15.8	20.0	19.1
Corrected yield (wt.%)	29.2	24.6	16.7	19.5	14.5	14.9	20.0	19.3

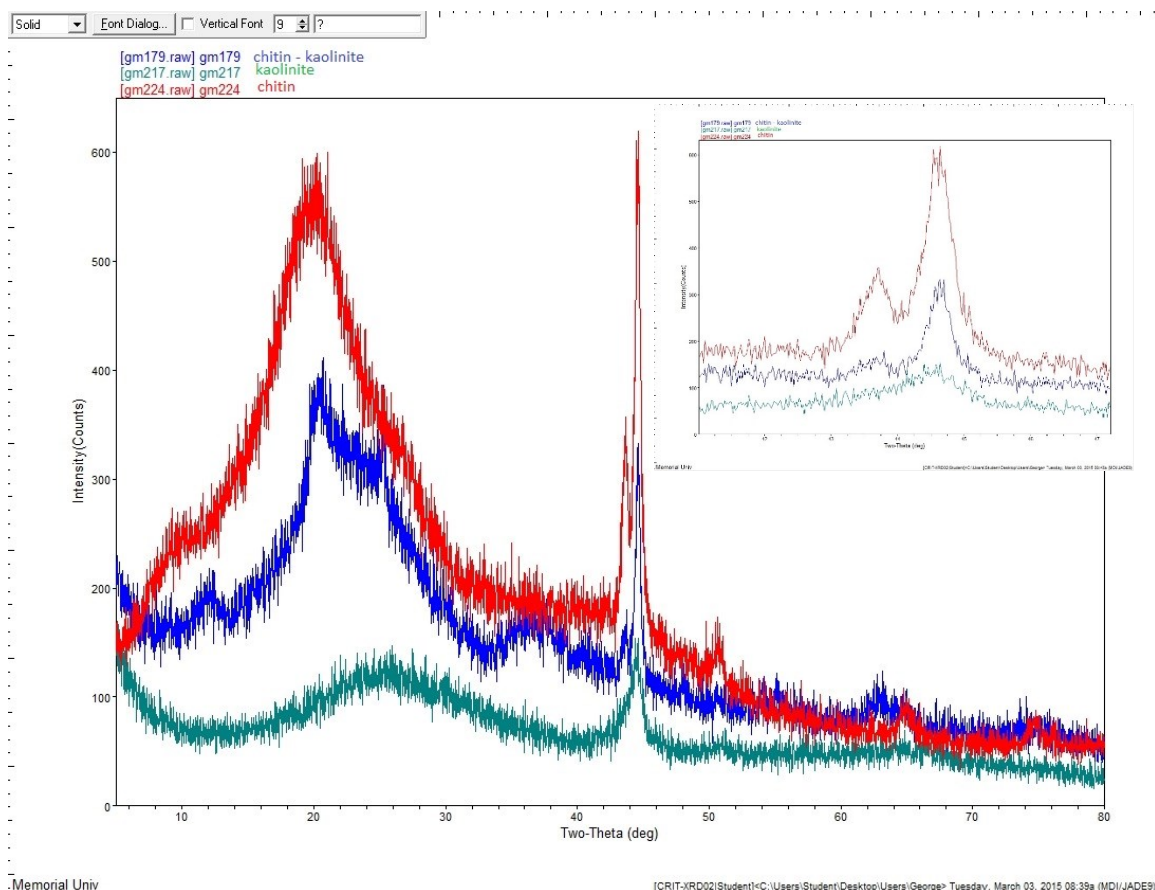


Figure A3– 18: XRD patterns (from 5 to 80° 2 θ , no separation) of α -chitin (red), and kaolinite (green) when milled with 68–70 \times 0.25" / 2 \times 0.5" balls [17.5% packing, 85.6 balls-to-powder (BtP) mass ratio] for 4 h, as well as 1:1 α -chitin:kaolinite mixture (blue) milled with 42.8 BtP (same packing) for the same time. Inset shows the region from 41 to 47° 2 θ in more detail.

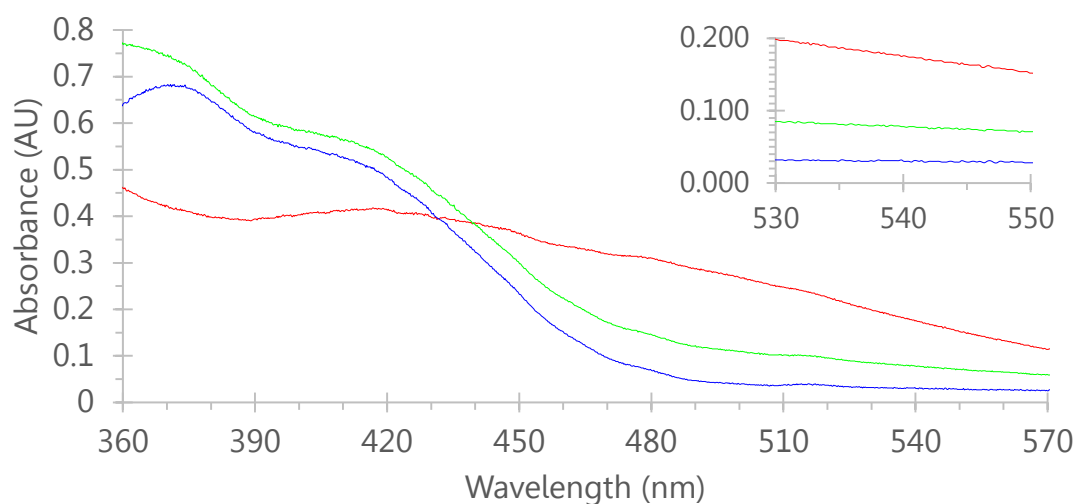


Figure A3– 19: UV-Vis spectra of 1500 μL of a 1.86 mM glucose solution after being reacted upon microwave irradiation for 5 min at 100 $^{\circ}\text{C}$ with 1500 μL IUPAC-like DNS reagents [0.088 mM 3,5-dinitrosalicylic acid, ca. 0.9 M tartaric acid disodium salt dihydrate, 62 mM phenol, 32 mM $\text{Na}_2\text{S}_2\text{O}_5$] of the following pH values: 12.80 (blue), 13.24 (green), and 13.60 (red). Inset focuses on the 530–550 nm region.

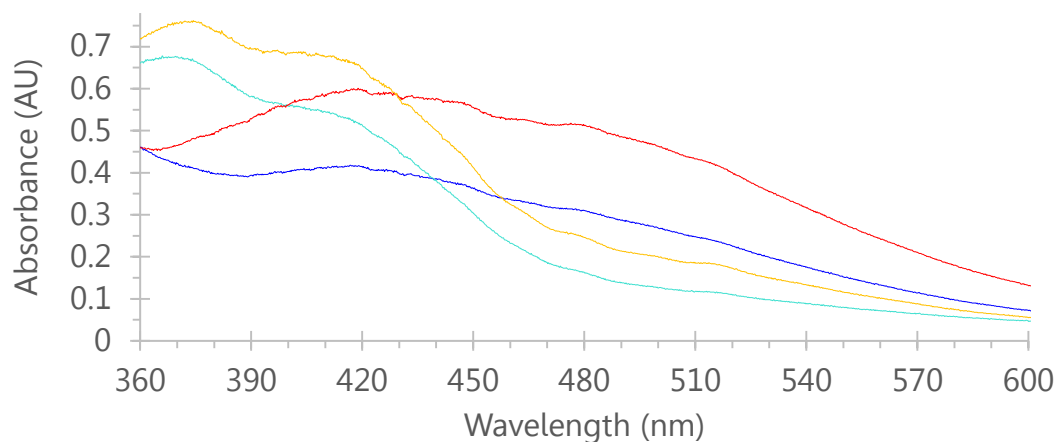


Figure A3– 20: UV-Vis spectra of 1500 μL of 1.86 (blue/red) and 0.93 (turquoise/orange) mM glucose solutions after being reacted upon microwave irradiation for 5 min at 100 $^{\circ}\text{C}$ with 1500 μL IUPAC-like [blue/turquoise; 0.088 mM 3,5-dinitrosalicylic acid, 0.40 M NaOH, ca. 0.9 M tartaric acid disodium salt dihydrate, 62 mM phenol, 32 mM $\text{Na}_2\text{S}_2\text{O}_5$] and sulfite-free [red/orange; 0.088 mM 3,5-dinitrosalicylic acid, 0.39 M NaOH, 0.77 M tartaric acid disodium salt dihydrate, 18 mM phenol] DNS reagents.

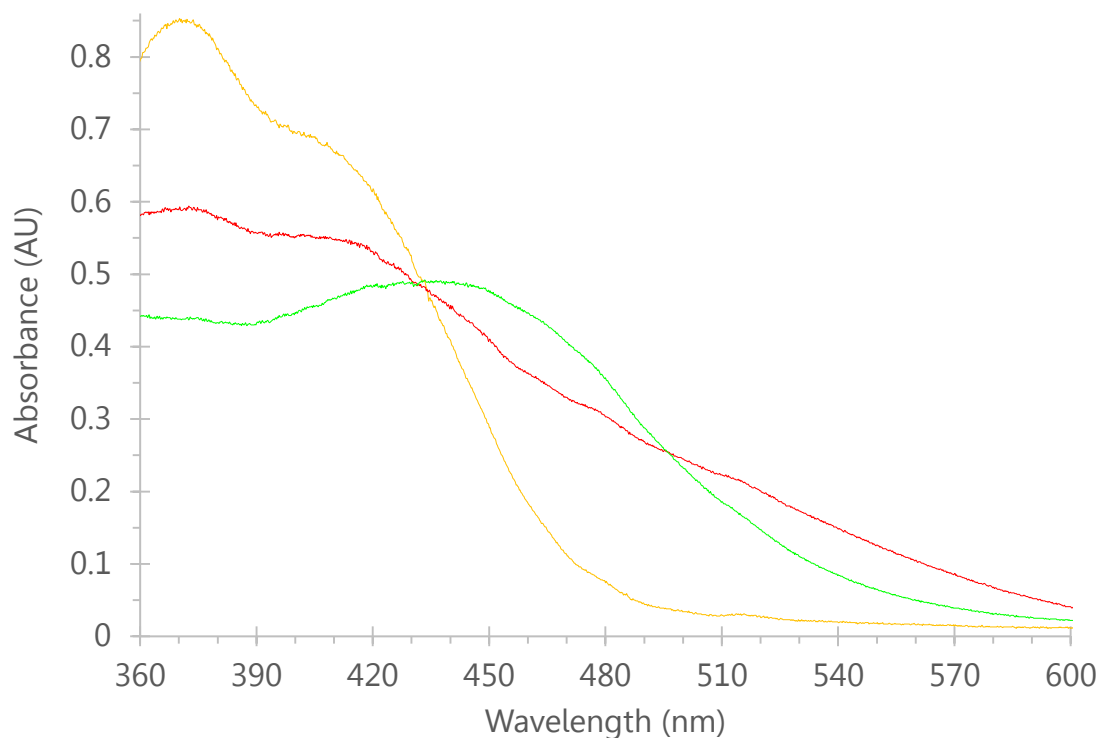


Figure A3– 21: UV-Vis spectra of 1500 μL of 0.72 mM *N*-acetyl-D-glucosamine solutions after being reacted upon microwave irradiation for 5 min at 100 $^{\circ}\text{C}$ with 1500 μL phenol-free DNS reagent [green; 0.088 mM 3,5-dinitrosalicylic acid, 0.375 M NaOH (pH 13.57), 1.068 M tartaric acid disodium salt dihydrate] and phenol-containing DNS reagent [red; 0.088 mM 3,5-dinitrosalicylic acid, 0.386 M NaOH (pH 13.59), 0.766 M tartaric acid disodium salt dihydrate, 17.8 mM phenol]. Signal in orange is for the initial reaction mixture (before the application of microwave irradiation).

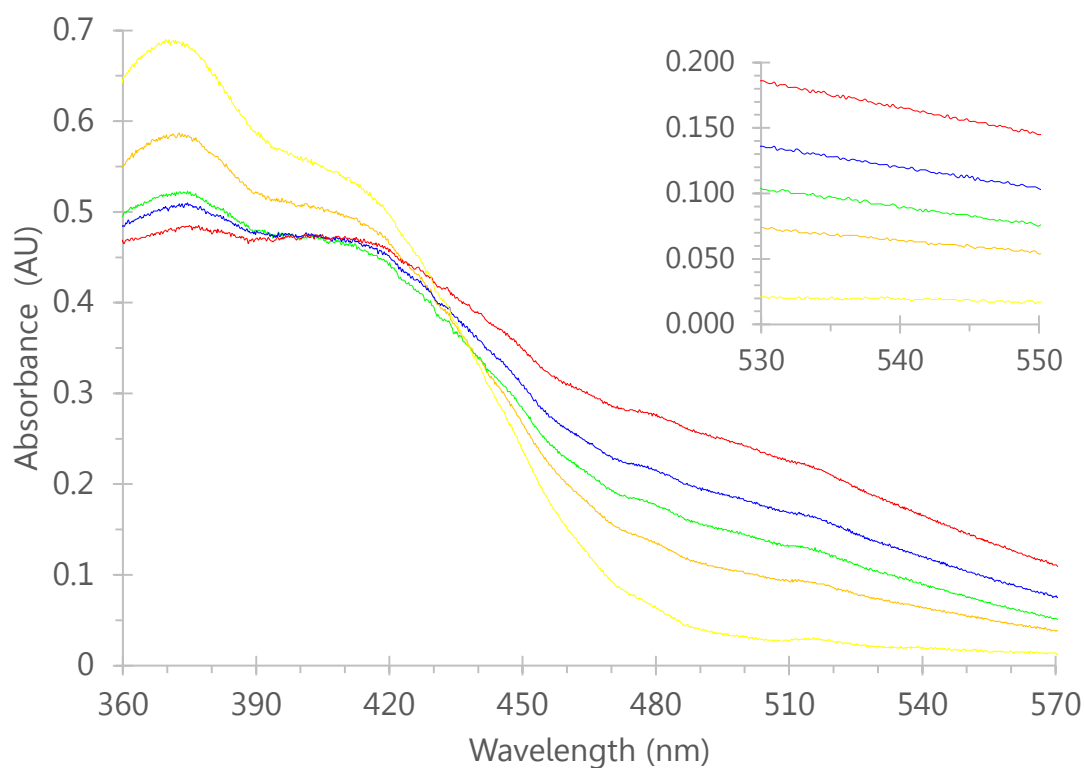


Figure A3– 22: UV-Vis spectra of 1500 μL standard glucose solutions of 0.964 (orange), 1.094 (green), 1.224 (blue), 1.483 (red) mM after being reacted upon microwave irradiation for 5 min at 100 $^{\circ}\text{C}$ with 1500 μL DNS reagent B [0.088 mM 3,5-dinitrosalicylic acid, 0.3997 M NaOH (pH 13.60), 1.063 M tartaric acid disodium salt dihydrate, 21.6 mM phenol]. Signal in yellow is the 1.224 mM glucose/DNS reagent B reaction mixture before its microwave treatment. The signal intensity of all initial reaction mixtures at 540 nm was in between 0.015 and 0.025. Calibration curve is shown on Figure 3–17.

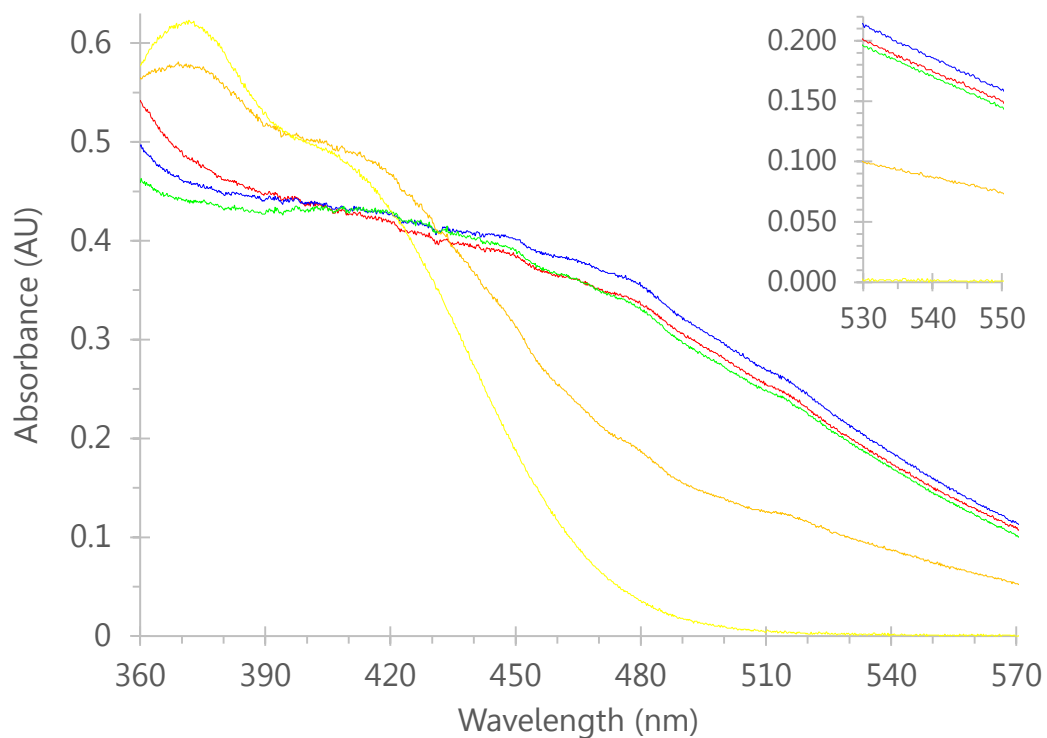


Figure A3– 23: UV-Vis spectra of 1500 μL standard *N*-acetyl-D-glucosamine (NAG) solutions of 0.594 (orange), 0.927 (green), 1.224 (blue), 1.484 (red) mM after being reacted upon microwave irradiation for 5 min at 100 $^{\circ}\text{C}$ with 1500 μL DNS reagent A [0.088 mM 3,5-dinitrosalicylic acid, 0.4079 M NaOH (pH 13.61), 0.766 M tartaric acid disodium salt dihydrate, 17.0 mM phenol]. Signal in yellow is the 0.594 mM NAG/DNS reagent A reaction mixture before its microwave treatment.

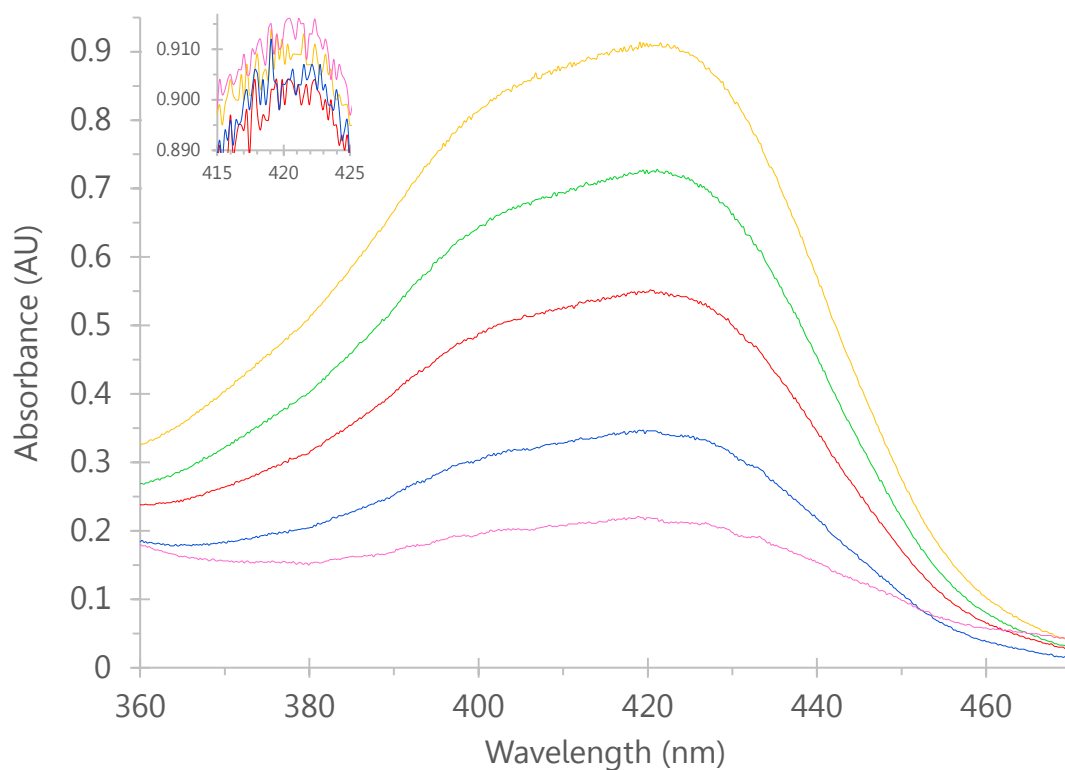


Figure A3– 24: UV-Vis spectra of 1500 μL standard *N*-acetyl-D-glucosamine (NAG) solutions of 100 (green), 200 (red), 300 (blue), and 400 (pink) μM after being reacted upon microwave irradiation for 10 min at 100 $^{\circ}\text{C}$ with 2000 μL Schales reagent. Signal in orange is the 100 μM NAG/Schaes reagent reaction mixture before its microwave treatment. Inset shows that the signal intensities of all initial reaction mixtures at 420 nm were in between 0.900 and 0.914. Calibration curve is shown on Figure 3–19.

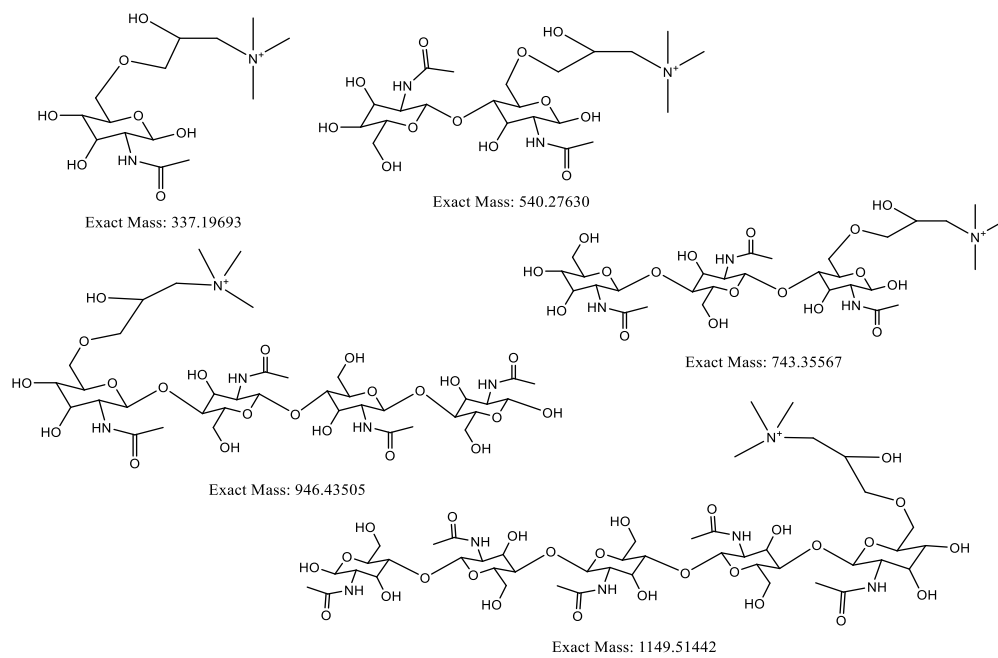


Figure A3– 25: Structures and exact masses of the MALDI-TOF MS analytes (monomer to pentamer).

A3.1 Details on m/z accuracy

Figure A3–26 records the m/z accuracy for the set of samples analyzed. Samples for 0.5, 2.0, and 6.0 h milling were derivatized and spotted/lasered on 11 and 12 of August 2015 respectively. The maximum difference from the exact mass was +0.095 for the (GlcNAc)₅ derivative peak. Sample for 4.0 h milling was derivatized and spotted/lasered on 24 and 25 of November 2015 respectively. The maximum difference from the exact mass was -0.215 for the (GlcNAc)₅ derivative peak. Calibrations of the instrument were not pursued as the recorded m/z differences for the analytes did not interfere with any other peaks. Figure A3–27 shows the dimer-GTMA peak for the 4.0 h milled sample at 540.1754, which is 0.1009 lower from its exact mass (540.2763). Its resolution (4864) is much higher than 2000 where it might have started being considered a problem for qualitative and quantitative analysis. The same stands for the rest of the analyte peaks shown in the inset table.

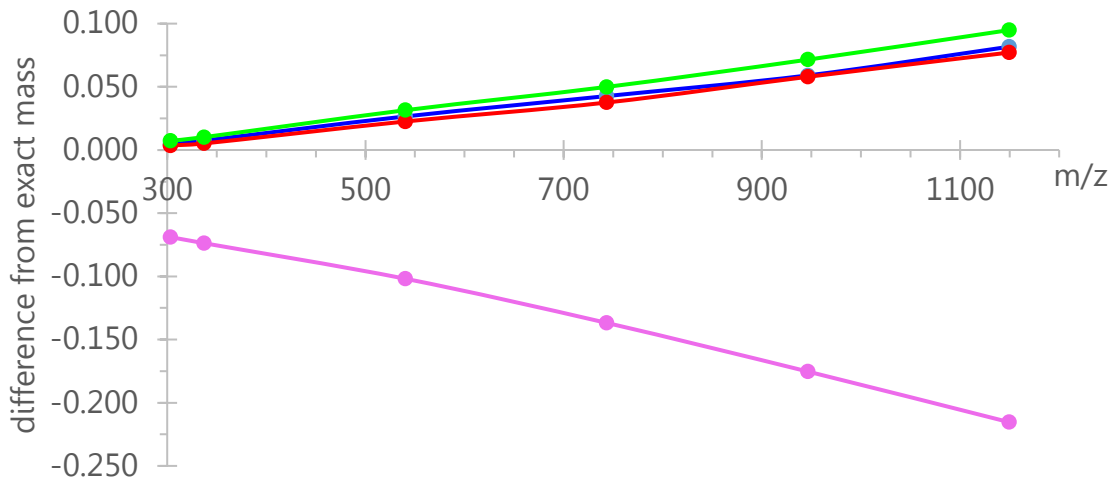


Figure A3– 26: m/z accuracy for the MALDI-TOF MS method. Number of spectra (among spots) are $n=4$ for 0.5 (blue), $n=4$ for 4 (pink), $n=5$ for 2 (red), $n=7$ for 6 (green) h milling soluble product samples ($2 \times 0.5''/68-70 \times 0.25''$ balls, with kaolinite). Exact masses of the analytes are shown in Figure A3–25.

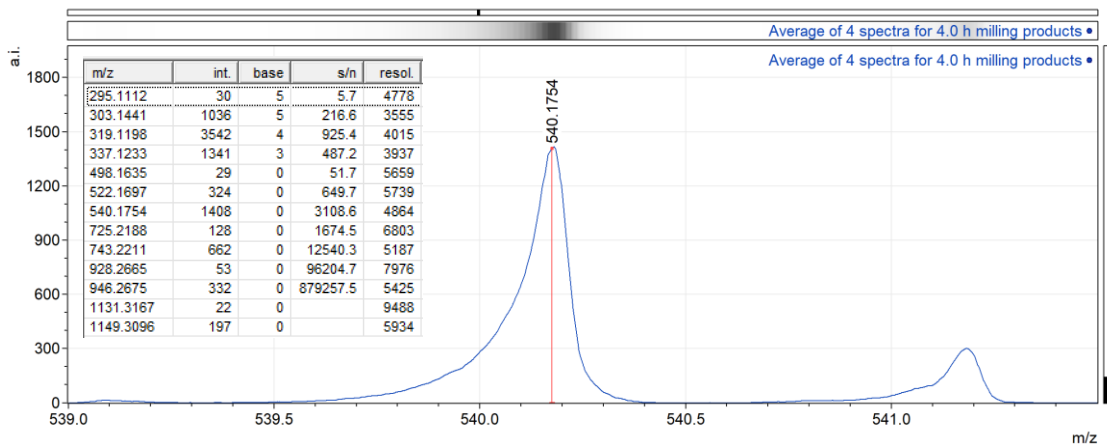


Figure A3– 27: The dimer-GTMA peak for the 4.0 h milled sample at m/z 540.1754 (protonated fragment included).

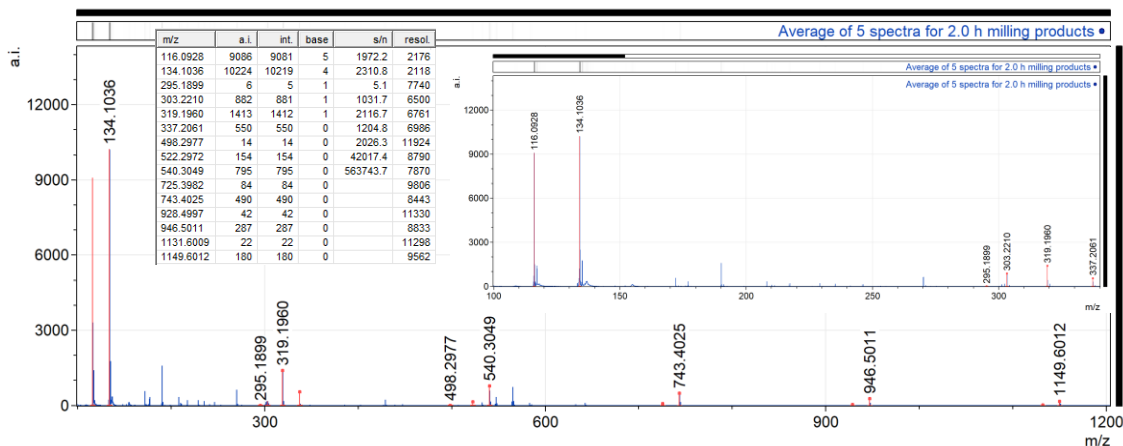


Figure A3– 28: Average spectra of the 2.0 h milling sample without subtraction of the blank derivatization reaction spectra. Inset shows the 100-340 m/z region in more detail. Inset table includes the corresponding peak list.

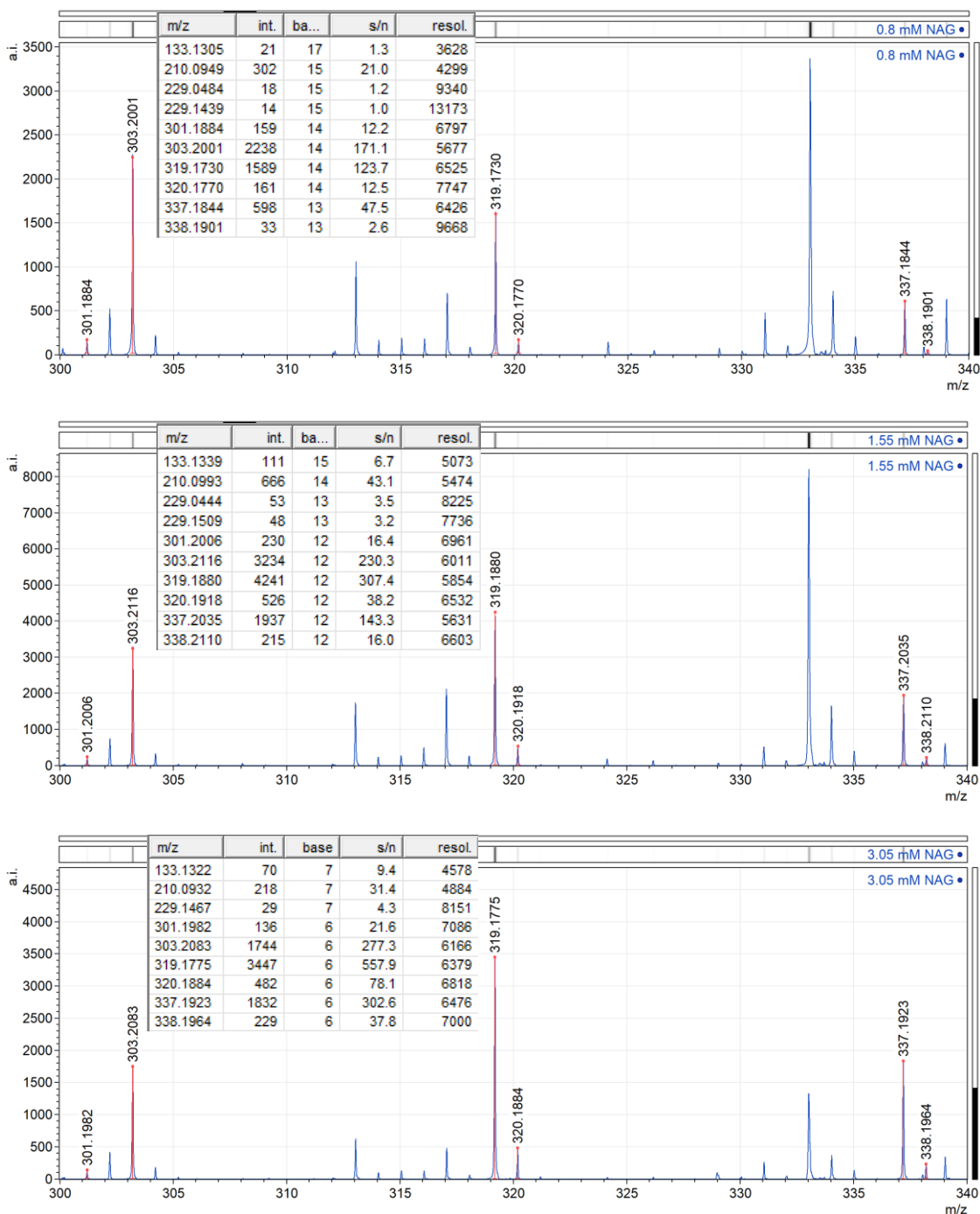


Figure A3–29: Spectra (m/z 300–340) of 0.80, 1.55, and 3.05 mM *N*-acetyl-D-glucosamine (NAG) standard solutions after derivitization with GTMA. Inset table shows the detailed peak list. Data was used to prepare NAG's calibration curve shown on Figure 3–25.

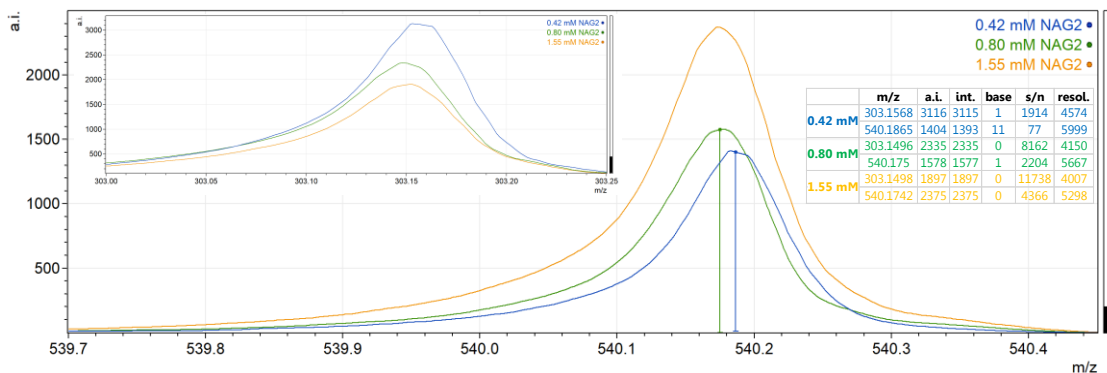


Figure A3– 30: Spectra (showing the analyte peak) of 0.42 (blue), 0.80 (green), and 1.55 (orange) mM *N,N'*-diacetylchitobiose (NAG₂) standard solutions after derivatization with GTMA. Inset spectra shows the IS peak and table records the detailed peak list. Data was used to prepare NAG₂'s calibration curve shown on Figure 3–25.

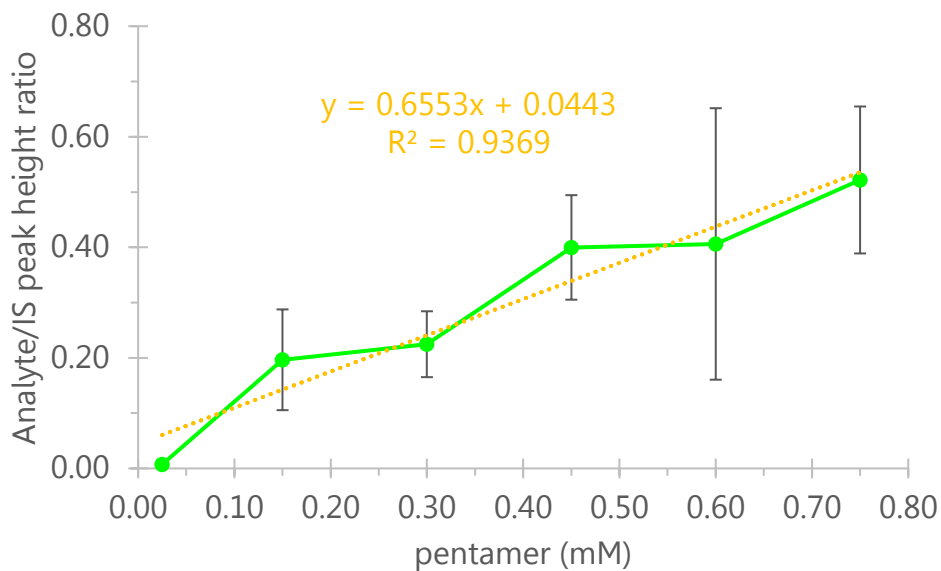


Figure A3– 31: Calibration curve for (GlcNAc)₅ prepared by GTMA derivatization and MALDI-TOF-MS. Error bars arise from quintuplicate acquisitions among spots.

Table A3– 3: Mass spectrometry peak lists for α -chitin water-soluble species of 0.5, 2.0, 6.0 h milling ($2 \times 0.5''$ /68–70 \times 0.25'' balls, with kaolinite) derivatized with GTMA. Spectra are shown in Figure 3–23.

0.5 h milling					2.0 h milling					6.0 h milling				
m/z	int.	base	s/n	resol.	m/z	int.	base	s/n	resol.	m/z	int.	base	s/n	resol.
116.0945	22748	15	1137.1	1793	116.0928	9081	5	1972.2	2176	116.0950	18142	19	1316.4	2198
133.1354	276	15	14.5	4388	133.1319	230	4	52.0	4110	133.1270	634	18	48.5	4012
134.1051	26847	15	1414.3	1291	134.1036	10219	4	2310.8	2118	134.1066	18741	18	1438.0	2560
229.1581	221	6	32.2	6825	229.1571	223	2	96.1	6464	229.1612	712	8	139.0	6386
295.1570	8	2	5.1	5620	295.1899	5	1	5.1	7740	295.1902	12	2	7.7	6955
303.2202	2505	1	1845.0	6357	303.2210	881	1	1031.7	6500	303.2209	862	2	622.5	6242
319.1955	1336	1	1309.3	6714	319.1960	1412	1	2116.7	6761	319.1979	2354	2	2174.3	6412
337.2070	311	1	486.5	7246	337.2061	550	0	1204.8	6986	337.2069	1001	1	1347.0	6668
498.2945	5	0	95.4	9402	498.2977	14	0	2026.3	11924	498.3039	9	0	65.8	7138
522.2947	171	0	3929.3	8209	522.2972	154	0	42017.4	8790	522.2988	174	0	1500.5	8344
540.3049	522	0	14025.4	7309	540.3049	795	0	563743.7	7870	540.3078	1031	0	10687.9	7451
701.2953	6	0	4783.2	4889	701.3990	7	0		13584	701.3691	5	0	2648.9	8772
701.3658	6	0	4552.0	4786	725.3982	84	0		9806	725.4010	50	0	57034.9	9102
725.3934	86	0	144959.5	8224	743.4025	490	0		8443	743.4069	462	0	3086770.4	8175
743.4013	293	0	2693994.7	7382	904.4963	3	0		21724	904.4905	1	0		20970
904.5084	1	0		10210	928.4997	42	0		11330	928.5075	11	0		11244
928.4949	45	0		9172	946.5011	287	0		8833	946.5076	187	0		9105
946.5053	154	0		7521	1131.6009	22	0		11298	1131.5732	2	0		7862
1131.6013	18	0		8108	1149.6012	180	0		9562	1149.6098	72	0		9685
1149.6037	74	0		6870										

Table A3– 4: Yield (g) calculation for GlcNAc and (GlcNAc)₂ when ball milling 1.00 g α-chitin with 68–70 × 0.25" / 2 × 0.5" balls (17.5 % packing, BtP 42.8) and kaolinite (1:1 g:g).^a

Measured quantity	Milling time (h)			
	0.5	2	4	6
A. Solubility %	16.7	50.3	73.7	75.8
B. Soluble products (mg)	167	503	737	758
Γ. Actual soluble mass (mg)	18.9	62.3	98.9	85.7
Δ. Water needed (mL)	66	61	56	66
E. [GlcNAc] (mM)	0.39	1.87	2.79	3.49
Z. [GlcNAc] ₂ (mM)	0.21	1.00	1.18	1.39
H. GlcNAc (mol)	2.6E-05	1.1E-04	1.6E-04	2.3E-04
Θ. (GlcNAc) ₂ (mol)	1.4E-05	6.1E-05	6.6E-05	9.2E-05
I. GlcNAc (g)	5.7E-03	2.5E-02	3.4E-02	5.1E-02
K. (GlcNAc) ₂ (g)	5.9E-03	2.6E-02	2.8E-02	3.9E-02

^a 1.00 g of α-chitin charged in the ball milling vial (along with 1.00 g kaolinite) will theoretically give 1000 mg (depolymerized) products (as we have observed no mass loss during ball milling).

Based on the solubilities of Figure 3–14, the masses of the soluble products (out of those 1000 mg) are expected to be those of measured quantity B.

When using 7.5 mL of water for the solubility tests, the actual masses of soluble products were those of measured quantity Γ.

The volumes of water needed to create the solutions for those theoretical masses of soluble products are expected to be those of measured quantity Δ.

Based on the concentrations given by MALDI-TOF MS (measured quantities E and Z), the number of mol of GlcNAc and (GlcNAc)₂ produced from ball milling 1.00 g of α-chitin are expected to be those of measured quantities H and Θ.

Yield (in g) for GlcNAc and (GlcNAc)₂ (MW are 221.1 and 424.2 g/mol respectively) from 1.00 g of α-chitin are those of measured quantities I and K.

Table A3– 5: Size exclusion chromatography (SEC) data for *N*-acetylglucosamine (NAG) and other chito-oligosaccharide standards.

Compound	Actual M_r	GPC M_n [a]	GPC M_p [b]	M_w/M_n	Retention Volume (mL)
NAG	221	306	289	1.04	19.22
(NAG) ₂	424	657	653	1.02	18.07
(NAG) ₄	831	1221	1263	1.02	17.02
(NAG) ₅	1034	1609	1650	1.01	16.58
(NAG) ₆	1237	2006	1947	1.00	16.32

[a] M_n was obtained via calibration against PEG standards

[b] M_p is the mode of the molecular weight distribution. M_p is quoted for very narrowly distributed polymers, such as polymer standards used in calibrations. Therefore, M_p might be a better reflection of the actual mass.

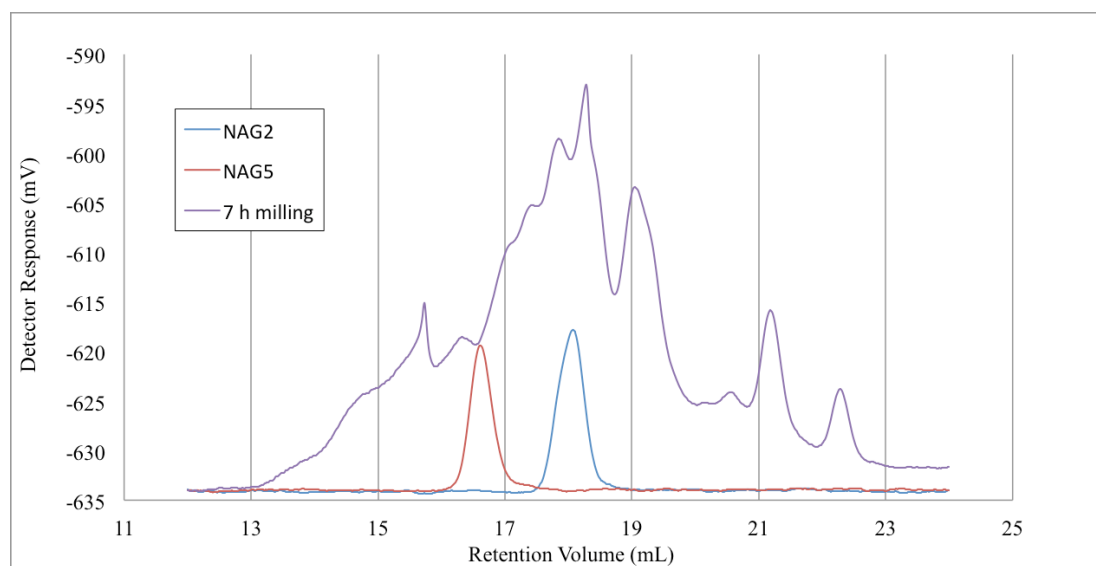


Figure A3– 32: Size-exclusion chromatogram for water-soluble products generated by grinding a 1:1 w/w mixture of chitin and kaolinite for 7 h (purple line) with 68–70 × 0.25" / 2 × 0.5" balls. Chromatograms of standards (NAG₂, blue line and NAG₅, red line) included for comparison.

Appendix A4

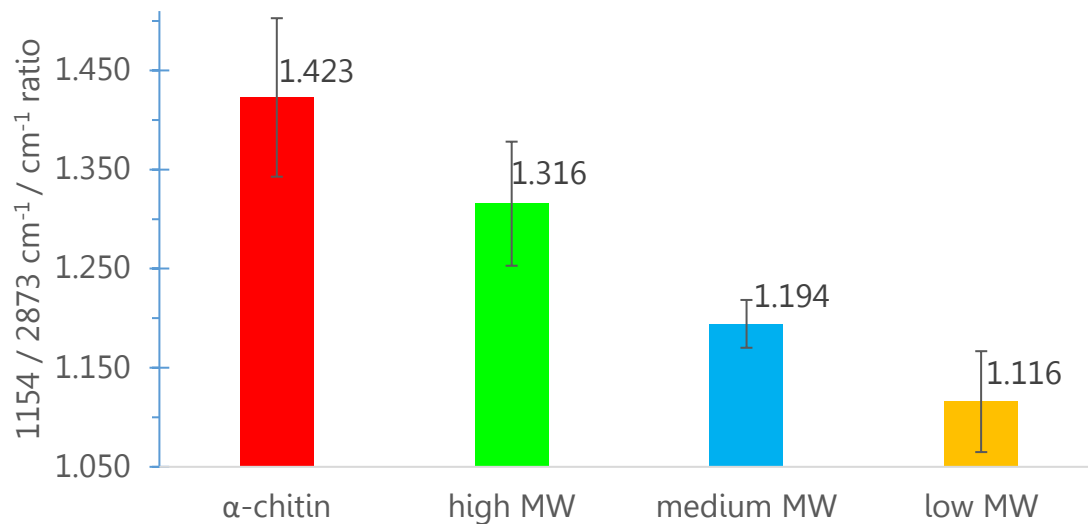


Figure A4– 1: FT-IR intensity ratio (1154 / 2873 cm⁻¹ / cm⁻¹) probing depolymerization of α-chitin samples prepared for dissolution and film casting studies. Complementary data recorded on Table 4–1.

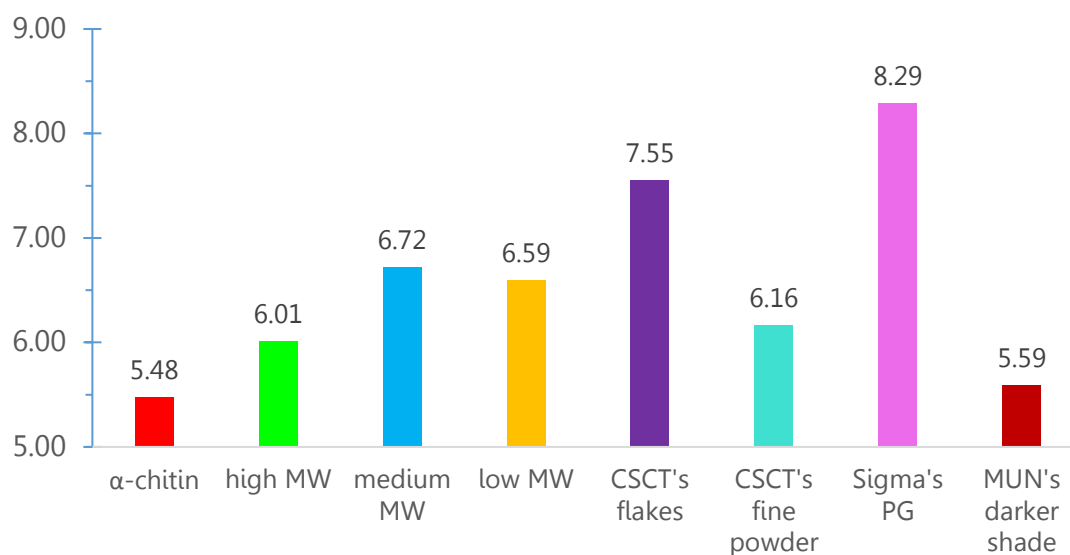


Figure A4– 2: Moisture contents (wt.%) of all available chitin samples. Values determined gravimetrically by drying 109 ± 21 mg sample on a ~25 L Vacutherm oven (Thermo Scientific) at 105 °C/50 mbar vacuum for ca. 15 h.

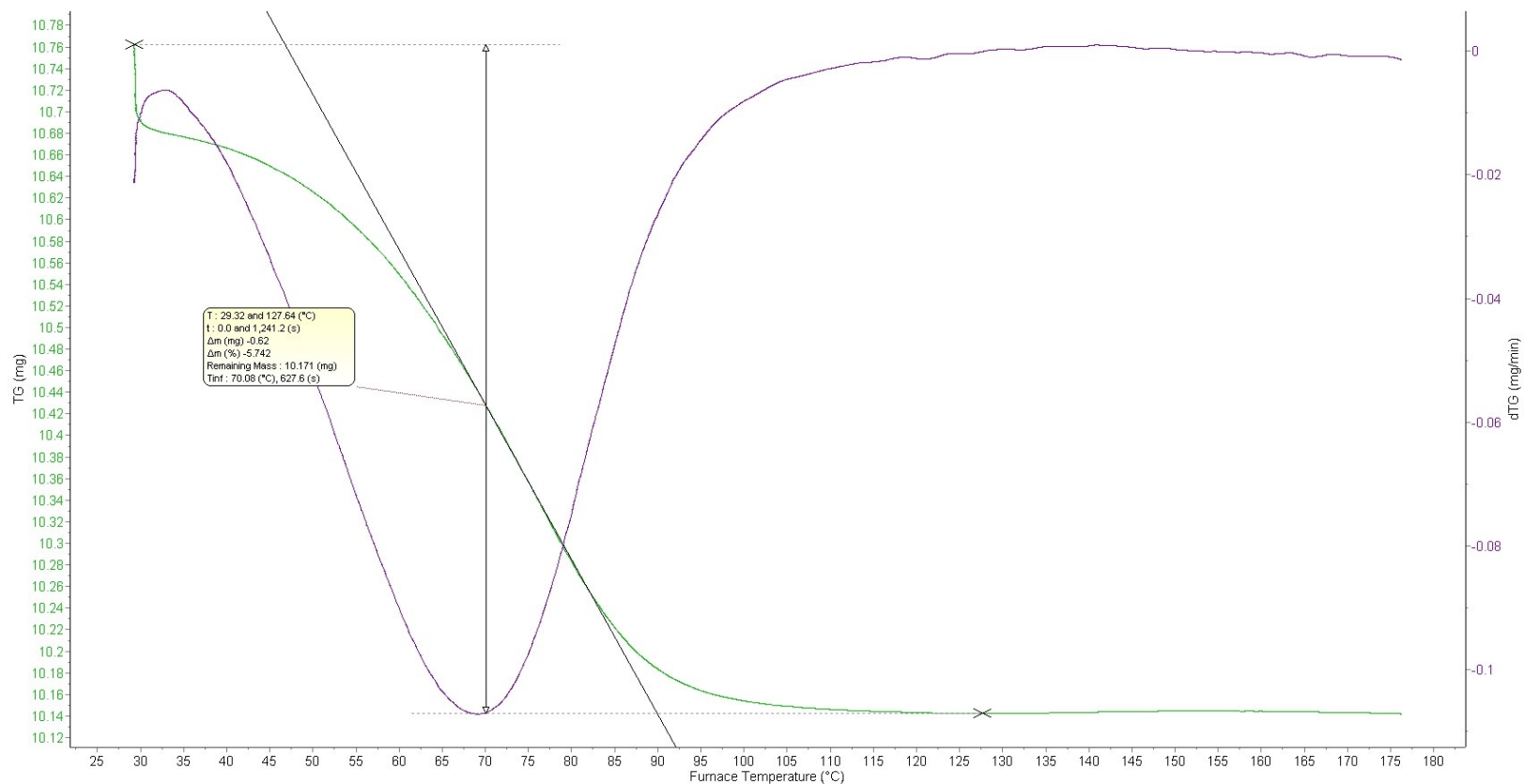


Figure A4– 3: Thermogravimetric analysis (TGA) curve (green) for moisture determination of high MW α -chitin. The heating rate from ca. 30 to >130 °C was ca. 6.3 °C/min. The mass loss in 1,241.2 s (ca. 20.7 min) was 5.74% (final temperature: 127.6 °C).

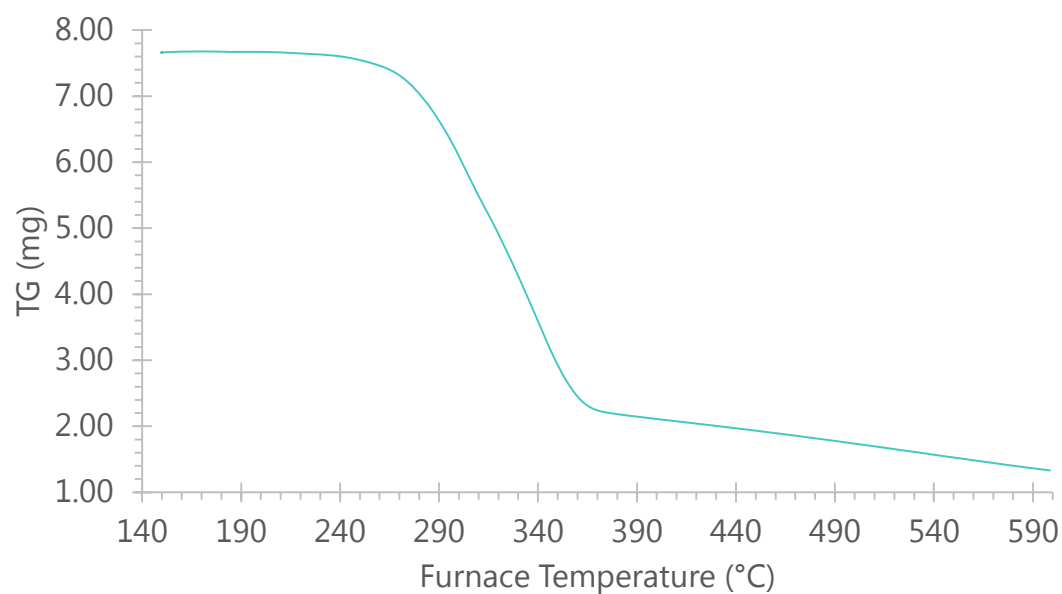


Figure A4– 4: Thermogravimetric analysis (TGA) curve for decomposition of high MW α -chitin. The heating rate was ca. 5.0 °C/min.

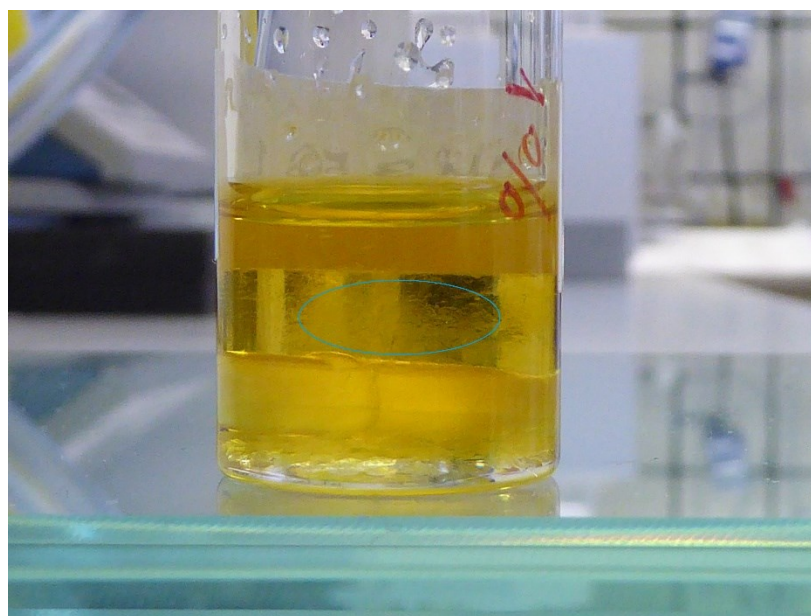


Figure A4– 5: Photograph of a 1.0 wt.% native α -chitin in 1:1 EmimAcO : DMSO after stirring at 100 °C for two days. Ellipse in blue above the white magnetic stir bar highlights a blurry region, which is characteristic of undissolved crystalline domains.



Figure A4– 6: Solidified honey-like coloured sample of 4.37 wt.% practical grade chitin in 20 wt.% NaOH.

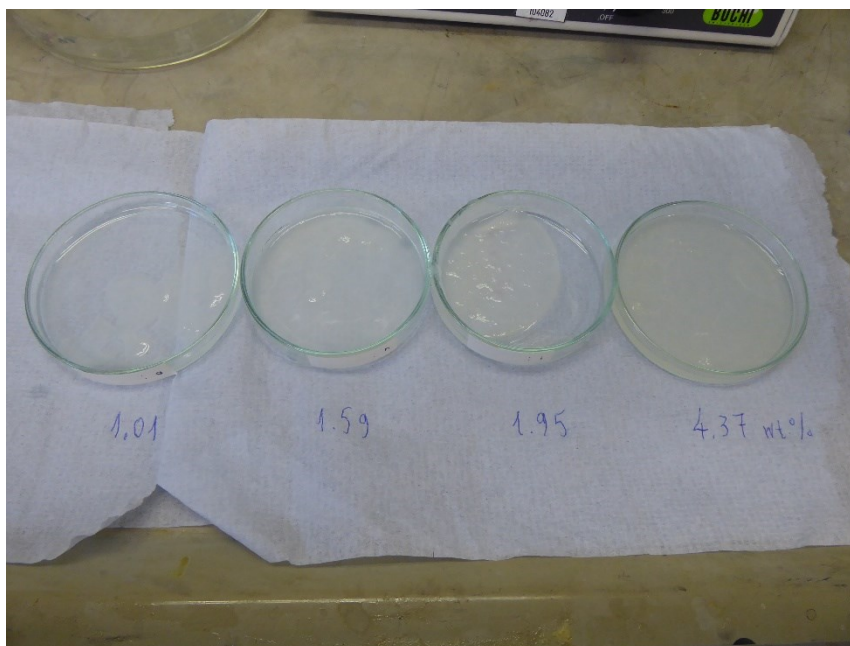


Figure A4– 7: Spread of wet practical grade (PG) chitin films after their anti-solvent (HCl) bath treatment. Concentrations from left to right: 1.01, 1.59, 1.95, 4.37 wt.%.

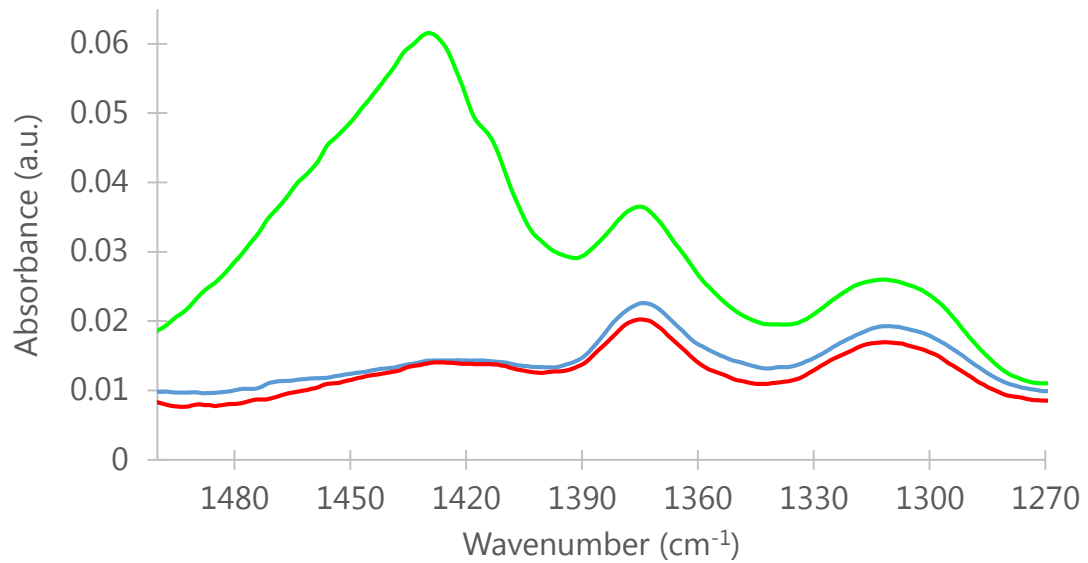


Figure A4– 8: Infrared spectra of deacetylation products 4–7 (red), 4–6 (blue) and 4–1 (green) acquired at CSCT.

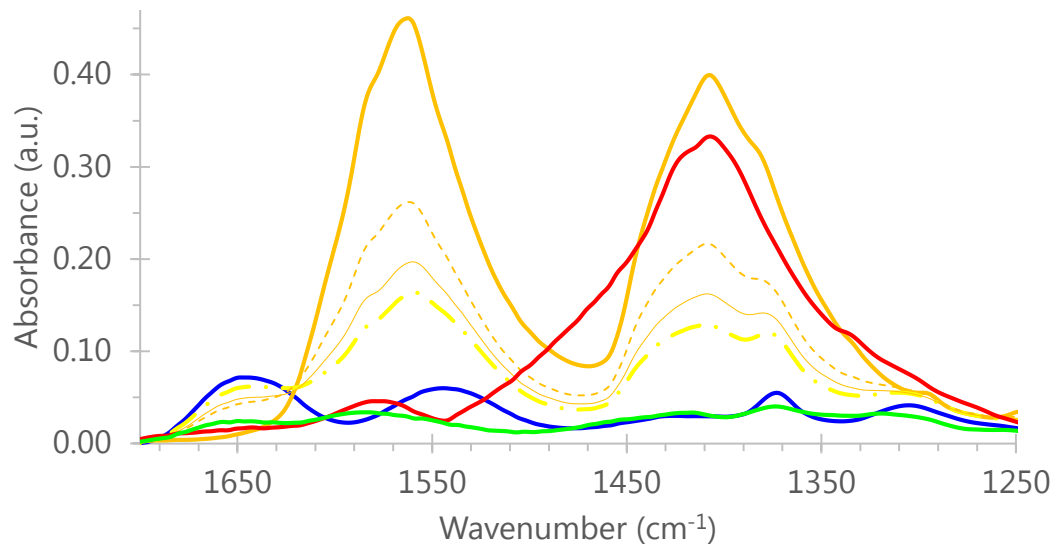


Figure A4– 9: Infrared spectra (amide region) of standard mixtures of 0 (blue solid), 35 (yellow long dash dot), 50 (orange thin solid), 65 (orange dash), 100 (orange solid) wt.% anhydrous sodium acetate (CH_3COONa) in milled α -chitin ($\sim 35\%$ CrI), product 4–1 before (red solid) and after (green solid) its washing treatment. Data were acquired at MUN.

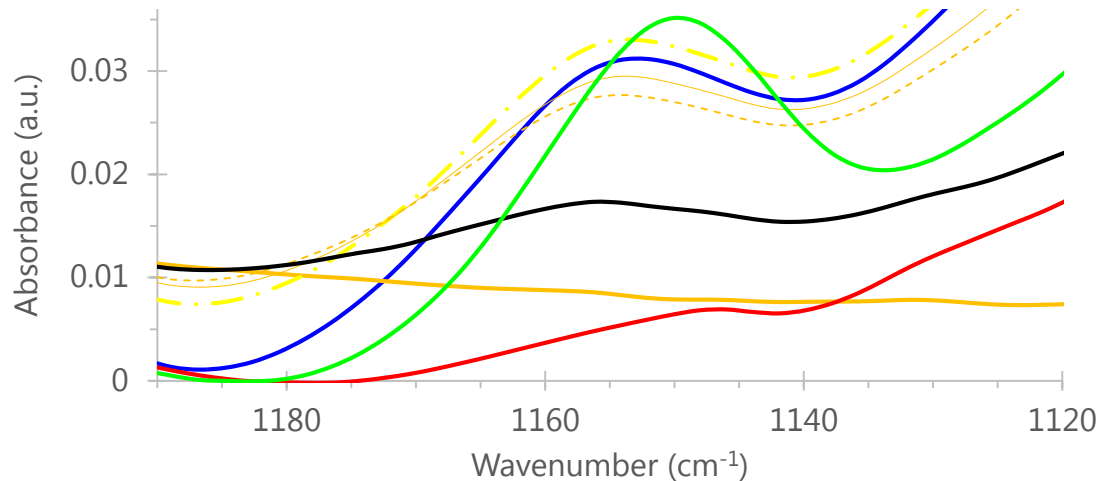


Figure A4– 10: Infrared spectra (glycosidic linkage region) of standard mixtures of 0 (blue solid), 35 (yellow long dash dot), 50 (orange thin solid), 65 (orange dash), 74 (black solid), 100 (orange solid) wt.% anhydrous sodium acetate (CH₃COONa) in milled α-chitin (~35% CrI), product 4–1 before (red solid) and after (green solid) its washing treatment. Data were acquired at MUN.

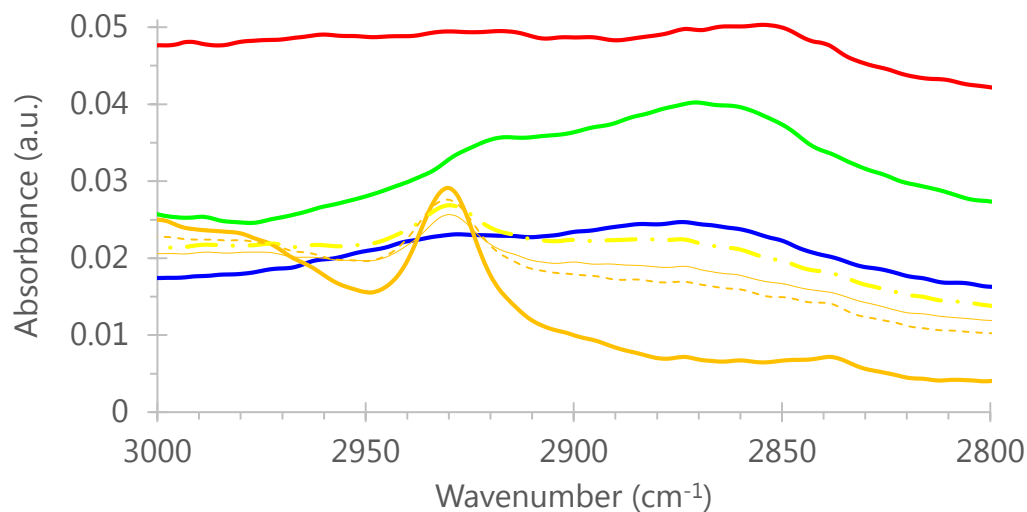


Figure A4– 11: Infrared spectra (carbon-hydrogen region) of standard mixtures of 0 (blue solid), 35 (yellow long dash dot), 50 (orange thin solid), 65 (orange dash), 100 (orange solid) wt.% anhydrous sodium acetate (CH₃COONa) in milled α-chitin (~35% CrI), product 4–1 before (red solid) and after (green solid) its washing treatment. Data were acquired at MUN.

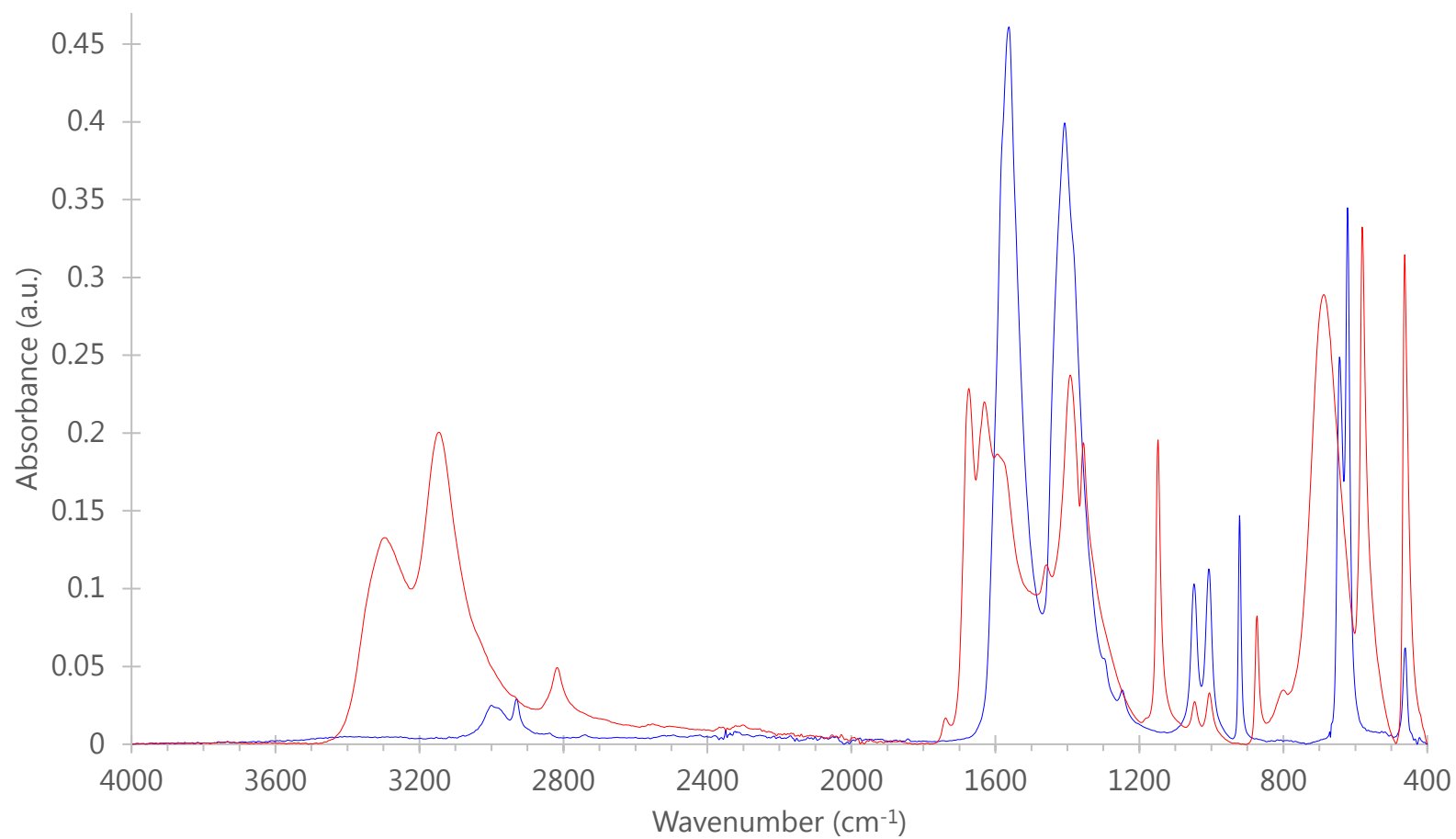


Figure A4– 12: Infrared spectra of ammonium (red) and sodium (blue) acetate.

A4.1 Conventional integrations in chitin solid-state NMR

Peak picking options were: standard method, only positive peaks, 10.00 noise factor, 10.00 sensitivity, 1000 max # of peaks, parabolic interpolation ticked, auto classify not ticked, interactive not ticked. Integration options were: peaks calculation method, default method parameters, autodetect integral regions, peak picking algorithm, 3.00% min area, apply automatic integration was not ticked.

When manual integrations were conducted (hence peaks were not picked) with method "Sum" [the algorithm was set as "peak picking" (same parameters as above)], the DA values of all samples in Figures 4–29 and 4–30 did not exceed 104.6% (95.1% was the lowest DA value). However, the majority of them were still above 100.0% (see Table A4–1). Interestingly, the DAs of the 14% packing set (Figure 4–30) where deacetylation is expected with increasing milling time and BtC, increased with increasing milling treatment. The reverse is observed for the 3% packing set where deacetylation is expected to be negligible. When spectra for PG chitin and 8/105 were opened with TopSpin (Bruker) and integrated (with no baseline correction) over the same frequency range, the resulting DAs were 95.04% and 102.3%. This suggests that the two softwares give almost identical results. However, the obtained DA values are not consistent with the so far analysis in this thesis.

When the "Sum" integration method was applied with autodetect regions [(hence MestreNova integrated each of the C1–C6 peaks separately (except the ones for

8/105 and 33/30 which exhibit significant peak overlap)], DAs for all six samples were in between 100.7% and 111.8% (no particular trend was observed for the amorphization effect). When the algorithm was derivative (instead of peak picking), DAs of the 8/105 sample for different sensitivities ranged from 115 to 172% [merging distance was 0.040 ppm and minimum area 3.00% (default settings)].

All these trials for manual and automatic conventional integration (calculation method "Sum") suggest that the method is not reliable probably due to challenging signal overlap in the 46-115 ppm region. Therefore, a deconvolution approach is hypothesized to improve the calculation of DA.

Table A4– 1: Manual integration data for chitin solid state NMR spectra in Figures 4–29 and 4–30.

with baseline correction				no baseline correction				
PG-chitin		Range (ppm)	Normalized	Absolute		Range (ppm)	Normalized	Absolute
	1	107.82 .. 53.61	600	8656143.1	1	107.87 .. 53.56	600	8475731.33
	2	26.57 .. 21.09	98.19	1416570.99	2	26.57 .. 21.09	95.07	1342929.11
13/10		Range (ppm)	Normalized	Absolute		Range (ppm)	Normalized	Absolute
(GM4.61z)	1	107.10 .. 52.47	600	10588166.67	1	107.15 .. 52.48	600	10588166.67
	2	26.64 .. 19.48	98.97	1746492.61	2	26.64 .. 19.48	98.97	1746492.61
33/30		Range (ppm)	Normalized	Absolute		Range (ppm)	Normalized	Absolute
(GM4.55)	1	107.74 .. 51.23	600	12264468.66	1	107.81 .. 51.21	600	11541248.09
	2	26.85 .. 17.43	100.91	2062619.95	2	26.85 .. 17.43	101.73	1956775.35
8/5		Range (ppm)	Normalized	Absolute		Range (ppm)	Normalized	Absolute
(GM4.70)	1	107.58 .. 51.81	600	10863169.37	1	107.54 .. 51.78	600	10119218.23
	2	26.54 .. 19.16	103.19	1868214.7	2	26.55 .. 19.17	104.59	1763906.75
8/45		Range (ppm)	Normalized	Absolute		Range (ppm)	Normalized	Absolute
(GM31)	1	107.02 .. 50.44	600	12048989.73	1	107.06 .. 50.39	600	11362396.28
	2	26.56 .. 17.47	102.22	2052702.08	2	26.56 .. 17.47	103.57	1961336.97
8/105		Range (ppm)	Normalized	Absolute		Range (ppm)	Normalized	Absolute
(GM35)	1	108.15 .. 50.06	600	12253660.49	1	108.14 .. 50.02	600	11507596.73
	2	26.86 .. 17.41	100.83	2059181.31	2	26.86 .. 17.41	102.3	1962083.74

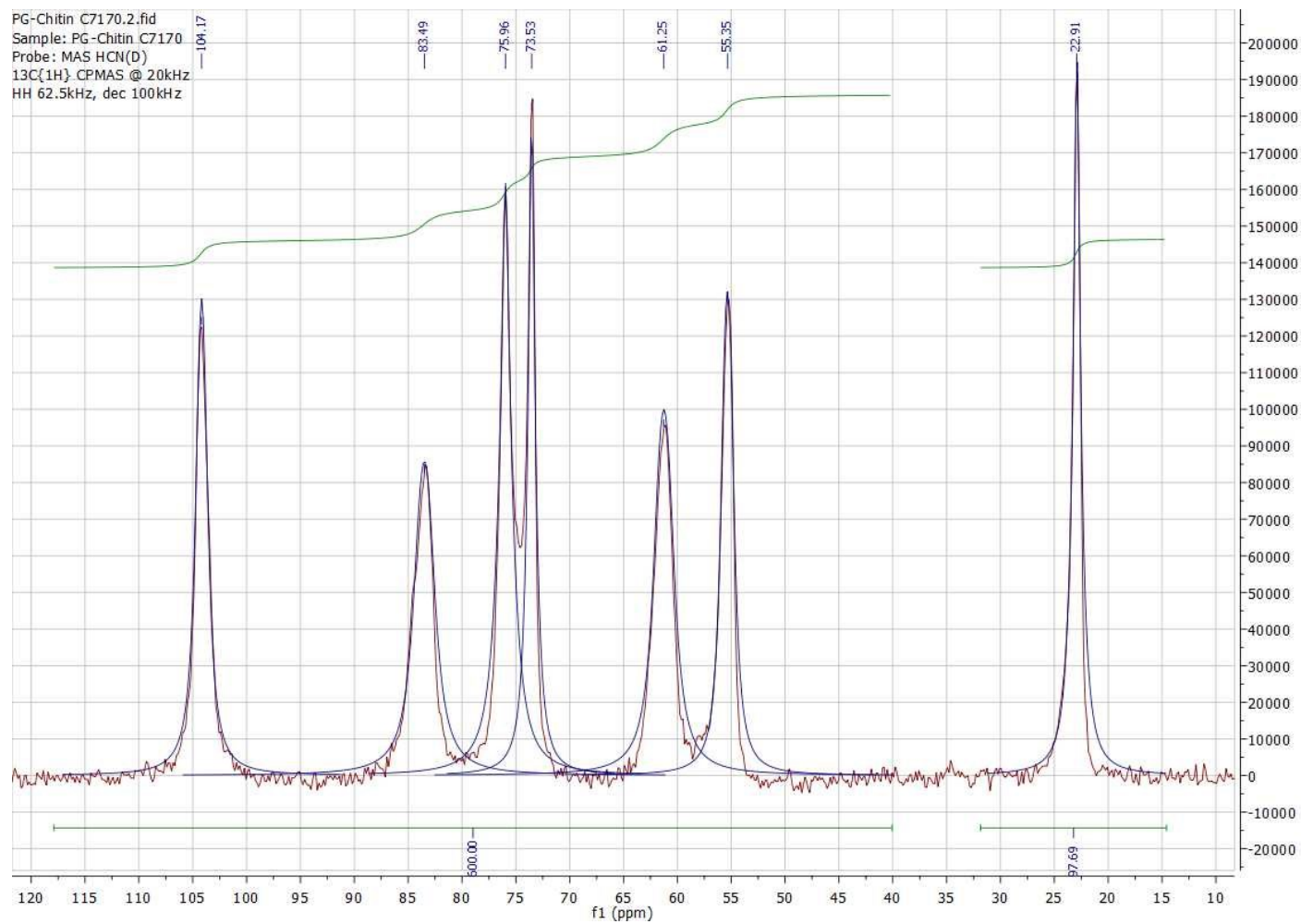


Figure A4– 13: Solid state CPMAS ^{13}C NMR spectra of PG chitin. DA obtained with MestreNova 11 GSD peak picking is 97.7% (optimization for narrow peaks, refinement level 2).

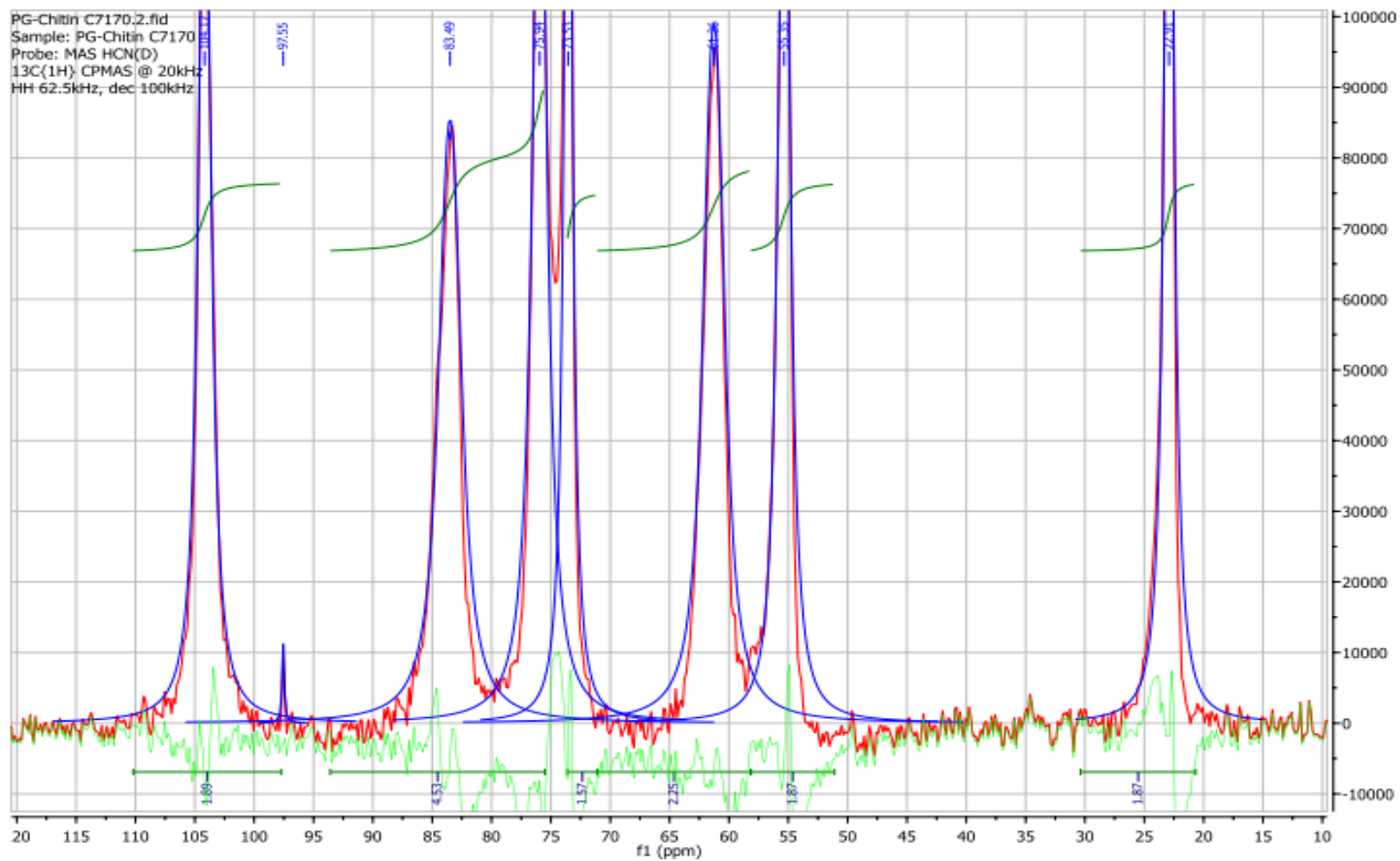


Figure A4– 14: Deconvolution and line fitting of solid state CP/MAS ^{13}C NMR spectra of PG chitin (red signal is for experimental data, blue is for the fitted line and green is the residue line) using MestreNova v. 10.0.2. Table A4–2 records the line fitting peak parameters and DA calculation.

Table A4– 2: Line fitting peak parameters and DA calculation for PG chitin (see spectrum in Figure A4-14).

Line Fitting					
Name: PG-chitin (narrow, 20 fit. cycles)					
From: 9.690 ppm					
To: 119.789 ppm					
Residual Error:7.63e+07					
#	ppm	Height	Width(Hz)	L/G	Area
1	104.17	130552.2	194	0.3	1721490.12
2	97.55	11261.52	31	-0.2	25762.694
3	83.49	85514.86	337	0.51	1901645.99
4	75.94	162654	186	-	2221005.23
5	73.53	177580.8	112	-0.1	1427292.07
6	61.26	99127.63	319	0.63	2046471.44
7	55.35	132235.3	195	0.49	1703901.06
8	22.91	196421.7	119	-	1705269

sum of #1-7 peak areas
11047568.6

DA 92.6%

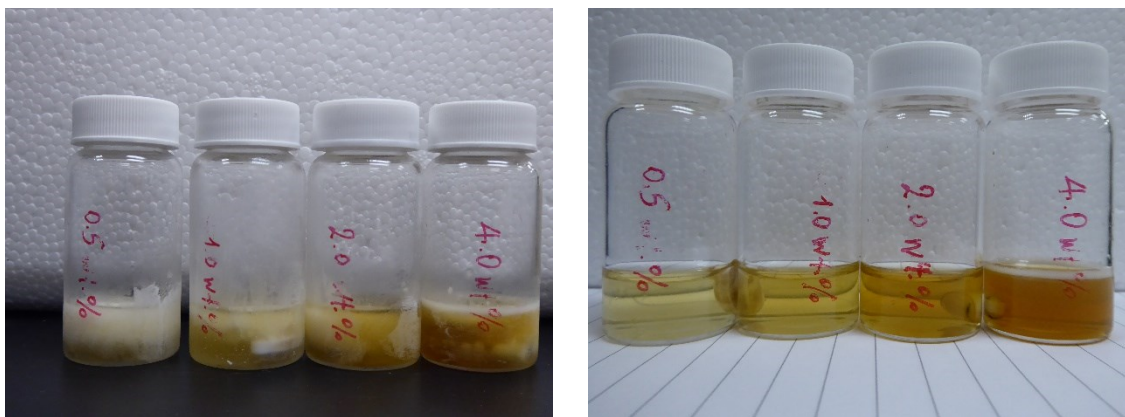


Figure A4– 15: Photographs of 0.5, 1.0, 2.0, 4.0 wt.% low MW α -chitin (see Table 4–1) in \sim 20 wt.% NaOH when frozen (left) and after thawing (right).

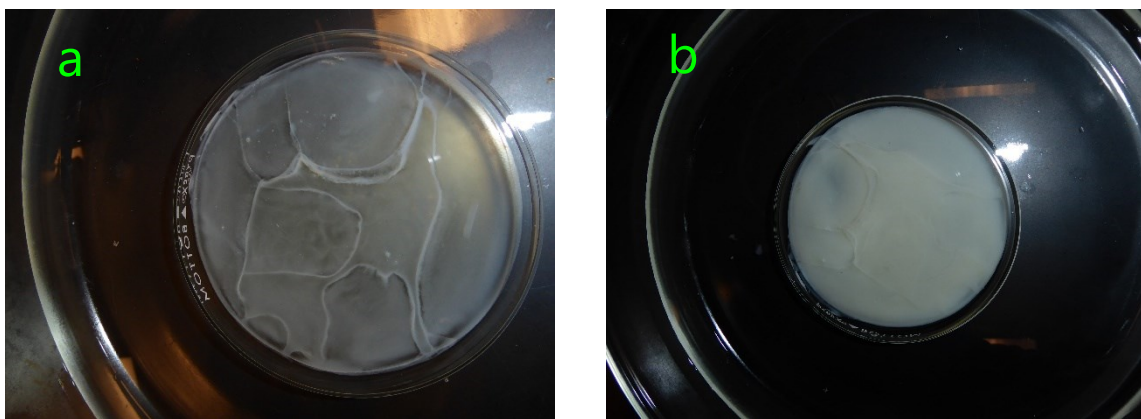


Figure A4– 16: Photographs of 4.77 wt.% 13/10 chitin in 19.00 wt.% NaOH immersed in a \sim 0.24 wt.% HCl bath for 10 min (a) and 4 h (b).